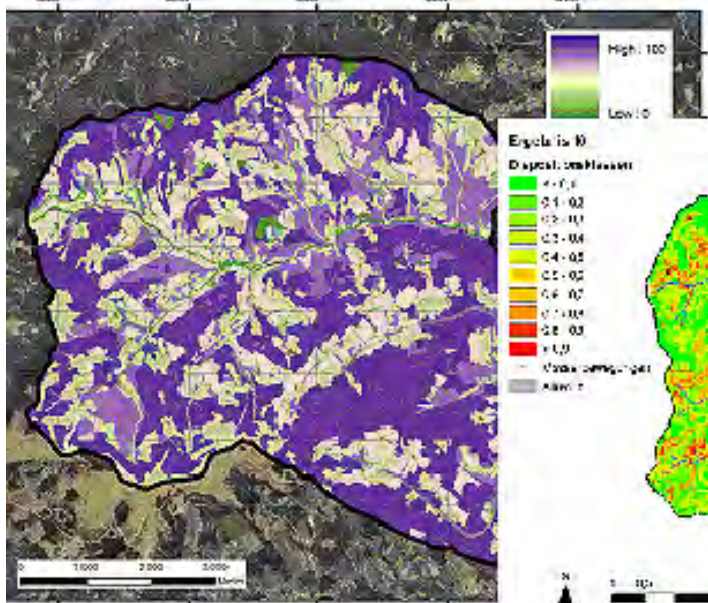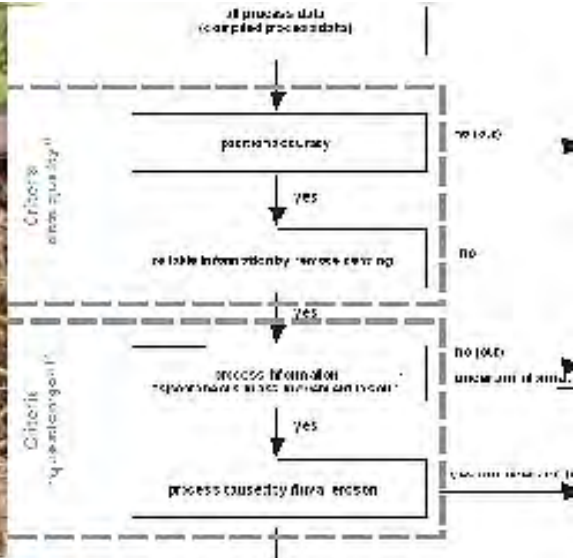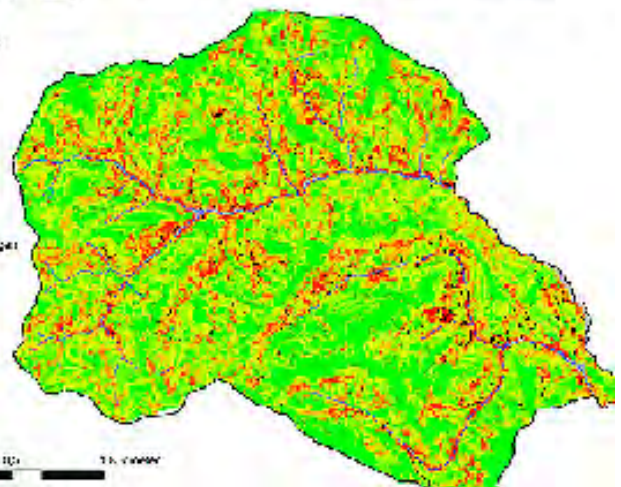# ENDREPORT - ADAPTSLIDE

ADAPTSLIDE

Wien, Juli 2011

Modelling of Landslide Susceptibility and affected Areas – Process-specific Validation of Databases, Methods and Results for the Communities of Gasen and Haslau

(AdaptSlide)

Modellierung von Rutschungsdispositionen und Prozessbereichen – Prozessspezifische Bewertung von Datengrundlagen, Methoden und Ergebnissen für das Gemeindegebiet von Gasen und Haslau

(AdaptSlide)

Vienna July 2011

Index of Authors:

Geological Survey of Austria (GBA)
Tilch Nils, Schwarz Leonhard

Federal Research and Training Centre for Forests, Natural Hazards and Landscape (BFW)
Hagen Karl, Aust Günter, Fromm Reinhard, Herzberger Edwin, Klebinder Klaus, Perzl Frank

Joanneum Research (JR)
Proske Herwig, Bauer Christian, Kornberger Birgit, Kleb Ulrike, Granica Klaus

Central Institute of Meteorology and Geodynamics (ZAMG)
Pistotnik Georg, Haiden Thomas

Content

Catalogue of Figures and Tables

Abstract:

Modelling of Landslide Susceptibility and affected Areas – Process-specific Validation of Databases, Methods and Results for the Communities of Gasen and Haslau (AdaptSlide)

Modellierung von Rutschungsdispositionen und Prozessbereichen – Prozessspezifische Bewertung von Datengrundlagen, Methoden und Ergebnissen für das Gemeindegebiet von Gasen und Haslau, (AdaptSlide)

In recent years several approaches to estimate landslide starting zones were developed. However, the practical value of the results for hazard assessment cannot be considered proven.

The AdaptSlide project provides a comprehensive and conclusive overview of currently available data bases, approaches and models to asses the susceptibility of spontaneous gravitational mass movements in loose material. Approaches to determine the whole affected areas have been developed. Process-orientated geological basic disposition maps, soil maps, remote sensing data, runoff disposition maps and precipitation maps were generated and assessed regarding cost-benefit aspects. The landslide susceptibility of the test-area (communities of Gasen and Haslau in SE_Austria) was modelled with several statistics-based approaches (Neural Network, Weight of Evidence, Logistic Regression) and one deterministic model (SINMAP). Model results have been validated and compared as far as possible; the limitation of current available validation methods was highlighted. A simple empirical model was developed to estimate the process area, based on landslide susceptibility maps. Methods were discussed regarding their potential to represent the impacts of climate and land use changes.

1. Introduction

In the recent years beside other natural hazards also landslides have caused substantial damage to settlements and infrastructure in mountainous regions like the Alps. In the future more frequent and more serious damage to property seems to be likely, because the relevant factors probably develop in an adverse way. Since the damage respectively the risk of losses of life and damage to property depends on the development of the process as well as on the development of the property, changes of both factors have to be considered.

A causal relationship between climatic developments and damage events with an ever increasing amount of damage seems to be obvious at first sight. For complex systems such as landslide processes it is important to critically question such a simplified representation of causal interrelationships. In order to be able to draw informed conclusions and to assess the effects of changes of individual system components like climate parameters or land-use, the "status quo" needs to be known, respectively the approaches and methods to estimate them and the incertitude's which have to be taken into account, using their results as basis for any kind of risk management.

Coming along with lately frequent landslide events in Austria (Gasen 2005 (BMLFUW 2006, Andrecs et al. 2007), Vorarlberg 2005 (BMLFUW 2006, Markart et al. 2007, Tilch & Kociu 2006, Tilch et al. 2009), Klingfurth 2009 (Chifflard & Tilch 2010, Tilch 2009), Feldbach and adjacent districts 2009 (Haberler et al. 2009, Schwarz et al. 2009)) a lack of area-wide slope susceptibility information, especially in case of spontaneous landsides in loose material showed up. The unexpected occurrence and the often rapid movement of such movements are specific characteristics of this kind of natural hazard, which cause high damage potential and hinder land-use planning measures.

A comprehensive and conclusive representation of currently available model chains is necessary to access reliable landslide susceptibility (spatial probability) and potential extent (runout and magnitude) approaches and models.

Hence, the Austrian Federal Ministry for Agriculture, Forestry, Environment and Water Management (BMLFUW) launched a cooperation of the Federal Research and Training Centre for Forests, Natural Hazards and Landscape (BFW), the Geological Survey of Austria (GBA), the Joanneum Research (JR) and the Central Institute of Meteorology and Geodynamics (ZAMG) to evaluate several databases and the potential of new technologies like Remote Sensing Technologies as LIDAR (airborne Laserscanning) and VHR (very high resolution) satellite images, with reference to the landslide relevant information content. Subsequently, the project aims to develop, improve and compare different methods of area-wide spontaneous landslide assessment in loose material. A further aim was to develop a method to estimate the extent of the process zones in an area-wide approach. The former three organizations already cooperated in a previous project (Tilch et al. 2009) under the guidance of the GBA, collecting data from a landslide-event in the communities of Gasen and Haslau 2005, and building up a database, which should allow further landslide-related activities.

Under the title „AdaptSlide (Modelling from slide disposition and process-area in the communities of Gasen and Haslau), project work has started in Oct. 2009, revering to this database. The project is part of the EU Alpine Space project Adaptalp

(Adaptation to Climate Change in the Alpine Space, Priority 3: Environment and Risk Prevention) which aims to describe possible adaptation strategies to climate change in the alpine space.

2. Aims and Strategies of the Project

The main aim of the AdaptSlide project was to develop, improve and compare different methods of area-wide spontaneous landslide assessment in loose material while optimizing the thematic data, thus ascertaining a reproducible approach to estimate landslide susceptibility. The main output to be produced are susceptibility maps for spontaneous shallow mass movements for the communities of Gasen and Haslau.

In detail aims and strategies of the project consider the following items: (1) the processing of input data, (2) the landslide susceptibility modelling with different approaches, (3) the comparison and validation of the results with adequate methods, (4) the modelling of process-areas, (5) the potential of the applied methods in modified basic conditions (e.g. climatic changes) and (6) the analysis of benefits and costs of the applied data and methods.

1) Aiming at the generation of a reliable database for the model development the first focal point is to evaluate the available landslide inventory carefully and to divide it into batches of different quality. In order to ensure a clear, transparent extraction of the data, a hierarchical method has to be developed and applied. With regard to the available input maps of environmental parameters high priority is given to the aspect of process-relevant processing utilising the different expertises and synergies of the involved project partners. Data are analysed critically with regard to their physical relevance to eliminate accidental correlations which may distort the modelling result. Different data sources (general available data and innovative ones) are used and different processing levels (low effort and high effort) are taken into account aiming at the evaluation of benefits and limits with regard to the modelling of landslide susceptibility.

2) The modelling part is arranged to evaluate different methods of modelling the susceptibility. Three statistical approaches representing different complexity of calculations are selected aiming at the identification of the best method. In order to take advantage of the excellent database and to demonstrate a completely different method a deterministic approach is applied as well. A general strategy for successively integrating different parameters for the statistical modelling is developed considering "level low" parameters and parameters with high correlation to the distribution of landslides first, followed by "level high" parameters. The number of parameters is extended one by one to quantify their influence. The best results according to different validation methods are selected and are re-calculated using simplified datasets without involving field-mapped landslide data in order to point out the significance of such data. Runs with process-oriented parameter combinations exclusively were also calculated, based on expert knowledge rather than on the strategy for successively integrating different parameter maps.

3) As different approaches are applied and many different parameter combinations are calculated, high priority has to be given to the validation and comparison of the results with adequate methods. The drawbacks of the state-of-the art validation methods characterizing the

whole test area without any local differentiation should be reduced by the joint interpretation of several methods. Aiming at visualizing the differences of selected modelling results, difference maps are calculated within one method as well as between two of the applied statistical methods.

4) As the resulting maps were designed to be finally used in landuse planning tasks, not only susceptibility maps of the landslide source areas were to be displayed. Since landslides in loose material frequently result in debris flow and thus affect much larger areas than the starting zones, a further aim was to estimate the whole process areas. Therefore the method need to be applicable on an area wide basis and should have moderate model input requirements. Since the method should complete the contents of landslide-disposition maps, it has to be attuned on such maps regarding e.g. the kind of starting information the scale and the display of results.

5) Analyses should comprise the potential of the methods and models to consider changing environmental conditions caused by climate change or variations in land use. Regarding precipitation scenarios models therefore are developed with the real precipitation distribution as presented by the respective August 2005 event analyses and regionalised afterwards with highest (worst case) intensities. Furthermore a different scenario with respect to landcover (change of distribution of forested/non-forested areas) are calculated in order to identify those areas with high sensitivities to landuse modifications.

6) Last but not least high relevance is given to the documentation of the efforts invested in each of the working steps to obtain detailed data with regard to benefits and costs. This documentation should result in recommendations for appropriate methods applicable under certain conditions and for certain aims (costs, value and limits of results). Also the question of the applicability of the investigated methods in different landscapes and regions is addressed.

3. Project Area (GBA)

The Gasen-Haslau area, which was studied for the ADAPTSLIDE-ADAPTALP project, is a region that last experienced numerous gravitational mass movements in August 2005, in the course of a period of high initial soil moisture and several days of continuous moderate precipitation. The events in question were mainly soil slips and earth flows, which often caused severe damage (Tilch & Koçiu 2006). Especially since the night of 21/22 August 2005, more than 770 gravitational mass movements took place over a period of several days in the region of the communities of Gasen and Haslau (Tilch et al. (2009), Fig. 3.1-1, area: approx. 50 km²). In many places, infrastructure (electric power lines, drinking water supply lines) or buildings (residential housing and commercial buildings) in towns, as well as connecting roads between localities were badly damaged. Many buildings had to be evacuated, and a large number of people were cut off from the outside world for days. In addition to considerable property damage, there was also one tragic event in the town of Gasen (see Fig. 3-1). During the night, an earth flow formed on the slope above one house. The material of this earth flow moved down into the valley and almost completely destroyed the house at the foot of the slope. Two people were killed.

Fig. 3-1: An earth flow/soil flow completely destroyed a home in the village of Gasen. Photo source: GBA photo archives

3.1. Location and Characteristics of the Project Area

The project area is located in the northeast part of the Austrian federal state of Styria, in the southern region of the Fischbacher Alps. The landscape is sub-mountainous in character; mountain heights varies between 800 and 1500 metres (above the Adriatic see level) within short distances, and the slopes are very steep in some places.

Due to the landscape genesis, the lower parts of the slopes are generally quite steep, while the upper slopes tend to be flatter. In consequence, both the flat areas

of the valley bottoms and the higher mountain slopes are populated, particularly those with southern exposure. The steeper slope areas and the slopes exposed north are mainly forested.

From a geologically view, the project area is located in the middle and lower section of the tectonic nappe group of the Graz Upper Austroalpine Paleozoic.
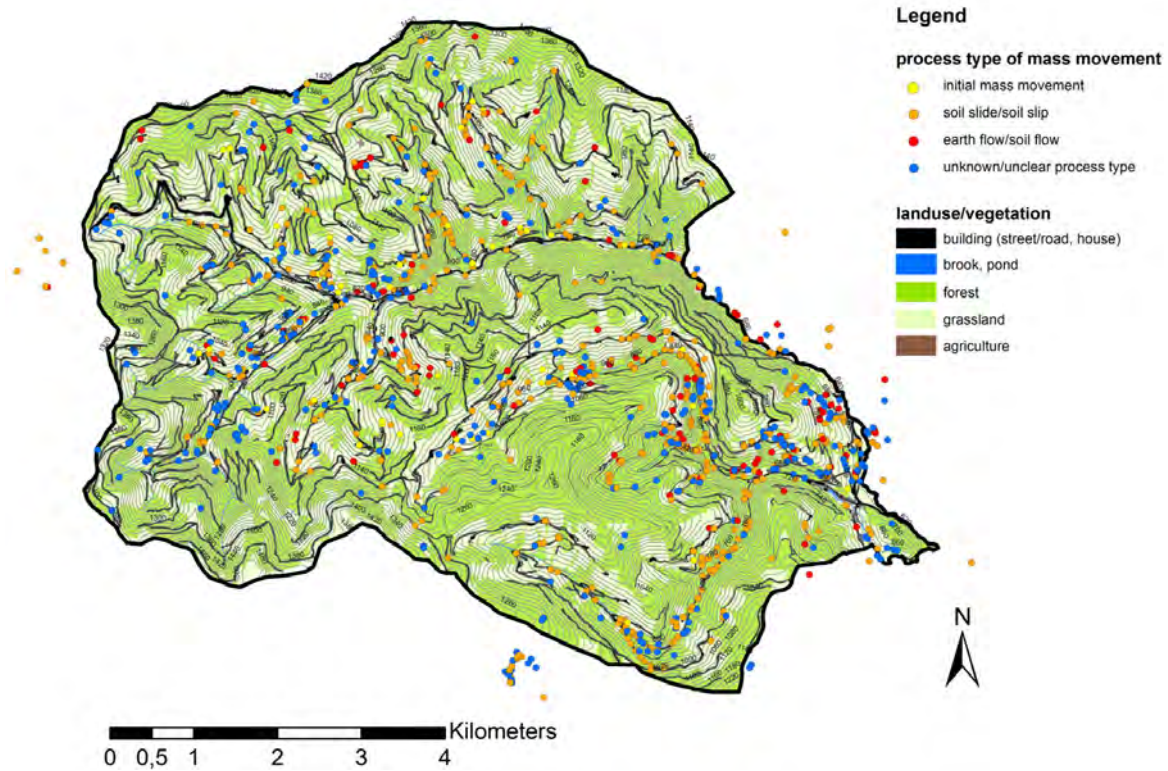
Fig. 3.1-1: Geographical position, inventory map of the gravitational mass movements of the event in August 2005, and land use/vegetation in the Gasen-Haslau project region. Key: Note designation of process types

Fig. 3.1-2: Impressions of the Gasen-Haslau project area on a dry summer day: looking north to the village of Gasen and the mixed land use on hillslopes. The lower slopes in the valleys are steeper, formed by dominant fluvial erosion along the valley floor. Photo source: GBA photo archives

A large part of the area is characterized by phyllitic mica schists and phyllites of the Exenberger series (Passailer phyllite and Heilbrunner phyllite). These hard rocks are mainly covered by more or less loamy sandy silts to silty sands with varying proportions of gravel. The western edge of the area is dominated by mainly carbonate rocks with marly soils.

In addition, black shale of the Devonian Arzberger Formation and orthogneisses of the Raabalpenkristallin are partially significant (Chapter 5.1). Whereas black shales mainly produce loamy to very loamy soils with gleys in hillside depressions, soils in the region of gneisses are predominantly sandy.

3.2.   Types of Gravitational Mass Movements

With a few exceptions, the gravitational mass movements that took place were spontaneous processes in soil. In the basis scar areas, usually the relatively unweathered rock or Cv-horizon became visible. Sometimes these horizons were masked or overlaid by material that fell or slide off the steep edge of the landslide scar. Depending on the thickness and composition of the soil layers, rotational (thicker soil layers) or translational (flatter soil layers) soil masses have been moved out (Fig. 3.2-1).
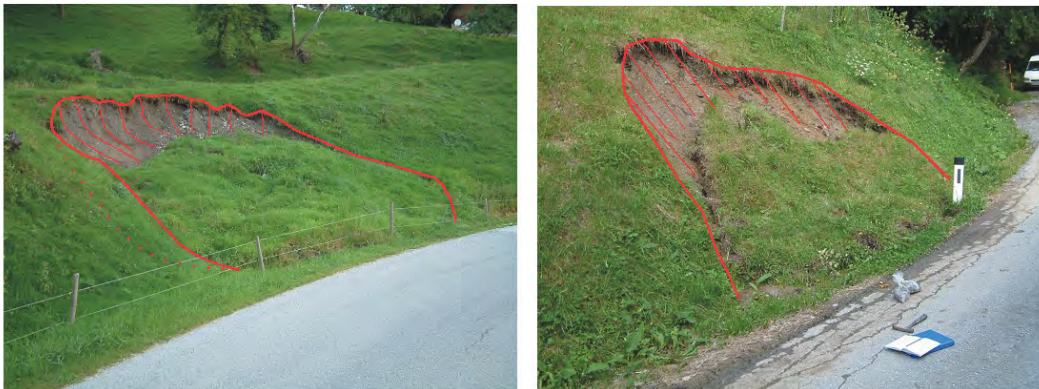
Fig. 3.2-1: Examples of gravitational mass movements in soil in Gasen-Halau project region: Rotational soil slide with a curved, concave-shaped sliding surface (left) and translational soil slide with a planar sliding surface (right). Photo source: GBA photo archives

During field mapping it was found out that most spontaneous mass movements could actually be assigned to only one dominant initial process type (cracking, mass movement type 1, stage 1). Out of this initial type, depending on local conditions (eg substrate, slope hydrology) different dominant types of processes evolved secondarily. On the one hand, soil slides have occurred, which caused an accumulation of the transported soil material near the scar area (mass movement type 2). In these process areas, the sliding process represents the final process stage (stage 3). On the other hand, some soil slides also turned into earth flows, so that the material was transported smoothly and rapidly down the slope (mass movement type 3, stage 4). Depending on the roughness (eg land use and micro-topography) as well as the length and inclination of the downhill slope, the material

speed and the transport distance varied. Especially on steep slopes with low surface roughness earth flows were able to travel long distances (Fig. 3.2-2, left) and reach high speeds. As a result, major damages were sometimes caused by relatively small masses of material (Fig. 3.2-2, right).

Fig. 3.2-2: The small source area and very long transition and accumulation area of a soil/debris flow (left) and the resulting damage/disaster (right). Photo source: village government photo archives

In a few instances, there were crater-like depressions with an irregular form and surface in the centre of earth-flow scar areas (Fig. 3.2-3). Only sliding or sliping initial processes can rather be excluded for such designed scar areas. These are probably evidences of spontaneous, hydrostatically caused (PWD) "slope explosions" (reference: Fig. Text 3.2-3). The released material was flowing out directly as an "earth flow" downhill, due to high water content and low consistency. These would thus be process areas in which extremely spontaneous earth flows formed without previous distinguishing characteristics or process indicators (stage 3).

The processes that take place within one process area are of course often so multi-faceted, complex, and variable in time that the mapped phenomena cannot always be unequivocally interpreted. Anyhow already in the course of field mapping it was possible to categorize all mapped unstable process areas in accordance with the respective dominant process type. (Fig. 3.2-4, Tab. 3.2-1). Not least, this was done against the background, that the process types and process stages include different hazard potentials. For example, earth flows generally have high hazard potential of impact, especially due to their high material velocity and large process extents.

Fig. 3.2-3: Crater-like source area with the main scarp of a soil/debris flow, formed by excess pore water pressure ("soil explosion"). Photo source: GBA photo archives

process type 1 / stage 1/2   process type 2 / stage 3   process type 3 / stage 4

Fig. 3.2-4: Classification of the gravitational mass movements in soil of the event "August 2005" in the Gasen-Haslau project region on the basis of movement type and development stage. Photo source: village government photo archives (left) and GBA photo archive (centre, right)

Tab. 3.2-1: Amount of the gravitational mass movements in soil (n=771) of the event "August 2005" in the Gasen-Haslau project region, classified by movement type and development stage of the process

	type/stadium of gravitational mass movement			
	1/1,2	2/3	3/4	
	incipient cracking	soil slide/soil slip	soil slip and earth flow	unknown/unclear process
movement	initial	sliding	sliding flowing	??
number	49	436	107	179
percentage [%]	6,4	56,5	13,9	23,2

4. Available Data (GBA, JR)

The following is a brief introduction to the process and spatial data/parameter maps that are important for the project in the sense of being available basic data.

4.1.   Process Data

Shortly after the events of August 2005, the crisis management group and several institutions (BFW*1, GBA*2, Engineering Office Geolith, WLV*3, State Government of Styria) working in various specialist disciplines gathered a large number of evidences and informations on the gravitational mass movements in question through field investigation. Later, there was archive research (GBA) and evaluation of current and older (1996, 2003) aerial photographs (Joanneum Research) in order to acquire as much information as possible on previous gravitational mass movements. This is very important, because only in this way a more objectified overall picture of the distribution of processes, significant process types and local-specific factors is possible (for example an event-independend viewing is possible).

All researched documents and information obtained in the field and through remote sensing were digitally processed as part of the project FloodRisk II (see Tilch et al. 2009) and cartographically represented by means of GIS technology. In order to avoid redundant information, all GIS data was synchronized by compiling the best, detailed information with regard to content (for example process and damage information) and/or quality (for example, localisation, extent of the process area) into one data set. This is necessary to clearly link all types of metadata (for example photographs, expert opinions and survey reports) internally and with the GIS data. Based on the data compiled in this way, various digital map products on different scales were produced for use in further spatial planning, such as:

- digital process cadastre/register, 1:10,000 (Fig. 4.1-1)

- digital thematic inventory map, 1:5,000 (Fig. 4.1-2)

- process index map for different scales and extensions

The digital thematic inventory map, which is based on aerial photographs taken soon after the event (not available for the entire area) and field investigation, provide information on the process areas affected. As training and calibration data, this is important basic material for subsequent process modelling. Data from the process cadastre/register is significant for the modelling of susceptibility maps.

All of this data and all of these maps were available in digital form at the beginning of the ADAPTSLIDE project.

Remote Sensing

Remote Sensing and Damage report

Field mapping

Field mapping and Remote Sensing

Field mapping and Damage report

Field mapping, Remote Sensing and Damage report

Expert report

Damage Report
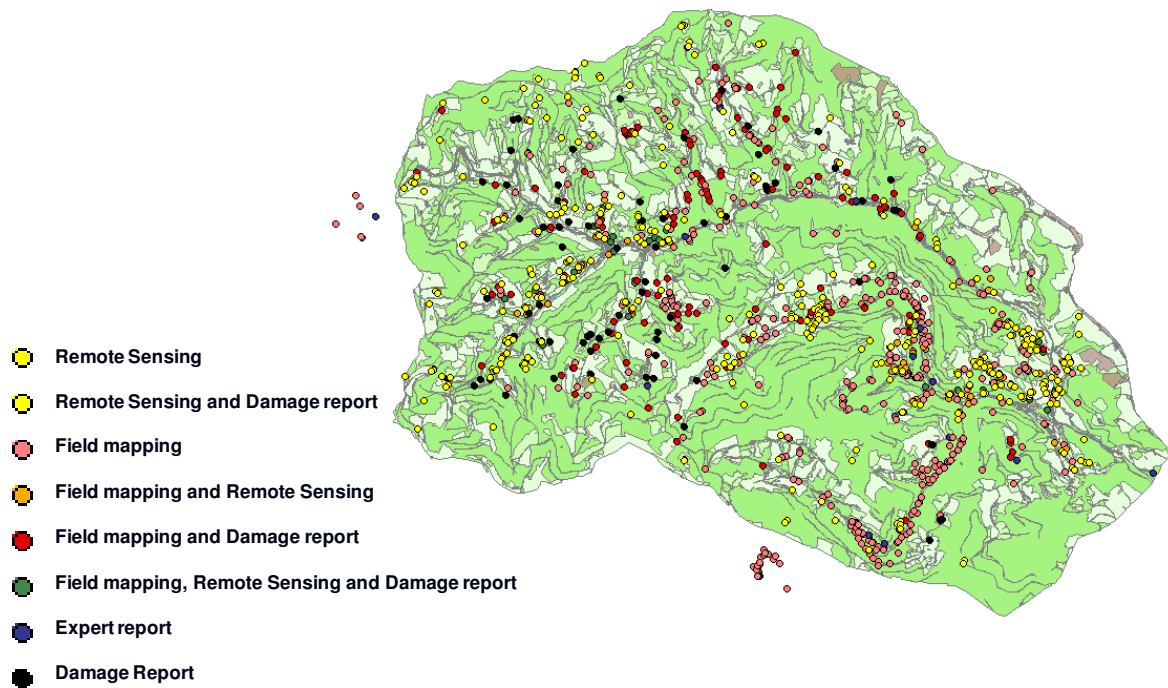
Fig. 4.1-1: Process cadastre/register with information about the type of data source/survey methods (Tilch et al. 2007)

Fig. 4.1-2: Thematic inventory map with information about the process sub-areas (left, Tilch et al. 2009) and a section of an aerial photo (right, data source: Joanneum Research)

4.2. **Available Spatial Data**

The concept of statistical modelling of susceptibility is based on the assumption that future landslides rather will happen under similar environmental circumstances as past ones did. Therefore for statistical modelling the second important input besides the landslide inventory is a set of maps of environmental parameters which are relevant to the process taken into focus. Spatial data always have to be checked with

regard to their physical relevance to eliminate accidental correlations which may distort the modelling result.

Different categories of parameter maps were created according to their processing status:

- directly derived maps
- elaborately derived maps
- combined maps

In this section only directly derived map are listed. For elaborately derived maps and combined maps requiring high processing effort please refer to section 5.

For direct derivation of maps of environmental data the following data sources were used:

- Digital Cadastral Map (DCM) of the Austrian Federal Office for Metrology and Surveying

- Digital Terrain Model (DTM) with a spatial resolution of 10 m of the Austrian Federal Office for Metrology and Surveying

The following parameters were derived directly from these basic datasets requiring only little processing effort:

- *Wegenetz_lg*   Influence area of Road Network „level low" based on DCM
- *Wald_DKM_lg*   Forest „level low" based on DCM
- *Wald_DKM_lg_80*   Forest „level low" ≥ 80% forest per pixel based on DCM
- *HN-DHM10*   Slope/inclination based on DTM 10m
- *HW-DHM10*   Plan Curvature based on DTM 10m
- *VW-DHM10*   Profile Curvature based on DTM 10m
- *HK-DHM10*   Curvature Classification based on DTM 10m
- *Flowaccumulation*   Flowaccumulation based on DTM 10m

Spatial data were aggregated to 50 m rasters to provide for spatial inaccuracies.

5. Production of Improved, Process-oriented Parameter Maps

Additional topics considered important with regard to the process in focus are:

- geology
- soil
- land cover
- runoff disposition
- precipitation

Available maps of these subjects did not adequately consider the parameters which control landslide activity. Therefore maps had to be reprocessed using additional datasources, field information and expert knowledge. Technical aspects of these adaptations are presented in detail in the sections 5.1. – 5.5.

Generally two different levels of processing effort applied for the generation of parameter maps can be distinguished:

- level low (abbreviation "lg" in parameter maps)
- level high (abbreviation "lh" in parameter maps)

"Level low" parameter maps are generated by means of simple, standard methods, while "level high" parameter maps are generated by advanced, higher developed methods with higher expenditure.

5.1. Geological Basic Disposition Maps (GBA)

5.1.1. Production of Conceptual Soil Maps using the GBA Methods

The main emphasis of the project is the production of susceptibility maps for spontaneous gravitational mass movements in soil in the Gasen-Haslau region. In order to facilitate large-scale, comprehensive assessment of susceptibility, it is necessary to have detailed and comprehensive information on the loose geosphere (soil and unconsolidated weathered rock in particular, referred in combination as the 'weathering veneer').

However, the generally available geological map (scale: 1:50,000) is only useful to a limited extent in dealing with issues of this kind, because it provides only partial information on the weathering veneer. A comprehensive conceptual soil map was therefore produced for the project area, which provides as detailed and realistic information as possible on the process-relevant weathering veneer.

A method developed by the Geological Survey of Austria was employed in producing the map. This is a simple, three-step, or an expanded five-step method (Fig. 5.1.1.1-2) , based on the available geological map that can be used for any location for which there is an existing area-wide geological map.

5.1.1.1 Method

The first step involves interpreting all geological units of the geological map (GK50, Fig. 5.1.1.1-1) as geotechnic-lithological units. Soil units are first interpreted on the basis of their general lithology and anistropy. Solid rock units are interpreted on the basis of (i) fracturing and weathering susceptibility (ii) and lithological heterogeneity/homogeneity. The result is a map of the geotechnically-lithologically units (GTL map).

As a second step, geotechnic-lithological soil units were assigned to 7 classes of substrates. If there were heterogeneous units or stratigraphical columns, the finest granular subunit was always taken as the base (in the sense of worst-case conditions). Furthermore, all solid rock units of the GTL map were assigned, using simple educt-product analogies corresponding to their distribution, to general or medium substrate classes respectively (general potential weathering products). This is done on the hypothesis that different (par)autochthone products (soil substrates) arise from different educts that have different mineral composition and potential fracture frequency, and thus different weathering susceptibility. Complex processes of slope denudation (for example periglacial processes) naturally lead to small-scale lithological-structural variances, as they do in many ways in the slope scale. However, these cannot be accounted for on the basis of the geological maps alone. They only allow identification of areas in which significant soil types predominate.

Given the background and aims of the project, there was chiefly assessment of those soil characteristics (grain-size distribution, texture of soil, dominant grain size) on the basis of which project-relevant soil characteristics and parameters (for example, hydraulic permeability, angle of internal friction) could subsequently be qualitatively to semi-quantitatively derived.

Reclassification of the solid rock units of the GTL map in potential areas of comparable soil substrates was done during this process on the basis of the following criteria:

- supported by rough-grains (sand-gravel) or fine grains (clay-silt)
- dominant soil type of the supporting, fine-grained soil (silt, clay)
- portion of rough and fine grains
- Heterogeneity and homogeneity of the units
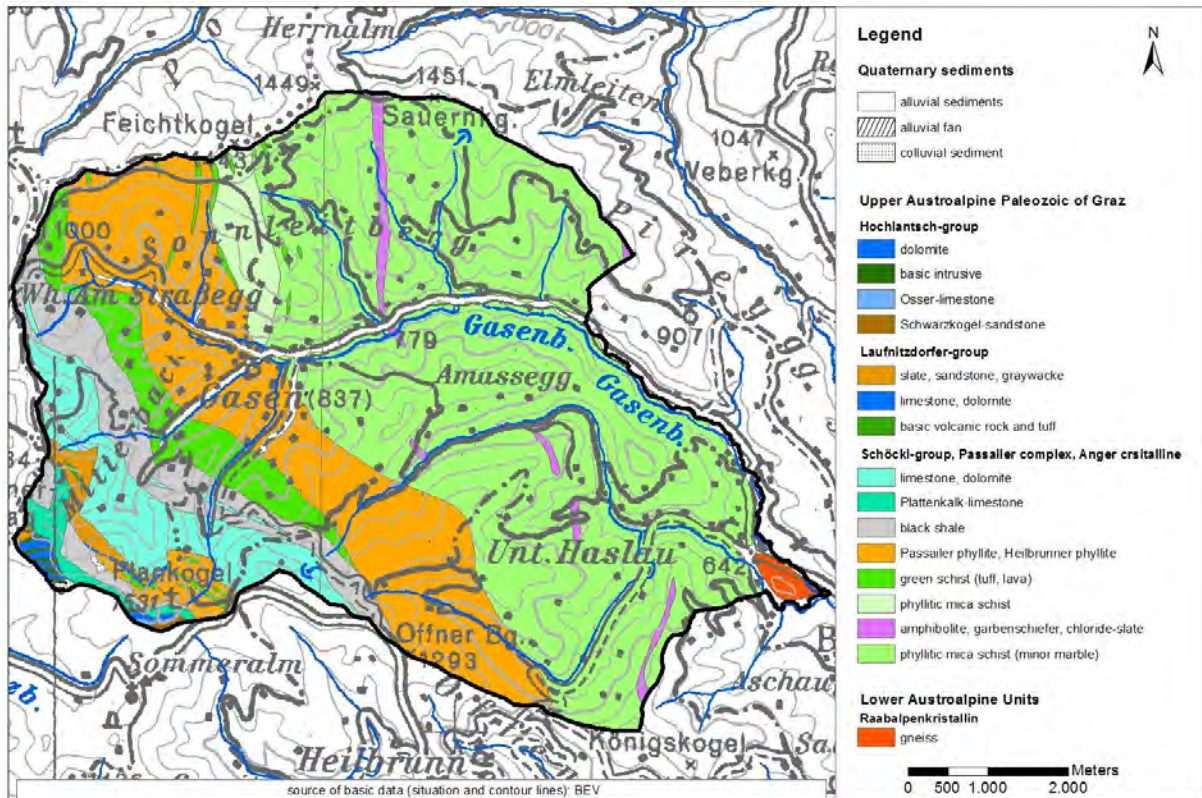
Fig. 5.1.1.1-1: Available digital geological map of the Geological Survey of Austria (1:50,000) of the project area (Flügel et al. 1990, Geofast 2005)
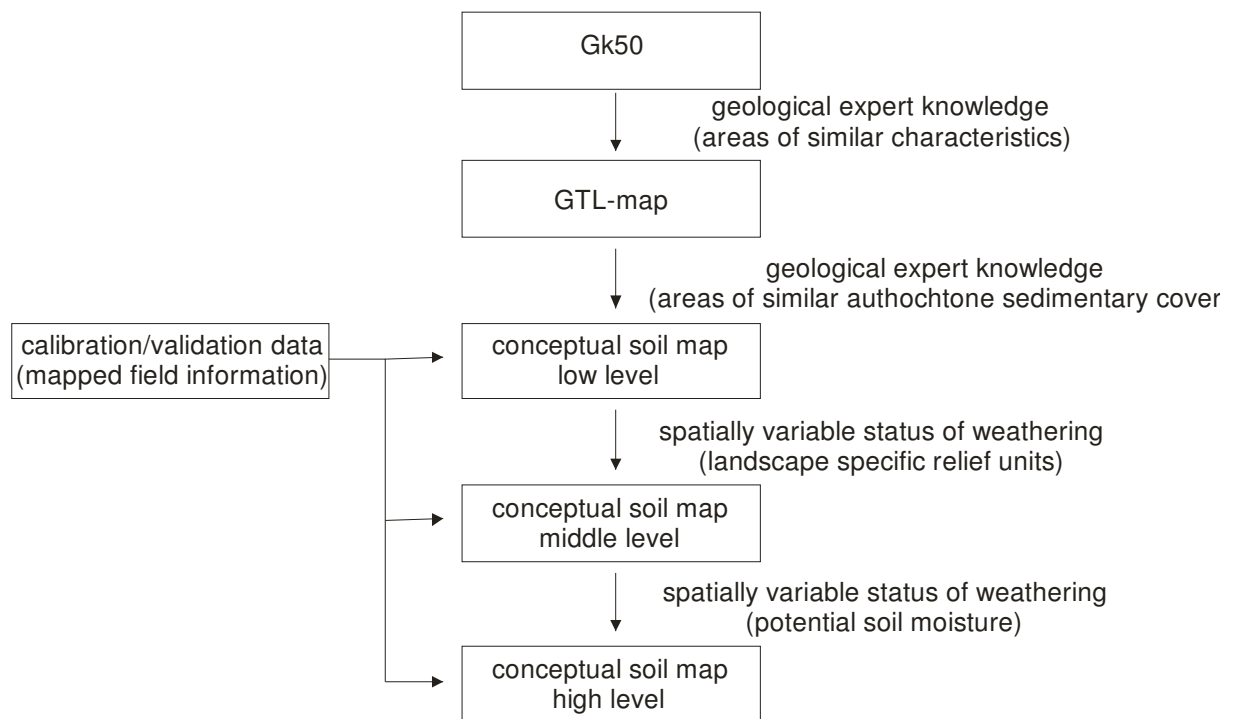
Fig. 5.1.1.1-2: Processing operation for producing substrate conceptual maps of different processing/quality levels

The distribution of substrate classes is oriented to the distribution of heterogeneous to homogenous units on the GTL map, or as the case may be the digital geological map. Therefore, the conceptual soil map (sub-map) produced is also based on a scale of 1:50,000 (sub map – low level).

Area-specific landscape developments are accounted for in an additional step, where the substrate classes (low level) of different relief units (hills, steep slopes, gentle slopes, etc.) are adapted according to the existing, different stage of weathering. This adaptation is done by upgrading or downgrading substrates from the different relief units by class. In this way, the conceptual soil map ‚sub map – middle level,' is produced.

In a final step, it is taken into account that locations with higher humidity are also potentially locations of more intensive chemical weathering, and that they will therefore tend to have greater loam deposits. The identification of areas with different, or as the case may be comparable humidity is done using the Topographic Wetness Index. Classification in the sense of delineating humidity classes is done on the basis of field knowledge. In this manner, dry locations are identified in rather steep slope locations and/or smaller catchment areas (for example ridges, divergent slopes), whereas wet areas tend to be identified in dell locations with larger slope catchment areas. Thus, for the latter locations, the substrate class might be modified by two substrate-class categories (for example, soil type 23 -> soil type 25).

The substrate classes identified in this way for all conceptual soil maps can be described in a combined way as follows:

    11: supported by rough-grained, gravel-rich soil/sediment, no portion of fine grained soil/sediment (no loam) (gravelly slope cover)

    12: supported by rough-grained, gravel-rich soil/sediment, very high portion of stones, small or very small portion of fine-grained soil/sediment (silty) and partly loamy (sandy slope cover)

    13: supported by rough-grained, sandy-gravelly soil/sediment, moderately portion of stones, moderately of fine-grained soil/sediment (silty) and partly or somewhat loamy (silty slope cover)

    14: supported by rough-grained, sandy-gravelly soil/sediment, moderately portion of stones, high portion of fine-grained soil/sediment (strongly silty) and partly or somewhat loamy (silty sand)

    23: supported by fine-grained silty soil, sandy, small portion of stones and moderate loamy (sandy loam)

    24: supported by fine-grained, silty-claylike soil/sediment, small portion of stones and strongly loamy (from clay-rich silt to silt)

    25: supported by fine-grained silty-claylike soil/sediment, small portion of stones and very strongly loamy (from silty clay to clay)

Because substrate information was available for the project area, the conceptual soil maps produced could be calibrated at different processing/quality levels. A total of 68 substrate data samples distributed among 52 locations in the area were available for this purpose (cf. Fig. 5.1.1.1-3).

Information on several substrate classes was available for 14 of these locations, which underscores the small-scale heterogeneity/variability of the substrate. For example, substrates of the classes 13 to 24 were found in one scar area. Substrate

heterogeneities of this kind cannot of course be accounted for using a method of producing substrate conceptual maps that has been simplified to this degree. However areas can be identified in which one substrate class potentially dominates due to the location factors included. It was particularly important here to concentrate on identifying the substrate class that was presumably the most sensitive toward the dependent variable (susceptibility).

Calibration of the substrate conceptual maps was done using all field information, irrespective of the small-scale substrate heterogeneities.

Using GIS retrieval, the mapped substrate information was compared to that of the conceptual maps, and the latter information subtracted. Here, positive values mean that the substrate class of the substrate conceptual map is shown as too high, corresponding in each case to the substrate discrepancy identified (-1 means, for example, that the substrate of the conceptual map is too high by one substrate class).
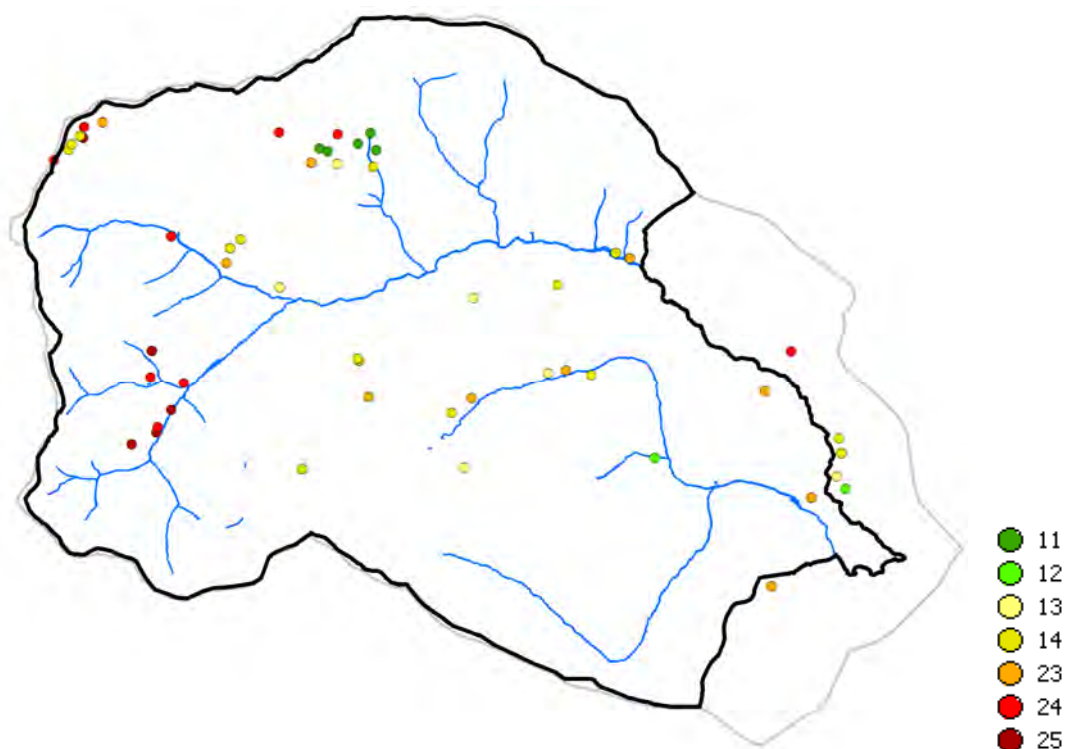
Fig. 5.1.1.1-3: Locations of observed soil classes in the project region Gasen-Haslau (grey line: observed area, black line: model area)

5.1.1.2 Results

Calibrated substrate conceptual map – low level

To begin with, the substrate conceptual map obtained (low level) was compared to the obtained field information. This demonstrated that in more or less the entire area, there was, on the one hand a relatively good match, and on the other, relatively large discrepancies between the substrate conceptual map and field information. This is attributed to the small-scale variability in the soil substrates. The major discrepancies occur primarily because the substrate conceptual map tends to show substrates that are too rough-grained in all substrate classes. For this reason, all substrate classes

on the substrate conceptual map were upgraded by one substrate class (adjustment by one substrate class in the direction of finer-grained soils, for example 11->12, 12->13). In this way, a calibrated conceptual map was obtained, and on the whole, a more balanced relationship between substrate overestimates and underestimates was achieved (Fig. 5.1.1.2-1, 5.1.1.2-2).
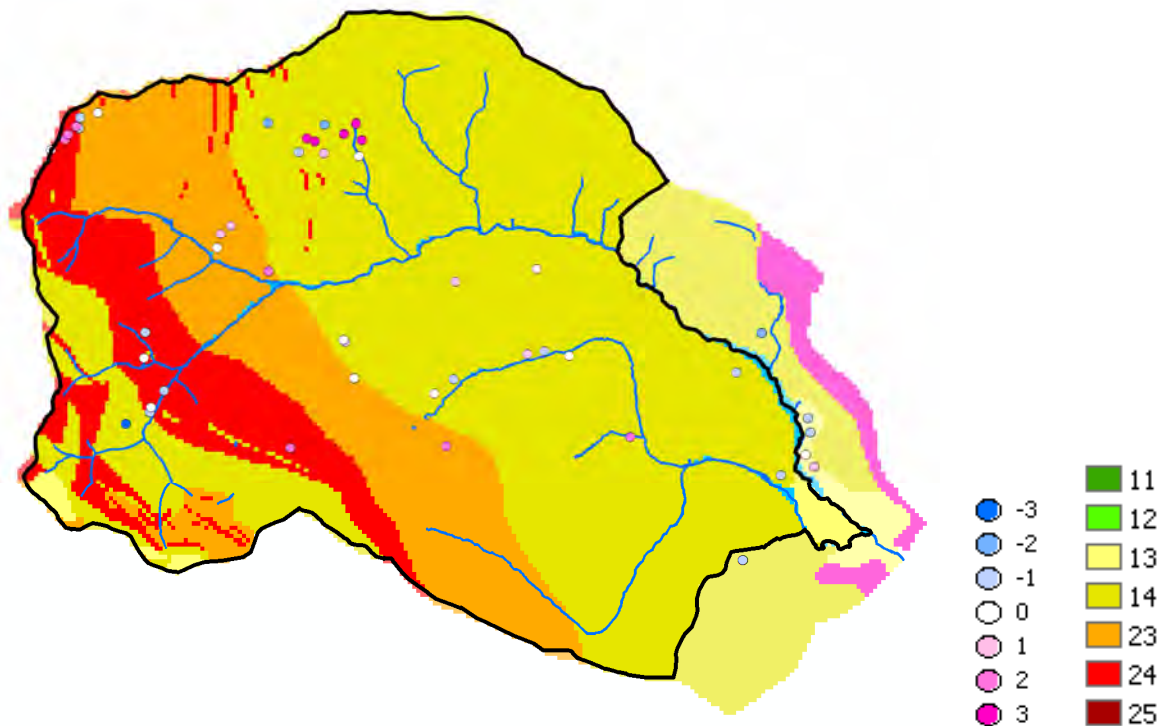
Fig. 5.1.1.2-1: Discrepancy between the substrate classes of the calibrated substrate conceptual map (low level) and the field information (negative values mean soils that are too gravel-rich on the substrate conceptual map)
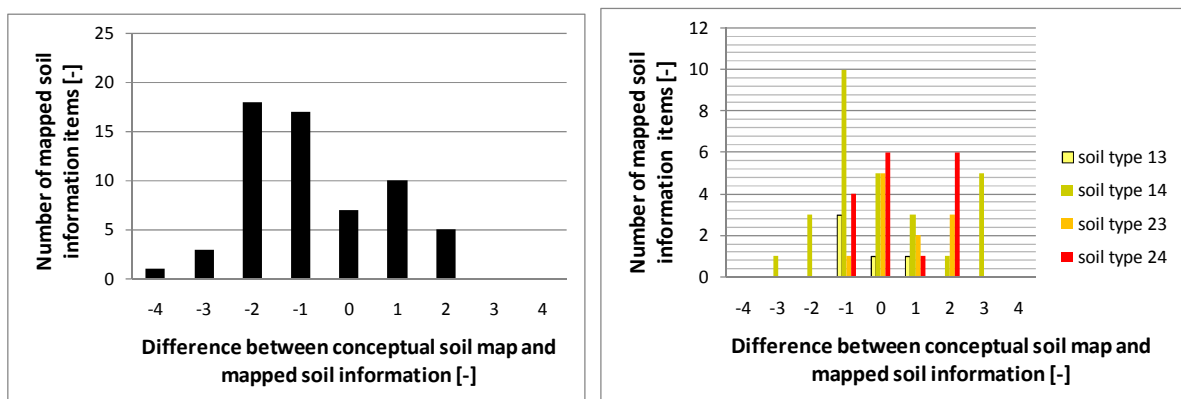
Fig. 5.1.1.2-2: Number of information items with a corresponding discrepancy (substrate-class discrepancy) compared to the calibrated substrate conceptual map (low level). Left: all data, irrespective of the substrate classes. Right: data in one substrate class of the substrate conceptual map. Negative values mean soils that are too gravel-rich on the substrate conceptual map

Calibrated conceptual map – middle level

The substrate conceptual map 'middle level' was calibrated analogously to the substrate conceptual map (low level). Due to the partial modification based on relief units, there is now a significantly wider spectrum of substrate classes. However, the discrepancy between the substrate conceptual map and the field information is more pronounced than it was with the non-calibrated, initial substrate conceptual map (low level). This is due mainly to the substrates being modified in the direction of coarse-grained substrates in the slope locations (-1) and steep slope locations (-2). There are obviously negative discrepancies (a substrate being identified as too gravel-rich) particularly in the region of the substrate classes 11 and 12 of the conceptual maps. But this is also seen in milder form in the substrate classes 13 and 14. The substrate classes of the substrate conceptual map (middle level) are therefore corrected as follows:

> Substrate class 11, 12 -> +2 substrate classes
>
> Substrate class 13, 14 -> +1 substrate class
>
> Substrate class 23, 24 -> +/-0, no change

The calibrated substrate conceptual map obtained in this manner (middle level, cf. Fig. 5.1.1.2-3) now displays a predominantly symmetrical spread of and within all substrate classes around the substrate classes investigated (Fig. 5.1.1.2-4). The percentage of major deviations is now relatively low as well.
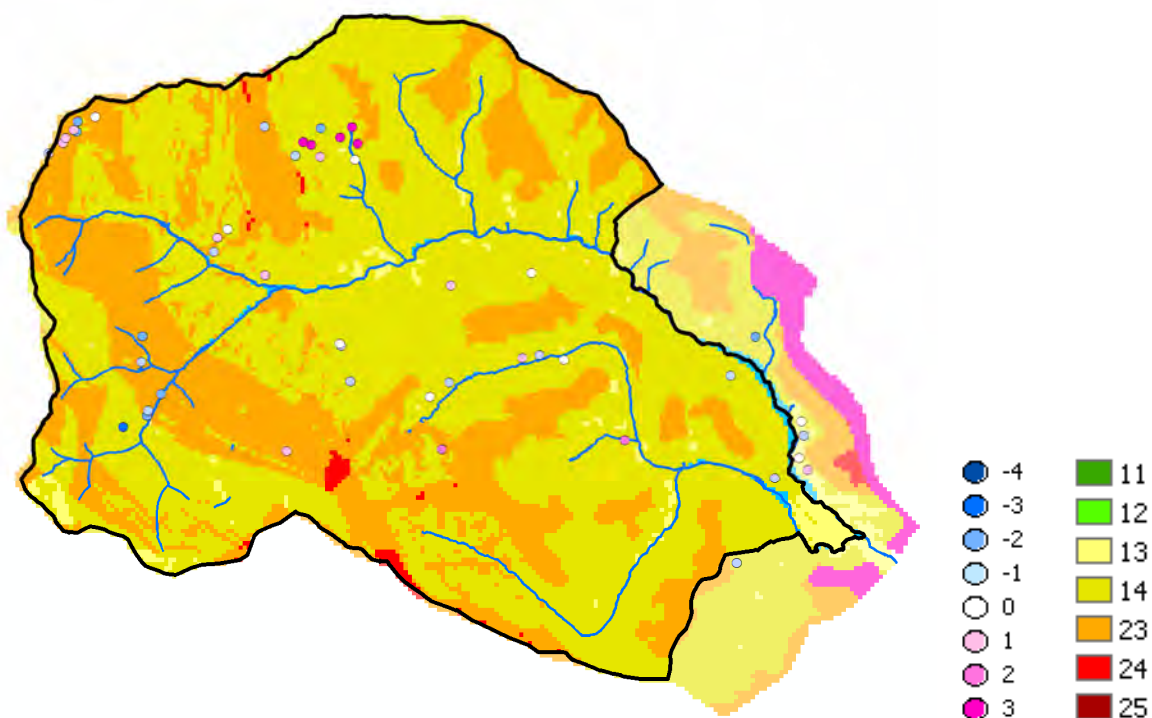
Fig. 5.1.1.2-3: Discrepancy between the substrate classes of the calibrated substrate conceptual map (middle level) and the field information (negative values signify soils that are too gravel-rich on the substrate conceptual map)
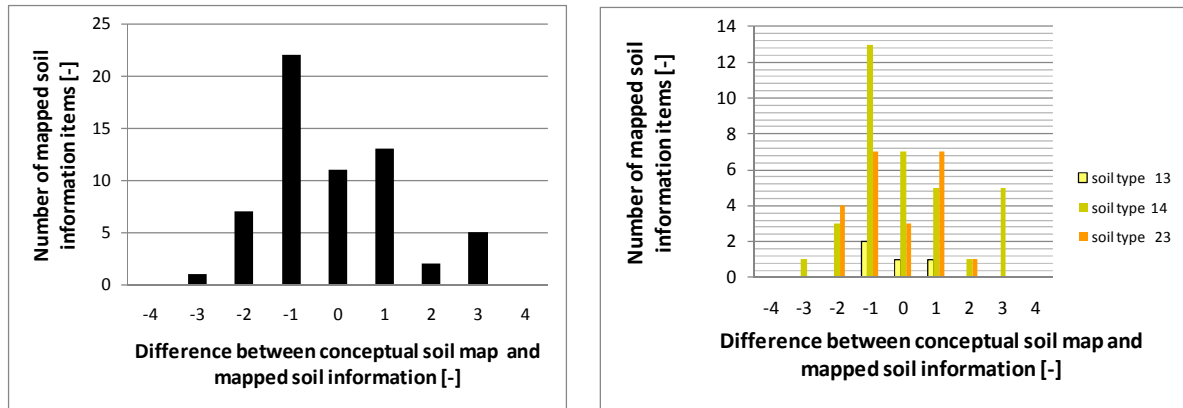
Fig. 5.1.1.2-4: Number of field information items with a corresponding discrepancy (substrate-class discrepancies) compared to the calibrated substrate conceptual map (middle level). Left: all data, irrespective of substrate classes. Right: data within one substrate class of the substrate conceptual map. Negative values signify soils that are too gravel-rich on the substrate conceptual map

Substrate conceptual map – high level

The improved substrate conceptual map 'high level' was calibrated along the same lines. After additional partial modification based on the Topographic Wetness Index, there is now a spectrum of substrate classes for the project area that is approximately as wide as that obtained in the field. It is also extremely positive that the discrepancies between these classes and those determined in the field are now usually quite small (Fig. 5.1.1.2-5 and Fig. 5.1.1.2-6). However, it is should also be noted that substrates richer in finer particles were often detected, particularly in the region of gravel-rich substrate classes (11, 12) (indicating a tendency toward negative discrepancies), and that by the same token, more gravel-rich substrates were detected in the region of finer-particle substrate classes (24, 25) (indicating a tendency toward positive discrepancies, cf. Fig. 5.1.1.2-6). This might mean that substrate extrema are too often identified, or shown as too widely distributed when using substrate conceptual maps. On the whole, however, it should be kept in mind that a relatively small amount of field information (68 items in total) is spread over a relatively large number of substrate classes, and that individual substrate classes therefore cannot be sufficiently analysed, or as the case may be calibrated.
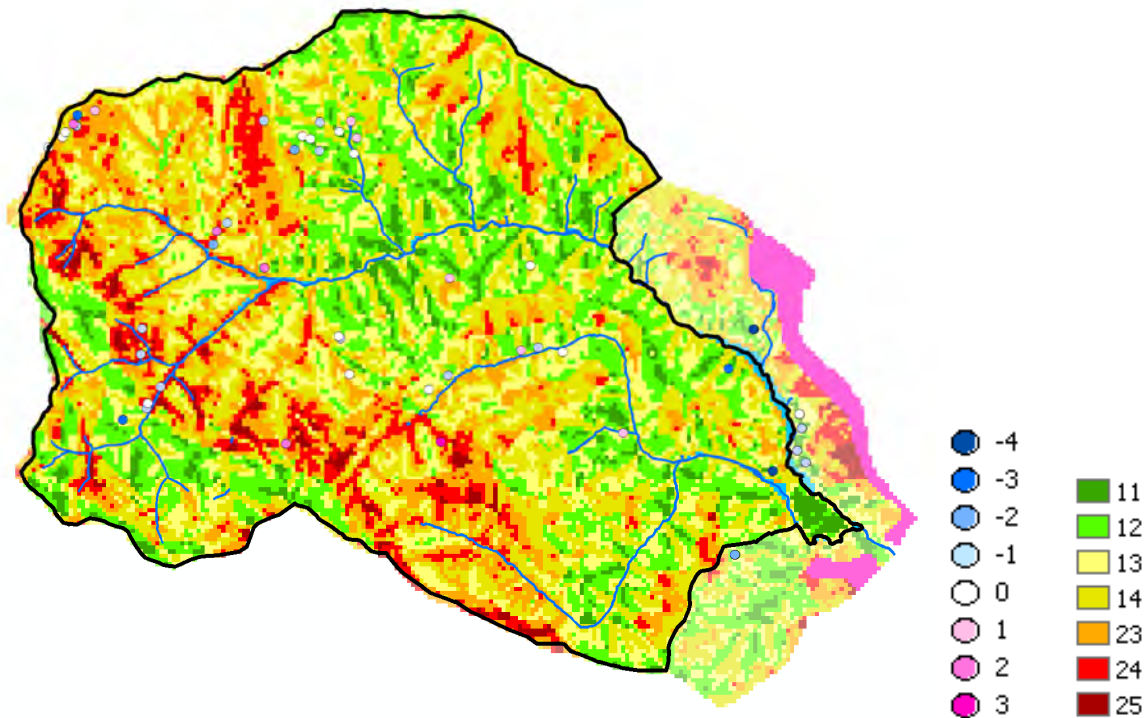
Fig. 5.1.1.2-5: Discrepancy between the substrate classes on the improved substrate conceptual map (high level) and field data (negative values signify soils that are too gravel-rich on the substrate conceptual map)

Nevertheless, there was an attempt to calibrate the improved substrate conceptual map (high level) on the basis of the available field information. Different methods were employed in doing so, however, no calibration method resulted in a generally valid adjustment that could be applied to the entire surface and all substrate classes.
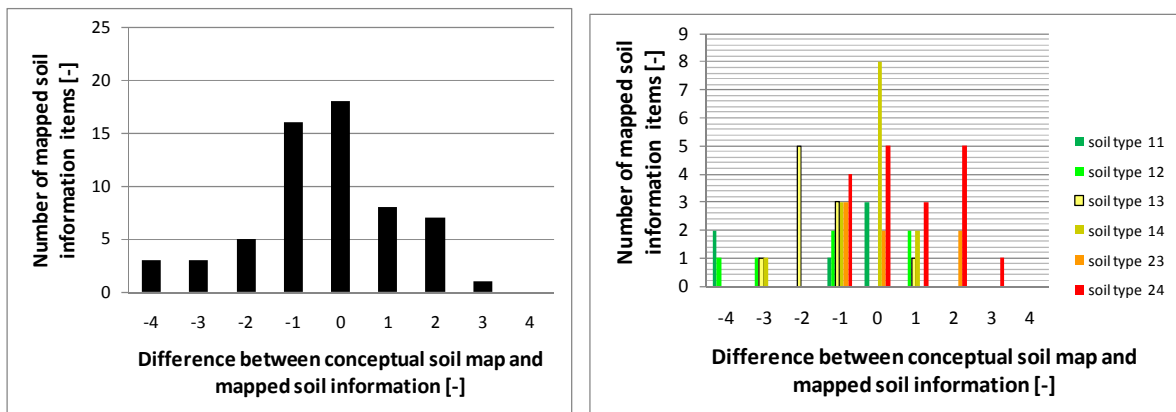
Fig. 5.1.1.2-6: Number of field information items showing the corresponding discrepancies (substrate class discrepancies) compared to the calibrated substrate conceptual map (high level). Left: all data, irrspective of substrate classes. Right: data within a substrate class of the substrate conceptual map. Negative values signify soils that are too gravel-rich on the substrate conceptual map

Nevertheless, it was seen that the modifications of the substrate conceptual map ('low level') in relation to relief and potential soil moisture did have a positive effect

on the result. Good results (+/- one substrate class) were obtained for all relief units and the soil-moisture classes. However, it should not be overlooked that in some locations, very poor results were achieved (deviations of 3 and 4 substrate classes). This was the case because, on the one hand:

➢ very different substrate classes (small-scale heterogeneity) occur even in very small areas. In one scar area, for example, a range of substrate classes from 14 to 25 was identified,

➢ and on the other hand, the natural, real spatial variability of the substrate classes simply cannot be depicted using a simplified method of this kind.

5.1.2. Derivation of Geological Basic Disposition Maps of different Processing/Quality Levels

Based on the substrate concept maps produced, geological basic disposition maps for different hazard-relevant process groups (hydrological processes and spontaneous mass movements) can now be derived in the following manner:

In identifying areas of different basic geological susceptibility, the primary focus of investigation was the soil characteristics (grain distribution, rock texture, predominant grain size), on the basis of which, relevant properties, or as the case may be specific values of soils can be assessed relatively under the inclusion of data from literature.

This produced, for example, the following critical slope angles, above which a slope can be considered process-susceptible (irrespective of cohesion, pore water pressure, and other factors that have similarly destabilizing effects):

Clay, silty clay	(substrates 24, 25)	>15°
Silt, sandy silt	(substrates 23)	>20°
Silty sand, clay-rich sand	(substrates 14)	>25°
Sand, gravel, and their combination	(substrates 11, 12, 13)	>30°

If there was a basic disposition to surface runoff, the assessable hydraulic conductivity (Kf) was the decisive indicator. In assessing basic disposition to spontaneous mass movements in soil, the angle of friction (angle of internal $\varphi\grave{}$) was used. Depending on the process group considered, the result was an aggregation/reclassification into soil provinces with comparable substrate characteristics Tab. 5.1.2-1 and Fig. 5.1.2-1).

In each case, the following 4 substrate provinces were found for the process-related basic dispositions :

Surface runoff (SOF)

1: no surface runoff, highly unlikely

2: very little surface runoff, rare, relatively unlikely

3: surface runoff possible, relatively likely

4: heavy surface runoff possible, highly likely

Disposition to spontaneous mass movements in soil (RutDisp)

1:      small landslide susceptibility ($\varphi\grave{} \geq 30°$)

2:      medium landslide susceptibility ($30° > \varphi\grave{} \geq 25°$)

3: high landslide susceptibility $(25° > \varphi` \geq 20°)$

4: very high landslide susceptibility $(\varphi` < 20°)$

Tab. 5.1.2-1: Reclassification of substrate classes into areas of comparable soil characteristics (Kf [-] und $\varphi`[°]$) and basic process disposition (surface runoff (SOF) and spontaneous landslides (RutDisp))

Soil type/class	Kf [-]	SOF [-]	$\varphi`$ [°]	SlideSusc [-]
11	4	1	30	1
12	3	2	30	1
13	2	2	30	1
14	2	3	25	2
23	2	3	20	3
24	1	4	15	4
25	1	4	15	4

The substrate conceptual maps, and thus also the process-based basic susceptibility maps, are of course subject to considerable uncertainty. For example, the Geological Map, an important database and the only generally accessible, surface-covering database for the geosphere in the project area, is available solely on a scale of 1:50,000. The substrate conceptual maps were produced on the basis of expert knowledge and general, regionally specific rules, and distinctive local features, such as dominant denudation processes, cannot therefore be accounted for.
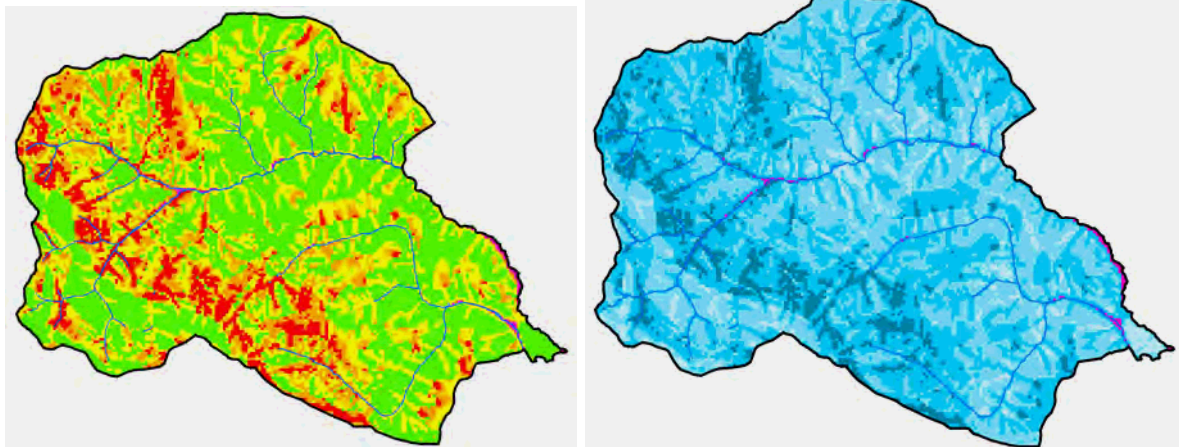
a.) geological susceptibility maps "high level"
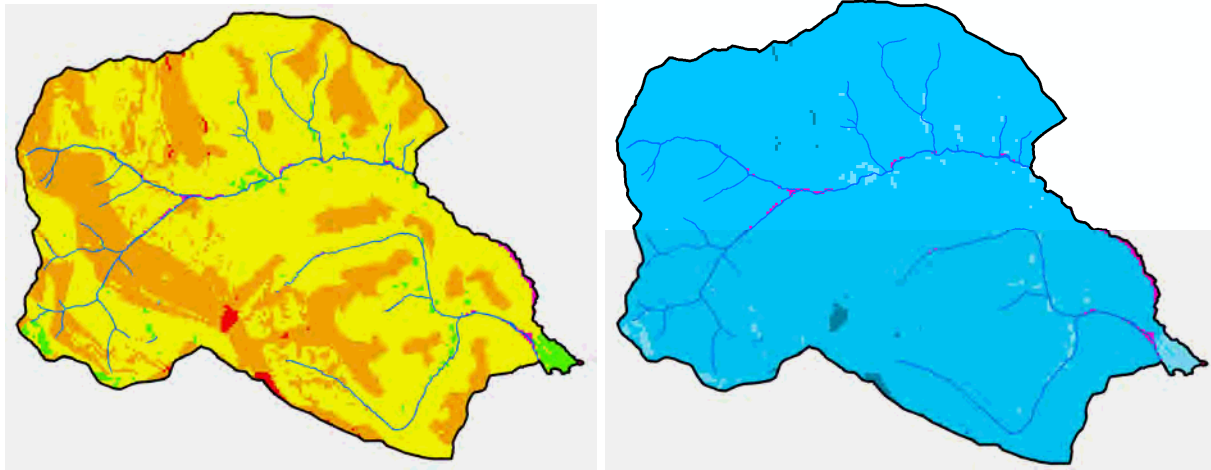
b.)   geological susceptibility maps "middle level"
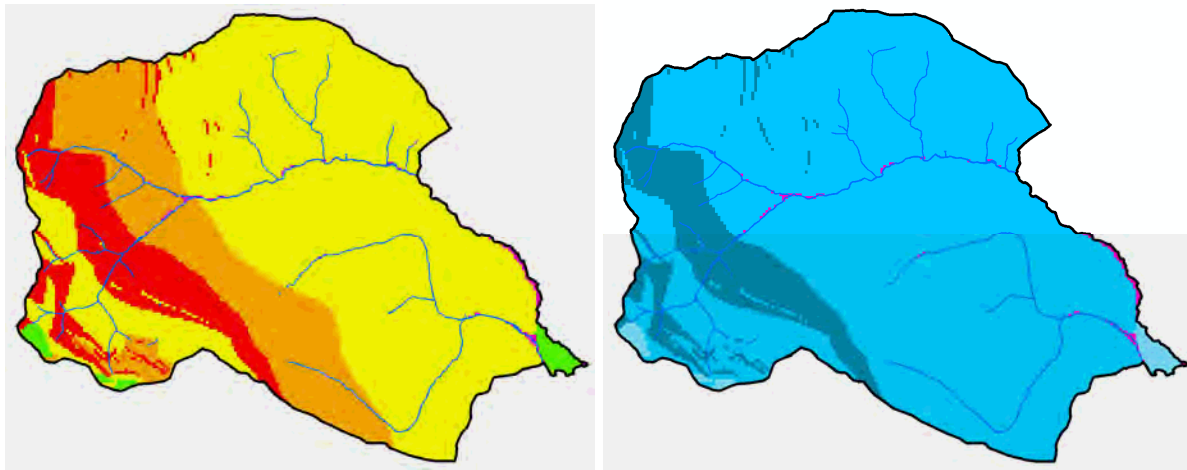
c.)   geological susceptibility maps "low level"

Fig. 5.1.2-1: Basic disposition maps for different process groups (spontaneous mass movements in soil (left) and surface runoff (right), and different processing/quality levels (a.) to (c.)

5.2.   Soil Map Based on the eBod and a Forest Site Classification (BFW)

When analyzing landslide susceptibility, basic information regarding the thickness of the soil and loose material, the physical behaviour (inner friction angle) and the water supply is certainly of high relevance. However, standard maps referring to these datasets are available neither in Austria nor in most other countries. Hence, efforts are made to develop these maps from other datasets. The Austrian Agricultural Soil Map and the Forest Site Maps contain basic soil information. The aim of this part of the project was to find out, whether this soil information can enhance the database for landslide-modelling.

5.2.1. Introduction: eBod

The Agricultural Soil Map which is divided into 219 mapping units, covers all agriculturally used areas of Austria; except are mountain pastures and hay meadows at high altitudes. The first survey of the soil mapping has been largely completed. The results of existing soil maps are available in analogue and digital form. Hence, in Austria, an almost area-wide, consistent (standardized) comprehensive map, describing the soils of the agriculturally used areas is available.

The soil mapping units are displayed as polygons. Within their boundaries the site parameters vary only in a small defined range. In addition to defining parameters of a more general nature such as slope inclination and groundwater depth, depth of horizon boundaries, those maps include also horizon specific parameters like texture and gravel content, the content of calcium carbonate and humus. On the basis of soundings and morphologic attributes of the terrain, the surveyor charts the distribution of the soil type units.

For each soil unit, at least one profile pit has to be opened in order to get a comprehensive description and to take soil samples for laboratory analysis (Bundesamt für Bodenkartierung und Bodenwirtschaft, 1967)

From 1998 onwards, the maps have been continuously transferred into a GIS system and since 2004 a web application (eBod, Fig. 5.2.1-1) is available.
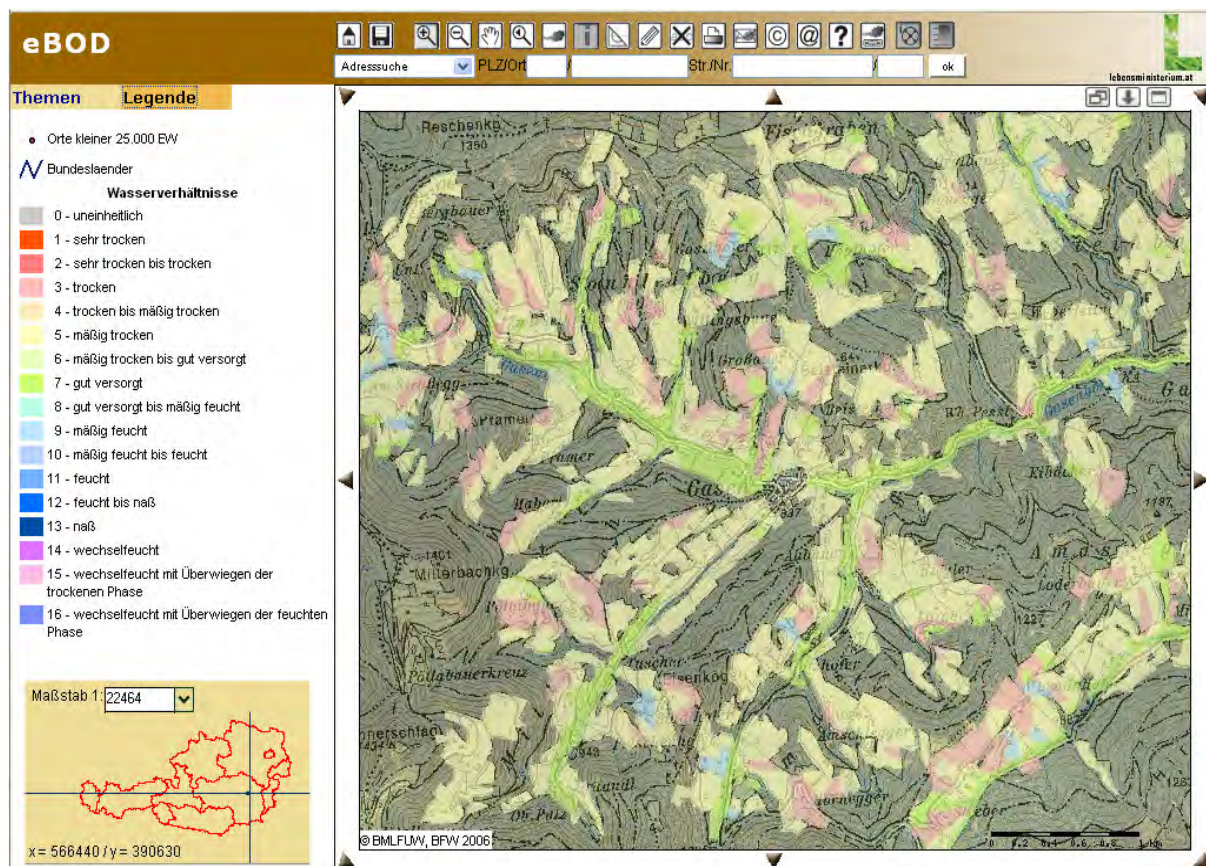
Fig. 5.2.1-1: Digital Soil Map of Austria (eBod, status 2010): Map section Gasen and surroundings – thematic layer of soil water conditions

This application is regularly updated and expanded with thematic maps, displaying for example the soil water status or soil erosion. Basic geodata like satellite images and aerial photos are additionally provided. The scale is variable, however, it is recommended to avoid a resolution lower than 1.10.000. When using a scale larger than 1: 30.000 the application will automatically switch to a raster image (cell size: 50 m) allowing overviews on a regional scale.

The test area (communities of Gasen and Haslau) is located in the mapping district 164 „Birkfeld", which was mapped in the early 1980ies.

5.2.2. Introduction: Forest Site Map

Forest site mapping in Austria uses information on topography, climate, geology, soil and vegetation. Contrary to the Agricultural Soil Mapping (eBod), Forest Site Maps are only available for parts of Austria. They cover some 15% of the forests, have been accomplished by public authorities and private institutions (owners) and show different scales and varying intensity of soil information (Schwarz, et al. 2001).

The Forest Site Map (scale 1:25.000) used for this investigation was published by BFW (Jelem, 1960). It comprises 35 different site units. The names of the units refer to the assessed parameters and – as in most Forest Site Maps - the site specific natural tree species (e.g.: "montane zone: spruce-larch-fir-forest on shaded slopes with rendzina").

5.2.3. Soils and Soil Physics in the Test Area

Generally, the mapping units within the test area do not differ significantly. Because of the absence of glacial erosion, the coverage of loose sediments is unusually thick. On the slopes, soil development is strongly influenced / shaped by colluvial processes. Therefore, slopes are covered by more or less (abundant) thick mantles of very loose, coarse or fine colluvial material originating mainly from weathering of gneiss, mica schists and phyllits. The dominating soil types are siliceous brown soils of loose sediments, mostly showing colluvial influence (Fig. 5.2.3-1). The soil texture is loamy sand or sandy silt with a gravel content of about 10 to 70 percent.

A random sample field survey concerning eBod, revealed soils characterized by an extremely low bulk density and the lack of aggregation stability. Since the soil units in the test area do not differ significantly, also soil parameters like texture, gravel content and bulk density are unlikely to vary considerably.

Fig. 5.2.3-1: Typical, abundant colluvial siliceous brown soil of loose sediments with explicit colluvial influence shown in a soil profile and starting point of a landslide in the test area

Platy structure and the high mica content suggest low inner friction angles. In the literature, a relationship between soil parameters and the shear parameters of the soils is documented (e.g. Schnell 1984). To use this information, it was necessary to convert the relations of soil size fractions' volume according to texture information into relations by weight following factors:

Coarse material: 2,5

Sand: 1,5

Silt: 2,0

Clay: 2,5

The calculated results for the soil types in the test-area are shown in Tab. 5.2.3-1.

Tab. 5.2.3-1: Classification according to DIN 18196 and estimation of shear parameters according to Schnell (1984) for the soil units in the test-area

unit	horizon depth from	horizon depth to	coarse fraction	sand	silt	clay	sum	> 2	< 0,06	group	c [kN/m²]	q [°]
a	0	15/30	31	22	39	7	100	31	46	UL	5	35
	15/30		89	4	7	1	100	89	8	GU	0	43
b	0	15/30	20	40	31	9	100	20	40	SU-	10	32
	15/30	50/70	32	34	26	8	100	32	34	SU-	10	32
	50/70		89	5	4	1	100	89	6	GU	0	43
c	0	10/25	13	34	43	9	100	13	52	UL	5	35
	10/25	35/45	54	23	18	5	100	54	23	GU-	5	35
	35/45		89	5	4	1	100	89	6	GU	0	43
d	0	15/30	13	34	43	9	100	13	52	UL	5	35
	15/30	45/65	32	27	34	7	100	32	41	UL	5	35
	45/65		89	4	6	1	100	89	7	GU	0	43
e	0	15/25	14	41	33	13	100	14	45	UL	5	35
	15/25	45/90	20	38	30	12	100	20	42	UL	5	35
	45/90		89	5	4	2	100	89	6	GU	0	43
f	0	15/30	20	32	40	9	100	20	49	UL	5	35
	15/30	70/90	20	32	40	9	100	20	49	UL	5	35
	70/90		53	18	23	5	100	53	28	GU-	5	35
g	0	15/35	14	41	33	13	100	14	45	UL	5	35
	15/35	80/100	49	25	19	7	100	49	27	GU-	5	35
	80/100		77	11	9	3	100	77	12	GU	0	43
h	0	15/25	32	33	26	10	100	32	35	SU-	10	32
	15/25	50/70	19	31	28	22	100	19	50	UM	10	33
	50/70		62	13	13	12	100	62	25	GU-	5	35
i	0	15/25	20	38	30	12	100	20	42	UL	5	35
	15/25	45/55	31	29	25	14	100	31	40	SU-	10	32
	45/55		68	15	12	5	100	68	17	GU-	5	35
j	0	15/25	7	27	50	17	100	7	66	UL	5	35
	15/25	45/65	25	22	40	14	100	25	53	UL	5	35
	45/65		53	18	23	5	100	53	28	GU-	5	35
k	0	20/30	10	31	43	16	100	10	59	UL	5	35
	20/30	80/90	10	31	43	16	100	10	59	UL	5	35
	80/90		10	31	43	16	100	10	59	UL	5	35
l	0	15/20	4	49	39	9	100	4	48	UL	5	35
	15/20	50/60	7	47	38	8	100	7	46	UL	5	35
	50/60	75/85	7	47	38	8	100	7	46	UL	5	35
	75/85		89	6	4	1	100	89	5	GW	-	45
m	0	15/20	32	34	26	8	100	32	34	SU-	10	32
	15/20	20/30	64	18	14	4	100	64	18	GU-	5	35
	20/30	50	89	5	4	1	100	89	6	GU	0	43
n	0	15/25	0	48	38	14	100	0	52	UL	5	35
	15/25	75/85	0	48	38	14	100	0	52	UL	5	35
	75/85		7	45	35	13	100	7	49	UL	5	35
o	0	20/40	6	20	64	9	100	6	73	UL	5	35
	20/40	70/90	6	20	64	9	100	6	73	UL	5	35
	70/90		0	22	68	10	100	0	78	UL	5	35
p	0	15/25	20	38	30	12	100	20	42	UL	5	35
	15/25		89	5	4	2	100	89	6	GU	0	43

The resulting shear parameters show only low variability, compared to the uncertainties originating from the classification of the input parameters.

Soil units are dominated by sand and silt and show medium to high gravel content. Soil depth varies widely between 10 and more than 100cm and is limited by the occurrence of predominant gravel content.

Of high relevance to slope stability and landslide-triggering is the presence of wet spots in the test area - frequently located at the lower parts of slopes. These spots are caused by pressure water - in case of intense rain the soils may lose cohesion and liquefy. The occurrence of these wet spots led to the classification of soil-unit-complexes within this mapping district (eBod). They typically show a gley horizon within the profile.

The event of 2005 suggests that these areas have frequently been starting zones of landslides. As these wet spots are only mapped partially within the eBod and are not recorded within the Forest Site Map, models estimating the susceptibility of slopes lack probably important information when using this dataset.

5.2.4. Soil Units and Correlation to Landslide Susceptibility

The landslide database was controlled by means of orthophotos and partially reappraised concerning land use and anthropogenic influence. Attributes concerning land use and vegetation (open land, forest, distances) were determined to analyse several effects of forest vegetation to the sliding disposition, like e.g. the influence of forest edges.

For a first survey to find out the influence of soil and site unit, the relative frequency of landslide starting zones in relation to the area of the respective unit was quantified. As Fig. 5.2.4-1 shows, the quotient of these two figures differs clearly between different units of eBod.

First investigations showed a clear correlation between the frequency of the observed landslides and the soil units of the agricultural soil mapping (Andrecs et al. 2007, Fig. 5.2.4-1).
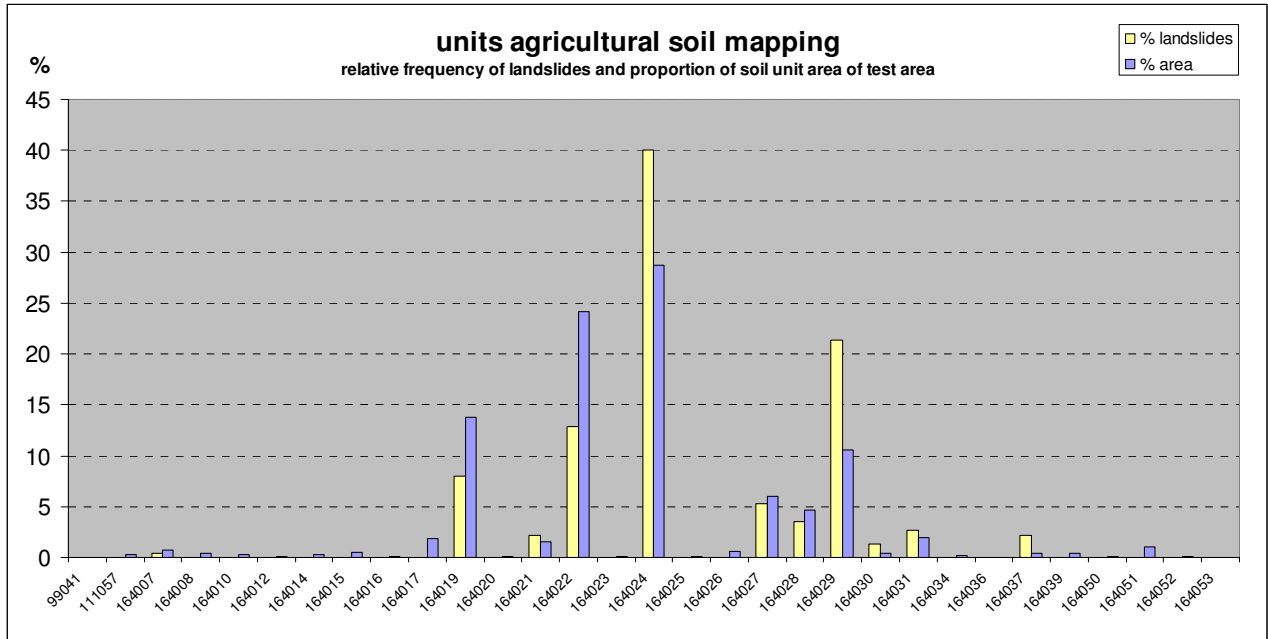
Fig. 5.2.4-1: Observed landslides in different soil units (eBod) in relation to the percentage of the area

Fig. 5.2.4-1 shows a concentration of landslides e.g. in soil unit 29, which is situated predominantly at back slopes and ditches. The high slope water supply in these areas causes high pore water pressures reducing cohesion and may lead to so called "slope explosions". In contrast, e.g. soil unit 22 shows low landslide densities because of the situation on hill slopes and high permeability of the soils in this unit.

Clear differences in the frequency of the observed landslides could also be detected between the forest site mapping units (Fig. 5.2.4-2).
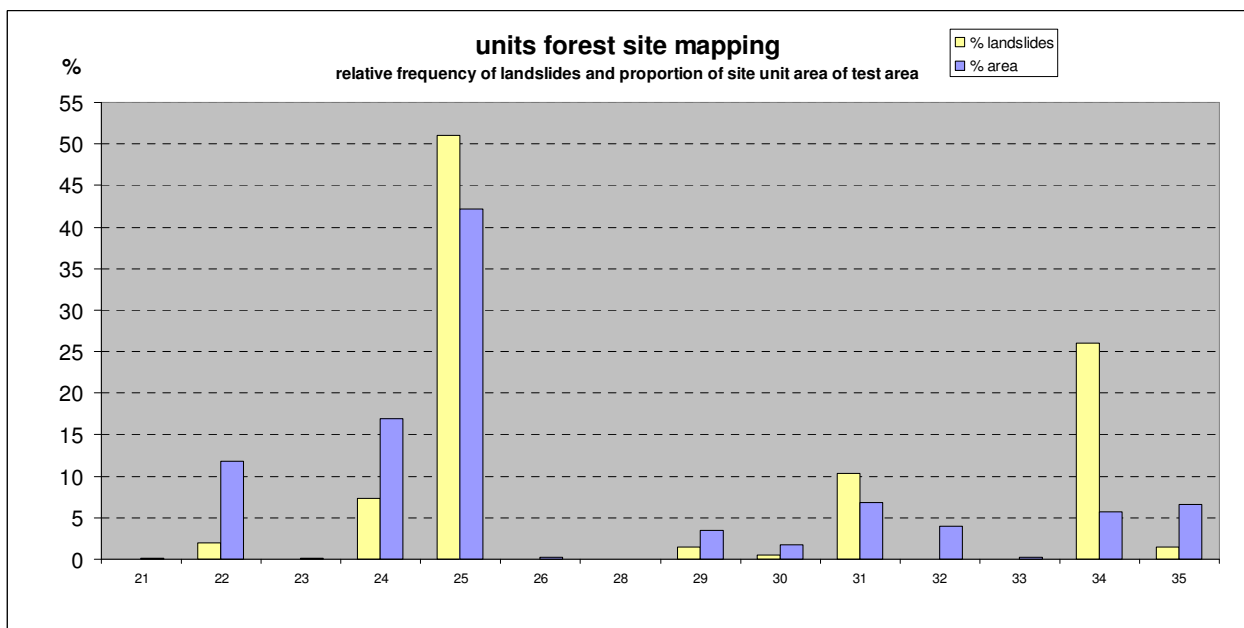
Fig. 5.2.4-2: Observed landslides in different forest site units (Forest Site Map) in relation to the percentage of the area

Fig. 5.2.4-2 shows a concentration of landslides especially in the forest site unit 34, which is located in ditches with colluvial accumulation of loose material. Conspicuous low slide densities are found e.g. in unit 22, which is situated on ridges and upper slopes on harder phyllits with higher quartz percentages and poor water supply.

The number of landslides within the soil and site units differ from the number at hypothesized equal distribution at the 0,1% level of significance.

Furthermore, it showed that about 70% of the observed land slides were influenced by road building (roads and road embankment). Within the forest, the proportion was even greater (75%). Due to the fact that we did not know, how extensively both total area and single units were affected by road construction the interaction between road construction and landslide-disposition could not be identified by statistical methods.

5.2.5. Unified Soil Map

The general aim of the project was to analyze the benefit of parameters and their combinations for the model results. Using area-wide calculating models to estimate the landslide susceptibility requires area-wide standardized parameter maps. Hence, the agricultural soil map and the Forest Site Map had to be merged into one map, new units referring to the agricultural as well as to the forest land had to be defined. However, this procedure causes a loss of information that has to be accepted.

Firstly, units within the eBod and within the Forest Site Map were combined and – thereby - simplified. Implementing this, an important issue is that the topographic position of the different units should not account for the grouping. Only soil intrinsic parameters such as parent material, root penetration depth, soil texture and water regime were relevant. For the test area 16 new soil units were found (Tab. 5.2.5-1).

Secondly, the two new, simplified maps had to be merged. This was achieved by comparing features of the units, while also considering the neighbourhood of the units.

Tab. 5.2.5-1: Unified soil units. The table shows the new units, the related units of eBod, Forest Site Map and World Reference Base for Soil Resources (WRB) classification

Unit	eBod – soil unit (BOFO)	Forest Site Map (STO)	WRB classification
a	164010	28	Leptic Regosol
b	164014,164015, 164016	29, 32, 35	Haplic Regosol
c	111057, 164017, 164019	22, 23	Leptic Regosol
d	164020, 164021, 164022, 164023, 164024, 164028	24	Leptic Regosol
e	99041, 164025, 164026, 164027	26, 30, 31	Haplic Cambisol
f	164029	33, 34	Haplic Cambisol
g	164030, 164031	-	Endogleyic Cambisol
h	164050, 164053	-	Haplic Regosol
i	164051, 164052	25	Haplic Regosol
j	164034, 164037	-	Haplic Regosol
k	164036	-	Haplic Cambisol
l	164039	-	Endogleyic Regosol
m	-	21	Hypersceletic Leptosol
n	164007	-	Endogleyic Regosol
o	164008	-	Haplic Gleysol
p	164012	-	Hypersceletic Leptosol

The characteristics of the new developed soil units are described below:

Unit a: *(STO: 28; BOFO: 164010)*
Slopes, ridges, terrain edges, strongly pending to steep
Leptic Regosol from talus material, partly also from solid rock (limestone, dolomite, greywacke), highly calcareous, shallow
Dry, high permeability, little water retention capacity
0 - 15/30cm: Silty sand or sandy silt
                            Coarse fraction medium to high
15/30 cm +:   Coarse fraction predominant

Unit b: *(STO: 29, 32, 35; BOFO: 164014, 164015, 164016)*
From pending to steep
Haplic Regosol from talus material (limestone, dolomite, lime schist), highly calcareous, medium deep
Moderately dry, moderate to high permeability, moderate water retention capacity; forest: „fresh"
0 - 15/30cm: Silty sand or loamy sand
                            Coarse fraction medium
15/30 – 50/70cm: Silty sand or loamy sand
                            Coarse fraction medium to high
50/70cm +:   Coarse fraction predominant

Unit c: *(STO: 22, 23; BOFO: 111057, 164017, 164019)*
Slopes, ridges, terrain edges, from even to steep
Leptic Regosol from talus material or (brittle) rock (phyllite, gneiss, mica schist), non calcareous, (shallow to) medium deep
Dry, high permeability, little to medium water retention capacity; forest: "fresh"

0 - 10/25cm:	Loamy sand or sandy silt
	Coarse fraction low to medium
10/25 – 35/45cm:	Loamy sand,
	Coarse fraction high to very high
35/45cm +:	Coarse fraction predominant or rock

Unit d: *(STO: 24; BOFO: 164020, 164021, 164022, 164023, 164024, 164028)*
Slopes, rarely hilltops, ridges, terrain edges; little pending to steep
Leptic Regosol from talus material or from (brittle) rock (phyllite, gneiss, mica schist, rarely quarzite), non calcareous, moderately deep to deep
Moderately dry, in small areas (little depressions or channels at the slope) water availability better, moderate to high permeability, moderate water retention capacity; forest: "fresh"

0- 15/30cm:	Loamy sand or sandy silt
	Coarse fraction low to medium
15/30 – 45/65cm:	Loamy sand or sandy silt
	Coarse fraction medium to high
45/65cm +:	Coarse fraction predominant, partly also (bed)rock

Unit e:*(STO: 26, 30, 31; BOFO: 99041, 164025, 164026, 164027)*
Upper slopes to down slope positions, little pending to steep
Haplic Cambisol from talus material or from brittle rock (phyllite, gneiss, mica schist), non calcareous, deep
water availability good, moderate permeability, moderate to high water retention capacity; forest: "very fresh"

0- 15/25cm:	Loamy sand
	Coarse fraction low to medium
15/25 – 45/90cm:	Loamy sand
	Coarse fraction medium
45/90cm +:	Coarse fraction predominant

Unit f: *(STO: 33, 34; BOFO: 164029)*
Bottom of slopes, gullies, gorges, lower slopes, strongly pending to steep,
Haplic Cambisol from talus material (phyllite, gneiss, mica schist), non calcareous, deep
Water availability good, moderate permeability, high water retention capacity; forest: "very fresh (to moist)"

0 - 15/30cm:	Sandy silt or loamy sand
	Coarse fraction medium
15/30 – 70/90cm:	Sandy silt or loamy sand
	Coarse fraction medium
70/90cm +:	Sandy silt or loamy sand
	Coarse fraction high to very high

Unit g:*(BOFO: 164030, 164031)*
Slope with little gullies, bottom of slopes, slope-depressions, at the edge of swelling muldes; very little to little pending
Endogleyic Cambisol from talus material (phyllite, gneiss, mica schist), non calcareous, deep
Moderately moist with pressurized water, high permeability, moderate water retention capacity;

0 - 15/35cm:	Loamy sand
	Coarse fraction low to medium
15/35 – 80/100cm:	Loamy sand, rarely sandy loam
	Coarse fraction medium to very high
80/100cm +:	Coarse fraction very high to predominant

Unit h *(BOFO: 164050, 164053)*
Plantations, slopes, even to moderate inclination
Haplic Regosol, soils dominated by (their) colour, from dark, brittle granite-phyllite, non calcareous, moderately deep to deep
Moderately dry to good water availability, moderate permeability, moderate to high water retention capacity;

0 - 15/25cm:	Loamy sand
	Coarse fraction medium to high
15/25 – 50/70cm:	Sandy loam
	Coarse fraction medium
50/70cm +:	Loamy sand, sandy loam or loam
	Coarse fraction medium to predominant

Unit i: *(STO: 25) (BOFO: 164051, 164052)*
Slopes, strongly to highly pending
Haplic Regosol, soils dominated by (their) colour, talus material (dark clay schist, partly also phyllite), non calcareous, moderately deep to deep
Moderately dry, moderate to high permeability, moderate water retention capacity

0 - 15/25cm:	Loamy sand
	Coarse fraction medium
15/25 – 45/55cm:	Loamy sand or sandy loam
	Coarse fraction medium to high
45/55cm +:	Loamy sand
	Coarse fraction high to predominant

Unit j: *(BOFO: 164034, 164037)*
Valley floors with gullies and troughs, alluvial fans, very little to little pending, rippled, humpy
Haplic Regosol from fine above coarse alluvial material, non calcareous, moderately deep
Moderately dry, high permeability, moderate water retention capacity

0 - 15/25cm:	Loamy sand or silt
	Coarse fraction low
15/25– 45/65cm:	Loamy sand or silt
	Coarse fraction low to high
45/65cm +:	Coarse fraction predominant

Unit k: *(BOFO: 164036)*
Valley floors, even to very little pending
Haplic Cambisol from fine alluvial or colluvial material, non calcareous, deep
Water availability good, moderate permeability, high water retention capacity

0 - 20/30cm:	Sandy silt, loamy sand or loamy silt
	Coarse fraction low (medium)
20/30– 80/90cm:	Sandy silt, loamy sand or loamy silt
	Coarse fraction low (medium)
0/90cm +:	Sandy silt, loamy sand or loamy silt
	Coarse fraction low (medium)

Unit l: *(BOFO: 164039)*
Valley floors, alluvial fan, even to very little pending, gently wavy
Endogleyic Regosol from fine alluvial and colluvial matersial, non calcareous, deep
Moderately moist by pressure and ground water, high permeability, low water retention capacity

0 - 15/20cm:	Silty sand or loamy sand
	Partly low gravel content

15/20– 50/60cm:	Silty sand or loamy sand
	Partly low gravel content
50/60 - 75/85cm:	Silty sand or loamy sand
	Partly low gravel content
75/85cm +:	Predominant gravel

Unit m: *(STO: 21)*
Ridges and upper slopes
Hyperskeletic Leptosol from phyllite, poor gneiss and schist, non calcareous, shallow
Moderately dry, high permeability, little water retention capacity

0 - 15/20cm:	Loamy sand or silty sand
	Coarse fraction medium to high
15/20– 20/30cm:	Silty sand or loamy sand
	Coarse fraction very high
20/30 – 50cm:	Silty sand or loamy sand
	Coarse fraction predominant
50cm +:	Rock (debris)

Unit n: *(BOFO 164007)*
Valley floors, alluvial fans, even to very little pending
Endogleyic Regosol, drained gleysol from fine alluvial material, non calcareous, deep
Moderately moist by pressurized water and ground water, moderate permeability, high water retention capacity

0 - 15/25cm:	Loamy sand
15/25– 75/85cm:	Loamy sand
75/85cm +	Loamy sand
	Coarse fraction low

Unit o: *(BOFO 164008)*
Troughs and gullies on valley floors and alluvial fans, even to very little pending, gently rippled, humpy
Haplic Gleysol from fine alluvial material, non calcareous, deep
Moist by pressurized water, moderate permeability, little water retention capacity

0 - 20/40cm:	sandy silt
	coarse fraction low
20/40– 90/90cm:	sandy silt
	coarse fraction low
70/90cm +:	sandy silt

Unit p: *(BOFO 164012)*
Valley floors, alluvial fans, even to little pending, mostly rippled, humpy, often next to channels
Hyperskeletic Leptosol from coarse alluvial materiel (mica schist, gneiss, quartzite), non calcareous, shallow
dry, high permeability, little water retention capacity

| 0 - 15/25cm: | loamy sand, coarse fraction medium |
| as of 15/25cm: | coarse fraction predominant |

When merging the polygons of the two datasets three different cases were found:

1. Areas with data of one of the two datasets (e.g. eBod Fig. 5.2.5-1).

2. Areas with data of both of the datasets: These areas are mostly very small and occur along the land use types where they overlap. They were attached to one of the neighbouring units by a GIS algorithm, overtaking the eBod information because of the assumed higher quality.

3. Areas without data: More than 10% of the area lacked any information (Fig. 5.2.5-3). This is due to the fact that the agricultural soil map did not cover all of the extensively used grassland, and the fact, that the Forest Soil Map did not cover the whole test area. Additionally, stripes and smaller areas along the two land use types due to geometric impreciseness were observed. In these cases, units and information were assigned by expert knowledge, considering the information of the surrounding polygons.

Merging eBod and the Forest Site Map did not meet the demand for a map covering the whole area.
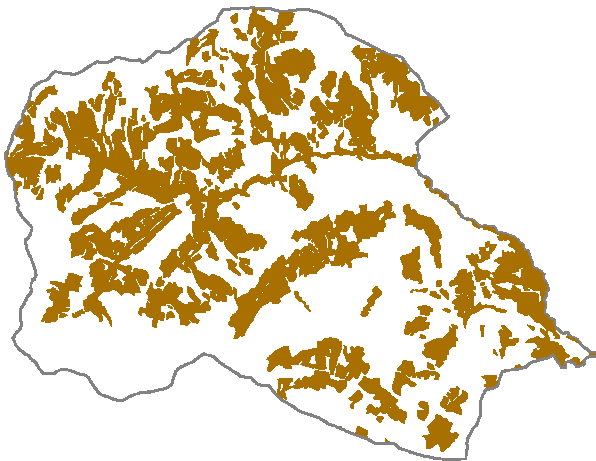
Fig. 5.2.5-1: Area-Coverage eBod (brown)

Fig. 5.2.5-2: Additional Coverage Forest Site Map (green)
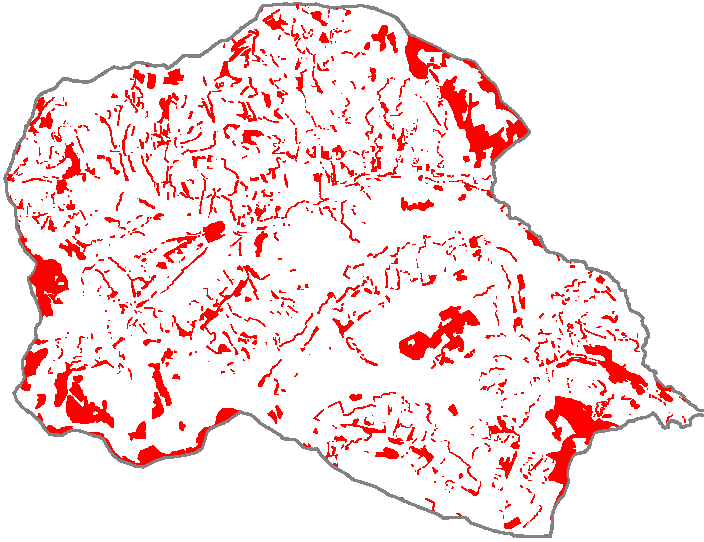
Fig. 5.2.5-3: Areas with lacking soil information. Merging eBod and the Forest Site Map did not meet the demand for a map covering the whole area

The resulting unified area-wide map, processed in the described way is shown in Fig. 5.2.5-4
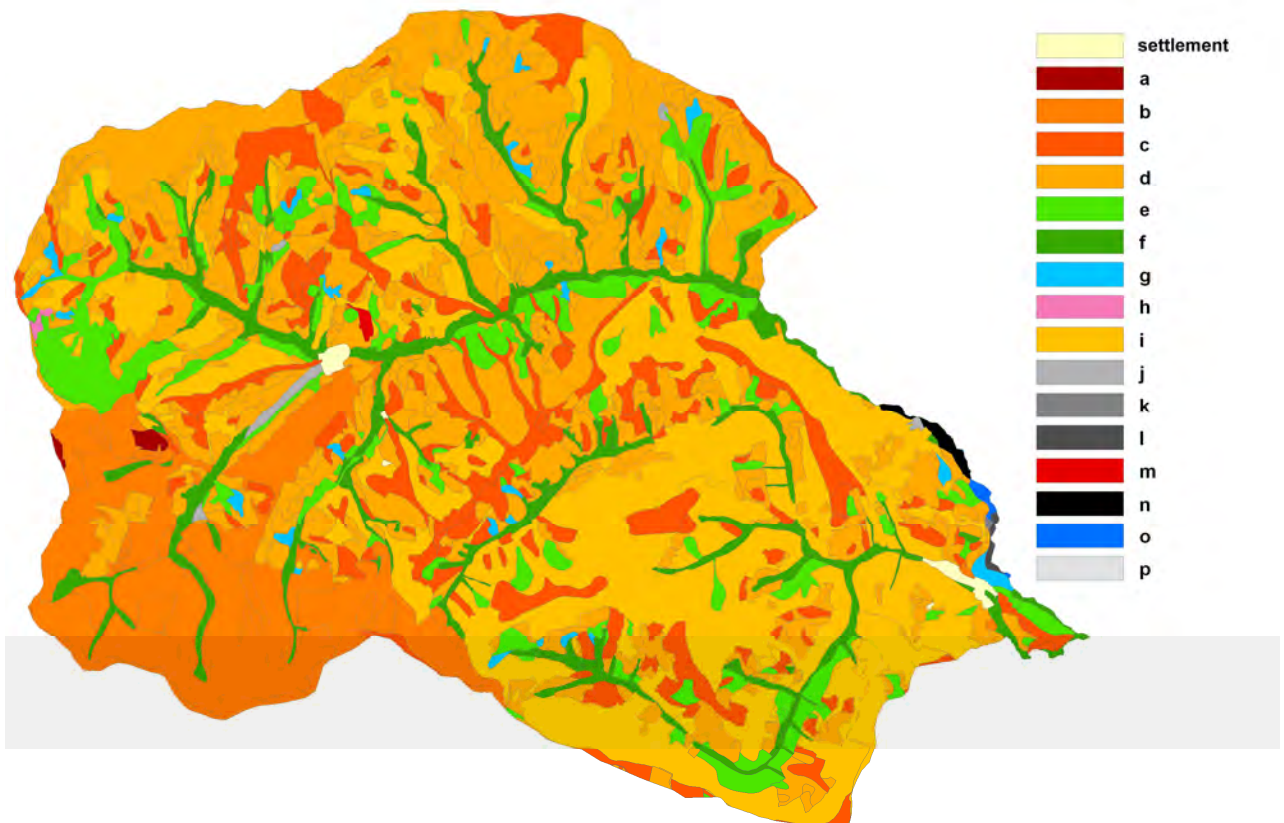
Fig. 5.2.5-4: Unified (merged and simplified) soil map

5.2.6. Landslide Disposition Map

The units were assigned an index for landslide susceptibility between 1 (low disposition) to 5 (high disposition) shown in Fig. 5.2.6-1. Here, especially soil depth, parent material, content of coarse material and water conditions were used. The allocation of soil units (Fig. 5.2.5-4) to disposition classes (Fig. 5.2.6-1) is based on expert knowledge, the way they are merged is shown in Tab. 5.2.5-2.

Tab. 5.2.6-1: Generated classes of landslide disposition based on the merged and simplified, area-wide soil units

landslide disposition	1	2	3	4	5
unit	a,m,n,o,p	k	b,c,d,h,,j	e,i,l	f,g
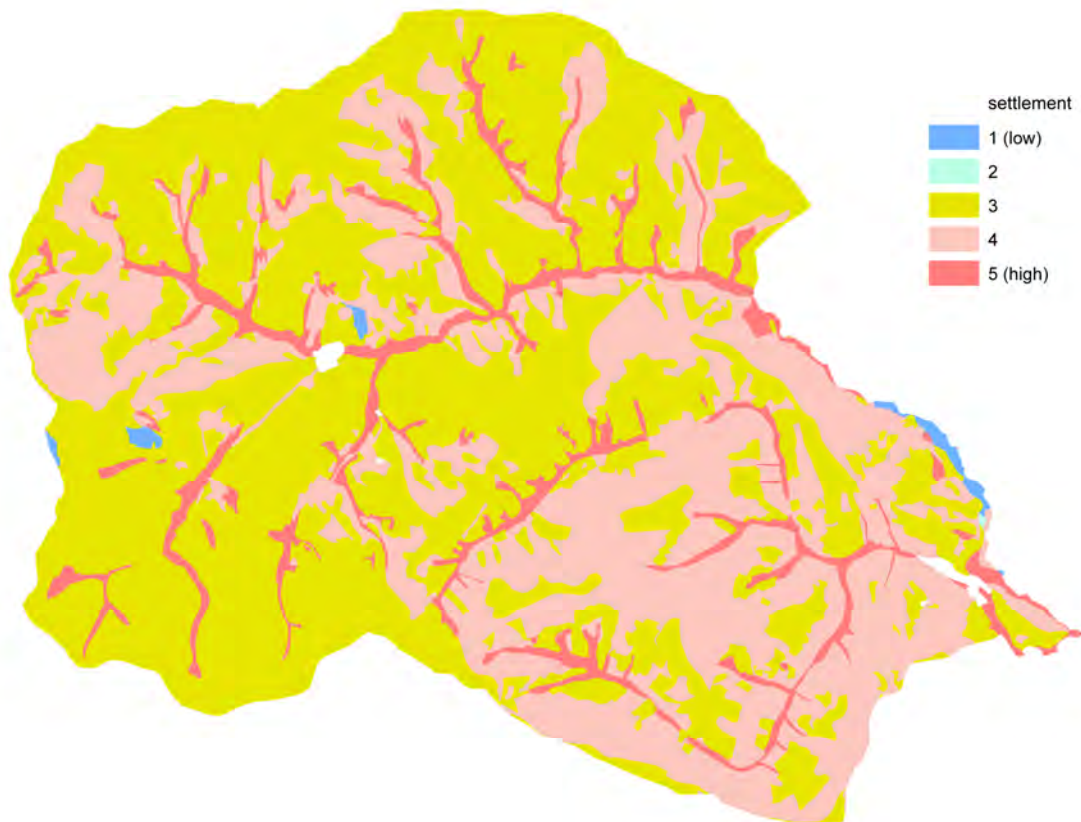
Fig. 5.2.6-1: Disposition for land slides in the unified map (assigned by expert knowledge)

The unified soil maps as well as hence generated disposition map are input-parameters for the comparison and evaluation of databases and database combinations with different approaches (Chapter 7 and 8). The soilmap is a considerable source of information for physically based approaches like the SINMAP model (Chapter 7.5).

5.3.   Remote Sensing Data (JR)

Due to technological progress and new sensors the potential of Remote Sensing Data with regard to environmental applications has grown significantly within the past few years. The main advantage of Remote Sensing Data is the possibility to perform area-wide investigations and analyses on an objective basis even on inaccessible areas. Remote sensing can replace costly and slow data collection on the ground, ensuring in the process that areas or objects are not disturbed.

Within the frame of AdaptSlide the following data sources were used:

- Satellite Data
- Aerial Photographs
- Airborne Laserscanner (LiDAR – Light Detection and Ranging)

5.3.1. Satellite Data

Available land cover data of the test area do not represent small-scale land cover heterogeneities. This is especially true for the forest / non-forest classification based on the Digital Cadastral Map. Aiming at reducing this deficit high-resolution satellite data were acquired and classified.
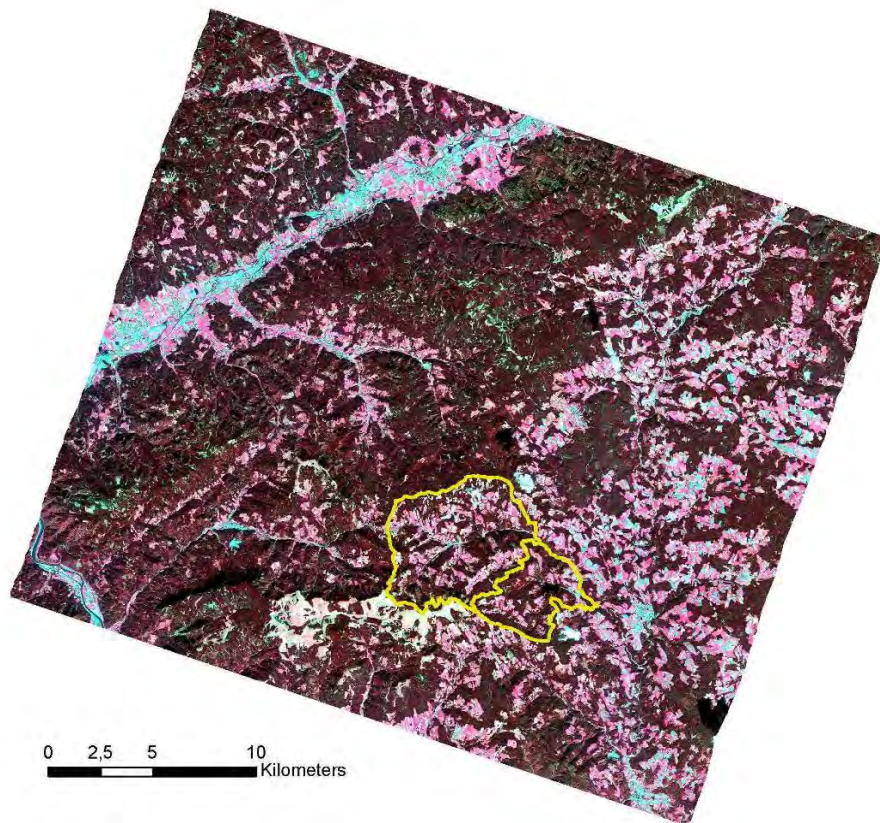
Fig. 5.3.1-1: SPOT5 scene taken on 30-09-2007 covering the test area Gasen-Haslau and most parts of the Fischbacher Alps (false colour representation; yellow: borders of communities Gasen and Haslau)

An archived SPOT5 scene taken on 30th of September 2007 best met the demands with respect to illumination and cloud cover (Fig. 5.3.1-1). Orbital platforms collect and transmit data from different parts of the electromagnetic spectrum. The data from the french SPOT5 system offer a resolution of 2,5 to 5 meters in panchromatic mode and 10 meters in multispectral mode covering wavelengths of 0,50 – 0,59; 0,61 – 0,68 and 0,79 – 0,89 µm (= green, red, near Infrared). The additional band at mid-infrared wavelengths (1,58 – 1,75 µm with 20 meters spatial resolution) provides efficient capabilities for vegetation surveys. The data do not only allow the classification with regard to the main tree species but also a rough assessment of growth classes and crown coverage.

Because of the late acquisition date of the SPOT5 scene additionally an AVNIR scene (Advanced Visible and Near Infrared Radiometer) of the Japanese ALOS system which was available at the institute was used. This sensor also provides data with a spatial resolution of 10 m in multispectral mode. The available scene which was slightly affected by clouds was taken on 15th of July 2007, thus showing excellent illumination conditions (Fig. 5.3.1-2).
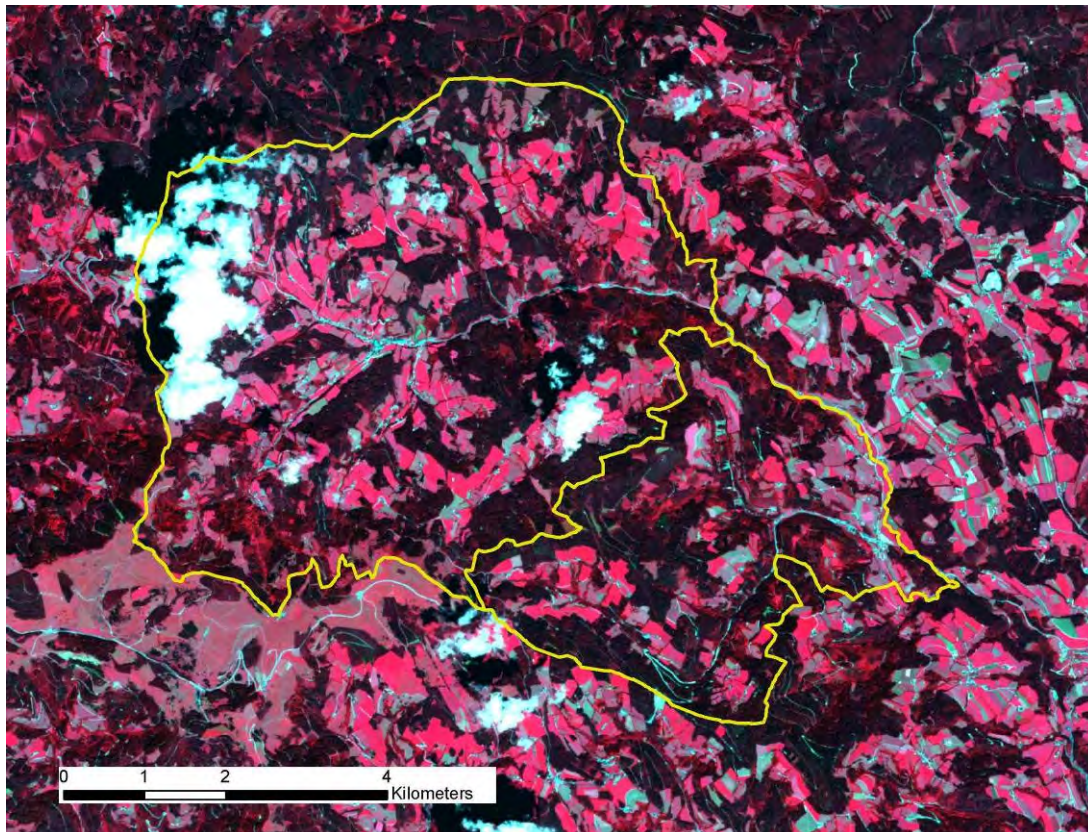
Fig. 5.3.1-2: Detail of unprocessed AVNIR scene taken on 15-07-2007 covering the test area Gasen-Haslau (false colour representation; yellow: borders of communities Gasen and Haslau)

5.3.1.1 Data Preprocessing - Geocoding

The test site is located in a mountainous region which brings about that it is a prerequisite to remove the displacement errors caused by the topographic relief. In order to optimize the absolute geometric location accuracy of the geocoded image

data, these errors are removed through the integration of a Digital Elevation Model (DEM), i.e. the consideration of terrain relief information. The spatial database of the geocoding was the DEM provided by the Austrian Federal Office for Metrology and Surveying (BEV) with a 10 m resolution.

This preprocessing step is executed by means of ground control points, with the points representing an approximately homogenous distribution with respect to position and height. The geocoding was performed with the RSG software (Remote Sensing software package Graz) of JOANNEUM RESARCH.

5.3.1.2 Data Preprocessing - Topographic Normalization

In mountainous terrains the illumination and reflexion within an image is strongly influenced by the topography. These variations have to be removed, in order to achieve that two objects having the same reflectance properties show the same spectral signature despite their different orientation to the sun's position. In this project, a new correction method was used for topographic normalization implementing an incidence normalization filter. This filter is based on the finding that the gray-values of a specific land-cover class show a linear dependency on the incidence angle of the sun relative to the underlying DEM. This fact is used in this program to calculate a unique slope and offset value K for every pixel in its grey-value/incidence angle feature space. Once a specific K value has been calculated for a pixel, a normalized gray-value is calculated by normalisation to the default incidence angle. The result of the normalization process can be observed through the disappearance of the "3D" effect, which is still present in the raw image. Based on these results, the analysis of the land cover signatures can be performed on an equal basis.

5.3.1.3 Classification

Following the data pre-processing the supervised land cover classification was performed. For SPOT5 and AVNIR imagery with a spatial resolution of 10 x 10 m the objects of interest are smaller than the pixel size. In this case, pixel-based approaches classifying the spectral signature of each pixel are well applicable for the derivation of landcover and especially forest parameters. Previous investigations (e.g. Schardt & Schmitt 1996, Granica et al. 2000, 2004) have shown very good results regarding the differentiation of tree species. This is illustrated in Fig. 5.3.1.3-1: the different species show well separated clusters in the feature space of the NIR (Near InfraRed) and the MIR (Mid InfraRed) band of the SPOT5 image.

The signature analysis has been performed on a number of bands and channels derived from the SPOT5 data. The parametric signatures are based on statistical parameters, e.g. mean and covariance matrix, that are derived from training samples. The training sites required for the supervised classification were selected on the basis of aerial photographs and by a ground truthing campaign, and according to the results of the signature analysis. Statistics have been derived for each training site as well as independently for each verification site and analyses on histograms and spectral curves have been made.

The spectral bands of the satellite images were taken as input features for the classification using a Maximum-Likelihood (ML) classifier. The ML decision rule is

based on the probability that a pixel belongs to a particular class. The basic equation assumes that these probabilities are equal for all classes, and that the classes have normal distributions. The variability of classes is taken into account by using the covariance matrix. Finally, to achieve the classification result, a detailed evaluation of several classification runs based on different parameter settings and combinations of training areas was performed.
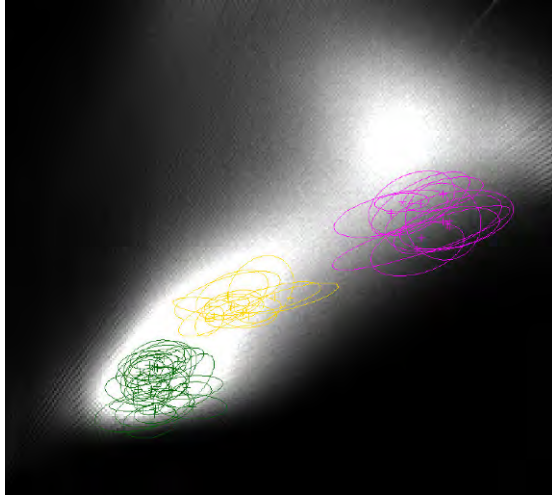
Fig. 5.3.1.3-1: two-dimensional representation of well separated training clusters in the feature space of the NIR (Near InfraRed, x-axis) and the MIR (Mid InfraRed, y-axis) band: green = spruce; yellow = larch; magenta = broadleaf

The result of the tree type classification with the original 10 m spatial resolution is shown in Fig. 5.3.1.3-1, the result after the aggregation to 50 m (based on majority) is shown in Fig. 5.3.1.3-3. The nomenclature of the tree type distribution is based on the percentage of coniferous (i.e.: sum of coniferous / (sum of coniferous + sum of broadleaf)). Pure tree types consist of more than 90 % of this particular species. The nomenclature is given in Fig. 5.3.1.3-2.

The result shows a high predominance of spruce stands in most parts of the study area. Larch is intermingled frequently and there are even stands dominated by larch. Pine can be found as well widespread in different mixture ratios. Deciduous woodland commonly is restricted to minor patches and strips often accompanying streams and ditches or the borders of the forest. Broadleaves can not be differentiated by means of spectral analysis. Based on field verifications beech, maple, birch and wild cherry were identified as dominating broadleaves in the study area.

The spectral signature of each pixel does not only contain tree species related information. Other factors affecting pixel values are for example age of trees, density of trees as well as the vertical structure of the forest, insect calamities or drought stress (Granica et al. 2004). This information can be used for the further parameterisation and subdivision of forest areas aiming at the analysis of the influence of the vegetation on landslide susceptibility. As the stage of stand development and the crown coverage were evaluated as relevant indicators, these parameters were derived from the spectral signature of each pixel of the available satellite data as well.

For the stand development four classes were defined (ref. to Fig. 5.3.1.3-4). The older classes ('timber' and 'old timber') are dominating the forests in most parts of the study area.

With regard to crown coverage as well four different classes are shown (ref. to Fig. 5.3.1.3-5). Crown coverage < 30 % is not considered 'forest area' but is classified open area. The dominating density class is 61 – 80 %.

For the accuracy assessment of these classifications the following aspects have to be taken into account:

- The stand development classes could be separated with higher accuracy than the crown coverage classes for coniferous.

- Generally the classification of coniferous woodland can be considered to be derived with higher accuracy than for deciduous woodland.
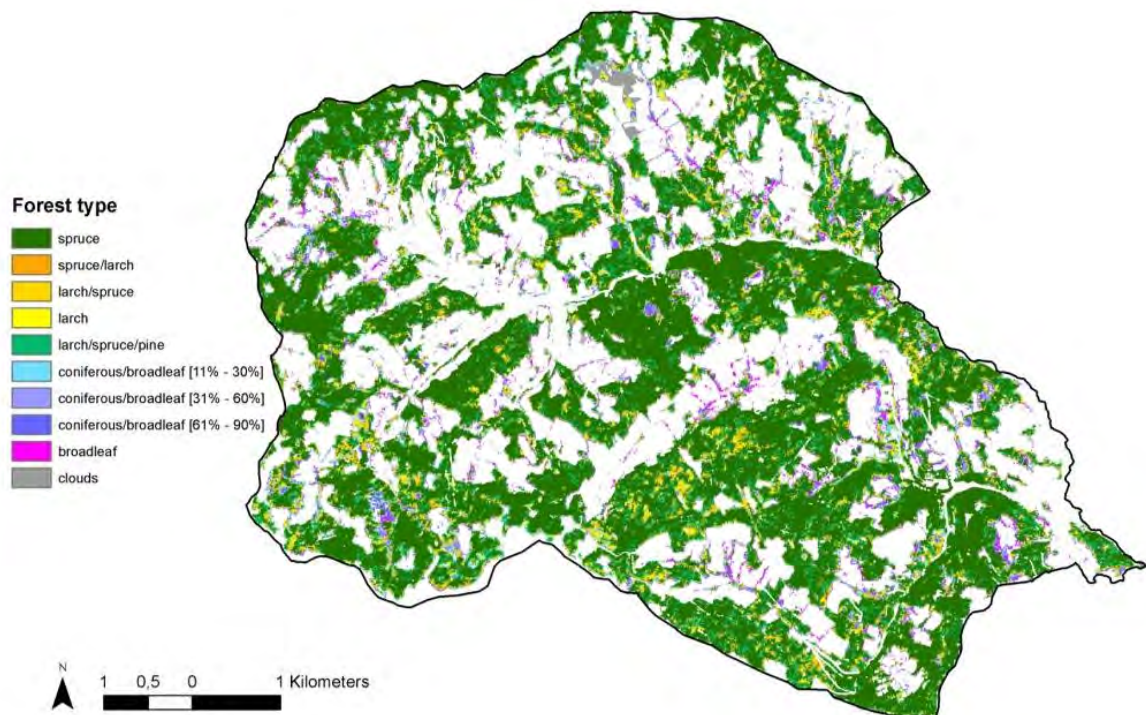
Fig. 5.3.1.3-2: Result of the tree type classification based on satellite data with high spatial resolution (SPOT5, ALOS)

Forest type (50m)

- spruce
- spruce/larch
- larch/spruce
- larch
- larch/spruce/pine
- coniferous/broadleaf [11% – 30%]
- coniferous/broadleaf [31% – 60%]
- coniferous/broadleaf [61% – 90%]
- broadleaf
- clouds

1 0,5 0   1 Kilometers
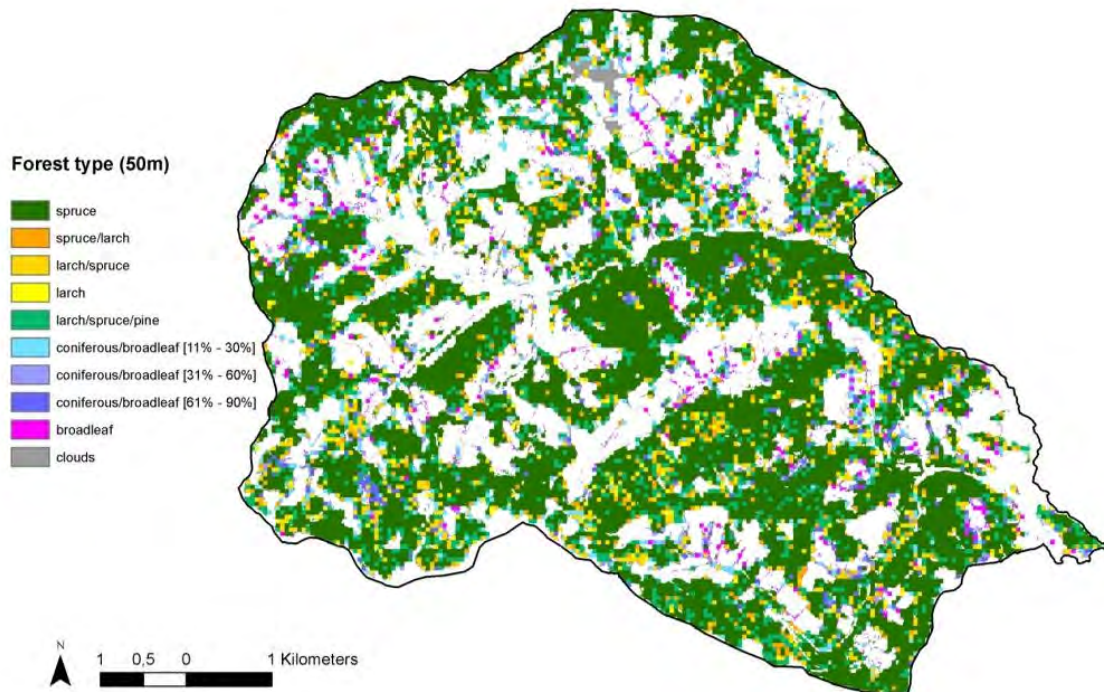
Fig. 5.3.1.3-3: Result of the tree type classification based on satellite data with high spatial resolution (SPOT5, ALOS) after aggregation to 50 m (based on majority)

The results of the crown coverage and the stand development classification with the original 10 m spatial resolution as well as the nomenclatures are shown in Fig. 5.3.1.3-4 and Fig. 5.3.1.3-5 respectively.

Stand development

- culture / thicket
- pole
- timber
- old timber
- clouds

1 0,5 0   1 Kilometers
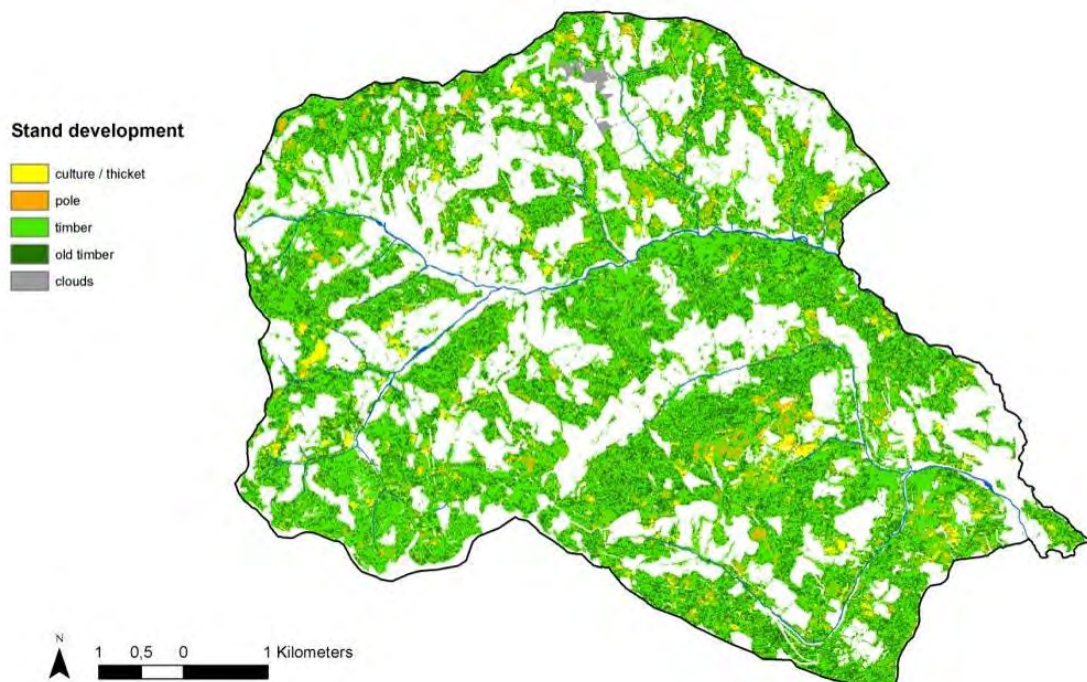
Fig. 5.3.1.3-4: Result of the stand development classification based on satellite data with high spatial resolution (SPOT5, ALOS)
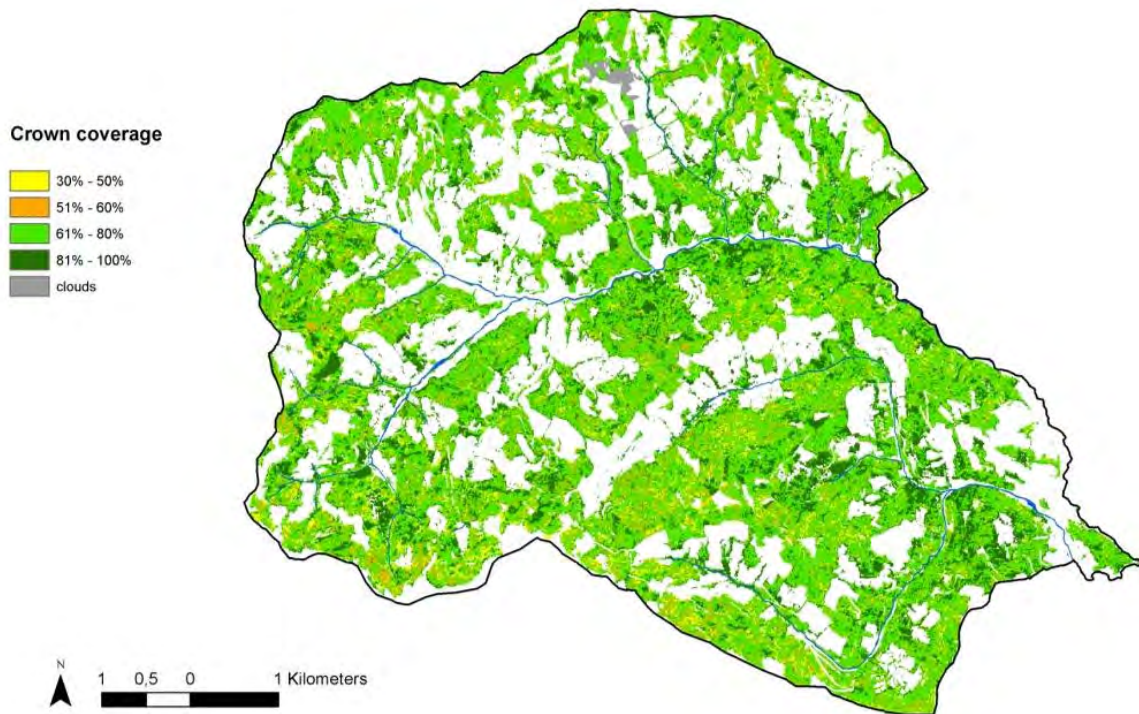
Fig. 5.3.1.3-5: Result of the crown coverage classification based on satellite data with high spatial resolution (SPOT5, ALOS)

The protective function of the forest cover in the study area with regard to shallow landslides is clearly detectable by means of the validation of the modelling results (Chapter 7.2 – 7.4).

The classifications of forest type, crown coverage and stand development were combined to an advanced process related forest dataset ("Wald_Sat_lh"). Characteristics of the root system (shallow root systems of e.g. spruce vs. deep tap root systems of e.g. larch and pine) and the capacity of evapotranspiration can be seen as most relevant with respect to the triggering of shallow landslides.

The forest types were reclassified to four types considering the above mentioned process relevant characteristics:

- coniferous dominated by spruce

- coniferous dominated by larch and/or pine

- mixture of coniferous and broadleaf

- forest dominated by broadleaves

The class "clouds" could be eliminated by visual interpretation of aerial photographs.

The original stand development classification (4 classes, ref. to Fig. 5.3.1.3-4) was kept assuming increase of stability with higher stand development classes.

By combining forest type and stand development four tentative classes were defined:

- Class 1: Stand class 1, all forest types + Stand class 2, forest type 1
- Class 2: Stand class 2, forest type 2, 3, 4 + Stand class 3, forest type 1
- Class 3: Stand class 3, forest type 2, 3 + Stand class 4, forest type 1
- Class 4: Stand class 3, forest type 4 + Stand class 4, forest type 2, 3, 4
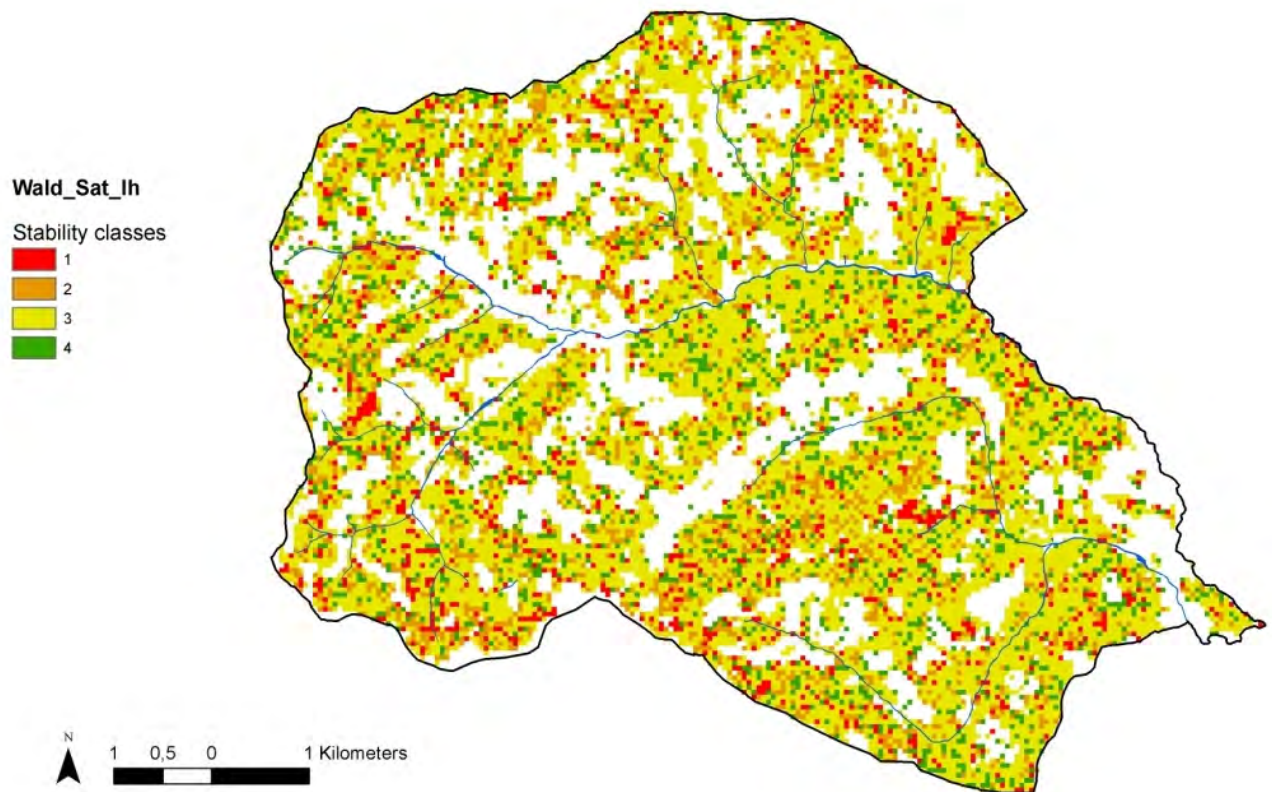
Fig. 5.3.1.3-6: Forest classification "Wald_Sat_lh" with four stability classes under consideration of additional forest parameters (forest type, crown coverage, stand development)

As well the original crown coverage classification (4 classes, ref. to Fig. 5.3.1.3-5) was kept assuming increase of stability with higher crown coverage classes. This hypothesis was confirmed by the bivariate statistics except for crown coverage classes 3 and 4 which hence were merged. The final stability classes were defined by adding correction factors for crown coverage classes 3 (+1), 4 and 5 (+2). This procedure theoretically results in 6 final classes with only the classes 3, 4, 5 and 6 remaining in the study area. These classes were redefined for the final four stability classes of "Wald_Sat_lh".

Finally the non-forested areas were classified as well. Four classes regarding to vegetation density were defined (Fig. 5.3.1.3-7) but these results were not taken into account for the modelling procedure.
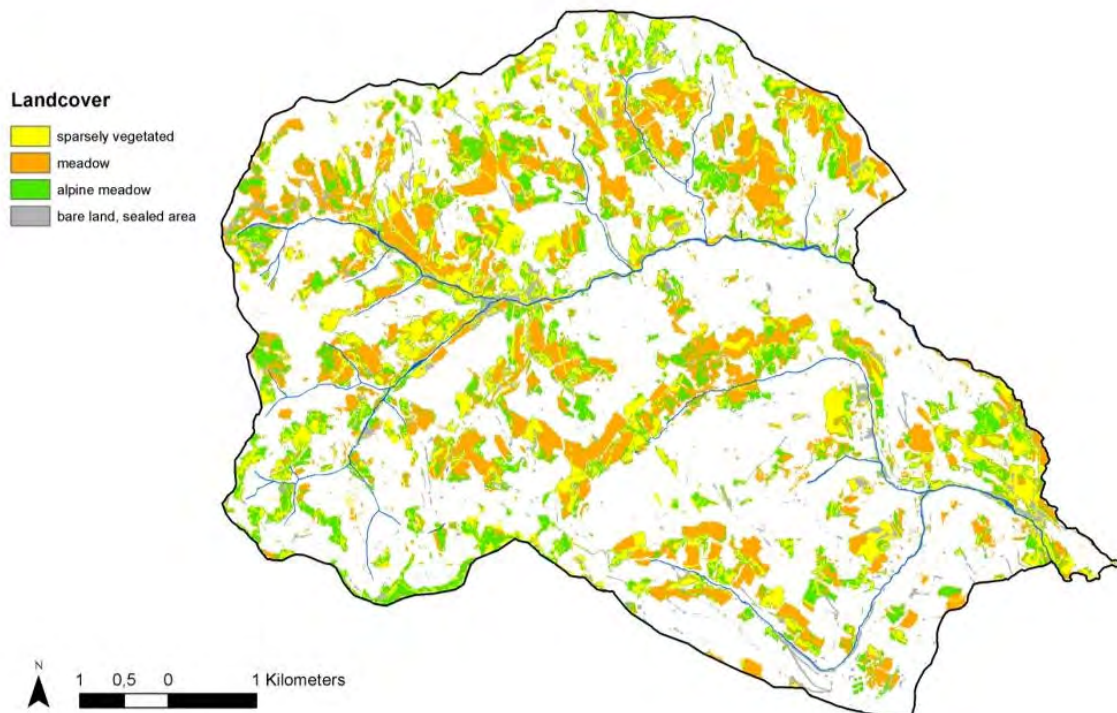
Fig. 5.3.1.3-7: Result of the classification of non-forested areas based on satellite data with high spatial resolution (SPOT5, ALOS)

From the landcover classification finally three different datasets were created as input to the modelling procedure.

1. A forest mask aggregated to 50 m with forest defined when at least 6 out of original 25 pixels are classified as forest ("Wald_Sat_lg", Fig. 5.3.1.3-8).

2. A forest mask aggregated to 50 m with forest defined when at least 20 out of original 25 pixels (= 80 %) are classified as forest ("worst case scenario", "Wald_Sat_lg_80" Fig. 5.3.1.3-9).

3. A forest classification with four stability classes under consideration of additional forest parameters (forest type, crown coverage, stand development, "Wald_Sat_lh", Fig. 5.3.1.3-6).

Generally it has to be stated that a lot of information supposed to be relevant for the triggering of shallow landslides was lost by the aggregation process (cf. Fig. 5.3.1.3-2 and Fig. 5.3.1.3-3).
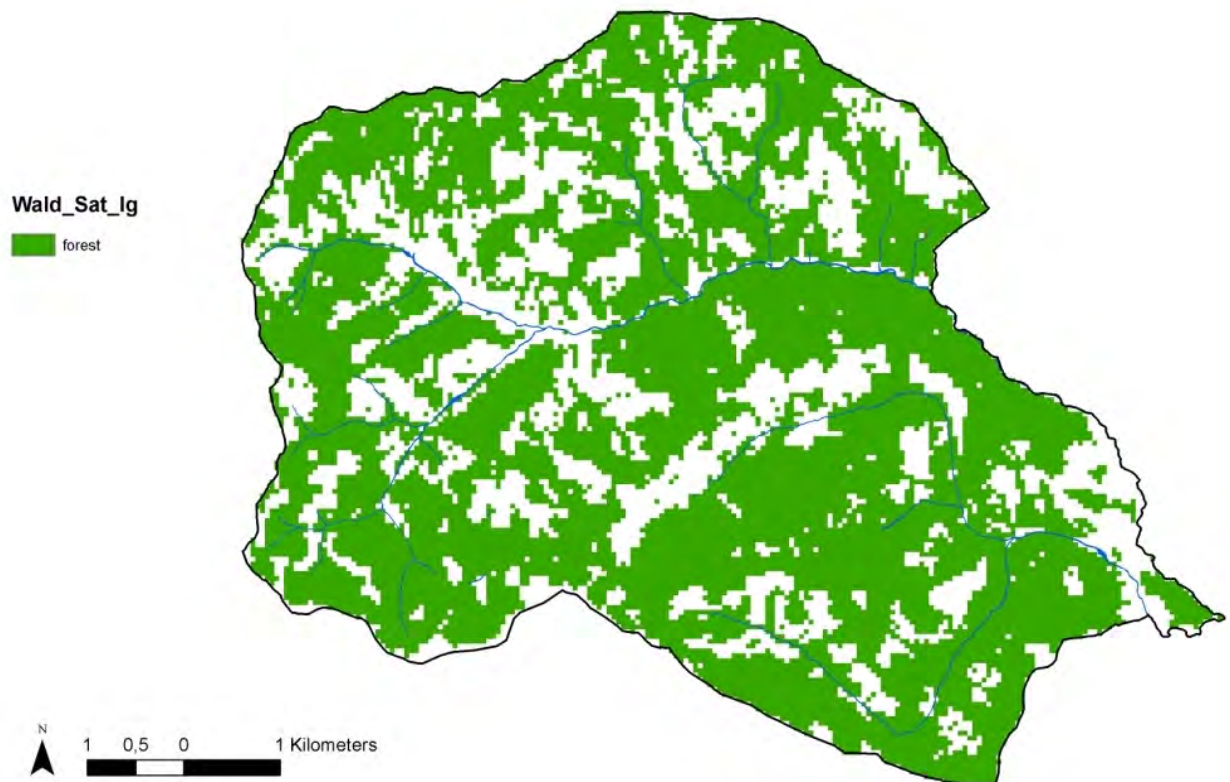
Fig. 5.3.1.3-8: Forest mask "Wald_Sat_lg" based on the classification of satellite data after aggregation to 50 m with forest defined when at least 6 out of 25 pixels are classified as forest

Fig. 5.3.1.3-9: Forest mask "Wald_Sat_lg_80" based on the classification of satellite data after aggregation to 50 m with forest defined when at least 20 out of 25 pixels are classified as forest

5.3.2. Aerial Photographs

Within the first phase of the project "Low-Cost Aerial Data Acquisition Platform for Disaster Operations" aerial photographs were taken from the most affected areas in Gasen and Haslau approximately 15 days after the event. This was performed within the frame of a pilot study funded by the Styrian government aiming at the rapid acquisition of image data, and with respect to ortho-rectification, mosaicing and associated accuracy analysis of the data (Wack et al. 2006).

The data capture was carried out with a high resolution digital camera (12 mega pixel) in connection with a L1L2 GPS phase receiver on board of a helicopter. Wherever possible, the images were captured with an overlap of about 70 % in order to enable the generation of a 3D surface model. The average height above ground was 400 m and yielded a ground sampling distance (GSD) of about 10 centimeters in nadir, and appropriately increasing with increasing off-nadir look angle. The images were taken at an oblique look direction from onboard the helicopter, and span an off-nadir angle range between about 0 and 60 degrees.
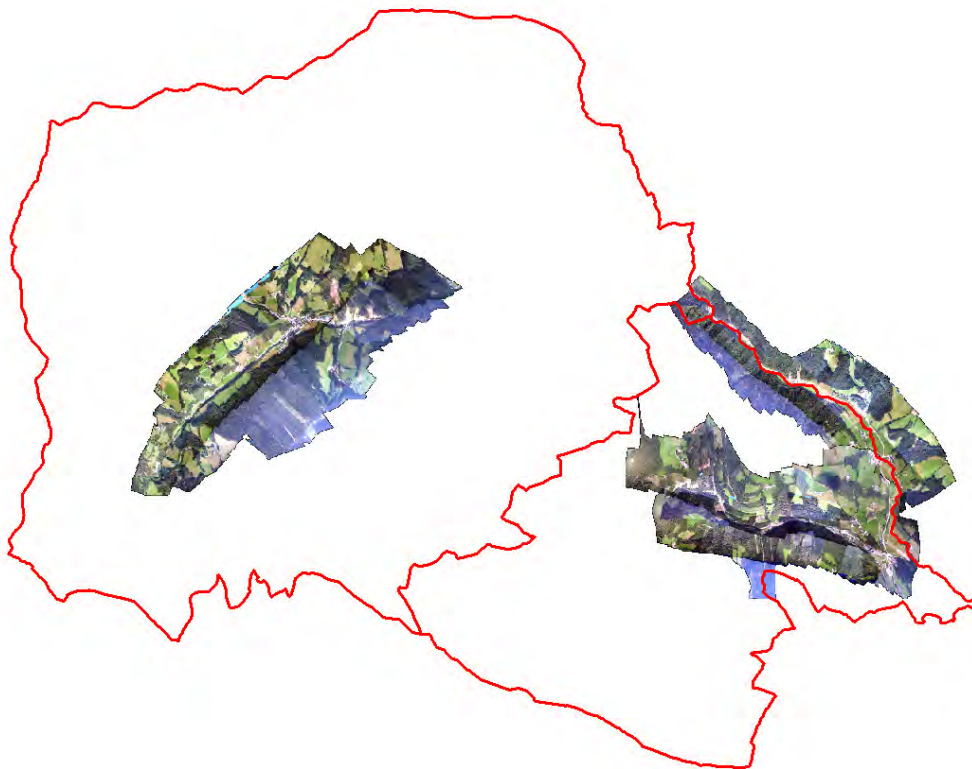
Fig. 5.3.2-1: Coverage of the aerial photographs taken in September 2005 within the borders of the communities of Gasen and Haslau (red)

For the coverage of three strongly affected areas (Fig. 5.3.2-1), three overlapping strips needed to be flown for each of them. In total more than 200 images were necessary to cover the entire area. A close-up of overlapping input images as acquired from three flight tracks (two images each per image strip) is shown in Fig. 5.3.2-2. The overlapping images show distinct geometric distortions among the individual image strips due to imaging and terrain effects, but also radiometric differences due to the disposition between camera exposure (view) and sun illumination.

For further processing, ground control points (GCPs) had to be made available in order to refine/adjust the unknown elements of the exterior orientation by means of a photogrammetric image block adjustment. According to the quality of the reference ortho-photo mosaic and elevation data on the one hand, and to the kind of features to be used due to vegetation coverage, the location accuracy of the GCPs can be assumed to be about 2 m in planimetry and height.
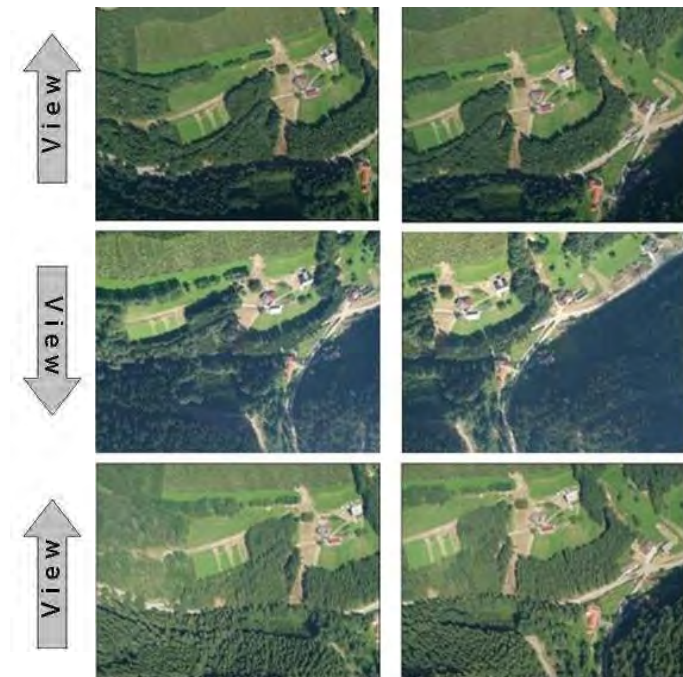
Fig. 5.3.2-2: Close-up of overlapping input images as acquired from three flight tracks

Based on the refined exterior orientation resulting from the block adjustment and using the reference DEM the individual images were ortho-rectified. These ortho-rectified images still show different displacement of outstanding objects like trees and buildings, in particular in case of different viewing direction (Fig. 5.3.2-2). In order to properly mosaic the images, the look angle information of each individual image was included into the mosaicing procedure. This approach yields an image mosaic with acceptable geometric fidelity. No manual interaction (e.g. to define cut-lines between overlapping ortho images) is necessary. Concerning its radiometric characteristics, however, the mosaic shows distinct in-homogeneities depending on individual camera exposure. The results achieved by the feasibility study have shown that a low cost image acquisition solution as used in this campaign is fairly sufficient for rapid hazard mapping, in order to e.g. identify damaged or endangered areas and infrastructure.

The resulting ortho-photo mosaics were visually interpreted to identify landslides using overlays with existing Digital Terrain Models (LiDAR DTM where available (refer to Chapter 5.3.3), DTM of JOANNEUM RESEARCH for remaining areas). Where possible, a subdivision was performed to define triggering, transport and deposition zones. The types of mass movements were classified according the approach of the Geological Survey. Finally the confidence level of the information was classified according the following scheme:

- assured: the identified feature is related to a landslide with high probability, the type of mass movement can be classified in most cases

- assumed: the identified feature is probably related to a landslide but misinterpretations may occur, the type of mass movement can be classified in some cases

- indicated: the identified feature may be related to a landslide but may be related to different processes like e.g. building activities as well; the type of mass movement can not be classified

Due to the delayed date of the data acquisition (15 days after the event) misinterpretations came about mainly in those areas which were affected by remedial measures and building activities.

Based on the analysis of the ortho-photo mosaics taken in September 2005 altogether 276 features were assigned to mass movements. Besides the ortho-photos from the described pilot study area wide visual interpretations of ortho-photos taken in 1996 (black and white, ground resolution 0,5 m) and 2003 (color, ground resolution 0,25 m) which were provided by the Geographic Information System Styria were performed. These analyses resulted in 31 (1996) and 167 (2003) features respectively which could be attributed to landslides (ref. to section 4.1).

5.3.3. LiDAR – Data: Assessement of Potential

Laser scanning (LiDAR = Light Detection And Ranging) is an active measurement system to acquire spatial information to describe the earth's surface. It is based on the physical principle of run-time measurement of the emitted, reflected and received laser pulse (Wehr & Lohr 1999). The reflection on the surface delivers important information about the characteristics due to different scattering of the signal (cf. Wagner et al. 2003). An important advantage of the LiDAR system is the possibility to acquire more than one reflection of each pulse. In forested areas the first reflection normally is returned from the canopy, giving information about the forest surface. The pulse can further penetrate the crown and is finally reflected from the ground delivering information about the height of the terrain. From these data a highly-accurate DTM also under densely forested areas can be generated (Wack & Wimmer 2002, Abraham & Adolt 2006).

Products derived from LiDAR data therefore hold high potentials with regard to the analysis and assessment of natural hazards in two main aspects:

- LiDAR DTMs are holding new possibilities for geomorphological analyses.

- LiDAR Digital Surface Models (DSMs) and Vegetation Height Models (VHMs) bring about new possibilities for the derivation of vegetation and forest parameters.

Fig. 5.3.3-1: Coverage of the LiDAR data within the test area (red lines: political borders of communities)

Airborne Laserscanning was arranged for the study area after the precipitation event of August 2005 by the Austrian Federal Ministry of Agriculture, Forestry, Environment and Water Management. Because of financial reasons unfortunately only a part of the study area was covered on the occasion of this campaign (Fig. 5.3.3-1). As the current LiDAR campaign of the Province of Styria did not cover the northern part of Eastern Styria so far, no area wide LiDAR dataset is available. Therefore despite the high potential LiDAR data offer were not considered for the modelling procedure in this study.

5.3.3.1 Geomorphological Potential

Geomorphological features often represent signs of surface instability in different scales and magnitudes. However, most techniques to observe geomorphological features do have constraints in vegetated terrain due to disadvantageous data acquisition principles such as all optical sensors. The option to "eliminate" vegetation by using last pulse data and filtering to achieve a DTM in contrary to a DSM is a crucial advantage in geomorphological applications. Therefore LiDAR data show high potential in recognition of micro-scale geomorphic features. Nevertheless it has to be considered that even LiDAR data do have problems in very densely vegetated terrain – coarse point distributions lead to smoother surfaces after interpolation and do often not represent microfeatures correctly. LiDAR is used more frequently in geomorphological applications since the last decade (e.g. McKean & Roering 2003, Chigira et al. 2004, Sekiguchi & Sato 2004, Haneberg et al. 2005). These works also cover the aspect of mapping micro topography applied in landslide recognition and their quantitative assessment.

With respect to landslide analyses two aspects are relevant:

- identification of landslides using geomorphological indicators

- derivation of detailed maps of geomorphometric parameters (e.g. slope, curvature) necessary as input for susceptibility modelling

One very promising approach aiming at the automatic detection of landslides is based on the calculation of surface roughness. This method was tested in some parts of the study area.

The surface of most landslides is rougher, on a local scale of a few meters, than adjacent unfailed slopes. This characteristic can be exploited to automatically detect and map landslides. In some cases even information about landslide mechanics as manifested by internal deformation features is deducible. One technique to quantify local topographic surface roughness is to measure the variability in slope and aspect in local patches of the DTM. Following the approach of McKean & Roering (2003), unit vectors are constructed perpendicular to each cell in the DTM. The vectors are defined in three dimensions (using polar coordinates) by their direction cosines. Local variability of vector orientations is then evaluated statistically. Orientation statistics were calculated in small sampling windows of a fixed size that were moved over the DTM. By calculating the statistical variability of orientation of the unit vectors of all cells in the sampling window, the elevation matrix is replaced with a map of local topographic roughness. The effect of the size of sampling window was tested by varying the window width between 3 and 7 cells and varying the grid cell dimensions between 1 and 10 m. One result of a calculation which was carried out in the region south of the village of Gasen is presented in Fig. 5.3.3.1-1.
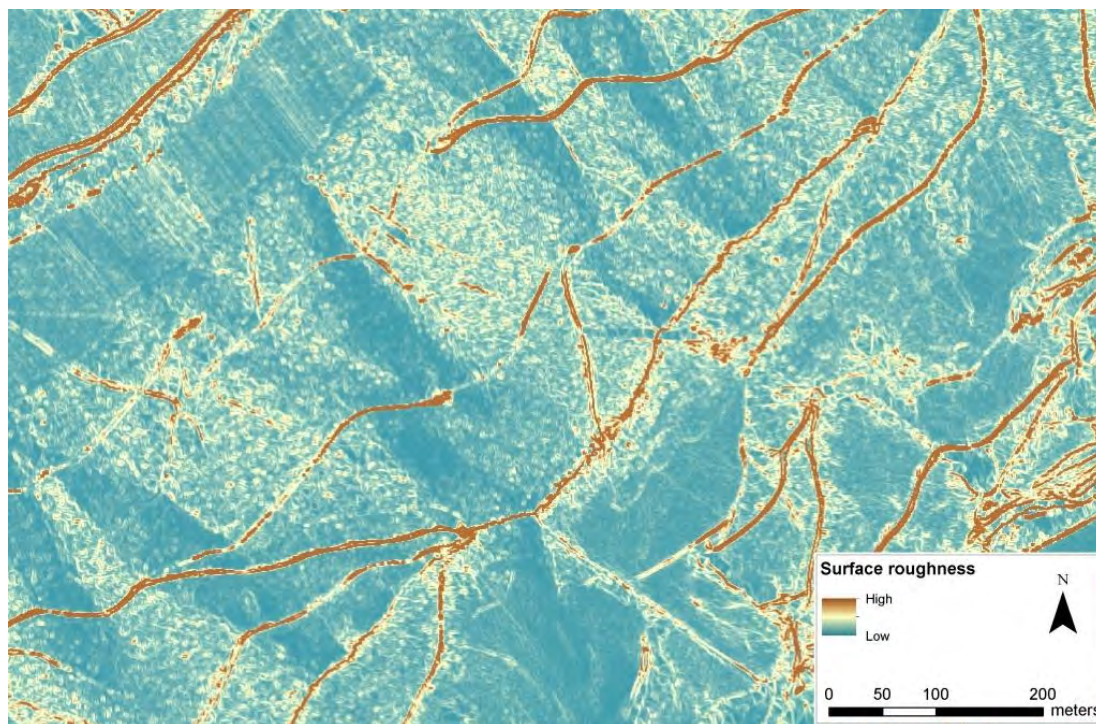
Fig. 5.3.3.1-1: Result of calculation of surface roughness based on LiDAR – DTM south of village of Gasen (window width: 3 x 3 cells, spatial resolution: 5 m)

Moreover geomorphological analyses of LiDAR DTMs may result in further relevant parameters with regard to the triggering of shallow landslides (e.g. forest roads and slope edges).

5.3.3.2 Forestal Potential

Vegetation remote sensing is a principal application of LiDAR. The calculation of a vegetation height model (VHM) can be performed by subtracting each DTM pixel value from the respective DSM pixel value representing the canopy surface of a forest. The result is a raster consisting of vegetation height values. Instead of using these pixel values directly, more significant information can be calculated by using objects of interest (e.g. individual tree crowns, tree groups or whole forest stands). According to the object of interest and to the calculation method, different heights can be obtained: maximum single tree height, mean stand height or the distribution of heights within a forest stand. The result can give valuable information about the age of a tree or forest stand, the structure of a forest stand, timber volume and even assortments. Tree age can be estimated by involving the height information directly from the data and an estimated mean annual growth (e.g. yield tables from literature). The structure of a forest stand can be estimated from the distribution of height values, whether it is an even-aged forest or a forest consisting of heterogeneously high trees. Finally, tree height is, among other factors, an important input variable for the calculation of timber volume. Aiming at automated subdivision of forest stands based on single tree detection from first pulse LiDAR data and SPOT5 satellite data, relevant parameters like stand wise average stem number, stem density or crown coverage were derived. An example of an automatic detection of single trees based on a LiDAR VHM which was carried out in the region south of the village of Gasen is given in Fig. 5.3.3.2-1.
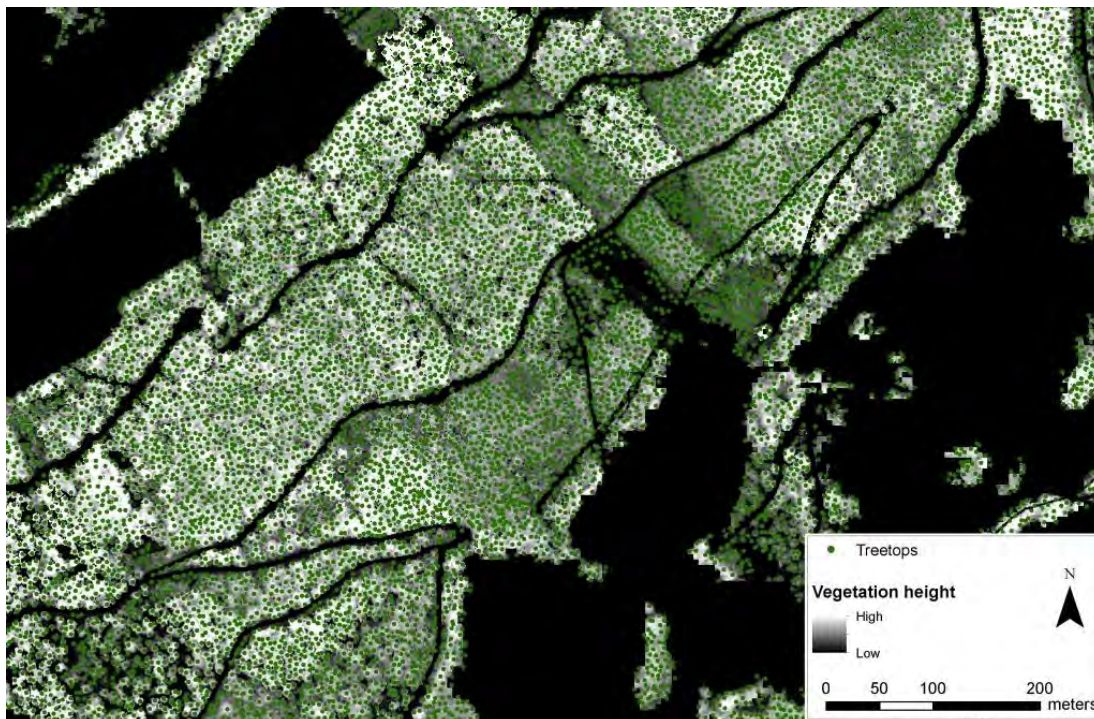
Fig. 5.3.3.2-1-3: Result of calculation of surface roughness based on LiDAR – DTM south of village of Gasen (window width: 3 x 3 cells, spatial resolution: 5 m)

5.4.   Runoff Disposition Map (BFW)

The water supply in the loose material represents a major factor for the investigation of the triggering parameters of spontaneous landslides. Both the amount of precipitation during storm events and the rate of infiltration into the loose material determine soil moisture and soil saturation. Thus, the information regarding the infiltration rate supports the evaluation of the slope susceptibility.

To verify this assumption, a runoff map for the test area was compiled showing different levels of processing efforts (low, medium, high).

5.4.1. Introduction

Different approaches for differentiation of runoff contributing areas in alpine regions are available.

Tables with ranges of runoff coefficients were first presented by Bunza and Schauer (1989). Rickli and Forster (1997) developed an approach for the assessment of runoff coefficients, using field data and interpretations of data from the literature. Löhmannsröben et al. (2000) described the most important factors influencing runoff behavior of different soil vegetation complexes, and named soil as the dominant factor for runoff behavior. Scherrer and Naef (2003), Naef et al. (2007) developed a sound approach for the characterization of dominant runoff processes on grassland areas. The application of their scheme requires comprehensive knowledge in the field of soil/plant/land-use and runoff development. For the assessment of woodland or sealed areas, this scheme can only be used with reservations.

A manual for easy use by practitioners in the assessment of runoff characteristics in the case of the recurrent design event has not been developed so far. For this purpose, results of about 700 simulations of torrential rain in the Eastern Alps were compiled and interpreted in a joint effort by the Bavarian Environmental Agency (Germany) and the Institute of Natural Hazards and Alpine Timberline at the BFW in Innsbruck (Austria). The results were published as "a simple code of practice for assessing of surface runoff coefficients for alpine soil/vegetation units in torrential rain" by Markart et al. (2004). Further methods to estimate the surface runoff on the base of available data has been developed (Klebinder et al. 2008).

5.4.2. Estimation of the Runoff Process

The methods used in the field investigations are described in detail by Markart et al. (2006). For the characterization and differentiation of the various runoff producing areas in about 25 catchments and regions of the Eastern Alps, research plots were selected for the runoff characteristics of the different soil/vegetation complexes. These are irrigated by means of a transportable spray irrigation installation for large plots. Further investigations comprised monitoring soil water status using TDR-probes, detailed characterization of vegetation (description of abundance, dominance and frequency on all plots, as well as analysis of plant biomass on several grassy plots) and analysis of the most important physical soil properties.

Tab. 5.4.2-1 Classification scheme of surface runoff

Runoff coefficients (AKL)	Surface runoff in % of precipitation
0	0
1	> 0 – 10
2	> 11 - 30
3	> 30 - 50
4	> 50 - 75
5	> 75
6	100

A lot of simulations of torrential rain using transportable spray irrigation installations have been made. These data were extrapolated from plot size to representative hydrological soil/vegetation units, while considering hydrological effects of vegetation cover, physical soil characteristics as well as type and intensity of cultivation, e.g. the intensity of man-made, mechanical impact (roads, ski tracks, water logging) or grazing (mechanical impact by livestock).

The surface runoff coefficient (Ψconst) describes the measured outflow in % of precipitation at the time of constant discharge. For the attribution of surface runoff coefficients, the schemes in (Tab. 5.4.2-1) are suggested. The value of Ψconst is allocated to the seven surface runoff classes (AKL). The colours following the system of a traffic light: Dark green indicates high infiltration potential and very low surface runoff, red = danger – high surface runoff potential, blue = sealed or totally wet areas.

5.4.3. Processing Levels and Scales

Runoff maps can be generated on various processing levels which follow different information values of the resulting maps. While the field investigated runoff maps represent accurate datasets with low uncertainty, runoff maps generated by the use and evaluation of existing information produce datasets with a higher uncertainty. However, processing time and costs of the latter are significantly lower. Thus, runoff maps based on area-wide field investigations are limited to micro- and meso-scale catchments.

5.4.4. Indicators for Runoff Disposition

5.4.4.1 Infiltration Potential of Soils

Infiltration of precipitation into the soil is primarily dependent on the proportion of makropores (Burch et al. 1989): The depth of penetration is influenced to a high extent by soil structure (depending on whether the soil is loose, dense or cohesive, Czell 1972).

Soil	Description	Example
Rich in skeleton, loose material	**Rich in skeleton, from coarse grained to mixed grained texture** with high content of coarse fraction (gravel, sand) **Hydraulic conductivity: high** **>> 1m /day**	
Loose soil, rich in fine fraction	**Mixed grained to fine grained soils** Böden with a maximum content silt and clay (together) of 40%, content of clay alone < 20%. **Hydraulic conductivity: high-medium,** **0,1-1m/day**	
Fine grained, dense, cohesive	Content of silt and clay (together) > 40%, **cohesive** (plastic). Hydrological effects of skeleton only in drought periods (shrinkage cracks). **Hydraulic conductivity: medium-very low, << 10 cm/ day**	

Fig. 5.4.4.1-1: Rough classification of infiltration potential of soils depending on soil physical properties after Markart et al. (2004)

Therefore, these soil features can be used as indicators for infiltration and runoff behavior ('Fig. 5.4.4.1-1):

- Contents of fine or coarse soil: The higher the amount of parts > 2 mm diameter, the higher the infiltration of water into the soil. The higher the contents of fine fraction, especially silt (0,063 mm to 0,002 mm $\varnothing$) and clay (< 0,002 mm $\varnothing$), the slower percolation into the soil matrix.

- Soil structure and layering: Loosely layered soils allow rapid infiltration of water into the soil. Content of draining pores - allowing rapid drainage and infiltration - decreases with increasing bulk density of soil.

- Soil depth: Especially on shallow and very shallow soils on steep slopes and over near surface bedrock seepage is limited. After flowing short distances along the bedrock, water comes back to the surface as return flow.

5.4.4.2 Surface Runoff at Different Land Cover Units and Indicator Function of Plants

Plants are important indicators for hydrological site characteristics. Besides indicating nutrition or compaction, they characterize the predominant humidity conditions of a site (Schauer 1992). Based on statistical analysis and empirical interpretation of rain

simulation experiments, it became possible to compile a catalogue of plants indicating predominant runoff behavior of forests, wet areas, grazed areas and sites with good infiltration characteristics in general (Markart et al. 2004).

Fig. 5.4.4.2-1 shows the surface runoff potential of major land cover units in Austria and can be summarized as follows:

- Sites covered by forests dominantly show low to medium runoff values.

- Grassland covers the whole range of runoff classes. However, there are clear tendencies by integrating soil and landuse indicators.

- Cropland covers medium and high runoff classes.

- Medium runoff potential e.g. is shown by mustard or rape.

- High runoff values are achieved by plots covered with maize (AKL 5).

- Bare soil before growth and after harvest shows AKL 5.

- Very high runoff potential is expected on sealed areas, AKL 5/6. Runoff is developing very fast on such areas.
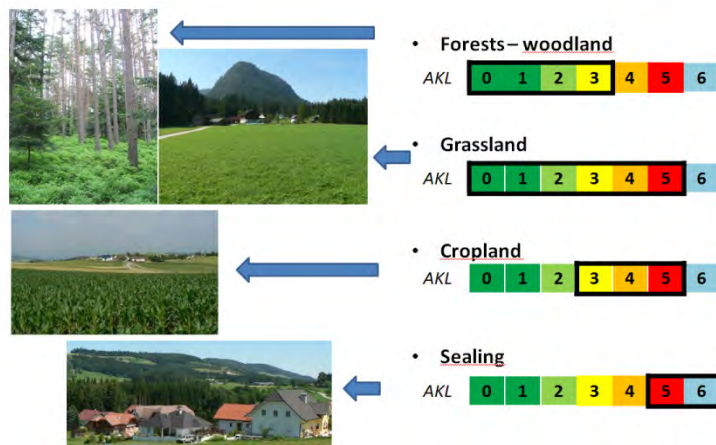
Fig. 5.4.4.2-1: Dominant surface runoff classes for typical land cover units in Austria

5.4.4.3 Effects of Cultivation and Mechanical Impacts on Surface Runoff Development

Tab. 5.4.4.3-1 comprises examples covering the effect of different ways and intensities of cultivation and land use on infiltration characteristics depending on soil physical properties (content of fine soil / coarse material and layering / bulk density). The information is based on statistical and empirical analyses of results from simulations of torrential rain on about 700 plots in Middle-Europe.

Tab. 5.4.4.3-1: Effects of cultivation and mechanical impacts on surface runoff development (from Markart et al. 2004)

Form of land use / encroachment	Consequences on surface runoff in dependence of soil conditions / physical properties			
	Coarse soil, rich in skeleton, loose	Coarse soil, rich in skeleton, including fine grained components, loose	Fine grained soil, loose	Fine grained soil, cohesive
Planed areas	+/-	-	--	--
Grazing - extensive	+/-	+/-	--	--
Grazing - intensive	-	--	---	--
Mechanical impact (e.g. driving) - extensive	+/-	-	--	-
Mechanical impact (e.g. driving) - intensive	-	--	--	--
Grading + additional impact (grazing, using of heavy machines, grooming of ski pistes))	+/-	--	---	--
Forestry use	(+/-)	(+/-)	(+/-)(-)	(-)/(--)
Drainage	+/-	+/-	+	++
Manuring	+/-	+/-	++	+
Revegetation, use of bioengineering methods	+/-	+	+++	++

Signs and symbols:
- negative impacts

      +/-   indifferent, marginal deterioration

      -    slight deterioration

      --   significant deterioration

      ---   extreme deterioration

      ()   temporarily, reversible

+ positive impacts

      +/-   indifferent, marginal amelioration

      +   slight amelioration

      ++   significant amelioration

      +++   extreme amelioration

5.4.5. Creation of Runoff Disposition Maps

With these indicators, a realistic differentiation of different runoff contributing soil - vegetation complexes will be possible. It is feasible to allocate all indicators during field investigations (level high). A few parameters can be identified from the existing datasets to get the level "low". Especially information from high-quality soil maps (like e.g. the ebod) can advance these runoff maps.

Tab. 5.4.5-1: Summary of indicators to estimate the surface runoff class

AKL	Gassland and pasture
0	Grassland; coarse soil, loose material and rich in skeleton with marginal mechanical impact
1	Grassland; fine grained and loose soil without additional use
2	Grassland; fine grained and loose soil with additional use in low intensity (short-term pasture, impacts from light-weight machines)
3	Grassland and pasture; still loose soil with additional use (grazing, mechanical impacts e.g. driving of machines) or signs of pseudogley and/or soils with high moisture (fewer wetness indicators)
4	Grassland; fine grained and cohesive soil (pseudogley, loam)
4/5	Grassland and pasture; fine grained and dense soil; intensively used areas with intensive pasture, driving with heavy machines; ski-runs with or without man-made changes in surface-morphology
5	Grassland and pasture; saturated soils, extremely dense soils
6	Wet areas with permanently saturated soil (e.g. fen, spring-areas)
	Cropland
3	Loose and fine-grained substrate with dense plant cover
4	Fine-grained – cohesive soil-substrate with dense plant cover; maize on sandy and loose soil
5	Plants without a complete surface coverage; fine grained and cohesive soils; maize
	Forests
0	Soil rich in boulders and skeleton, loose soils
1	Fine-grained and loose soils covered by forests with dense ground vegetation
2	Fine-grained and loose soils; spruce without ground vegetation; no additional use e.g. grazing or driving with heavy machines
3	Fine-grained and cohesive soil-substrate (pseudogley, loam); forests with dense ground vegetation; Spruce without or with poor ground covering vegetation on fine-grained soils
4	Fine-grained cohesive and/or dense soils (e.g. dense pseudogleys); forests with poor ground vegetation

5.4.6. From Surface Flow to Subsurface Flow

While the surface runoff process is strongly connected to the type and state of the vegetation cover as well as the current and former landuse types, the subsurface flow is dominated by the soil characteristics (e.g. hydrological productivity, storage capacity and degree of soil saturation).

Interflow near the surface which can be a major factor in the release process of shallow landslides, affects both soil and vegetation. Especially the existence of preferential flow paths (macropores, mouse tubes, root tubes, etc.) has an impact on the development of this part of the general runoff process.

To assess the water which can infiltrate the soil (subsurface flow SSF), the surface runoff coefficient Ψconst was subtracted from the value 1 (1 is equivalent to the infiltration of the entire precipitation).

SSF = 1 - Ψconst

To calculate the subsurface flow, the mean value of each Surface Runoff Class (AKL) was determined. The result of this calculation was used to define the weight - factor for the computation of the accumulated subsurface flow conducted in the SAGA GIS environment. SAGA offers a flow tracing module which allows to use the DEMON routing algorithm (Costa-Cabral and Burges, 1994).

Available Datasets

Different datasets are available to create the runoff disposition maps for the low and medium process level.

Soil information or information about the unconsolidated rock

   1) The conceptual map of unconsolidated rock in the high process level (GBA)

   2) The soil map, compiled from the digital soil map (eBod) and the Forest Site Map (BFW)

Information about landcover and landuse

The database from the digital cadastral map (DKM) was used. The map presents a high resolution and informative database for settlement and agriculture used areas, the content for forests are slight.

Information about topography-related issues

To generate hydrological essential databases, the digital elevation model (DEM) with 10 meter resolution was used. The DEM was used for deriving:

   1) A map of incoming solar radiation which describes the potential soil moisture, calculated in SAGA GIS by using standard parameter settings.

   2) A map of flow accumulation which describes the potential saturation of soils.

5.4.7. Assessment of the Runoff Disposition Map „Low Level"

The assessment of the runoff disposition on this level generally uses available datasets, which are upgraded by the expertise of the scientist. They are generated with moderate processing effort without fieldwork and specify knowledge on local conditions or facts. The currently existing knowledge about runoff generation process is used, as far as possible; an adaption of this knowledge to special issues of the investigation area is practicable.

Mostly geographic information systems (GIS) are used to generate additional necessary information (e.g. topographic wetness index calculated from the DEM). The GIS allows to develop an estimation scheme and to produce maps.

Assessing the runoff disposition for the low processing level, the landuse dataset was combined with the conceptual map of unconsolidated rock in the high process level. Each soil-landuse combination was defined by a runoff disposition class (AKL, Tab. 5.4.7-1).

Tab. 5.4.7-1: Surface runoff classes (AKL, estimation matrix using soil information and landuse)

Landuse	pure skeleton (talus) - shallow (AC soil profile) - not loamy or cohesive **11**	skeleton based - high fraction of rock and moderate percentage of sandy or silty soil matrix - not loamy **12**	skeleton based - mixed corn fraction - sand and gravel - moderate percentage of rock and silty soil matrix - slightly loamy (silty talus) **13**	skeleton based- mixed corn fraction - sand and gravel - moderate percentage of rock and high part of silty soil matrix - slightly loamy (uS) **14**	matrix based - silty - moderate percentage of rock - moderate loamy (sU) **23**	matrix based - silty to clay - moderate percentage of rock - strongly loamy and cohesive (tU to T) **24**	matrix based - clay to sil) - moderate percentage of rock - strongly loamy and cohesive (uT to T) **25**
10 Buildings	6	6	6	6	6	6	6
11 Commercial Area	6	6	6	6	6	6	6
12 Technical infrastructur	5	5	5	5	3	5	5
13 Streets	6	6	6	6	6	6	6
14 Buildung area	5	5	5	5	5	5	5
15 Buildung area greened	2	3	3	4	4	5	5
16 Recreation area	5	5	5	5	5	5	5
20 Forest	0	0	1	2	2	3	4
30 Cropland	2	2	2	3	3	4	4
31 Argricultural used areas	1	1	1	2	2	3	4
32 Grassland	0	1	2	3	3	4	4
33 Orchard	1	2	2	2	2	3	4
34 Pasture	3	3	3	4	4	5	5
35 Pasture close to farms	3	3	3	4	4	5	5
36 Alp, mountain pasture	1	3	3	4	4	5	5
90 Rivers	6	6	6	6	6	6	6
91 Lakes	6	6	6	6	6	6	6

To include the topographical parameters which are derived from the DEM, the defined AKL-values were modified to higher or lower AKLs.

Tab. 5.4.7.-2: Modification of surface runoff classes using topographic parameters

RADIATION \ FLOWACCUMULATION	<=1000	1000-2000	>2000
>1600	-2	-1	0
1000-1600	-1	0	1
<= 1000	0	1	2

Tab. 5.4.7-2 shows the modification matrix, where high radiation in combination with a low flow accumulation follows through a lower surface runoff. The range of modification accounts for +/- two AKLs, the modification is limited to the minimum and maximum values for each landuse class. The "low level" subsurface flow map is shown in Fig. 5.4.7-1.
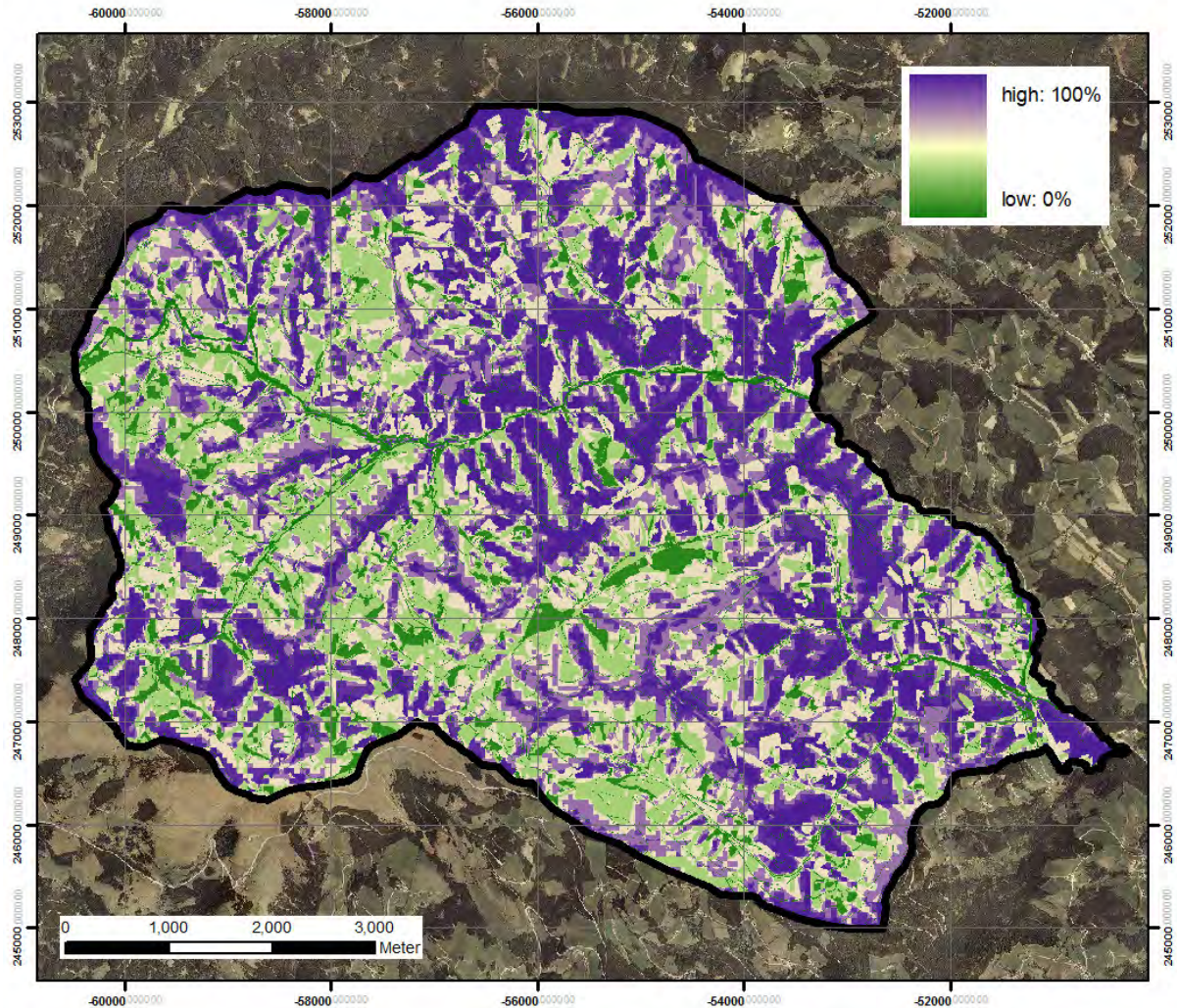
Fig. 5.4.7-1: Subsurface flow (in percent of the precipitation), processing level low

5.4.8. Assessment of the Runoff Disposition Map „Medium Level"

Generally, the assessment of the runoff disposition on a medium level is based on further specified datasets, which are generally not available. On this level, a portion of the project time will be devoted to the investigation area, in order to get extended knowledge about the environment, selective analysis of the bio- pedo- and hydroinventory and to upgrade basic information datasets. The estimation schemes and the production of the runoff maps will be conducted using a GIS.

The procedure to generate the map is modified to the procedure described in the low level method:

- Instead of the conceptual map of unconsolidated rock (GBA) the soil map (BFW) was used.

- To simplify the procedure and to uniform the way of map creation, the pedo-physical parameters from the soil map were transformed (Tab. 5.4.8-1) to the soil classification system from the map of the conceptual map of unconsolidated rock, thereby using the estimation scheme (Tab. 5.4.7-1) from the low level procedure.

Tab. 5.4.8-1: Transfer from the soil map units(BFW) to the units of the conceptual soil map (GBA)

units from soil map	a	b	c	d	e	f	g	h	i	j	k	l	m	n	o	p
soil substrate	13	14	13	14	23	23	14	24	23	23	23	23	12	23	23	23

- Including the soil saturation in the assessment, the parameters were interpreted in reference to the soil moisture described in the soil map (BFW) (Tab. 5.4.7-2). The modification account for +/- one AKL and is limited to the minimum and maximum value of each landuse class.

Tab. 5.4.8-2: Modification of surface runoff class (AKL) using soil moisture information from soil map

Landuse	Units from soilmap															
	a	b	c	d	e	f	g	h	i	j	k	l	m	n	o	p
Buildings	0	0	0	0	0	0	0	0	0	0	0	0	0	0	0	0
Commercial Area	0	0	0	0	0	0	0	0	0	0	0	0	0	0	0	0
Technical infrastructur	0	0	0	0	0	0	0	0	0	0	0	0	0	0	0	0
Streets	0	0	0	0	0	0	0	0	0	0	0	0	0	0	0	0
Buildung area	0	0	0	0	0	0	0	0	0	0	0	0	0	0	0	0
Buildung area greened	-1	-1	-1	-1	0	0	1	0	-1	-1	0	1	-1	1	1	-1
Recreation area	-1	-1	-1	-1	0	0	1	0	-1	-1	0	1	-1	1	1	-1
Forest	-1	0	0	0	1	1	1	0	-1	-1	0	1	-1	1	1	-1
Cropland	-1	-1	-1	-1	0	0	1	0	-1	-1	0	1	-1	1	1	-1
Argricultural used areas	-1	-1	-1	-1	0	0	1	0	-1	-1	0	1	-1	1	1	-1
Grassland	-1	-1	-1	-1	0	0	1	0	-1	-1	0	1	-1	1	1	-1
Orchard	-1	-1	-1	-1	0	0	1	0	-1	-1	0	1	-1	1	1	-1
Pasture	-1	-1	-1	-1	0	0	1	0	-1	-1	0	1	-1	1	1	-1
Pasture close to farms	-1	-1	-1	-1	0	0	1	0	-1	-1	0	1	-1	1	1	-1
Alp, mountain pasture	-1	-1	-1	-1	0	0	1	0	-1	-1	0	1	-1	1	1	-1
Rivers	0	0	0	0	0	0	0	0	0	0	0	0	0	0	0	0
Lakes	0	0	0	0	0	0	0	0	0	0	0	0	0	0	0	0

The "medium level" subsurface flow map is shown in Fig. 5.4.8-1
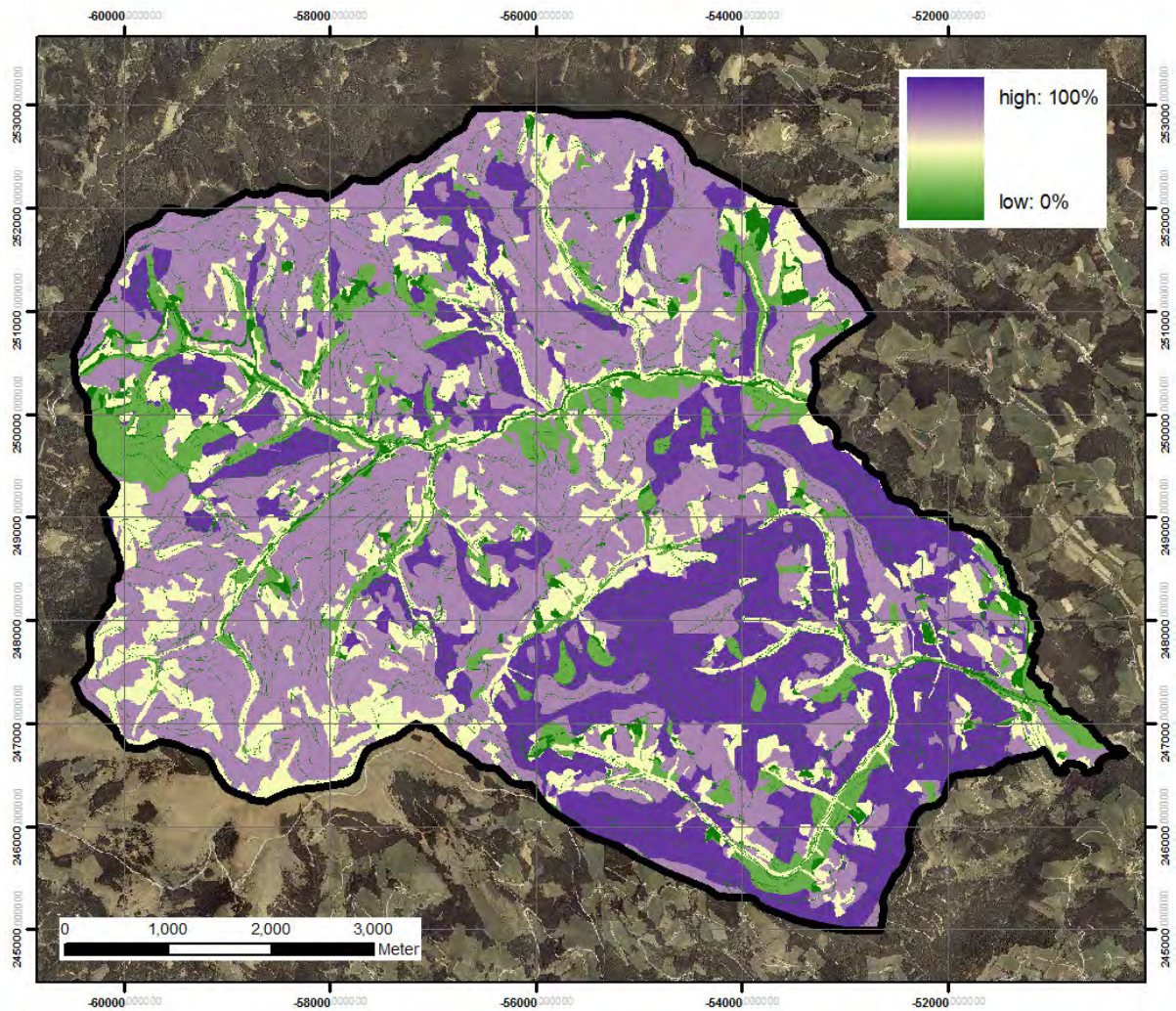
Fig. 5.4.8-1: Subsurface flow (in percent of the precipitation), processing level medium

5.4.9. Assessment of the Runoff Disposition Map „High Level"

The assessment of the runoff disposition occurs by area-wide fieldwork. All indicators for runoff mapping were investigated and integrated to estimate the corresponding runoff class. For this purpose, the decision scheme from Markart et al. (2004) was used. Fig. 5.4.9-1 shows the "high level" subsurface flow map.
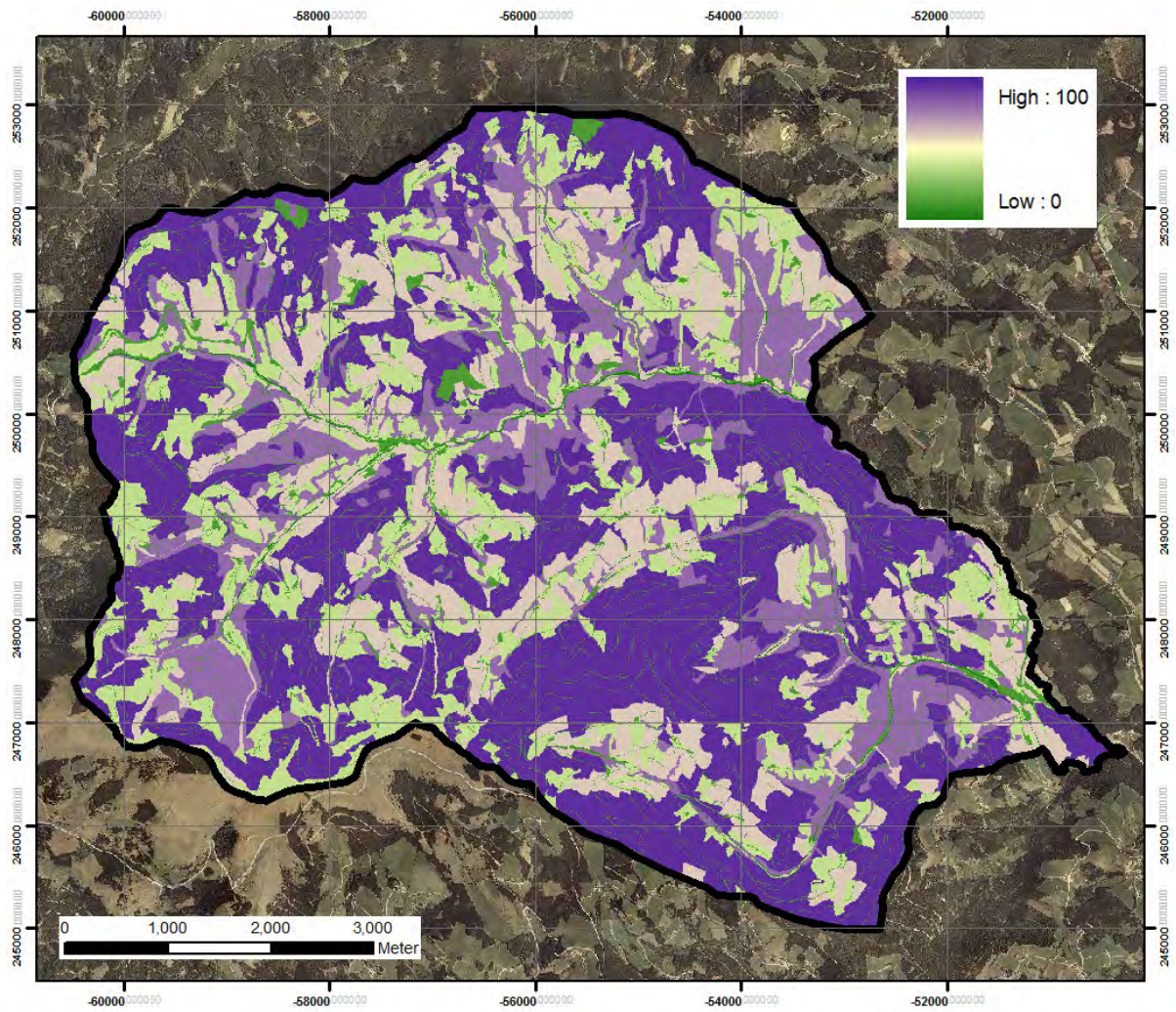
Fig. 5.4.9-1: Subsurface flow (in percent of the precipitation), processing level high

5.5.   Precipitation Maps (ZAMG)

5.5.1. Introduction

On 20th and 21st August 2005, a torrential rain event caused widespread flooding and landslides in the area of Gasen/Haslau in Eastern Styria (Andrecs et al. 2007). In the context of the "ADAPTSLIDE" project, the Central Institute of Meteorology and Geodynamics ("Zentralanstalt für Meteorologie und Geodynamik", ZAMG) was asked to conduct a recalculation of precipition analyses of this event, including a spatially differentiated estimation of uncertainties.

5.5.2. Data Base

The operational precipitation analyses of the INCA system are based on a non-linear combination of radar and rain gauge data (Haiden et al. 2009) in order to combine the advantages of both methods, namely the accuracy of rain gauge measurements and the high spatial resolution of radar data. The latter are available on a 1*1-kilometre grid, which is also used for the whole INCA system. Concerning the rain gauges, for the area of Styria so far only automatic stations of ZAMG have been used. For the present project, 24-hourly measurements of 7 additional stations of the Hydrological Service ("Hydrografisches Zentralbüro", HZB) in the area of Gasen were available.

These additional stations may prove valuable in further resolving the spatial structure of the precipitation fields, since the typical distance between two neighbouring ZAMG stations is in the order of 10 to 20 kilometres, and Fischbach is the only ZAMG station inside the area of investigation. A comparison between operational INCA precipitation analyses and reanalyses including the 24-hourly HZB stations that has been conducted earlier, has shown the interesting result that two HZB gauges, namely Fladnitzberg and Hohenau, had received considerably more precipitation on 20th August than the operational analyses had displayed (Haiden 2008).

5.5.3. Methodology

In order to quantify the uncertainties, "ensemble analyses" were computed by artificially omitting the data of one of the rain gauges in the investigation area, following the idea of cross validation. Thus, this method yields 8 different analyses, plus the operational analysis (without the HZB data) and the reanalysis (including the HZB data).

Furthermore it was investigated if the spread of these ensemble analyses (i.e. the uncertainty) could further be reduced by a modification of the radar data scaling, in particular concerning the extent to which radar data are "allowed" to be scaled upward by corresponding rain gauge measurements. In the operational INCA system, the maximum threshold of this upward scaling is set rather conservatively, since this has proven to show on average the best results (Haiden et al. 2009). If the radar data strongly deviate from the rain gauge measurements, however, like on 20th August in Fladnitzberg and Hohenau, a more flexible scaling with a higher threshold may create better analyses.

5.5.4. Results

5.5.4.1 Comparison of Operatinal INCA Analyses and HZB Rain Gauge Measurements

Tab. 5.5.4.1-1: HZB rain gauge measurements (left column) and precipitation operationally analysed in INCA at their corresponding grid points (right column) on 20th (top), 21st (center) and 22nd August (bottom)

HZB station number	name	measurement [mm/24h]	INCA analysis [mm/24h]
111328	Kreuzwirt	13,8	7,8
111369	Hohenau/Raab	134,5	66,5
111401	Fladnitzberg	99,9	55,5
111435	Alpl	43,2	15,8
112003	Breitenau/Mixnitz	57,9	46,1
112540	Stanz	40,1	45,8
123117	Birkfeld	52,0	39,2

HZB station number	Name	measurement [mm/24h]	INCA analysis [mm/24h]
111328	Kreuzwirt	34,7	41,6
111369	Hohenau/Raab	56,4	62,5
111401	Fladnitzberg	69,4	68,2
111435	Alpl	66,4	59,4
112003	Breitenau/Mixnitz	55,6	58,8
112540	Stanz	66,7	60,3
123117	Birkfeld	55,0	45,7

HZB station number	Name	measurement [mm/24h]	INCA analysis [mm/24h]
111328	Kreuzwirt	2,6	2,4
111369	Hohenau/Raab	5,7	6,1
111401	Fladnitzberg	9,0	9,1
111435	Alpl	3,3	4,1
112003	Breitenau/Mixnitz	7,8	11,3
112540	Stanz	4,4	8,0
123117	Birkfeld	10,6	3,5

Tab. 5.5.4.1-1 opposes the measurements of the HZB rain gauges to the operational INCA precipitation analyses at the corresponding grid points. On 20th August, the precipitation was underestimated by a factor of 2 at the stations of Hohenau and Fladnitzberg that were especially affected by the strong precipitation event, and even by a factor of 3 at the station of Alpl (though with lower absolute amounts). The analyses show a better quality on 21st and 22nd August. Absolute precipitation

amounts on 21st are of a similar magnitude as on 20th, whereas precipitation was less plentiful on 22nd August.

5.5.4.2 Computation of Ensemble Precipitation Analyses by Omitting one Station in Each Case

In the following, ensemble precipitation analyses for 20th (Fig. 5.5.4.2-1), 21st (Fig. 5.5.4.2-2) and 22nd August 2005 (Fig. 5.5.4.2-3) are depicted. Each of these figures contains in this order the operational precipitation analysis and the precipitation reanalysis (large pictures), the 8 ensemble analyses in a narrower sense (panel of small pictures), and finally the absolute and relative ensemble spread (large pictures again), respectively. The absolute ensemble spread is computed by subtracting the lowest precipitation analysis from the highest one, and the relative ensemble spread by dividing these values by the precipitation reanalysis (i.e. including the 24-hourly HZB data), which for comprehensible reasons may be regarded as the best one available.

Each INCA precipitation analysis is composed of an analysis obtained by station interpolation and a radar analysis, which are combined in such a way that on the one hand station measurements are reproduced at their according grid points, and on the other hand the structures obtained from the radar field are reproduced in-between. The station interpolation follows an inverse distance weighting algorithm in consideration of an elevation dependency of precipitation (Haiden and Pistotnik, 2009). It can be seen in the pictures that the introduced uncertainties also radiate into the surroundings of the investigation area, exhibiting still moderate effects in a distance of about 50 kilometres; this range is governed by the choice of using the 8 nearest stations, respectively, for the inverse distance weighting.

Due to the discrepancy between radar and station measurements on 20th August, there is a considerable uncertainty margin on that day, peaking around 60 mm in the vicinity of Fladnitzberg and Hohenau (Fig. 5.5.4.2-1c, top). It is noteworthy that the maximum of the relative uncertainty is displaced further to the Northeast, where it locally reaches more than 200% of the reference value close to Fischbach (Fig. 5.5.4.2-1c, bottom). This is attributable to the fact that the extreme peak of precipitation at Fladnitzberg and Hohenau is still represented by the respective other station if one of them is omitted, whereas further Northeast the Fischbach measurement yields a local precipitation minimum which is filled by the higher values of the surrounding HZB stations upon leaving out this value.

There are smaller uncertainties on 21st August, when their absolute as well as relative maxima are situated between Kreuzwirt and Birkfeld and amount to 20 to 25 mm, or approximately 60% of the reference value, respectively (Fig. 5.5.4.2-2c).

Analysis uncertainties are even smaller, namely around 5 mm only, on 22nd August (Fig. 5.5.4.2-3c, top). The relative uncertainty shows similar values to the day before, but the low signal-to-noise ratio indicates that this calculation method reaches its limits if the precipitation amounts are as little as on this day (Fig. 5.5.4.2-3c, bottom.)
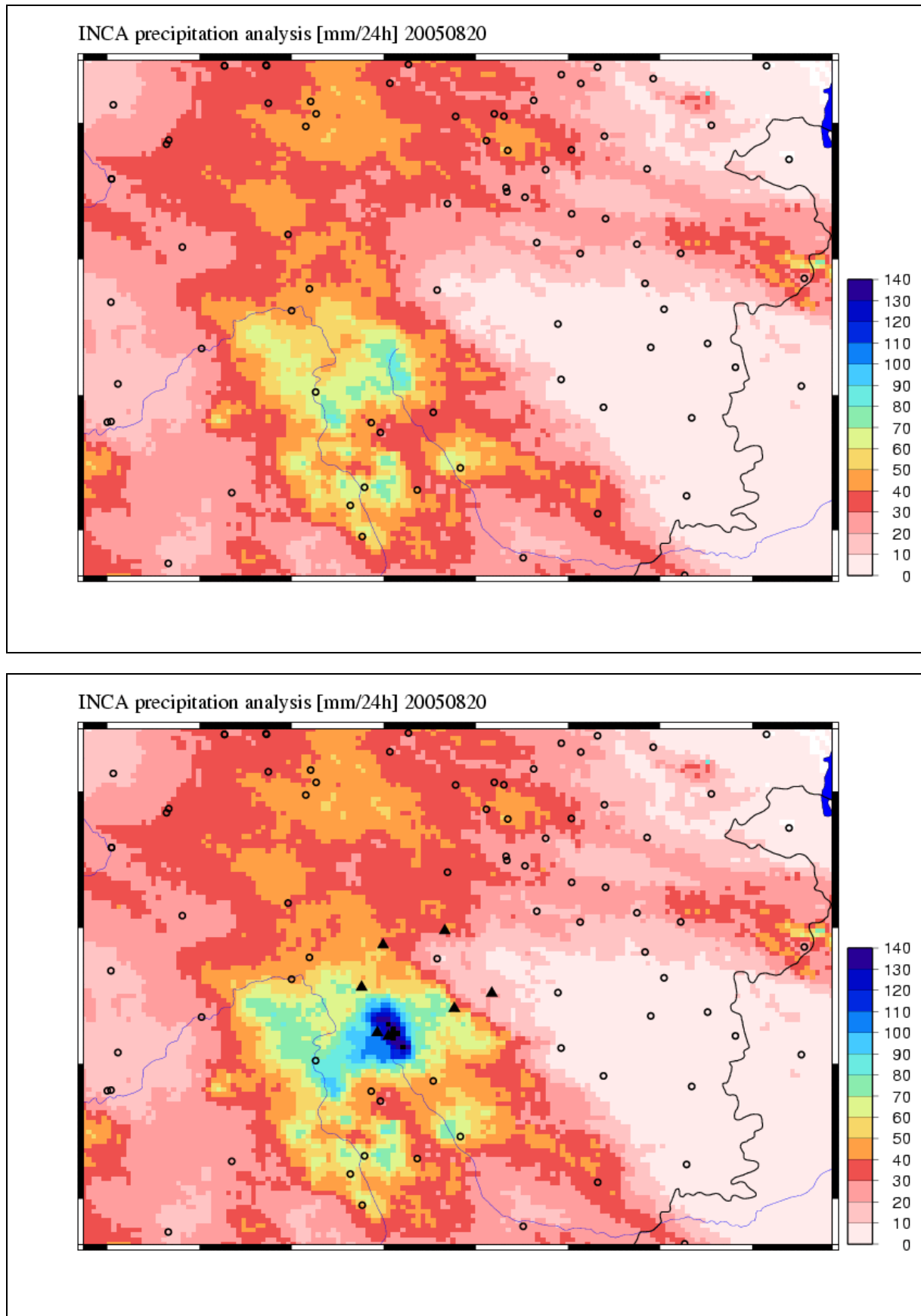
Fig. 5.5.4.2-1a: 24-hourly INCA precipitation analysis from 20th Aug. 2005 06 UTC to 21st Aug. 2005 06 UTC without (top) and with HZB data (bottom). Circles denote ZAMG stations, triangles HZB stations
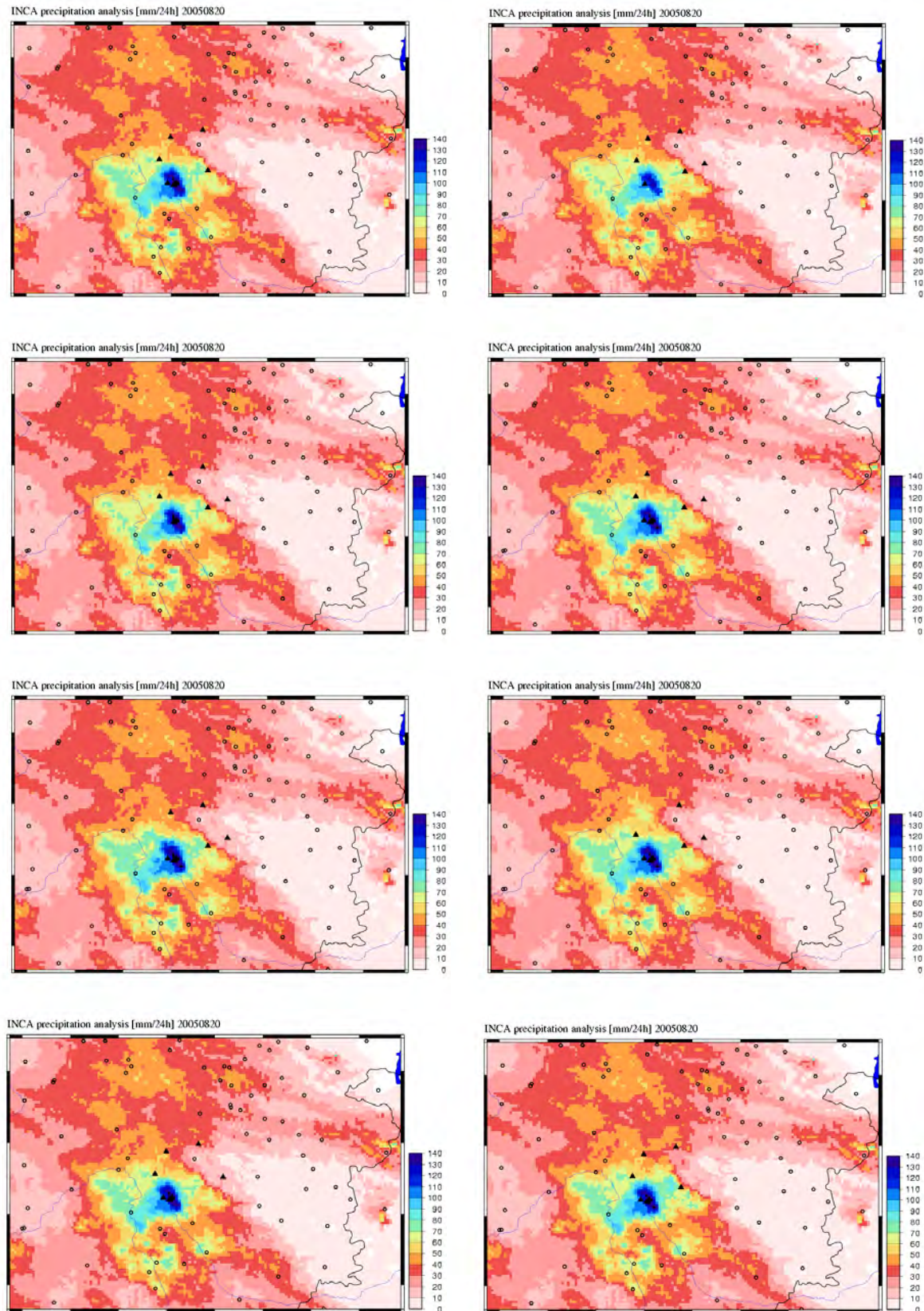
Fig. 5.5.4.2-1b: 24-hourly INCA ensemble precipitation analyses from 20th Aug. 2005 06 UTC to 21st Aug. 2005 06 UTC, created by omitting one station respectively (from top left line-by-line to bottom right: HZB stations Kreuzwirt, Hohenau/Raab, Fladnitzberg, Alpl, Breitenau/Mixnitz, Stanz and Birkfeld plus ZAMG station Fischbach)

INCA precipitation spread (mm/24h) 20050820

relative INCA precipitation spread [%] 20050820
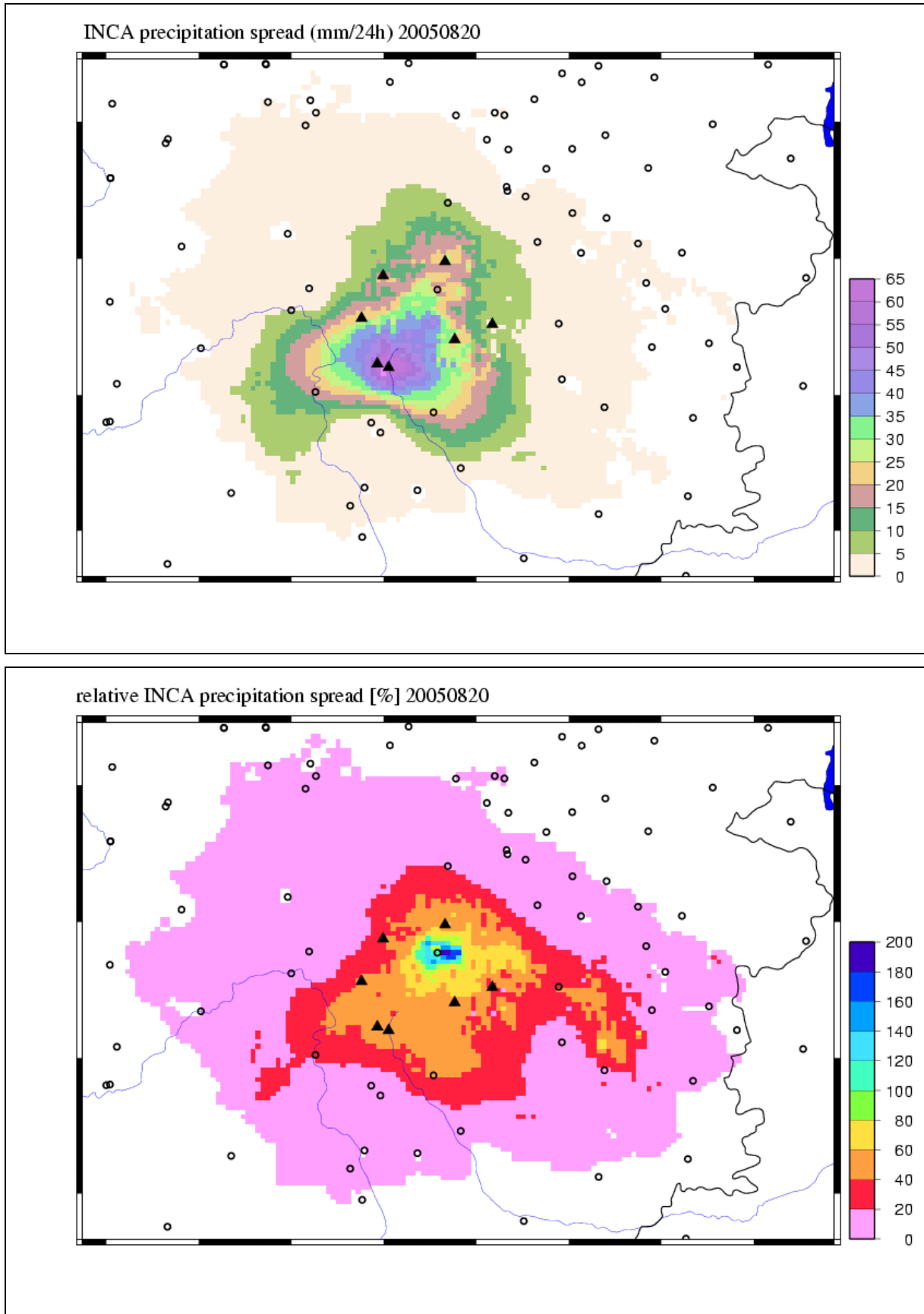
Fig. 5.5.4.2-1c: Absolute (top, [mm/24h]) and relative spread (bottom, [%]) of the precipitation ensembles of 20th Aug. 2005 from Fig. 1a and 1b
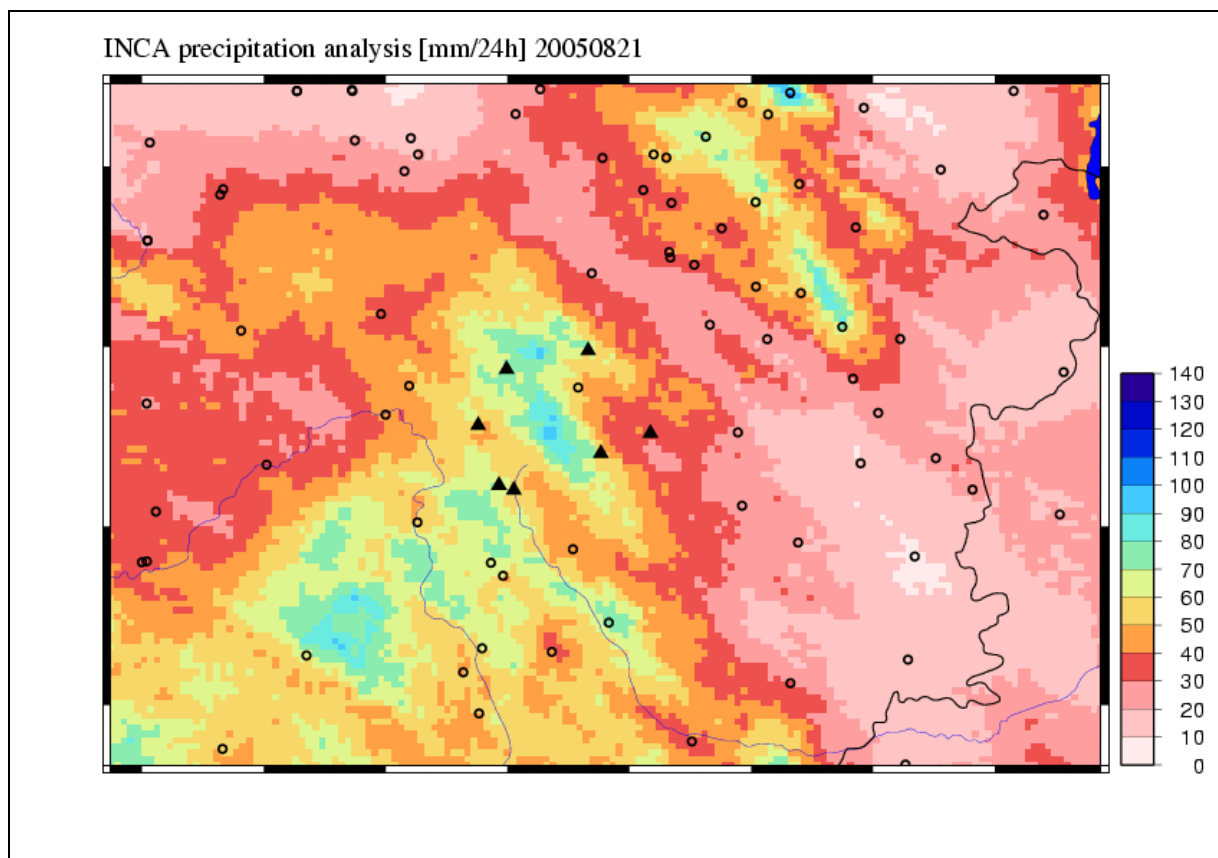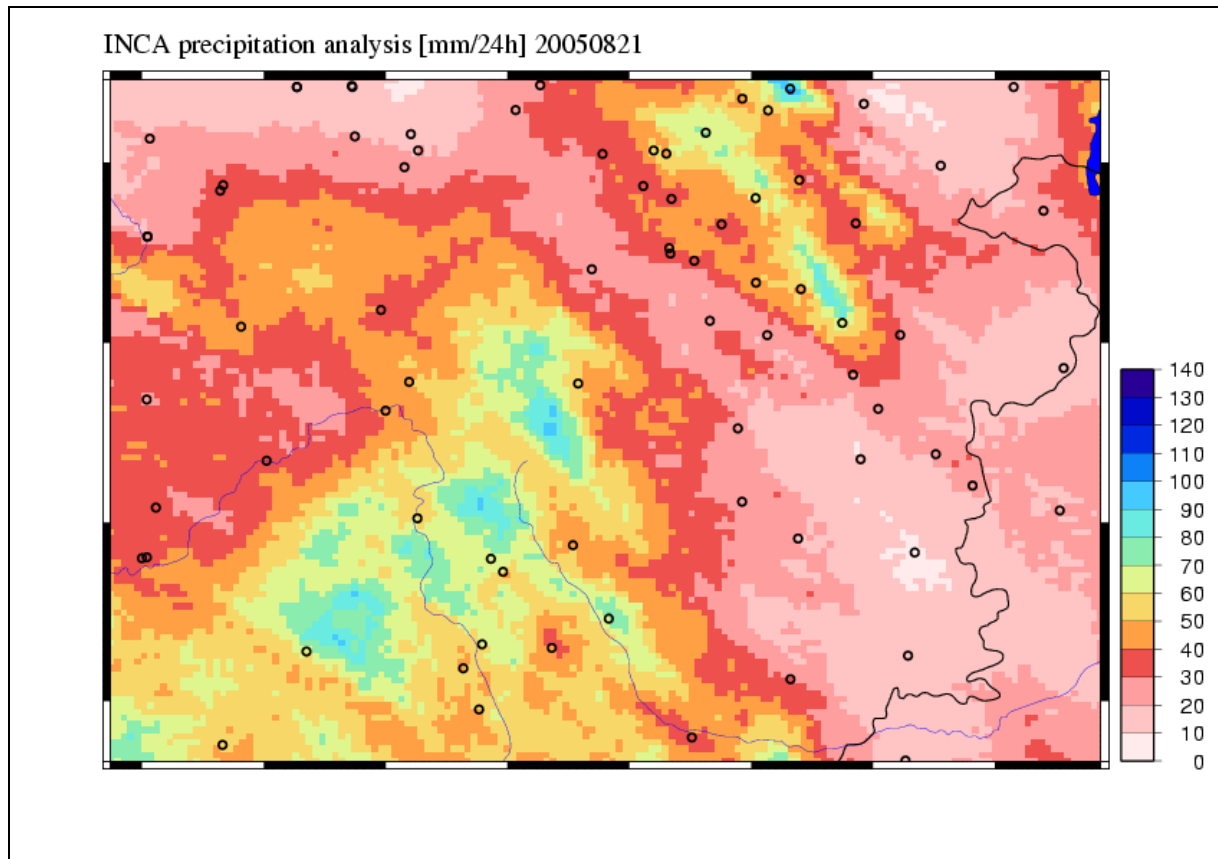
Fig. 5.5.4.2- 2a: 24-hourly INCA precipitation analysis from 21st Aug. 2005 06 UTC to 22nd Aug. 2005 06 UTC without (top) and with HZB data (bottom). Circles denote ZAMG stations, triangles HZB stations
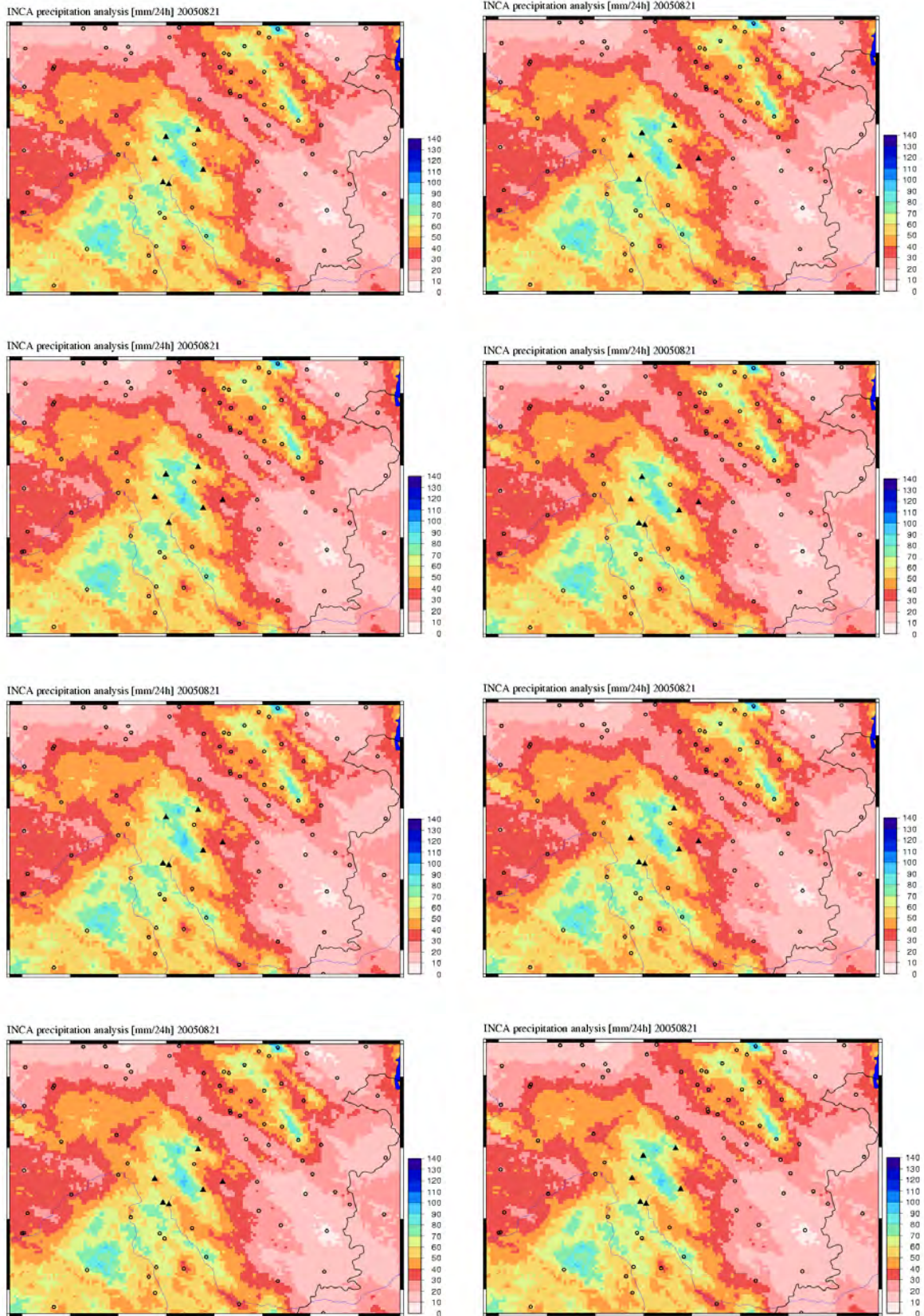
Fig. 5.5.4.2-2b: 24-hourly INCA ensemble precipitation analyses from 21st Aug. 2005 06 UTC to 22nd Aug. 2005 06 UTC, created by omitting one station respectively (from top left line-by-line to bottom right: HZB stations Kreuzwirt, Hohenau/Raab, Fladnitzberg, Alpl, Breitenau/Mixnitz, Stanz and Birkfeld plus ZAMG station Fischbach)
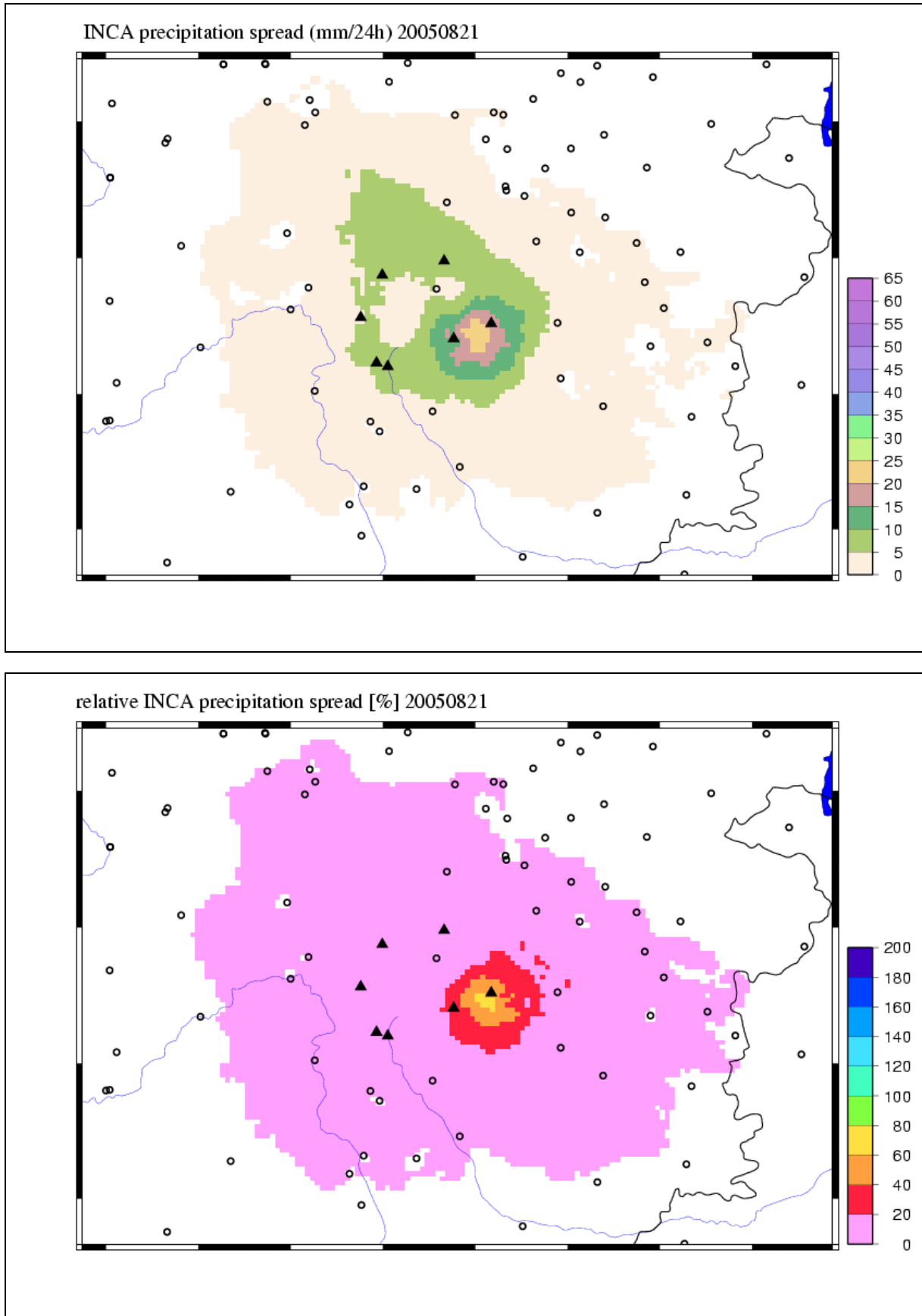
Fig. 5.5.4.2-2c: absolute (top, [mm/24h]) and relative spread (bottom, [%]) of the precipitation ensembles of 21st August 2005 from Fig. 5.5.4.2-2a and 5.5.4.2-2b
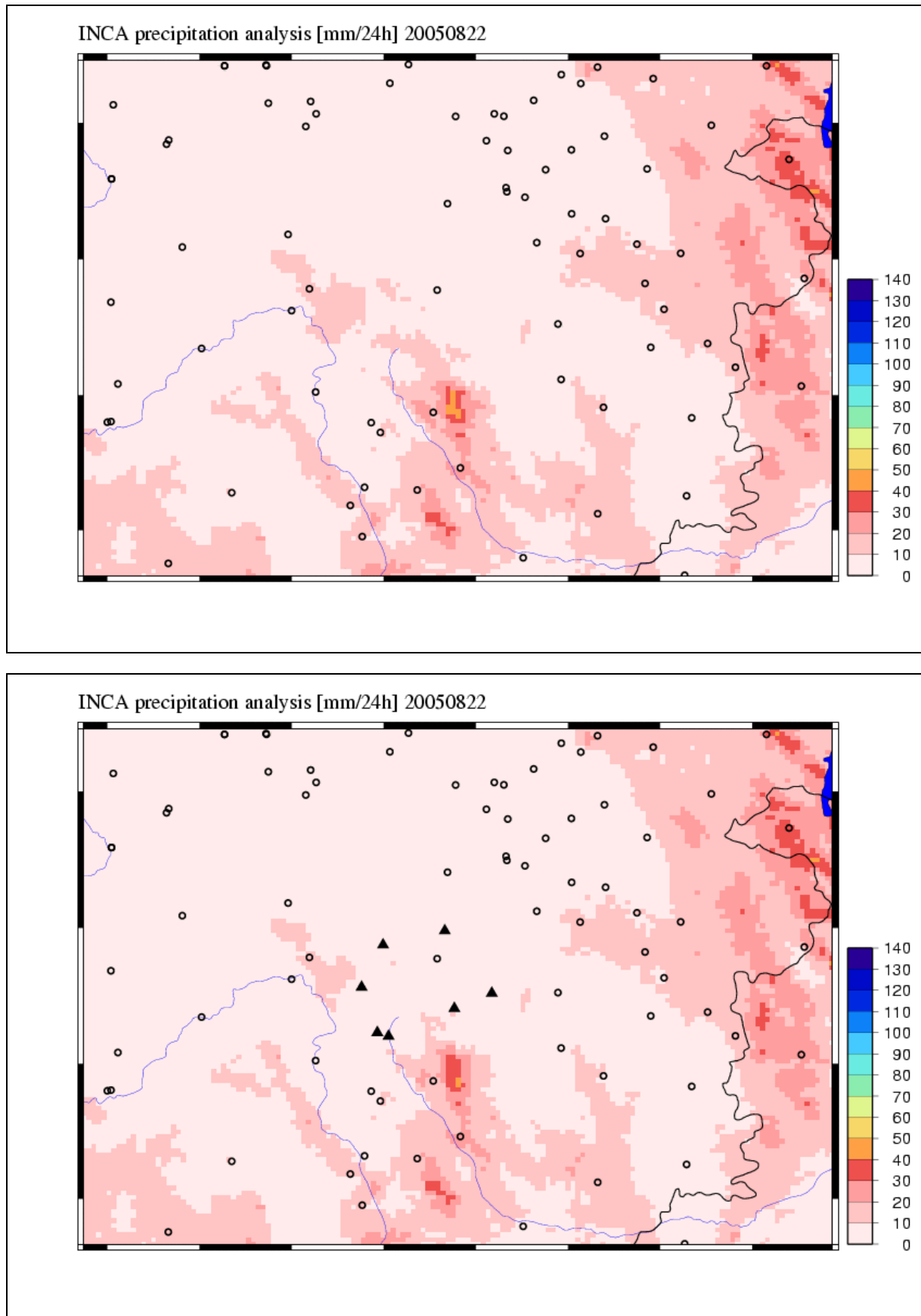
Fig. 5.5.4.2-3a: 24-hourly INCA precipitation analysis from 22nd Aug. 2005 06 UTC to 23rd Aug. 2005 06 UTC without (top) and with HZB data (bottom). Circles denote ZAMG stations, triangles HZB stations
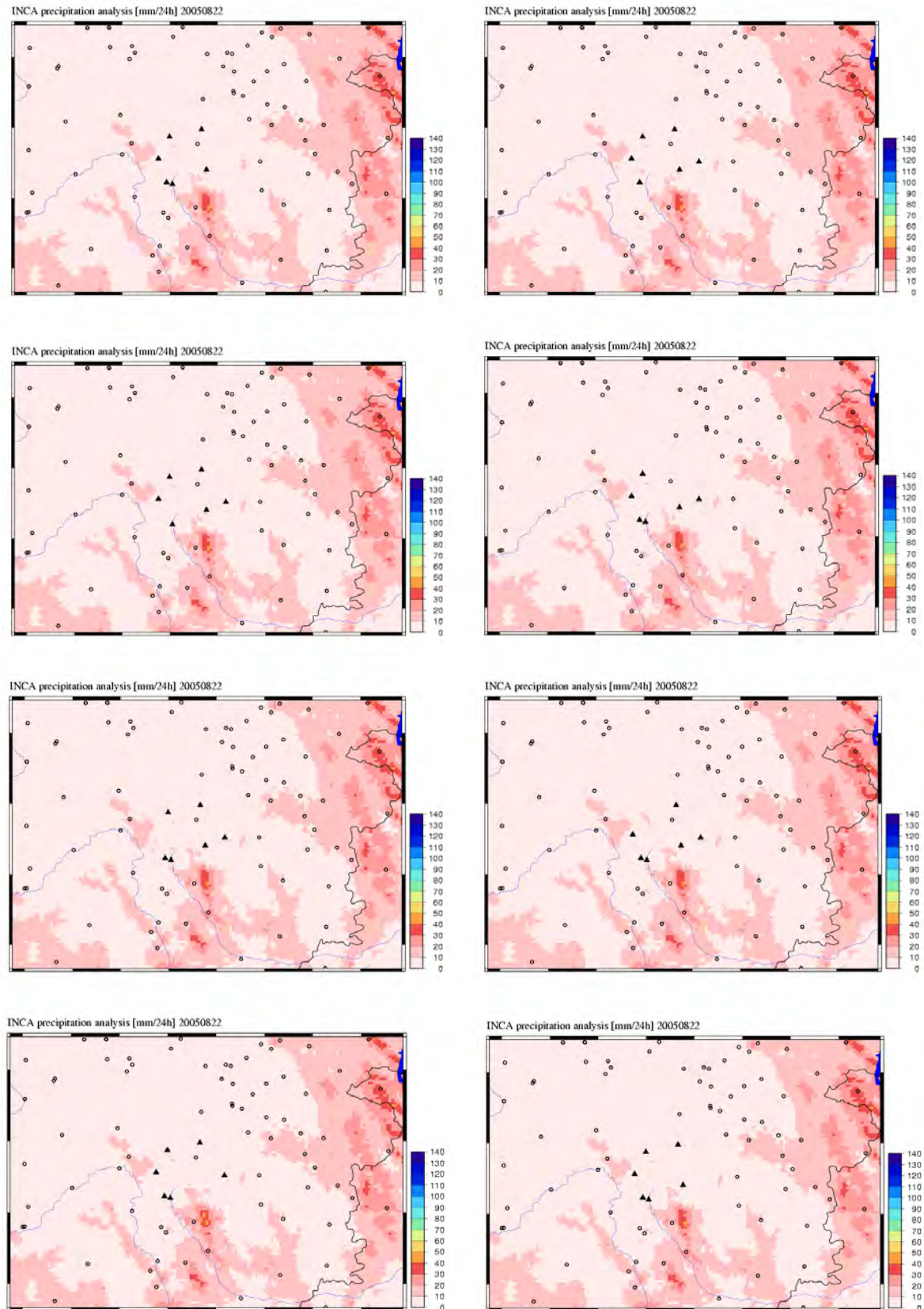
Fig. 5.5.4.2- 3b: 24-hourly INCA ensemble precipitation analyses from 22nd Aug. 2005 06 UTC to 23rd Aug. 2005 06 UTC, created by omitting one station respectively (from top left line-by-line to bottom right: HZB stations Kreuzwirt, Hohenau/Raab, Fladnitzberg, Alpl, Breitenau/Mixnitz, Stanz and Birkfeld plus ZAMG station Fischbach)
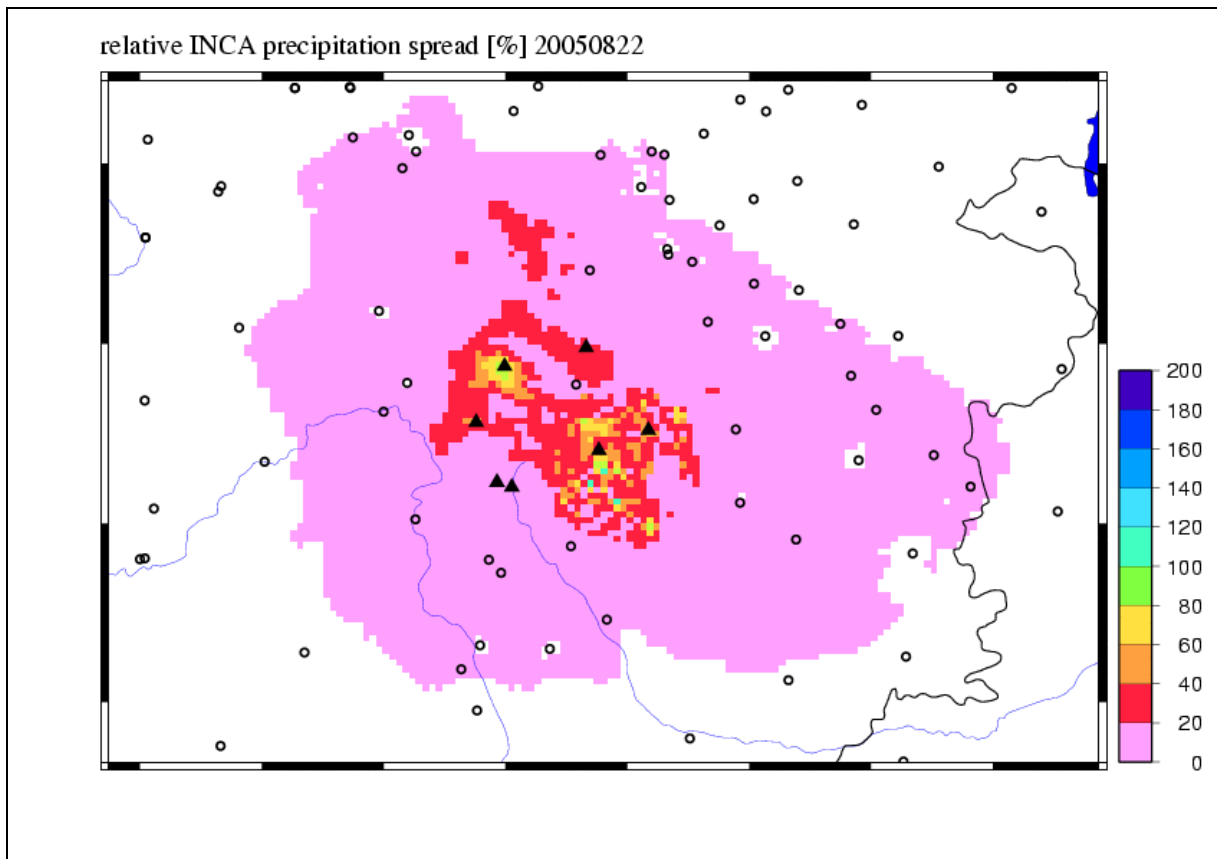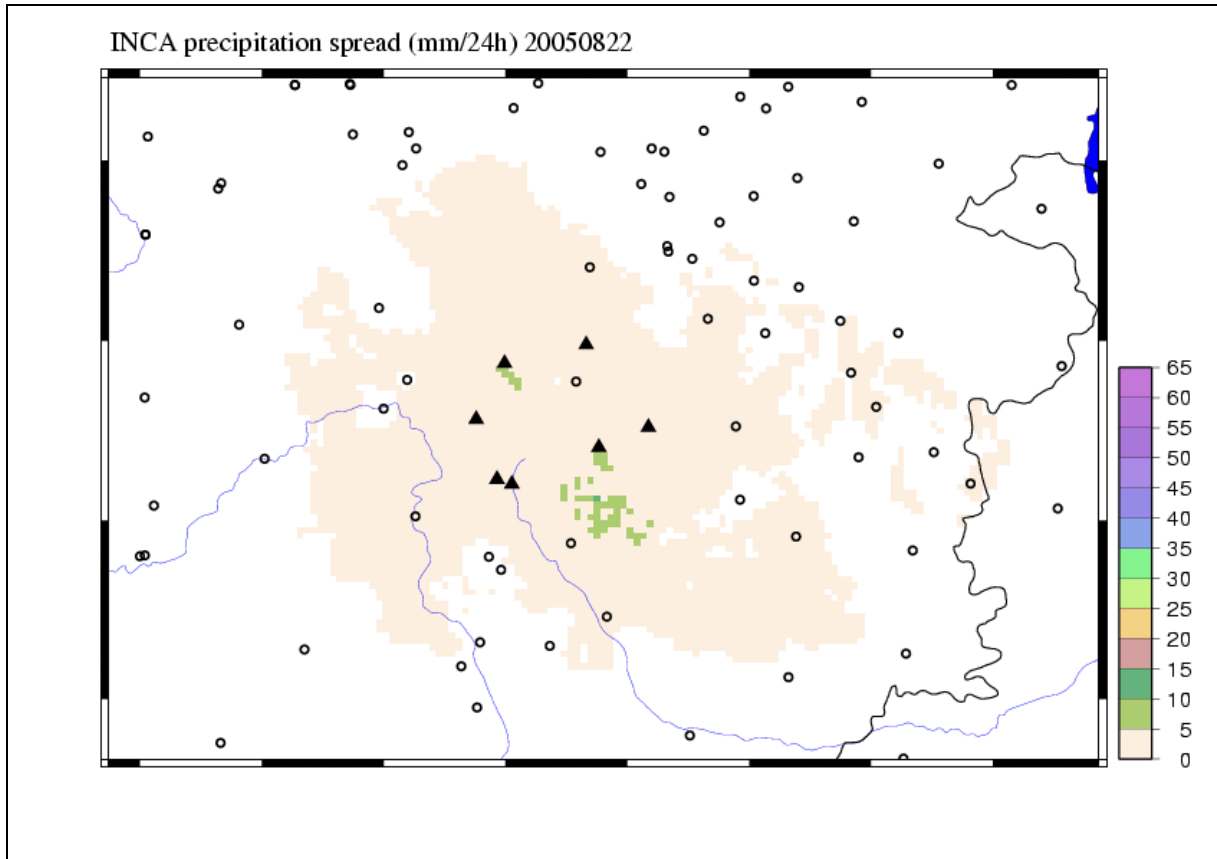
Fig. 5.5.4.2-3c: absolute (top, [mm/24h]) and relative spread (bottom, [%]) of the precipitation ensembles of 22nd August 2005 from Fig. 5.5.4.2-3a and 5.5.4.2-3b

5.5.4.3 Tests with a Modified Radar Scaling

Differences between gauge and radar measurements of precipitation are ubiquitous. Its most important reasons are on the one hand the limitation of the radar sight due to earth curvature as well as mountains and other obstacles, and on the other hand the lack of knowledge about spatial variations of precipitation intensities, which may happen at very small scales and can therefore not sufficiently be resolved by radar, let alone station measurements. Neglecting the fact that also rain gauge measurements are subject to uncertainties (especially when influenced by wind), they can be considered to represent the "truth" which is only available at a few discrete points, whereas the radar measurements are continuously available but posing a less accurate estimation.

It is a logical consequence to calibrate the radar analysis with the help of rain gauge measurements. This is also done in a double-stage process within the INCA system, first on a monthly basis according to climatological experience and subsequently according to rain gauge measurements. In certain circumstances, a calibration like this may be precarious, as an upward calibration of radar measurements may yield unrealistically high precipitation peaks, especially during situations with high precipitation intensities and high spatial variability, as it is characteristic for summertime convective precipitation events (i.e., showers and thunderstorms).

As a consequence, the maximum "allowed" calibration factor is limited with the value of 4 in the operational INCA system, yielding on average the best results according to previous studies (Haiden et al. 2009). Any possible residual of the span between radar and station measurements is bridged not until in the following and final step, the combination between radar and station analysis; in doing so, the actual occurrence of a residual span is rated as a hint of a poor radar sight, and consequently the weight of the radar field is reduced and its structures are less accentuated. Poor radar sight mainly applies to the Alpine area, where the INCA precipitation analyses are thus usually characterized by the coarse structures from the station interpolation and not by the fine, but occasionally not trustworthy structures from the radar field.

Translating this into the present investigation, it means that the extremely high precipitation measurements at Fladnitzberg and Hohenau on 20th August 2005 that were not in line with the radar data, produced a broad "blob" of precipitation which was actually unrealistic for this convective precipitation event. That is why it was investigated if a more flexible calibration of the radar field with higher limits would yield a better analysis with more realistic and more accentuated precipitation peaks. For this purpose, the maximum allowed calibration factor was set to 5 first and to unlimited afterwards. As it turned out that the needed calibration factors rarely rose above 5, these two test runs hardly differ, which is why only the results of the unlimited calibration are presented here.
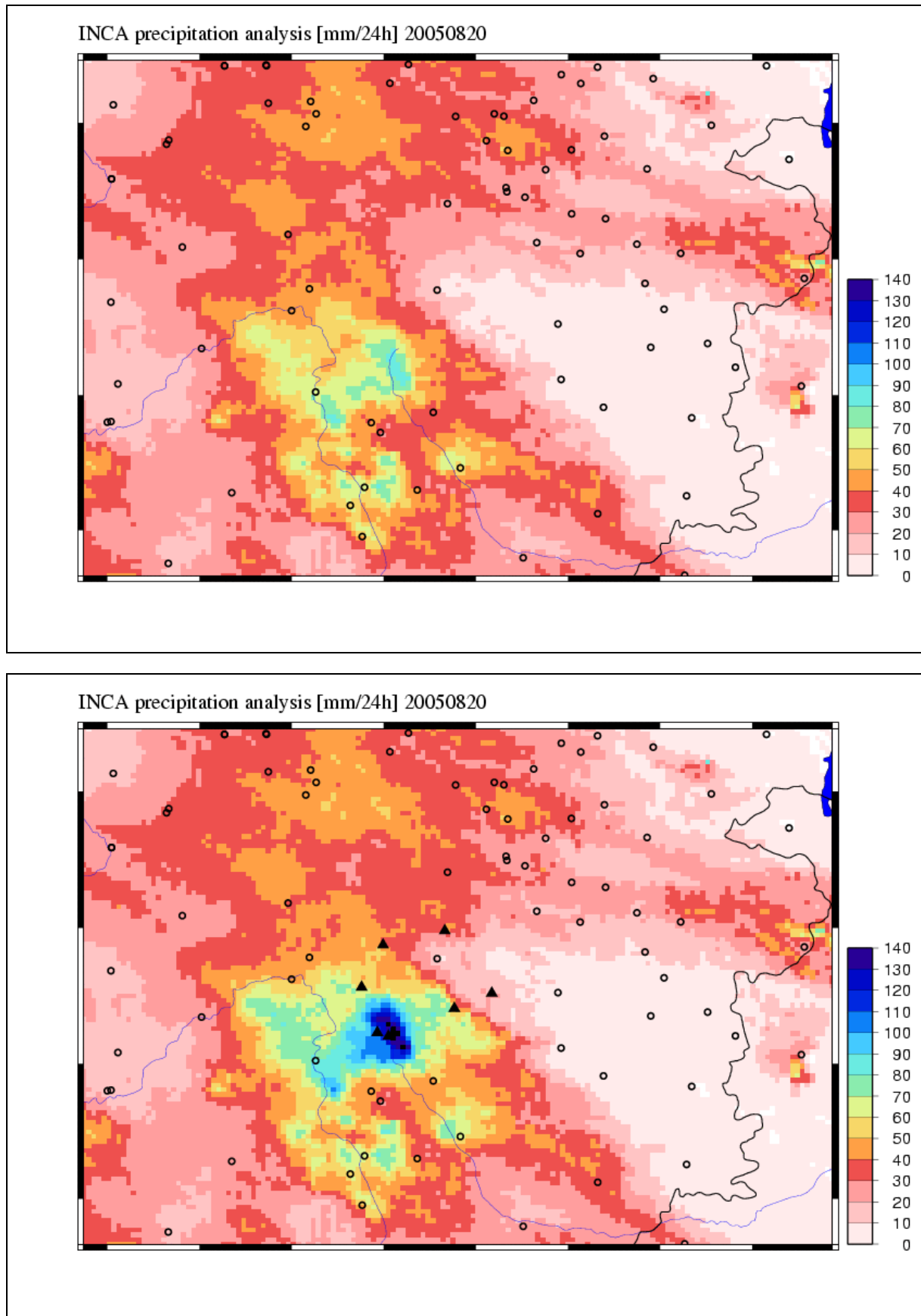
Fig. 5.5.4.3-1a: 24-hourly experimental INCA precipitation analysis with modified radar calibration from 20th Aug. 2005 06 UTC to 21st Aug. 2005 06 UTC without (top) and with HZB data (bottom). Circles denote ZAMG stations, triangles HZB stations
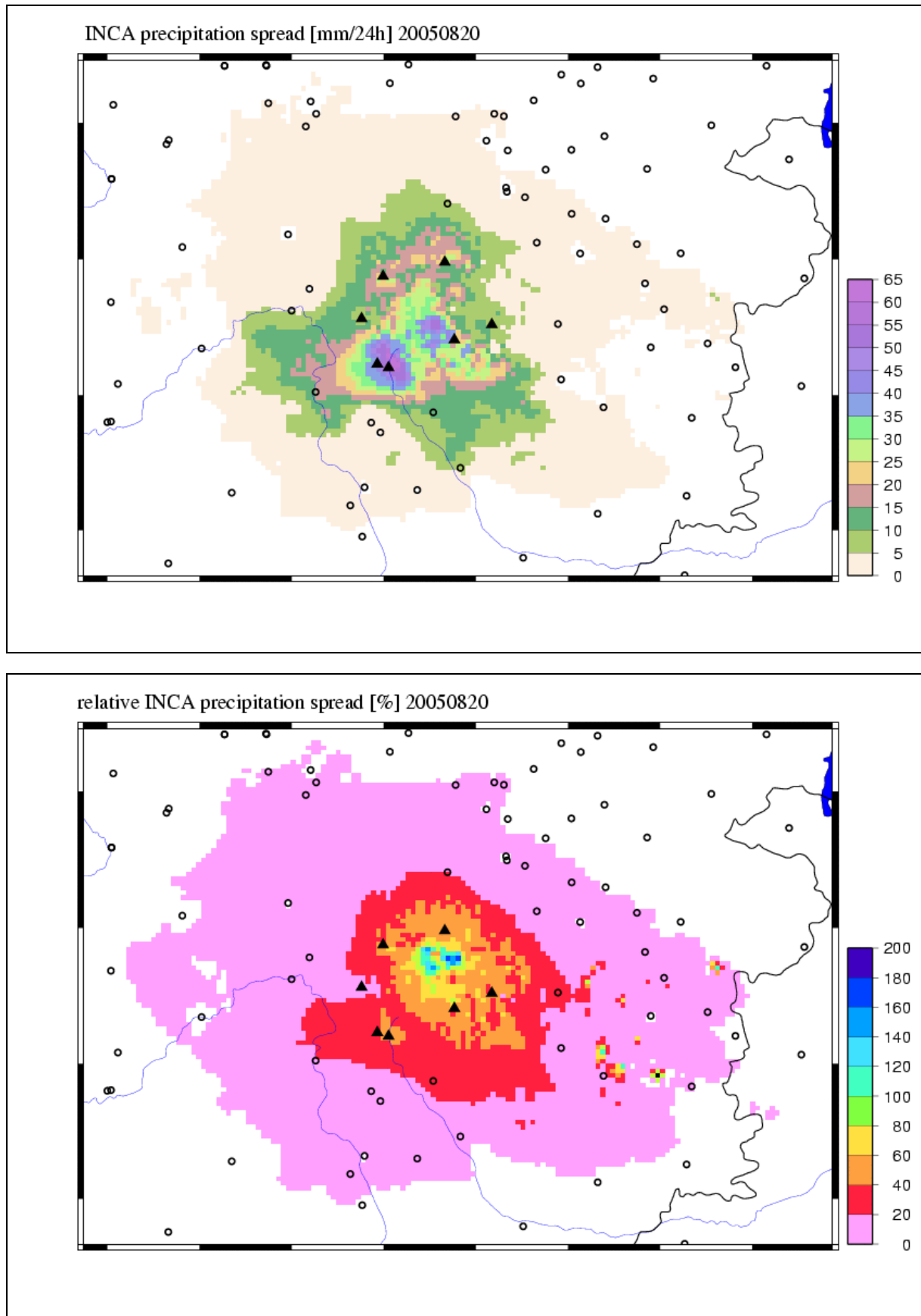
Fig. 5.5.4.3-1b: Absolute (top, [mm/24h]) and relative spread (bottom, [%]) of the experimental ensemble precipitation analyses from 20th Aug. 2005 06 UTC to 21st Aug. 2005 06 UTC
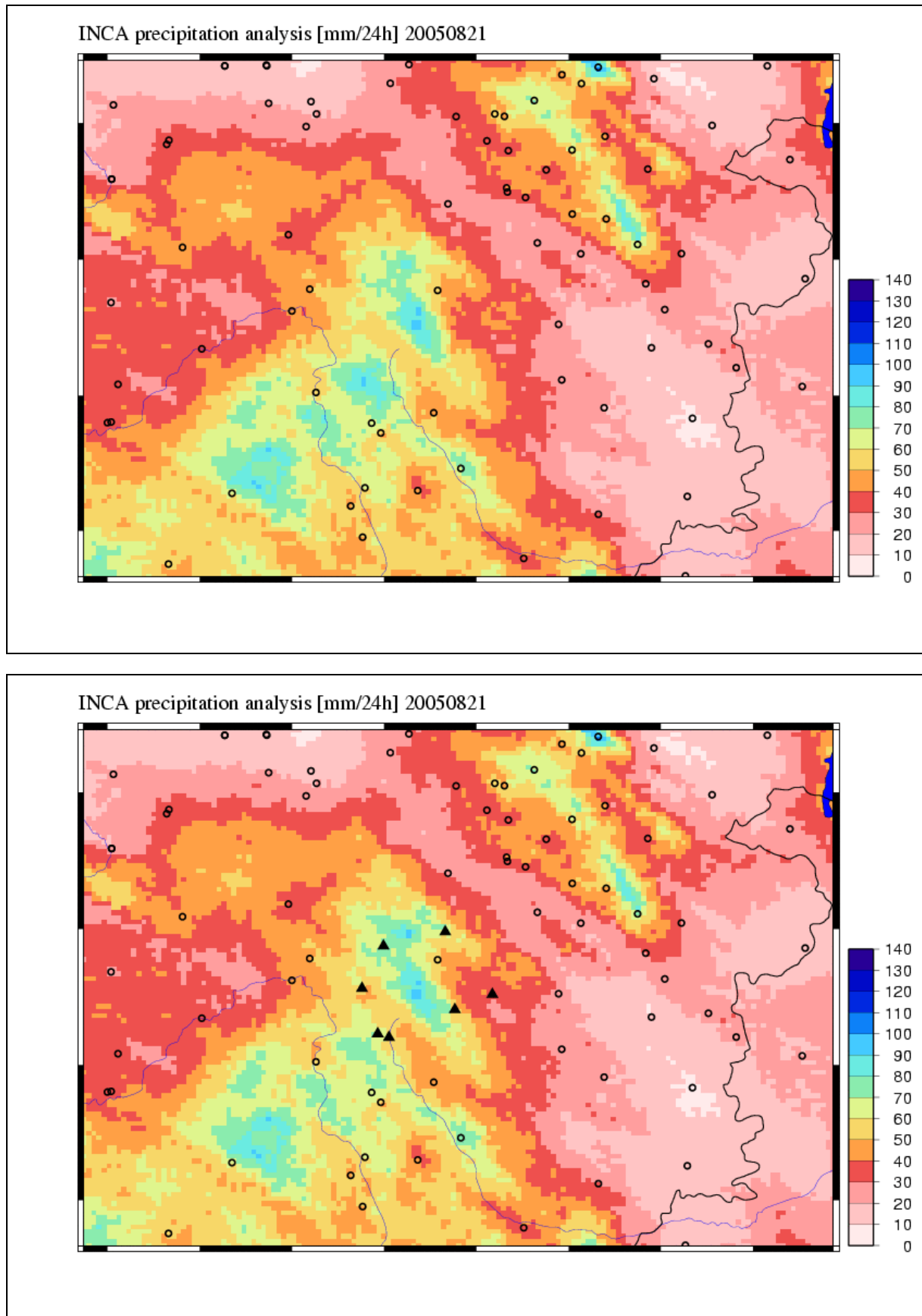
Fig. 5.5.4.3-2a: 24-hourly experimental INCA precipitation analysis with modified radar calibration from 21st Aug. 2005 06 UTC to 22nd Aug. 2005 06 UTC without (top) and with HZB data (bottom). Circles denote ZAMG stations, triangles HZB stations

INCA precipitation spread [mm/24h] 20050821

relative INCA precipitation spread [%] 20050821
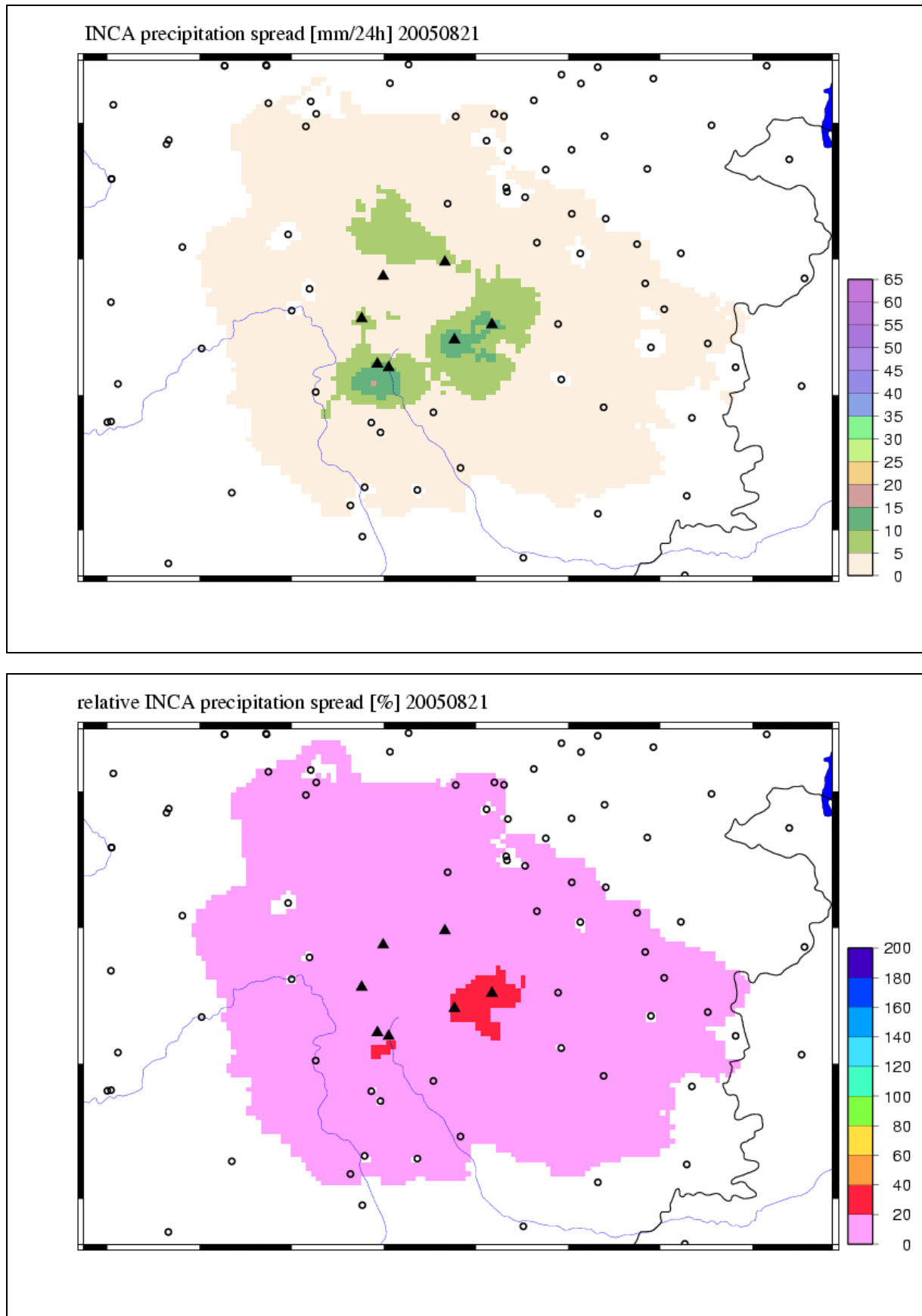
Fig. 5.5.4.3-2b: Absolute (top, [mm/24h]) and relative spread (bottom, [%]) of the experimental ensemble precipitation analyses from 21st Aug. 2005 06 UTC to 22nd Aug. 2005 06 UTC

Fig. 5.5.4.3-3a: 24-hourly experimental INCA precipitation analysis with modified radar calibration from 22nd Aug. 2005 06 UTC to 23rd Aug. 2005 06 UTC without (top) and with HZB data (bottom). Circles denote ZAMG stations, triangles HZB stations

INCA precipitation spread [mm/24h] 20050822

relative INCA precipitation spread [%] 20050822
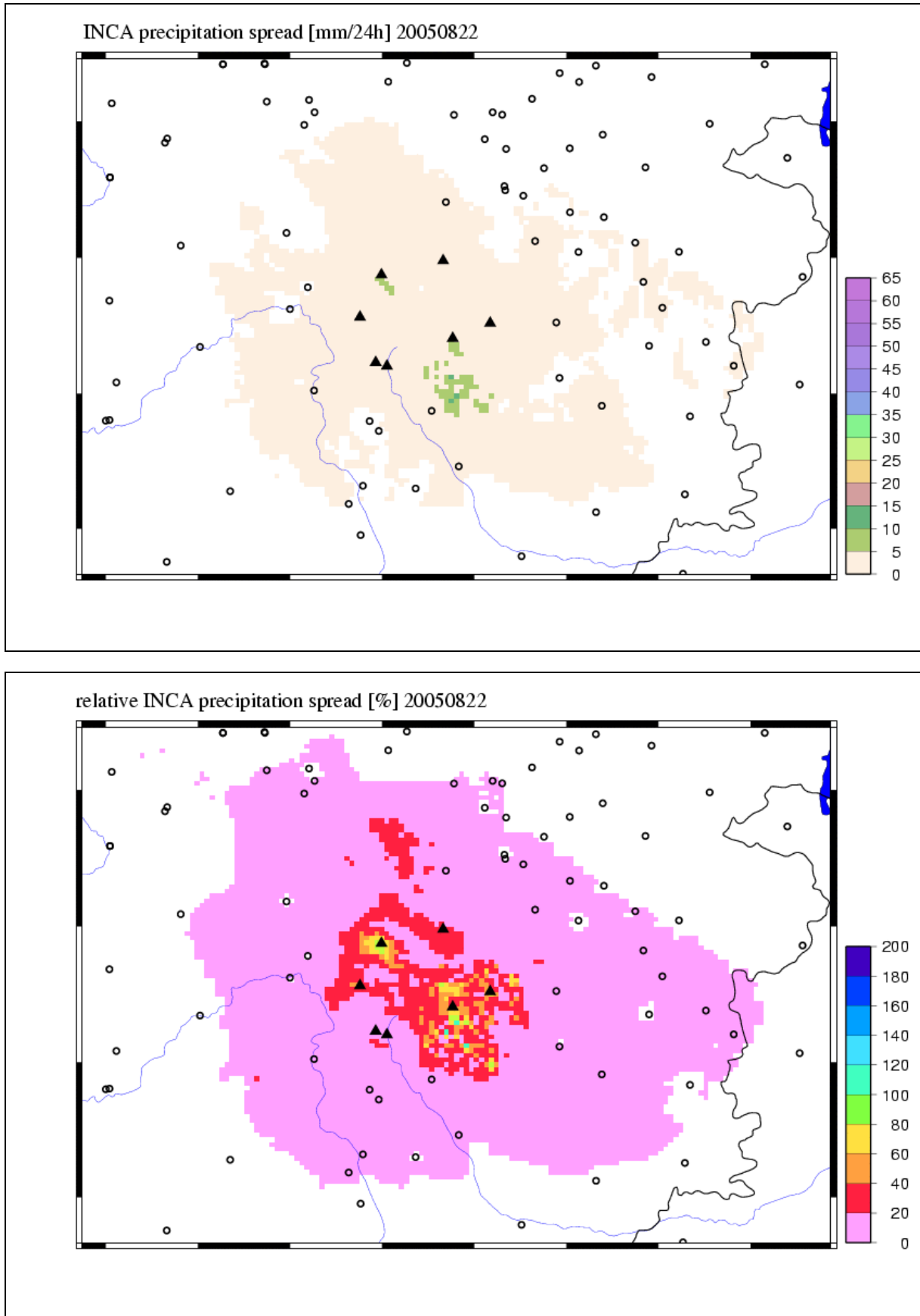
Fig. 5.5.4.3-3b: Absolute (top, [mm/24h]) and relative spread (bottom, [%]) of the experimental ensemble precipitation analyses from 22nd Aug. 2005 06 UTC to 23rd Aug. 2005 06 UTC

The question whether the ensemble of experimental analysis was indeed better than the ensemble of the operational analysis was addressed in two ways:

- Is the uncertainty margin of the experimental ensemble analyses smaller than in the reference?

- Can the measurements of the HZB stations be better reproduced than in the operational reference?

Fig.s 5.5.4.3-1 to 5.5.4.3-3 show the analyses without HZB data, the analyses with HZB data (it was abandoned to present the remaining 8 ensemble analyses this time) and the absolute and relative spread of the 10 ensemble analysis, as before but with the modified radar calibration.

The reduction of the uncertainty margin is obvious on 20th August (Fig. 5.5.4.3-2a) and on 21st August (Fig. 5.5.4.3-2b; compare with Fig. 5.5.4.2-1c and 5.5.4.3-2c, respectively). On 22nd August hardly any differences are visible any more, which is mainly due to the less plentiful precipitation amounts on that day. Computing the mean ensemble span over a square of 100x100 kilometres centered on Gasen confirms the reduction of the span on 20th and 21st August as well as a marginal rise on 22nd August (Tab. 5.5.4.3-1).

Tab. 5.5.4.3-1: Comparison of the mean span of ensemble precipitation analyses with operational (left column) and experimental radar calibration (right column) in an area of 100x100 kilometres around Gasen

Date	mean span of reference ensembles [mm/24h]	mean span of experimental ensembles [mm/24h]
20th Aug. 2005	4,34	3,72
21st Aug. 2005	1,58	1,21
22nd Aug. 2005	0,30	0,32

To answer the question if the reduced ensemble span in fact encompasses the "truth" and not another value, it was additionally investigated by means of cross validation if the measurements of the HZB stations can be better reproduced by the INCA analyses with modified radar calibration than by the operational INCA analysis (Tab. 5.5.4.3-2). Results are inconclusive here: The rain gauge measurements on 20th August (especially the extreme peaks at Hohenau and Fladnitzberg) are captured considerably better on 20th August (especially the extreme peaks at Hohenau and Fladnitzberg) but predominantly poorer on 21st August. The root mean square error (RMSE) from the 7 HZB stations drops from 33.2 mm to 27.9 mm on 20th August while it rose from 6.2 mm to 7.7 mm on 21st August. On 22nd August, the analysed values according to both methods are almost identical, pointing out that the discrepancies between radar and rain gauge measurements are only small on that day.

Tab. 5.5.4.3-2: Comparison of INCA precipitation analyses with operational radar calibration (left column) and INCA precipitation analyses with experimentally modified radar calibration (central column), each of them without using HZB data, with the HZB rain gauge measurements tehmselves (right column) on 20th (top), 21st (center) and 22nd August (bottom)

HZB station	name	operational INCA analysis	exp. INCA analysis	measurement [mm/24h]
111328	Kreuzwirt	7,8	7,8	13,8
111369	Hohenau/R.	66,5	78,6	134,5
111401	Fladnitzberg	55,5	63,7	99,9
111435	Alpl	15,8	15,9	43,2
112003	Breitenau/M.	46,1	49,7	57,9
112540	Stanz	45,8	47,0	40,1
123117	Birkfeld	39,2	40,7	52,0

HZB station	name	operational INCA analysis	exp. INCA analysis	measurement [mm/24h]
111328	Kreuzwirt	41,6	41,1	34,7
111369	Hohenau/R.	62,5	67,3	56,4
111401	Fladnitzberg	68,2	77,1	69,4
111435	Alpl	59,4	61,2	66,4
112003	Breitenau/M.	58,8	62,2	55,6
112540	Stanz	60,3	64,5	66,7
123117	Birkfeld	45,7	44,2	55,0

HZB station	name	operational INCA analysis	exp. INCA analysis	measurement [mm/24h]
111328	Kreuzwirt	2,4	2,4	2,6
111369	Hohenau/R.	6,1	6,1	5,7
111401	Fladnitzberg	9,1	9,1	9,0
111435	Alpl	4,1	4,1	3,3
112003	Breitenau/M.	11,3	11,3	7,8
112540	Stanz	8,0	8,0	4,4
123117	Birkfeld	3,5	3,6	10,6

5.5.5. Summary and Interpretation

A re-computation of INCA precipitation analyses shows the strong influence, which may unfold by the use of additional HZB stations with 24-hourly data that are not available in real-time. The creation of ensemble analyses by omitting single stations in the investigation area was used to quantify the uncertainties, which grow bigger when the precipitation gradients are stronger and additional measurements thus become more important. Hence especially the extremely high readings of two HZB stations (Fladnitzberg and Hohenau) and the comparably low value of ZAMG station Fischbach are reflected in a considerable uncertainty margin on 20th August, whereas the sharpness of analysis increased on 21st and 22nd August.

Tests with a modified radar calibration showed that a more flexible calibration would significantly improve the results on 20th August, whereas it would impair analysis quality on 21st August. These findings are conflicting with an earlier, more extensive investigation, according to which the maximum threshold of the calibration factor was set to the operational value of 4. Thus, the tests and experiences with the radar calibration suggest that the operationally used one yields the best results on average, but may be suboptimal in some extreme cases; this leads to the recurrent and not universally solvable problem if the best results on average or the most realistic representations of extreme events are desired.

Finally, also the question which meteorological reasons caused the radar and rain gauge measurements to differ that strongly on 20th August 2005 is interesting. The weather situation on that day was characterized by a low pressure system that moved from France via Northern Italy to the Balkan states. Ahead of it, especially on 20th August a very warm and unstably stratified air mass was transported to Austria from the Southeast. As the water surface temperature of the Adriatic Sea usually has its annual maximum at this time and a correspondingly high amount of water evaporates, the content of water vapour was very high in this air mass, and so was its potential to produce strong precipitation events which was indeed released as it reached the Alpine range and was forced to rise.

Due to the high content of water vapour, the cloud base was unseasonably low (for example, the weather observers on duty at Graz Thalerhof airfield reported a cloud base about 300 metres above ground, or about 700 metres above sea level only). This means that a considerable amount of droplet growth, and thus enhancement of precipitation still occurred in very low levels, which can hardly be scanned by radar, since its nearest location is situated on Zirbitzkogel at 2300 metres above sea level. As long as the rain gauge measurements are representative for their respective environment, the radar calibration and the final combination of the radar analysis with the interpolated "station analysis" are capable of correcting these errors. In the case presented here, however, embedded convection was responsible for very localized and extreme precipitation peaks, which did not hit any of the operationally available stations.

Summing up, an unfortunate coincidence of a "winterly" low cloud base (with its implications in the precipitation characteristics and the radar sight) and a "summerly" high variability and intensity of this precipitation event, whose peaks could not be represented by any of the operationally available stations, seems to have caused the poor quality and the high uncertainty of the INCA precipitation analyses on 20th August 2005. The weather phenomenon which caused it, namely a low pressure system moving along a path protruding deeply South into the Mediterranean region and thus being able to ingest very warm and humid air masses, is very rare in summer, in fact it does not occur at all in many years; hence a situation like this and its impact on the performance of precipitation analyses is not expected to occur often. On the other hand, if this weather pattern happens to occur again in summer, it can initiate a precipitation event with similar characteristics anytime again.

6. Datamanagement (GBA, JR)

6.1.   Process Data

6.1.1. Extracting Data Batches of Varying Quality

The process data (Fig. 6.1.1-1, 1008 points), which are available for modelling process-oriented susceptibility maps, are very heterogeneous in terms of data quality and the content due to different data sources (archive, remote sensing, field observation), exploration methods, and investigation aims (eg. process- and damage-oriented cadaster/inventories). It is therefore necessary to divide this data into data batches with different relevance for different modelling objectives, and different data quality (content, location, etc.). In doing so, the following factors must be taken into account: Which data is reliable/unreliable information due to:

a. geographical localization

b. general process information (gravitational mass movements)

c. process type (spontaneous gravitational mass movements in soil)

d. process-triggering factors

e. the event date

f. the attribution of real, location-specific characteristics/features/conditions
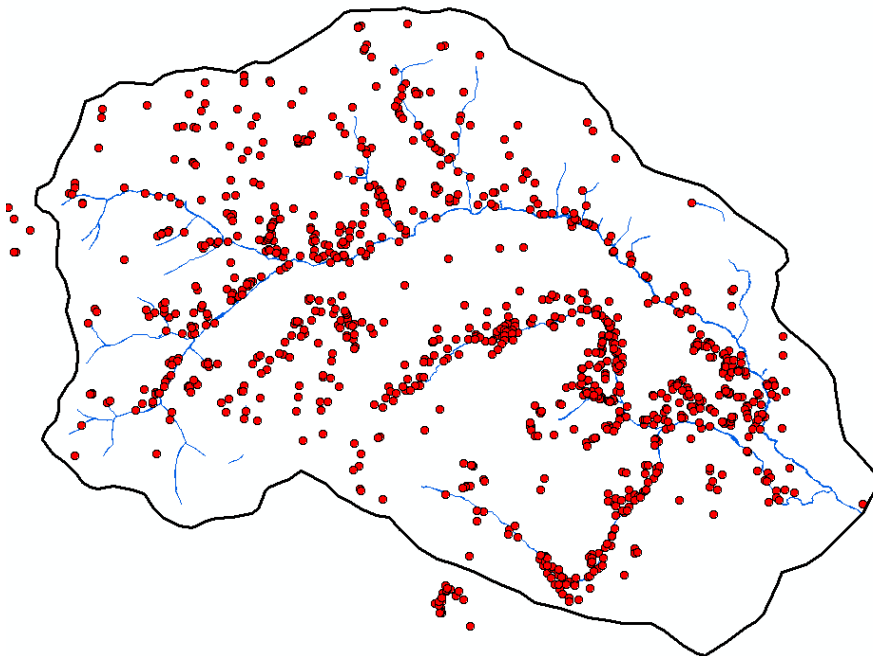
Fig. 6.1.1-1: Geographical positions of the process data (1008 point-information) available for modelling susceptibility maps for the Region of "Gasen-Haslau"

In order to ensure a clear, transparent extraction of the data into batches of different data-quality, a hierarchical extraction method was developed and applied (Fig. 6.1.1-2). The following criteria were employed for the gradual (step by step) extraction of data batches of different quality and application-objectives:

1. As a first step, all process information points (11 points) were removed that were unsuitable for detailed or large-scale modelling due to uncertain or deficient geographical location. The data extracted cannot be used for further modelling and validation of susceptibility maps.

2. Then all process information points were removed for which it was unclear whether they actually supplied any information on a gravitational mass movement (217 points). This means that all those points have been removed that were based on uncertain indications, obtained from the use of indirect investigation methods (such as aerial photo analysis). These points were assessed as 'conjectural' or 'indicative.' Depending on the potential event date/period, the data batch was then decomposed in turn into model-external test data (103 points) and time-related test data (114 points) of poor quality (5 points: definitely not a mass movement).

3. After that, all data points were removed that did not relate to mass movements in soil (107), or for which it was unclear whether they related to mass movements (3 points). This, for example, involved information on progressively, not spontaneous mass movements (for example creeping slopes) or rock slides. Similarly, points were removed, for which the type of mass-movement could not be sufficiently defined (attribution: 'non-specific mass movement'). Depending on the potential event date/period, this data batch was also decomposed into test data (39 points) and time-related test data (68 points) of medium quality.

4. As a further step, all data points were removed that contained reliable or unreliable information on the process-triggering factor 'fluvial bank erosion' (181 points). This is very important, because for process-oriented identification of areas of different/comparable process susceptibility, only those process information should be included in the modelling, for which comparable, dominant, process-controlling variables and location parameters/conditions can be adopted. Thus, a susceptibility map for mass movements, which are induced by hydrological, fluvial processes, would require parameter maps that could approximately represent the hydrological and hydraulic conditions along/in the brooks and rivers. For this reason, the project ADAPTSLIDE also concentrates on the susceptibilities of those processes that were/are triggered in the slope areas solely due to hydro(geo)logical slope processes.

all process data
(compiled process data)

Criteria "data quality"

position accuracy — no (out)

yes

reliable information by remote sensing — no

yes

Criteria "question/goal"

process information "spontaneous mass movement in soil" — no (out) / uncertain information

yes

process caused by fluvial erosion — yes (or uncertain) (out)

event August 2005 — no

yes

complete mapped attributes — no

yes

extraction of data, which are relevant for the project area

Aug 2005 — no — "time-related test data with low quality"

yes

"test data with low quality"

Aug 2005 — no — "time-related test data with middle quality"

yes

"test data with middle quality"

"time-related test data with high quality"

"test data with high quality"

"Data set "high quality" for modelling
train-, test- und validation-data)

extraction of use-oriented data sets
by statistical methods

"train data"

"test data"

"validation data"

Fig. 6.1.1-2: Schematic representation of the hierarchical method of extracting data sets (i) for different objectives, (ii) different relative quality and (iii) data with project-related relevance

5. After that, all data points were removed that provided information about process events from other event periods than August 2005 (34 points: time-related test data with high quality). It is particularly important to take this into account when event-specific parameter maps (for example precipitation maps) are used to model the process susceptibility. On the one hand, the intention can be to produce event-specific susceptibility maps and in that way to check the functionality of a model. On the other hand, for general land-use planning, it is important to have more general susceptibility maps that are not limited to specific events.

6. Furthermore, all those data points were extracted that had incomplete attribution of important location-specific parameters/factors (16 points). This is particularly important when model calculations are supposed to be done using training data whose parameter attributions are based on field observation (i.e. are more likely to be real, location-specific parameters). By including all other data points with incomplete attribution, only model training with the available parameter maps, which are based on generally available data, is possible. This means that the quality and the functionality of a model-technique is distorted and can therefore only be analyzed badly (i.e. what is rather recognized by the model, and what rather not). So it can happen, for example, that on the basis of a model technique correct relationships are quite well recognized, but the regionalisation of these relationships fails due to poor quality of the available regionalization data. Data with incomplete parameter attribution is therefore classified as test data with high data quality.

7. The aim of the ADAPTSLIDE project is to produce susceptibility maps for spontaneous mass movements in soil for the districts of Gasen and Haslau (Fig. 6.1.1-3, red lines). Because the process data obtained extends into other district areas as well (Fig. 6.1.1-3), the modelled area is smaller than the area investigated. Consequently, process data that has no relevance for the districts of Gasen and Haslau (21 points) should be extracted from the data set that is relevant for modelling. However, in so doing, it must be kept in mind that the process areas of mass movements that induced outside district boundaries might well extend into areas of these districts. Thus, all data points situated outside district boundaries, but whose scar areas are located upslope from district boundaries, were not removed from the data sets that are relevant for modelling. In the same way the delineation of the modelling area for susceptibility maps was drawn, so that all those slope areas were included into the modelling, whose potential process areas extend into the municipal area (Fig. 6.1.1-3 and 6.1.1-4, yellow area).
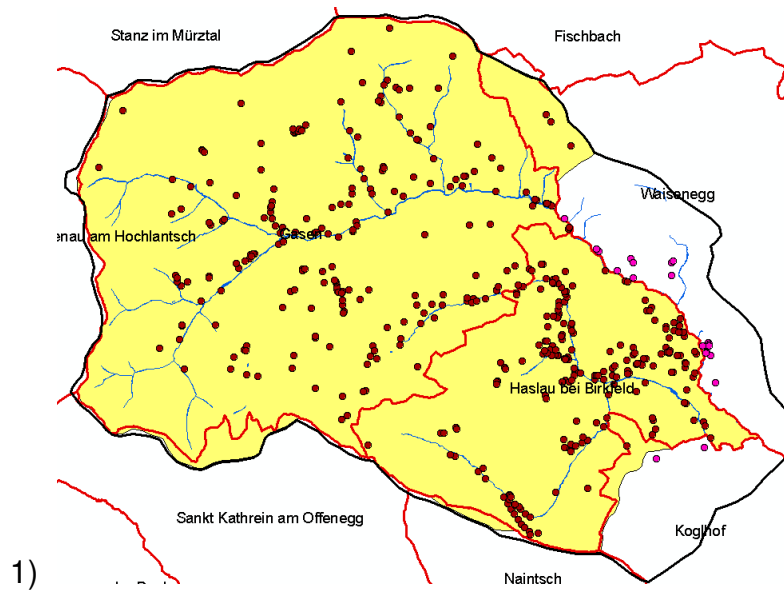
Fig. 6.1.1-3: Modelling-relevant area for the districts of Gasen and Haslau, including project-relevant points (red) and non project-relevant points (pink)

Based on the aim of the project, the high-quality process data set available for modelling process susceptibility is reduced to 413 points (Tab. 6.1.1-1). Similarly, all other test and prediction data of different quality that have been of significance for the modelling in the project area, were ultimately extracted (Fig. 6.1.1-4, Tab. 6.1.1-1).
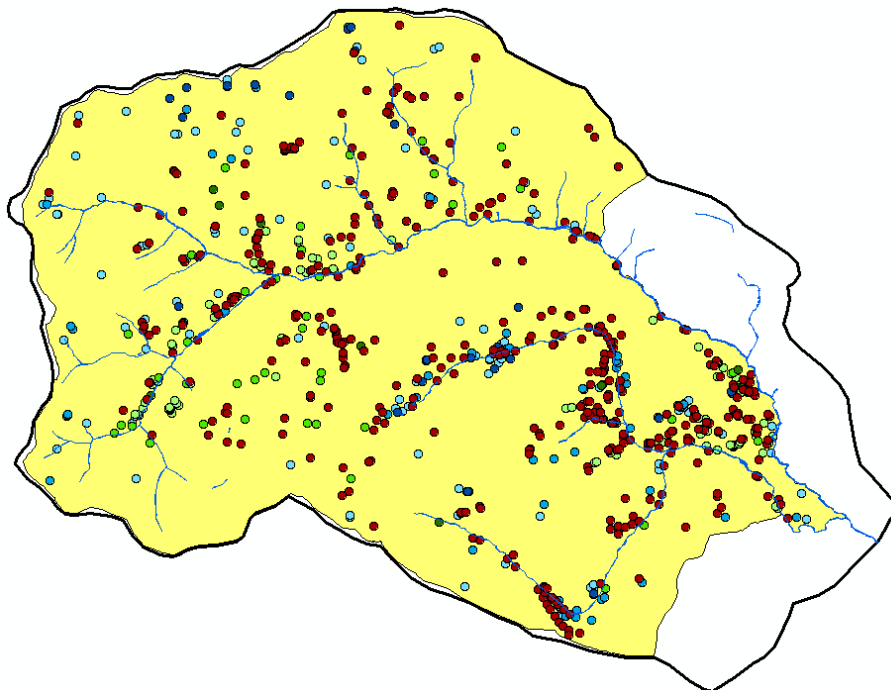
Fig. 6.1.1-4: Available data of very high relative quality (training, test, and validation data) and additional test data and prediction data of different relative quality (legend, Tab. 6.1.1-1) used for modelling susceptibility to spontaneous mass movements in soil in the project area Gasen-Haslau (yellow area)

Tab. 6.1.1-1: Process data sets, which were extracted for the model area, and which are characterized by different quality

Data Set	Number of points	Legend, map in Fig. 6.1.1-4
Final process data set for modelling	413	dark red
Test data (high quality)	12	dark green
Test data (medium quality)	39	green
Test data (low quality)	92	light green
Time-related test data (high quality)	34	dark blue
Time-related test data (medium quality)	57	blue
Time-related test data (low quality)	112	light blue

6.1.2. Splitting of Process Data of High Quality (Training-, Validation-, Testdata)

Data splitting is the act of partitioning available data into two (or more) portions; usually for validatory purposes. Generally one portion of the data is used to develop a predictive model and the other one to evaluate the model's performance (Picard & Berk 1990). In the case of Artificial Neural Network (ANN) development to ensure generalization three representative parts have to be created: training-, validation- and testdata (cf. section 7.2). The sampling methodology used for data splitting can have a significant effect on the quality of the subsets used for training, testing and validating an ANN. Poor data splitting can result in inaccurate and highly variable model performance (May et al. 2010).

The dataset "high quality for modelling", (Tab. 6.1.1-1) hence was divided into three representative portions: training-data (40 %), validation-data (30 %) and test-data (30 %). Each element (or pixel) is randomly assigned to one of the three portions bearing in mind that data are characterized by inhomogeneity with regard to defined parameters. Each element is characterized by a number of properties with these properties irregular distributed over the study area. A simple random sampling would lead to portions which are not representative anymore. So the partition of the data is performed by stratified random sampling without replacement. For the sampling the following stratification was used (abbreviations see Tab. 6.2-1):

- Curvature Classification based on DTM 10m ("HK-DHM10", 9 categories)
- Exposition (8 categories)
- Influence area of Road Network „level low" based on Digital Cadastral Map (DCM) and field mapping ("Wegenetz_lg_mb", 2 categories)
- Forest „level low" based on DCM and field mapping ("Wald_DKM_lg_mb", 2 categories)
- Geological basic disposition „level low" based on conceptual soil map "level low" ("Sub_GK_lg", 5 categories)
- Precipitation "level low" ("NS_lg", 4 categories)

This selection results in 5760 strata, but not all of these strata are available in the underlying data. Furthermore, the landslide pixels of the trainings and validation data

are duplicated to achieve approximately the same proportion of elements with and without landslides.

The results of the data splitting are given in Tab. 6.1.2-1. Distribution of landslide training- validation and testdata is illustrated in Fig. 6.1.2-1.

Tab. 6.1.2-1: Results of splitting of process data of high quality (training-, validation-, testdata)

Data Set	pixels without landslides		landslides	
	number	%	number	%
Training data	8033	40,07	171	41,40
Validation data	6020	30,03	126	30,51
Test data	5995	29,90	116	28,09
Σ	20048	100	413	100
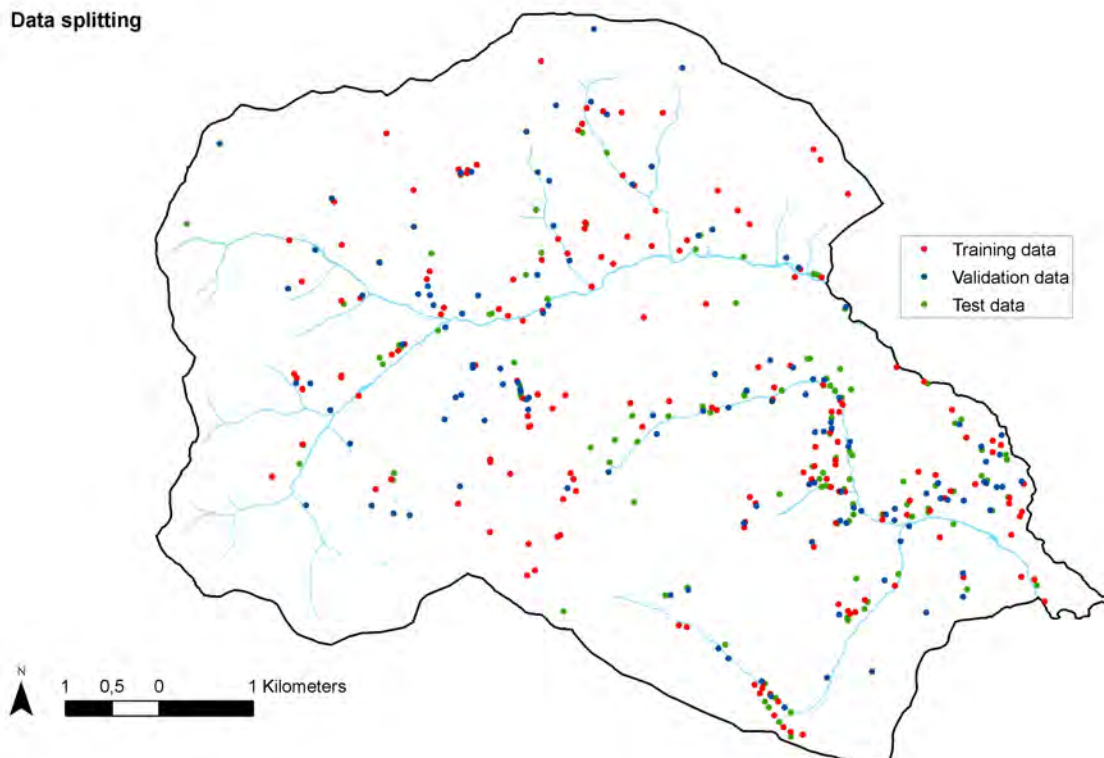
Fig. 6.1.2-4: Distribution of training-, validation- and testdata of landslide points after data splitting in the study area

Apart from the training-, validation- and testdataset, a fourth dataset, called "regionalisation dataset" was created. This dataset was generated without considering the landuse information mapped at the locations of the process data.

Only information which was derivable from maps like the DCM or satellite images was used. The dataset covers the whole study area by a 50 m raster and shows only one value per 50 x 50 m pixel (training-, validation- and test data can include also more than one mass movement value per 50 x 50 m pixel).

6.2.   Management of Parameter Maps

All environmental parameters which were integrated in the modelling procedure are listed in Tab. 6.2-1. The first column gives the abbreviations which are used in the modelling Chapter 7.2 – 7.4.

Bivariate statistics were calculated taking into account the distribution of mass movements and all environmental datasets aiming at identifying those parameters which show high correlations to mass movements occurrence. The results are shown in Tab. 6.2-2. Variables with high correlations were integrated first in the modelling operations.

Bivariate statistics as well were calculated between all environmental parameters aiming at identifying intercorrelations between modelling parameters. φ-Coefficient was used to determine strength of association for binary parameters whereas Cramer's V was used for non-binary parameters. Parameters showing high intercorrelations (i.e. Cramer's V or φ-Coefficient > 0,3) were not used in the same modelling run (Tab. 6.2-3).

Tab. 6.2-1: List of parameters integrated in the statistical modelling

Parameterbezeichung / Abbreviation of parameter	Beschreibung Deutsch	English description
HK-DHM10	Hangklassifikation aufgrund DHM 10m	Curvature Classification based on DTM 10m
HW-DHM10	Horizontalwölbung aufgrund DHM 10m	Plan Curvature based on DTM 10m
VW-DHM10	Vertikalwölbung aufgrund DHM 10m	Profile Curvature based on DTM 10m
Wegenetz_lg_mb	Einflussbereich Wegenetz „level gering" aufgrund DKM und MB-Kartierung	Influence area of Road Network „level low" based on Digital Cadastral Map (DCM) and field mapping
Wegenetz_lh_mb	Einflussbereich Wegenetz „level hoch" aufgrund DKM, Luftbild und MB-Kartierung	Influence area of Road Network „level high" based on DCM and field mapping
Wegenetz_lg	Einflussbereich Wegenetz „level gering" aufgrund DKM (Regionalisierungsdaten)	Influence area of Road Network „level low" based on DCM (Regionalisation Data)
Wegenetz_lh	Einflussbereich Wegenetz „level hoch" aufgrund DKM (Regionalisierungsdaten)	Influence area of Road Network „level high" based on DCM (Regionalisation Data)
Wald_DKM_lg_mb	Wald „level gering" aufgrund DKM und MB-Kartierung	Forest „level low" based on DCM and field mapping
Wald_Sat_lg_mb	Wald „level gering" aufgrund Satellitenbild und MB-Kartierung	Forest „level low" based on Satellite Data and field mapping
Wald_DKM_lg	Wald „level gering" aufgrund DKM (Regionalisierungsdaten)	Forest „level low" based on DCM (Regionalisation Data)
Wald_DKM_lg_80	Wald „level gering" ≥ 80% Wald pro Zelle aufgrund DKM	Forest „level low" ≥ 80% forest per pixel based on DCM
Wald_Sat_lg	Wald „level gering" aufgrund Satellitenbild (Regionalisierungsdaten)	Forest „level low" based on Satellite Data (Regionalisation Data)

Wald_Sat_lg_80	Wald „level gering" ≥ 80% Wald pro Zelle aufgrund Satellitenbild	Forest „level low" ≥ 80% forest per pixel based on Satellite Data
Wald_Sat_lh	Wald „level hoch" aufgrund Satellitenbild	Forest „level high" based on Satellite Data
Flowaccumulation	Fließakkumulation aufgrund DHM 10m	Flowaccumulation based on DTM 10m
QDisp_lg_GK_lg_fa	Unterirdischer Abfluss - Disposition „level gering" basierend auf Geol. Karte „level gering" und Fließakkumulation	Subsurface flow disposition „level low" based on Geol. Map „level low" and Flowaccumulation
QDisp_lg_GK_lh_fa	Unterirdischer Abfluss - Disposition „level gering" basierend auf Geol. Karte „level hoch" und Fließakkumulation	Subsurface flow disposition „level low" based on Geol. Map „level high" and Flowaccumulation
QDisp_lg_GK_lg_fa_NS_lh	Unterirdischer Abfluss - Disposition „level gering" basierend auf Geol. Karte „level gering", Fließakkumulation und Niederschlag „level hoch"	Subsurface flow disposition „level low" based on Geol. Map „level low", Flowaccumulation and Precipitation "level high"
QDisp_lg_GK_lh_fa_NS_lh	Unterirdischer Abfluss - Disposition „level gering" basierend auf Geologischer Karte „level hoch", Fließakkumulation und Niederschlag „level hoch"	Subsurface flow disposition „level low" based on Geol. Map „level high", Flowaccumulation and Precipitation "level high"
QDisp_lg_GK_lg_fa_NS_lg	Unterirdischer Abfluss - Disposition „level gering" basierend auf Geologischer Karte „level gering", Fließakkumulation und Niederschlag „level gering"	Subsurface flow disposition „level low" based on Geol. Map „level low", Flowaccumulation and Precipitation "level low"
QDisp_lg_GK_lh_fa_NS_lg	Unterirdischer Abfluss - Disposition „level gering" basierend auf Geologischer Karte „level hoch", Fließakkumulation und Niederschlag „level gering"	Subsurface flow disposition „level low" based on Geol. Map „level high", Flowaccumulation and Precipitation "level low"
QDisp_lg_BK_fa	Unterirdischer Abfluss - Disposition „level gering" basierend auf Bodenkarte und Fließakkumulation	Subsurface flow disposition „level low" based on Soil Map and Flowaccumulation
QDisp_lg_BK_fa_NS_lg	Unterirdischer Abfluss - Disposition „level gering" basierend auf Bodenkarte, Fließakkumulation und Niederschlag „level gering"	Subsurface flow disposition „level low" based on Soil Map, Flowaccumulation and Precipitation "level low"

QDisp_lh_fa	Unterirdischer Abfluss - Disposition „level hoch" mittels Feldkartierung und Fließakkumulation	Subsurface flow disposition „level high" based on field mappingand Flowaccumulation
QDisp_lh_fa_NS_lg	Unterirdischer Abfluss - Disposition „level hoch" mittels Feldkartierung, Fließakkumulation und Niederschlag „level gering"	Subsurface flow disposition „level high" based on field mapping, Flowaccumulation and Precipitation "level low"
QDisp_lg_BK_fa_NS_lh	Unterirdischer Abfluss - Disposition „level gering" mittels Bodenkarte, Fließakkumulation und Niederschlag „level hoch"	Subsurface flow disposition „level low" based on Soil Map, Flowaccumulation and Precipitation "level low"
QDisp_lh_fa_NS_lh	Unterirdischer Abfluss - Disposition „level hoch" mittels Feldkartierung, Fließakkumulation und Niederschlag „level hoch"	Subsurface flow disposition „level high" based on field mapping, Flowaccumulation and Precipitation "level high"
NS_lg	Niederschlag „level gering"	Precipitation "level low"
NS_lh	Niederschlag „level hoch"	Precipitation "level high"
HN-DHM10	Hangneigung aufgrund DHM 10m	Slope/inclination based on DTM 10m
Sub_GK_lg	Geologische Grunddisposition „level gering" mittels Substratkonzeptkarte „level gering"	Geological basic disposition „level low" based on conceptual soil map "level low"
Sub_GK_lh	Geologische Grunddisposition „level hoch" mittles Substratkonzeptkarte „level hoch"	Geological basic disposition „level high" based on conceptual soil map „level high"
BK	Grunddisposition aufgrund Bodenkarte	Basic disposition based on Soil Map

Explanation of abbreviations:
Deutsch: DHM: Digitales Höhenmodell (Topographie); DKM: Digitale Katastralmappe
English:DTM: Digital Terrain Model; DCM: Digital Cadastral Map

Tab. 6.2-2: Correlations of landslide distribution with environmental parameters

Parameter	φ-Coefficient	Parameter	φ-Coefficient
HK-DHM10	0.324	QDisp_lg_GK_lh_fa	0.265
HW-DHM10	0.206	QDisp_lg_GK_lg_fa_NS_lh	0.267
VW-DHM10	0.323	QDisp_lg_GK_lh_fa_NS_lh	0.265
Wegenetz_lg_mb	0.292	QDisp_lg_GK_lg_fa_NS_lg	0.253
Wegenetz_lh_mb	0.180	QDisp_lg_GK_lh_fa_NS_lg	0.259
Wegenetz_lg	0.290	QDisp_lg_BK_fa	0.246
Wegenetz_lh	0.298	QDisp_lg_BK_fa_NS_lg	0.236
Wald_DKM_lg_mb	0.385	QDisp_lh_fa	0.214
Wald_Sat_lg_mb	0.425	QDisp_lg_BK_fa_NS_lh	0.263
Wald_DKM_lg	0.155	QDisp_lh_fa_NS_lh	0.222
Wald_DKM_lg_80	0.134	NS_lg	0.067
Wald_Sat_lg	0.238	NS_lh	0.209
Wald_Sat_lg_80	0.301	HN-DHM10	0.257
Wald_Sat_lh	0.263	Sub_GK_lg	0.096
Flowaccumulation	0.261	Sub_GK_lh	0.457
QDisp_lg_GK_lg_fa	0.267	BK	0.178

Tab. 6.2-3: Results of calculation of correlations between all environmental parameters: strength of association is shown as φ-Coefficient for binary parameters, Cramer's V for non-binary parameters.

	HK-DHM10	HW-DHM10	VW-DHM10	Wegenetz_lg_mb¹	Wegenetz_lh_mb¹	Wegenetz_lg¹	Wegenetz_lh¹	Wald_DKM_lg_mb¹	Wald_Sat_lg_mb¹	Wald_DKM_lg¹	Wald_DKM_lg_80¹	Wald_Sat_lg¹	Wald_Sat_lh	Flowaccumulation	QDisp_lg_GK_lg_fa	QDisp_lg_GK_lh_fa	QDisp_lg_GK_lg_fa_NS_lh	QDisp_lg_GK_lh_fa_NS_lh	QDisp_lg_GK_lg_fa_NS_lg	QDisp_lg_GK_lh_fa_NS_lg	QDisp_lg_BK_fa	QDisp_lg_BK_fa_NS_lg	QDisp_lh_fa	QDisp_lg_BK_fa_NS_lh	QDisp_lh_fa_NS_lh	NS_lg	NS_lh	HN-DHM10	Sub_GK_lg	Sub_GK_lh	BK
HK-DHM10	1	0.597	0.515	0.081	0.080	0.082	0.081	0.112	0.089	0.109	0.065	0.094	0.054	0.359	0.363	0.374	0.363	0.374	0.363	0.375	0.357	0.357	0.357	0.360	0.362	0.034	0.054	0.125	0.054	0.191	0.149
HW-DHM10	0.597	1	0.243	0.048	0.042	0.049	0.043	0.129	0.118	0.130	0.080	0.125	0.066	0.361	0.364	0.369	0.363	0.369	0.363	0.371	0.358	0.358	0.356	0.360	0.360	0.024	0.037	0.120	0.043	0.200	0.113
VW-DHM10	0.515	0.243	1	0.132	0.107	0.134	0.109	0.115	0.089	0.111	0.063	0.094	0.051	0.240	0.245	0.257	0.245	0.257	0.243	0.257	0.238	0.240	0.240	0.248	0.251	0.034	0.049	0.147	0.056	0.133	0.160
Wegenetz_lg_mb¹	0.081	0.048	0.132	1	0.777	0.991	0.771	0.060	0.020	0.052	0.021	0.028	0.031	0.077	0.069	0.077	0.069	0.077	0.067	0.075	0.069	0.071	0.075	0.073	0.078	0.066	0.073	0.088	0.049	0.045	0.080
Wegenetz_lh_mb¹	0.080	0.042	0.107	0.777	1	0.768	0.994	0.107	0.070	0.102	0.084	0.076	0.078	0.044	0.042	0.048	0.043	0.048	0.039	0.044	0.039	0.043	0.043	0.042	0.051	0.052	0.078	0.079	0.052	0.036	0.096
Wegenetz_lg¹	0.082	0.049	0.134	0.991	0.768	1	0.773	0.059	0.020	0.051	0.019	0.026	0.030	0.077	0.069	0.078	0.069	0.078	0.067	0.076	0.070	0.072	0.076	0.074	0.080	0.065	0.073	0.088	0.051	0.046	0.079
Wegenetz_lh¹	0.081	0.043	0.109	0.771	0.994	0.773	1	0.109	0.067	0.102	0.083	0.074	0.077	0.046	0.045	0.051	0.045	0.051	0.041	0.047	0.042	0.046	0.051	0.044	0.053	0.052	0.079	0.079	0.053	0.037	0.097
Wald_DKM_lg_mb¹	0.112	0.129	0.115	0.060	0.107	0.059	0.109	1	0.781	0.980	0.710	0.789	0.790	0.061	0.033	0.050	0.033	0.050	0.030	0.047	0.044	0.043	0.074	0.047	0.077	0.084	0.082	0.295	0.061	0.176	0.270
Wald_Sat_lg_mb¹	0.089	0.118	0.089	0.020	0.070	0.020	0.067	0.781	1	0.800	0.671	0.986	0.986	0.062	0.025	0.037	0.025	0.037	0.024	0.034	0.042	0.043	0.070	0.051	0.070	0.083	0.078	0.275	0.049	0.193	0.240
Wald_DKM_lg¹	0.109	0.130	0.111	0.052	0.102	0.051	0.102	0.980	0.800	1	0.725	0.809	0.809	0.064	0.026	0.042	0.026	0.042	0.024	0.040	0.044	0.042	0.069	0.045	0.071	0.083	0.078	0.292	0.059	0.187	0.269
Wald_DKM_lg_80¹	0.065	0.080	0.063	0.021	0.084	0.019	0.083	0.710	0.671	0.725	1	0.677	0.679	0.061	0.020	0.025	0.020	0.025	0.023	0.020	0.025	0.024	0.062	0.062	0.066	0.084	0.101	0.269	0.079	0.197	0.235
Wald_Sat_lg¹	0.094	0.125	0.094	0.028	0.076	0.026	0.074	0.789	0.986	0.809	0.677	1	1	0.061	0.031	0.044	0.031	0.044	0.027	0.040	0.044	0.045	0.076	0.053	0.077	0.084	0.080	0.284	0.053	0.191	0.246
Wald_Sat_lh	0.054	0.066	0.051	0.031	0.078	0.030	0.077	0.790	0.986	0.809	0.679	1	1	0.037	0.021	0.027	0.021	0.027	0.020	0.026	0.029	0.029	0.041	0.032	0.043	0.047	0.048	0.146	0.044	0.113	0.144
Flowaccumulation	0.359	0.361	0.240	0.077	0.044	0.077	0.046	0.061	0.062	0.064	0.061	0.061	0.037	1	0.657	0.638	0.657	0.638	0.670	0.644	0.696	0.675	0.655	0.639	0.614	0.029	0.027	0.067	0.034	0.251	0.122
QDisp_lg_GK_lg_fa	0.363	0.364	0.245	0.069	0.042	0.069	0.045	0.033	0.025	0.026	0.020	0.031	0.021	0.657	1	0.771	1	0.772	0.888	0.775	0.707	0.707	0.697	0.661	0.666	0.049	0.045	0.073	0.065	0.221	0.127
QDisp_lg_GK_lh_fa	0.374	0.369	0.257	0.077	0.048	0.078	0.051	0.050	0.037	0.042	0.025	0.044	0.027	0.638	0.771	1	0.771	0.998	0.730	0.915	0.690	0.697	0.692	0.701	0.706	0.049	0.046	0.094	0.052	0.205	0.134
QDisp_lg_GK_lg_fa_NS_lh	0.363	0.363	0.245	0.069	0.043	0.069	0.045	0.033	0.025	0.026	0.020	0.031	0.021	0.657	1	0.771	1	0.772	0.888	0.775	0.707	0.707	0.697	0.661	0.666	0.049	0.045	0.073	0.065	0.221	0.127
QDisp_lg_GK_lh_fa_NS_lh	0.374	0.369	0.257	0.077	0.048	0.078	0.051	0.050	0.037	0.042	0.025	0.044	0.027	0.638	0.772	0.998	0.772	1	0.730	0.915	0.690	0.697	0.706	0.700	0.706	0.049	0.046	0.052	0.205	0.094	0.134
QDisp_lg_GK_lg_fa_NS_lg	0.363	0.363	0.243	0.067	0.039	0.067	0.041	0.030	0.024	0.024	0.023	0.027	0.020	0.670	0.888	0.730	0.888	0.730	1	0.753	0.688	0.687	0.682	0.638	0.641	0.053	0.037	0.071	0.063	0.224	0.121
QDisp_lg_GK_lh_fa_NS_lg	0.375	0.371	0.257	0.075	0.044	0.076	0.047	0.047	0.034	0.040	0.020	0.040	0.026	0.644	0.775	0.915	0.775	0.915	0.753	1	0.694	0.704	0.698	0.678	0.685	0.050	0.038	0.049	0.209	0.093	0.130
QDisp_lg_BK_fa	0.357	0.358	0.238	0.069	0.039	0.070	0.042	0.044	0.042	0.044	0.025	0.044	0.029	0.696	0.707	0.690	0.707	0.690	0.688	0.694	1	0.881	0.752	0.710	0.671	0.037	0.033	0.068	0.052	0.243	0.130
QDisp_lg_BK_fa_NS_lg	0.357	0.358	0.240	0.071	0.043	0.072	0.046	0.043	0.043	0.042	0.024	0.045	0.029	0.675	0.707	0.697	0.707	0.697	0.687	0.704	0.881	1	0.744	0.739	0.687	0.057	0.047	0.070	0.057	0.240	0.133
QDisp_lh_fa	0.357	0.356	0.240	0.075	0.043	0.076	0.051	0.074	0.070	0.069	0.062	0.076	0.041	0.655	0.697	0.692	0.697	0.706	0.682	0.698	0.752	0.744	1	0.667	0.728	0.036	0.031	0.068	0.044	0.236	0.137
QDisp_lg_BK_fa_NS_lh	0.360	0.360	0.248	0.073	0.042	0.074	0.044	0.047	0.051	0.045	0.062	0.053	0.032	0.639	0.661	0.701	0.661	0.700	0.638	0.678	0.710	0.739	0.667	1	0.757	0.055	0.061	0.072	0.052	0.233	0.140
QDisp_lh_fa_NS_lh	0.362	0.360	0.251	0.078	0.051	0.080	0.053	0.077	0.070	0.071	0.066	0.077	0.043	0.614	0.666	0.706	0.666	0.706	0.641	0.685	0.671	0.687	0.728	0.757	1	0.054	0.054	0.073	0.046	0.227	0.148
NS_lg	0.034	0.024	0.034	0.066	0.052	0.065	0.052	0.084	0.083	0.083	0.084	0.084	0.047	0.029	0.049	0.049	0.049	0.049	0.053	0.050	0.037	0.057	0.036	0.055	0.054	1	0.520	0.090	0.165	0.065	0.105
NS_lh	0.054	0.037	0.049	0.073	0.078	0.073	0.079	0.082	0.078	0.078	0.101	0.080	0.048	0.027	0.045	0.046	0.045	0.046	0.037	0.038	0.033	0.047	0.031	0.061	0.054	0.520	1	0.085	0.169	0.071	0.170
HN-DHM10	0.125	0.120	0.147	0.088	0.079	0.088	0.079	0.295	0.275	0.292	0.269	0.284	0.146	0.067	0.073	0.094	0.073	0.052	0.071	0.049	0.068	0.070	0.068	0.072	0.073	0.090	0.085	1	0.113	0.298	0.135
Sub_GK_lg	0.054	0.043	0.056	0.049	0.052	0.051	0.053	0.061	0.049	0.059	0.079	0.053	0.044	0.034	0.065	0.052	0.065	0.205	0.063	0.209	0.052	0.057	0.044	0.052	0.046	0.165	0.169	0.113	1	0.310	0.066
Sub_GK_lh	0.191	0.200	0.133	0.045	0.036	0.046	0.037	0.176	0.193	0.187	0.197	0.191	0.113	0.251	0.221	0.205	0.221	0.094	0.224	0.093	0.243	0.240	0.236	0.233	0.227	0.065	0.071	0.298	0.310	1	0.045
BK	0.149	0.113	0.160	0.080	0.096	0.079	0.097	0.270	0.240	0.269	0.235	0.246	0.144	0.122	0.127	0.134	0.127	0.134	0.121	0.130	0.130	0.133	0.137	0.140	0.148	0.105	0.170	0.135	0.066	0.045	1

¹ binary variables   ≥ 0.300   ≥ 0.700

A general strategy was developed for successively integrating different parameters for the statistical modelling, which followed the following principles:

1. At first only "level low" parameters are considered, followed by "level high parameters".

2. Variables with high correlation to the distribution of landslides are integrated first.

3. The number of variables is extended successively one by one to find out their influence. If there are two or more variables of equal level all of them are tested. The modelling is then continued subsequently with the variable showing the best validation results.

4. Following the step-by-step "level low" and "level high" modelling the best result according to the validation is selected ("best_lg" and "best_lh" respectively). From these results single parameter maps are eliminated or replaced with other maps as one map used with different combinations of maps may contribute to the result to varying degrees. If a variable does not improve the result it will not be used subsequently.

5. The "best_lg" and the "best_lh" results are as well re-calculated with the regionalisation data.

In Fig. 6.2-1 the parameter tree with all spatial datasets used in the modelling procedure is presented. Here "level low" parameter maps (Chapter 5) are presented in yellow, "level high" in red boxes. The orange boxes are "level middle" parameter maps, which have to be considered as intermediate steps, not used for modelling.

When considering the parameter maps used for modelling, it was important to choose only parameters, whose process-oriented connection to slope instability can be explained physically. The tree shows 9 main branches indicated by numbers 1 - 9, each one representing one important process-orientated aspect for the development of mass movements. These 9 branches are forest (1), roads (2), geosphere-information (3), precipitation (4), subsurface flow (5), slope inclination (6), vertical curvature (7), horizontal curvature (8) and curvature classification (9). Within the main branches, there exist several sub-branches, which show the variations of this particular parameter. The rule, which had to be obeyed when varying the parameter combinations according to the strategy of parameter integration, was that in each run, only one parameter per main branch was allowed. In this way it was ensured that one process-orientated aspect is not emphasized too much.
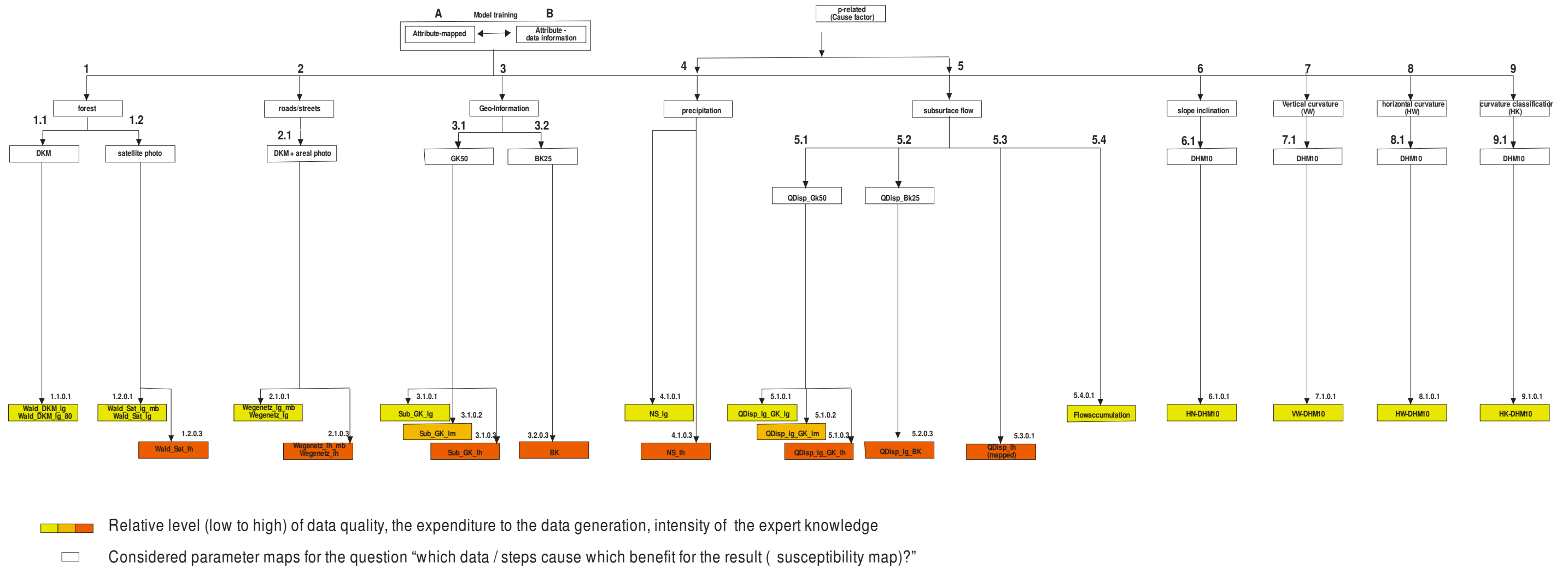
Fig. 6.2-1: Parameter tree of available spatial datasets with regard to type of information and processing

7. Methods Modelling Landslide Disposition

7.1. Validation Methods (GBA)

Suitable validation methods are required in order to provide a satisfactory answer to the central question of the Adaptslide Project: "Which modelling technology/method and parameter map/combination of parameter maps produces which improvements in susceptibility maps. Only then is it possible to make meaningful comparisons between individual results. The validation-method issue is not a trivial one, because full knowledge of all past (and future) mass movements in one area is impossible. Several different validation methods have therefore been developed over a period of several decades in order to model landslide susceptibility maps. However, each method has its advantages and disadvantages. Thus, for the Adaptslide Project, different validation methods were used in order to make as objective as possible a statement on the quality of a susceptibility map. When selecting the validation methods used, there was, whenever possible, an attempt to counterbalance the disadvantages of one method with the advantages of another. At the GBA, that effort also led to the development of an additional, own validation method.

In general, a distinction can be made between the validation of training data ("success rate" according to Chung and Fabbri 1999) and the validation of test data ("prediction rate" according to Chung and Fabbri 1999; Chapter 6.1.2). The modelling is calculated using the training data, whereas the test data is control data that is not used in modelling. The test data can be differentiated both spatially and time-related from the training data. However, the validation of training data indicates only how well the model reproduces an already known distribution of mass movements ("goodness of fit"). The validation of test data is more important for assessing the quality of the result, because it shows how well the model performs when used with independent and unknown data. So the "goal of network training is not to learn an exact representation of the training data itself, but rather to build a statistical model of the process that generates the data" (Bishop 1995). This is called the model's generalization capability and is checked through validation of the test data. This validation therefore indicates how well the model's results can be applied to areas where data on mass movements is lacking, or how well potential future mass movements can be identified using the model.

When neural networks are used, the validation of training and validation data is done separately for reasons associated with modelling technology, the validation data being used first as a measure of the model performance. Test data are used only to check the final result. Finally the comparison of the validation results of different modelling technologies (logistic regression, neural networks, weight of evidence and SINMAP) was performed by the test data (Chapter 7.2. - 7.5).

A brief description of the validation methods used for the project, along with their advantages and disadvantages, is given in the Chapters 7.1.1 - 7.1.6.

7.1.1. Validation according to the "Spatial Prediction Model" Approach (Chung and Fabbri 1999, 2003)

This approach (Fig. 7.1.1-1) is probably the validation method that is currently most often used and is represented in the form of an x/y diagram. All pixels in the results are placed in descending order along the x-axis (axis of abscissa), according to their degree of susceptibility. The y-axis (axis of ordinates) indicates the cumulated percentage of mapped mass movements for the area in the respective susceptibility class. The gradient of the curve produced in this manner corresponds to the "ratio of effectiveness", which indicates the predictive power of a susceptibility class, and which can also be seen as a kind of standardized indicator of mass-movement density within a specific susceptibility class. Low gradients are therefore the aim when there are low susceptibility values, and steep gradients when there are high susceptibility values. In graphic terms, a result improves the farther the curve lies toward the upper left. In simpler terms, instead of the curve, the area under the curve (AUC) can also be used as the validation measurement, even though this value cannot of course reproduce the run of the entire curve.

This validation approach has the following advantages: the standardized measurement of mass-movement density is more meaningful than the simple number of mass movements per class, which is strongly dependent on the spatial extent of the susceptibility class. Furthermore, the method does not depend on a threshold value. This is an advantage because the threshold value (between stable and unstable) does not have to be fixed in advance. It can be determined on the basis of the validation and the use of the model in a specific context (Begueria 2006). A second, and even greater advantage is that validations without threshold values in the case of the same or similar model runs (particularly for neural networks) are much more stable with respect to fluctuations/uncertainties in results due to model technology than are the validation methods that refer to threshold values. With validation methods that are dependent on threshold values, even slight fluctuations around the threshold value can heavily influence the validation result, whereas methods that are independent of threshold values remain largely unaffected. And finally, with standardized density measurement and independence of a threshold value, comparisons can be made between the results of different modelling technologies.

This method has the following disadvantages: because of its independency on defined disposition classes and threshold values, poor results (for example, those with few mass movements in high classes or many mass movements in low classes) can be validated as "very good" due to displacement of the susceptibility classes. Furthermore, a reduction or enlargement of the area under investigation can completely displace the susceptibilities on the x-axis, which can result in a major change in the validation results for the same mass-movement points. As a consequence, several different areas can no longer be compared, because if they are, a high disposition class in one area might correspond to a low disposition class in another area. Furthermore, the method produces only a summarized area-wide validation, so that poor results in individual sub-areas can be compensated for a good result in another sub-area. And finally, using this method, only the mass-movement points (= true positives and false positives) are assessed (y-axis), whereas the non mass-movement points (= true negatives and false negatives) are included only indirectly via the x-axis.
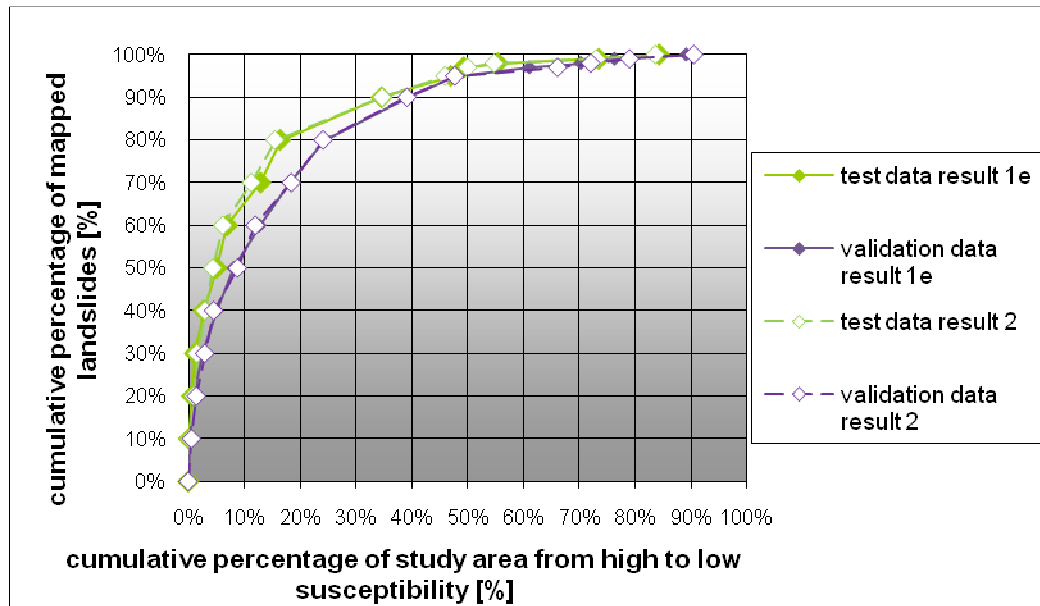
Fig. 7.1.1-1: Validation according to Chung & Fabbri (1999)

7.1.2. Recognition Rate (=Sensitivity)

This validation method simply reproduces the percentage of correctly classified landslides (= true positives) relative to the total number of landslides (= true positives and false positives, Begueria 2006). This requires the specification of a threshold value for the transition from stable to unstable, which is usually assumed to be 0.5 (as it is for Adaptslide).

The advantage of this method is that it is very simple to grasp, calculate and employ (particularly for comparative purposes), because it consists of only one validation value. In addition, this method also relates to the disposition classes, so that susceptibility maps with many mass movements in low classes or few mass movements in high classes always have poor validation.

The method has the following disadvantages: because it is dependent on a - threshold value, that value must be defined in advance. On the whole, this method involves major simplification, and with the same or similar model runs (particularly in the case of neural networks), it is much more susceptible to fluctuations/uncertainties that are due to modelling technology. In addition, this method incorporates only the number of mass movements per class, not the more meaningful mass-movement density. Furthermore, this method relates only to the mass movements and enables only a summarized area-wide validation (see above).

7.1.3. Distribution of Landslides over Susceptibility Classes

This widely used method provides a (cumulative) presentation of mass movements in each susceptibility class (Fig. 7.1.3-1). A good result is obtained when there are few landsides in the low classes (corresponding to the steep lines) and many landslides in the high classes (corresponding to the flat lines). Roughly speaking, this means that a result is better the farther the curve runs toward the upper left.
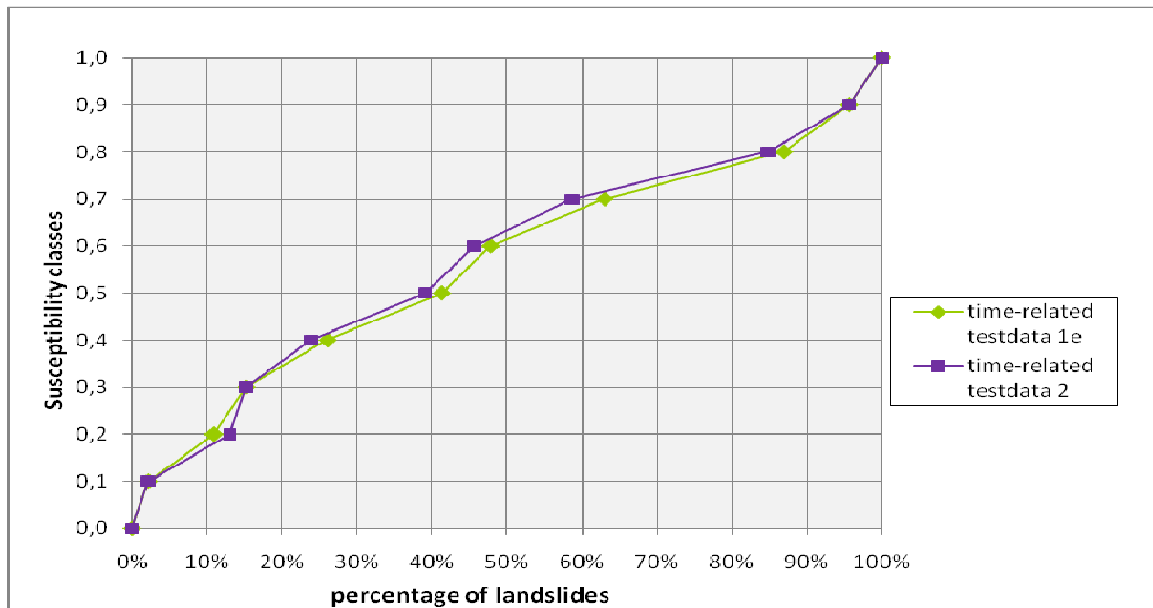
Fig. 7.1.3-1: Cumulative distribution of landslides over the susceptibility classes of time-related test data 1e and 2

The advantages of this method are that it refers to the susceptibility classes, it is highly descriptive, and that, aside from the definition of as many susceptibility classes as possible, it is independent of threshold values. The method therefore clearly provides more differentiation and is less subject to fluctuation than the recognition rate, which is incorporated into the method in any case.

The major disadvantage of this method is that it is not easily quantifiable (AUC is not used), which therefore leaves great scope for subjective interpretation. In addition, it does not include mass-movement density. Furthermore, the method refers only to mass movements and enables only a summarized area-wide validation (see above).

7.1.4. Receiver Operating Characteristic (ROC)

The ROC method presents sensitivity and specificity together in one validation. Specificity represents the correctly classified landslide-free pixels (= true negatives) in relation to the total number of landslide-free pixels (= true negatives and false negatives). In this validation, the threshold value moves in the histogram of landslides/no-landslides distribution from the lowest to the highest susceptibilities (Fig. 7.1.4-1), a point being entered on the ROC curve at every threshold value (Fig. 7.1.4-2). If the threshold value is low (to the left on the histogram), a high number of true positives will be achieved, but also a low number of true negatives. The opposite applies with a high threshold value (Begueria 2006). The result improves, the farther the curve lies to the upper right. Here too, the AUC can mostly be used as a validation figure.
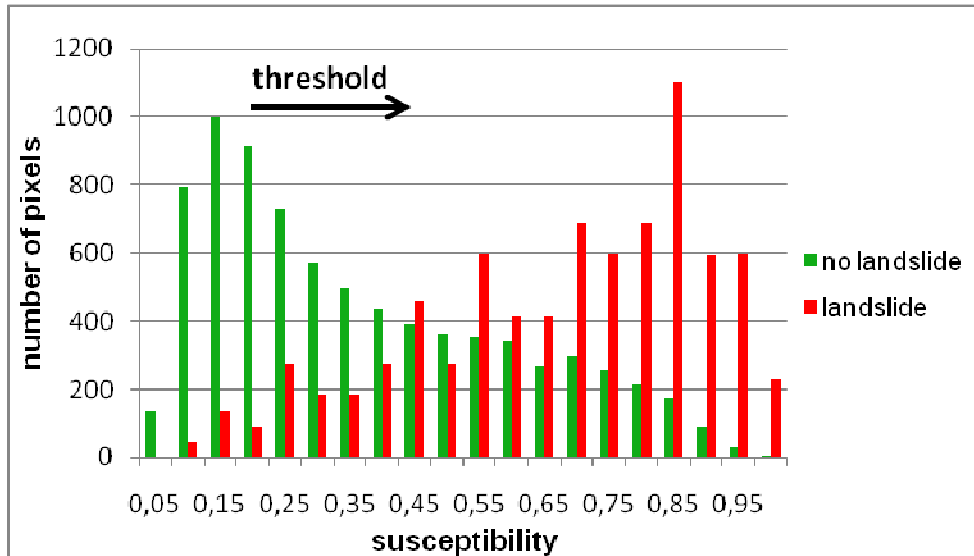
Fig. 7.1.4-1: ROC – Histogram of train data of result 1e: landslide / no-landslide pixels
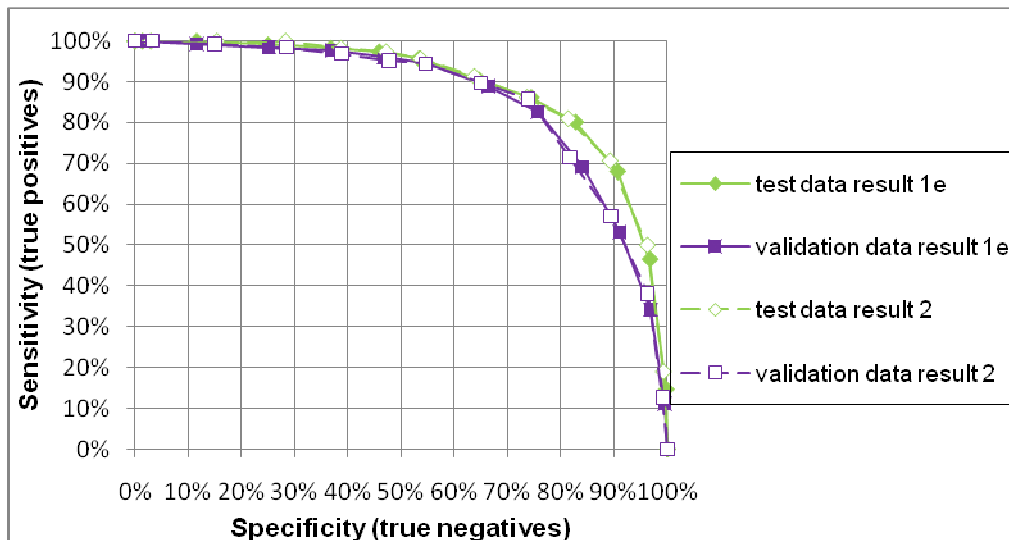
Fig. 7.1.4-2: Curve of Receiver Operating Characteristic (ROC)

The advantage of ROC compared to the other validation methods described is that both mass movements and non-mass movements can be taken into account in the validation. Other advantages include the method's independence from threshold values and the herefrom resulting stability concerning fluctuations at same or similar model runs (particularly in the case of neural networks, see above).

The disadvantages of this validation method are that the susceptibility classes are only indirectly included, density is not really incorporated, and it enables only a summarized area-wide validation.

7.1.5. GBA Method

The GBA method is, in principle, a further development of the recognition rate, or of the "distribution of landslides over susceptibility classes". The former has the disadvantage, among others, that it shows only one threshold value (see above), and

the latter that it is difficult to quantify (see above). The GBA method, which is also based on the "distribution of landslides over susceptibility classes", tries to overcome these disadvantages. This is done by calculating one value for the high and one value for the low susceptibilities, these two values then being added together. This splitting into two values makes it possible to analyze model quality in isolation, i.e. for stable areas only or for unstable areas only. The values used are the gradient angle of the upper or lower classes in the mass movement distribution, the quality of the results increasing with an increasing angle.

This method has the following advantages: it is based on susceptibility classes, it is not dependent on individual threshold values and is therefore reasonably stable with respect to fluctuations at the same or similar model runs (however not as stable as the method according to Chung & Fabbri (1999) and ROC), and it enables consideration in isolation of stable and unstable areas.

The disadvantages of this method are that it incorporates only mass-movement points, mass-movement density is not taken into account, and it too only enables a summarized area-wide validation.

7.1.6. Use of Validation Methods

The way in which the different validation methods described above are combined in order to produce an overall validation are described in the respective chapters on modelling (cf. Chapter 7.2, 7.3, 7.4 and 7.5). The validation methods according to Chung & Fabbri (1999) and the ROC are used in order to compare the different modelling methods.

7.2. Modelling and Validation of Susceptibility Maps by Using Neural Networks (GBA)

7.2.1. Fundamentals

Neural networks

Neural networks are particularly suitable for modelling when the functional context of a plurality of variables is not explicitly known and/or it is complex and not linear. The multilayer perceptron used here consists of an input layer, a hidden layer, and an output layer (Fig. 7.2.1-1). In the input layer, variables are added to the network. In the output layer, the information "mass movement yes/no" is defined for the network, or susceptibility is calculated. In the layers there are nodes (containing an activation function) connected by synapses (weights are found here).
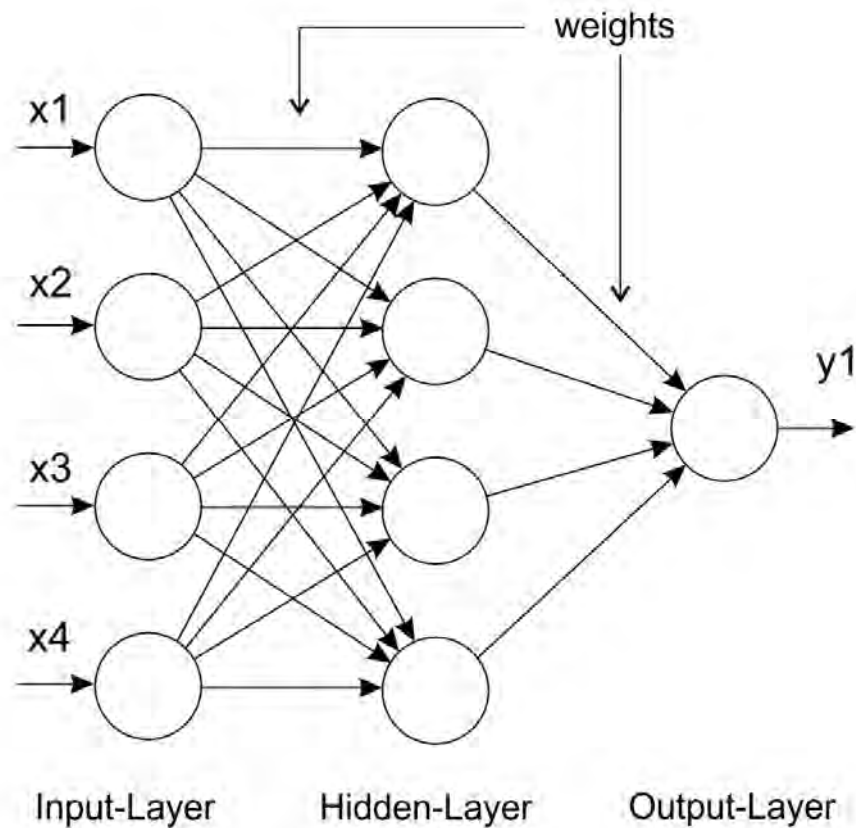
Fig. 7.2.1-1: Schematic representation of a multilayer perceptron

During the training phase, the network is trained through given network's input variables and given output [the known mass-movement information (yes/no)]. The network then searches for an ideal connection between input variables and mass-movement data by optimizing the weights. This optimization is done through minimization of the MS error (mean square error between predefined and calculated output), the calculated output representing the susceptibility within the range [0, 1]. With the help of a learning algorithm [here delta bar delta (Bishop 1995)], there is a search for the minimum error surface. For training, the data set must be split into training and validation data (Chapter 6.1.2), the network being trained with training data and being validated parallel by the validation data, which shows the model performance. The ideal weight is reached when the error curve of the validation data displays its absolute minimum, this is the moment when the training is stopped. In order to optimize performance during training, the user can vary the number of hidden layers, the number of nodes, the learning algorithm, or various network parameters.

The network generated in this way is saved and led to the test phase, in which independent test data (Chapter 6.1.2 and 7.1) is now added to the network. This data again contains the input variables, but no predefined output. The network now calculates the output (= susceptibility) independently, and through comparison of the calculated output with the known output, the performance of the network and the capability of generalization (Chapter 7.1) can be tested (Smith 1993). Finally, the

network for the AdaptSlide project is fed with the regionalisation data (Chapter 6.1.2) without predefined output in order to produce the 50 m raster map.

Validation strategy for neural networks

When modelling with neural networks, there must be continuous attention to the data set used for validation. This is highly important, because the selection of the best result depends on it. The validation data running synchronously, is therefore also used during the training phase. However there are two different approaches to the comparison of results that are produced using different parameter constellations: the first approach, which is widely used, stipulates that the validation data must always be used here as well, whereas the independent test data is used only once, at the very end, in order to validate the final results. It is assumed that the test data is genuinely independent only in this form, and that if there has been repeated previous use of the data, it would have been indirectly incorporated into the selection of results, thereby losing its independence.

The second approach applies the use of the test data when comparing the results of different parameter constellations. It is assumed that only the test data is genuinely independent and therefore suitable for use during objective comparison of results. The validation data, on the other hand, indirectly influences training, as it has already been used during the training phase as a stop criterion. It is therefore dependent data and as such not suitable for independent comparison of results.

Because both approaches have their pros and cons, the first validation approach was ultimately chosen for the validation of neural networks due to its wider use. It was ultimately necessary to use the second approach to compare the results of a plurality of modelling technologies, because the other models used for the project were calculated without validation data. It was therefore impossible to avoid some duplication of methodology when validating the results of neural networks.

In order to determine when the validation of a result can be assessed as better, worse, or equally as good as others, it was necessary to determine the limits within which a result can be considered reproducible and how, in turn, the uncertainty of results affect the results of different validation methods. This is not a trivial issue with regard to neural networks, because this method, due to the constantly different, random initialization of the initial weights with the same parameter settings, always produces slightly different results. Numerous test runs were therefore carried out with the same parameter settings before actual modelling, in order to obtain threshold values for the margin of fluctuation in the validation values of a result with the same settings for each validation method (Chapter 7.1). If, during modelling, the differences in validation values of two results lay within these threshold values, the results were assessed as equally good; if they lay outside these values, the result was deemed better/worse.

As described before, there are different validation methods, each with certain advantages and disadvantages. In order to obtain the most meaningful validation possible, which takes into account and equalizes various method-specific aspects, these validation methods are combined into a validation strategy. To that end, an unequivocal, clearly applicable validation scheme was developed for validation of the results obtained using neural networks. This is a multi-stage, progressive procedure in which there is a transition to the next validation stage only when the validation criterion of the stage in question has shown that both of the results compared are

equally good, taking into account the respective margin of fluctuation (model uncertainty).

The validation scheme, which is implemented primarily with validation data, is explained below on the basis of the following prior considerations: Because the recognition rate displays major fluctuations due to the use of only one threshold-value criterion, the recognition rate was used only as a first criterion in the sense of a minimum requirement at a low level (>70%). If this criterion was not met, the result was immediately rejected. In the second validation stage, therefore, the recognition rate was only incorporated as one sub-criterion when there were differences of > 10%. When there were smaller differences, it was not taken into account.

The validations according to Chung & Fabbri (1999), the ROC and the method developed by GBA were considered particularly significant, so these validations were taken into account in the second decision-step. Since it turned out that validation according to Chung & Fabbri (1999) and ROC always produced quite similar results, these methods were combined into one sub-criterion. The GBA method was then chosen as second sub-criterion. Only when the two sub-criteria produce the same results, the third validation step is applied, in which the validation results of the time-related data are compared. These are subjected to purely visual examination (without AUC) due to the low number of points, with the aid of the two sub-criteria: "validation according to Chung & Fabbri (1999)" and "cumulative mass-movement distribution across the susceptibility classes."

If both results can still be assessed as equally good, the test data is compared during a fourth validation stage in accordance with the second validation step. If no better/poorer result is obtained after applying the complete step-wise strategy for validation, preference will be given, when comparing two parameter maps with the same theme, to the map whose preparation involved the least effort. The strategy for validation with its individual validation steps can be summarized as follows:

1st step: decision criterion: recognition rate > 70%, otherwise rejection

2nd step: decision criterion: comparison of sub-criteria

- Recognition rate (only in the case of differences > 10%)

- Validation according to Chung & Fabbri (1999) + ROC

- GBA method

3rd step: decision criterion: time-related data ["Mass-movement distribution across susceptibility classes," validation according to Chung & Fabbri (1999)].

4th step: decision criterion: Test data according to the scheme in the 2nd stage

5th step: decision criterion: parameter map involving less effort

7.2.2. Results of Modelling and Modelling Validation

7.2.2.1 Modelling Results using "Level Low" Parameter Maps

The strategy for model integration of parameter maps described in Chapter 6.2 result in 31 "level low" model runs for modelling by means of neural networks, which are listed, including the respective parameter combinations, in Tab. 7.2.2.1-1. The parameter combinations of individual network runs do not necessarily correspond to the parameter combinations of runs with the other modelling methods used in the project (Chapter 7.3, 7.4. and 7.5). In modelling with neural networks, run 10 was selected, after the first 11 "level low" runs, as the best "level low" run ("best_lg"), so that all subsequent "level low" runs were variations of the parameter combinations of run 10 (Chapter 6.2).

Tab. 7.2.2.1-1 part 1: Model runs "level low" and the parameter maps used (abbreviation of parameter maps, see Tab. 6.2-1)

# Run	Parameter maps used	Relation to other runs
Run 1	Wald_DKM_lg_mb, VW-DHM10, HN-DHM10	
Run 2	Wald_Sat_lg_mb, VW-DHM10, HN-DHM10	as Run 1, but using Wald_Sat_lg_mb instead of Wald_DKM_lg_mb
Run 3	Wald_Sat_lg_mb, VW-DHM10, HN-DHM10, Wegenetz_lg_mb	as Run 2, but adding Wegenetz_lg_mb
Run 3dkm	Wald_DKM_lg_mb, VW-DHM10, HN-DHM10, Wegenetz_lg_mb	as Run 3, but using Wald_DKM_lg_mb instead of Wald_Sat_lg_mb
Run 4	Wald_Sat_lg_mb, VW-DHM10, HN-DHM10, Wegenetz_lg_mb, Flowaccumulation	as Run 3, but adding Flowaccumulation
Run 5	Wald_Sat_lg_mb, VW-DHM10, HN-DHM10, Wegenetz_lg_mb, QDisp_lg_GK_lg_fa	as Run 4, but using QDisp_lg_GK_lg_fa instead of Flowaccumulation
Run 6	Wald_Sat_lg_mb, VW-DHM10, HN-DHM10, Wegenetz_lg_mb, QDisp_lg_GK_lh_fa	as Run 3, adding QDisp_lg_GK_lh_fa, as Run 4, but using QDisp_lg_GK_lh_fa instead of Flowaccumulation; as Run 5, but using QDisp_lg_GK_lh_fa instead of QDisp_lg_GK_lg_fa
Run 7	Wald_Sat_lg_mb, HK-DHM10, HN-DHM10, Wegenetz_lg_mb, QDisp_lg_GK_lg_fa	as Run 5, but using HK-DHM10 instead of VW-DHM10
Run 9	Wald_Sat_lg_mb, HK-DHM10, VW-DHM10, HN-DHM10, Wegenetz_lg_mb, QDisp_lg_GK_lg_fa	as Run 5, but adding HK-DHM10
Run 10	Wald_Sat_lg_mb, VW-DHM10, HN-DHM10, Wegenetz_lg_mb, QDisp_lg_GK_lg_fa, Sub_GK_lg	as Run 5, but adding Sub_GK_lg
Run 11	Wald_Sat_lg_mb, VW-DHM10, HN-DHM10, Sub_GK_lg	as Run 2, but adding Sub_GK_lg
Run 12	Wald_DKM_lg_mb, VW-DHM10, HN-DHM10, Wegenetz_lg_mb, QDisp_lg_GK_lg_fa, Sub_GK_lg	as Run 10a, but using Wald_DKM_lg_mb instead of Wald_Sat_lg_mb
Run 13	VW-DHM10, HN-DHM10, Wegenetz_lg_mb, QDisp_lg_GK_lg_fa, Sub_GK_lg	as Run 10, without Wald_Sat_lg_mb
Run 14	Wald_Sat_lg_mb, VW-DHM10, HN-DHM10, Wegenetz_lg_mb, QDisp_lg_GK_lh_fa, Sub_GK_lg	as Run 10, but using QDisp_lg_GK_lh_fa instead of QDisp_lg_GK_lg_fa
Run 15	Wald_Sat_lg_mb, VW-DHM10, HN-DHM10, Wegenetz_lg_mb, Sub_GK_lg	as Run 10, but without QDisp_lg_GK_lg_fa
Run 16	Wald_Sat_lg_mb, VW-DHM10, HN-DHM10, QDisp_lg_GK_lg_fa, Sub_GK_lg	as Run 10, but without Wegenetz_lg_mb
Run 17= Run 18	Wald_Sat_lg_mb, HN-DHM10, Wegenetz_lg_mb, QDisp_lg_GK_lg_fa, Sub_GK_lg	as Run 10, but without VW-DHM10
Run 19 = Run 26	Wald_Sat_lg_mb, VW-DHM10, HN-DHM10, Wegenetz_lg_mb, QDisp_lg_GK_lg_fa, Sub_GK_lg, HK-DHM10	as Run 10, but adding HK-DHM10

Tab. 7.2.2.1-1 part 2: Model runs "level low" and the parameter maps used (abbreviation of parameter maps, see Tab. 6.2-1)

# Run	Parameter maps used	Relation to other runs
Run 20	Wald_Sat_lg_mb, VW-DHM10, HN-DHM10, Wegenetz_lg_mb, QDisp_lg_GK_lg_fa, Sub_GK_lg, NS_LG	as Run 10, but adding NS_lg
Run 21	Wald_Sat_lg_mb, VW-DHM10, HN-DHM10, Wegenetz_lg_mb, Sub_GK_lg, QDisp_lg_GK_lg_fa_NS_lg	as Run 10, but using QDisp_lg_GK_lg_fa_NS_lg instead of QDisp_lg_GK_lg_fa
Run 22	Wald_Sat_lg_mb, VW-DHM10, HN-DHM10, Wegenetz_lg_mb, Sub_GK_lg, QDisp_lg_GK_lh_fa_NS_lg	as Run 14, but using QDisp_lg_GK_lh_fa_NS_lg instead of QDisp_lg_GK_lh_fa; as Run 21 but using QDisp_lg_GK _lh_fa_NS_lg instead of QDisp_lg_GK_lg_fa_NS_lg
Run 23	Wald_Sat_lg_mb, VW-DHM10, HN-DHM10, Wegenetz_lg_mb, Sub_GK_lg, QDisp_lg_GK_lh_fa, NS_LG	as Run 10, but using QDisp_lg_GK_lh_fa + NS_lg instead of QDisp_lg_GK_lg_fa; as Run 20 but using QDisp_lg_GK_lh_fa instead of QDisp_lg_GK_lg_fa; as Run 14, but adding NS_lg
Run 24	Wald_Sat_lg_mb, VW-DHM10, HN-DHM10, Wegenetz_lg_mb, Sub_GK_lg, QDisp_lg_BK_fa	as Run 10, but using QDisp_lg_BK_fa instead of QDisp_lg_GK_lg_fa
Run 25	Wald_Sat_lg_mb, VW-DHM10, HN-DHM10, Wegenetz_lg_mb, Sub_GK_lg, QDisp_lg_BK_fa_NS_lg	as Run 10, but using QDisp_lg_BK_fa_NS_lg instead of QDisp_lg_GK_lg_fa; Run 24 using QDisp_lg_BK_fa_NS_lg instead of QDisp_lg_BK_fa
Run 27	Wald_Sat_lg_mb, VW-DHM10, HN-DHM10, Wegenetz_lg_mb, Sub_GK_lh, QDisp_lg_GK_lh_fa, HK-DHM10	as Run 10, but using QDisp_lg_GK_lh_fa instead of QDisp_lg_GK_lg_fa, Sub_GK_lh instead of Sub_GK_lg + HK_DHM10; as Run 19 but using QDisp_lg_GK_lh_fa instead of QDisp_lg_GK_lg_fa, Sub_GK_lh instead of Sub_GK_lg; as Run 6 but adding HK_DHM10 and Sub_GK_lh
Run 28	Wald_Sat_lg_mb, VW-DHM10, HN-DHM10, Wegenetz_lg_mb, QDisp_lg_GK_lg_fa, Sub_GK_lg, HK-DHM10, NS_lg	as Run 19, but adding NS_lg; as Run 10, but adding HK-DHM10 and NS_lg
Run 29	Wald_Sat_lg, VW-DHM10, HN-DHM10, Wegenetz_lg, QDisp_lg_GK_lg_fa, Sub_GK_lg	as Run 10, but using Wegenetz_lg instead of Wegenetz_lg_mb and Wald_Sat_lg instead of Wald_Sat_lg_mb
Run 30	Wald_Sat_lg, VW-DHM10, HN-DHM10, Wegenetz_lg, Sub_GK_lg, QDisp_lg_BK_fa	as Run 24, but using Wegenetz_lg instead of Wegenetz_lg_mb and Wald_Sat_lg instead of Wald_Sat_lg_mb; as Run 10, but using QDisp_lg_BK_fa instead of QDisp_lg_GK_lg_fa, Wegenetz_lg instead of Wegenetz_lg_mb and Wald_Sat_lg instead of Wald_Sat_lg_mb
Run 31	Wald_Sat_lg, VW-DHM10, HN-DHM10	as Run 2, but Wald_Sat_lg instead of Wald_Sat_lg_mb; as Run 10, but without Wegenetz_lg_mb, QDisp_lg_GK_lg_fa, Sub_GK_lg and Wald_Sat_lg instead of Wald_Sat_lg_mb
Run 32	Wald_Sat_lg, VW-DHM10, HN-DHM10, Wegenetz_lg_mb, QDisp_lg_GK_lg_fa, Sub_GK_lg	as Run 10, but using Wald_Sat_lg instead of Wald_Sat_lg_mb

The following discussion describes the results of the model runs carried out using "level low" parameter maps. The results are evaluated based on the validation strategy presented in Chapter 7.2.1 (Tab. A1 in Annex) and compared (validation comparisons: Tab. A2 in the Annex). In comparing results, particular attention is given to the issue of whether a new parameter map leads to improvement or deterioration in modelling validation results in the sense of the general question asked by the Adaptslide project ("Which effort produces which benefit?"). For this reason, the result comparisons are also summarized by each new involved parameter map. In addition, there is discussion of the changes in susceptibility map

and parameter influences on the model that are brought about by the new parameter map.

Forest "level low" (*Wald_DKM_lg_mb, Wald_Sat_lg_mb*)

Comparison of the parameter maps *forest "level low":*

- Forest „level low" based on Satellite Data and field mapping (Wald_Sat_lg_mb)

- Forest „level low" based on digital cadastral map and field mapping (*Wald_DKM_lg_mb*)

The parameter *forest* was generally a very important parameter for modelling, because its integration invariably produced clear improvement in the model performance. The reason for that was that with this parameter, there was a reduction in susceptibilities inside forest, and an increase in susceptibilities outside forest. Both of the "level low" forest parameter maps used produced equally good results. Thus, for the following model calculations employing other parameter map combinations, there was a decision, based on the criterion "relevance to event August 2005," in favour of *forest map based on of satellite data.*

The parameter *forest* was generally a very important parameter for modelling, because its integration invariably produced clear improvement in the model performance. The reason for that was that with this parameter, there was a reduction in susceptibilities inside forest, and an increase in susceptibilities outside forest. Both of the "level low" forest parameter maps used produced equally good results. Thus, for the following model calculations employing other parameter map combinations, there was a decision, based on the criterion "relevance to event August 2005," in favour of *forest map based on of satellite data.*

First, the two parameter maps for forest had to be compared by means of runs 1 and 2, where run 1 incorporated *Wald_DKM_lg_mb* and run 2 *Wald_Sat_lg_mb*. In addition to forest, both runs included only the 2 additional parameters profile curvature (*VW-DHM10*) and slope (*HN-DHM10*) (Tab. 7.2.2.1-1). The susceptibility maps for runs 1 und 2 (Fig. 7.2.2.1-1) now presented a very similar image with a tendency toward lower susceptibilities in forest and higher values in steep terrain (often lower valley flanks) and in vertical-concave areas.
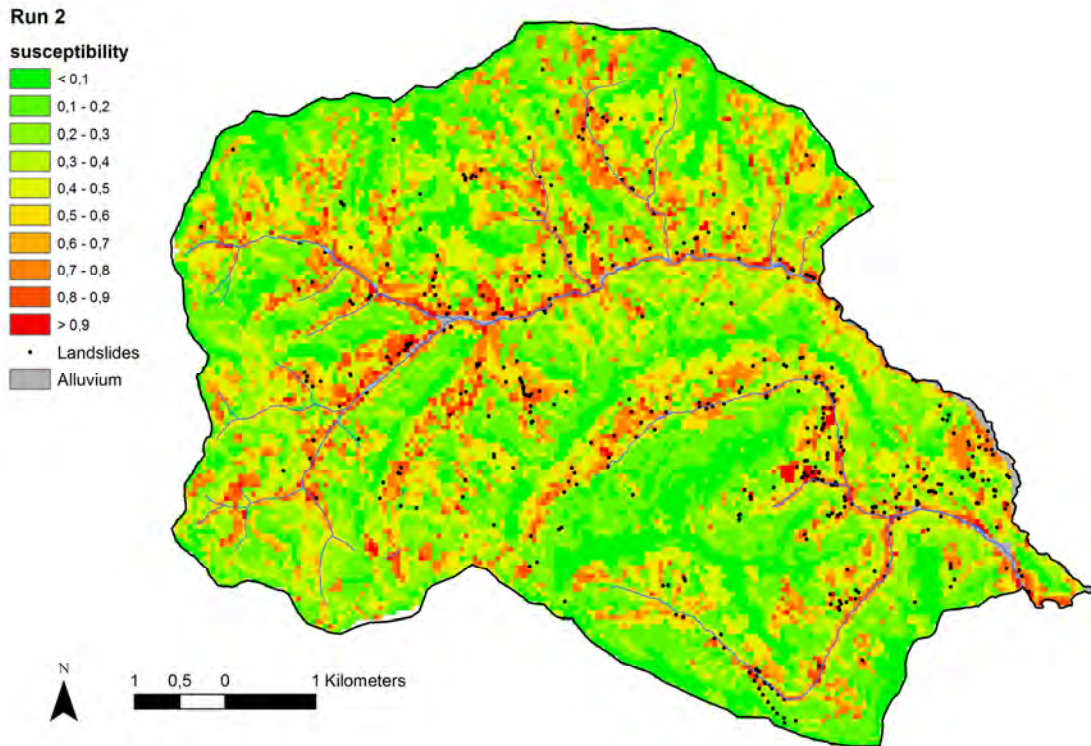
Fig. 7.2.2.1-1: Susceptibility map of run 2

However, due to the GBA validation strategy used, the results of runs 1 and 2 were seen as equally good, because the differences between all validation measurements were within the threshold values (Tab. A2 in Annex). This is also obvious from the validation curve according to Chung & Fabbri (1999, Fig. 7.2.2.1-2).
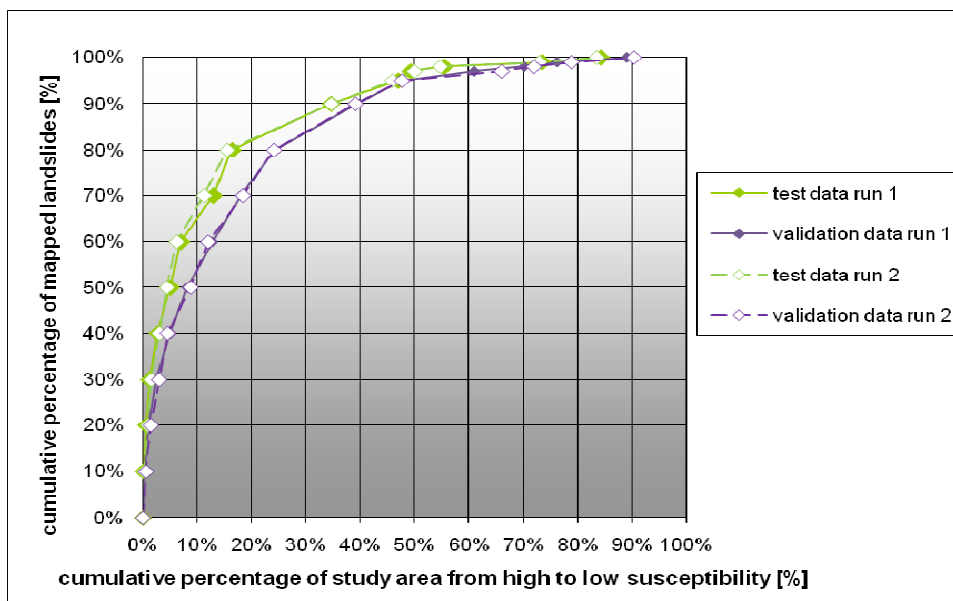
Fig. 7.2.2.1-2: Validation according to Chung and Fabbri (1999)

The influences of the three parameters employed, which are captured by a sensitivity analysis, are also approximately equal, the parameter forest being the most influential in both cases (Fig. 7.2.2.1-3).
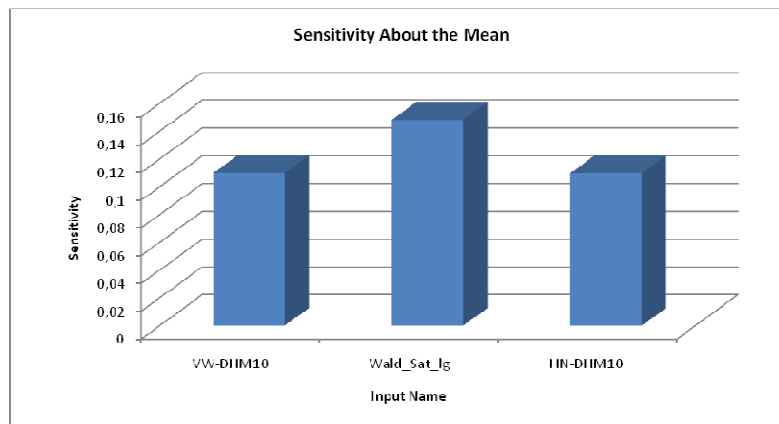
Fig. 7.2.2.1-3: Sensitivity analysis of run 2

In addition, the influence of these two forest maps was compared by means of the runs 3dkm and 3 (see: *Road network "level low"*-), and the runs 10 and 12 (Tab. 7.2.2.1-1). Here too, the results were more or less equally good, with only run 3dkm performing very slightly better than run 3. Thus, as neither of the two forest parameter maps used led to genuinely better results, preference was given to the forest map *Wald_Sat_lg_mb* in further work, because of its presumably greater actuality to the event.

Finally, in run 13 (Tab. 7.2.2.1-1) the parameter *Wald_Sat_lg_mb* was not taken into account, while the other parameters corresponded to those of run 10 (see Geological basic disposition). It was seen that this result led to obviously poorer validation results (Tab. A2 in Annex). This is explained by the fact that the number of pixels showing medium susceptibilities was obviously higher than it was in run 10, so that there was an increase in susceptibilities in forest and a decrease in susceptibilities outside forest. In addition, very high values were seen in the difference map for runs 13 and 10, which also manifested the strong influence of forest. It can therefore be concluded that the parameter *Wald_Sat_lg_mb* is a highly significant factor in obtaining better and clear results and is therefore a very important parameter in modelling.

Road network "level low"- (=*Wegenetz_lg_mb*)

Significance of the parameter maps *influence area of road network –"level low"* (*Wegenetz_lg_mb*):

The use of this parameter leads to an improvement in model performance. It has a major influence on the result, leading to a strong rise in susceptibility in areas influenced by roads and a strong decrease in susceptibility in areas at some distance from roads.

In order to study the influence of the parameter *influence areas of road network "level low"* on model performance, the results of the runs 1 and 3dkm, 2 and 3 and 16 and 10 were compared. The runs 3dkm, 3 and 16 hereby represent the respective parameter combinations of runs 1, 2 and 10, with the addition of the parameter *Wegenetz_lg_mb* (Tab. 7.2.2.1-1).

The difference map comparing run 3 to run 2 (Fig. 7.2.2.1-4) shows that integration of the parameter *Wegenetz_lg_mb* into the modelling produces major changes in map appearance, making the roads on the difference map visible. In the influence-area of roads, there is an increase (blue), and at some distance from roads, a decrease in susceptibility, so the neural network reacts to these parameters in the desired and expected manner. The sensitivity analysis also shows considerable influence of the parameter *Wegenetz_lg_mb*, although it is somewhat weaker than the influence of the other parameters. The same picture was seen when the results of the runs 3dkm and 1 were compared, as well as the results of runs 10 and 16.
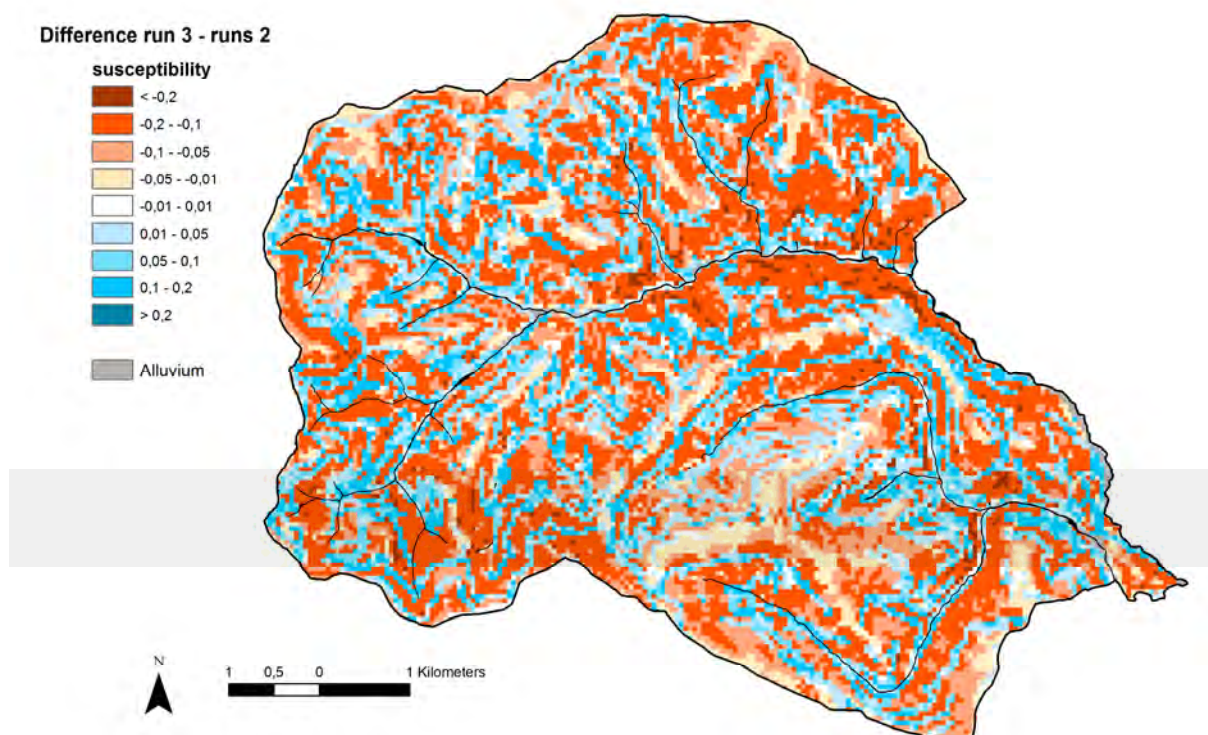
Fig. 7.2.2.1-4: Difference map of run 3 – run 2

The validation comparisons (Tab. A2 in Annex) showed that in all cases, the results of runs with the parameter *Wegenetz_lg_mb* (run 3dkm, 3 and 10) were better than those without that parameter (run 1, 2 und 16). Incorporation of the parameter *Wegenetz_lg_mb* therefore led to improvement in model performance, making this an important parameter.

Flow accumulation

Significance of the parameter map *Flowaccumulation*

This parameter has a moderate influence on the result and leads to a slight improvement in model performance. Increasing flow accumulation tends to be accompanied by a rise in susceptibility.

In order to study the influence of the parameter *Flowaccumulation* on the model performance, the results of runs 4 and 3 were compared. Run 4 was calculated using the parameters of run 3 and the parameter *Flowaccumulation* (Tab. 7.2.2.1-1). The sensitivity analysis and the difference maps demonstrate that the parameter Flowaccumulation does have an impact on model performance, but that it is clearly smaller than any of the other parameters. With increasing flow accumulation, there is a tendency toward greater susceptibility. Finally, the validation comparison (Tab. A2 in Annex) shows better values for run 4 than for run 3, which leads to the conclusion that the parameter *Flowaccumulation* generally contributes to improved model performance.

Subsurface flow disposition "level low"

Comparison of the parameter maps *subsurface flow disposition –"level low"*:

- Subsurface flow disposition "level low" based on geological map "level low" and flow accumulation (*QDisp_lg_GK_lg_fa)*

- Subsurface flow disposition "level low" based on geological map "level high" und flow accumulation (*QDisp_lg_GK_lh_fa)*

- Subsurface flow disposition "level low" based on soil map und flow accumulation (*QDisp_lg_BK_fa)*

The use of subsurface flow disposition parameter maps generally leads to an improvement in the model performance, and this also applies in comparison with *Flowaccumulation*. When this parameter is integrated, there tends to be an increase in susceptibility in areas of higher subsurface flow disposition. However, when the 3 subsurface flow disposition variants used were compared, it was noted that the susceptibility maps produced usually showed only minor deviations, and the validations were therefore practically just as good. These minor differences can be attributed to subsurface flow disposition usually having only a moderate influence on results, and the substituted substrate map making up only a part of this parameter. So taking different variants of subsurface flow disposition into account could not produce significantly better results.

Subsurface flow disposition "level low" base on geological map "level low" and flow accumulation (*QDisp_lg_GK_lg_fa)*

This subsurface flow disposition parameter was included in modelling in run 5, in addition to the parameters from run 3 (Tab. 7.2.2.1-1). The influence of *QDisp_lg_GK_lg_fa* on the model performance was now studied by comparing the results of runs 5 and 3, and 15 and 10 respectively. There was comparison to the parameter *Flowaccumulation* through runs 5 and 4 (Tab. 7.2.2.1-1).

After integration of the parameter *QDisp_lg_GK_lg_fa*, a tendency was now seen, in the result of run 5 (Fig. 7.2.2.1-5), toward a reduction in susceptibility in areas of lower subsurface flow disposition and an increase in areas of higher subsurface flow disposition, so that the parameter`s influence into the modelling was in the expected and desired manner.
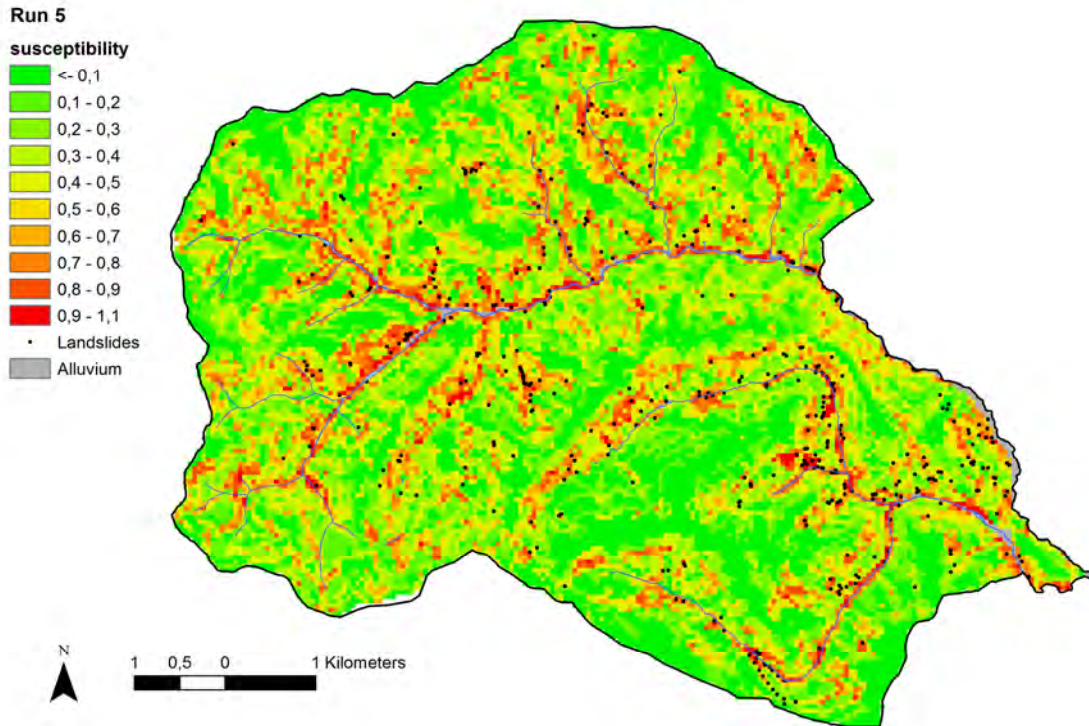
Fig. 7.2.2.1-5: Susceptibility map of run 5

However, as shown by the sensitivity analysis of run 5 (Fig. 7.2.2.1-6), the parameter *QDisp_lg_GK_lg_fa* (as before in the case of parameter *Flowaccumulation*) has only a rather moderate influence on the result, whereas the other parameters all have a stronger influence.
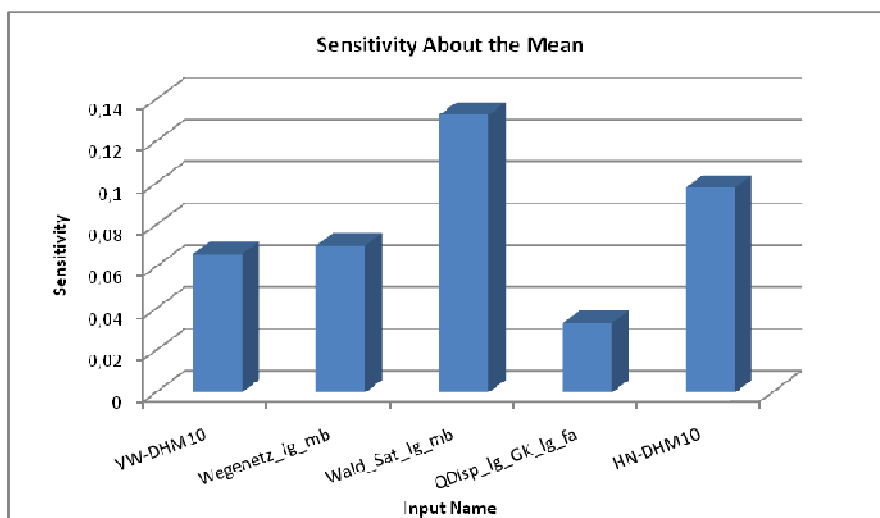
Fig. 7.2.2.1-6: Sensitivity analysis of run 5

The comparison of the validation results (Tab. A2 in Annex) now shows that the results with *QDisp_lg_GK_lg_fa* (run 5 or 10) are better than the results achieved without these parameters (run 3 or 15). In comparison to run 4 (with *Flowaccumulation*), run 5 performs slightly better. Integration of the parameter *QDisp_lg_GK_lg_fa* into the modelling therefore led to an improvement in the model performance, whereas slight improvements were also achieved with respect to *Flowaccumulation*.

Subsurface flow disposition "level low" based on geological map "level high" and flow accumulation (*QDisp_lg_GK_lh_fa)*

In run 6, this subsurface flow disposition parameter was incorporated into the modelling in addition to the parameters from run 3 (Tab. 7.2.2.1-1). The influence of this parameter on the model performance was now studied by comparing the results of runs 6 and 3, and 14 and 15 respectively (Tab. 7.2.2.1-1). Comparisons were made between the parameters *QDisp_lg_GK_lh_fa* and *QDisp_lg_GK_lg_fa* by juxtaposing the runs 6 and 5, 10 and 14, 22 and 21 and 23 und 20 respectively (Tab. 7.2.2.1-1). In runs 21 and 22, subsurface flow disposition was calculated with integrated "level low"-precipitation (see precipitation).

As in the case of *QDisp_lg_GK_lg_fa*, this runoff parameter was seen as having only a moderate influence, even though it influenced the modelling in the expected way. An improvement in the model performance through integration of this parameter could be verified only in the validation comparison between runs 6 and 3, whereas the result of run 14, interestingly enough, was just as good as that of run 15. However, in the comparison of run 6 to run 4, the parameter *QDisp_lg_GK_lh_fa* was seen as slightly better than *Flowaccumulation*.

In the comparison between the runs with *QDisp_lg_GK_lh_fa* and those with *QDisp_lg_GK_lg_fa*, there were, in general, only slight changes in the map's appearance. One example that can be cited is the difference map for runs 6 and 5 (Fig. 7.2.2.1-7). The slight differences seen here can be attributed to subsurface flow disposition being only a moderate factor in the results in both cases, and the substituted geological map ("level low" to "level high") being, in turn, only one part of this parameter. More significant changes are seen only in the difference map between runs 10 and 14.
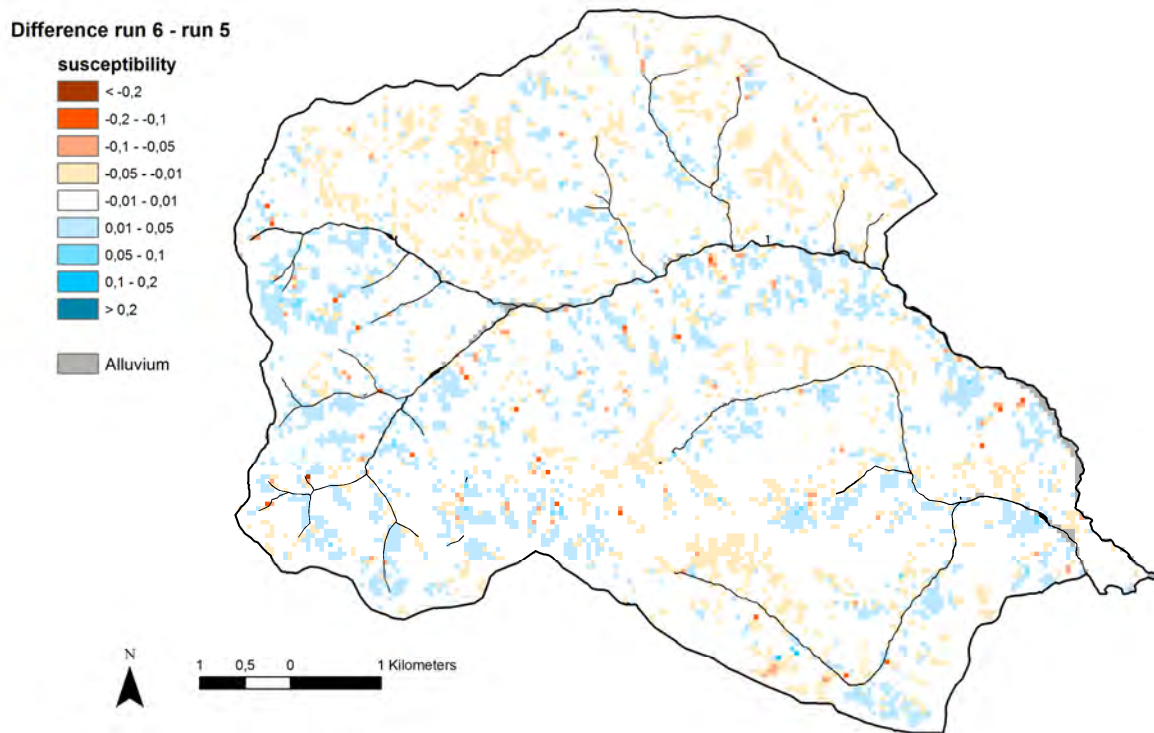
Fig. 7.2.2.1-7: Difference map of run 6 – run 5

Given what were in most cases minor changes in the map, the validation comparisons of runs 6 and 5, 22 and 21, and 23 and 20 respectively were seen as equally good (Tab. A2 in Annex). Only run 14, which included the parameter *QDisp_lg_GK_lh_fa*, produced an even poorer validation result than run 10.

In comparison to *QDisp_lg_GK_lg_fa*, the parameter *QDisp_lg_GK_lh_fa* resulted neither in significant changes in map appearance nor improvement in model performance (in the case of run 14, there was actually a deterioration in model performance). Therefore, in the interest of simplification, and because of the deterioration seen with *QDisp_lg_GK_lh_fa* in run 14, the parameter *QDisp_lg_GK_lg_fa* was preferred in further processing.

Subsurface flow disposition "level low" based on soil map und flow accumulation (*QDisp_lg_BK_fa*)

In run 24 (Tab. 7.2.2.1-1), this runoff parameter was incorporated into modelling in addition to the parameters from run 3 and the geological basic disposition "level low" (*Sub_GK_lg*). Here too, sensitivity analysis showed that this parameter had only moderate influence on the result, although it influenced the modelling in the expected manner (*QDisp_lg_GK_lg_fa*). Comparison to *QDisp_lg_GK_lg_fa* was carried out by means of run 10 (see Geological basic disposition). It was shown here, as with the subsurface flow disposition variants (see above), that the susceptibility maps from runs 10 and 24 deviated very little from each other, and the validation comparison also presented both results as equally good (Tab. A2 in Annex).

Curvature classification

Significance of the parameter map *curvature classification* (*HK-DHM10)*

This parameter always leads to a slight deterioration in model performance.

The parameter was incorporated into modelling in run 7, the parameter combination of run 7 differing from that of run 5 by the replacement of *VW-DHM10* with *HK-DHM10* (Tab. 7.2.2.1-1). Due to the curvature classification, the susceptibility map for run 7 is somewhat more agitated than that for run 5, which can be attributed to the parameter *HK-DHM10*, which is strongly differentiating on a small scale. Because *HK-DHM10* is split into 9 parameters (one parameter per class), these individual parameters play a much weaker role than *VW-DHM10* in the modelling. A validation comparison (Tab. A2 in the Annex) shows that the result without *HK-DHM10* (run 5) is slightly better than that containing this parameter (run 7).

There was also a comparison of runs that incorporated *HK-DHM10* in addition to *VW-DHM10* (runs 9 and 5, runs 19 und 10) (Tab. 7.2.2.1-1). The validation comparisons (Tab. A2 in Annex) for these runs also showed the results without curvature classification as slightly better. In general, therefore, the inclusion of curvature classification resulted in all cases in a slight deterioration in model performance, which is why this parameter was not included in further modelling.

Geological basic disposition "level low"

Significance of the parameter map *geological basic disposition* "level low" *(Sub_GK_lg)*

Despite its very weak and "contrary" influence on the result, this parameter leads to a slight improvement in model performance.

This parameter was incorporated into the modelling in run 10, in addition to the parameters from run 5 (Tab. 7.2.2.1-1). The influence of *Sub_GK_lg* on the model performance was then studied by comparing runs 10 and 5, and also runs 11 and 2 (run 11 is run 2 with the addition of *Sub_GK_lg*, Tab. 7.2.2.1-1).

The susceptibility map from run 10, which together with run 24 represents the best "level low" result without precipitation, is shown in Fig. 7.2.2.1-8. It also displays a tendency toward higher susceptibilities outside forest, on steeper slopes, on vertical concave slopes, in areas of high subsurface flow disposition and in areas affected by roads.

Run 10

susceptibility

- ▮ < - 0,1
- ▮ 0,1 - 0,2
- ▮ 0,2 - 0,3
- ▮ 0,3 - 0,4
- ▮ 0,4 - 0,5
- ▮ 0,5 - 0,6
- ▮ 0,6 - 0,7
- ▮ 0,7 - 0,8
- ▮ 0,8 - 0,9
- ▮ > 0,9
- · Landslides
- ▮ Alluvium
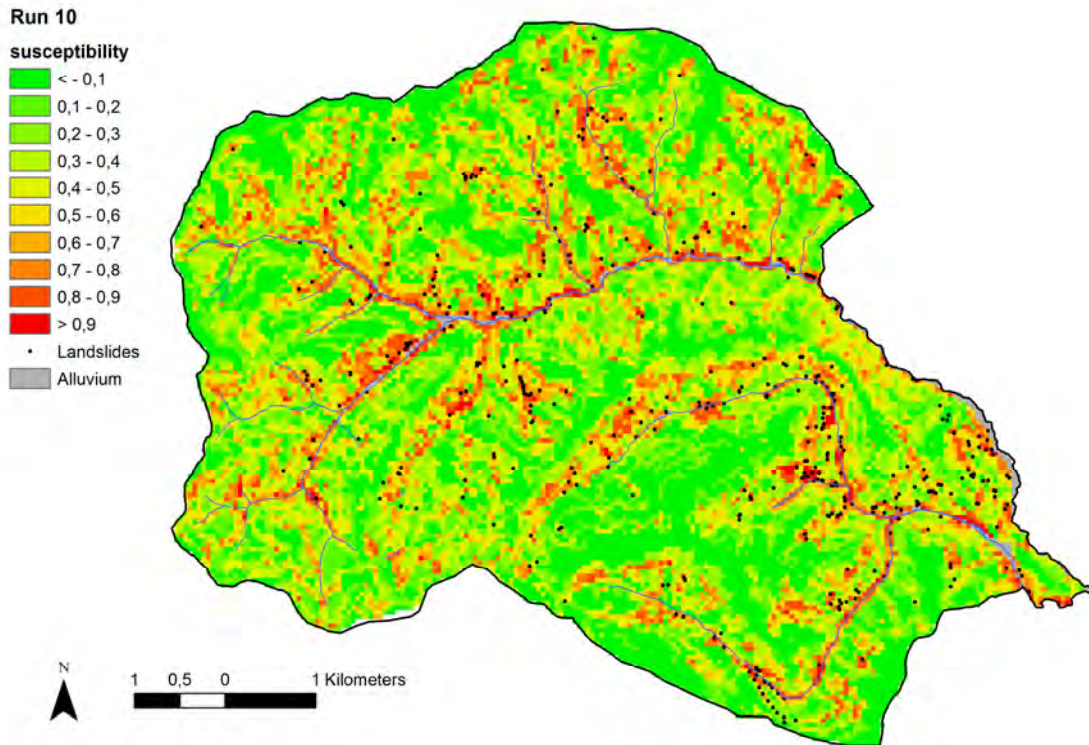
Fig. 7.2.2.1-8: Susceptibility map of run 10

The influence of geology (*Sub_GK_lg*) is obvious in the difference map from runs 10 and 5 (Fig. 7.2.2.1-9), however in a way opposite to that expected. Higher susceptibilities in run 10 (blue) appear in a region of lower geological basic disposition (phyllitic mica schist), whereas lower susceptibilities (red) appear in lithological units classified as landslide-prone (black shale, green shale). These differences between runs 10 and 5 are quite small, however, which can be explained by the very slight influence of the parameter *Sub_GK_lg* on the model result (Fig. 7.2.2.1-10).
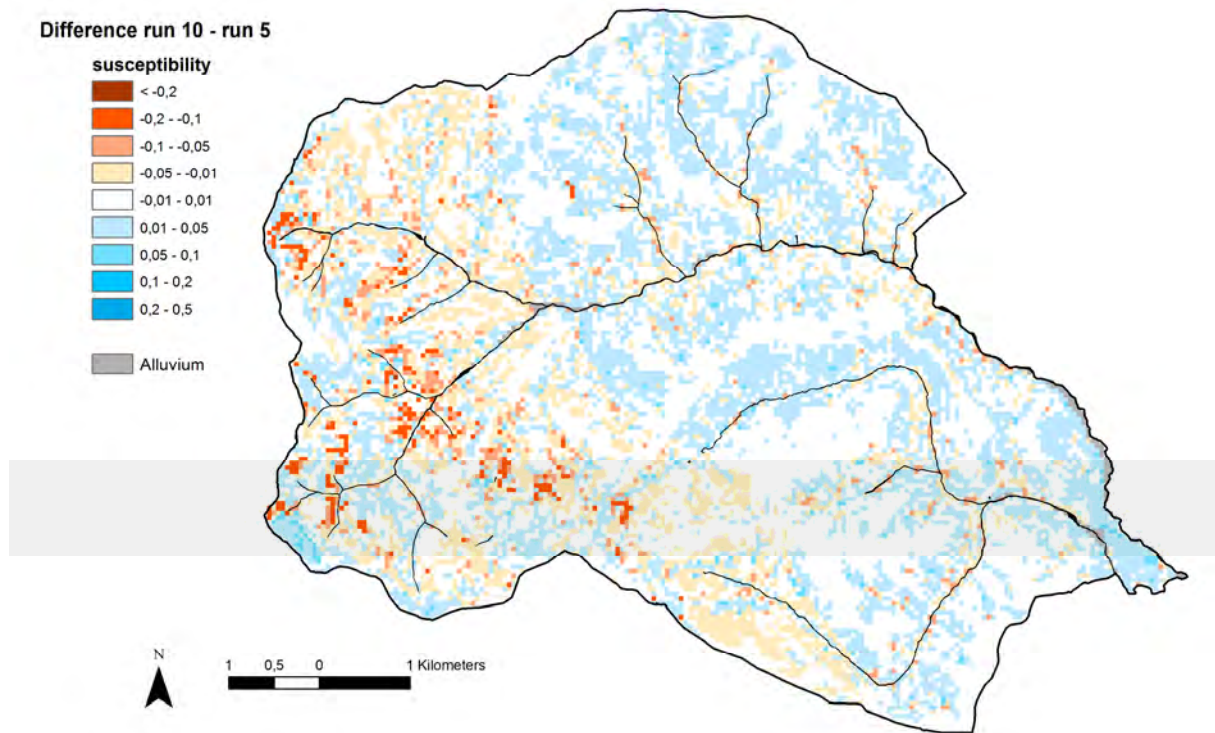
Fig. 7.2.2.1-9: Difference map of run 10 – run 5
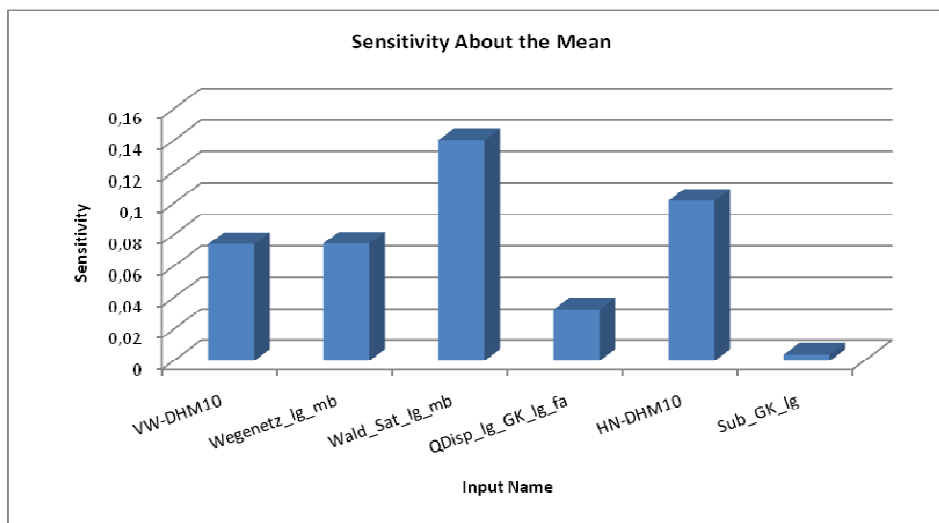
Fig. 7.2.2.1-10: Sensitivity analysis of run 10

The "contrary" influence of *Sub_GK_lg* can therefore be explained either by the statistical connection between mass-movement distribution and geological units being too weak and therefore unclear to the neural network, or the geological basic disposition leading, precisely in landslide-prone areas, to greater mass erosion, which in turn results in lower slopes, and thus less landslide-susceptibility.

The validation comparison from runs 10 and 5 (Tab. A2 in Annex) now showed that the result of run 10, despite the "contrary" influence of *Sub_GK_lg*, indicated slightly better performance than run 5. This was also confirmed by the comparison between

runs 11 and 2 (which also produced very similar map images, Tab. A2 in Annex). The integration of *Sub_GK_lg* into the modelling, despite the very weak and "contrary" influence of this parameter, thus led to a slight improvement in the model performance, which is why the parameter was also retained for further calculations.

Profile curvature

🔆 Significance of the parameter map *profile curvature* (*VW-DHM10)*

This parameter has a relatively strong influence on the result and leads to an improvement in the model performance. The integration of this parameter leads to a rise in susceptibility in concave areas.

In order to study the influence of this parameter on model performance*, VW-DHM10* was excluded in run 17, whereas the other parameters corresponded to those of run 10 (Tab. 7.2.2.1-1). It was shown that profile curvature led to a rise in sensibility in concave areas, which are often found on lower valley slopes. The validation comparison now showed that run 10 led to a better result than run 17 (Tab. A2 in Annex). The integration of profile curvature also led to an improvement in the model performance, and it is therefore an important parameter for modelling.

Precipitation "level low" *(NS_lg)*

🔆 Comparison of the parameter maps *precipitation –*"level low":

- Precipitation "level low" as an independent parameter *(NS_lg)*

- Precipitation "level low" integrated with subsurface flow disposition "level low" based on geological map "level low" and flow accumulation (*QDisp_lg_GK_lg_fa_NS_lg)*

- Precipitation "level low" integrated with subsurface flow disposition "level low" based on geological map "level high" and flow accumulation (*QDisp_lg_GK_lh_fa_NS_lg)*

- Precipitation "level low" integrated with subsurface flow disposition "level low" based on soil map and flow accumulation *(QDisp_lg_BK_fa)*

As an independent parameter, *precipitation "level low"* has a strong influence on the modelling result and therefore produces major changes in map appearance, with a rise in susceptibility in areas of heavy precipitation and a decrease in susceptibility in areas with little precipitation. In integrated form, however, this parameter scarcely influences modelling results and usually results in only very slight changes in map appearance. Thus, the integration of *precipitation "level low"* as an independent parameter also leads to changes in validation, whereas validation usually does not change when *precipitation* is used as an integrated parameter. But in neither case was there a recognizable tendency toward improvement in model performance due to the integration of *precipitation "level low."*

Precipitation *"level low"* was included in the modelling both as an independent parameter and in integrated form as part of subsurface flow disposition (Tab. 6.2-1). In order to investigate the influence of *NS_lg* on the model performance, runs with the same parameter combination were compared, but with or without *NS_lg*. The parameter *NS_lg* was combined in both independent and integrated form with the subsurface flow dispositions *QDisp_lg_GK_lg_fa* (runs 20, 21 and 28),

QDisp_lg_GK_lh_fa (runs 23 und 22) and *QDisp_lg_BK_fa* (runs 34 und 25) respectively, whereas in the case of the independent parameter, this was done with the "level high" subsurface flow disposition *QDisp_lh_fa_NS_lg* (run 64) as well.

Fig. 7.2.2.1-11 now shows the susceptibility map for run 23 as an example of results with *NS_lg* as an **independent parameter**. Conspicuous here are the higher susceptibilities in the centre of the study area, which are also located in the region of the higher precipitation "level low." The neural network thus responds to the parameter *NS_lg*, and does so in the expected direction.
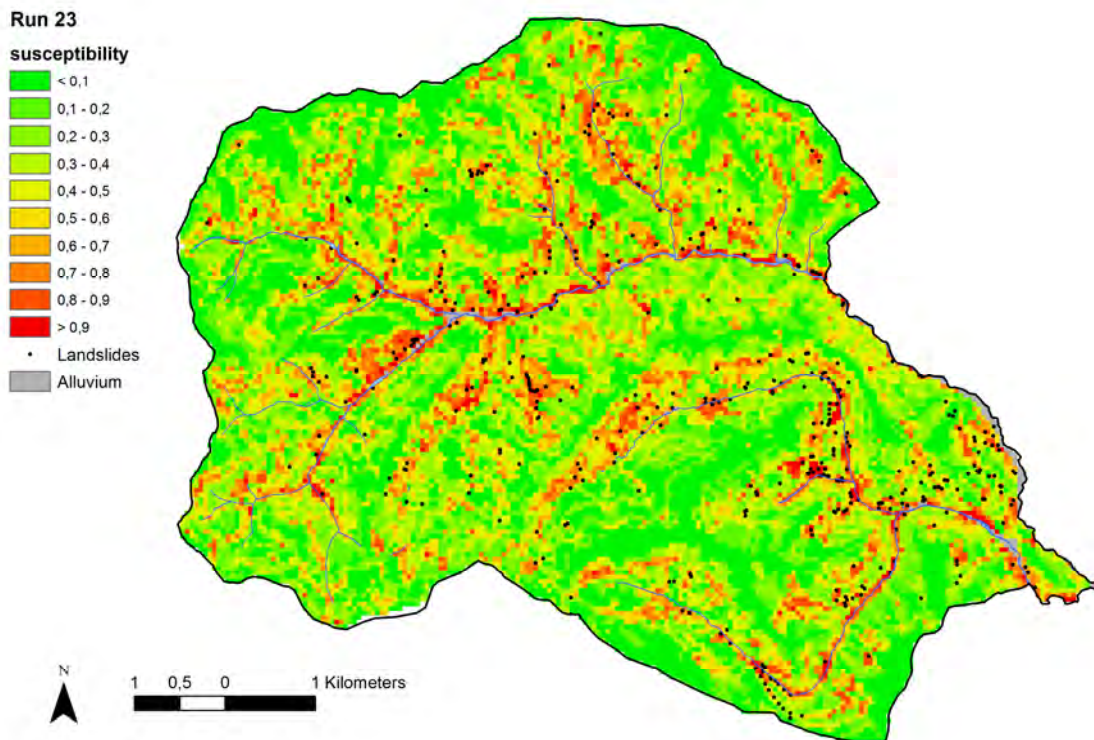
Fig. 7.2.2.1-11: Susceptibility map of run 23

This circumstance can be seen even more clearly in the difference map for runs 23 and 24 (Fig. 7.2.2.1-12), even though *NS_lg* is rather weakly reflected in modelling. However, when comparing run 23 to other runs (for example to run 10), it was noted that the results in the validations were equally good (Tab. A2 in the Annex), whereas the difference maps often showed high values. That is an indication of shortcomings in the validation methods used.

The sensitivity analysis of run 23 (Fig. 7.2.2.1-13) shows that *NS_lg* has little influence on the model result.
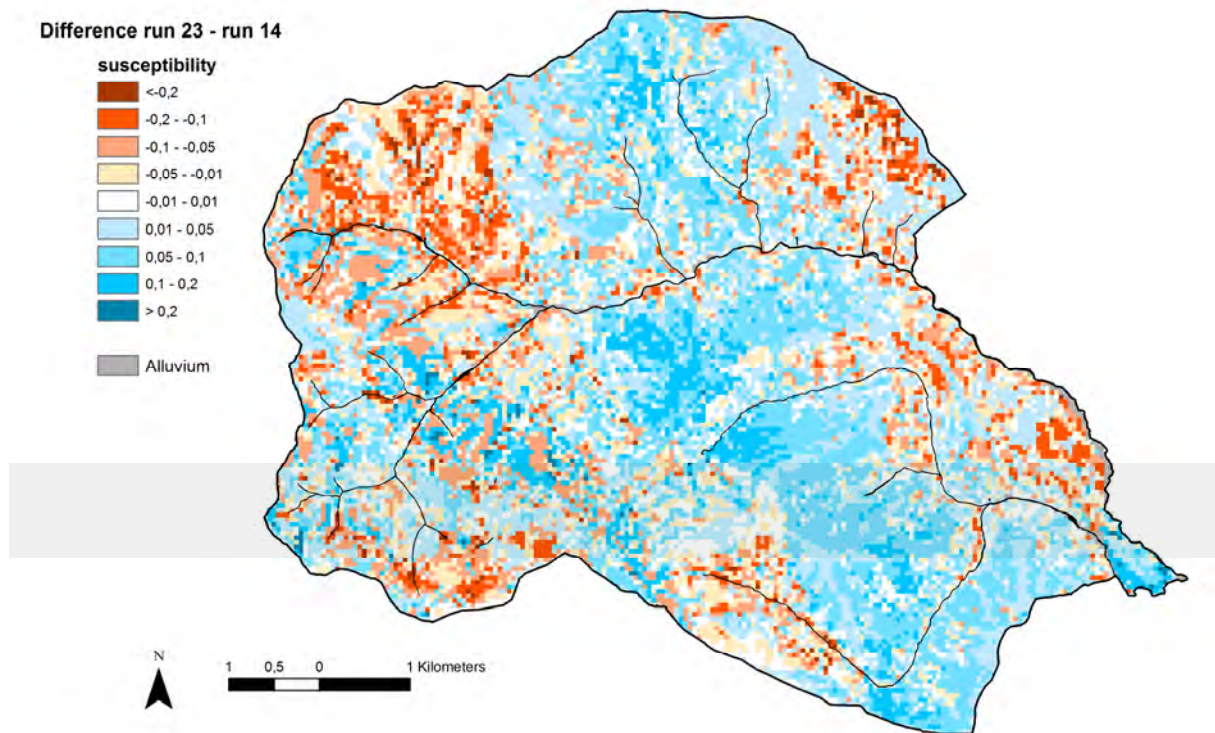
Fig. 7.2.2.1-12: Difference map of run 23 – run 14
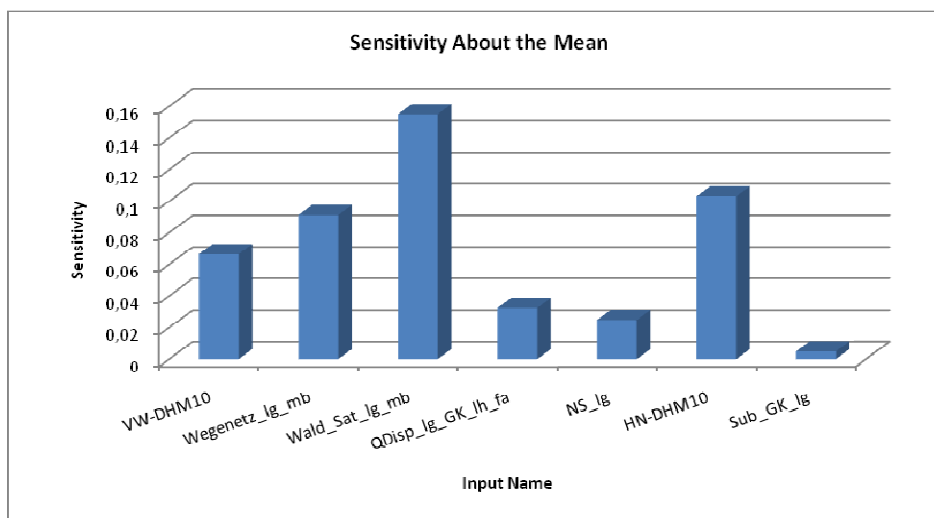
Fig. 7.2.2.1-13: Sensitivity analysis of run 23

The validations of modelling with *NS_lg* as an independent parameter therefore produced no clear picture: in the validation comparison, the runs 20, 34 and 64, which were expanded with the parameter *NS_lg*, were (very) slightly worse than the corresponding runs 10, 33 and 46 without *NS_lg*. When comparing the runs 23 and 14 (both containing *QDisp_lg_GK_lh_fa*) or runs 28 and 19 (both containing *HK-DHM10*), the runs 23 and 28 containing *NS_lg* were (very slightly) better (Tab. A2 in Annex, parameters of runs: see Tab. 7.2.2.1-1).

Fig. 7.2.2.1-14 shows the difference map for the runs 21 and 10, which exemplifies the results that have *NS_lg* as an **integrated parameter**. The differences are very small, the parameter geology (*Sub_GK_lg*) tracing more strongly in the distribution of differences than the parameter precipitation (*NS_lg*). The small differences, as in the case of subsurface flow disposition can be attributed to the parameter *QDisp_lg_GK_lg_fa_NS_lg* that contains *NS_lg*, playing a quite moderate role in the result (Fig. 7.2.2.1-15) and *NS_lg* in turn making up only one part of this parameter.
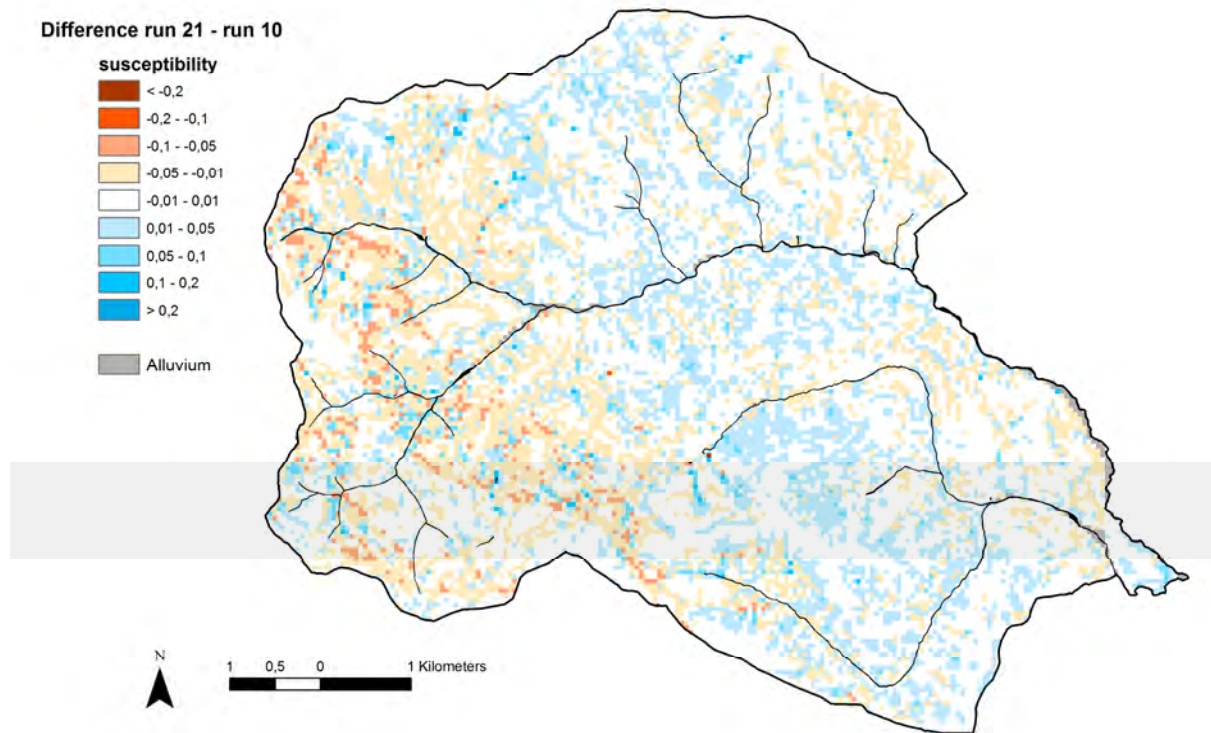
Fig. 7.2.2.1-14: Difference map of run 21 – run 10

The sensitivity analysis of run 21 (Fig. 7.2.2.1-15) demonstrates that the parameter containing NS_lg, which is *QDisp_lg_GK_lg_fa_NS_lg*, is influencing the modelling result only in a moderate way and to the same degree as *QDisp_lg_GK_lg_f*a in run 10 (Fig. 7.2.2.1-10). Hence the integration of *NS_lg* into the parameter *QDisp_lg_GK_lg_fa_NS_lg* did not result in any appreciable changes for this parameter.
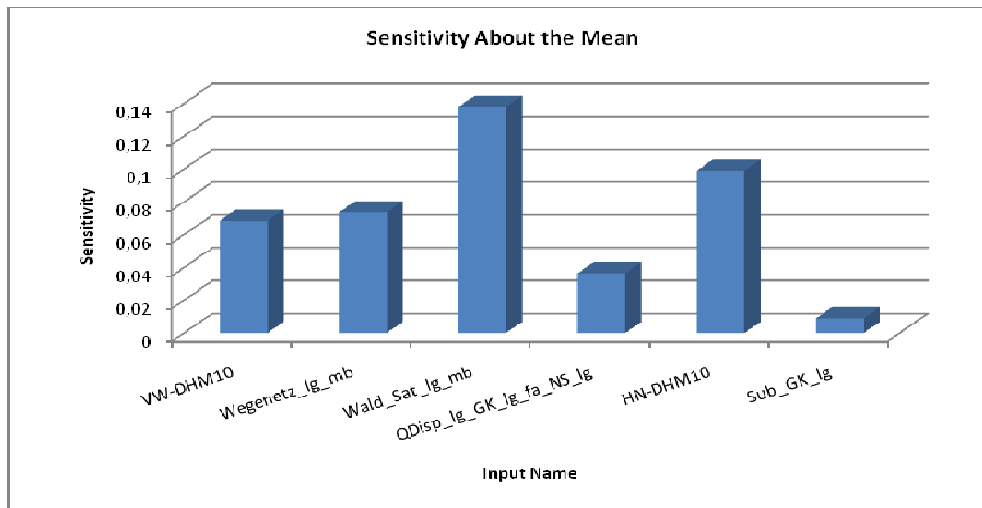
Fig. 7.2.2.1-15: Sensitivity analysis of run 21

In the validation comparison (Tab. A2 in Annex), two of the three runs studied (21 and 25) that had *NS_lg* as an integrated parameter were assessed as just as good as the respective runs (10 and 25) without *NS_lg*. Only run 22 produced slightly better results than run 14.

Forest and road network without land-use mapping

> Significance of the parameter maps *forest* and *road network without land-use mapping* (*Wald_Sat_lg, Wegenetz_lg)*
>
> Use of the parameter maps **without** land-use mapping (regionalisation data) results in a very strong deterioration in the model performance compared to parameter maps **with** mapped land-use. This applies particularly to the parameter *forest*. When *forest* is integrated *without* land-use mapping, the neural network can no longer recognize its stabilizing effect as clearly, and the parameter is no longer showing great influence on the modelling result. The mapping of land-use information (particularly forest and roads) is therefore enormously significant in the event documentation of mass movements..

The influence of regionalisation data (= forest and road network data without land-use mapping (*Wald_Sat_lg, Wegenetz_lg*, see Chapter 6.1.2)) on the model performance was studied on the basis of runs 29 to 32 (Tab. 7.2.2.1-1). In order to do so, there was comparison of the runs with regionalisation data and the corresponding runs with the same parameter combination but with mapped land-use data *(Wald_Sat_lg_mb, Wegenetz_lg_mb)* (runs 2, 10 and 24). The runs 29 und 30 included both parameters (*Wald_Sat_lg, Wegenetz_lg*), while the runs 31 and 32 incorporated only the parameter *Wald_Sat_lg*.

The susceptibility map for run 29 (Fig. 7.2.2.1-16) is an example of the runs done with regionalisation data. It has the same parameters as run 10, but includes *Wald_Sat_lg* and *Wegenetz_lg*. It shows higher susceptibilities in and lower susceptibilities outside forest than for run 10. The reason for this is that the neural network, due to the partially erroneous values in the regionalisation data, can no longer as clearly recognize the stabilizing effect of forest, and *Wald_Sat_lg* therefore

is no longer showing as great influence on the modelling result as *Wald_Sat_lg_mb* does in run 10. According the roads, however, there was an unexpected, slight increase in susceptibilities, which cannot be explained.
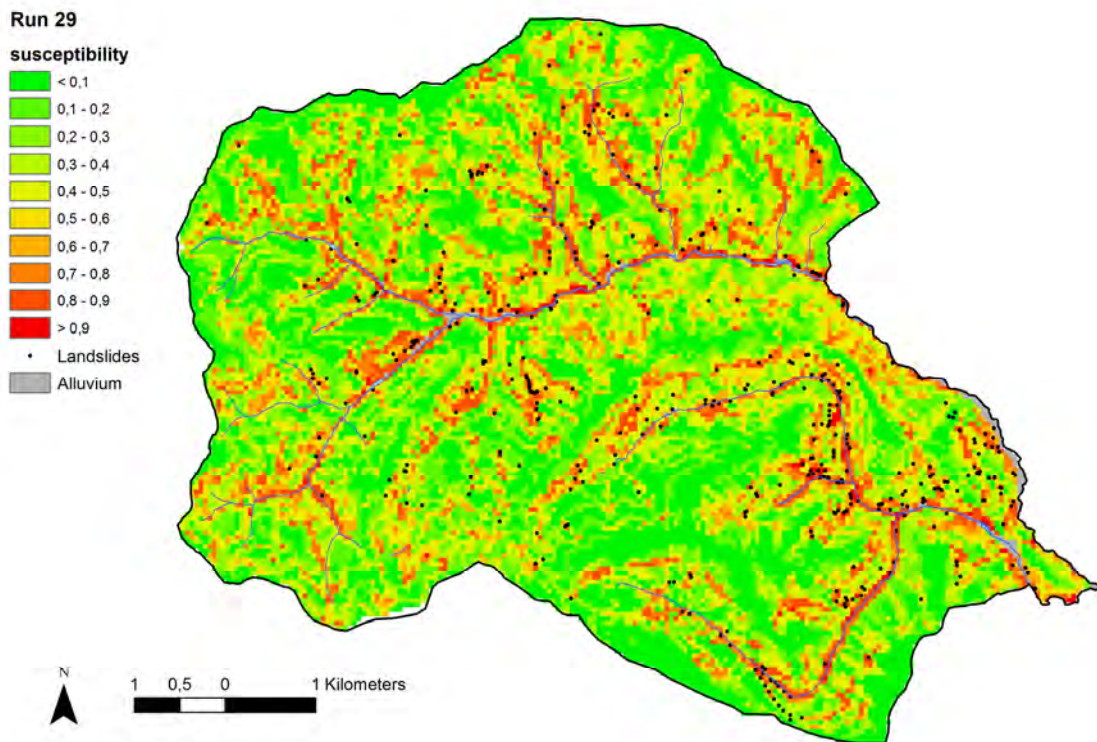
Fig. 7.2.2.1-16: Susceptibility map of run 29

The validation comparison (Tab. A2 in Annex) showed the clearest picture of any obtained in this project: all of the runs (29 to 32) calculated with regionalisation data performed worse than the corresponding runs with mapped land-use (runs 2, 10 and 24, cf. Fig. 7.2.2.1-17). In contrast to the use of regionalisation data, the use of parameters with mapped land-use greatly improved the model performance, particularly as regards the parameter *forest* (areas stabilized by tree roots). The mapping of land-use information (especially forest and roads) as part of event-documentation of mass movements is therefore enormously important, particularly when the data is subsequently incorporated into susceptibility modelling.

Validation comparison of all "level low" runs and selection of the best "level low" runs with neural networks

Comparison of all "level low" parameter maps

Generally speaking, major differences in the validation of runs occurred only with the inclusion of the parameters *forest, road network, subsurface flow disposition,* and *profile curvature* (and certainly also with the inclusion of *slope*, although this was not studied). In the case of all other parameters, the differences in validation results were quite small. This applied particularly to comparisons of variants of *one* parameter (*forest, subsurface flow disposition* and *precipitation*). The biggest differences in validation, and thus the biggest improvements in the model performance were achieved in the case of parameters with mapped land-use information, as opposed to parameters without mapped land-use information (= regionalisation data), and with inclusion of the parameter *forest*.

This fact is apparent from a comparison of all runs with "level low" parameter maps according to the validation strategy developed by GBA (see Chapter 7.2.1 and Tab. A2 in Annex) and is also clearly seen in the validation of the test data for "level low" events according to Chung and Fabbri 1999 (Fig. 7.2.2.1-17). So there is essentially a broad array of run-curves in which only the runs with regionalisation data (the dashed lines for the runs 29, 30, 31 and 32) and run 13 (without the parameter *forest*) swerve downward.
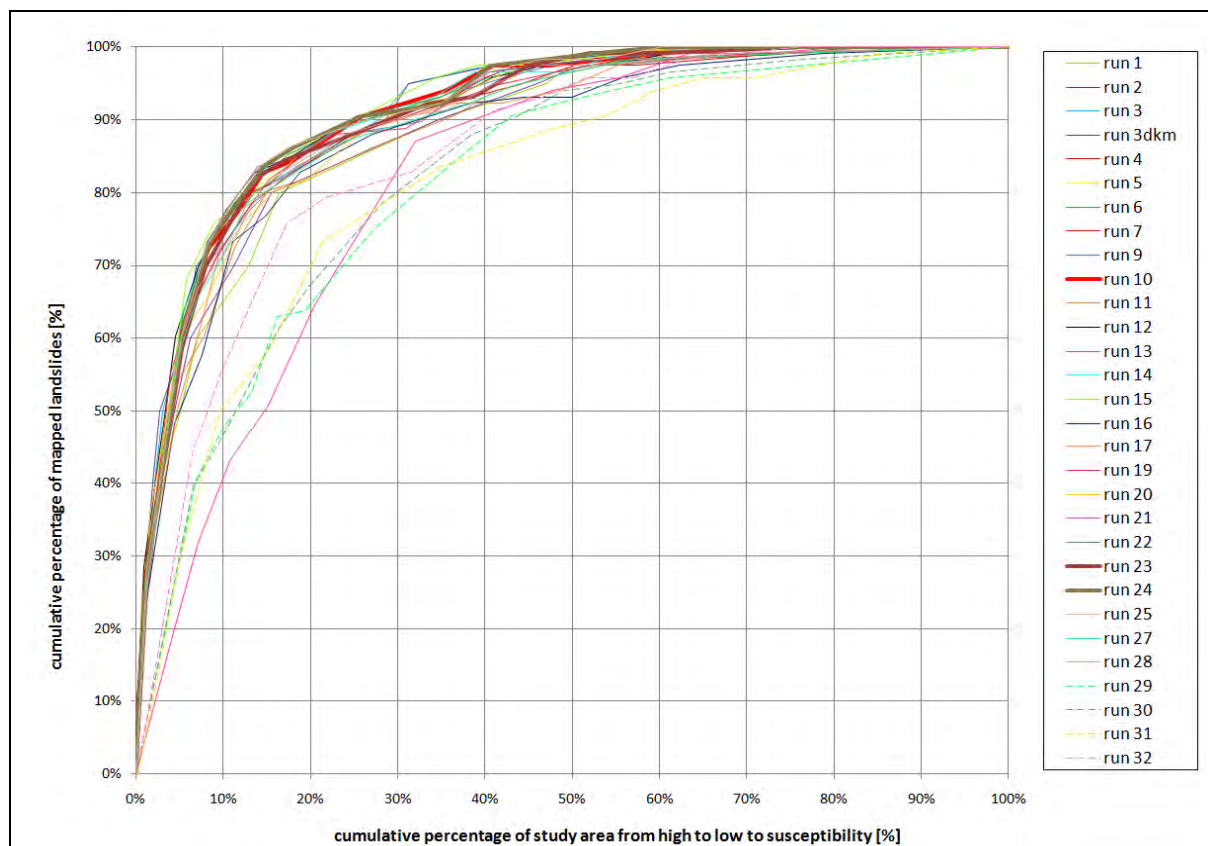
Fig. 7.2.2.1-17: Validation according to Chung & Fabbri (1999) of the test data of "low-level" runs

Based on the validation comparisons (see Tab. A2 in Annex), seven runs were assessed as equally good. From this group, the runs 10, 23 and 24 were selected as the "best 5 level low." The remaining four runs were rejected due to their close similarity to other runs because of the parameters "integrated *NS_lg*" and *Wald_dkm_lg_mb*. The three runs selected all include the parameters *Wald_Sat_lg_mb, VW-DHM10, HN-DHM10, Wegenetz_lg_mb* and *Sub_GK_lg*, and differ only in having different subsurface flow dispositions (*QDisp_lg_GK_lg_fa* in run 10, *QDisp_lg_GK_lh_fa* in run 23 and *QDisp_lg_BK_fa* in run 24, Tab 7.2.2.1-1). In addition, run 23 had *NS_lg* as an independent parameter, which was significant for the subsequent calculation of scenarios (cf. Chapter 11.1). Furthermore, runs 5 (*QDisp_lg_GK_lg_fa*) and 6 (*QDisp_lg_GK_lh_fa*), which were only marginally worse, were included in the "best 5 level low." They displayed the same parameters as the three best runs, however without *Sub_GK_lg*. Run 10, one of the best runs, showed in the test data an AUC for Chung & Fabbri 1999 of 91.34 and 91.68% for ROC, a recognition rate of 90.5%, and for the GBA validation method, a value of 55.29.

7.2.2.2 Modelling Results Using "Level High" Parameter Maps

For modelling based on neural networks, the procedure for model integration of parameter maps described in Chapter 7.1 produced 33 model runs using parameter maps of the processing/quality grade "level high," which are listed, including the respective parameter combinations, in Tab. 7.2.2.2.1. The parameter combinations of individual network runs do not necessarily correspond to the parameter combinations of runs with the other modelling methods used in the project (see Chapters 7.3, 7.4, and 7.5.). In modelling with neural networks, run 33 was selected as the best "level high" run ("best_lh") after the first 13 "level high" runs (after run 48_E), so that all subsequent "level high" runs were variations of the parameter combinations of run 33 (see Chapter 7.1).

Tab. 7.2.2.2.1_part 1: Model runs "level high" and the parameter maps used (abbreviation of parameter maps: Tab. 6.2.1)

# Run	Parameter maps used	Relation to other Runs
Run 33	Waldsat_lg_mb, VW-DHM10, HN-DHM10, Wegenetz_lg_mb, QDisp_lg_BK_fa, BK	as Run10, but using QDisp_lg_BK_fa instead of QDisp_lg_GK_lg_fa and BK instead of Sub_GK_lg
Run 34	Waldsat_lg_mb, VW-DHM10, HN-DHM10, Wegenetz_lg_mb, QDisp_lg_BK_fa, BK, NS_LG	as Run 10, but using QDisp_lg_BK_fa instead of QDisp_lg_GK_lg_fa and BK instead of Sub_GK_lg and adding NS_LG; as Run 33, but adding NS_lg
Run 35	Waldsat_lh_mb, VW-DHM10, HN-DHM10	as Run 2, but using Waldsat_lh_mb instead of Waldsat_lg_mb; as Run 31, but using Waldsat_lh_mb instead of Waldsat_lg_mb
Run 36	Waldsat_lh_mb, VW-DHM10, HN-DHM10, Wegenetz_lg_mb, QDisp_lg_GK_lg_fa, Sub_GK_lg	as Run 10, but using Waldsat_lh_mb instead of Waldsat_lg_mb; as Run 32, but using Waldsat_lh_mb instead of Waldsat_lg_mb
Run 37 = Run 39	Waldsat_lg_mb, VW-DHM10, HN-DHM10, Wegenetz_lh_mb	as Run 3, but using Wegenetz_lh_mb instead of Wegenetz_lg_mb
Run 38 = Run 3		
Run 40 = Run 42	Waldsat_lg_mb, VW-DHM10, HN-DHM10, Wegenetz_lg_mb, QDisp_lh_fa	as Run 5, but using QDisp_lh_fa instead of QDisp_lg_GK_lg_fa
Run 41 = Run 5		
Run 43	Waldsat_lg_mb, VW-DHM10, HN-DHM10, Wegenetz_lg_mb, QDisp_lg_GK_lg_fa, Sub_GK_lh	as Run10, but using Sub_GK_lh instead of Sub_GK_lg
Run 44 = Run 10		
Run 45 = Run 43	Waldsat_lg_mb, VW-DHM10, HN-DHM10, Wegenetz_lg_mb, QDisp_lg_GK_lg_fa, SUB_GK_LH	as Run10, but using Sub_GK_lh instead of Sub_GK_lg
Run 46 = Run 48	Waldsat_lg_mb, VW-DHM10, HN-DHM10, Wegenetz_lg_mb, QDisp_lh_fa, BK	as Run 33, but using QDisp_lh_fa instead of QDisp_lg_BK_fa
Run 47 = Run 33		

Tab. 7.2.2.2-1_part 2: Model runs "level high" and the parameter maps used (abbreviation of parameter maps: Tab. 6.2.1)

Run 48_A	Waldsat_lg_mb, VW-DHM10, HN-DHM10, Wegenetz_lg_mb, QDisp_lg_GK_lh_fa, Sub_GK_lh	as Run10, but using QDisp_lg_GK_lh_fa instead of QDisp_lg_GK_lg_fa and Sub_GK_lh instead of Sᴜʙ_GK_lg; as Run 14, but using Sub_GK_lh instead of Sub_GK_lg, as Run 6 adding Sub_GK_lh, as Run 27 – HK-DHM10
Run 48_B	Waldsat_lg_mb, VW-DHM10, HN-DHM10, Wegenetz_lg_mb, QDisp_lh_fa, Sub_GK_lh	as Run10, but using QDisp_lh_fa instead of QDisp_lg_GK_lg_fa and Sub_GK_lh instead of Sub_GK_lg; as Run 40 adding Sub_GK_lh, as Run 46, but using Sub_GK_lh instead of BK
Run 48_C	Waldsat_lg_mb, VW-DHM10, HN-DHM10, Wegenetz_lg_mb, QDisp_lg_BK_fa, Sub_GK_lh	as Run10, but using QDisp_lg_BK_fa instead of QDisp_lg_GK_lg_fa and Sub_GK_lh instead of Sub_GK_lg; as Run 33, but using Sub_GK_lh instead of BK, as Run 24, but using Sub_GK_lh instead of Sub_GK_lg; as Run 43, but using QDisp_lg_BK_fa instead of QDisp_lg_GK_lg_fa
Run 48_D	Waldsat_lg_mb, VW-DHM10, HN-DHM10, Wegenetz_lg_mb, QDisp_lg_GK_lh_fa, BK	as Run10, but using QDisp_lg_GK_lh_fa instead of QDisp_lg_GK_lg_fa and BK instead of Sub_GK_lg; as Run 33, but using QDisp_lg_GK_lh_fa instead of QDisp_lg_BK_fa, as Run 6 adding BK, as Run 14, but using BK instead of Sub_GK_lg
Run 48_E	Waldsat_lh_mb, VW-DHM10, HN-DHM10, Wegenetz_lh_mb, QDisp_lg_GK_lh_fa, BK	as Run10, but using QDisp_lg_GK_lh_fa instead of QDisp_lg_GK_lg_fa and BK instead of Sub_GK_lg and Waldsat_lh_mb instead of Waldsat_lg_mb; as Run 48_D, but using Wegenetz_lh instead of Wegenetz_lg, as Run 48_A, but using Wegenetz_lh instead of Wegenetz_lg and BK instead of Sub_GK_lh
Run 53	Waldsat_lg_mb, VW-DHM10, HN-DHM10, Wegenetz_lh_mb, QDisp_lg_BK_fa, BK	as Run10, but using QDisp_lg_BK_fa instead of QDisp_lg_GK_lg_fa, BK instead of Sub_GK_lg, Wegenetz_lh_mb instead of Wegenetz_lg_mb; as Run 33 but using Wegenetz_lh_mb instead of Wegenetz_lg_mb
Run 55	Waldsat_lg_mb, HK-DHM10, VW-DHM10, HN-DHM10, Wegenetz_lh_mb, QDisp_lg_BK_fa, BK	as Run10, but using QDisp_lg_BK_fa instead of QDisp_lg_GK_lg_fa, BK instead of Sub_GK_lg, adding HK-DHM10; Run 33 adding HK-DHM10
Run 56	Waldsat_lg_mb, VW-DHM10, HN-DHM10, Wegenetz_lg_mb, QDisp_lg_GK_lg_fa, BK	as Run10, but using BK instead of Sub_GK_lg, as Run 33, but using QDisp_lg_GK_lg_fa instead of QDisp_lg_BK_fa, as Run 46, but using QDisp_lg_GK_lg_fa instead of QDisp_lh_fa; as Run 48_D, but using QDisp_lg_GK_lg_fa instead of QDisp_lg_GK_lh_fa
Run 57	Waldsat_lg_mb, VW-DHM10, HN-DHM10, Wegenetz_lg_mb, QDisp_lg_BK_fa, BK	as Run10, but using Flowaccumulation instead of QDisp_lg_GK_lg_fa and BK instead of Sub_GK_lg, as Run 33, but using Flowaccumulation instead of QDisp_lg_BK_fa
Run 58	Waldsat_lg_mb, VW-DHM10, HN-DHM10, Wegenetz_lg_mb, QDisp_lg_BK_fa, NS_lh, BK	as Run10, but using NS_lh, QDisp_lg_BK_fa instead of QDisp_lg_GK_lg_fa and BK instead of Sub_GK_lg, Run 33 adding NS_lh, as Run 34, but using NS_lh instead of NS_lg
Run 59	Waldsat_lg_mb, VW-DHM10, HN-DHM10, Wegenetz_lg_mb, QDisp_lg_GK_lg_fa, Sub_GK_lg, NS_lh	as Run10, but using NS_lh; as Run 20, but using NS_lh instead of NS_lg
Run 60	Waldsat_lg_mb, VW-DHM10, HN-DHM10, Wegenetz_lg_mb, QDisp_lg_GK_lh_fa_NS_lh, BK	as Run10, but using QDisp_lg_GK_lh_fa_NS_lh instead of QDisp_lg_GK_lg_fa and BK instead of Sub_GK_lg, as Run 33, but using QDisp_lg_GK_lh_fa_NS_lh instead of QDisp_lg_BK_fa; as Run 48_D, but using QDisp_lg_GK_lh_fa_NS_lh instead of QDisp_lg_GK_lh_fa
Run 61	Waldsat_lg_mb, VW-DHM10, HN-DHM10, Wegenetz_lg_mb, QDisp_lg_GK_lg_fa_NS_lh, Sub_GK_lg	as Run10, but using QDisp_lg_GK_lg_fa_NS_lh instead of QDisp_lg_GK_lg_fa, as Run 21, but using QDisp_lg_GK_lg_fa_NS_lh instead of QDISP_lg_GK_lg_fa_NS_lg
Run 62	Waldsat_lg_mb, VW-DHM10, HN-DHM10, Wegenetz_lg_mb, QDisp_lg_GK_lh_fa_NS_lh, Sub_GK_lg	as Run10, but using QDisp_lg_GK_lh_fa_NS_lh instead of QDisp_lg_GK_lg_fa, as Run 22, but using QDisp_lg_GK_lh_fa_NS_lh instead of QDisp_lg_GK lh_fa_NS_lg, as Run 61, but using QDisp_lg_GK_lh_fa_NS_lh instead of QDisp_lg_GK_lg_fa_NS_lh

Tab. 7.2.2.2-1_part 3: Model runs "level high" and the parameter maps used (abbreviation of parameter maps: Tab. 6.2-1)

Run 63	Waldsat_lg_mb, VW-DHM10, HN-DHM10, Wegenetz_lg_mb, QDisp_lh_fa_NS_lh, BK	as Run 10, but using QDisp_lh_fa_NS_lh instead of QDisp_lg_GK_lg_fa and BK instead of Sub_GK_lg, as Run 33, but using QDisp_lh_fa_NS_lh instead of QDisp_lg_BK_fa, as Run 46, but using QDisp_lh_fa_NS_lh instead of QDisp_lh_fa
Run 64	Waldsat_lg_mb, VW-DHM10, HN-DHM10, Wegenetz_lg_mb, QDisp_lh_fa, BK, NS_lg	as Run10, but using QDisp_lh_fa instead of QDisp_lg_GK_lg_fa and BK instead of Sub_GK_lg adding NS_lg; as Run 33, but using QDisp_lh_fa instead of QDisp_lg_BK_fa adding NS_lg; as Run 46 adding NS_lg
Run 65 = Run 66	Waldsat_lg_mb, VW-DHM10, HN-DHM10, Wegenetz_lg_mb, QDisp_lh_fa, BK, NS_lh	as Run10, but using QDisp_lh_fa instead of QDisp_lg_GK_lg_fa and BK instead of Sub_GK_lg adding NS_lh; as Run 33, but using QDisp_lh_fa instead of QDisp_lg_BK_fa adding NS_lh; Run 46 adding NS_lh; as Run 63, but using QDisp_lh_fa + NS_lh instead of QDisp_lh_fa_NS_lh; as Run 64, but using NS_lh instead of NS_lg
Run 68	Waldsat_lg_mb, VW-DHM10, HN-DHM10, Wegenetz_lg_mb, QDisp_lg_BK_fa_NS_lh, BK	as Run10, but using QDisp_lg_BK_fa_NS_lh instead of QDisp_lg_GK_lg_fa and BK instead of Sub_GK_lg, as Run 33, but using QDisp_lg_BK_fa_NS_lh instead of QDisp_lg_BK_fa, as Run 58, but using QDisp_lg_BK_fa_NS_lh instead of QDisp_lg_BK_fa adding NS_lh
Run 69	Waldsat_lg_mb, VW-DHM10, HN-DHM10, Wegenetz_lh_mb, HK-DHM10, QDisp_lh_fa, Sub_GK_lh	as Run 27, but using QDisp_lh_fa instead of QDisp_lg_GK_lh_fa and Wegenetz_lh_mb, instead of Wegenetz_lg_mb,
Run 70	Waldsat_lg_mb, VW-DHM10, HN-DHM10, Wegenetz_lh_mb, HK-DHM10, QDisp_lh_fa_NS_lh, Sub_GK_lh	as Run 69, but using QDisp_lh_fa_NS_lh instead of QDisp_lh_fa; as Run 28 but using Wegenetz_lh_mb instead of Wegenetz_lg_mb and QDisp_lh_fa_NS_lh instead of Sub_GK_lh and QDisp_lg_GK_lh_fa
Run 71	Waldsat_lg, VW-DHM10, HN-DHM10, Wegenetz_lg, QDisp_lg_BK_fa, NS_lh, BK	as Run 58, but using Waldsat_lg instead of Waldsat_lg_mb, Wegenetz_lg instead of Wegenetz_lg_mb; as Run10, but using NS_lh, QDisp_lg_BK_fa instead of QDisp_lg_GK_lg_fa, BK instead of Sub_GK_lg, Waldsat_lg instead of Waldsat_lg_mb and Wegenetz_lg instead of Wegenetz_lg_mb
Run 72	Waldsat_lg, VW-DHM10, HN-DHM10, Wegenetz_lg, QDisp_lg_BK_fa, BK	as Run 33, but using Waldsat_lg instead of Waldsat_lg_mb, Wegenetz_lg instead of Wegenetz_lg_mb; as Run10, but using QDisp_lg_BK_fa instead of QDisp_lg_GK_lg_fa, BK instead of Sub_GK_lg, Waldsat_lg instead of Waldsat_lg_mb and Wegenetz_lg instead of Wegenetz_lg_mb; as Run 30, but using BK instead of Sub_GK_lg, as Run 71 without NS_lh
Run 73	Waldsat_lg, VW-DHM10, HN-DHM10, Wegenetz_lg, QDisp_lg_GK_lh_fa, Sub_GK_lh, NS_lh	as Run P2, but using Waldsat_lg instead of Waldsat_lg_mb, Wegenetz_lg instead of Wegenetz_lg_mb; as Run10, but using QDisp_lg_GK_lh_fa instead of QDisp_lg_GK_lg_fa, Sub_GK_lh instead of Sub_GK_lg, NS_lh, Waldsat_lg instead of Waldsat_lg_mb and Wegenetz_lg instead of Wegenetz_lg_mb
Run P1	Waldsat_lg_mb, VW-DHM10, HN-DHM10, Wegenetz_lg_mb, QDisp_lh_fa, Sub_GK_lg	as Run 10, but using QDisp_lh_fa instead of QDisp_lg_GK_lg_fa
Run P2	Waldsat_lg_mb, VW-DHM10, HN-DHM10, Wegenetz_lg_mb, QDisp_lg_GK_lh_fa, Sub_GK_lh, NS_lh	as Run10, but using QDisp_lg_GK_lh_fa instead of QDisp_lg_GK_lg_fa, Sub_GK_lh instead of Sub_GK_lg, adding NS_lh; as Run 48_A adding NS_lh

The following discussion is presenting the results of the model runs performed using "level high" parameter maps. The results are analysed in a manner analogous to the "low level" runs (Chapter 7.2.2.1.) and compared -- summarized by parameter map -- on the basis of the validation strategy presented in 7.2.1.

Basic disposition based on soil map (BK)

💡 Significance of the parameter map *basic disposition based on soil map (BK):*

The integration of this parameter resulted in a very mild deterioration in model performance. This is also the case compared to the parameter map *geological basic disposition "level low,"* whereas compared to the parameter map *geological basic disposition "level high,"* there was a slight improvement in the model performance. The influence of this parameter on the result is moderate and thus clearly greater than that of the *geological basic dispositions* "level low" and "level high. The parameter is influencing the result in the expeted direction, which is shown in higher susceptibilities in the regions of higher basic disposition based on the soil map.

In run 33, this parameter was included in the modelling together with *subsurface flow disposition "level low"* based on the soil map and flow accumulation (*QDisp_lg_BK_fa*), in addition to the parameters from run 3. In order to investigate the influence of this parameter on the model performance, the results of runs 48_D and 6 were compared, with run 48_D having the same parameter combination as run 6, but also containing the parameter map *BK*. A comparison was made to the parameter *Sub_GK_lg* through juxtaposition of runs 33 and 24, 56 and 10, 48_D and 14, and finally 46 and P1. There was a comparison to the parameter Sub_GK_lh through juxtaposition of the runs 46 and 48_B and 33 and 48_C (for the parameter combinations of the runs, Tab. 7.2.2.1-1 and 7.2.2.2-1).

It was shown that in all runs, the parameter *BK* influenced results in the expected direction. There were lower susceptibilities in areas with lower basic disposition based on the soil map, whereas higher susceptibilities occurred in areas of higher basic disposition. As the sensitivity analysis of run 33 shows (Fig. 7.2.2.2-1), the influence of this parameter on the result can generally be termed moderate, however it is still obviously greater than that of *Sub_GK_lg* (Fig. 7.2.2.1-10) and *Sub_GK_lh*.
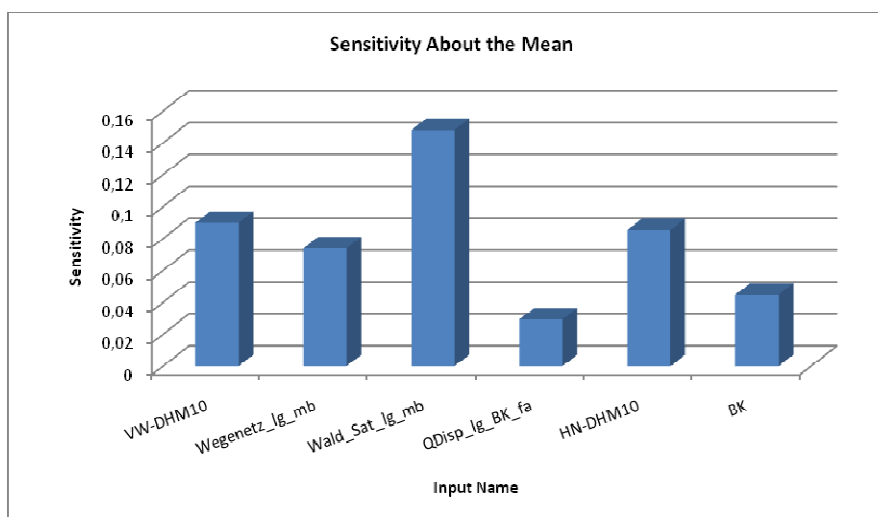
Fig. 7.2.2.2-1: Sensitivity analysis of run 33

The validation comparison of the runs 48_D and 6 (Tab. A2 in Annex) showed that the integration of this parameter into the modelling leads to a very slight deterioration

in model performance. Compared to the parameter *Sub_GK_lg*, consideration of this parameter, despite the strong influence on the result, also lead to a (very) slight deterioration in model performance, whereas compared to the parameter map *Sub_GK_lh*, there was a slight improvement in model performance.

Geological basic disposition "level low" *(Sub_GK_lg)*

Significance of the parameter map *geological basic disposition "level low" based on the conceptual soil map (Sub_GK_lg):*

Compared to the parameters *geological basic disposition "level high"* and *basic disposition based on the soil map*, this parameter led to a mild improvement in model performance (see above and below). This is remarkable, because its influence on modelling is weak and acts in the "opposite" direction than expected, whereas the two other parameters have a moderate influence on modelling in the expected direction.

This parameter had already been included in modelling in the "level low" runs (Chapter 7.2.2.1), however it is also included here, in the "level high" parameter maps, due to the comparisons to *Sub_GK_lg* and *BK*. Based on the comparison of the runs P1 to run 40, the integration of *Sub_GK_lg* in modelling, compared to the non-inclusion of this parameter, can also be analysed at "level high." Here too, it was shown, analogously to the "level low" runs, that the integration of *Sub_GK_lg* resulted in a slight improvement in model performance, even though the parameter had only a weak influence and in the "opposite" direction than expected on the modelling.

The comparisons to the two other basic disposition maps *BK* and *Sub_GK_lh* will be explained in more detail on the respective parameter maps. However, it was shown that *Sub_GK_lg*, compared to *Sub_GK_lh*, led to a slight improvement in the model performance, and that compared to BK, a tendency was seen toward a very slight improvement in the model performance (Tab. A2 in Annex). That is quite remarkable, because *Sub_GK_lg* shows a weak influence on the model result and acts in the "opposite direction," whereas the two other parameters have a moderate influence, and in the expected direction in modelling.

Geological basic disposition "level high" *(Sub_GK_lh)*

Significance of the parameter map *geological basic disposition* "level high" based on conceptual soil map *(Sub_GK_lh):*

Integration of this parameter does not result in any clear tendency toward improvement in the model performance. However, it was seen, when compared to both the "level low" map and the *basic disposition based on soil map*, that this parameter led to a slight deterioration in the model performance. That was remarkable, because the "level high" map has a stronger influence on modelling compared to the "level low" map, and in contrast to the "level low" map, it influences modelling in the expected direction.

This parameter was included in modelling in run 43, in addition to the parameters from run 5. In order to study the influence of this parameter on model performance,

there was a comparison of the results of the runs 43 and 5, and also those of runs 48_A and 6, and those of 48_B and 40. Here, the first of the runs compared has in each case the same parameter combination as the second run, however with the addition of the parameter *Sub_GK_lh* (Tab. 7.2.2.2-1). In order to compare the two parameter maps *Sub_GK_lh* and *Sub_GK_lg*, the runs 43, 48_A, 48_C and 48_B were juxtaposed to the runs 10, 14, 24 und P1 respectively, the former group containing "level high" maps and the latter "level low" maps (Tab. 7.2.2.1-1). The comparison to parameter *BK* was then made via the runs 48_B and 46, and 48_C and 33 (see *BK*).

The difference map for run 43 compared to run 5 (Fig. 7.2.2.2-2) now shows that the "level high" parameter map *Sub_GK_lh*, in contrast to the "level low" parameter map *Sub_GK_lg* (Chapter 7.2.2.1), influences modelling in the expected direction. Thus, in run 43, higher susceptibilities (blue) occur in the region of higher geological basic disposition (generally black shale, green shale), whereas lower susceptibilities (red) occur in the areas that are classified as less landslide-prone (generally phyllitic mica schist). The sensitivity analysis of run 43 (Fig. 7.2.2.2-3) shows that the parameter *Sub_GK_lh* has a moderate influence on the model result. The influence of this parameter is therefore obviously stronger than that of *Sub_GK_lg* (Fig. 7.2.2.1-10), however it is also weaker than that of *BK* (Fig. 7.2.2.2-1).
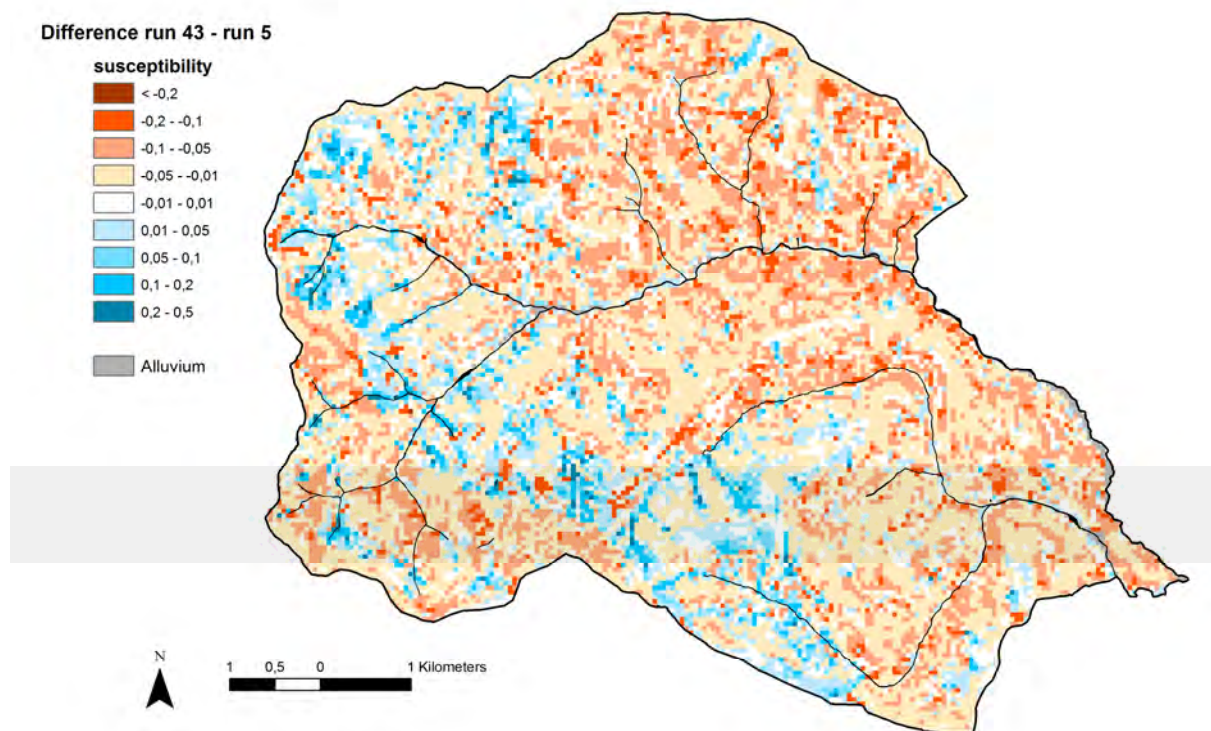
Fig. 7.2.2.2-2: Difference map of run 43 - 5
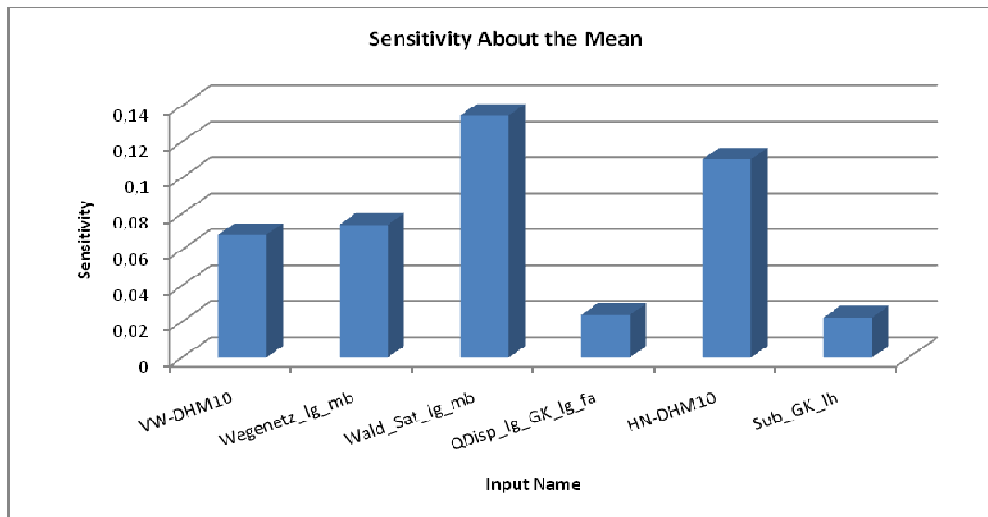
Fig. 7.2.2.2-3: Sensitivity analysis of run 43

The validation comparisons (Tab. A2 in Annex) concerning integration of the parameter map *Sub_GK_lh* into modelling now show no unequivocal picture. Whereas in runs 43 and 48_A, there is a slight deterioration in the model performance due to the inclusion of *Sub_GK_lh*, in run 48_B, the inclusion of this parameter produces a very slight improvement. On the other hand, the validation comparisons relating to *Sub_GK_lg* and *BK* present a very clear picture: in all four comparisons to the "level low" parameter map, as well as in the two comparisons to basic disposition based on the soil map (see *BK*), use of the "level high" parameter maps leads to a slight deterioration in the model performance.

This demonstrates that none of the attempts to integrate more realistic or process-oriented basic disposition maps of the geosphere into models led to improvement in the model performance. However, this does not necessarily mean that the geological basic disposition map "level high," for example, is not more realistic and more process-oriented than the "level low" map, because it should be kept in mind that model performance is ultimately measured by the validation method/strategy used. The somewhat poorer validation results obtained through integration of the parameter map *Sub_GK_lh* might also be due to the validation methods employed simply not being able to depict the improvements the map produced, because the methods used are always area-wide and thus incapable of detecting partial improvements (cf. Chapter 7.1). This deficit highlights the need for new, partial validation methods. Furthermore, it is also conceivable that the improvement in *Sub_GK_lh* simply cannot be detected by the model, because the available data (other parameter maps and process data) is not of sufficient quality to reproduce the complex events in nature on a 1:1 basis.

Comparison of all "geosphere" parameter maps

- geological basic disposition "level low" based on conceptual soil map "level low"*(Sub_GK_lg):*

- geological basic disposition "level high" based on conceptual soil map "level high" *(Sub_GK_lh):*

- Basic disposition based on soil map *(BK):*

In the case of these three parameters, only integration of the "level low" map leads to a slight improvement in model performance. However, this parameter map influences modelling in the "opposite" direction than expated. This means that there is a decrease in susceptibility in areas with higher geological basic disposition. However, the other two parameter maps influence modelling in the expected direction. The strongest influence on the result is seen in the *basic disposition based on the soil map*, followed by the "level high" parameter map, and then by the "level low" parameter map, which has only a very weak influence. The first two have a moderate influence on the result.

Compared to the other two parameter maps, the "level low" parameter map, despite its weak influence in the "opposite" direction, leads to a slight improvement in the model performance. When comparing the other two maps, the "level high" parameter map shows poorer model performance.

However, this does not necessarily mean that the *geological basic disposition map "level high"* is less realistic or process-oriented than the "level low" map. The poorer model performance measured by the validation methods described might in fact be attributable to the inadequacy of the area-wide validation methods used, which in turn highlights the necessity of developing a new, partial validation method. Furthermore, it might actually be impossible to adequately depict the total complexity of nature.

Subsurface flow disposition "level low" & "level high"

Comparison of the parameter maps *subsurface flow disposition "level low" & "level high":*

- Subsurface flow disposition "level low" based on the geological map "level low" and flow accumulation (*QDisp_lg_GK_lg_fa)*

- Subsurface flow disposition "level low" based on the geological map "level high" and flow accumulation (*QDisp_lg_GK_lh_fa)*

- Subsurface flow disposition "level low" based on soil map and flow accumulation (*QDisp_lg_BK_fa)*

- Subsurface flow disposition "level high" based on field mapping and flow accumulation (*QDisp_lh_fa)*

The influence of these four "subsurface flow disposition" parameter maps on results is largely moderate and thus similarly high. In addition, the susceptibility maps produced using these parameter maps usually display only slight differences (with the exception of some results for *subsurface flow disposition "level high" based on field mapping*). The validation results for these four parameter maps are also very

similar, those for *subsurface flow disposition "level low" based on soil map* being slightly better, and those for *subsurface flow disposition "level low" based on the geological map "level high"* being slightly poorer than those for the other subsurface flow disposition maps.

The great similarity in results and model performance was already noted in the "level low" analyses and can be attributed to subsurface flow disposition usually showing only a moderate influence in the result, and the substituted parameter map "geosphere" in turn being only one of several components used in producing the parameter maps "subsurface flow disposition."

It was therefore seen that both "level high" variants (both the variant with mapped subsurface flow disposition and the variant with geological basic disposition "level high") in comparison to the level low variants, did not lead to improvement in the model performance. But in this context as well, it should also be investigated whether the cause for this might be the area-wide validation methods used (see comparison of all "geosphere" parameter maps).

In the following discussion of "level high" runs, only the results of the parameter map "field mapping and flow accumulation" (*QDisp_lh_fa*)" will be discussed in detail. As the three parameter maps *QDisp_lg_GK_lg_fa*, *QDisp_lg_GK_lh_fa* and *QDisp_lg_BK_fa* were analysed in detail in discussion of the "level low" runs (Chapter 7.2.2.1), there will be only summary discussion of the significance of these parameter maps for the model result.

<u>Subsurface flow disposition "level low" based on the geological map "level low" and flow accumulation (*QDisp_lg_GK_lg_fa*)</u>

In the validation comparison of the runs with this parameter (56 and 61) to the runs with the parameter QDisp_lg_GK_lh_fa (48_D and 62), model performance remained equally good. Compared to the runs with QDisp_lg_BK_fa (24, 48_C and 33), the results of runs with this parameter (10, 43 and 56) ranged from equally good to somewhat poorer (for run parameters, Tab. 7.2.2.1-1 and 7.2.2.2-1). Compared to the runs with the mapped subsurface flow disposition QDisp_lh_fa (40, 46 and P1), there was actually a tendency toward a slightly better model performance in the runs with this parameter (runs 5, 10 and 56). Here too, it was shown that this parameter had only a moderate influence on the result and its sensitivity, and that the maps of results usually differed little from those of the other subsurface flow disposition parameters. Somewhat larger differences in map appearance were seen only in comparisons with maps produced using the parameter QDisp_lh_fa. The validations and influences of this parameter are therefore, in general, quite similar to those of the other subsurface flow disposition parameters (significant differences appeared only to a limited extent in the comparison to QDisp_lh_fa), so it is impossible to make any clear statement on the influence of this parameter on the model performance.

<u>Subsurface flow disposition "level low" based on geological map "level high" and flow accumulation (*QDisp_lg_GK_lh_fa*)</u>

The validation comparisons of the runs with this parameter to the runs with *QDisp_lg_GK_lg_fa* show the same model performance (see *QDisp_lg_GK_lg_fa*). On the other hand, compared to the runs with *QDisp_lg_BK_fa* (33) and *QDisp_lh_fa* (P1), the runs with this parameter (48_D or 14) show a slight deterioration in model

performance (for run parameters, see Tab. 7.2.2.1.-1 and 7.2.2.2-1). Thus, compared to the other runoff parameters, this parameter tends to produce a slight deterioration in model performance. In the case of this parameter as well, sensitivity and map appearance for the result usually differ little from those of the other subsurface flow disposition parameters, the exception being the difference map for the result with *QDisp_lh_fa*.

Subsurface flow disposition "level low" based on soil map and flow accumulation *(QDisp_lg_BK_fa)*

The validation comparisons of the runs with this parameter to the results for the runs with the other subsurface flow disposition parameters tended to show a slight to very slight improvement in model performance based on this parameter. This also applies to the validation comparisons with *QDisp_lh_fa*, where model performance, after the integration of *QDisp_lg_BK_fa*, is slightly better in one case (run 33 and 46) and equally good in another (run 24 and P1) (run parameters, Tab. 7.2.2.1-1 and 7.2.2.2-1). On the other hand, sensitivities and suscepitbity maps are usually similar to those of the other subsurface flow disposition parameters, whereas compared to *QDisp_lh_fa* there are greater differences in the susceptibility maps (run 46 and 33).

Subsurface flow disposition "level high" based on field mapping and flow accumulation *(QDisp_lh_fa)*

This parameter was included in modelling in run 40, in addition to the parameters from run 3. Therefore, in order to study the influence of this parameter on model performance, these two runs were compared. The comparison to *QDisp_lg_GK_lg_fa* was performed by juxtaposing the runs 40 and 5, 46 and 56, and P1 and 10; the comparison to *QDisp_lg_GK_lh_fa* by juxtaposing runs P1 and 14, and the comparison to *BK* by juxtaposing the runs 46 and 33 and P1 and 24 (for run parameters, Tab. 7.2.2.1-1 and 7.2.2.2-1).

It was shown that the influence of this parameter on the result was moderate, as it was in the case of the other subsurface flow disposition variants. Only in run 46 there was actually a stronger influence. It was noted that some of the susceptibility maps produced using this parameter showed greater deviations compared to those using the other subsurface flow disposition parameters than the others did among themselves. This applied to the difference maps for the runs 40 compared to 5, P1 compared to 14, 46 to 56, and 46 to 33.

With integration of this parameter into the modelling, there was a slight improvement in the model performance (see Tab. A2 in Annex). However, compared to the runs with *QDisp_lg_GK_lg_fa* and *BK*, there was a very slight deterioration in the model performance with this parameter, whereas compared to *QDisp_lg_GK_lh_fa*, there was a slight improvement. On the whole, therefore, no definite statement can be made on the influence of this parameter on model performance compared to the other subsurface flow disposition parameters.

Forest "level high" based on satellite data

💡 Significance of the parameter map *forest* "level high" based on satellite data (*Wald_Sat_lh)*:

This parameter map is just as influential in modelling as the "level low" satellite data forest map *without* mapped forest distribution, however its influence is obviously weaker than the "level low" satellite data forest map *with* mapped forest distribution. Integrating this parameter into modelling improved the model performance. However, compared to the "level low" satellite data forest map *without* mapped forest distribution (and this is the decisive comparison), there was a slight deterioration in model performance, and compared to the "level low" satellite data forest map *with* mapped forest distribution, there was an obvious deterioration in model performance. On the whole, therefore, the forest map "level high" did not contribute to an improvement, but rather to deterioration in the model performance.

This parameter was included in modelling in run 35. In order to study the influence of this parameter on the model performance, run 36 was compared to run 13 (which has the same parameters as run 36, but without forest). A comparison to the previously used forest map *Wald_Sat_lg_mb* was made with run 35 by means of run 2, which contains the same parameters as run 35, however instead of *Wald_sat_lh,* run 2 contains the mapped forest distribution *Wald_Sat_lg_mb*. However, because the parameter *Wald_Sat_lh* contains no mapped forest distribution, it can only be compared on an equal basis with the parameter *Wald_Sat_lg*, which also contains no mapped forest distribution. This was done through the comparison with run 31 (for run parameters, Tab. 7.2.2.1-1 and 7.2.2.2-1).

The sensitivity analysis of run 35 showed that *Wald_sat_lh* had an influence on the result that was approximately equal to that of the other forest map without mapped forest distribution (*Wald_sat_lg*), but that it was definitely weaker than that of the forest map with mapped forest distribution (*Wald_Sat_lg_mb*. When comparing the susceptibility maps for the runs 2 and 35 (analogous to run 31), this lead in run 35 to a rise in susceptibility in forest and a decrease in susceptibility outside forest. Furthermore, the difference map for runs 35 and 31 also showed somewhat higher susceptibilities outside forest in run 31, whereas in forest, there could be great variation in the differences. The dichotomous variable *Wald_sat_lg* thus produces stronger differentiation between forest/non-forest than the polytomous variable *Wald_sat_lh*, whereas inside the forest, only the latter can, by the nature of things, produce differention.

The validation comparisons (Tab. A2 in Annex) now showed that the integration of this parameter, compared to non-consideration of this parameter, clearly improved model performance. However, compared to *Wald_Sat_lg_mb*, model performance strongly deteriorated. The most significant comparison, however, is that to *Wald_Sat_lg*, and even here there was also a slight deterioration in the result of *Wald_sat_lh*. The forest map "level high" thus made no contribution to improving the model performance (resulting rather in deterioration). Because the influence of this parameter also decreased, it should probably not be assumed that there would be noticeable improvement with the use of a different, partial validation method (see comparison of the parameter maps *basic disposition of the geosphere*).

Influence area of road network "level high" based on DCM, aerial photography and field mapping

---

💡 Significance of the parameter map "level high" *(Wegenetz_lh_mb)*

The integration of this parameter leads to a slight improvement in model performance, however compared to *road network* "level low," there is also deterioration of varying degrees in model performance. This parameter also has a weaker influence on modelling than the "level low" variant. The reason for this is that through enlargement of the surface by coding "influence area yes," the correlation between this parameter and the mass movement distribution is definitely weakened.

This parameter was included in modelling in run 37, in addition to the parameters from run 2. The change caused by the integration of this parameter could be studied from the comparison of these two runs. Comparisons to the parameter road network "level low" were performed by juxtaposing the runs 37 and 3, 48_E and 48_D, and 53 and 33 (for run parameters, Tab. 7.2.2.1-1 and 7.2.2.2-1).

As the sensitivity analysis of run 37 (Fig. 7.2.2.2-4) now shows, in a manner representative of the runs with this parameter, *Wegenetz_lh_mb* has only a moderate and therefore decidedly weaker influence than *Wegenetz_lg_mb* on modelling.
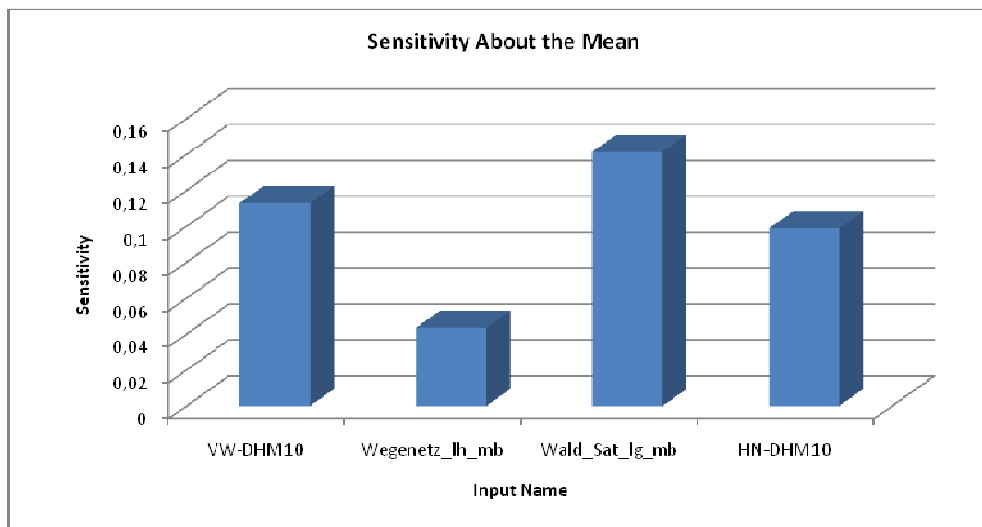
Fig. 7.2.2.2-4: Sensitivity analysis of run 37

The difference map of runs 37 and 3 (Fig. 7.2.2.2-5) shows that in the case of those roads that are included in both road system maps (*Wegenetz_lh_mb* and *Wegenetz_lg_mb*, roads visible on the diagram), run 3 shows higher susceptibilities (red), while in the roads that appear only in *Wegenetz_lh_mb*, run 37 produces higher susceptibilities (blue). This proves that *Wegenetz_lg_mb* is more influential in modelling than *Wegenetz_lh_mb*, but that *Wegenetz_lh_mb* nevertheless has an influence on the susceptibility map. The fact that *Wegenetz_lh_mb* has a weaker influence is attributed to the area with the coding "influence area yes" being much larger here than in *Wegenetz_lg_mb*, even though this does not result in an increase in the number of mass movements lying within the influence area of the roads (because attribution is done according to land-use coding). However, this also

weakens the correlation between mass movement distribution and the influence area of roads.
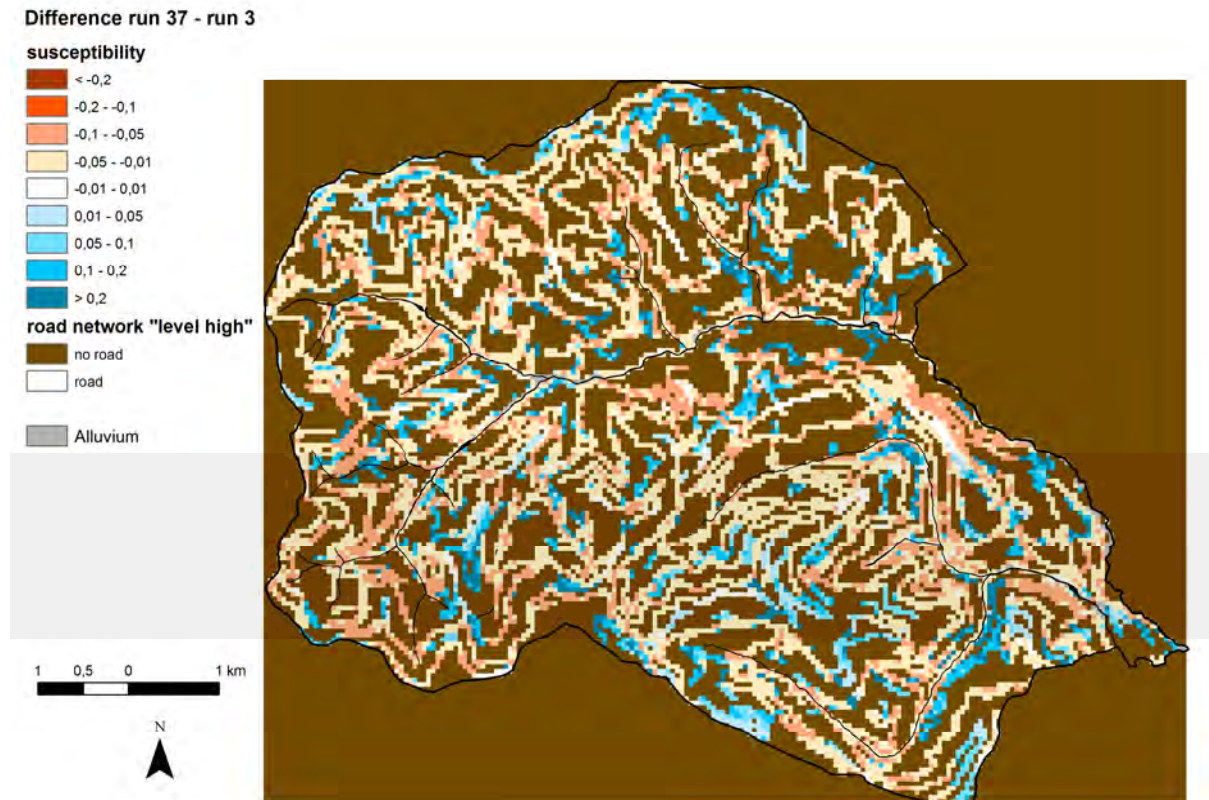
Fig. 7.2.2.2-5: Difference map of run 37 - 3

A comparison of the validations (Tab. A2 in Annex) now showed that integration of this parameter did lead to a slight improvement in the model performance, but that in all three cases, compared to *Wegenetz_lg_mb*, there was a deterioration (of varying intensity) in model performance. Completion of the road network by means of satellite image analysis did not improve model performance either, rather the opposite. Because this also diminished the influence of this parameter, it seems unlikely that improvements would be seen if it were used with another, partial validation method (see comparison of parameter maps *basic disposition of the geosphere)*.

Curvature classification

Significance of the parameter map *curvature classification* (*HK-DHM10)*
This parameter always results in a (mild) deterioration in model performance.

Because this parameter has been studied in connection with the "level low" runs, it will not be discussed in detail here. In order to study changes in model performance resulting from this parameter, the runs 55 and 33 and 27 and 48A were compared in the "level high" analyses (for run parameters, Tab 7.2.2.1-1 and 7.2.2.2-1). It was seen here, as in the "level low" runs, that the integration of this parameter always resulted in a (slight) deterioration in model performance (Tab. A2 in Annex). Here

too, in the sensitivity analysis, the class 0 (= dell: horizontal and vertical concave) had the greatest influence on the result, although this was not visible in the difference map.

Precipitation *"level high" (NS_lh)*

Comparison of the parameter maps *precipitation* – "level high":

- Precipitation "level high" as an independent parameter *(NS_lh)*

- Precipitation "level high" integrated into subsurface flow disposition "level low" based on the geological map "level low" and flow accumulation (*QDisp_lg_GK_lg_fa_NS_lh*)

- Precipitation "level high" integrated into subsurface flow disposition "level low" based on the geological map "level high" and flow accumulation (*QDisp_lg_GK_lh_fa_NS_lh*)

- Precipitation "level high" integrated into subsurface flow disposition "level low" based on soil map and flow accumulation *(QDisp_lg_BK_fa_NS_lh)*

- Precipitation "level high" integrated into subsurface flow disposition "level high" based on field mapping and flow accumulation (*QDisp_lh_fa_NS_lh*)

As an independent parameter, precipitation "level high" has a strong influence on modelling and therefore causes major changes in the susceptibility map, with a rise in susceptibility in areas of high precipitation and a decrease in susceptibility in areas of low precipitation. Here, the influence of precipitation "level high" on the result is clearly even greater than at precipitation "level low," which results in mild improvement in model performance compared to the "level low" results.

In integrated form, however, this parameter has hardly any influence on modelling and usually causes only very slight changes in the susceptibility map. However no tendency toward improvement in model performance through integration of precipitation "level high" could be seen compared to non-consideration of this parameter (analogue to "level low"), neither in independent nor in integrated form.

Precipitation "level high" was included in modelling in both independent and integrated form. In both cases, it was combined with the subsurface flow dispositions *QDisp_lg_GK_lg_fa* (runs 59 and 61), *QDisp_lg_GK_lh_fa* (runs 60, 62 and P2), *QDisp_lg_BK_fa* (runs 58 and 68) and *QDisp_lh_fa* (runs 63 and 65) respectively (Chapter 5.4; for run parameters, Tab. 7.2.2.1-1 and 7.2.2.2-1).

Fig. 7.2.2.2-6 now shows the susceptibility map from run 58 as an example of results with *NS_lh* as an **independent parameter**. There are noticeably higher susceptibilities extending from the centre to the southeast of the area, which is the region of high precipitation "level high." As before with "level low," the neural network reacts to the parameter NS_lh, and in the expected direction. This can be seen even more clearly in the difference map for runs 58 and 33 (Fig. 7.2.2.2-7). That map also clearly demonstrates that strong differences occur, from which it can be concluded that *NS_lh* is a strong factor in modelling.
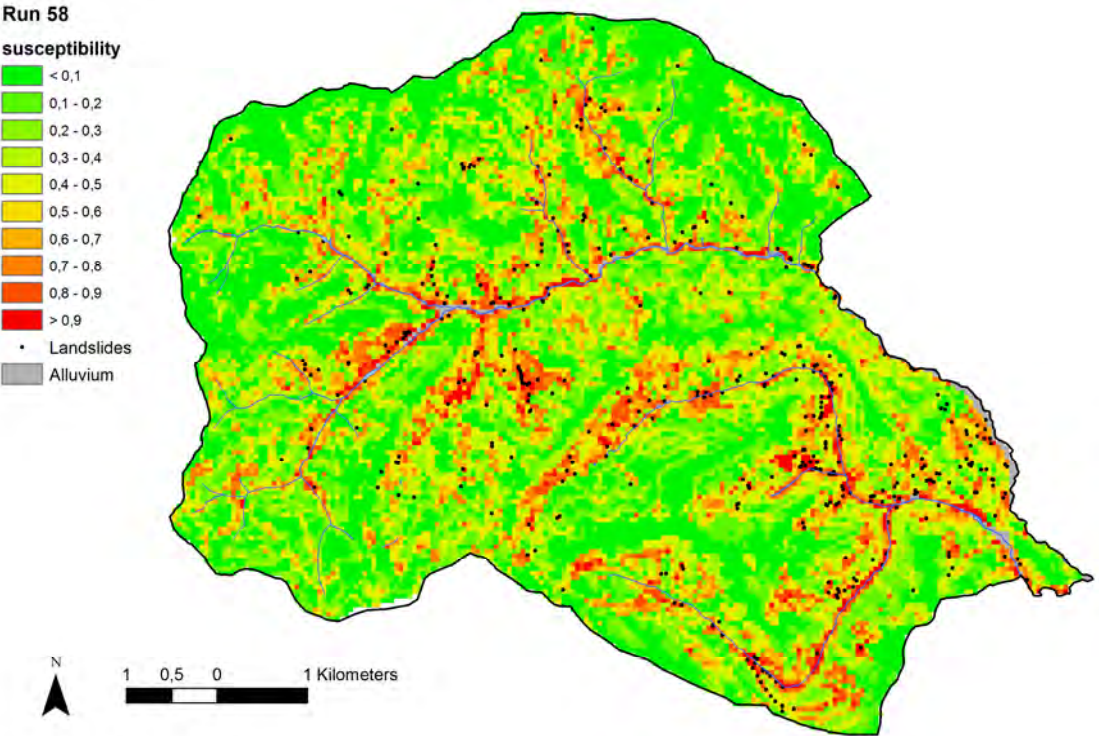
Fig. 7.2.2.2-6: Susceptibility map of run 58
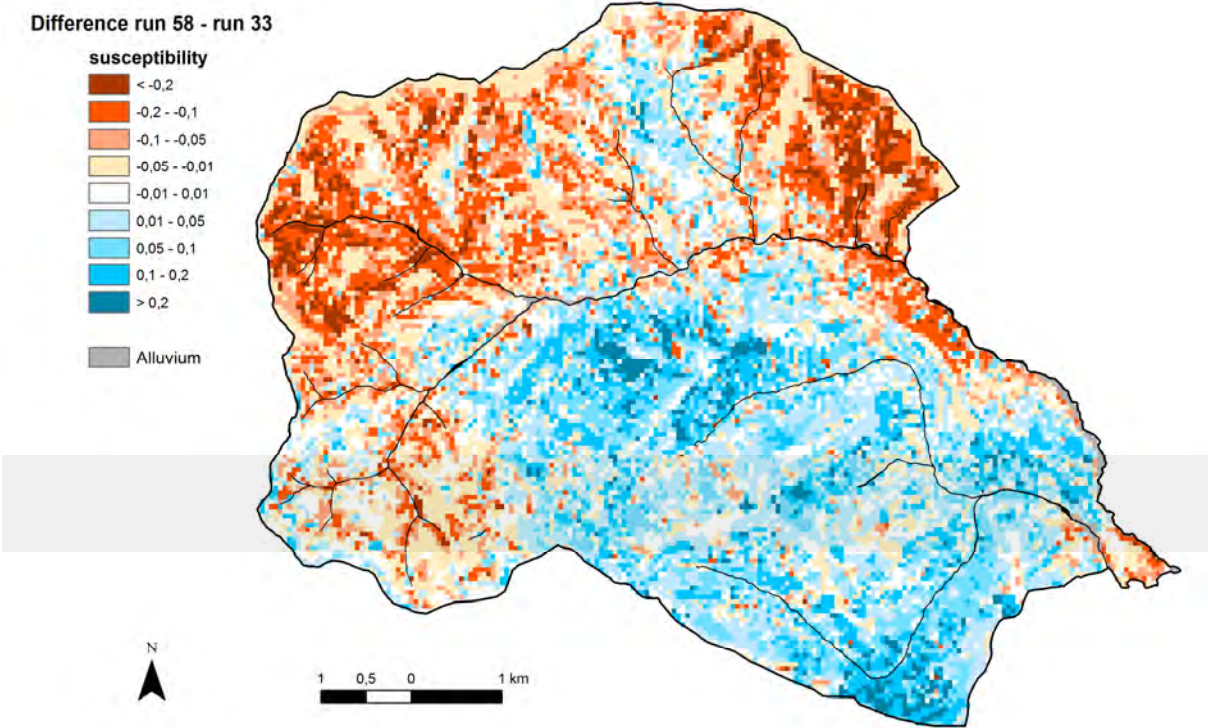
Fig. 7.2.2.2-7: Difference map of run 58 – run 33

The sensitivity analysis of network 58 (Fig. 7.2.2.2-8) shows that precipitation "level high," as previously assumed, has actually a strong influence on the modelling result (equal to that of the road network), and that it obviously plays a bigger role than precipitation "level low" (Fig. 7.2.2.1-13).
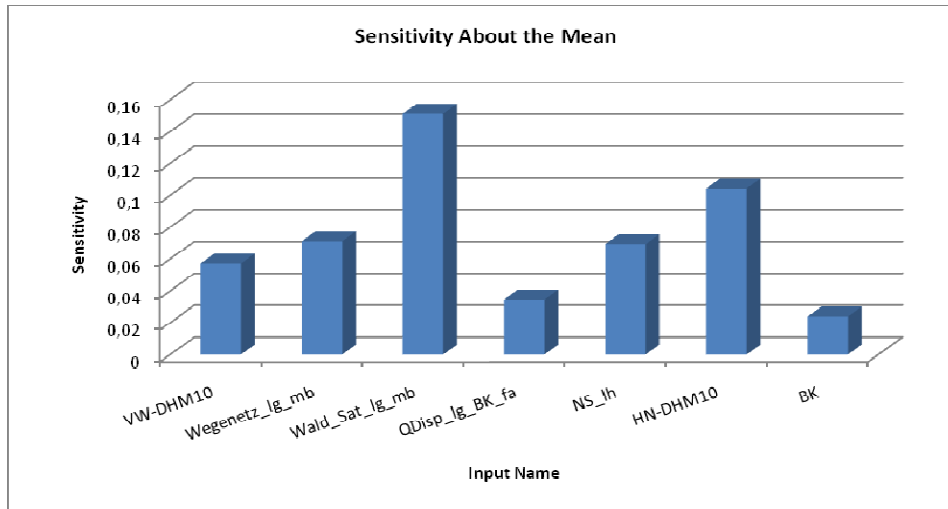
Fig. 7.2.2.2-8: Sensitivity analysis of run 58

In order to investigate the influence of *NS_lh* as an independent parameter on model performance, there was a comparison of runs with the same parameter combination, but with *NS_lh* (runs 58, 59, 65 and P2) and without *NS_lh* (runs 33, 10, 46 and 48_A). The comparisons of *NS_lh* to *NS_lg* were performed by juxtaposing runs 58 and 34, 59 and 20, and 65 and 64 (for run parameters, Tab. 7.2.2.1-1 and 7.2.2.2-1).

Due to the strong influence of *NS_lh* on modelling, it came as something of a surprise that the integration of this parameter now brought no visible improvement in model performance (Tab. A2 in Annex). The four comparisons of runs with and without this parameter were equally good in two cases; in one case, a run with this parameter was slightly better; and in one case slightly worse. Based on this equality in model performance, despite strongly differing susceptibility maps, it can once again be concluded that there is a need for a new, partial validation method that can better differentiate and reflect the differences in results in model performance (see comparison of the parameter maps *basic disposition of the geosphere*).

However, compared to the runs with "level low" precipitation, it was seen that the integration of "level high" precipitation always led to a slight improvement in model performance.

In order to investigate the influence of *NS_lh* as an **integrated parameter** on model performance, there was a comparison of runs with the same parameter combination, but with (runs 60, 61, 63, 68 and 70) and without *NS_lh* (runs 48_D, 10, 46, 33 and 69). The comparisons to *NS_lg* were made by juxtaposing the runs 61 and 21, and 62 and 22. Finally, by juxtaposing runs 65 and 63, and 58 and 68, a comparison was made to *NS_lh* as an independent parameter (for run parameters, Tab. 7.2.2.1-1 and 7.2.2.2-1).

It was now seen, as in the case of "level low" precipitation, that precipitation "level high," in integrated form, usually exerted only a weak influence on the modelling result, and that this influence was also weaker than that of *NS_lh* as an independent parameter. Quite small differences are therefore seen in the difference maps of runs with and without integrated precipitation "level high," and precipitation distribution is scarcely traced. Furthermore, in the sensitivity analysis as well, the integration of *NS_lh* in integrated form generally changes very little (there are exceptions, however), so that subsurface flow dispositions with integrated precipitation "level high" (*QDisp_lg_GK_lg_fa_NS_lh,* *QDisp_lg_GK_lh_fa_NS_lh,* *QDisp_lg_BK_fa_NS_lh* and *QDisp_lh_fa_NS_lh*) also show a moderate influence on the result in most cases. Generally speaking, therefore, it has to be said that the neural network hardly reacts in any significant way to integrated precipitation "level high." That in turn can be attributed to the subsurface flow disposition containing *NS_lh*, usually having only a moderate influence on the result, and *NS_lh* in turn making up only part of that parameter.

Given the slight influence of NS_lh in integrated form, it is not surprising that the validation comparisons (Tab. A2 in Annex) showed no improvement (rather a slight deterioration) in model performance with the integration of this parameter. It was even demonstrated that *NS_lh* in integrated form, compared to *NS_lh* in independent form, resulted in mild deterioration in model performance. Finally, the comparison of the two integrated parameters *NS_lg* and *NS_lh* showed that this did not lead to any change in model performance.

<u>Forest and road network without land-use mapping</u>

<div style="border:1px solid">

💡 <u>Significance of the parameter maps *forest* and *road network without land-use mapping* (*Wald_Sat_lg, Wegenetz_lg)*</u>

Use of the parameter maps *without* land-use mapping (regionalisation data) results in a very strong deterioration in the model performance compared to parameter maps *with* mapped land-use. When *forest* is integrated *without* land-use mapping, the neural network can no longer recognize its stabilizing effect as clearly, and the parameter is no longer showing great influence on the modelling result. The mapping of land-use information (particularly forest and roads) is therefore enormously significant in the event documentation of mass movements.

</div>

The influence of regionalization data [= forest and road network data without land-use mapping (*Wald_Sat_lg, Wegenetz_lg,* see Chapter 6.1.2)] on the model performance was studied by means of the runs 71, 72 and 73. For this purpose, there was a comparison between the runs with regionalization data and those with the same parameter combinations, but with mapped land-use data (*Wald_Sat_lg_mb*, *Wegenetz_lg_mb*) (runs 58, 33 and P2, for run parameters, Tab. 7.2.2-1).

Here too, a comparison to the runs with mapped land-use showed the same phenomenon as with the "level low" runs: the parameter *Wald_Sat_lg* has a weaker influence on modelling, so that in forest, there is an increase, and outside forest there is a decrease in susceptibility. The parameter *Wegenetz_lg* has an unexpectedly strong influence on modelling, so that there is often an increase in susceptibility (with the exception of run 72) in the influence area of roads.

The validation comparison (Tab. A2 in Annex) showed, as seen at the "low level" results, the clearest picture of any obtained in this project: all of the runs (71, 72 and 73) calculated with regionalisation data performed worse than the corresponding runs with mapped land-use (runs 58, 33 and P2, see also Fig. 7.2.2.2-9). In contrast to the use of regionalisation data, the use of parameters with mapped land-use greatly improved the model performance, particularly as regards the parameter *forest* (areas stabilized by tree roots). The mapping of land-use information (especially forest and roads) as part of event-documentation of mass movements is therefore enormously important, particularly when the data is subsequently incorporated into susceptibility modelling.

Validation comparison of all "level high" runs and selection of the best "level high" runs with neural networks

---

 Comparison of all "level high" parameter maps

Generally speaking, the validation results of all "level high" runs, with and without consideration of one parameter, were very similar. Thus the integration of the new "level high" parameter maps of the geosphere (*basic disposition based on soil map* or *geological basic disposition based on the conceptual soil map*) and the precipitation map "level high" resulted in scarcely any changes in model performance compared to non-consideration of these parameters. A similar situation applied with respect to the *subsurface flow disposition "level high" based on field mapping* parameter, and for *road network "level high,"* both of which, compared to non-consideration of these parameters, resulted in only slight improvements in validation results. Major differences in validation, and thus the biggest improvements in model performance, could be only achieved – as before with the "level low" runs – in the case of parameters with mapped land-use information as opposed to parameters without mapped land-use information (= regionalization data), and with the inclusion of the parameter *forest "level high"* as opposed to non-consideration of this parameter (for comparisons between "level low" and "level high" variants, see Chapter 7.2.2.3).

This fact is apparent from a comparison of all runs with "level high" parameter maps according to the validation strategy developed by GBA (Chapter 7.2.1 and Tab. A2 in Annex) and is also clearly seen in the validation of the test data for "level low" events according to Chung and Fabbri (1999) (Fig. 7.2.2.2-9). So there is essentially a broad array of run-curves in which only the runs with regionalisation data (the dashed lines for the runs 71, 72 and 73) as well as the runs containing *Wald_Sat_lh* (35 and 36) swerve downward. However, as *Wald_Sat_lh* contains no mapped land-use information, 35 and 36 should be considered regionalization data, so that this curve sequence will once again fit into the overall picture.
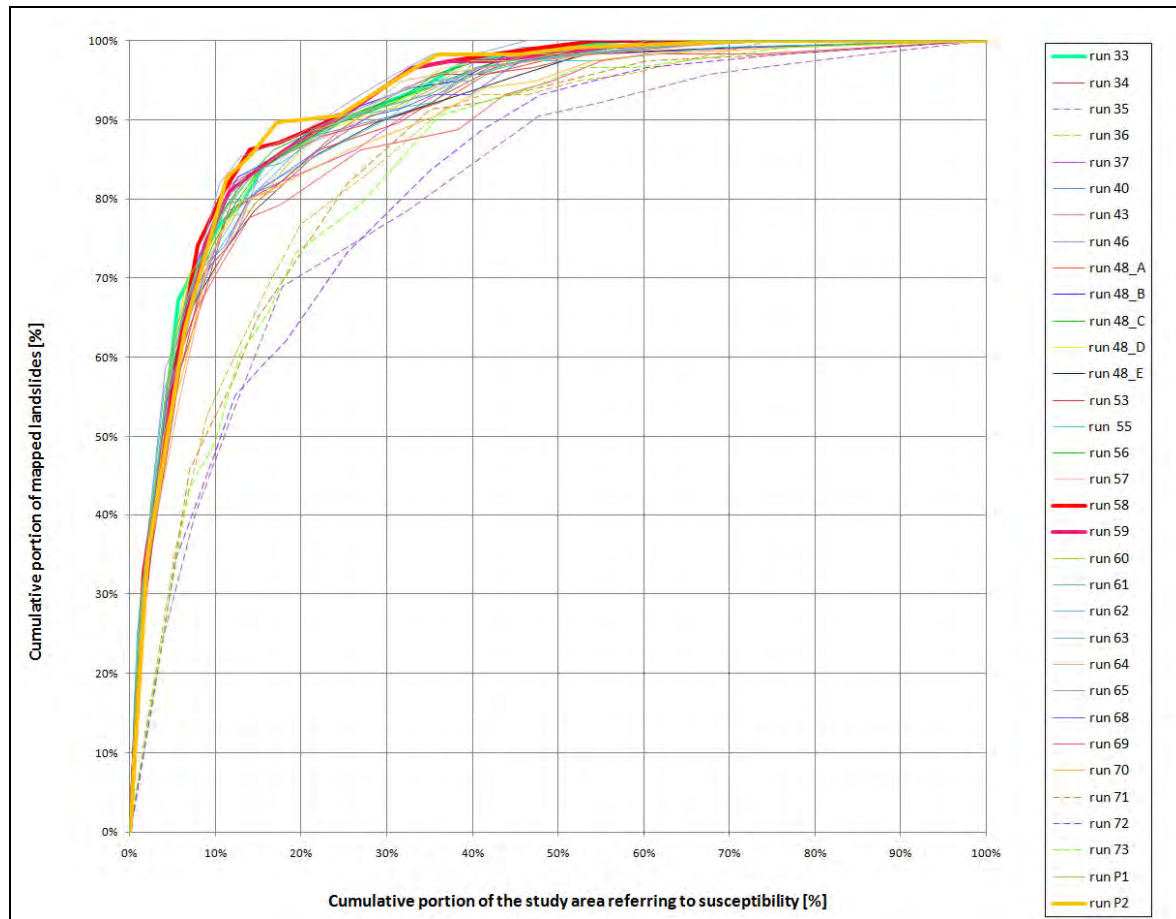
Fig. 7.2.2.2-9: Validation according to Chung & Fabbri (1999) for the test data of "level high" runs

As with the "level low" variants, there were, in the case of the "level high" variants, several results among the best runs, which, based on the validation comparisons, were classified as "equally good." The runs 33, 58, 59 and P2, which were validated as equally good, as well as run 61, which turned out to be very slightly worse as the others, were selected as the "best 5"–"level high" runs (thick lines in Fig. 7.2.2.2-9).

It is remarkable in this context that four of the "best five" runs (with the exception of run 33) display the parameter NS_lh, which appears in 58, 59 and P2 as an independent parameter and in 61, on the other hand, in integrated form. It is also striking that all of the "best five" "level high" runs include *Waldsat_lg_mb, VW-DHM10, HN-DHM10, Wegenetz_lg_mb* and also one of the "level low" subsurface flow disposition parameters. This clearly demonstrates, based on the better validation results, that the "level low" variants are preferable to the "level high" variants (see Chapter 7.2.2.4). In runs 33 and 58 the additional parameters were *QDisp_lg_BK_fa* and *BK*; in run 59, *QDisp_lg_GK_lg_fa* and *Sub_GK_lg*; in run 61, *QDisp_lg_GK_lg_fa_NS_lh* and *Sub_GK_lg*; and in run P2, *QDisp_lg_GK_lh_fa, Sub_GK_lh and NS_lh* (for run parameters, see Tab 7.2.2.2-1). Thus, for the "best 5"-"level high" runs, all three geosphere basic disposition maps were used, and the two best runs contained *BK* (run 58) and *Sub_GK_lh* (run P2). In the test data, run 58, one of the two best runs, showed an AUC for Chung & Fabbri (1999) of 92.64%, and 92.99% for ROC, a recognition rate of 90.5%, and with the GBA validation method, a value of 57.88.

7.2.2.3 Modelling results using process-oriented parameter maps

---

Significance of modelling results using process-oriented parameter maps

A deterioration in model performance was seen in all runs that used process-oriented parameter combinations exclusively, the "level high" runs showing even greater deterioration in model performance than the "level low" runs.

Runs with process-oriented parameter combinations exclusively were introduced into the method of model integration of parameter maps according to the description in Chapter 6.2, for both "level low" and "level high" runs. These parameter combinations were established in advance, based on the authors' expert knowledge, and were thus different from the other parameter combinations, which were found through successive search, validation, and selection. That this procedure was justified can be seen from that fact that four of the five runs with process-oriented parameter combinations were not among the lot of runs found through successive searches.

In the case of "level low" variants, the runs 26 (=19), 27 and 28 exhibited process-oriented parameter combinations. For the "level high" variants, these were the runs 69 and 70. The "level low" variants were comprised of the parameters *Wald_sat_lg_mb, Wegenetz_lg_mb, HN-DHM10, VW-DHM10* and *HK-DHM10*; run 26 also containing *QDisp_lg_GK_lg_fa* and *Sub_GK_lg*; whereas run 27 contained *QDisp_lg_GK_lh_fa* and *Sub_GK_lh*. And finally, run 28 was calculated with the parameters of run 26 (=19) plus *NS_lg*. The "level high" variants exhibited both the parameters *Wald_sat_lg_mb, Wegenetz_lh_mb, HN-DHM10, VW-DHM10, HK-DHM10* and *Sub_GK_lh*; run 69 also containing the parameter *Qdisp_lh_fa*, and run 70 the additional parameter *QDisp_lh_fa_NS_lh*, which had been augmented with the integrated precipitation (for run parameters, see Tab 7.2.2.1-1 and 7.2.2.2-1).

Here too, phenomena appeared that had also been observed in previous runs: because all runs with process-oriented parameter combinations contain the curvature classification *HK-DHM10*, which is highly differentiating on a small scale, their susceptibility maps usually present a rather agitated appearance. Here, the class 0 (=dell) is the curvature class with the strongest influence on model result. In the "level high" runs with *Wegenetz_lh_mb*, it was shown that this parameter had again an obviously weaker influence than the corresponding "level low" parameter *Wegenetz_lg_mb*.

In order to make statements on model performance, the runs with process-oriented parameter combinations were now subjected to validation comparisons with one of the best "best 5" runs from "level low" and "level high" respectively. Here, both "level low" comparisons (with run 10) and "level high" comparisons (with run 58) presented the same picture: in all runs with process-oriented parameter combinations, there was a deterioration in model performance. The level high" runs usually displayed even greater deterioration in model performance than the "level low" runs, where the runs 26 and 28 were only slightly worse than run 10. This meant that the model performance in the "level low" runs was also somewhat better than that in the "level high" runs.

7.2.2.4 Comparison of "Level Low" and "Level High" Results

💡 Comparison of "level low" and "level high" results and selection of the best results

The validation comparisons of "level high" with "level low" runs showed that the "level high" parameter maps only rarely contributed toward an improvement in model performance. Slight improvements compared to "level low" were largely seen only with *"level high" precipitation as an independent parameter*. In the case of all other "level high" parameter maps, however, there was no improvement compared to the respective "level low" parameter maps, and in many cases there was actually a deterioration in the model performance.

Validation comparisons of the "best 5"-"level low"- with the "best 5"-"level high"-runs showed that the differences between all results were quite small. However the results of the "level high" runs were at least slightly better than those of the "level low" runs. This can be explained by all of the best "level high" runs being calculated with the parameter *"level high" precipitation as an independent parameter*. That also applied to the overall best results 58, 59 and P2. The results of runs with combinations of process-oriented parameter maps were even worse than those of the "low level" runs. That too would be good, if it was checked by means of new partial validation methods that remain to be developed.

Essentially, the conclusions provided by "level low" runs (Chapter 7.2.2.1) were largely confirmed by the "level high" runs (Chapter 7.2.2.2): the clearest and probably most important conclusion that can be drawn from the "level low" and "level high" results is that the use of parameter maps **with** mapped land-use of forest and roads led to a definite improvement in the model performance compared to parameter maps that are based exclusively on generally available data. This also underlines the enormous importance of mapping land-use information (particularly forest and roads) when documenting gravitational mass-movement events. It was also clear in both level-categories that *forest* is an important parameter that strongly contributes to improved model performance, and that *road network, subsurface flow disposition* and *geological basic disposition "level low"* tend to improve model performance to varying degrees. This is particularly remarkable in the case of *geological basic disposition*, because this parameter is influencing the model just very weakly and not in the expected (desired) direction, but rather in the opposite direction.

It was also seen in both level-categories that taking into account different subsurface flow disposition maps usually resulted in very similar susceptibility maps and validation results. A similar situation was seen when incorporating precipitation in integrated form. On the other hand, the integration of precipitation as an independent parameter map led to an obviously different distribution of susceptibilities (there was a clear pattern of precipitation distribution). However, this resulted in scarcely any improvement in the model performance. Furthermore, there was a slight deterioration in model performance in both level-categories due to curvature classification.

The following conclusions were derived from the "level low" runs only

- both forest maps (based on satellite images or DCM) resulted in the same model performance.

- profile curvature and flow accumulation led to a strong and slight improvement in model performance respectively.

The conclusions gained from "level high" runs only were that:

- *basic disposition based on the soil map* results in a slight deterioration in model performance,

- *geological basic disposition "level high"* does not show any tendency toward improvement/deterioration in model performance.

Comparison of the validation results of "level high" and "level low" runs demonstrated that "level high" parameter maps **rarely contributed to improvement** in model performance (Tab. A1 and A2 in Annex). Slight improvements compared to "level low" were in fact only seen with *"level high"* precipitation as independent parameter, which also had a much stronger influence on modelling than *precipitation "level low."* However, just how slight these improvements actually are is demonstrated by the fact that when both precipitation "*level low*" and *precipitation "level high"* were compared to runs without the parameter precipitation, no improvement in model performance was seen.

However, with all other "level high" parameter maps, there is no improvement compared to the respective "level low" parameter map. Thus, in the case of *precipitation "level high" in integrated form*, there was no change in model performance, and in the case of the two parameter maps for geosphere *(geological basic disposition "level high," basic disposition based on soil map)*, the *forest map "level high,"* the *road system "level high"* and the *subsurface flow disposition "level high" by means of field mapping*, there was even a deterioration in model performance.

In the case of subsurface flow disposition, the inclusion of a "level high" map in the "level low" subsurface flow disposition (as in the case of *subsurface flow disposition "level low" based on the geological map "level high," subsurface flow disposition "level low" based on the soil map*), resulted in virtually no improvement in model performance compared to the "level low" parameter map. The only exception here was *subsurface flow disposition "level low" based on soil map*, which in the case of two runs was slightly better than *subsurface flow disposition "level low" based on geological map "level low".*

The fact that most "level high" parameter maps produced no improvement, or even a deterioration in model performance, is remarkable, and in part incomprehensible, but it can also be **explained** to some extent. The most surprising thing is probably that *geological basic disposition "level low,"* despite its "contrary" and very weak influence on modelling, results in better model performance than the rather more accurate and more influential parameters *geological basic disposition "level high* and *basic disposition based on the soil map.*

In contrast, model performance being worse with the use of *road system "level high"* can probably be explained by the fact that here, the area with coding "influence area yes" becomes much larger than it is in the case of the "level low" variant, while the number of mass movements that lie within the influence area of the roads does not increase (assignment is done by means of land-use coding). However, this also leads to the connection between mass-movement distribution and the influence area of roads becoming weaker (Chapter 7.2.2.2). The similarity in model performance through integration of the parameters *subsurface flow disposition* and *precipitation in integrated form* can be attributed in both level-categories to the fact that the different underlying substrate maps as well as the precipitation map are only part of the

parameter *subsurface flow disposition*, so that the susceptibility maps generated are usually very similar (Chapters 7.2.2.1 & 7.2.2.2).

The absence of improvement with use of the other "level high" parameter maps can only be explained as follows:

- ➢ On the one hand, it might be the case that the "level high" parameter map used do not reproduce the corresponding situation any more realistically or in a way that is any more process-oriented than the "level low" map. So it is questionable whether the effort required to produce the "level high" parameter map for modelling is actually worthwhile.

- ➢ On the other hand, it might also be the case that individual "level high" maps actually are more realistic and process-oriented than the corresponding "level low" maps, but that the validation method, due to the simplifying, summarised area-wide validation (Chapter 7.1) is unable to recognise these improvements in the susceptibility map.

This deficit underlines the necessity of new partial validation methods. Furthermore, there is also the possibility that the improvements in the parameter map cannot be recognised by the model, because the available data is inadequate, given the complexity of the material.

The following picture emerged from **a validation comparison of the "best 5"-"level low" with the "best 5"-"level high"** runs and the runs **with process-oriented parameter-map combinations:**

Basically, all three model-run groups led to quite similar results. Closer examination showed that the "level high" runs (33, 58, 59, 61 and P2) tended to exhibit slightly better model performance than that of the "level low" runs (5, 6, 10, 23 and 24), which was however in turn somewhat better than model performance in process-oriented runs. For "level low" and "level high" runs, this can be seen in Tab. 7.2.2.4-1 and in Fig. 7.2.2.4-1 for all three groups. The latter does not cover the entire validation according to the validation strategy used (Chapter 7.2.1) but rather only the validation according to Chung & Fabbri (1999) of the validation data (it was used primarily for assessment of the neural-networks runs), but the described connection is still clearly visible. Fig. 7.2.2.4-2 displays the same situation for the test data that was used later in order to compare the modelling methods (Chapters 7.1 and Chapter 8). Here the curve spread is somewhat larger.
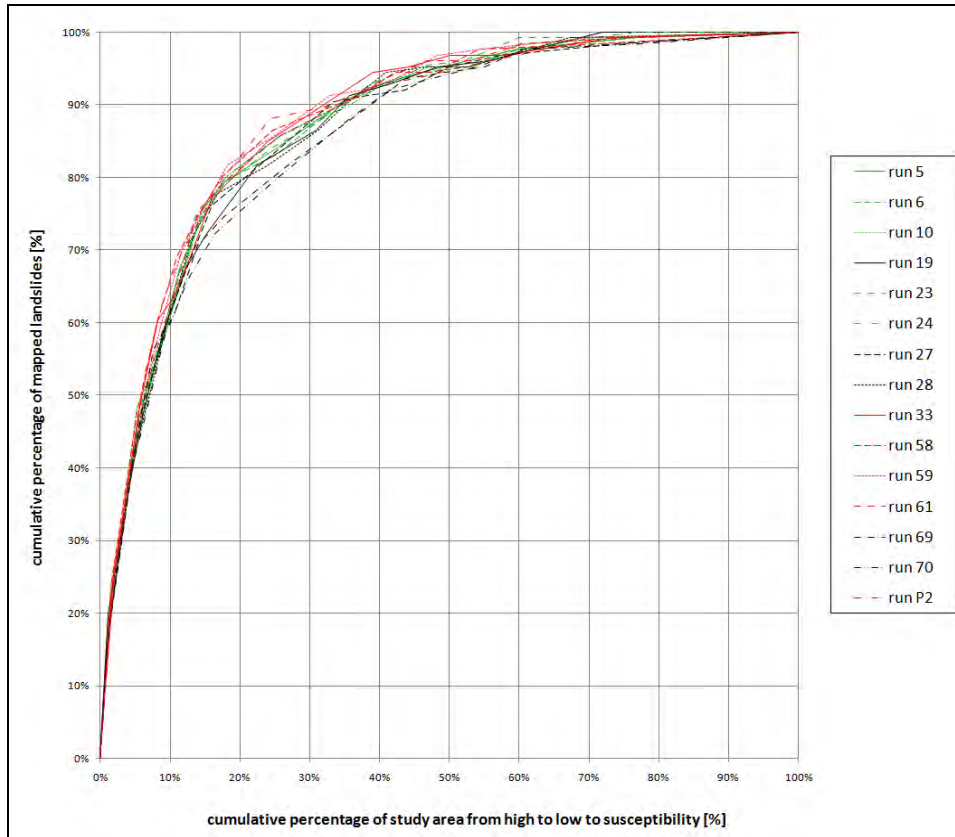
Fig. 7.2.2.4-1: Validation according to Chung & Fabbri (1999) for the validation data of the "best 5"-"level low" (green) and "level high" runs (red), as well as the runs with process-oriented parameter combinations (black)
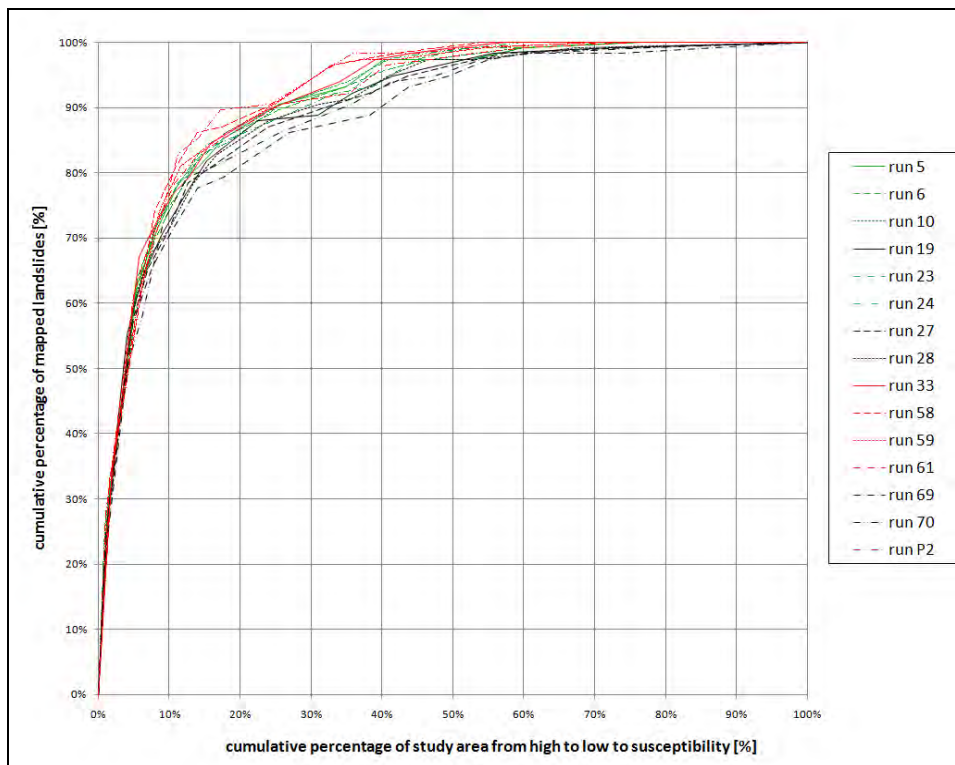
Fig. 7.2.2.4-2: Validation according to Chung & Fabbri (1999) of the test data of the "5 best"-"level low" (green) and "level high" runs (red), as well as the runs with process oriented parameter combinations (black)

The poorer model performance seen for the runs with process-oriented parameter combinations might now be due to the maps themselves or to the validation methodology used. This once again points out the necessity of new partial validation methods.

Initially, the tendency toward slightly better validation results for the "level high" runs might be surprising, as it has been shown that the "level high" parameter maps, except for the precipitation map, usually contribute to a deterioration in the model performance (see above and Chapter 7.2.2.2). But it should be considered here, in the first place, that the "level high" runs largely use "level low" parameters, because almost all of the "level high" parameters were rejected due to poorer validation results.

A second, important reason for this was the **selection of the overall best results** (the best results of "level low" and "level high"). This was done using Tab. 7.2.2.4-1, in which all of the best five runs from "level low" and "level high" were compared on the basis of the validation strategy in Chapter 7.2.1. As noted above, the table shows that the validation results are very similar, which is why several best results had to be selected. The results of runs 58, 59 and P2 were selected as the best overall results from modelling with neural networks, because they were the only results that were never worse than the others, and also, compared to each other, they produced equally good validation results.

The table now shows the reason for the apparent contradiction in the better validation results for the "level high" runs, despite the general deterioration when using the "level high" parameter maps. The three best runs (58, 59 and P2), which are also nearly always better than the "level low" runs, all include the parameter *precipitation "level high" in independent form*. This is also the only "level high" parameter that actually resulted in a slight improvement compared to the "level low" runs. On the other hand, "level high" runs without this parameter usually led to validation results that were poorer than those obtained using corresponding "level low" parameter maps exclusively (Chapter 7.2.2.2). Thus, the best "level high" run without precipitation (run 33) for example, shows somewhat poorer validation results than the two "level low" runs 10 and 24.

Tab. 7.2.2.4-1: Validation comparison of the "best 5" – "level low" and "best 5" – "level high" runs according to the validation strategy in Chapter 7.2.1 (-: equal, x: not meaningful)

		Best 5 „level low"					Best 5 „level high"				
Compared to		5c	6	10	23(NS)	24	33	58(NS)	59(NS)	61(NSi)	P2(NS)
Best 5 „level low"	**5c**	x	-	**Slightly worse**	-	**Slightly worse**	-	**Slightly worse**	**Slightly worse**	-	Very slightly worse
	6	-	x	**Slightly worse**	-	**Slightly worse**	**Slightly worse**	**Slightly worse**	**Slightly worse**	-	Very slightly worse
	10	**Slightly better**	**Slightly better**	x	-	-	Very slightly better	Very slightly worse	-	-	**Slightly worse**
	23(NS)	-	-	-	x	Very slightly worse	Very slightly worse	Very slightly worse	Very slightly worse	-	**Slightly worse**
	24	**Slightly better**	**Slightly better**	-	Very slightly better	x	Very slightly better	Very slightly worse	-	**-**	Very slightly worse
Best 5 „level high"	**33**		**slightly better**	very slightly worse	Very slightly better	Very slightly worse	x	-	-	-	-
	58(NS)	**Slightly better**	**Slightly better**	Very slightly better	Very slightly better	Very slightly better	-	x	-	Very slightly better	-
	59(NS)	Slightly better	Slightly better	-	Very slightly better	-	-	-	x	-	-
	61 (Nsi)	-	-	-	-	-	-	Very slightly worse	-	x	Very slightly worse
	P2(NS)	Very slightly better	Very slightly better	**Slightly better**	**Slightly better**	Very slightly better	-	-	-	Very slightly better	x

7.3. Modelling and Validation of Landslide Susceptibility Maps by means of Weight of Evidence (JR)

7.3.1 Basic Principles

The Weight of Evidence (WoE) modelling method is a quantitative 'datadriven' method used to combine datasets. The method was initially applied to non-spatial, quantitative, medical diagnoses to combine evidence from clinical diagnoses to predict diseases (Spiegelhater & Kill-Jones 1984, Spiegelhater 1986). In geosciences the method first was applied for mineral potential mapping by implementing it in a GIS framework (Bonham-Carter et al. 1989). Sabto (1991) and Van Westen (1993) applied the method for landslide susceptibility analysis based on GIS technology. Today numerous examples from many parts of the world exist making use of the WoE-method for landslide susceptibility analysis (e.g. van Westen 1993, Guzzetti et al. 1999, Lee et al. 2002, Klingseisen & Leopold 2006 a, b, Mathew et al. 2007, Rezaei Moghaddam et al. 2007, Thiery et al. 2007, Long 2008, Proske et al. 2008, Barbieri & Cambuli 2009, Jayathissa 2010).

WoE is basically the Bayesian approach in a log-linear form. Prior probabilities (PriorP) and posterior probabilities (PostP) are the most important concepts in the Bayesian approach. PriorP is the probability that a terrain unit contains the response variable before taking predictive variables into account, and its estimation is based on the response variable density for the study area. This initial estimate can be modified by the introduction of other evidences. PostP is then estimated according to the response variable density for each class of the predictive variables. The model is based on the calculation of positive (W+) and negative (W-) weights, whose magnitude depends on the observed association between the response variable and the predictive variable.

$$W^+ = \ln \frac{P(B \mid \mathrm{RV})}{P(B \mid \overline{\mathrm{RV}})} \qquad (1)$$

$$W^- = \ln \frac{P(\overline{B} \mid \mathrm{RV})}{P(\overline{B} \mid \overline{\mathrm{RV}})} \qquad (2)$$

P   Probability

RV   Response Variable

In Eqs. (1) and (2), B is a class of the predictive variable and the overbar sign '−' represents the absence of the class and/or response variable. The ratio of the probability of response variable presence to that of response variable absence is

called odds (Bonham-Carter 1994). The WoE for all predictive variables is combined using the natural logarithm of the odds (logit), in order to estimate the conditional probability of landslide occurrence. When several predictive variables are combined, areas with high or low weights correspond to high or low probabilities of presence of the response variable. Further details of the method are given by many authors (e.g. Bonham-Carter 1994, Porwal et al. 2003, Neuhäuser and Terhorst 2007, Barbieri & Cambuli 2009).

As mentioned by Bonham-Carter (1994), the results of the WoE method are strongly dependent on the number of events introduced in the model (e.g. on the estimation of probabilities) and on the quality of the landslide inventory map. The WoE method requires the assumption that input maps are conditionally independent. Expert selection or different types of statistical tests can be employed to test the dependency of the factors with respect to landslides. Pairwise comparison is the most employed method for testing conditional independence in the modelling approach (Regmi et al. 2010, ref. to Chapter 6.2 and Tab. 6.2.3).

The WoE model is generally applied using binary evidential themes i.e. with factor maps which contain two classes, representing the presence or absence of the factor. Real world geospatial data are usually multi-class or continuous. Hence this requires the analysis of many individual maps for each factor class separately (e.g. each slope class separately for the slope theme).

7.3.2. Modelling and Validation Results

Using the WoE method, the spatial relationship between landslide-occurrence location and landslide-related factors was calculated.

As the method is a pixel-based one the response variable (landslide occurrence) can be considered in a binary manner (1 / 0) solely. The WoE modelling results therefore are not fully comparable with the results of Artificial Neural Network (ANN) modelling (section 7.2) and Logistic Regression modelling (section 7.4) where the occurrence of more than one landslide per pixel (which is the case for 39 raster cells in the study area) could be taken into account.

Approx. 70 % of the available landslide-dataset "high quality for modelling" (cf. Tab. 6.1.1.1) were used to calculate the weights. This training dataset corresponds to the original "training-" and "validation" portion of the complete dataset (Chapter 6.1.2). The remaining 30 %, corresponding to the original "test" portion of the dataset were used for the validation of the modelling results.

In practice, in WoE positive and negative weights (W+ and W-) are calculated, the magnitude of which depends on the measured association between the response variable (the landslides) and the predictor variables (causative factors). The modelling process was based on an Arc Macro Language (AML) script created in ArcInfo. The calculated weights were standardized for each map (0 – 1).

As described in section 6.2 a general strategy in successively involving different parameters for the statistical modelling was followed. Basically at first only "level low" parameters were considered, followed by addition or substitution of "level high" parameters.

Based on different combinations of these parameter maps in total 63 modelling runs were calculated.

The results are presented in the following sections.

The validation of the results made use of the following methods:

1. Modelled probability (cut-off value 0,5)
2. Chung & Fabbri Curve (Chung & Fabbri 2003)
3. Receiver Operating Characteristic (ROC) - Curve

These methods as well as some fundamental problems are described in detail in section 7.1. The calculation was applied to the training dataset ("success rate") as well as to the test dataset ("prediction rate").

The modelling strategy (i.e. which parameter maps were kept in the further modelling steps and which of the maps were rejected) was based on the results of the validation. The strategy was based on the combined assessment of the validation results of both the LR and the WoE modelling.

With regard to the comparison of two different modelling runs the following aspects were taken into account:

- Differences < 1,0 % related to modelled probability (method 1) were not taken into account
- Differences < 0,5 % related to areas under curve (methods 2 and 3) were not taken into account.
- The methods 2 and 3 was given higher significance than method 1.
- The validation results of the LR modelling was given higher significance than the results of the WoE modelling.
- the prediction rate was given higher significance than the success rate.
- The results of the ANN modelling (Geological Survey) were taken into account as well to allow for similar modelling sequences in both the modelling groups.
- In case that none of the above mentioned decision criteria supported a clear decision, expert-knowledge of the involved scientific groups was taken into account.

The results of the validations are summed up in Tab. 7.3.2-1.

Generally the WoE modelling results are characterized by a high number of pixels situated in the medium part of the susceptibility spectrum compared to the other two statistical methods. This is expressed by a high portion of yellow areas in the maps (Fig. 7.3.2.1-5 to 7.3.2.1-7 and Fig. 7.3.2.2-5 to 7.3.2.2-6). ANN as well as LR show much better differentiation between high and low susceptibilities.

Tab. 7.3.2-1: Results of Validations of Modelling Runs calculated with Weight of Evidence

Run	Probability	ROC (AUC)	Chung/Fabbri (AUC)
1	56.10%	82.10%	82.12%
	71.20%	86.80%	87.76%
2	56.10%	82.20%	82.31%
	71.20%	86.90%	87.87%
3	61.10%	84.70%	84.58%
	79.80%	90.50%	91.06%
4	63.60%	83.50%	83.29%
	72.10%	86.70%	87.16%
5	60.70%	84.00%	83.76%
	69.20%	87.00%	87.35%
6	63.20%	83.90%	83.72%
	73.10%	87.40%	87.79%
7	74.30%	83.10%	82.90%
	83.70%	86.60%	86.98%
8	82.10%	81.90%	81.80%
	93.30%	85.60%	86.30%
9	71.10%	82.10%	81.91%
	76.90%	84.30%	84.86%
10	68.90%	84.10%	83.87%
	78.80%	87.40%	87.85%
11	62.90%	82.30%	82.34%
	76.00%	87.00%	87.78%
12	68.60%	84.00%	83.81%
	78.80%	87.40%	87.82%
13	58.60%	75.40%	75.34%
	60.60%	78.00%	78.61%
14a	68.20%	84.10%	83.91%
	75.00%	87.00%	87.39%
14b	68.90%	83.70%	83.56%
	76.90%	86.80%	87.25%
15	71.40%	84.80%	84.72%
	84.60%	90.50%	90.99%
16	67.90%	82.10%	81.91%
	71.20%	84.20%	84.73%
18	80.00%	84.10%	83.97%
	89.40%	89.20%	89.65%
19	86.40%	82.10%	81.92%
	92.30%	85.80%	86.36%
20	82.50%	85.10%	84.97%
	85.60%	90.60%	91.08%
21	65.70%	84.00%	83.82%
	75.00%	87.30%	87.64%
22	70.00%	84.00%	83.85%
	81.70%	87.20%	87.56%
23	72.50%	84.30%	84.10%
	85.60%	87.60%	87.95%
24	69.30%	80.70%	80.53%
	69.20%	82.20%	82.63%

Run	Probability	ROC (AUC)	Chung/Fabbri (AUC)
25	68.60%	80.70%	80.57%
	69.20%	82.40%	82.78%
26	68.90%	81.70%	81.49%
	76.00%	83.50%	83.96%
27	73.90%	82.70%	82.49%
	76.90%	84.60%	85.02%
28	73.90%	82.90%	82.73%
	76.90%	84.70%	85.13%
29	58.20%	78.30%	78.23%
	64.40%	78.30%	79.11%
31	33.90%	74.90%	75.07%
	41.30%	78.00%	79.20%
32	56.10%	78.30%	78.13%
	68.30%	80.50%	81.12%
33	69.30%	82.70%	82.53%
	74.00%	86.00%	86.39%
34	67.10%	82.80%	82.61%
	74.00%	86.20%	86.68%
35	38.90%	75.30%	75.43%
	46.20%	77.90%	78.87%
36	58.90%	78.50%	78.41%
	68.30%	80.70%	81.22%
37	65.40%	84.60%	84.56%
	79.80%	88.90%	89.62%
40	62.10%	84.00%	83.80%
	74.00%	87.90%	88.35%
41	66.10%	83.90%	83.69%
	73.10%	86.10%	86.64%
42	64.60%	84.00%	83.75%
	71.20%	86.40%	86.94%
43	74.30%	84.90%	84.70%
	79.80%	87.60%	87.97%
43a	70.70%	84.70%	84.53%
	76.90%	87.90%	88.24%
44	72.10%	84.20%	84.00%
	78.80%	86.60%	87.11%
45	73.20%	84.60%	84.36%
	76.90%	86.70%	87.15%
46	63.60%	82.80%	82.65%
	71.20%	87.00%	87.35%
47	69.60%	82.70%	82.55%
	73.10%	84.70%	85.30%
48	64.60%	82.80%	82.65%
	71.20%	85.70%	86.06%
55	78.20%	83.90%	83.69%
	82.70%	86.80%	87.24%
57	73.90%	84.20%	84.02%
	75.00%	86.60%	87.13%

Run	Probability	ROC (AUC)	Chung/Fabbri (AUC)
58	82.90%	85.80%	85.56%
	86.50%	89.40%	89.68%
59	80.00%	84.60%	84.42%
	89.40%	88.80%	89.10%
60	74.30%	84.90%	84.71%
	79.80%	87.60%	87.97%
61	68.20%	84.10%	83.91%
	75.00%	87.00%	87.39%
62	68.60%	84.10%	83.87%
	78.80%	87.40%	87.85%
63	75.00%	84.90%	84.64%
	79.80%	87.90%	88.24%
64	70.00%	85.00%	84.79%
	75.00%	87.90%	88.27%
66	81.80%	84.60%	84.40%
	89.40%	88.80%	89.22%
67	75.00%	83.20%	83.00%
	83.70%	87.30%	87.76%
68	77.10%	84.10%	83.94%
	82.70%	86.70%	87.14%
69	72.10%	82.30%	82.14%
	73.10%	83.70%	84.17%
70	74.30%	82.40%	82.24%
	76.00%	83.80%	84.29%
71	75.00%	81.30%	81.13%
	76.00%	82.40%	83.11%
72	74.30%	80.00%	79.85%
	77.90%	82.10%	82.82%

■ Successrate
■ Predictionrate

7.3.2.1. Modelling Results using Parameter Maps of Low Processing Effort

"Level low" parameter maps are generated by means of simple, standard methods (cf. Fig. 6.2-1). Based on different combinations of these parameter maps 32 modelling runs were calculated. The modelling procedure and the included parameter maps can be followed by Tab. 7.3.2.1-1.

The modelling runs were started with some very simple combinations of parameter maps taking into account only a few basic parameters (runs 1, 2 and 3). The exchange of *Wald_DKM_lg_mb* by *Wald_Sat_lg_mb* only resulted in very low improvements of the validation results. Nevertheless, during further progress of the modelling *Wald_Sat_lg_mb* was kept assuming that this dataset presented higher relevance than the data of the Digital Cadastral Map (expert knowledge).

After involvement of the influence of the road network the validation results show a significant improvement of both success and prediction rates (> 90 % for prediction rates, cf. Tab. 7.3.2-1)

In the following modelling runs parameters connected to subsurface flow (*Flowaccumulation, QDisp*) were involved. As based on the field investigations,

subsurface flow was rated to be highly relevant from the process-oriented point of view by the involved experts, such maps were kept in the further modelling procedure even accepting that the results of the validation were worsening.

The susceptibility maps derived from runs 5 and 6 are shown in the Fig. 7.3.2.1-5. and 7.3.2.1-6.

In run 10 the first parameter map considering geological / pedological aspects was involved (*Sub_GK_lg)* which lead to only a marginal improvement compared to run 6. The involvement of *Sub_GK_lg* in run 11 as well did not show any significant difference compared to run 2. Nevertheless based on additional expert-knowledge this parameter map was kept in the further modelling steps.

Run 13 was a test run without any forest map and resulted in a significant decrease of the validation results.

The cumulated Chung & Fabbri as well as ROC-curves of runs 1 to 13 are presented in Fig. 7.3.2.1-1 to 7.3.2.1-4 showing clearly

➢ the very good results of run 3 (without any involvement of maps connected to subsurface flow),

➢ the bad result of run 13 (without any involvement of forest maps) and

➢ the strong grouping of all the remaining runs.

Runs 14a and 14b are variations of run 10 including *Sub_GK_lg* with different subsurface flow parameter maps. The validation results are very similar to those of run 10. The susceptibility map derived from run 14a is shown in Fig. 7.3.2.1-7.

Run 15 adds *Sub_GK_lg* to the parameters involved in run 3 resulting in more or less the same validation results (with prediction rates of Chung & Fabbri and ROC method > 90 %).

Run 16 which does not consider the influence of the road network results in significantly lower AUC values.

The following modelling runs test different derivatives of the subsurface flow, partly involving the distribution of precipitation (run 20, run 23, and run 28). Highest AUC values of both success and prediction rates (> 90 % for prediction rates, cf. Tab. 7.3.2-1) are calculated with results of run 20.

Runs 29 to 32 are calculated using regionalisation data (*Wald_DKM_lg, Wegenetz_lg*) instead of field-based datasets. This replacement results in a significant decrease of all calculated validation indices.
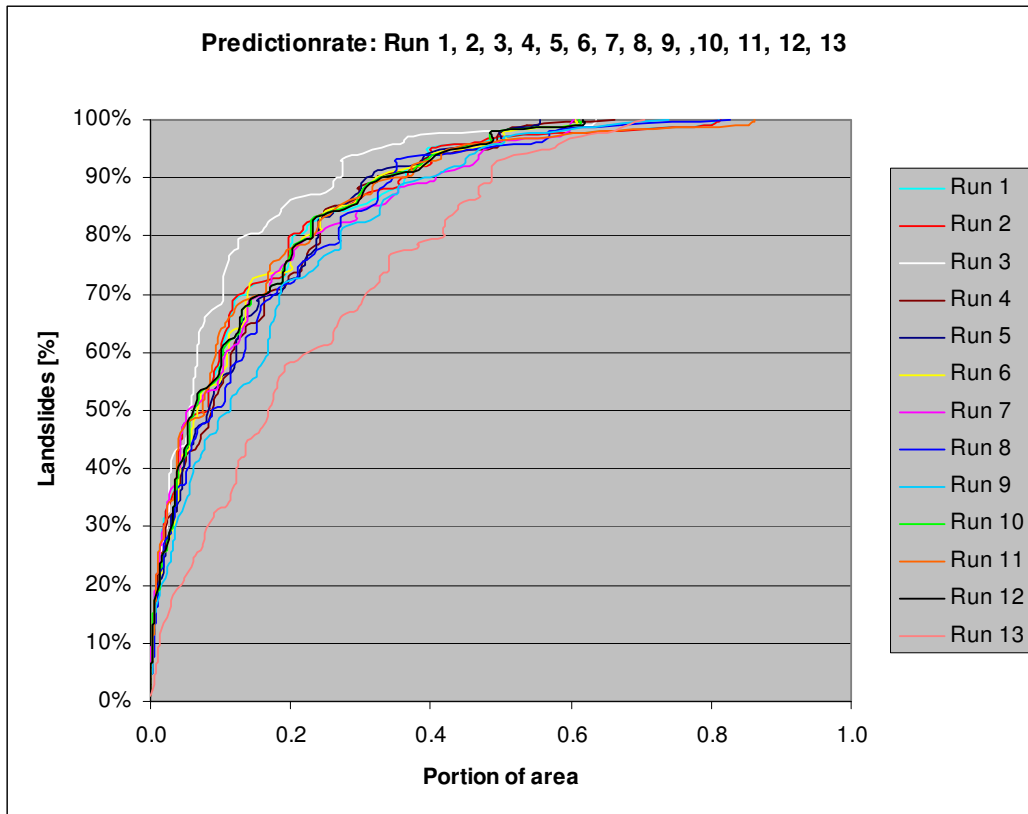
Fig. 7.3.2.1-1: Cumulated Chung & Fabbri curves of runs 1 to 13 (predictionrate)
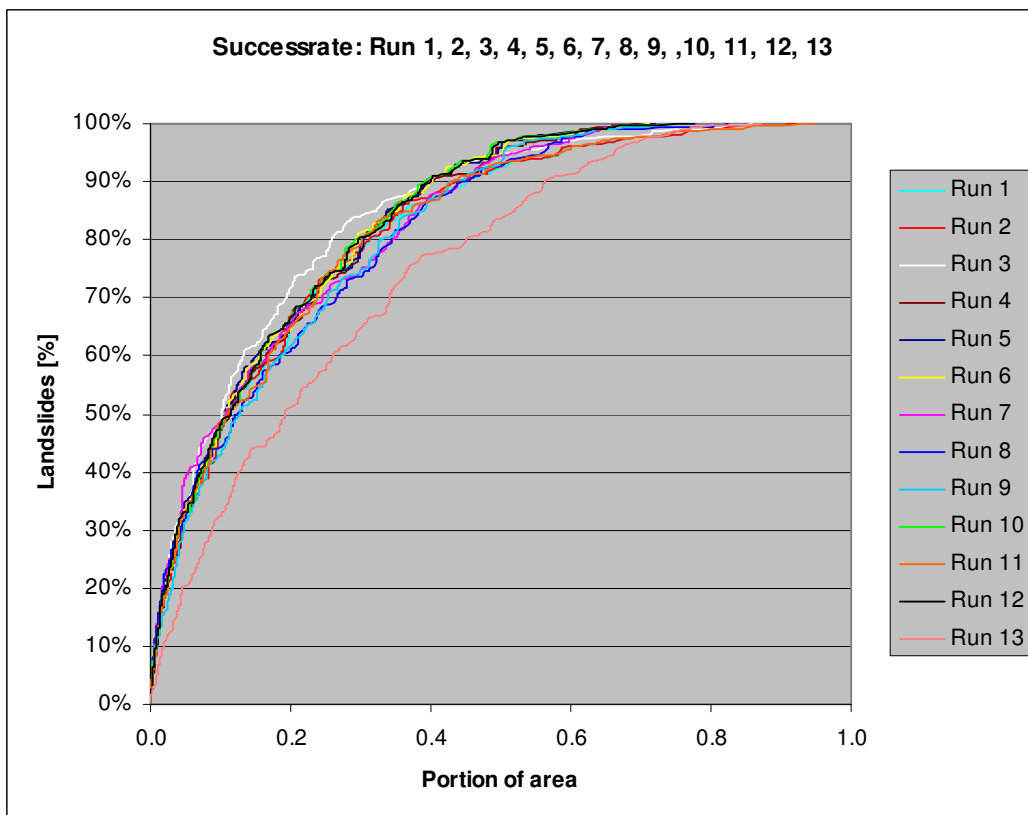
Fig. 7.3.2.1-2: Cumulated Chung & Fabbri curves of runs 1 to 13 (successrate)
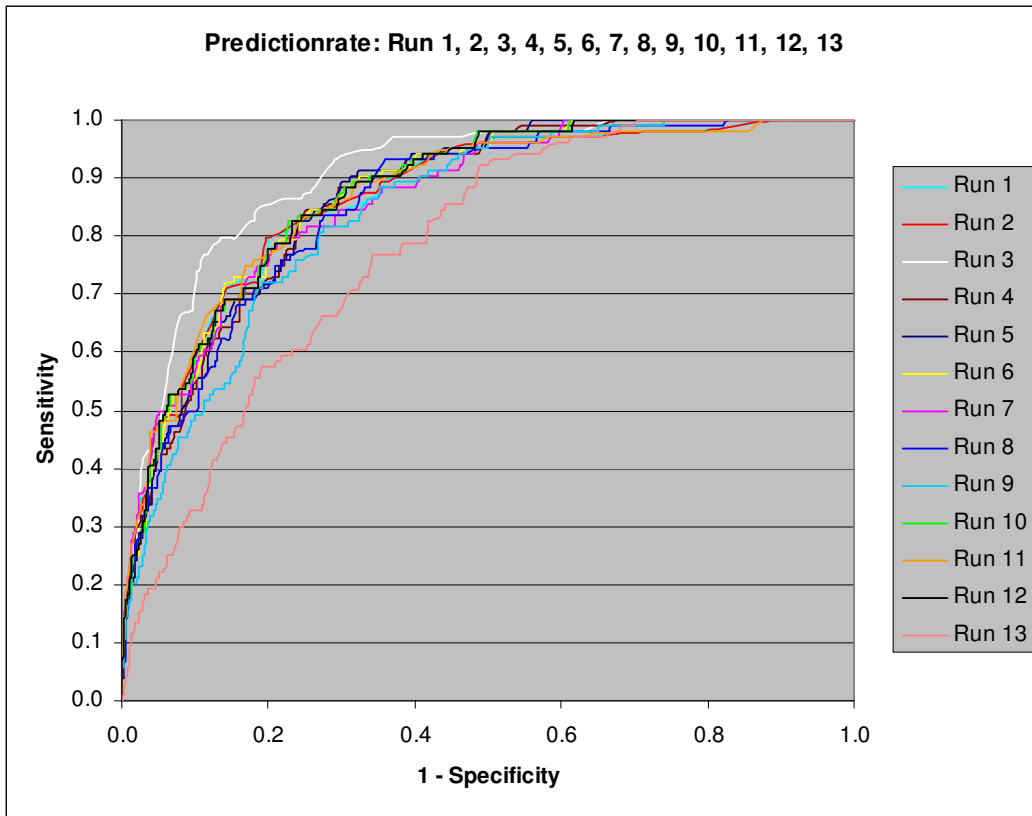
Fig. 7.3.2.1-3: Cumulated ROC curves of runs 1 to 13 (predictionrate)
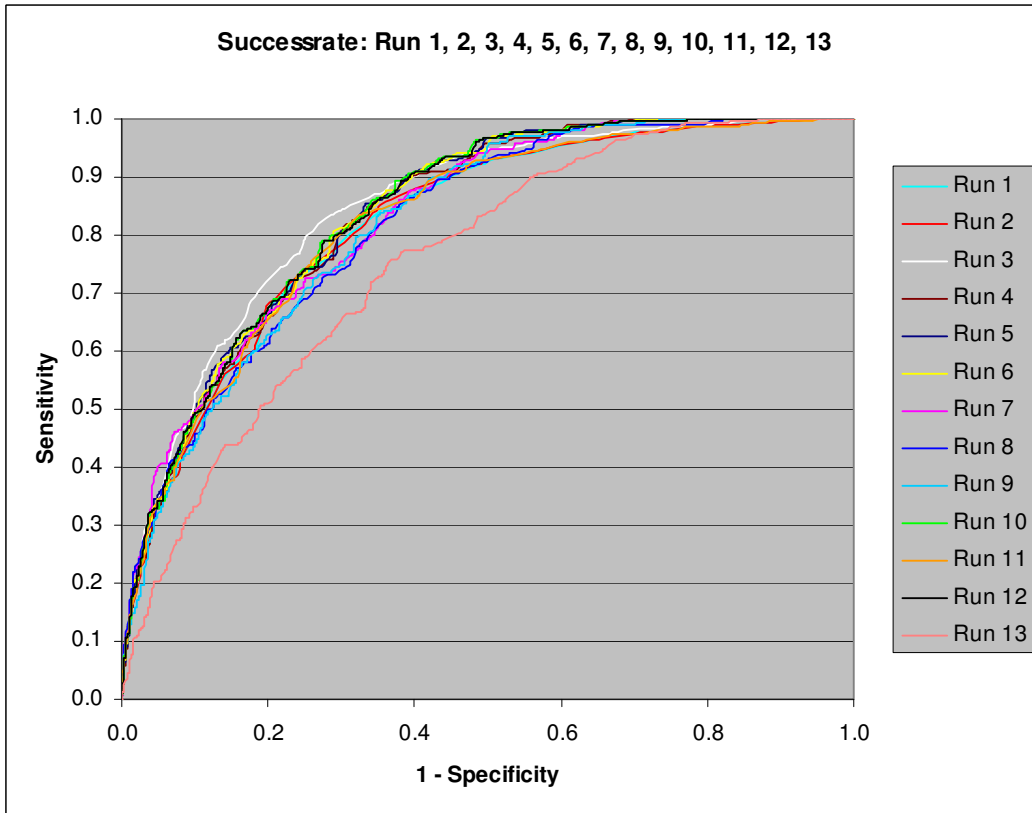
Fig. 7.3.2.1-4: Cumulated ROC curves of runs 1 to 13 (successrate)

Tab. 7.3.2.1-1: Model runs using Parameter Maps of Low Processing Effort only

Run	Parameter Maps (abbreviations cf. Tab. 6.2.2)						
	Slope	Curvature	Forest	Street Network	Hydro(geo)logy	Geology / Pedology	Precipitation
1	HN-DHM10	VW-DHM10	Wald_DKM_lg_mb				
2	HN-DHM10	VW-DHM10	Wald_Sat_lg_mb				
3	HN-DHM10	VW-DHM10	Wald_Sat_lg_mb	Wegenetz_lg_mb			
4	HN-DHM10	VW-DHM10	Wald_Sat_lg_mb	Wegenetz_lg_mb	Flowaccumulation		
5	HN-DHM10	VW-DHM10	Wald_Sat_lg_mb	Wegenetz_lg_mb	QDisp_lg_GK_lg_fa		
6	HN-DHM10	VW-DHM10	Wald_Sat_lg_mb	Wegenetz_lg_mb	QDisp_lg_GK_lh_fa		
7	HN-DHM10	HK-DHM10	Wald_Sat_lg_mb	Wegenetz_lg_mb	QDisp_lg_GK_lh_fa		
8	HN-DHM10	HW-DHM10	Wald_Sat_lg_mb	Wegenetz_lg_mb	QDisp_lg_GK_lh_fa		
9	HN-DHM10	VW-DHM10, HW-DHM10	Wald_Sat_lg_mb	Wegenetz_lg_mb	QDisp_lg_GK_lh_fa		
10	HN-DHM10	VW-DHM10	Wald_Sat_lg_mb	Wegenetz_lg_mb	QDisp_lg_GK_lh_fa	Sub_GK_lg	
11	HN-DHM10	VW-DHM10	Wald_Sat_lg_mb			Sub_GK_lg	
12	HN-DHM10	VW-DHM10	Wald_DKM_lg_mb	Wegenetz_lg_mb	QDisp_lg_GK_lh_fa	Sub_GK_lg	
13	HN-DHM10	VW-DHM10		Wegenetz_lg_mb	QDisp_lg_GK_lh_fa	Sub_GK_lg	
14a	HN-DHM10	VW-DHM10	Wald_Sat_lg_mb	Wegenetz_lg_mb	QDisp_lg_GK_lg_fa	Sub_GK_lg	
14b	HN-DHM10	VW-DHM10	Wald_Sat_lg_mb	Wegenetz_lg_mb	Flowaccumulation	Sub_GK_lg	

15	HN-DHM10	VW-DHM10	Wald_Sat_lg_mb	Wegenetz_lg_mb		Sub_GK_lg	
16	HN-DHM10	VW-DHM10	Wald_Sat_lg_mb		QDisp_lg_GK_lh_fa	Sub_GK_lg	
18	HN-DHM10		Wald_Sat_lg_mb	Wegenetz_lg_mb	QDisp_lg_GK_lh_fa	Sub_GK_lg	
19	HN-DHM10	HW-DHM10	Wald_Sat_lg_mb	Wegenetz_lg_mb	QDisp_lg_GK_lh_fa	Sub_GK_lg	
20	HN-DHM10	VW-DHM10	Wald_Sat_lg_mb	Wegenetz_lg_mb	QDisp_lg_GK_lh_fa	Sub_GK_lg	NS_lg
21	HN-DHM10	VW-DHM10	Wald_Sat_lg_mb	Wegenetz_lg_mb	QDisp_lg_GK_lg_fa_NS_lg	Sub_GK_lg	
22	HN-DHM10	VW-DHM10	Wald_Sat_lg_mb	Wegenetz_lg_mb	QDisp_lg_GK_lh_fa_NS_lg	Sub_GK_lg	
23	HN-DHM10	VW-DHM10	Wald_Sat_lg_mb	Wegenetz_lg_mb	QDisp_lg_GK_lh_fa	Sub_GK_lg	NS_lg
24	HN-DHM10	VW-DHM10	Wald_Sat_lg_mb	Wegenetz_lg_mb	QDisp_lg_BK_fa	Sub_GK_lg	
25	HN-DHM10	VW-DHM10	Wald_Sat_lg_mb	Wegenetz_lg_mb	QDisp_lg_BK_fa_NS_lg	Sub_GK_lg	
26	HN-DHM10	VW-DHM10, HK-DHM10	Wald_Sat_lg_mb	Wegenetz_lg_mb	QDisp_lg_GK_lg_fa	Sub_GK_lg	
27	HN-DHM10	VW-DHM10, HK-DHM10	Wald_Sat_lg_mb	Wegenetz_lg_mb	QDisp_lg_GK_lh_fa	Sub_GK_lh	
28	HN-DHM10	VW-DHM10, HK-DHM10	Wald_Sat_lg_mb	Wegenetz_lg_mb	QDisp_lg_GK_lh_fa	Sub_GK_lh	NS_lg
29	HN-DHM10	VW-DHM10	Wald_DKM_lg	Wegenetz_lg	QDisp_lg_GK_lh_fa	Sub_GK_lg	
30	HN-DHM10	VW-DHM10	Wald_DKM_lg	Wegenetz_lg	QDisp_lg_GK_lh_fa	Sub_GK_lg	NS_lg
31	HN-DHM10	VW-DHM10	Wald_DKM_lg				
32	HN-DHM10	VW-DHM10	Wald_Sat_lg	Wegenetz_lg	QDisp_lg_GK_lh_fa	Sub_GK_lg	
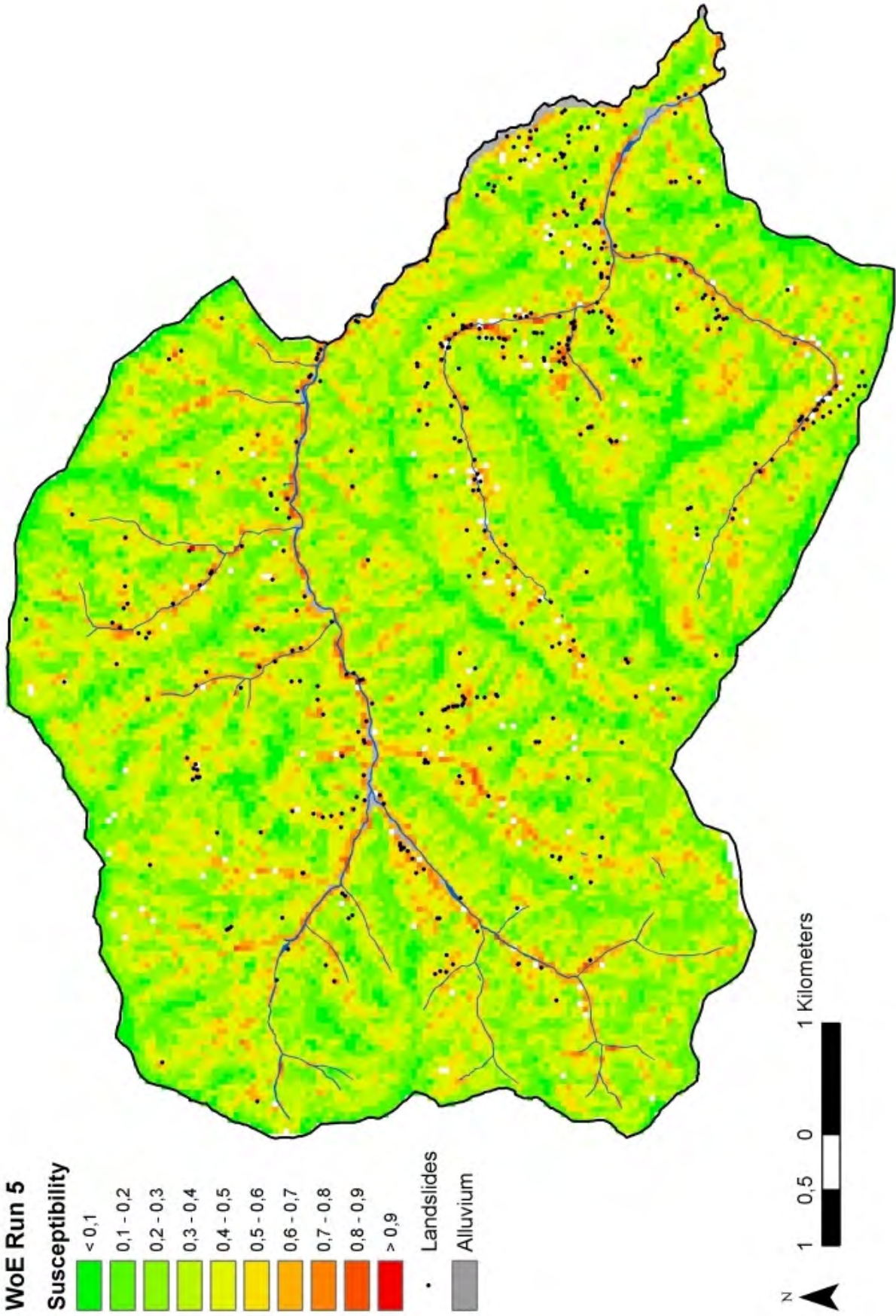
Fig. 7.3.2.1-5: Result of WoE modelling run 5

WoE Run 6

Susceptibility

- < 0,1
- 0,1 - 0,2
- 0,2 - 0,3
- 0,3 - 0,4
- 0,4 - 0,5
- 0,5 - 0,6
- 0,6 - 0,7
- 0,7 - 0,8
- 0,8 - 0,9
- > 0,9

- Landslides
- Alluvium
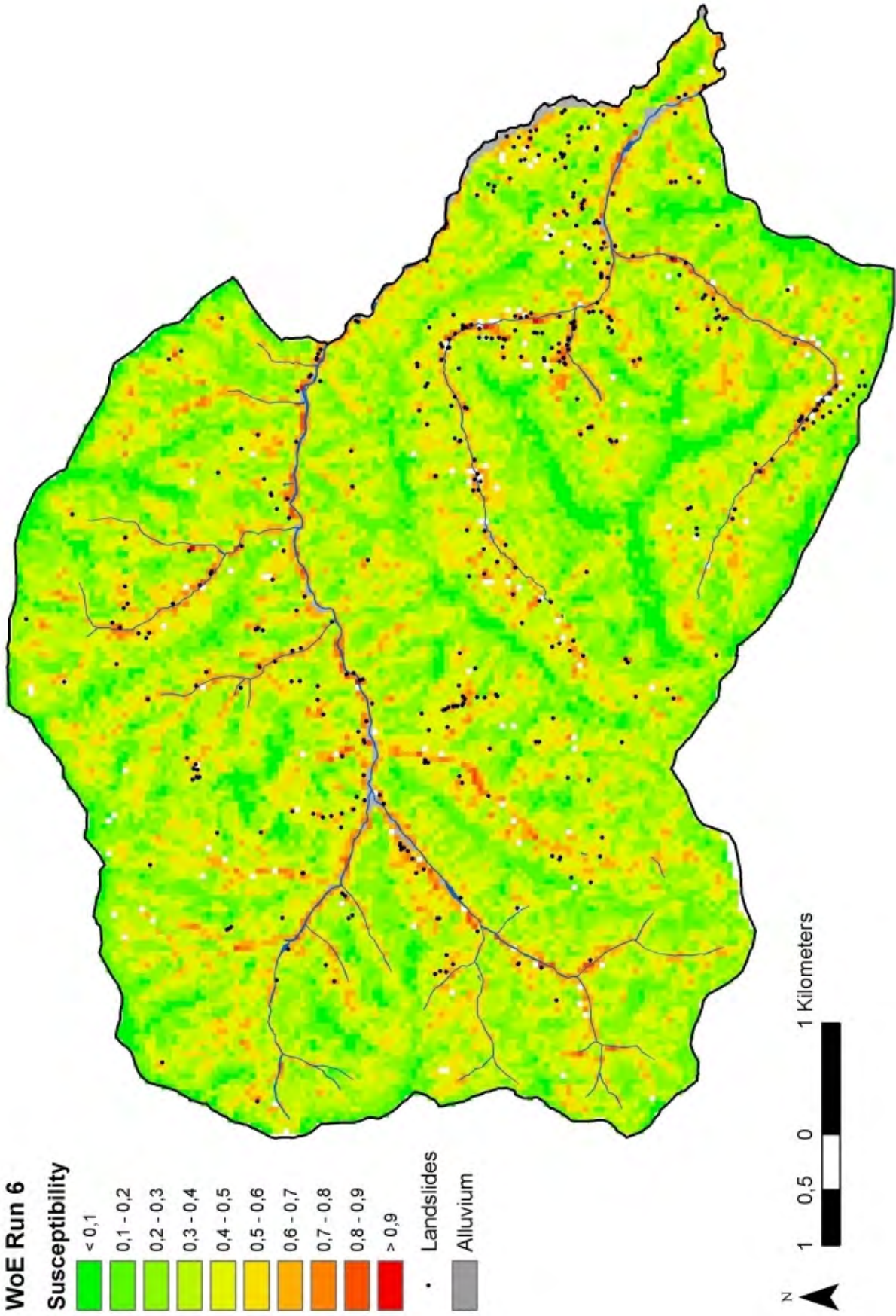
Fig. 7.3.2.1-6: Result of WoE modelling run 6

WoE Run 14a

Susceptibility

- < 0,1
- 0,1 - 0,2
- 0,2 - 0,3
- 0,3 - 0,4
- 0,4 - 0,5
- 0,5 - 0,6
- 0,6 - 0,7
- 0,7 - 0,8
- 0,8 - 0,9
- > 0,9

· Landslides

Alluvium
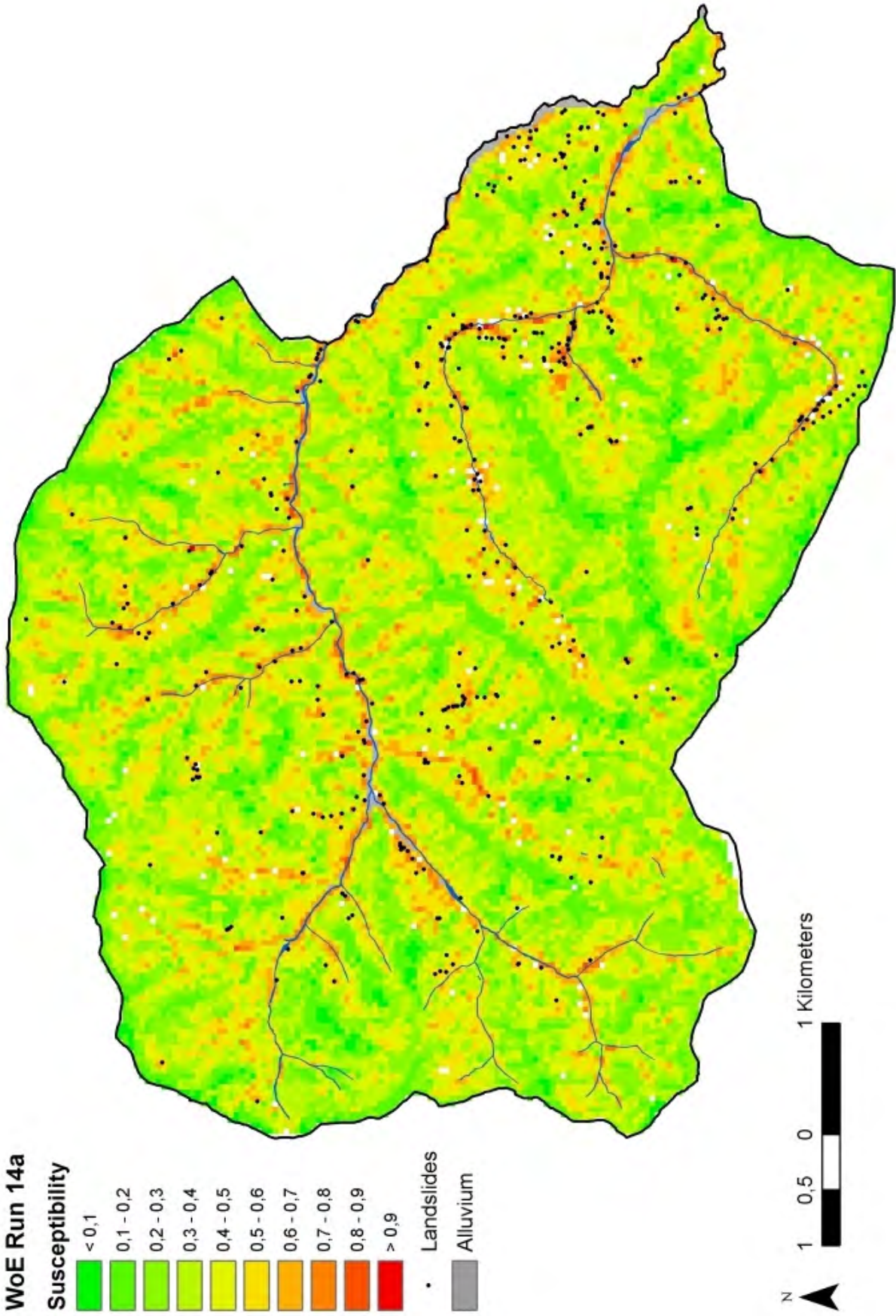
Fig. 7.3.2.1-7: Result of WoE modelling run 14a

For visualisation of differences of particular modelling runs maps of differences were calculated.

In the following examples negative differences between the two considered maps are displayed in red (higher susceptibility in the second map than in the first map), positive differences are displayed in blue (higher susceptibility in the first map than in the second map).

In the example shown in Fig. 7.3.2.1-8 the parameter map *Wegenetz_lg_mb* additionally is involved in the second run (run 3) compared to the first run (run 2). The influence area of the road network is characeterized by significantly higher landslide susceptibility resulting in negative differences.
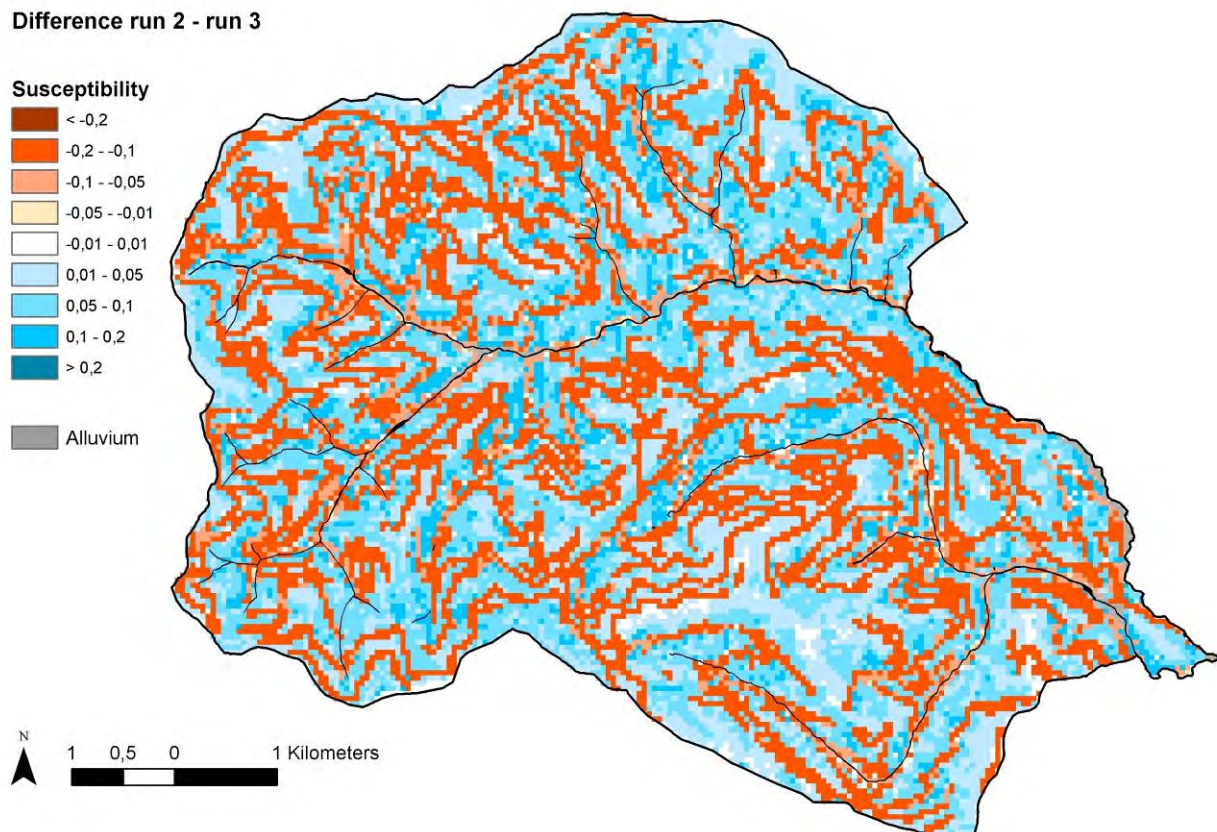
Fig. 7.3.2.1-8: Map of differences between WoE run 2 and 3

Fig. 7.3.2.1-9 (differences between run 5 and 6) is an example where contrasts are very low generally. In run 6 *QDisp_lg_GK_**lh**_fa* is used instead of *QDisp_lg_GK_**lg**_fa*. Significant differences therefore are restricted to areas where there are relevant differences between the "level low" and "level high" versions of the conceptual soil map (ref. to section 5.1).

Differences between run 9 and run 10 (Fig. 7.3.2.1-10) clearly display the geological situation in the western part as *Sub_GK_lg* is added in run 10. The involvement of this parameter map generally results in lower susceptibilities in most of the study area.
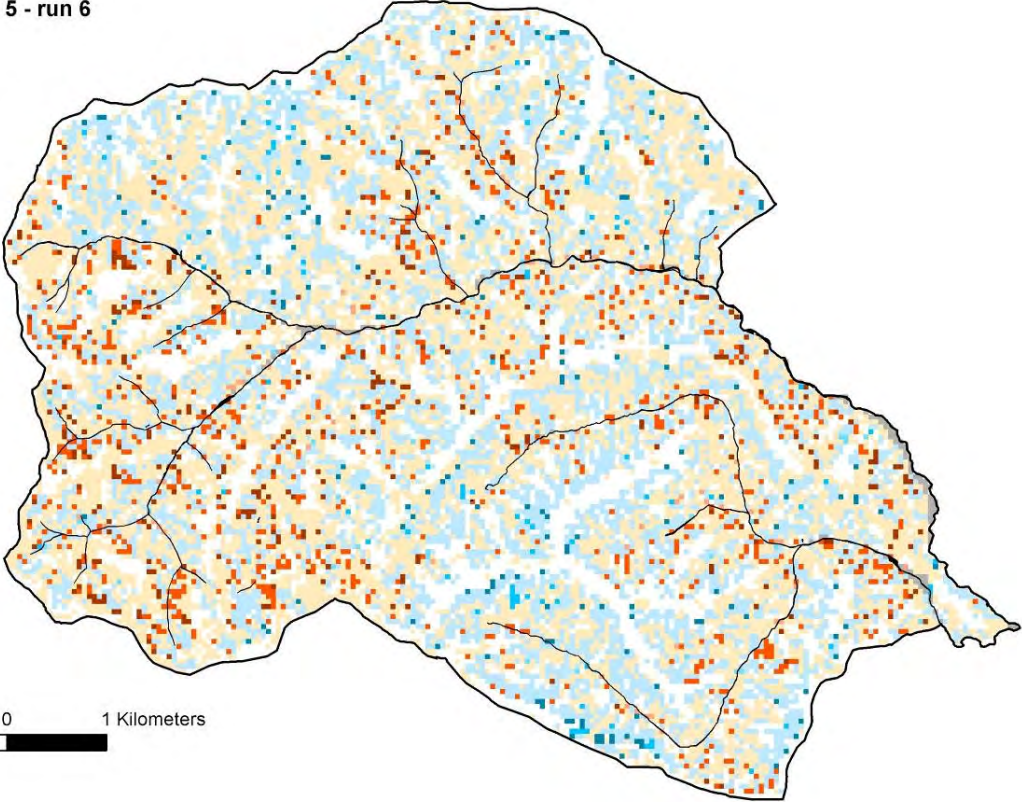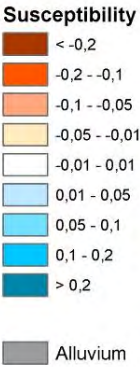
Fig. 7.3.2.1-9: Map of differences between WoE run 5 and 6
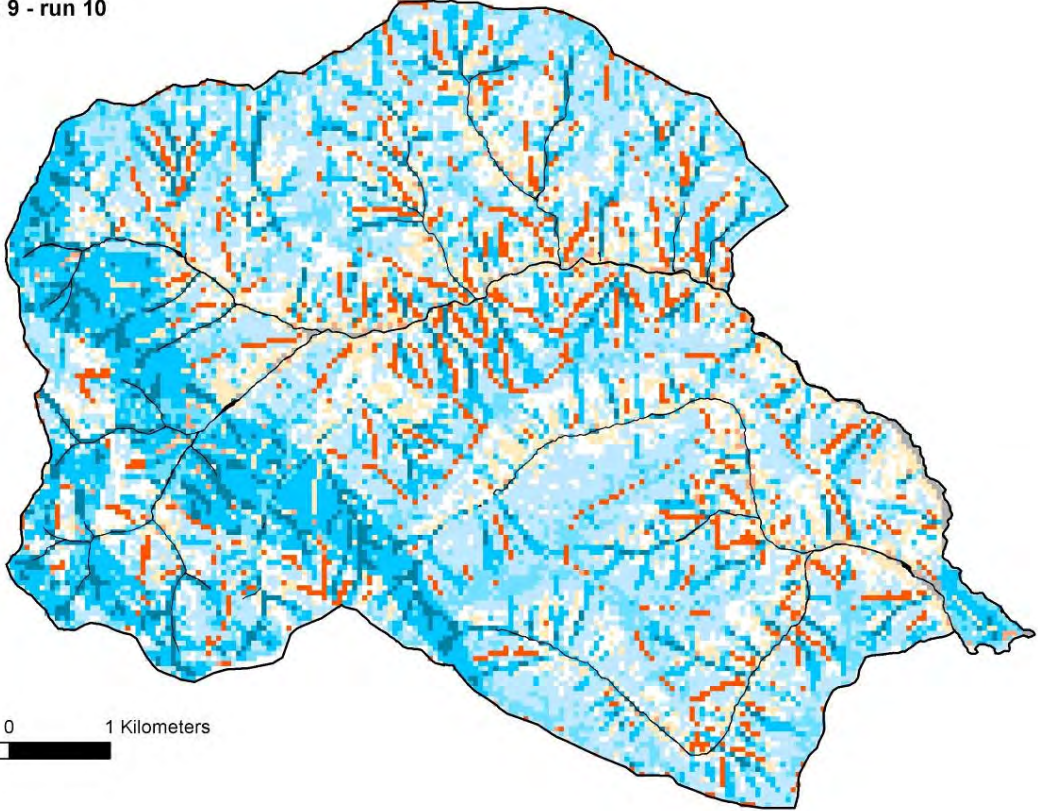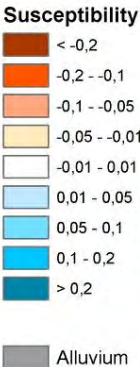
Fig. 7.3.2.1-10: Map of differences between WoE run 9 and 10

Difference run 10 - run 13

Susceptibility

■	< -0,2
■	-0,2 - -0,1
■	-0,1 - -0,05
■	-0,05 - -0,01
□	-0,01 - 0,01
■	0,01 - 0,05
■	0,05 - 0,1
■	0,1 - 0,2
■	> 0,2

■	Alluvium
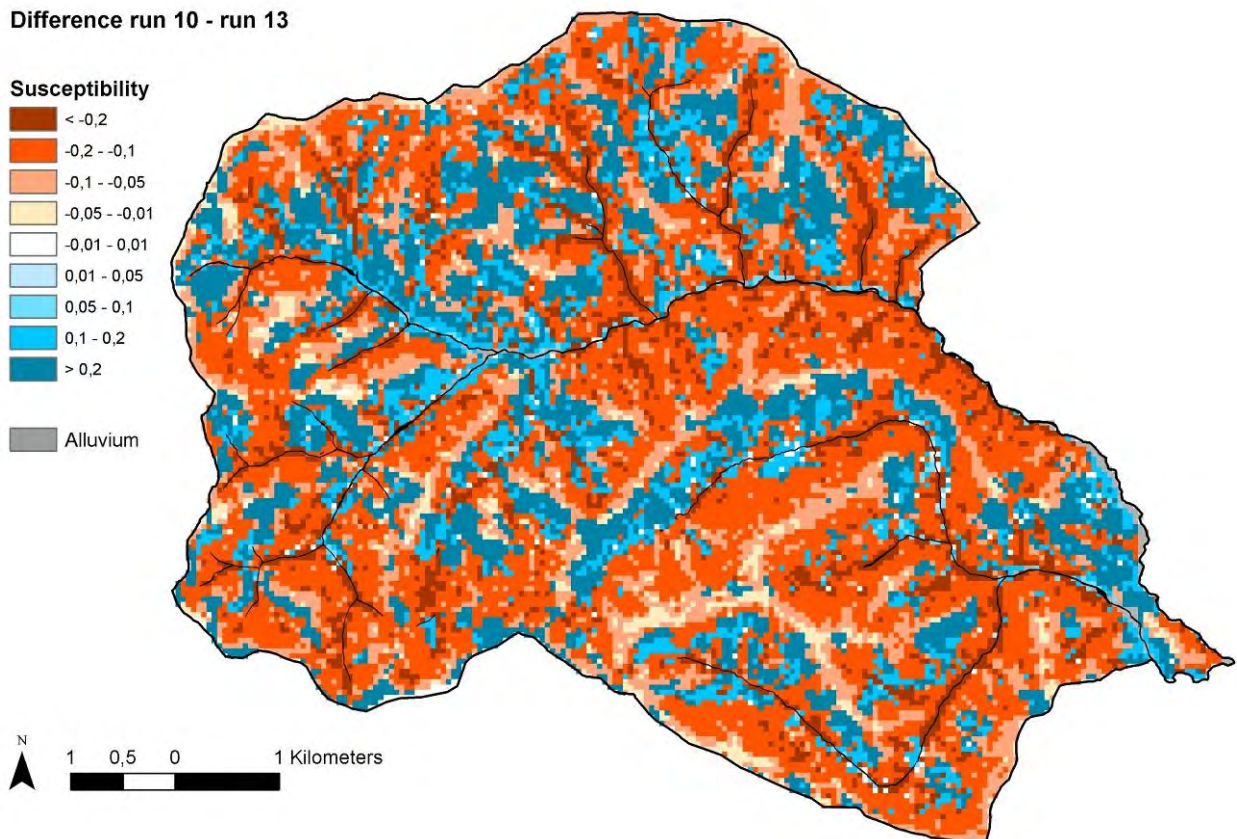
Fig. 7.3.2.1-11: Map of differences between WoE run 10 and 13

Very high contrasts (positive as well as negative) are apparent in the map of differences between runs 10 and 13 (Fig. 7.3.2.1-11). The structure clearly reflects the forest cover as run 13 was calculated without any forest-related parameter map. Therefore forested areas are modelled with much higher susceptibilities in run 13 compared to run 10 resulting in negative differences and vice versa in open land.

7.3.2.2. Modelling Results using Parameter Maps of High Processing Effort

"Level high" parameter maps are generated by advanced, higher developed methods with higher expenditure (cf. Fig. 6.2-1). Based on different combinations of these parameter maps 31 modelling runs were calculated. The modelling procedure can be followed by Tab. 7.3.2.2-1.

Runs 33 and 34 involve *BK* as geological / pedological oriented parameter map for the first time. Compared to the consideration of *Sub_GK_lg* all validation indices are improved significantly by this measure.

Runs 35 and 36 aim at the evaluation of *Wald_Sat_lh*. With regard to the consideration of *Wald_DKM_lg* the validation did not reproduce any improvements despite much higher processing efforts. This finding is ascribed to the fact that a lot

of information supposed to be relevant for the triggering of shallow landslides was lost by the aggregation process (cf. Chapter 5.3).

The involvement of different parameter maps with regard to hydro(geo)logy (e.g. runs 41 and 42 or 43 and 43a or 47 and 48) generally does not change the validation indices significantly although the susceptibility patterns do show differences. This issue which obviously is related to the applied validation methods is addressed in section 7.1.

The involvement of *Sub_GK_lh* in runs 43 and 43a produces some improvements of the validation results (approx. 1,5 % AUC). Compared to modelling with *Sub_GK_lg* instead of *Sub_GK_lh* the validation indices do not change significantly. The susceptibility map based on run 43a is shown in Fig. 7.3.2.2-5.

Following the general modelling strategy, the selected "best" results (selected by joint evaluation of WoE and LR modelling) both "level low" (run 10) and "level high" (run 43a) were recalculated with one of the parameter maps replaced. In general, this procedure did not result in any significant improvements of the validation indices.

Run 58 for the first time involves the parameter map *NS_lh*. Compared to run 43a without any map related to precipitation the prediction rates improve by approx. 1,5 % AUC. Similar improvements are noticed compared to run 64 applying *NS_lg* instead of *NS_lh*. Run 58 consequently represented the best validation indices of the WoE "level high" modelling phase. The susceptibility map derived from run 58 is shown in Fig. 7.3.2.2-6.

Fig. 7.3.2.2-1 to 7.3.2.2-4 give the Chung & Fabbri as well as the ROC curves of the five best "level high" calculations. A strong grouping of most of the curves with the best result shown by run 58 (yellow curves) can be observed in all diagrams.

Runs 71 and 72 are calculated using regionalisation data (*Wald_DKM_lg, Wegenetz_lg*) instead of field-based datasets. Equal to the effect observed at the "level low" modelling, this replacement results in a significant decrease of all calculated validation numbers (approx. 7 to 8 % AUC).
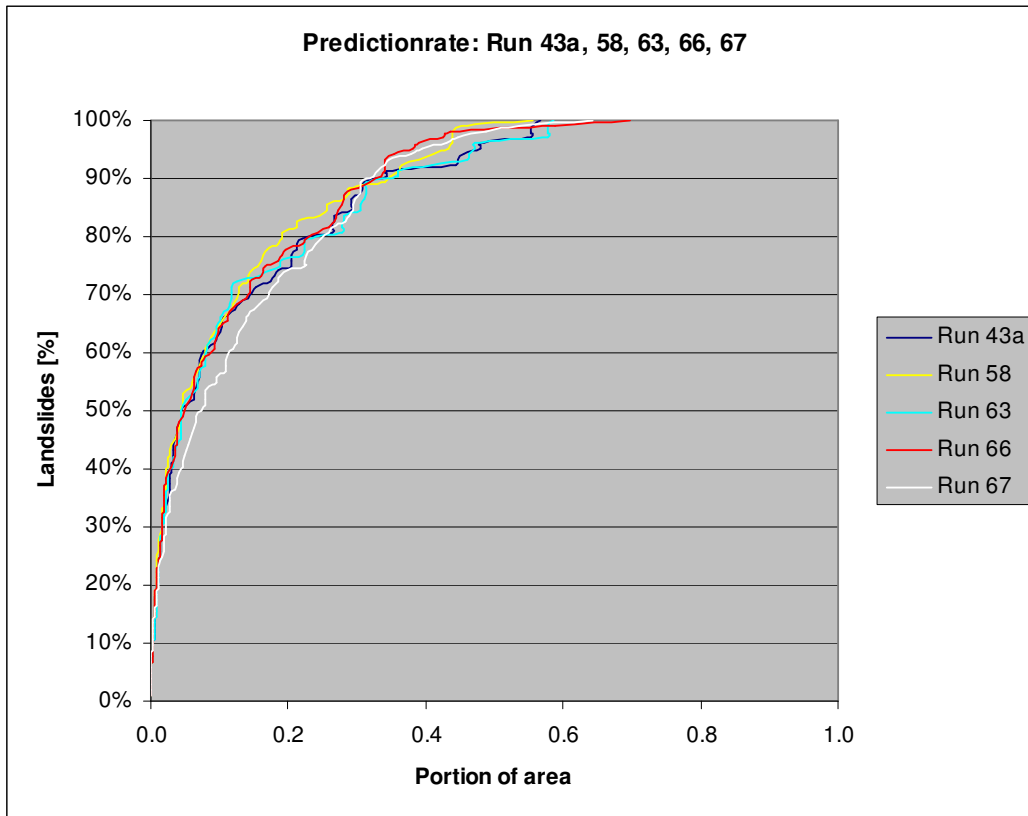
Fig. 7.3.2.2-1: Cumulated Chung & Fabbri curves of runs 43a, 58, 63, 66 and 67 (predictionrate)
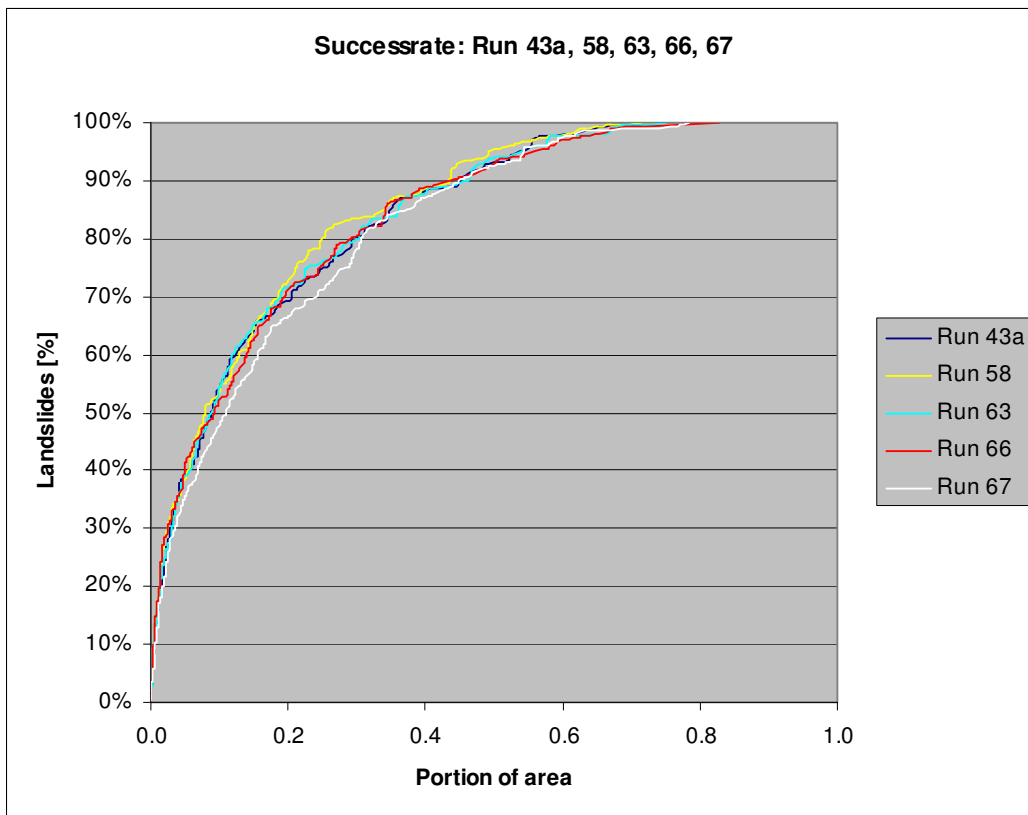
Fig. 7.3.2.2-2: Cumulated Chung & Fabbri curves of runs 43a, 58, 63, 66 and 67 (successrate)
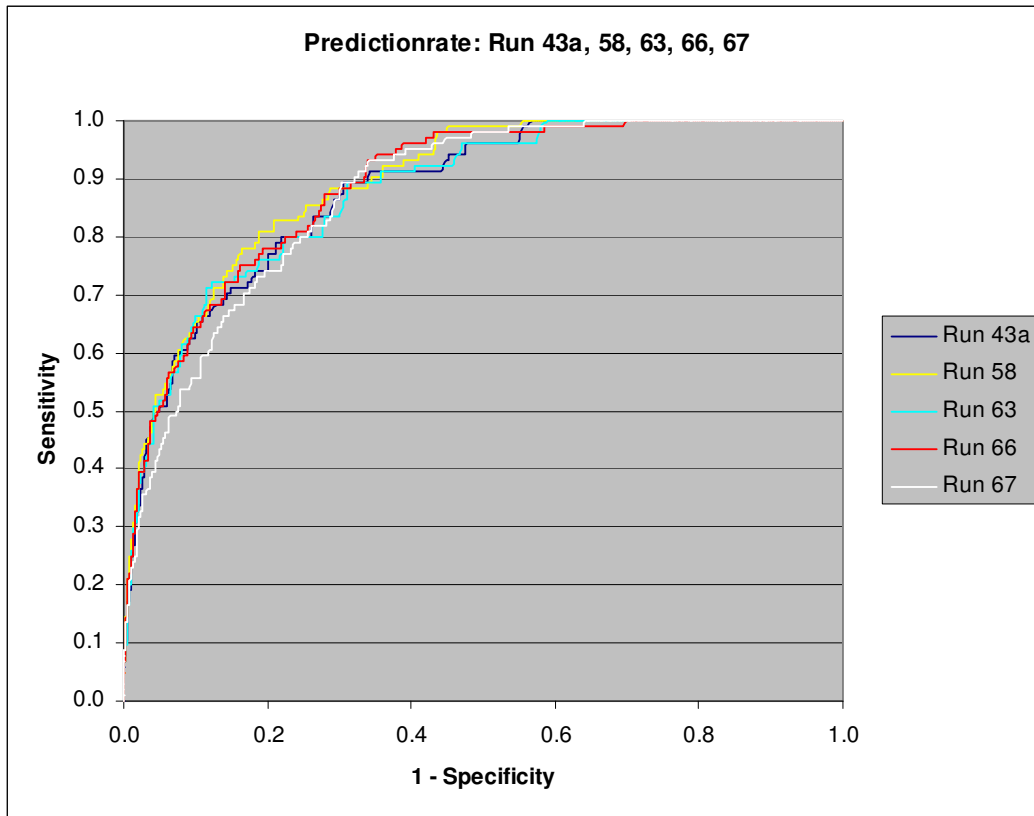
Fig. 7.3.2.2-3: Cumulated ROC curves of runs 43a, 58, 63, 66 and 67 (predictionrate)
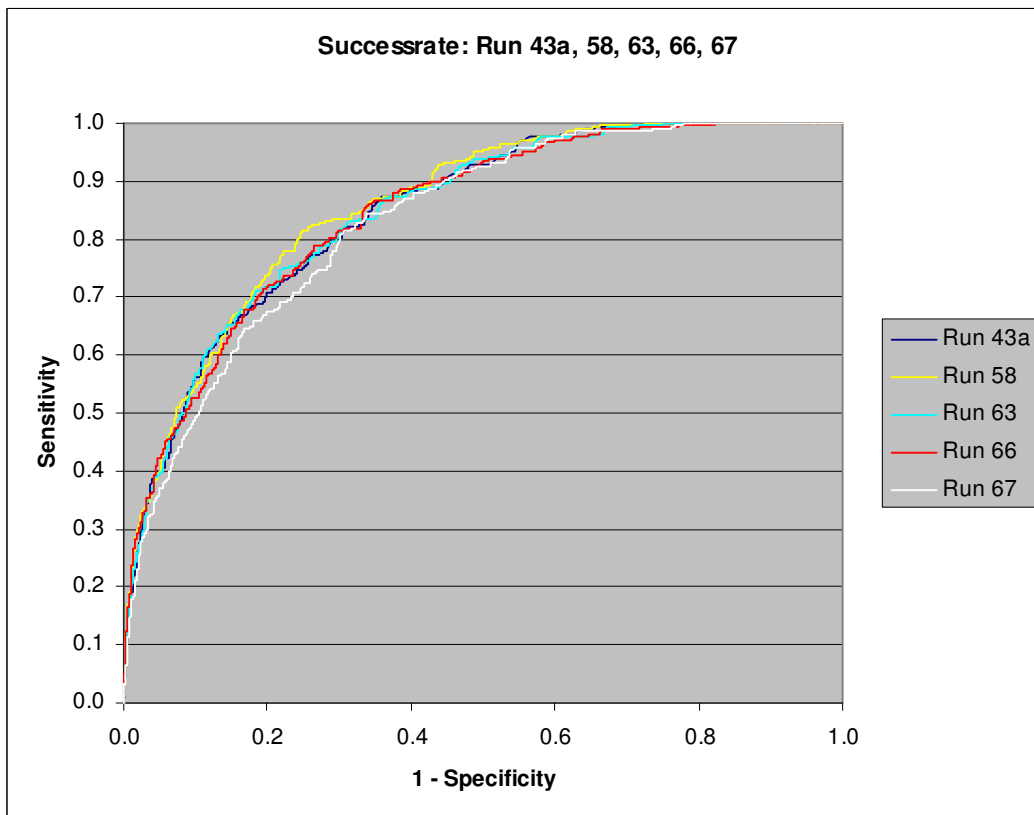
Fig. 7.3.2.2-4: Cumulated ROC curves of runs 43a, 58, 63, 66 and 67 (successrate)

Tab. 7.3.2.2-1: Model runs using Parameter Maps of High Processing Effort additionally (* run 73 modelled only with LR, see Chapter 7.4)

Run	Parameter Maps (abbreviations cf. Tab. 6.2.2)						
	Slope	**Curvature**	**Forest**	**Street Network**	**Hydro(geo)logy**	**Geology / Pedology**	**Precipitation**
33	HN-DHM10	VW-DHM10	Wald_Sat_lg_mb	Wegenetz_lg_mb	QDisp_lg_BK_fa	BK	
34	HN-DHM10	VW-DHM10	Wald_Sat_lg_mb	Wegenetz_lg_mb	QDisp_lg_BK_fa_NS_lg	BK	
35	HN-DHM10	VW-DHM10	Wald_Sat_lh				
36	HN-DHM10	VW-DHM10	Wald_Sat_lh	Wegenetz_lg_mb	QDisp_lg_GK_lh_fa	Sub_GK_lg	
37	HN-DHM10	VW-DHM10	Wald_Sat_lg_mb	Wegenetz_lh			
40	HN-DHM10	VW-DHM10	Wald_Sat_lg_mb	Wegenetz_lg_mb	QDisp_lh_fa		
41	HN-DHM10	VW-DHM10	Wald_Sat_lg_mb	Wegenetz_lh	QDisp_lg_GK_lh_fa		
42	HN-DHM10	VW-DHM10	Wald_Sat_lg_mb	Wegenetz_lh	QDisp_lh_fa		
43	HN-DHM10	VW-DHM10	Wald_Sat_lg_mb	Wegenetz_lg_mb	QDisp_lg_GK_lh_fa	Sub_GK_lh	
43a	HN-DHM10	VW-DHM10	Wald_Sat_lg_mb	Wegenetz_lg_mb	QDisp_lh_fa	Sub_GK_lh	
44	HN-DHM10	VW-DHM10	Wald_Sat_lg_mb	Wegenetz_lh	QDisp_lh_fa	Sub_GK_lg	
45	HN-DHM10	VW-DHM10	Wald_Sat_lg_mb	Wegenetz_lh	QDisp_lh_fa	Sub_GK_lh	
46	HN-DHM10	VW-DHM10	Wald_Sat_lg_mb	Wegenetz_lg_mb	QDisp_lh_fa	BK	
47	HN-DHM10	VW-DHM10	Wald_Sat_lg_mb	Wegenetz_lh	QDisp_lg_BK_fa	BK	
48	HN-DHM10	VW-DHM10	Wald_Sat_lg_mb	Wegenetz_lh	QDisp_lh_fa	BK	

55	HN-DHM10	HK-DHM10	Wald_Sat_lg_mb	Wegenetz_lg_mb	QDisp_lh_fa	Sub_GK_lh	
57	HN-DHM10	VW-DHM10	Wald_Sat_lg_mb	Wegenetz_lg_mb	Flowaccumulation	Sub_GK_lh	
58	HN-DHM10	VW-DHM10	Wald_Sat_lg_mb	Wegenetz_lg_mb	QDisp_lh_fa	Sub_GK_lh	NS_lh
59	HN-DHM10	VW-DHM10	Wald_Sat_lg_mb	Wegenetz_lg_mb	QDisp_lg_GK_lh_fa	Sub_GK_lg	NS_lh
60	HN-DHM10	VW-DHM10	Wald_Sat_lg_mb	Wegenetz_lg_mb	QDisp_lg_GK_lh_fa_NS_lh	Sub_GK_lh	
61	HN-DHM10	VW-DHM10	Wald_Sat_lg_mb	Wegenetz_lg_mb	QDisp_lg_GK_lg_fa_NS_lh	Sub_GK_lg	
62	HN-DHM10	VW-DHM10	Wald_Sat_lg_mb	Wegenetz_lg_mb	QDisp_lg_GK_lh_fa_NS_lh	Sub_GK_lg	
63	HN-DHM10	VW-DHM10	Wald_Sat_lg_mb	Wegenetz_lg_mb	QDisp_lh_fa_NS_lh	Sub_GK_lh	
64	HN-DHM10	VW-DHM10	Wald_Sat_lg_mb,	Wegenetz_lg_mb	QDisp_lh_fa	Sub_GK_lh	NS_lg
66	HN-DHM10	VW-DHM10	Wald_Sat_lg_mb	Wegenetz_lg_mb	QDisp_lh_fa	Sub_GK_lh, BK	NS_lh
67	HN-DHM10	VW-DHM10	Wald_Sat_lg_mb	Wegenetz_lg_mb	QDisp_lg_BK_fa	BK	NS_lh
68	HN-DHM10	VW-DHM10	Wald_Sat_lg_mb	Wegenetz_lg_mb	QDisp_lg_BK_fa_NS_lh	Sub_GK_lh, BK	
69	HN-DHM10	VW-DHM10, HK-DHM10	Wald_Sat_lg_mb	Wegenetz_lh	QDisp_lh_fa	Sub_GK_lh	
70	HN-DHM10	VW-DHM10, HK-DHM10	Wald_Sat_lg_mb	Wegenetz_lh	QDisp_lh_fa_NS_lh	Sub_GK_lh	
71	HN-DHM10	VW-DHM10	Wald_DKM_lg	Wegenetz_lg	QDisp_lh_fa	Sub_GK_lh	NS_lh
72	HN-DHM10	VW-DHM10	Wald_DKM_lg	Wegenetz_lg	QDisp_lh_fa	Sub_GK_lh, BK	NS_lh
73*	HN-DHM10	VW-DHM10	Wald_Sat_lg_mb	Wegenetz_lh_mb	QDisp_lh_fa	Sub_GK_lh	NS_lh

WoE Run 43a

Susceptibility

- < 0,1
- 0,1 – 0,2
- 0,2 – 0,3
- 0,3 – 0,4
- 0,4 – 0,5
- 0,5 – 0,6
- 0,6 – 0,7
- 0,7 – 0,8
- 0,8 – 0,9
- > 0,9

. Landslides

Alluvium
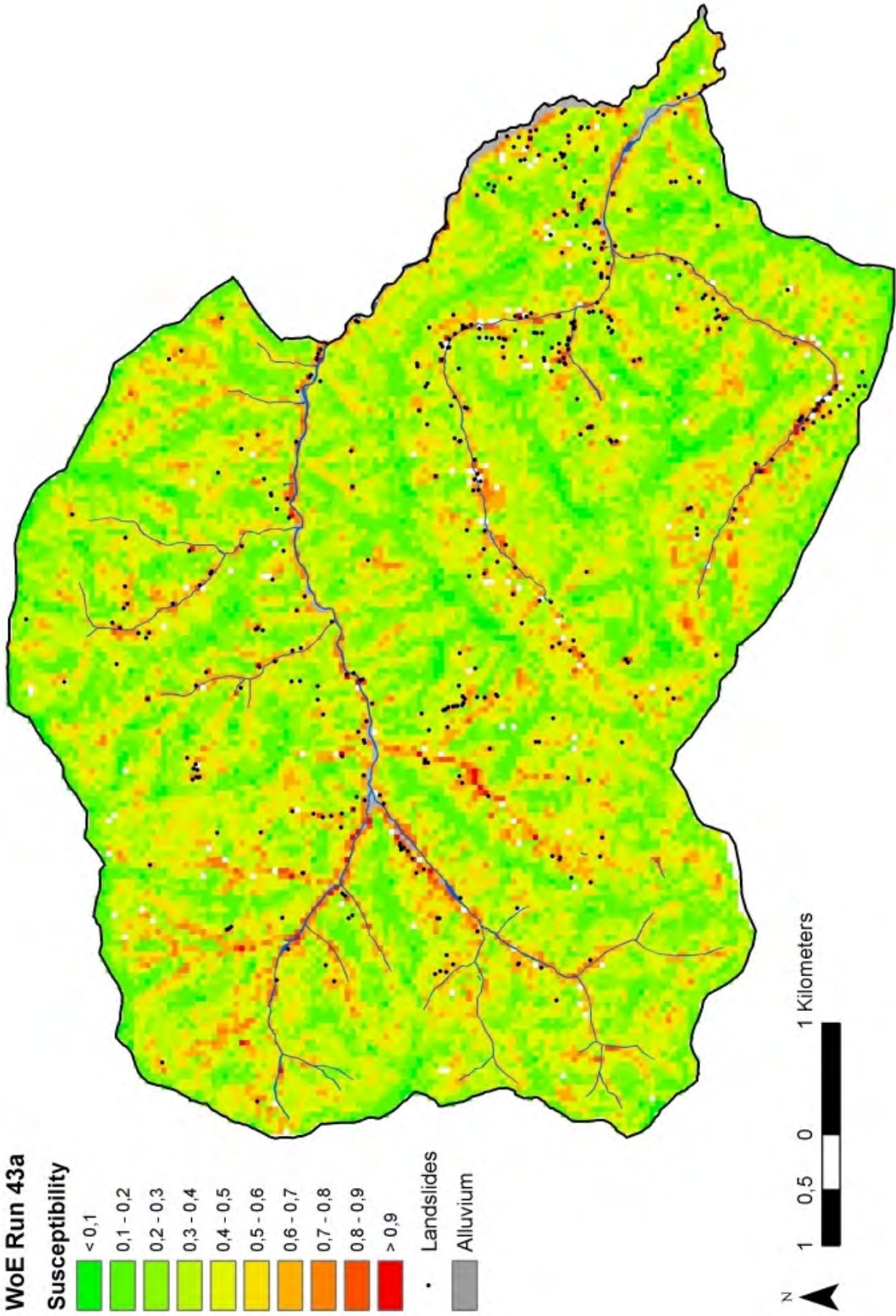
Fig. 7.3.2.2-5: Result of WoE modelling run 43a

WoE Run 58

Susceptibility

- < 0,1
- 0,1 – 0,2
- 0,2 – 0,3
- 0,3 – 0,4
- 0,4 – 0,5
- 0,5 – 0,6
- 0,6 – 0,7
- 0,7 – 0,8
- 0,8 – 0,9
- > 0,9

. Landslides

Alluvium

1   0,5   0   1 Kilometers

N
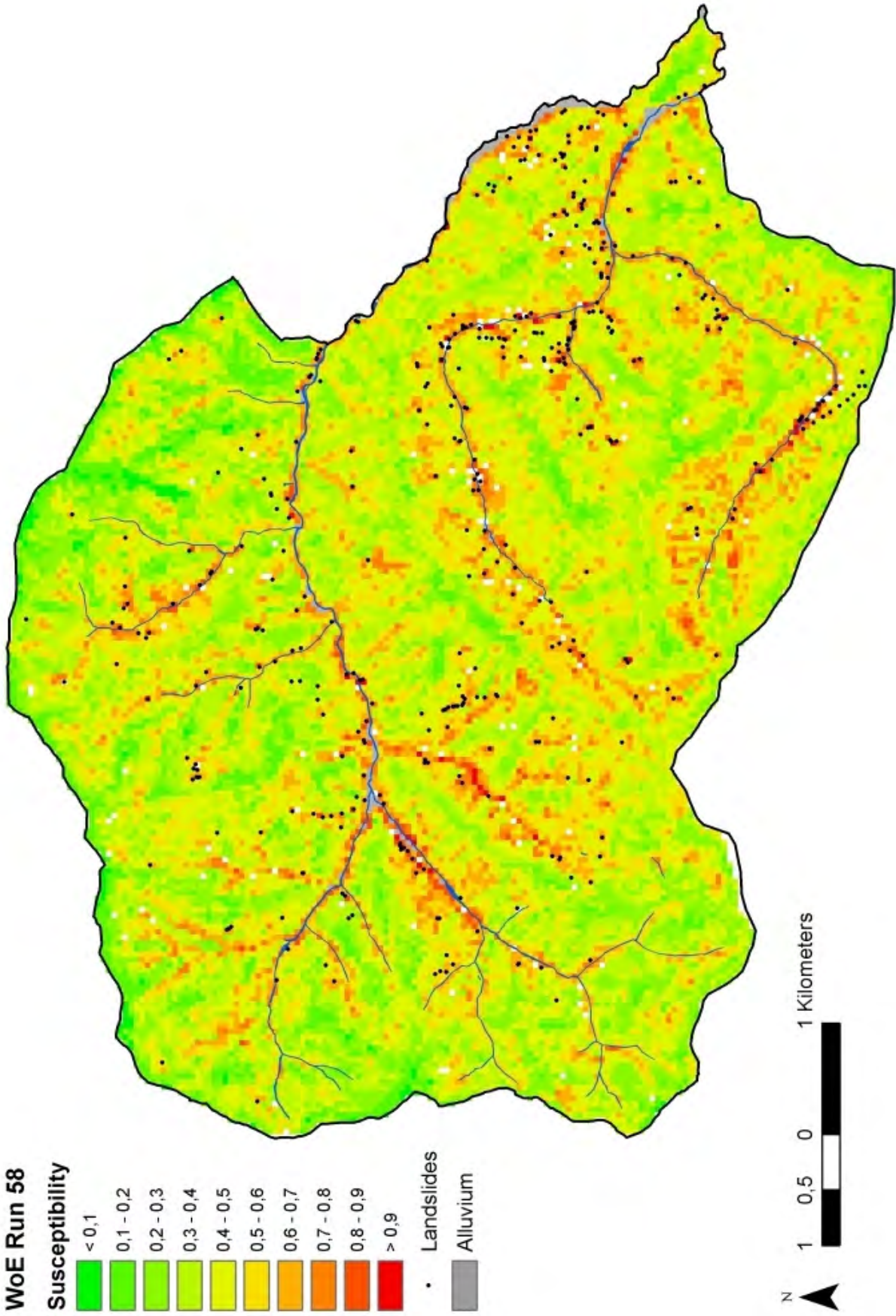
Fig. 7.3.2.2-6: Result of WoE modelling run 58

7.3.2.3. Modelling Results using Process Oriented Combinations of Parameter Maps

Besides the systematic modelling following the general approach as described in section 6.2 and the validation results some runs were calculated under specific consideration of expert knowledge of the Geological Survey. Whereas run 26 only involves "level low" parameter maps, runs 27 and 28 as well as runs 69 and 70 consider at least one "level high" parameter map.

Following the validation indices the results of these modelling runs do not show any significant differences compared to the systematic modelling. However, it has to be noticed that the number of adequate modelling runs based on expert knowledge has been too low to confirm this conclusion definitely.

7.3.2.4. Comparison of Results of different Processing Levels

As is shown in Chapter 11 and in the Annex (Tab. A6) the single replacement of one "level low" parameter map by the adequate "level high" parameter map in most cases does not result in a significant improvement of the validation indices (> 1 % AUC).

However, the cumulative estimation of the involvement of "level high" parameter maps by calculating the arithmetic means of the validation indices (only runs without regionalisation datasets were taken into account) shows a notable improvement of all "level high" validation indices compared to the "level low" results (Tab. 7.3.2.4-1). Although this result has to be interpreted with reservations because of the general modelling approach (e.g. identification of best parameter combination and further calculation based on this selection) the conclusion can be drawn that by combination of several "level high" parameter maps tentatively better results can be achieved.

Tab. 7.3.2.4-1: Arithmetic means of validation indices of "level low" and "level high" modelling runs

	Probability	ROC (AUC)	Chung/Fabbri (AUC)
level low (n = 28)			
Successrate	69,12 %	83,16 %	82,73 %
Predictionrate	77,51 %	86,26 %	86,76 %
level high (n = 18)			
Successrate	72,89 %	84,18 %	83,99 %
Predictionrate	79,32 %	87,66 %	87,89 %

Aiming at getting an impression of the local differences between the "level low" and the "level high" modelling runs the five best results of the "level low" modelling stage were selected according to the joint assessment of the validation indices of both the WoE and the LR modelling method. The selected modelling runs are 5, 6, 14a, 23 and 24. To create a common susceptibility map of these five runs the mid-range value was calculated. The same procedure was followed using the "level high" results of runs 43a, 58, 63, 66 and 67.

The differences between the two resulting maps were calculated and are presented in Fig. 7.3.2.2-7. Generally considerable differences – positive as well as negative - can be registered all over the area. These differences can mainly be ascribed to the following facts:

1. the different involvement of the precipitation-related parameter maps: in the five best results of the "level low" modelling stage only one run involves *NS_lg* whereas in the five best results of the "level high" modelling stage three runs involve *NS_lh.*

2. the different involvement of the geology-related parameter maps: in the five best results of the "level low" modelling stage three runs involve *Sub_GK_lg* whereas in the five best results of the "level high" modelling stage *Sub_GK_lh* is involved in most cases and *BK* is involved in two runs.
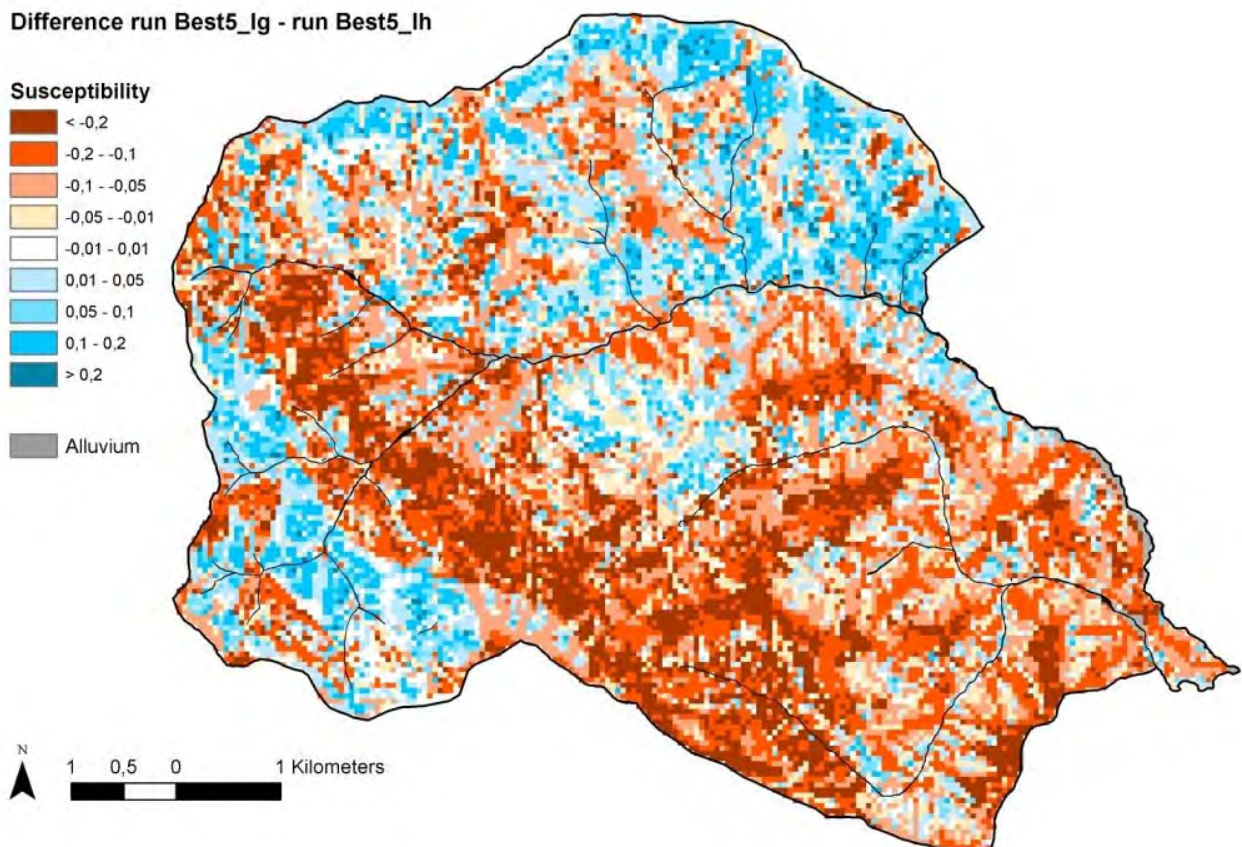
Fig. 7.3.2.2-7: Map of differences between WoE best five maps of "level low" modelling stage and WoE best five maps of "level high" modelling stage

7.4.   Modelling and Validation of Landslide Susceptibility Maps by means of Logistic Regression (JR)

Logistic multiple regression identifies variables that are significant in predicting the probability of occurrence. The approach allows a spatial distribution of probabilities or susceptibility values to be calculated within the GIS environment and was successfully used in numerous landslide susceptibilty studies (e.g. Carrara et al. 1999, Dai and Lee 2002 a,b, Dai et al. 2004, Ayalew & Yamagishi 2005, Pradhan et al. 2006, Zhu & Huang 2006, Alemayehu 2007, Bell 2007, Chen & Wang 2007, Greco et al. 2007)

7.4.1. Basic Principles

Logistic regression (LR) is a statistical method to describe a discrete i.e. binary dependent variable through several explanatory variables. With a LR the probability of an event occurring in an element can be estimated. This can be helpful for classifying elements into one of two populations. In this case, the elements are the units of analysis (pixels) and the populations are either the presence or the absence of landslides. The goal of LR would be to find the best fitting model to describe the relationship between the presence or absence of landslides (dependent variable) and a set of independent parameters.

The advantage of logistic regression is that, through the addition of an appropriate link function to the usual linear regression model, the variables may be either continuous or discrete, or any combination of both types and they do not necessarily have normal distributions. This is an important pro given the usually non-normal distribution of most environmental data (Hair et al. 1998, Pradhan et al 2006).

The dependent variable can have only 2 values (an event occurring or not occurring), and predicted values can be interpreted as probability because they are constrained to fall in the interval between 0 and 1.

Quantitatively, the relationship between the probability of occurrence and its dependency on several variables can be expressed as:

$$p = 1 / (1 + e^{-z}) \qquad\qquad\qquad (1)$$

where p is the probability of an event occurring. The probability varies from 0 to 1 on an S-shaped curve and z is the linear combination of explanatory variables. Logistic multiple regression involves fitting to the data an equation of the form

$$z = b_0 + b_1x_1 + b_2x_2 + \ldots + b_nx_n \qquad\qquad\qquad (2)$$

where b_0 is the intercept of the model, the b_i (i = 0, 1, 2, …, n) are the slope coefficients of the logistic multiple regression model and the x_i (i = 0, 1, 2, …, n) are the independent variables. The model formed is then a logistic multiple regression of presence or absence of landslides (present conditions) on the independent variables (pre-failure conditions).

In order to appropriately interpret Eqs. (1) and (2), one has to use the coefficients as a power to the natural log(e). The result represents the odds ratio or the probability that an event will occur divided by the probability that it fails to do so. If a coefficient is positive, its transformed log value will be > 1, meaning that the event is more likely to occur. If a coefficient is negative, the latter will be < 1 and the odds of the event occurring decreases. A coefficient of 0 has a transformed log value of 1, and it does not change the odds one way or the other. For a positive coefficient, the probability plotted against the values of an independent variable follows an S-shaped curve (Ayalew & Yamagishi 2005). For a negative coefficient the S-shape is turned around.
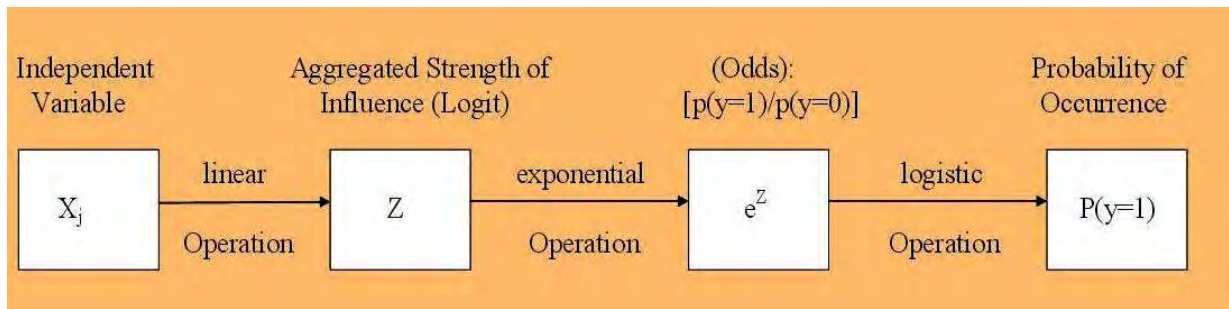
Fig. 7.4.1-1.: Basic Interrelations between the Components of Logistic Regression

Although logistic multiple regressions finds a "best fitting" equation just as linear regression does, the principles on which it does so are rather different. Instead of using a least-squared deviations criterion for the best fit, it uses a maximum likelihood method, which maximizes the probability of getting the observed results given the appropriate regression coefficients.

The technique of logistic multiple regression yields coefficients for each parameter. These coefficients serve as weights in an algorithm that can be used in the GIS database to produce a map depicting the probability of landslide susceptibility.

Further methodological aspects of the method are given by many authors (e.g. Backhaus et al. 2000, Chen & Wang 2007, Hosmer & Lemeshow 1989, Kleinbaum 1998).

7.4.2. Modelling and Validation Results

Using the logistic multiple regression method, the spatial relationship between the locations of landslides and environmental parameters was calculated.

Approx. 70 % of the available landslide-dataset "high quality for modelling" (cf. Tab. 6.1.1-1) were used as input to the logistic multiple regression algorithm. This training dataset corresponds to the original "training-" and "validation" portion of the complete dataset (cf. Chapter 6.1.2). The remaining 30 %, corresponding to the original "test" portion of the dataset were used for the validation of the modelling results.

The algorithm was calculated within R, a freely downloadable desktop statistical software package, to obtain the coefficients for the logistic multiple regression model. After the calculation was executed the results were imported to the GIS.

As described in Chapter 6.2 a general strategy in successively involving different parameters for the statistical modelling was followed. Basically at first only "level low" parameters were considered, followed by addition or substitution of "level high" parameters.

Based on different combinations of these parameter maps 64 modelling runs were calculated of which 63 were identical with the WoE modelling (Chapter 7.3). One additional run was added at the end of the "level high" modelling procedure (run 73). The parameters included in the calculations are shown in Tab 7.3.2-1. The modelling results are presented in the following sections.

The validation of the results made use of the following methods:

1. Modelled probability (cut-off value 0,5)
2. Chung & Fabbri Curve
3. Receiver Operating Characteristic (ROC) - Curve

These methods as well as some fundamental problems are described in detail in Chapter 7.1. The calculation was applied to the training dataset ("success rate") as well as to the test dataset ("prediction rate").

The modelling strategy (i.e. which parameter maps were kept in the further modelling steps and which of the maps were rejected) was based on the results of the validation. The strategy was based on the combined assessment of the validation results of both the LR and the WoE modelling and is described in Chapter 7.3.2.

The results of the validation are summed up in Tab. 7.4.2.1-1.

Generally the LR modelling results are characterized by a much better differentiation between high and low susceptibilities than the WoE modelling which appears in a low number of pixels situated in the medium part of the susceptibility spectrum. This is expressed by a low portion of yellow areas in the maps (Fig. 7.4.2.1-5 to 7.4.2.1-7 and 7.4.2.2-1 to 7.4.2.2-2).

7.4.2.1. Modelling Results using Parameter Maps of Low Processing Effort

"Level low" parameter maps are generated by means of simple, standard methods (cf. Fig. 6.2-1). Based on different combinations of these parameter maps 32 modelling runs were calculated. The list of model runs calculated with LR is the same as with WoE – thus the modelling procedure and the included parameter maps can be followed by Tab. 7.3.2.1-1.

The modelling runs were started with some very simple combinations of parameter maps taking into account only a few basic parameters (runs 1, 2 and 3). The exchange of *Wald_DKM_lg_mb* by *Wald_Sat_lg_mb* only resulted in very low improvements of the validation results. Nevertheless, during further progress of the modelling *Wald_Sat_lg_mb* was kept assuming that this dataset presented higher relevance than the data of the Digital Cadastral Map (expert knowledge).

After involvement of the influence of the road network the validation results show a significant improvement of both success and prediction rates (> 90 % for prediction rates, cf. Tab. 7.4.2.1-1)

In the following modelling runs parameters connected to subsurface flow (*Flowaccumulation, QDisp*) were involved. As based on the field investigations, subsurface flow was rated to be highly relevant from the process-oriented point of view by the involved experts, such maps were kept in the further modelling procedure despite the fact that the results of the validation were not improving significantly compared to run 3.

The susceptibility maps derived from runs 5 and 6 are shown in the Fig.s 7.4.2.1-5. and 7.4.2.1-6.

Tab. 7.4.2.1-1: Results of Validations of Modelling Runs calculated with Logistic Regression

Run	Probability	ROC (AUC)	Chung/Fabbri (AUC)
1	78.82%	83.50%	83.16%
	85.45%	88.60%	88.63%
2	79.17%	83.70%	83.31%
	85.45%	88.70%	88.75%
3	77.78%	85.80%	85.38%
	87.27%	91.40%	91.25%
4	77.78%	86.40%	85.99%
	85.45%	91.10%	90.84%
5	77.43%	86.40%	85.96%
	85.45%	90.80%	90.61%
6	77.78%	86.40%	85.97%
	85.45%	90.70%	90.55%
7	76.04%	85.30%	84.84%
	87.27%	90.00%	89.90%
8	75.35%	85.20%	84.75%
	86.36%	89.70%	89.65%
9	77.78%	86.40%	85.98%
	85.45%	90.70%	90.54%
10	79.51%	86.50%	86.02%
	85.45%	90.70%	90.57%
11	79.17%	83.70%	83.35%
	85.45%	88.80%	88.83%
12	79.17%	86.40%	86.01%
	85.45%	90.80%	90.68%
13	67.36%	77.00%	76.72%
	81.82%	82.00%	82.06%
14a	78.13%	86.40%	86.01%
	86.36%	90.80%	90.62%
14b	78.82%	86.50%	86.06%
	86.36%	91.10%	90.88%
15	77.78%	85.80%	85.41%
	88.18%	91.50%	91.31%
16	77.78%	84.60%	84.17%
	83.64%	88.00%	88.02%
18	77.43%	85.20%	84.75%
	84.55%	89.60%	89.52%
19	76.04%	85.20%	84.81%
	86.36%	89.80%	89.68%
20	76.74%	86.00%	85.57%
	87.27%	91.50%	91.27%
21	78.82%	86.50%	86.05%
	85.45%	90.80%	90.61%
22	78.13%	86.40%	86.00%
	85.45%	90.70%	90.56%
23	78.47%	86.60%	86.17%
	87.27%	90.70%	90.49%
24	78.47%	86.50%	86.09%
	86.36%	91.00%	90.78%

Run	Probability	ROC (AUC)	Chung/Fabbri (AUC)
25	78.47%	86.50%	86.09%
	86.36%	91.00%	90.77%
26	78.82%	86.40%	86.00%
	87.27%	90.80%	90.65%
27	77.78%	86.50%	85.99%
	87.27%	90.90%	90.69%
28	77.08%	86.60%	86.11%
	86.36%	90.80%	90.61%
29	75.00%	81.60%	81.29%
	72.73%	82.10%	82.32%
31	65.97%	76.20%	75.93%
	73.64%	80.10%	80.34%
32	72.92%	81.40%	81.03%
	79.09%	85.40%	85.26%
33	78.47%	86.60%	86.12%
	88.18%	91.30%	91.03%
34	77.08%	86.60%	86.12%
	87.27%	91.30%	91.03%
35	68.75%	77.60%	77.32%
	77.27%	80.90%	81.14%
36	73.61%	81.90%	81.59%
	81.82%	85.00%	84.92%
37	78.82%	86.30%	85.84%
	86.36%	90.60%	90.49%
40	76.74%	86.40%	85.91%
	87.27%	91.40%	91.16%
41	79.51%	86.90%	86.44%
	85.45%	89.90%	89.83%
42	79.17%	86.80%	86.33%
	86.36%	90.40%	90.26%
43	77.78%	86.50%	86.04%
	88.18%	91.10%	90.94%
43a	76.74%	86.40%	85.94%
	87.27%	91.50%	91.29%
44	78.13%	86.90%	86.45%
	85.45%	90.40%	90.38%
45	78.82%	86.80%	86.33%
	86.36%	90.40%	90.28%
46	77.08%	86.50%	86.01%
	87.27%	91.70%	91.41%
47	79.17%	87.00%	86.59%
	86.36%	90.60%	90.43%
48	78.47%	86.90%	86.42%
	85.45%	90.70%	90.55%
55	75.69%	85.20%	84.78%
	87.27%	90.90%	90.87%
57	77.08%	86.50%	86.04%
	87.27%	91.50%	91.23%

Run	Probability	ROC (AUC)	Chung/Fabbri (AUC)
58	78.82%	87.50%	87.05%
	90.00%	93.00%	92.66%
59	78.82%	87.60%	87.13%
	88.18%	92.40%	92.07%
60	77.78%	86.60%	86.10%
	88.18%	91.20%	90.94%
61	79.17%	86.60%	86.15%
	86.36%	91.10%	90.95%
62	78.82%	86.50%	86.09%
	85.45%	90.70%	90.58%
63	76.39%	86.40%	85.96%
	87.27%	91.40%	91.20%
64	77.08%	86.50%	86.06%
	88.18%	91.50%	91.22%
66	78.82%	87.60%	87.07%
	90.00%	93.10%	92.74%
67	79.86%	87.60%	87.16%
	90.00%	92.80%	92.40%
68	78.13%	86.70%	86.21%
	89.09%	91.40%	91.20%
69	78.82%	86.80%	86.32%
	86.36%	90.40%	90.29%
70	79.17%	86.80%	86.35%
	86.36%	90.30%	90.16%
71	75.00%	82.90%	82.55%
	81.82%	85.20%	85.37%
72	74.31%	83.00%	82.59%
	84.55%	85.50%	85.62%
73	78.47%	86.60%	86.14%
	89.09%	92.20%	91.86%

▢ Successrate (yellow)
▢ Predictionrate (blue)

In run 10 the first parameter map considering geological / pedological aspects was involved (*Sub_GK_lg)* which lead to only a marginal improvement compared to run 6. The involvement of *Sub_GK_lg* in run 11 as well did not show any significant difference compared to run 2. Nevertheless based on additional expert-knowledge this parameter map was kept in the further modelling steps.

Run 13 was a test run without any forest map and resulted in a significant worsening of the validation results.

The cumulated Chung & Fabbri as well as the ROC-curves of runs 1 to 13 are presented in Fig. 7.4.2.1-1 to 7.4.2.1-4 showing clearly (1) the bad result of run 13 (without any involvement of forest maps) and (2) the good results and the strong grouping of all the remaining runs.
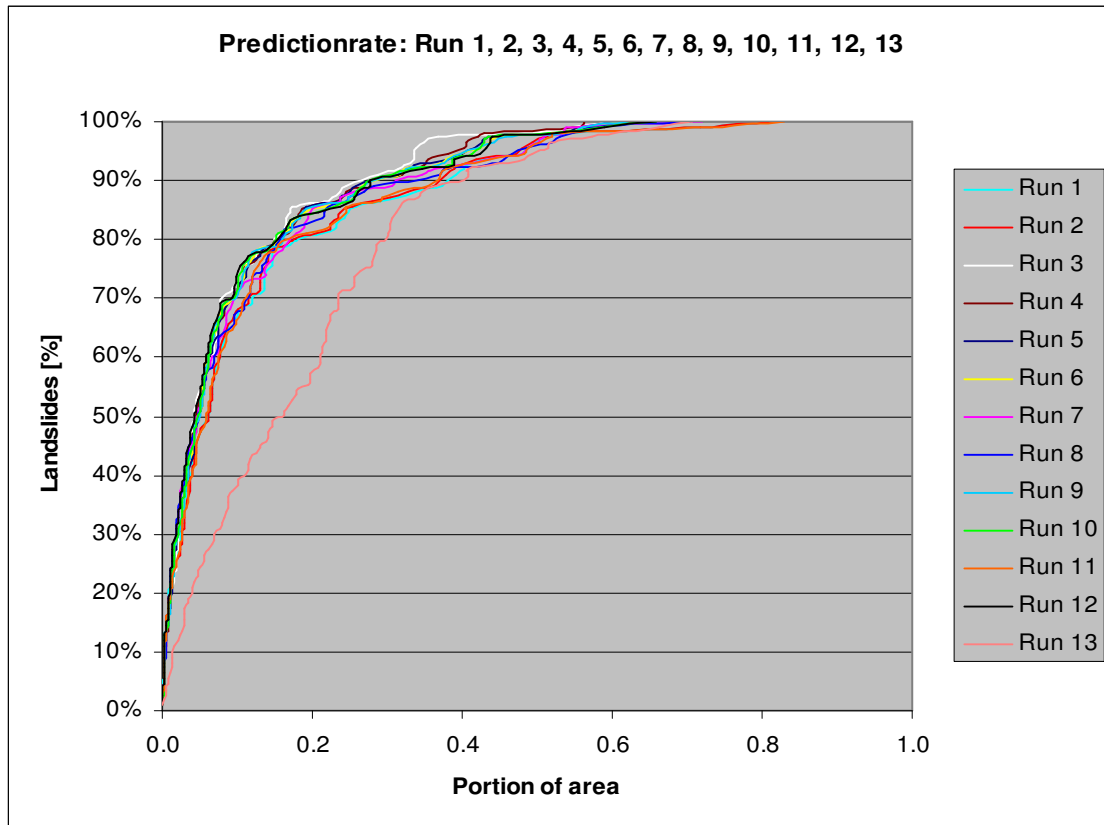
Fig. 7.4.2.1-1: Cumulated Chung & Fabbri curves of runs 1 to 13 (predictionrate)
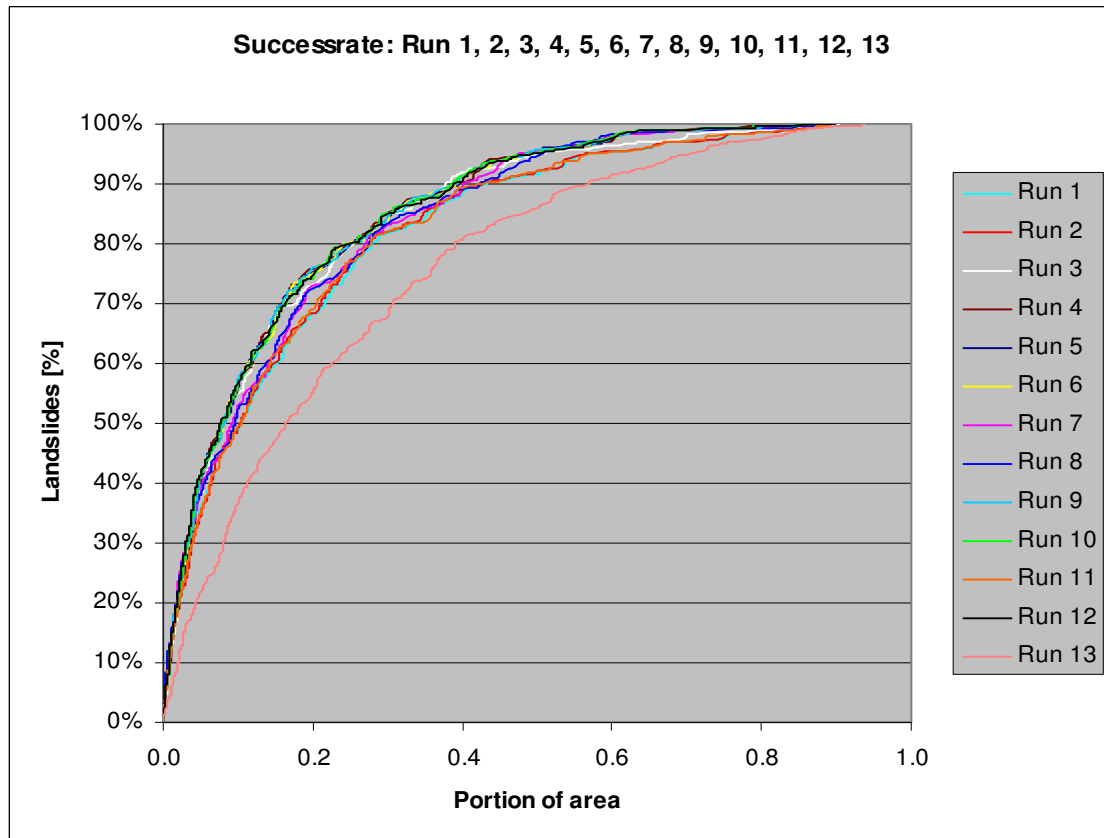
Fig. 7.4.2.1-2: Cumulated Chung & Fabbri curves of runs 1 to 13 (successrate)
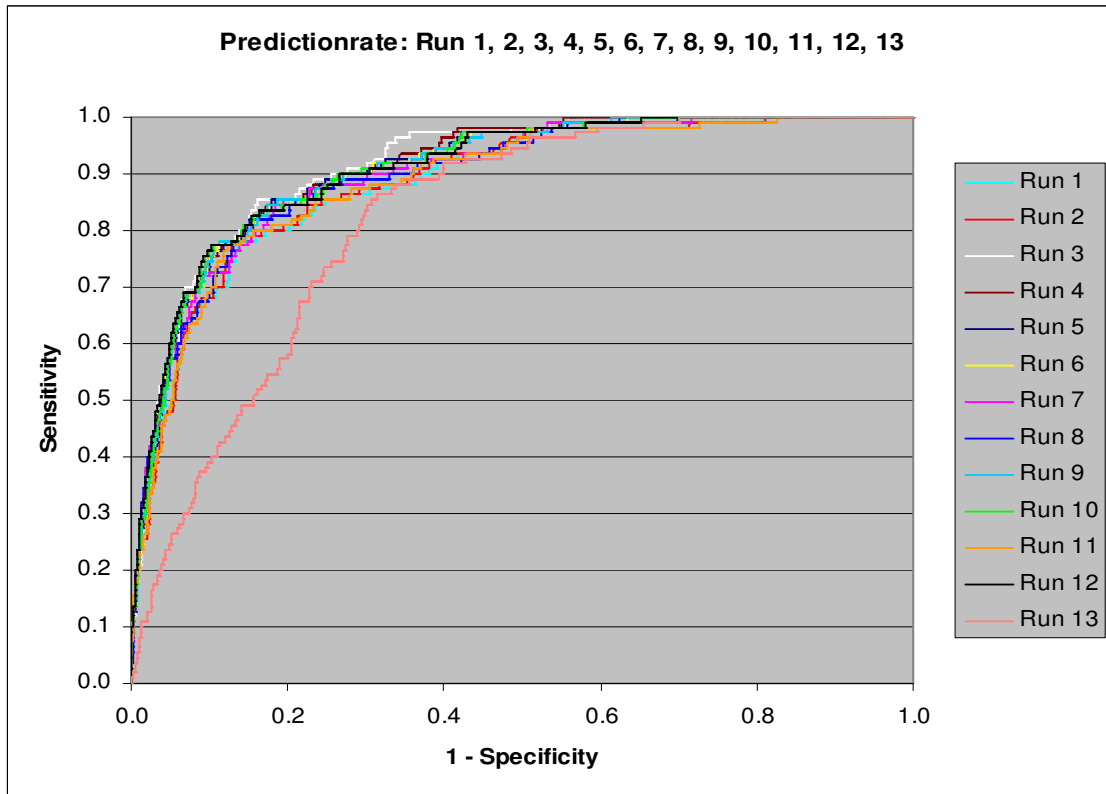
Fig. 7.4.2.1-3: Cumulated ROC curves of runs 1 to 13 (predictionrate)
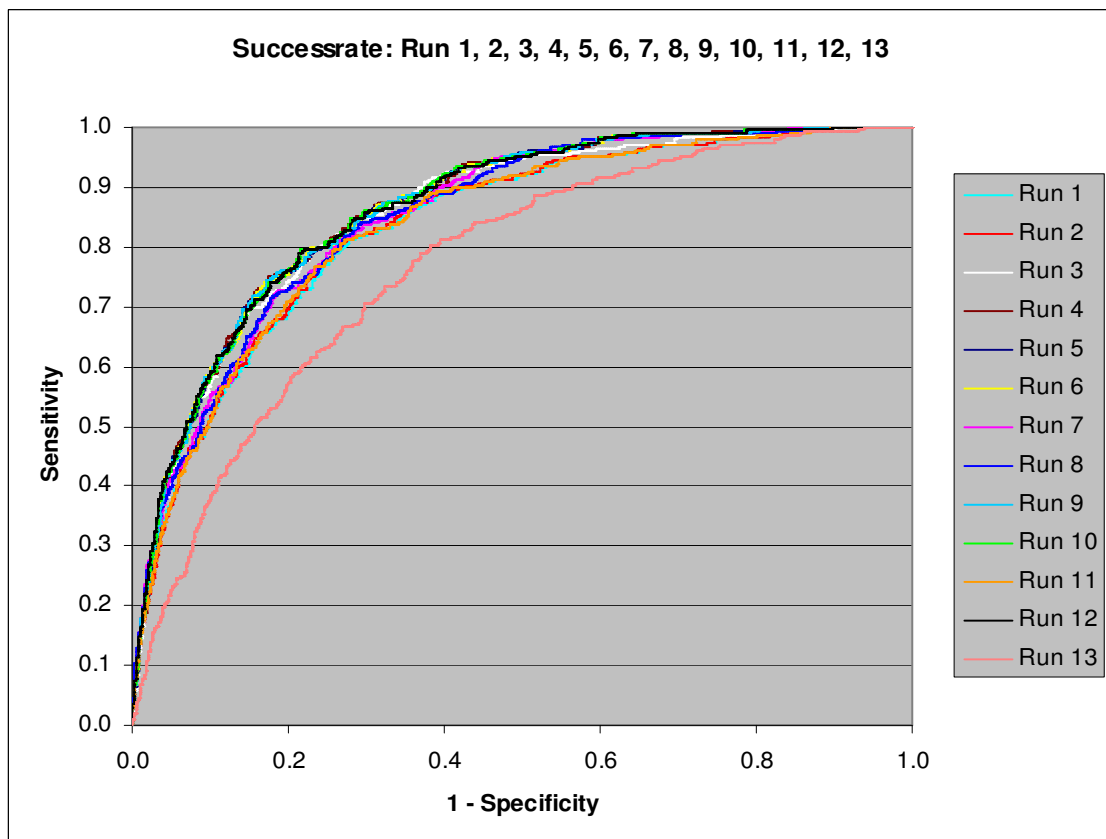
Fig. 7.4.2.1-4: Cumulated ROC curves of runs 1 to 13 (successrate)
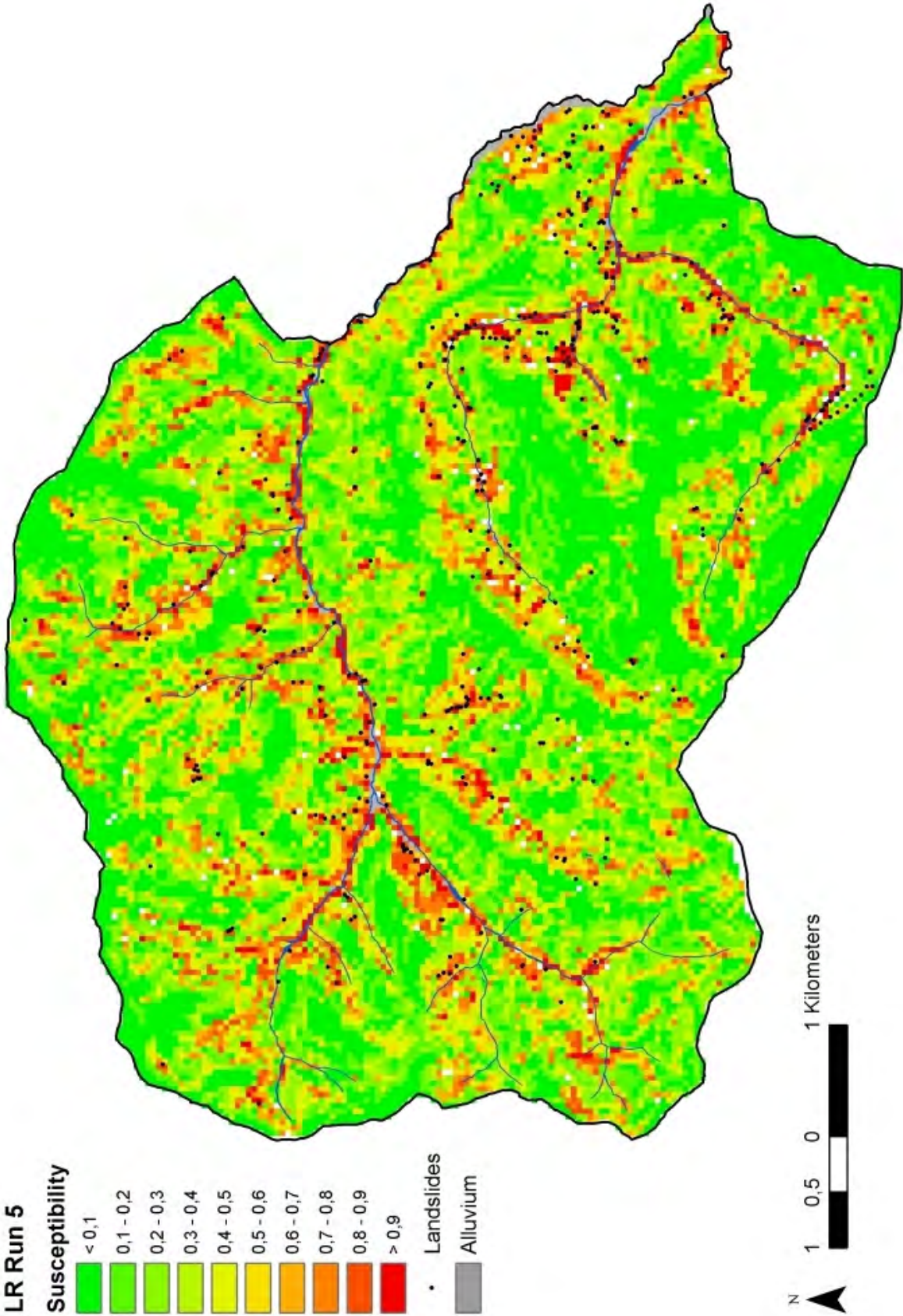
Fig. 7.4.2.1-5: Result of LR modelling run 5

LR Run 6

Susceptibility

- < 0,1
- 0,1 - 0,2
- 0,2 - 0,3
- 0,3 - 0,4
- 0,4 - 0,5
- 0,5 - 0,6
- 0,6 - 0,7
- 0,7 - 0,8
- 0,8 - 0,9
- > 0,9

Landslides

Alluvium

1   0,5   0   1 Kilometers

N
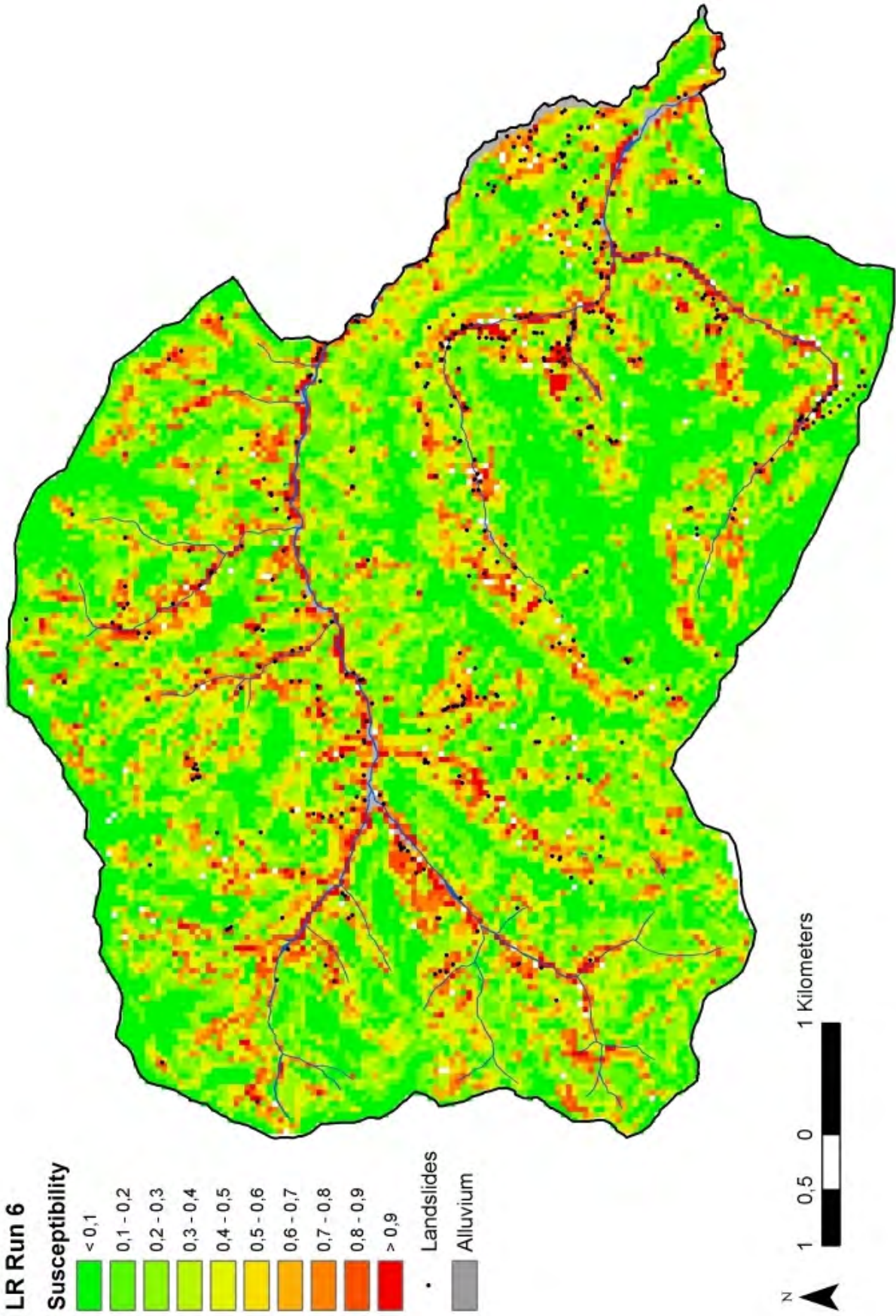
Fig. 7.4.2.1-6: Result of LR modelling run 6
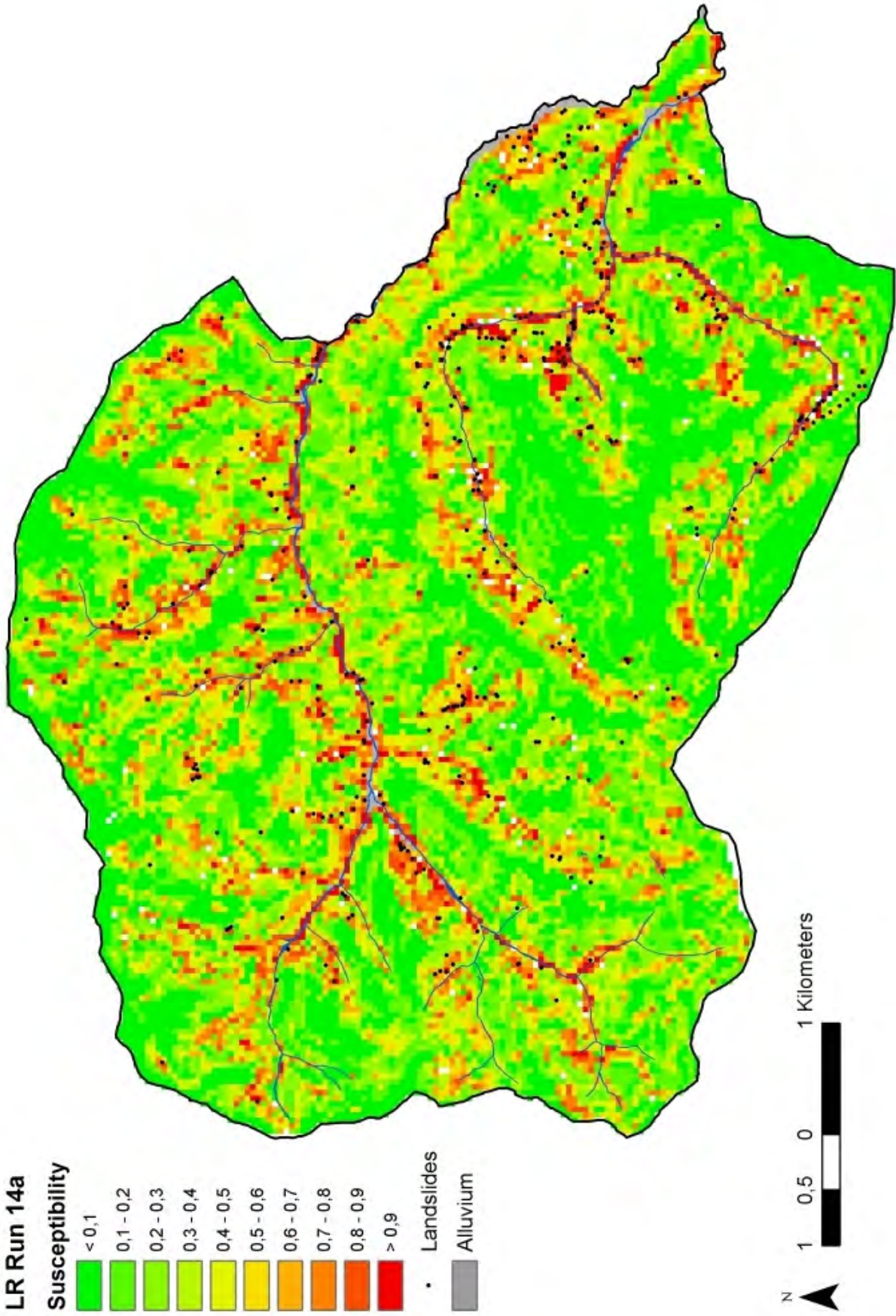
Fig. 7.4.2.1-7: Result of LR modelling run 14a

Runs 14a and 14b are variations of run 10 including *Sub_GK_lg* with different subsurface flow parameter maps. The validation results are very similar to those of run 10. The susceptibility map derived from run 14a is shown in Fig. 7.4.2.1-7.

Run 15 adds *Sub_GK_lg* to the parameters involved in run 3 resulting in more or less the same validation results (with prediction rates of Chung & Fabbri and ROC method > 90 % AUC).

Run 16 which does not consider the influence of the road network results in significantly lower AUC values.

The following modelling runs tested different derivatives of the subsurface flow, partly involving the distribution of precipitation (run 20, run 23, and run 28). Highest AUC values of both success and prediction rates (> 90 % for prediction rates, cf. Tab. 7.3.2-1) are calculated with results of run 20.

Runs 29 to 32 are calculated using regionalisation data (*Wald_DKM_lg, Wegenetz_lg*) instead of field-based datasets. This replacement results in a significant decrease of all calculated validation indices.

For visualisation of differences of particular modelling runs maps of differences were calculated. In the following examples negative differences between the two considered maps are displayed in red (higher susceptibility in the second map than in the first map), positive differences are displayed in blue (higher susceptibility in the first map than in the second map).

In the example shown in Fig. 7.4.2.1-8 the parameter map *Wegenetz_lg_mb* additionally is involved in the second run (run 3) compared to the first run (run 2). The influence area of the road network is characeterized by significantly higher landslide susceptibility resulting in negative differences. This effect is by far not as distinct as in the WoE modelling method (Fig 7.3.2.1-8) which can be ascribed to the complex coupling of regression coefficients in the LR method compared to the additive approach of the WoE method. On the other hand high portions of the test area are characterized by blue colours representing high positive differences, showing that after involvement of *Wegenetz_lg_mb* in run 3 lower susceptibilities are modelled in these areas.

Differences between run 9 and run 10 (Fig. 7.4.2.1-9) clearly display the geological situation in the western part as *Sub_GK_lg* is added in run 10. Again this effect is much flattened compared to the WoE approach (cf. Fig 7.3.2.1-10). Differences generally are very small pointing out the low impact of *Sub_GK_lg* on the modelling result.
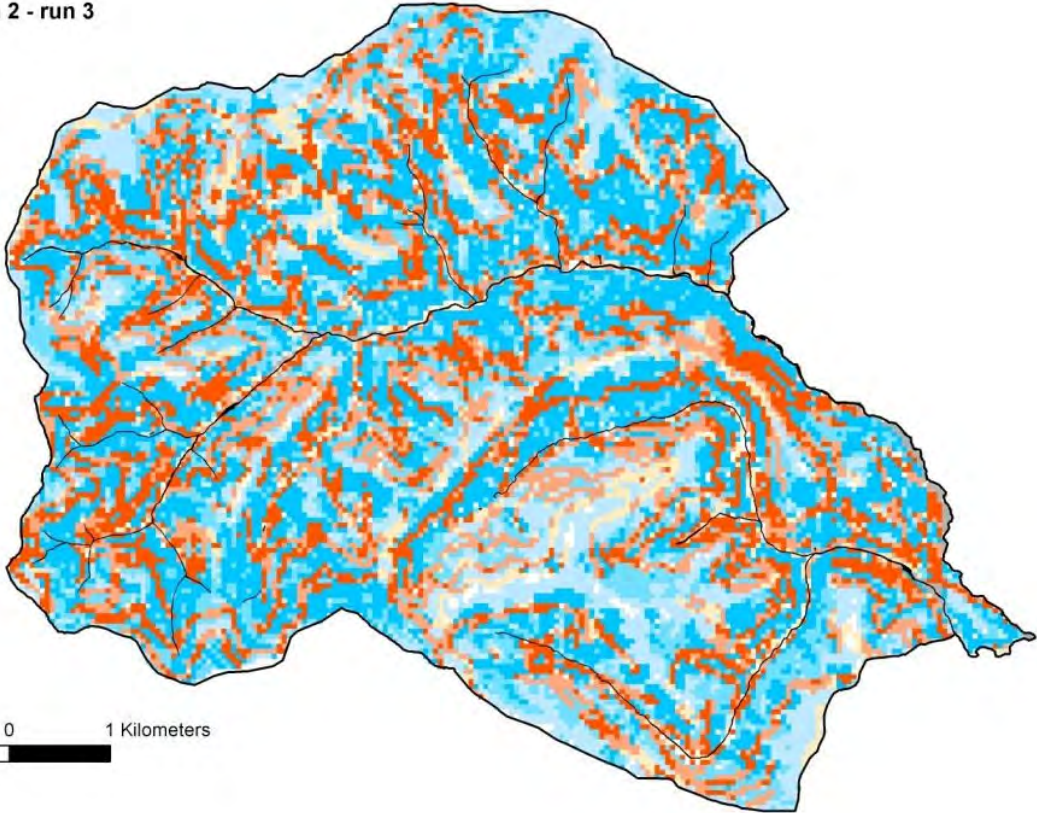
Fig. 7.4.2.1-8: Map of differences between LR run 2 and 3
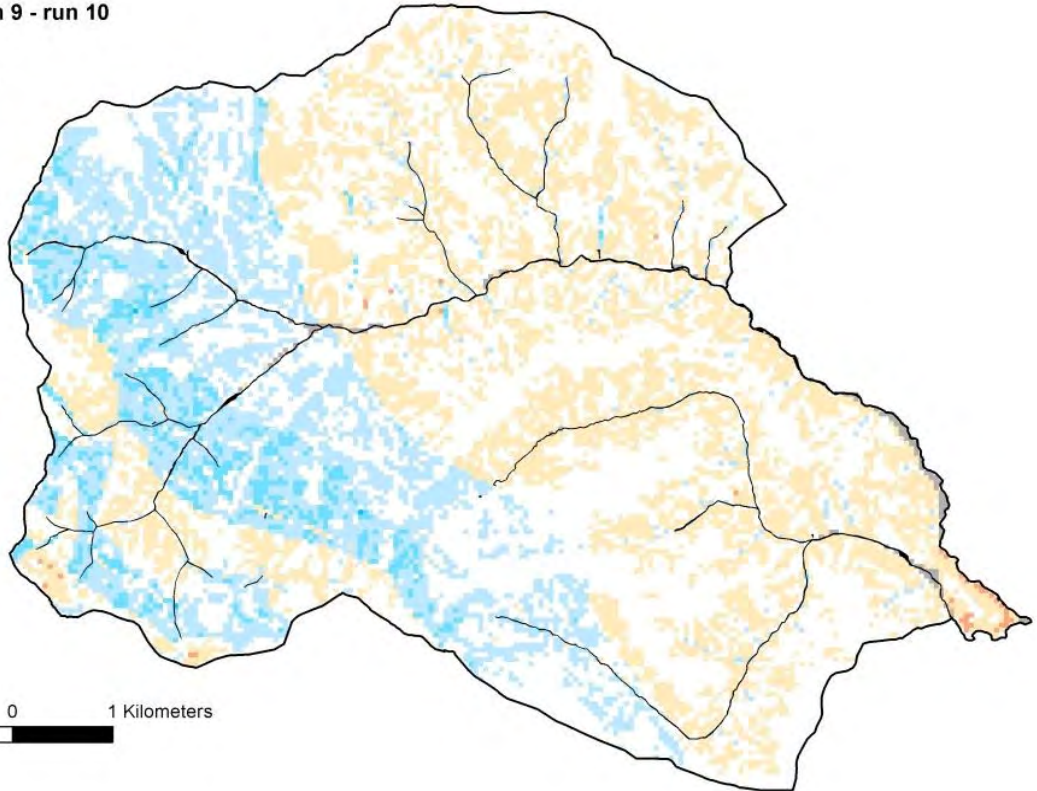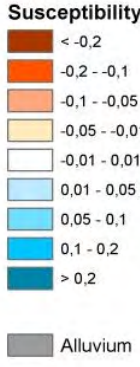
Fig. 7.4.2.1-9: Map of differences between LR run 9 and 10

The use of the regression technique allows a sensitivity analysis to be based on the magnitude of the regression coefficients. Standardized regression coefficients are used as sensitivity measures since the standardization process removes the effect of units and places all parameters on a comparable level (Hamby 1994). Their values are scaled in the range of -1 to 1. The sign of the standardized regression coefficients indicates the direction of change of the response function with respect to the direction of change in the input. In other words, the simulation model is more sensitive to the parameters that have larger-magnitude standardized regression coefficients in the regression equation. The coefficients are indicative of the amount of influence the parameter has on the model as a whole.

The coupling of regression coefficients is demonstrated by the example shown in Fig. 7.4.2.1-10. By adding the stabilizing influence of *Waldsat_lg_mb* in run 10, the destabilizing influence of *HN_DHM10* as well as *VW_DHM10* increases significantly compared to run 13.
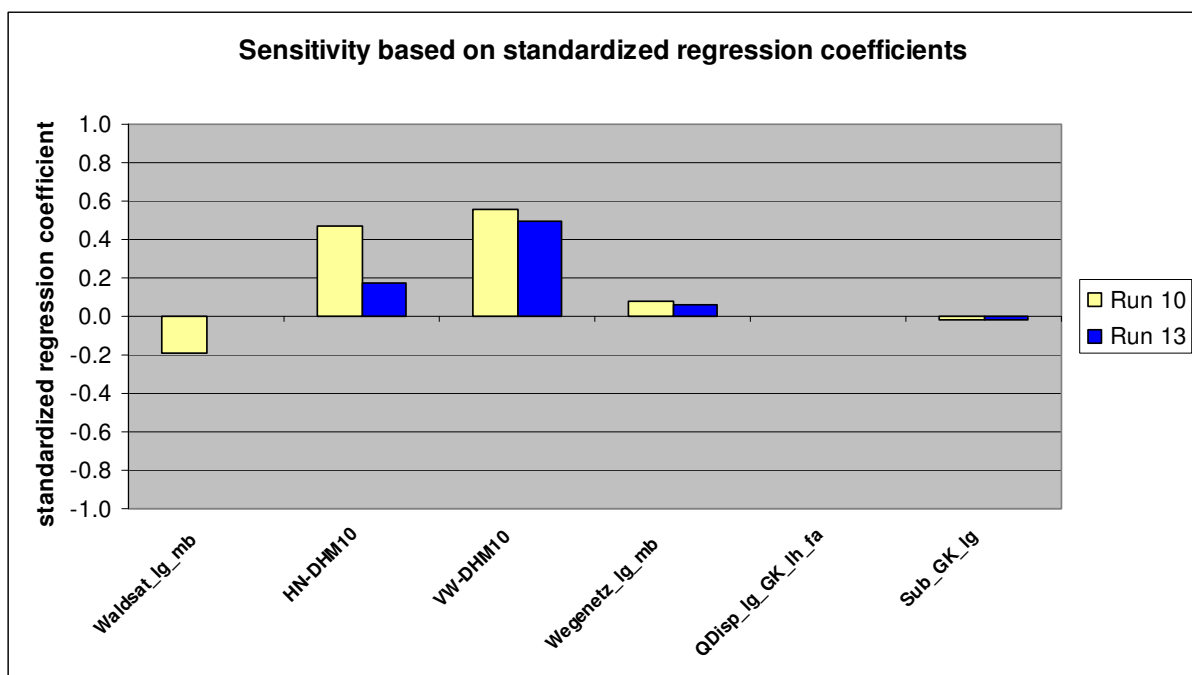
Fig. 7.4.2.1-10: Sensitivity of independent variables of run 10 compared to run 13

A second interesting example is given in Fig. 7.4.2.1-11 comparing runs 3 and 5. By adding *QDisp_lg_GK_lg_fa* in run 5 which exerts only a very low destabilizing influence on the dependent variable, the destabilizing influence of *VW_DHM_10* decreases significantly whereas the destabilizing influence of *HN_DHM_10* increases marginally.
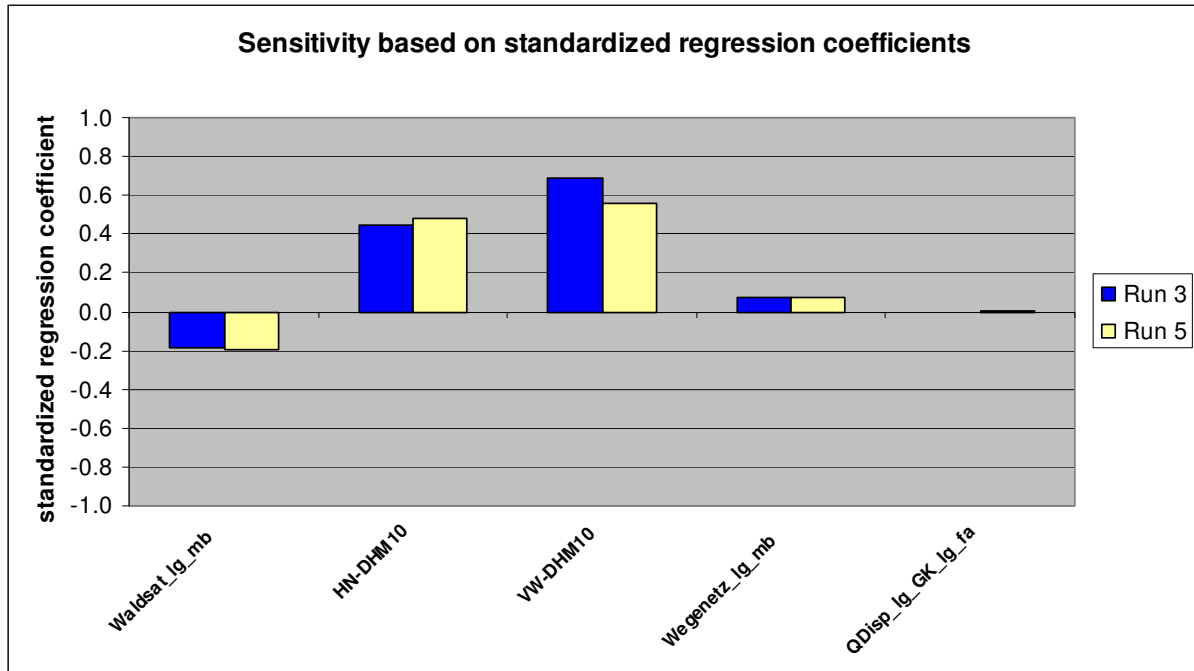
Fig. 7.4.2.1-11: Sensitivity of independent variables of run 3 compared to run 5

7.4.2.2. Modelling Results using Parameter Maps of High Processing Effort

"Level high" parameter maps are generated by advanced, higher developed methods with higher expenditure (cf. Fig. 6.2-1). Based on different combinations of these parameter maps 32 modelling runs were calculated. In general the list of model runs calculated with LR is the same as with WoE (refer to Tab. 7.3.2-3). One additional run was added at the end of the modelling procedure (run 73).

Runs 33 and 34 involve *BK* as geological / pedological oriented parameter map for the first time. In contrast to the WoE approach no significant change can be registered at all compared to the consideration of *Sub_GK_lg*. Generally the validation indices are very high with prediction rates > 91 % AUC.

Runs 35 and 36 aim at the evaluation of *Wald_Sat_lh*. With regard to the consideration of *Wald_DKM_lg* the validation did not reproduce any improvements despite much higher processing efforts. This finding is ascribed to the fact that a lot of information supposed to be relevant for the triggering of shallow landslides was lost by the aggregation process (cf. section 5.3).

The involvement of different parameter maps with regard to hydro(geo)logy (e.g. runs 41 and 42 or 43 and 43a or 47 and 48) generally does not change the validation indices significantly although the susceptibility patterns do show differences. This issue which obviously is related to the applied validation methods is addressed in section 7.1.

The involvement of *Sub_GK_lh* in runs 43 and 43a produces some improvements of the validation results (approx. 1,1 % AUC). Compared to modelling with *Sub_GK_lg* instead of *Sub_GK_lh* the validation indices do not change significantly. The susceptibility map based on run 43a is shown in Fig. 7.4.2.2.1.

Following the general modelling strategy, the selected "best" results (selected by joint evaluation of WoE and LR modelling) both "level low" (run 10) and "level high" (run 43a) were recalculated with one of the parameter maps replaced. In general, this procedure did not result in any significant improvements of the validation indices.

Run 58 for the first time involves the parameter map *NS_lh*. Compared to run 43a without any map related to precipitation the prediction rates improve by approx. 1,5 % AUC. Similar improvements are noticed compared to run 64 applying *NS_lg* instead of *NS_lh*. Run 58 consequently represented the best validation indices of the LR "level high" modelling phase with with prediction rates between 92 and 93 % AUC. The susceptibility map derived from run 58 is shown in Fig. 7.4.2.2-2.

Runs 71 and 72 are calculated using regionalisation data (*Wald_DKM_lg, Wegenetz_lg*) instead of field-based datasets. Equal to the effect observed at the "level low" modelling, this replacement results in a significant decrease of all calculated validation numbers (approx. 7 to 8 % AUC).

Compared to the WoE approach one extra run was calculated with the LR method. As the "level high" calculations using *Wegenetz_lh* did not consider the field data as represented in *Wegenetz_lh_mb*, in run 73 this dataset was considered to evaluate its influence. In comparison to run 58 where *Wegenetz_lg_mb* was involved instead the validation results marginally changed for the worse indicating that no improvement of the modelling result can be ascribed to the higher processing effort.

LR Run 43a
Susceptibility

- < 0,1
- 0,1 - 0,2
- 0,2 - 0,3
- 0,3 - 0,4
- 0,4 - 0,5
- 0,5 - 0,6
- 0,6 - 0,7
- 0,7 - 0,8
- 0,8 - 0,9
- > 0,9
- Landslides
- Alluvium
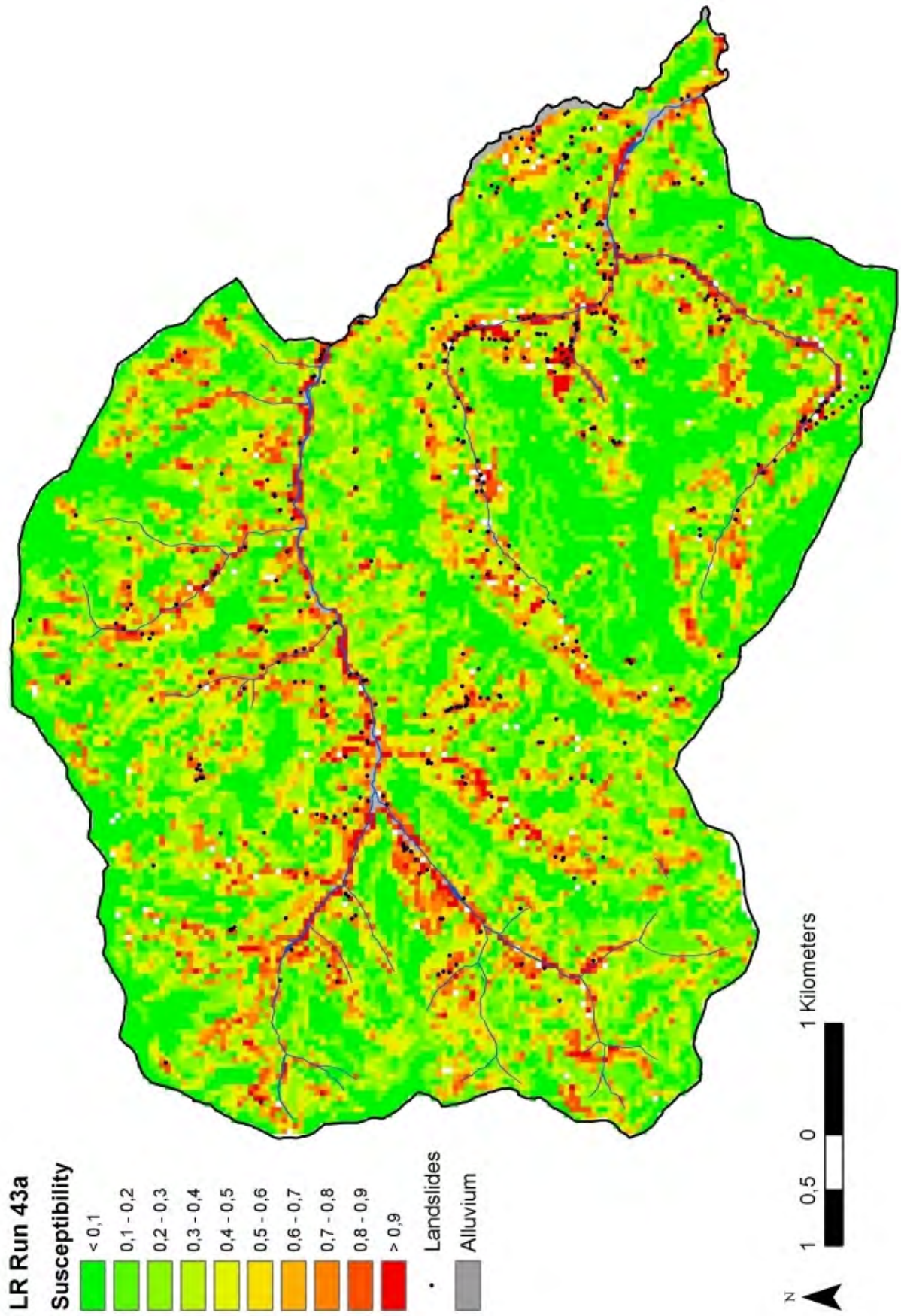
Fig. 7.4.2.2-1: Result of LR modelling run 43a

LR Run 58

Susceptibility

- < 0,1
- 0,1 - 0,2
- 0,2 - 0,3
- 0,3 - 0,4
- 0,4 - 0,5
- 0,5 - 0,6
- 0,6 - 0,7
- 0,7 - 0,8
- 0,8 - 0,9
- > 0,9
- Landslides
- Alluvium
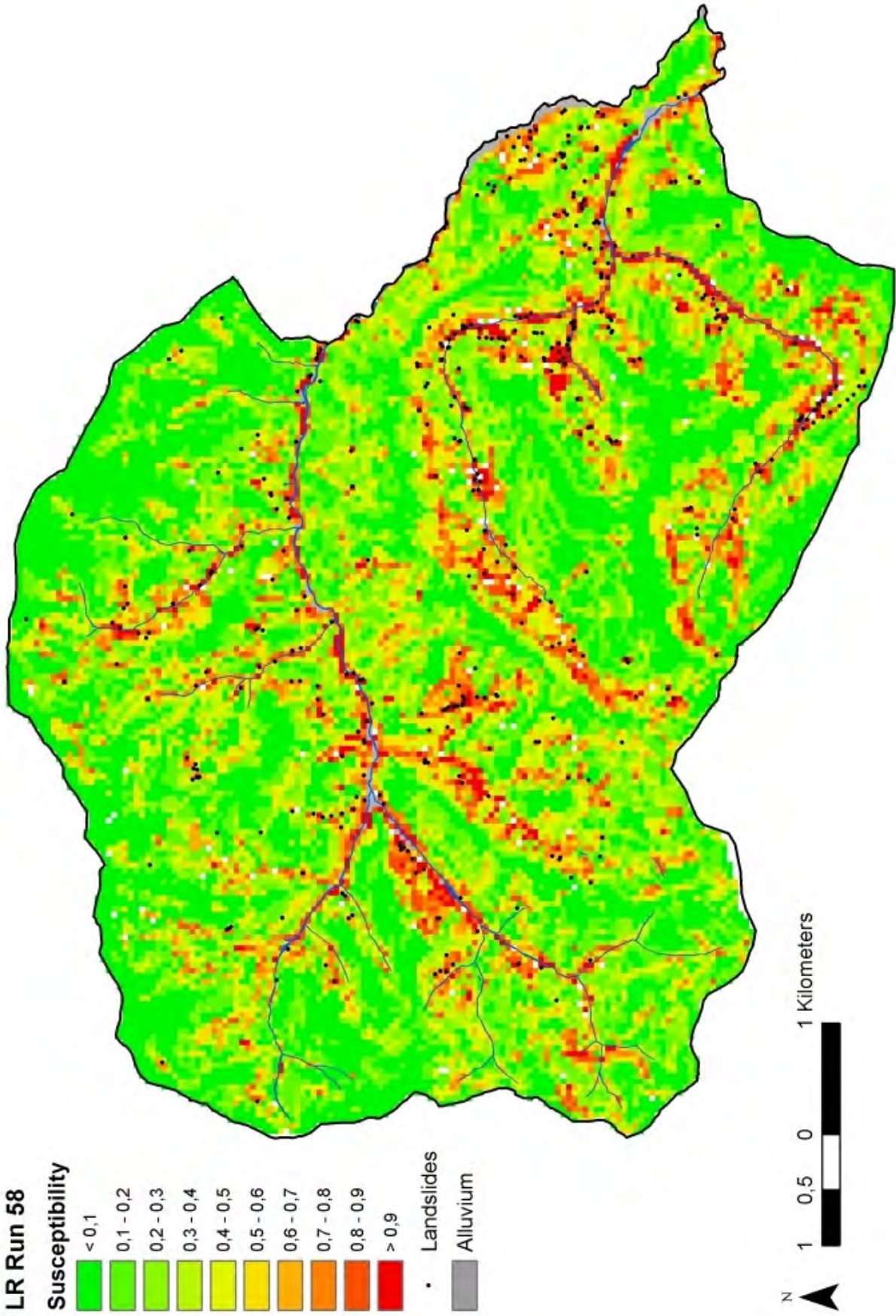
Fig. 7.4.2.2-2: Result of LR modelling run 58

Additionally some runs showing the best validation indices and involving *NS_lh* (run 58, 66 and 67) were recalculated with the scenario of uniform precipitation (arithmetic mean of the realistic precipitation as presented in *NS_lh*) to exclude influences caused by the specific precipitation pattern of the August 2005 event. These runs were named 58mc, 66mc and 67mc, the "mc" standing for "mean case".

The typical pattern of differences between run 58 and run 58mc is visualized in a difference map in Fig. 7.4.2.2-3. Positive deviances originating from lower susceptibilities in the "mc"-scenario mainly show up in the southeastern part of the test area where, according to *NS_lh* (cf. Chapter 5.5), precipitation was higher than average. Negative deviances can be registered in the western and northern part of the test area.
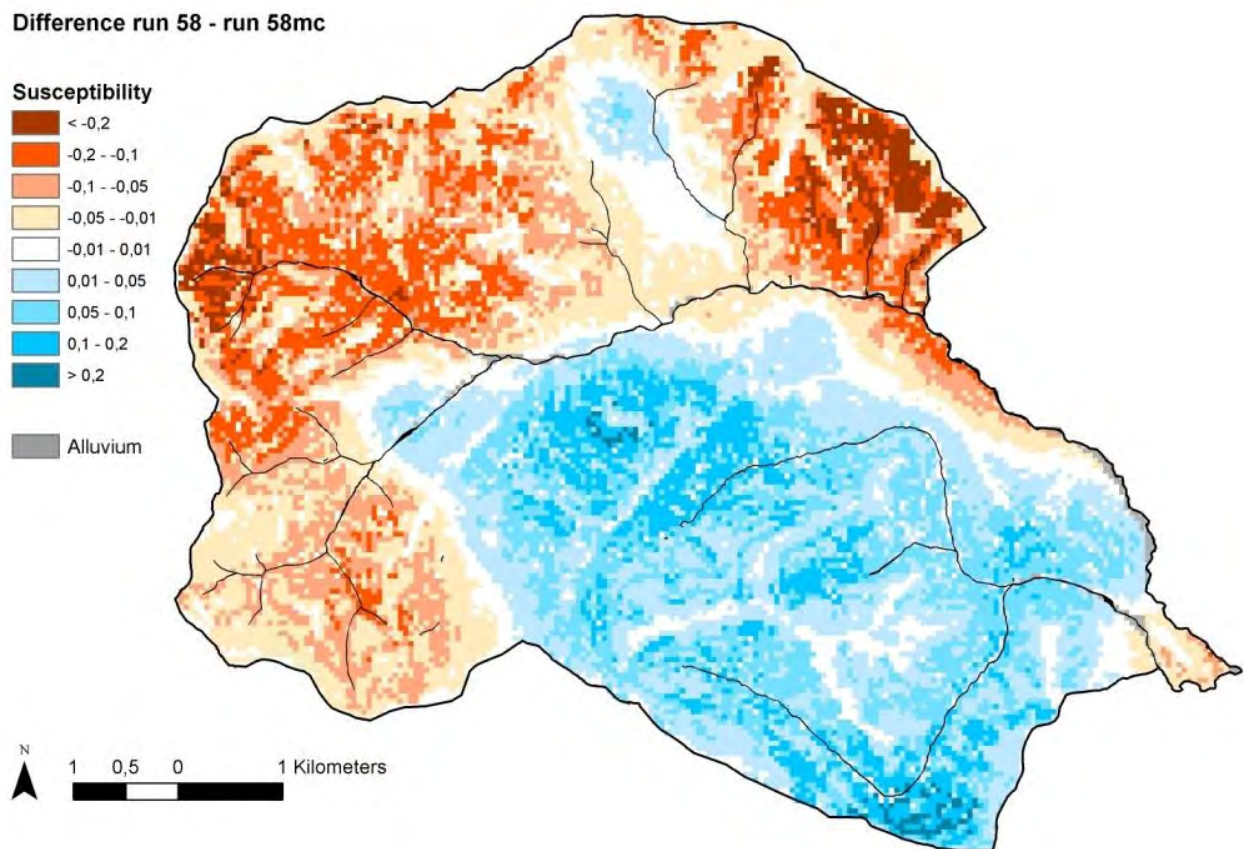
Fig. 7.4.2.2-3: Map of differences between LR run 58 and 58mc

The cumulated Chung & Fabbri - curves of runs 43a, 58mc, 63, 66mc and 67mc are presented in Fig. 7.4.2.2-4 and 7.4.2.2-5 showing the extraordinary strong grouping of the curves with regard to both datasets. Nevertheless it has to be stated that the "mc"-scenarios do not represent the specific environmental situation of the triggering event which means that the validation of these runs is adulterated to some extent.
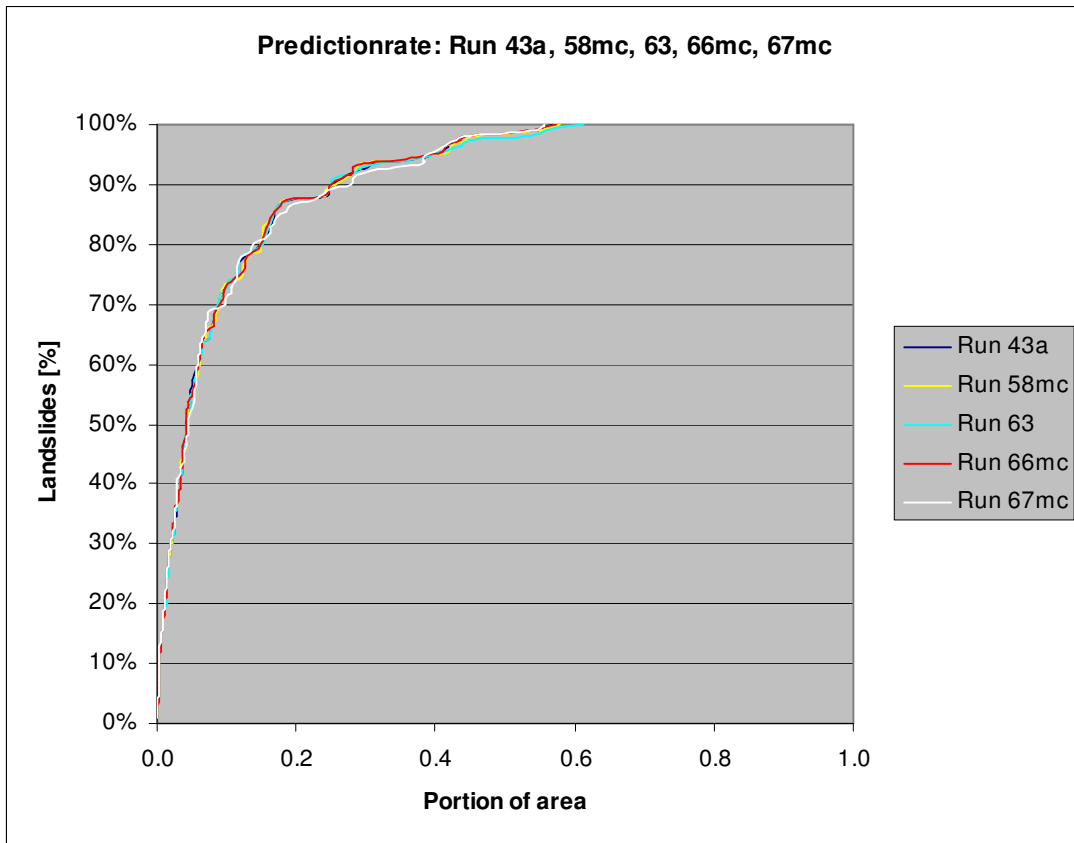
Fig. 7.4.2.2-4: Cumulated Chung & Fabbri curves of runs 1 to 13 (predictionrate)
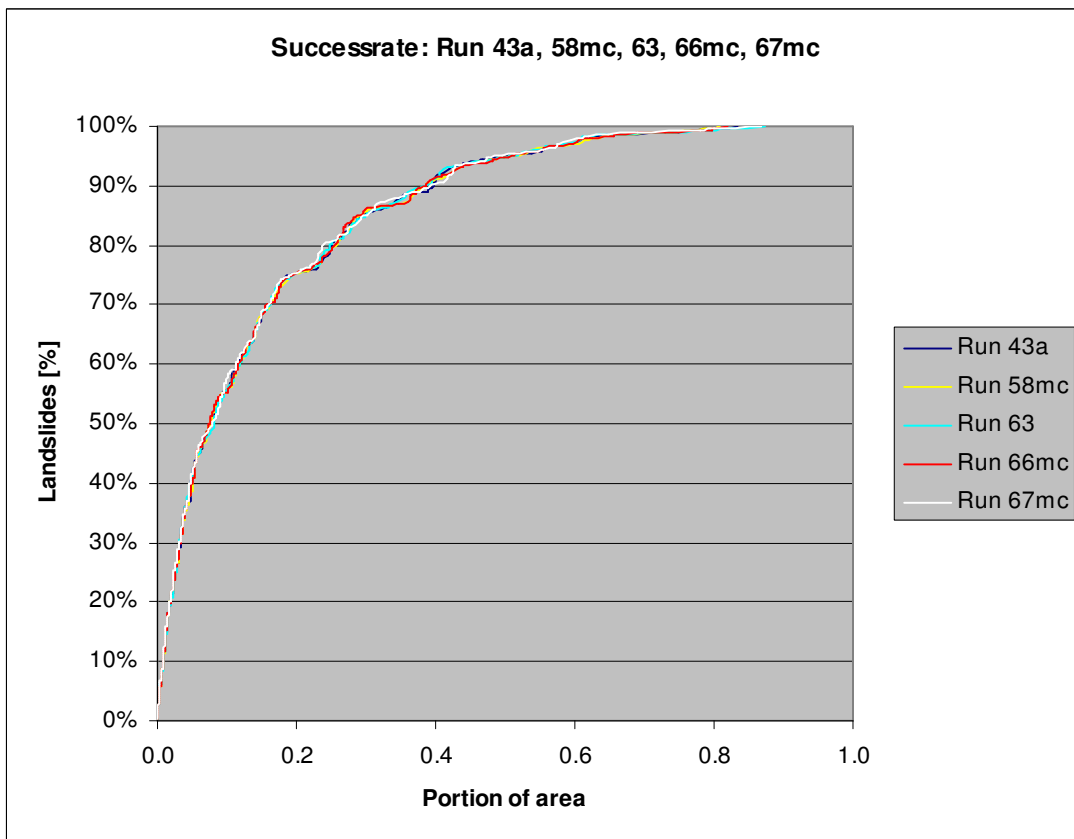
Fig. 7.4.2.2-5: Cumulated Chung & Fabbri curves of runs 1 to 13 (successrate)

7.4.2.3. Modelling Results using Process Oriented Combination of Parameter Maps

Besides the systematic modelling following the general approach as described in Chapter 6.2 and the validation results some runs were calculated under specific consideration of expert knowledge of the Geological Survey. Whereas run 26 only involves "level low" parameter maps, runs 27 and 28 as well as runs 69 and 70 consider at least one "level high" parameter map.

Following the validation indices the results of these modelling runs do not show any significant differences compared to the systematic modelling. However, it has to be noticed that the number of adequate modelling runs based on expert knowledge has been too low to confirm this conclusion definitely.

7.4.2.4. Comparison of Results of different Processing Levels

As is shown in Chapter 11 and in the Annex (Tab. A5) the single replacement of one "level low" parameter map by the adequate "level high" parameter map in most cases does not result in a significant improvement of the validation indices (> 1 % AUC).

However, the cumulative estimation of the involvement of "level high" parameter maps by calculating the arithmetic means of the validation indices (only runs without regionalisation datasets were taken into account) shows a notable improvement of most "level high" validation indices compared to the "level low" results (Tab. 7.4.2.4-1). Although this result has to be interpreted with reservations because of the general modelling approach (e.g. identification of best parameter combination and further calculation based on this selection) the conclusion can be drawn that by combination of several "level high" parameter maps tentatively better results can be achieved.

Tab. 7.4.2.4-1: Arithmetic means of validation indices of "level low" and "level high" modelling runs

	Probability	ROC (AUC)	Chung/Fabbri (AUC)
level low (n = 28)			
Successrate	77,57 %	85,53 %	85,10 %
Predictionrate	85,94 %	90,10 %	89,98 %
level high (n = 19)			
Successrate	77,83 %	86,68 %	86,21 %
Predictionrate	87,99 %	91,66 %	91,41 %

Aiming at getting an impression of the local differences between the "level low" and the "level high" modelling runs the five best results of the "level low" modelling stage were selected according to the joint assessment of the validation indices of both the WoE and the LR modelling method. The selected modelling runs are 5, 6, 14a, 23mc and 24. To create a common susceptility map of these five runs the mid-range value was calculated. The same procedure was followed using the "level high" results of runs 43a, 58mc, 63, 66mc and 67mc.

The differences between the two resulting maps were calculated and are presented in Fig. 7.4.2.4-1. Generally differences – positive as well as negative – are significantly lower than in the WoE approach (cf. Fig. 7.3.2.2-7) This is also due to the fact that instead of the real precipitation pattern the "mean case" scenarios were used for the results of runs 23, 58, 66 and 67. The remaining differences can mainly be ascribed to the different involvement of the geology-related parameter maps: in the five best results of the "level low" modelling stage three runs involve *Sub_GK_lg* whereas in the five best results of the "level high" modelling stage *Sub_GK_lh* is involved in most cases and *BK* is involved in two runs.
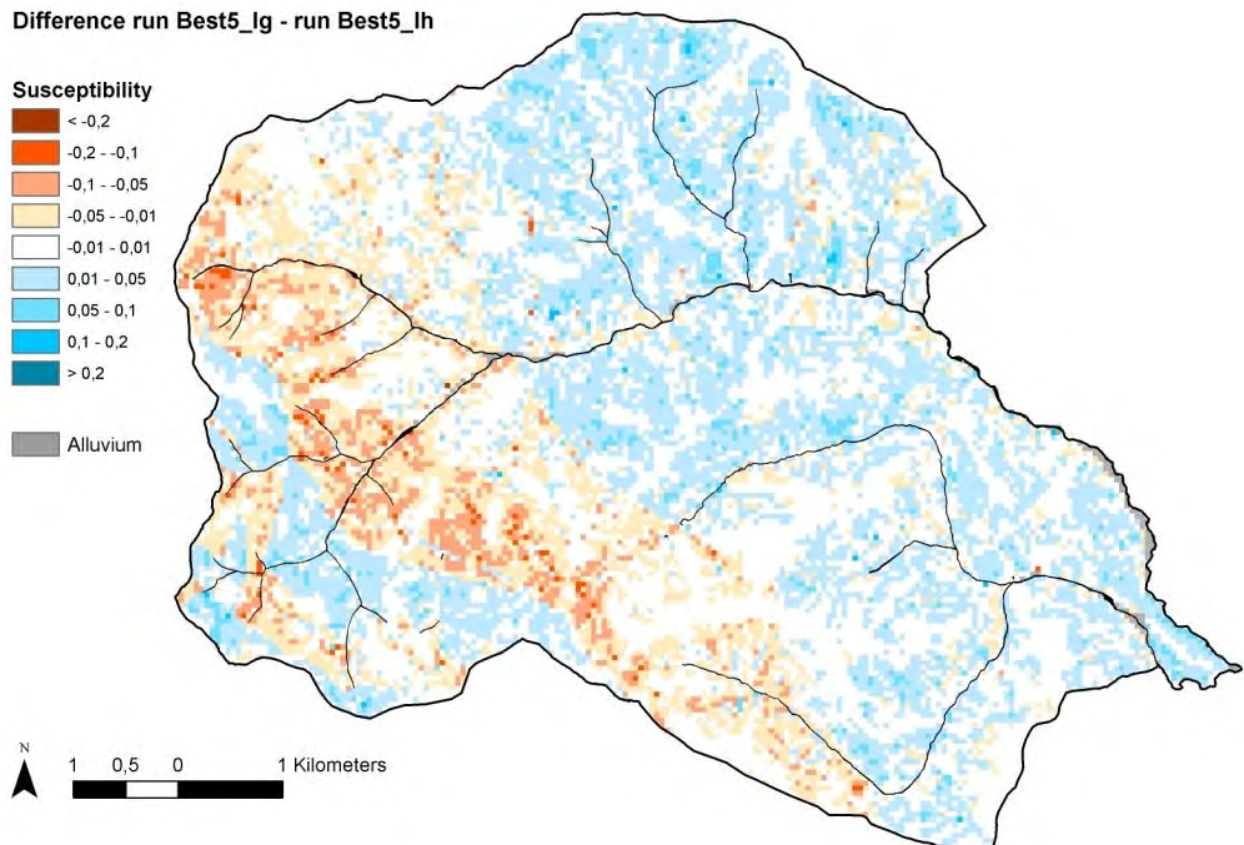
Fig. 7.4.2.4-1: Map of differences between LR best five maps of "level low" modelling stage and LR best five maps of "level high" modelling stage

7.5.   Modelling and Validation of Landslide Susceptibility Maps by means of Deterministic Modelling by SINMAP (JR)

Physically based models are useful in that they allow for relatively fine scale hazard mapping (Pack et al. 1998, Pack et al. 2005) and tend to be less site specific than multivariate statistical analyses (Montgomery and Dietrich, 1994). Information on geotechnical parameters is necessary in order to use this approach. Given the complexity of geotechnical conditions in slopes, deterministic methods are unreliable unless calibrated by correlating with a landslide inventory (Fell et al. 2008).

Despite problems related to the collection of sufficient input data, physically based models are increasingly used in hazard analysis even over large areas (e.g. Lan et al. 2003, Fowze et al. 2007, Kuthari 2007, Thiebes et al. 2007, Sulaiman & Rosli 2010). They are applicable only when the landslide types are restricted to shallow translational ones. The advantage of these "white box models" is that they have a physical basis. The information about the stability of a slope is expressed in terms of its factor of safety. However, these safety factors should never be used as absolute values - they are only indicative and can be used to test different scenarios (Pack et al. 2005). The calculated safety factor may as well be established in a GIS and the results referred to susceptibility.

In this work the SINMAP 2.0 (Stability Index MAPping) software created by Pack et al. (2005) was used for deterministic modelling. SINMAP 2.0 is an ArcGIS 9.0 plug-in that implements the computation and mapping of a slope stability index based upon geographic information, primarily digital elevation data. SINMAP is grid based, requiring ArcGIS version 9.0 or higher.

The use of the SINMAP approach is supported by the following arguments (Arpa Piemonte 2005):

- it is consolidated and universally accepted;

- it is easy to implement and requires knowledge of only a small number of parameters;

- it provides results which are acceptable in relation to the low costs involved and the data required;

- it provides results which are sufficiently valid for processes linked to long-lasting meteorological events.

7.5.1. Basic Principles

Montgomery and Dietrich (1994) first combined a contour-based steady-state hydrologic model with the infinite slope stability model, that balances the destabilizing components of gravity and the restoring components of friction and cohesion on a failure plane parallel to the ground surface with edge effects neglected, to define slope stability classes based upon slope and specific catchment area.

The SINMAP approach is similar to that of Montgomery and Dietrich in that it combines steady-state hydrologic concepts with the infinite slope stability model. It has its theoretical basis in the infinite plane slope stability model with wetness (pore pressures) obtained from a topographically based steady state model of hydrology. Digital elevation model (DEM) methods are used to obtain the necessary input information (slope and specific catchment area).

The SINMAP approach is based on the following hypotheses:

- infinite slope

- even surface of failure parallel to the slope and situated at the contact of the altered near-surface strata and the bedrock

- soil strength criteria (Mohr-Coulomb) expressed in terms of effective stresses

- steady-state flow parallel to the slope

- no significant deep drainage and no significant flow in the bedrock

SINMAP derives its terrain stability classification from inputs of topographic slope and specific catchment area and from parameters quantifying material properties and climate (primarily a hydrologic wetness parameter).

Following Hammond et al. (1992) the infinite slope stability model factor of safety (ratio of stabilizing to destabilizing forces) is given by (simplified for wet and dry density the same)

$$FS = \frac{C_r + C_s + \cos^2\theta[\rho_s g(D - D_w) + (\rho_s g - \rho_w g)D_w]\tan\phi}{D\rho_s g\sin\theta\cos\theta} \tag{1}$$

C_r	root cohesion
C_s	soil cohesion
θ	slope angle
ρ_s	saturated bulk density of the soil
ρ_w	density of water
g	acceleration due to gravity
D	vertical soil depth
D_w	vertical height of the water table within the soil layer
ϕ	internal friction angle of the soil

The SINMAP approach with the hydrologic model is to interpret the soil thickness as specified perpendicular to the slope, rather than soil depth measured vertically.

With this change FS reduces to:

$$FS = \frac{C + \cos\theta[1 - wr]\tan\phi}{\sin\theta} \tag{2}$$

where $w = D_w/D = h_w/h$ is the relative wetness

$C = (C_r + C_s) / (h \rho_s g)$ is the combined cohesion made dimensionless relative to the perpendicular soil thickness

$r = \rho_w / \rho_s$ is the water to soil density ratio.

Cohesion (due to soil and root properties) is combined with the soil density and thickness into a dimensionless cohesion factor, C (the relative contribution to slope stability of the cohesive forces). With the form of equation (2) it is assumed that the soil thickness (perpendicular to the slope) is constant.

Pore water pressure is computed assuming a hydrologic steady state with depth of saturated soil computed sufficient to sustain a lateral discharge proportional to the specific catchment area (the upslope area per unit contour length). The parameter "specific catchment area" is tied closely to recent hydrologic models that represent runoff generation by saturation (e.g. TOPMODEL, Beven and Kirkby 1979).

Detailed mathematical derivations of the theory are provided by Pack et al. (2005).

7.5.2. Parameterisation and Calibration

The data required to implement the theory include properties that can be highly variable in both space and time. These parameters are allowed to be uncertain following uniform probability distributions between specified lower and upper limits which may be adjusted (and calibrated) for geographic "calibration regions" based upon soil, vegetation or geological data.

Required parameters are:

- T/R (lower bound): lower bounding value for the ratio of soil transmissivity (hydraulic conductivity times soil thickness) to the effective steady state recharge rate [m].

- T/R (upper bound): upper bounding value for the ratio of transmissivity to the effective recharge rate [m].

- Dimensionless Cohesion C (lower bound): lower bounding value for both root and soil cohesion.

- Dimensionless Cohesion C (upper bound): upper bounding value for both root and soil cohesion.

- Phi [°] (lower bound): lower bounding value of the soil friction angle.

- Phi [°] (upper bound): upper bounding value of the soil friction angle.

- Soil Density [kg/m3].

The ratio T/R, which has units of [m], quantifies the soil's capacity for lateral drainage of water in relation to the relative wetness in terms of assumed steady state recharge. Although the term 'steady state' is used, the quantity R is not a long term (e.g. annual) average of recharge. Rather it is the effective recharge for a critical period of wet weather likely to trigger landslides. The ratio T/R, which is treated as a single parameter, therefore combines both climatic and hydrogeological factors.

C is a dimensionless combined root and soil cohesion factor in relation to the perpendicular soil thickness and density. This may be thought of as the ratio of the cohesive strength relative to the weight of the soil, or the relative contribution to slope stability of the cohesive forces (Dixon 2008).

The spatial database of the modelling was the DEM provided by the Austrian Federal Office for Metrology and Surveying (BEV) with a 10 m resolution. The SINMAP software automatically creates six grids from digital DEM data: pit-filled DEM, slope, flow direction, contributing area, saturation, and stability index. In addition to grid data, point data for landslides are required if the user wants to compare locations of predicted instability with areas of actual instability (Pack et al. 2005).

SINMAP also generates a slope-area chart ('S-A Plot') of study area data to aid in parameter calibration. The plot shows the relationship between contributing areas and groundslope and is generated by SINMAP routines (which do not work in ArcGIS 10). S-A Plots of the study area data are illustrated in Fig. 7.5.2-1 – 7.5.2-8. Four types of information are shown on the S-A Plot:

1. Normal cell data. Specific catchment area versus slope is plotted for a limited sampling of grid cell points across the study area that does not have landslides.

2. Landslide cell data. Landslides are plotted based upon the slope and specific catchment area values of the cell in which each landslide point lies.

3. Stability index region lines. These five lines provide boundaries for regions within slope-specific catchment area space that have similar potential for stability or instability.

4. Saturation region lines. These three lines provide boundaries for regions within slope-specific catchment area space that have similar wetness potential.
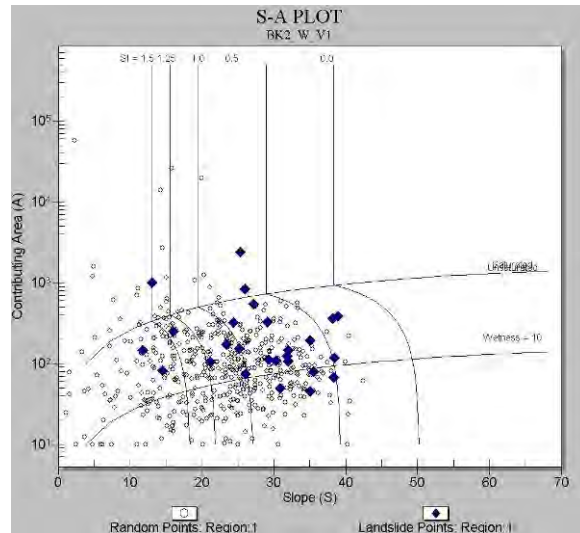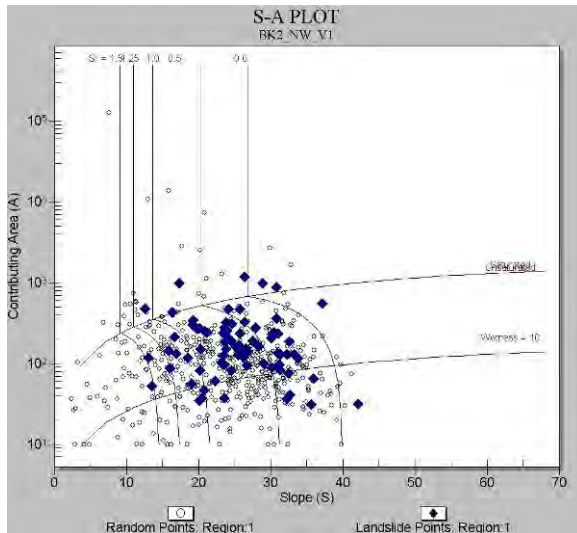
Fig. 7.5.2-1: S-A Plot of calibration region BK2 / non-forest with parameter settings of run V1

Fig. 7.5.2-2: S-A Plot of calibration region BK2 / forest with parameter settings of run V1
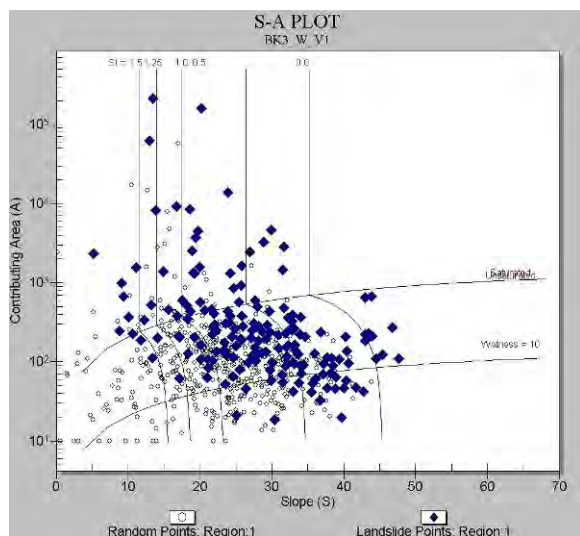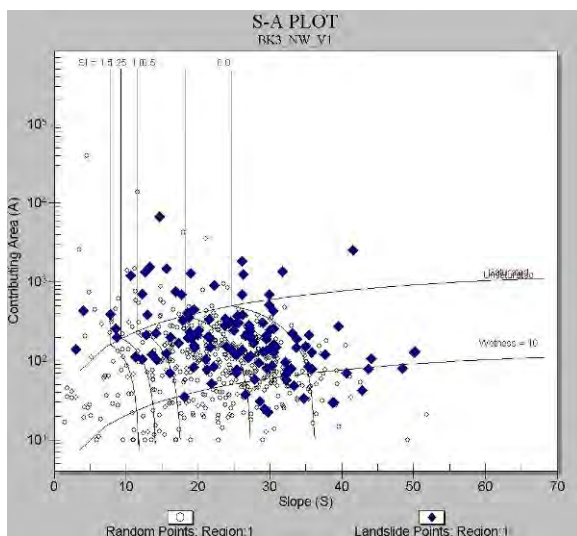
Fig. 7.5.2-3: S-A Plot of calibration region BK3 / non-forest with parameter settings of run V1

Fig. 7.5.2-4: S-A Plot of calibration region BK3 / forest with parameter settings of run V1
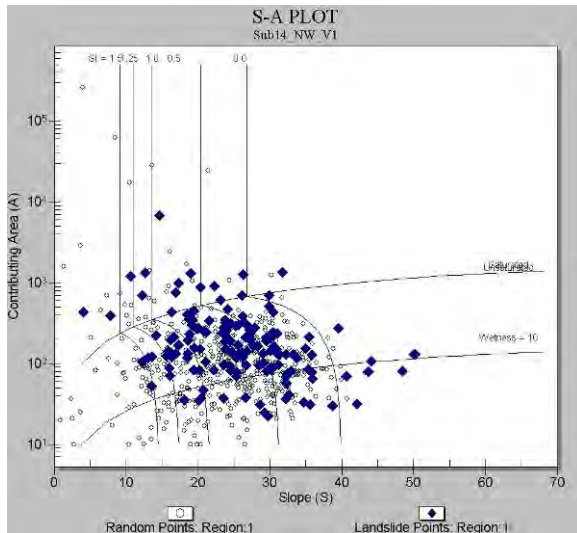
Fig. 7.5.2-5: S-A Plot of calibration region Sub14 / non-forest with parameter settings of run V1
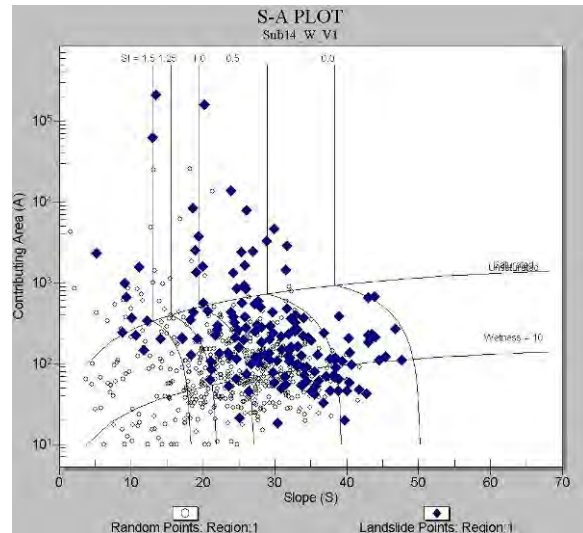
Fig. 7.5.2-6: S-A Plot of calibration region Sub14 / forest with parameter settings of run V1
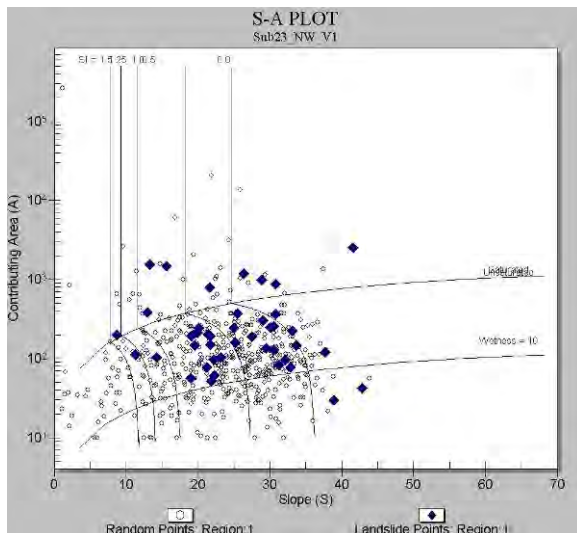
Fig. 7.5.2-7: S-A Plot of calibration region Sub23 / non-forest with parameter settings of run V1
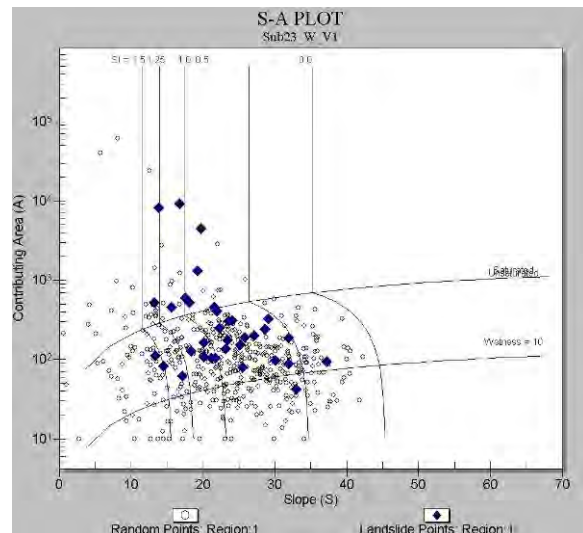
Fig. 7.5.2-8: S-A Plot of calibration region Sub23 / forest with parameter settings of run V1

The geometric points (blue rhombi) represent landslide locations. The single points represent a random selection of points within the calibration region. The slope and contributing areas are generated from the DEM. The vertically oriented curves are the breaks between stability index areas.

- Points to the left of the SI line of 1.5 are in the stable region.
- Points between 1.5 and 1.25 SI lines fall into the moderately stable region.
- Points between the 1.25 line and the 1.0 line fall in the quasi-stable region.
- Points between the 1.0 and the 0.5 line fall into the lower threshold region.
- Points between the 0.5 and the 0.0 line fall into the upper threshold region.
- Points to the right of the 0.0 line fall into the defended region.

The location of the 1.0 SI line is controlled by the lower bounds of the C and Phi parameters. The location of the 0.0 SI line is controlled by the upper bounds of the C and Phi parameters. The area between the 0.0 SI line and the 1.0 SI line represents the uncertainty associated with the parameter (Dixon 2003).

Horizontal lines represent the wetness which is controlled by the T/R calibration parameter. All points above the upper line are saturated.

The position of the upper line is controlled by the upper bounds of the T/R ratio. In this study the upper bounding of the T/R values was set equal to the lower bounding values thus defining saturated conditions, which implies that the water reached the soil surface at the time of slope failure. The lower line represents 10 percent wetness.

Calibrating the input parameters to the landslide points involves shifting the lines of the SA plot to fit the landslide occurrence by changing the upper and lower boundaries of the input parameters. A stability index of 1.0 may be interpreted as a factor of safety. Very few landslides should occur to the left of the 1.0 line since the factor of safety is >1.0. The calibration results thus in "capturing" a high proportion of observed landslides in regions with low stability index, while minimizing the extent of low stability regions and consequent attribution of terrain to regions where landslides have not been observed (Dixon 2003).

Model runs were based on two different versions with regard to the definition of geographic calibration regions.

1. The parameter map "Sub_GK_lg" (Geological basic disposition „level low" based on conceptual soil map "level low" (ref. to section 5.1.), 4 final classes after elimination of original class Sub100 – alluvial deposits, no landslides) was combined with the parameter map "Wald_Sat_lg" (Forest "level low" based on Satellite Data, 2 classes) resulting in 8 classes.

2. The parameter map "BK" (Basic disposition based on Soil Map (ref. to section 5.2.), 3 final classes after merging original classes 3 and 4) was combined with the parameter map "Wald_Sat_lg" (Forest "level low" based on Satellite Data, 2 classes) resulting in 6 classes.

Calibration of C and Φ was based on S/A plots. An overview of the parameters applied for the defined calibration regions is given in Tab. 7.5.2-1 and 7.5.2-2.

The hydrological parameters (T/R ratio) were set to saturated conditions, which implies that the water reached the soil surface at the time of failure. The T-values were estimated according the range of saturated conductivity suggested for the studied soil types dominated by fine-grained particles (sand, silt, clay, ref. to section 5.1 and 5.2) and a uniform value of 1 m as soil thickness. These assumptions result in T-values of 0,15 – 0,2 m²/24h. The recharge (R-value) of the modelling run V1 was set to the event precipitation value of August 21st 2005 (approx. 125 mm/24 h, ref. to section 5.5 and Andrecs et al. 2007). These assumptions result in a T/R-value of 1200 for the fine grained soil types (Sub23, Sub24; BK3) and 1500 for the less fine grained soil types (Sub13, Sub14; BK1, BK2).

Two additional different climatic scenarios were modelled by variation of the R values, V2 representing lower precipitation (67 % of the August 2005 event - approx. 85 mm/24 h), V3 showing a worst case scenario (150 % of the August 2005 event - approx. 185 mm/24 h).

With regard to landcover, scenarios were calculated by eliminating the influence of forested areas (stabilizing effects of root cohesion).

Tab. 7.5.2-1: Parameter definition for calibration region regarding parameter map "Sub_GK_lg" (for description of substratum units please refer to Chapter 5.1)

Calibration region	C low[1]	C high[2]	Phi low[1] [°]	Phi high[2] [°]	Soil Density [kg/m³]
Sub13_nf*	0,05	0,2	18	32	1950
Sub13_f**	0,2	0,4	16	30	1950
Sub14_nf	0,1	0,2	16	30	1950
Sub14_f	0,2	0,4	16	30	1950
Sub23_nf	0,1	0,2	12	26	1950
Sub23_f	0,2	0,2	12	24	1950
Sub24_nf	0,1	0,2	20	28	1950
Sub24_f	0,2	0,4	18	28	1950

[1] lower bound   [2] upper bound   * non-forested   ** forested

Tab. 7.5.2-2: Parameter definition for calibration region regarding parameter map "BK" (for description of soil units please refer to Chapter 5.2)

Calibration region	C low1	C high2	Phi low1 [°]	Phi high2 [°]	Soil Density [kg/m³]
BK1_nf*	0,05	0,2	18	32	1950
BK1_f**	0,2	0,4	16	30	1950
BK2_nf	0,1	0,2	16	30	1950
BK2_f	0,2	0,4	16	30	1950
BK3_nf	0,1	0,2	12	26	1950
BK3_f	0,2	0,2	12	24	1950

[1] lower bound   [2] upper bound   * non-forested   ** forested

7.5.3. Modelling Results

The most important output of the SINMAP software is the stability index (SI), the numerical value of which is used to classify the terrain stability at each grid location in the study area. Wetness Index (saturation) is also returned as a by-product of the stability index calculations. The stability index is defined as the probability that a location is stable assuming uniform distributions of the parameters over the uncertainty ranges defined by lower and upper bounds. This SI value ranges between 0 (most unstable) and 1 (least unstable). Where the most conservative (destabilizing) set of parameters in the model still results in stability, the stability index is defined as the factor of safety (ratio of stabilizing to destabilizing forces) at this location under the most conservative set of parameters. This yields a value greater than1.

Tab. 7.5.3-1 gives an example of how stability classes may be defined in terms of the stability index (SI).

Tab. 7.5.3-1: Definition of Stability Classes by Pack et al. (2005)

Condition	Class	Predicted State	Parameter Range	Possible Influence of Factors Not Modeled
SI > 1.5	1	Stable slope zone	Range cannot model instability	Significant destabilizing factors are required for instability
1.5 > SI > 1.25	2	Moderately stable zone	Range cannot model instability	Moderate destabilizing factors are required for instability
1.25 > SI > 1.0	3	Quasi-stable slope zone	Range cannot model instability	Minor destabilizing factors could lead to instability
1.0 > SI > 0.5	4	Lower threshold slope zone	Pessimistic half of range required for instability	Destabilizing factors are not required for instability
0.5 > SI > 0.0	5	Upper threshold slope zone	Optimistic half of range required for stability	Stabilizing factors may be responsible for stability
0.0 > SI	6	Defended slope zone	Range cannot model stability	Stabilizing factors are required for stability

The selection of breakpoints (1,5; 1,25; 1; 0,5; 0,0) is subjective, requiring judgement and interpretation in terms of the class definitions. In the example given by Pack et al. (2005) the terms 'stable', 'moderately stable', and 'quasi-stable' are used to classify regions that according to the model should not fail with the most conservative parameters in the parameter ranges specified. SI for these cases is the factor of safety that gives a measure of the magnitude of destabilizing factors (e.g. increased wetness due to road drainage, local loading, or local enhancement of pore pressures due to soil pipe effects) required for instability. The terms 'lower threshold' and 'upper threshold' are used to characterize regions where, according to the parameter uncertainty ranges quantified by the model, the probability of instability is less than or greater than 50 % respectively. External factors are not required to induce instability in these regions. Instability may arise simply due to a combination of parameter values within the bounds with which uncertainty and variability can be quantified. The term 'defended slope' is used to characterize regions where, according to the model, the slope should be unstable for any parameters within the parameter ranges specified. Where such slopes occur in the field they are held in place by forces not represented in the model, or the model is inappropriate, as in the case of bedrock outcrops. In the present study the selection of breakpoints and the definition of classes follows this example.

The results of the SINMAP modelling runs are shown in Fig. 7.5.3-1 to 7.5.3-12 for both approaches with regard to the definition of geographic calibration regions. The upper map represents the modelling result with the present forest cover, the lower map shows the scenario without stabilizing influence of root cohesion as defined by the C-values. From this comparison the high sensitivity with regard to the selected C-values becomes evident. From the comparison of the maps based on *"Sub_GK_lg"* (Fig. 7.5.3-1 to 7.5.3-6) with maps based on *"BK"* (Fig. 7.5.3-7 to 7.5.3-12) the high dependency on the selection of basics for the definition of calibration regions becomes apparent.

The maps present the landslides which were taken into account for the validation of the results as well. As the model is restricted to shallow translational movements only types 2 (landslide scar) and 3 (slope debris flow) were considered. To get a higher number of reference data, the 2nd category with regard to data quality was added to the original dataset thus integrating landslide sites triggered by events before and after August 2005 ("time-related test data with high quality") and sites characterized by incomplete assignment of attributes ("test data with high quality", ref. to section 5.1). A final number of 420 landslides thus were taken into account for the calibration and validation operations. The only reasonable validation method is by calculating the ratio of landslides situated in areas defined by stability indices < 1,0. The respective values are shown in Tab. 7.5.3-2.

Tab. 7.5.3-2: Results of SINMAP Validation

Run	No. of Landslides with SI < 1,0	Percentage of Landslides with SI < 1,0
Sub_Gk_V1	327	77,86 %
Sub_Gk_V2	318	75,71 %
Sub_Gk_V3	342	81,43 %
BK_V1	353	84,05 %
BK_V2	347	82,62 %
BK_V3	364	86,67 %

This superficial validation indicates that the use of the base map "*BK*" improves the results by about 5 to 7 % compared to the base map *"Sub_GK_lg"*.

Generally regions with high landslide densities are situated in areas classified as unstable in most cases. In addition some areas without any landslides are classified as unstable as well (e.g. in the western and in the north-eastern part of the test area). The most obvious reason for this misclassification may of course be the selection of the base maps defining the calibration regions. As described in sections 5.1 – 5.5 a number of additional base maps coming into consideration for this task was created within the frame of this project (*e.g. Wald_Sat_lh, QDisp_lh_fa_NS_lh, Sub_GK_lh, NS_lh)*. Due to limited resources the deterministic modelling building upon this basis could not be realised within the AdaptSlide project but has to be kept for further studies.
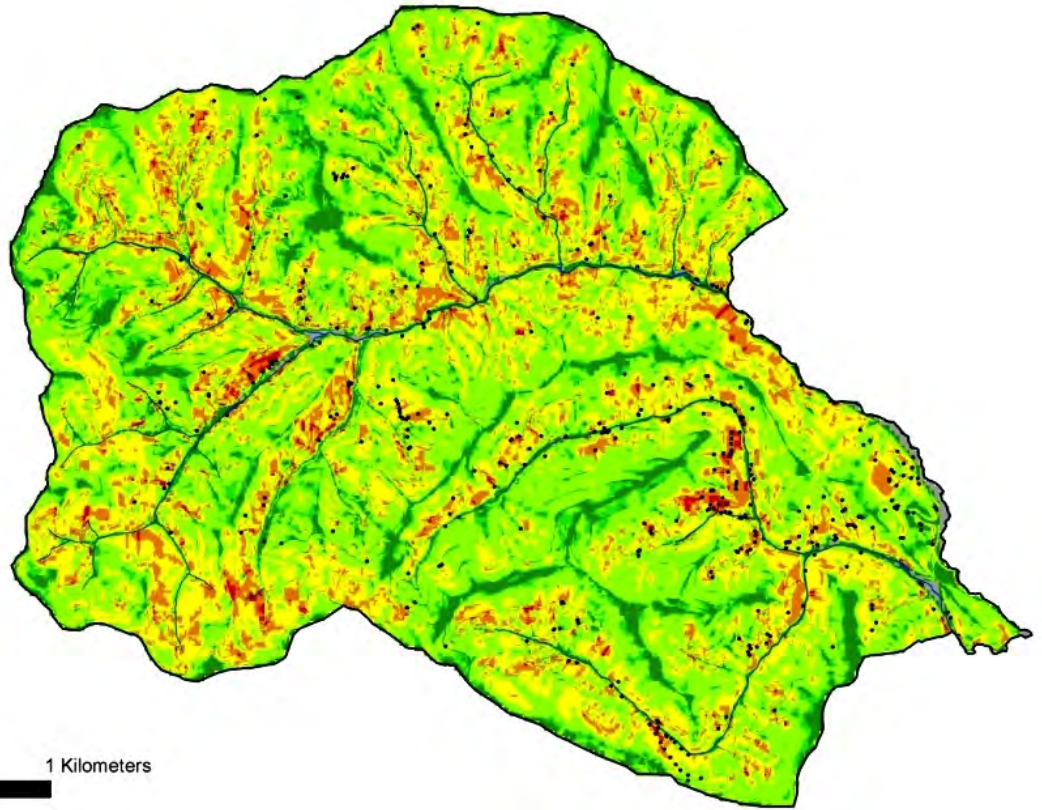
Fig. 7.5.3-1: Result of SINMAP Model run V1 (event August 2005) based on "Sub_GK_lg"
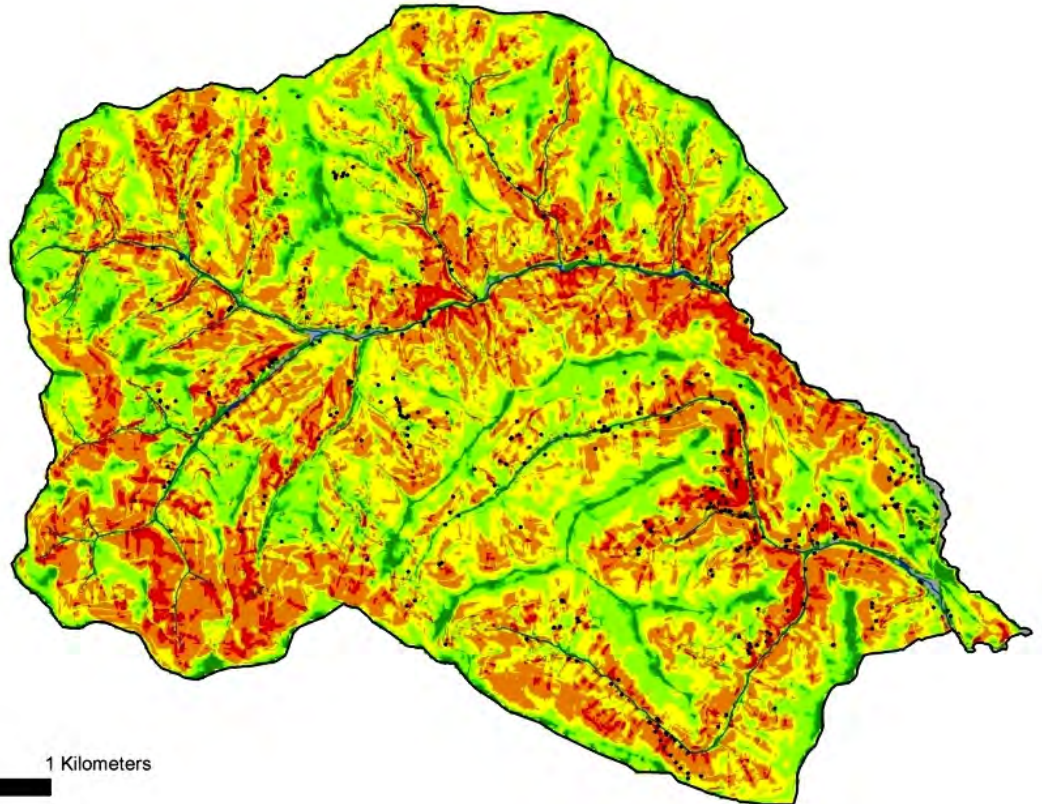
Fig. 7.5.3-2: Result of SINMAP Model run V1 (event August 2005) based on "Sub_GK_lg" without forest effect
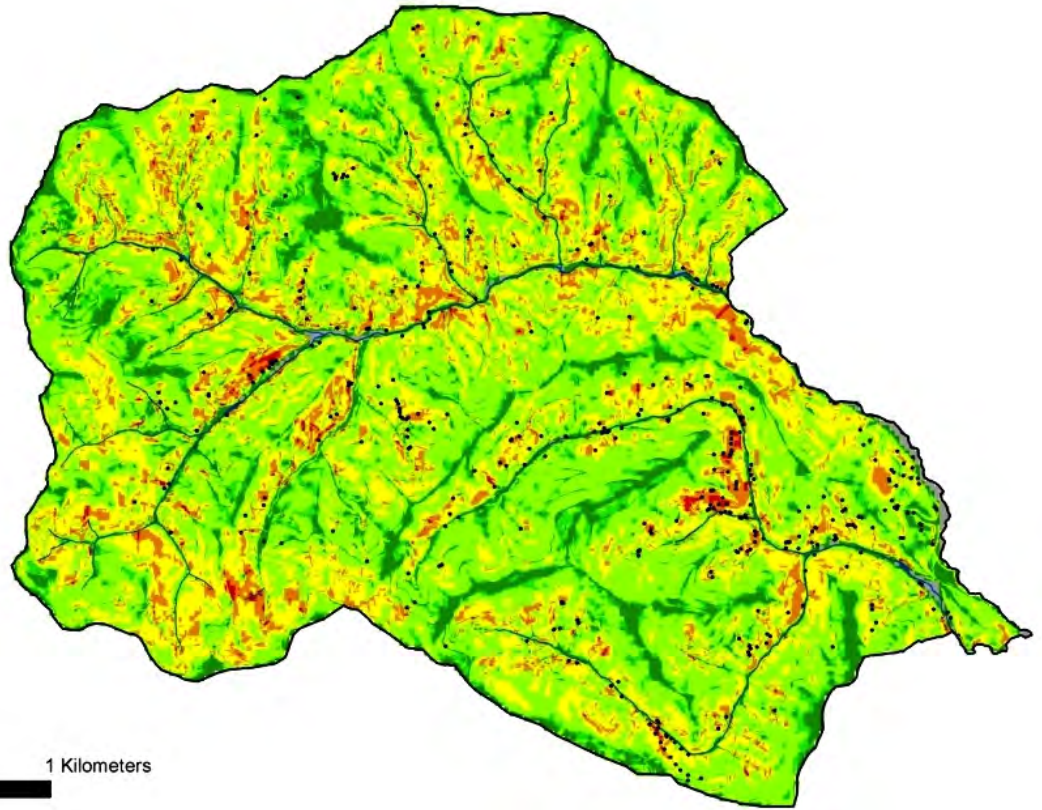
Fig. 7.5.3-3: Result of SINMAP Model run V2 (scenario low) based on "Sub_GK_lg"
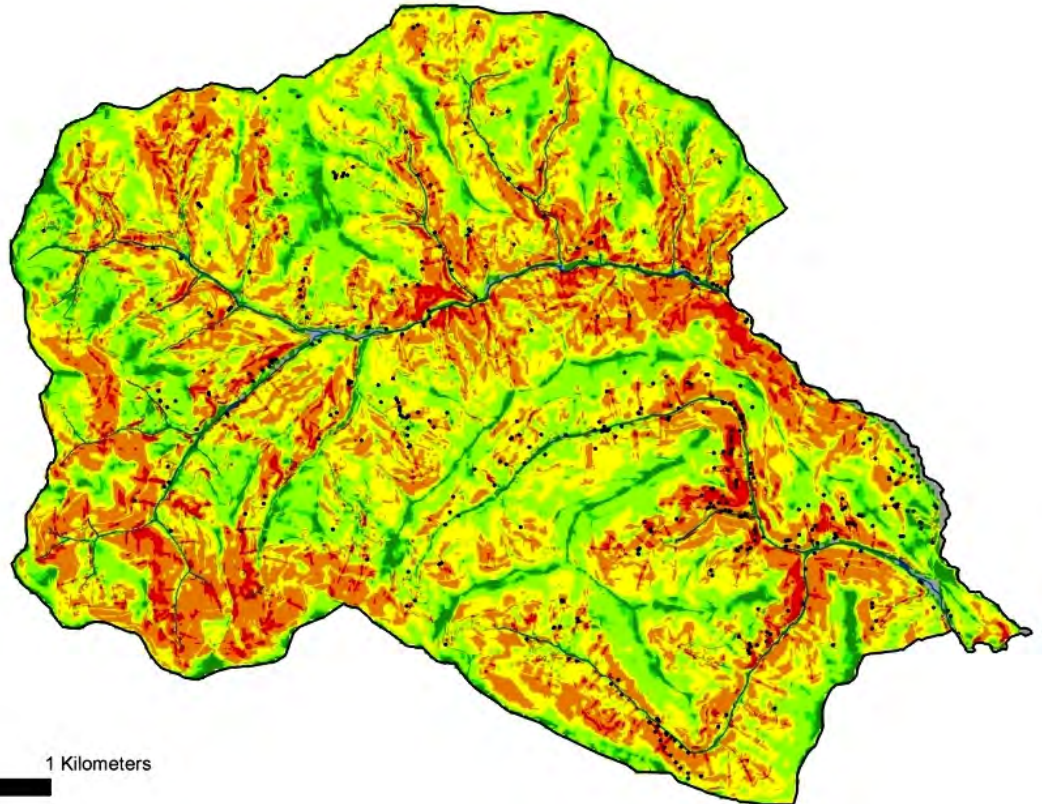
Fig. 7.5.3-4: Result of SINMAP Model run V2 (scenario low) based on "Sub_GK_lg" without forest effect
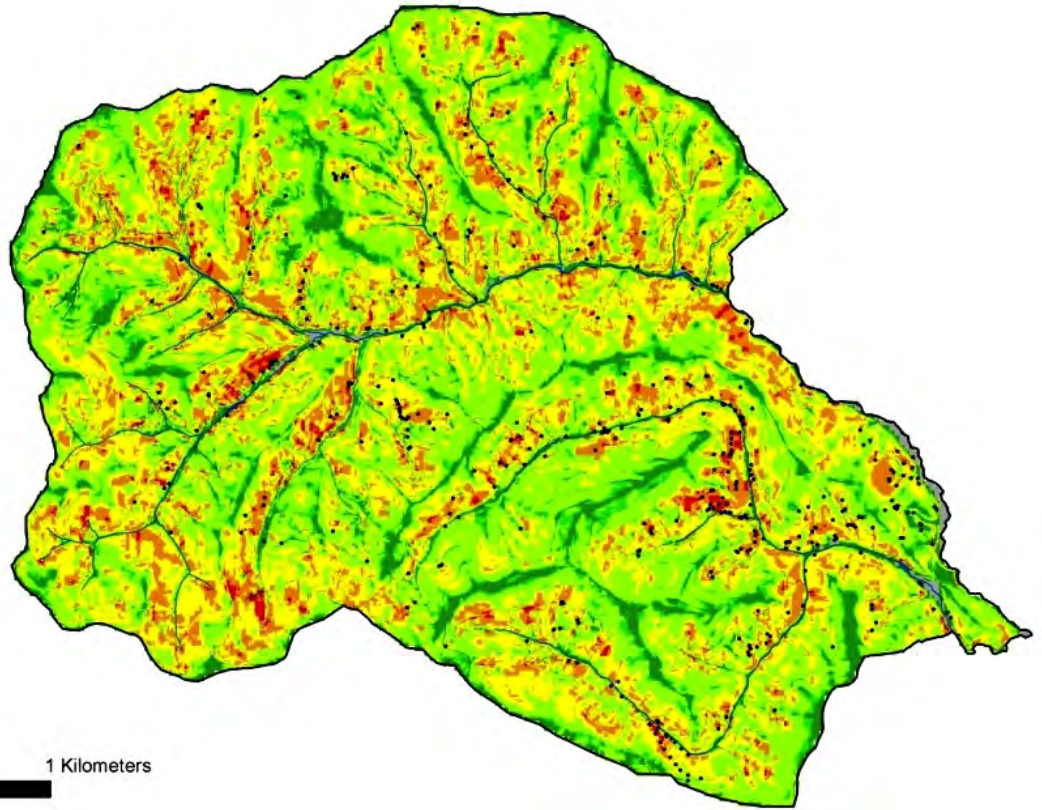
Fig. 7.5.3-5: Result of SINMAP Model run V3 (scenario high) based on "Sub_GK_lg"
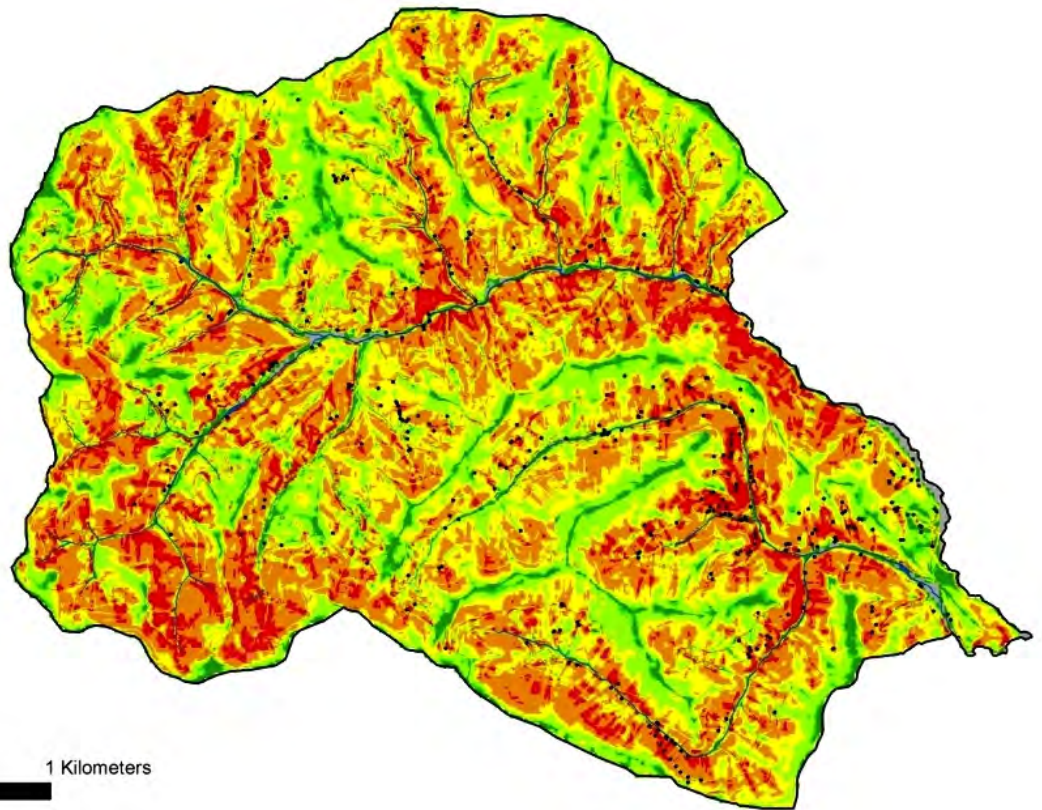
Fig. 7.5.3-6: Result of SINMAP Model run V3 (scenario high) based on "Sub_GK_lg" without forest effect
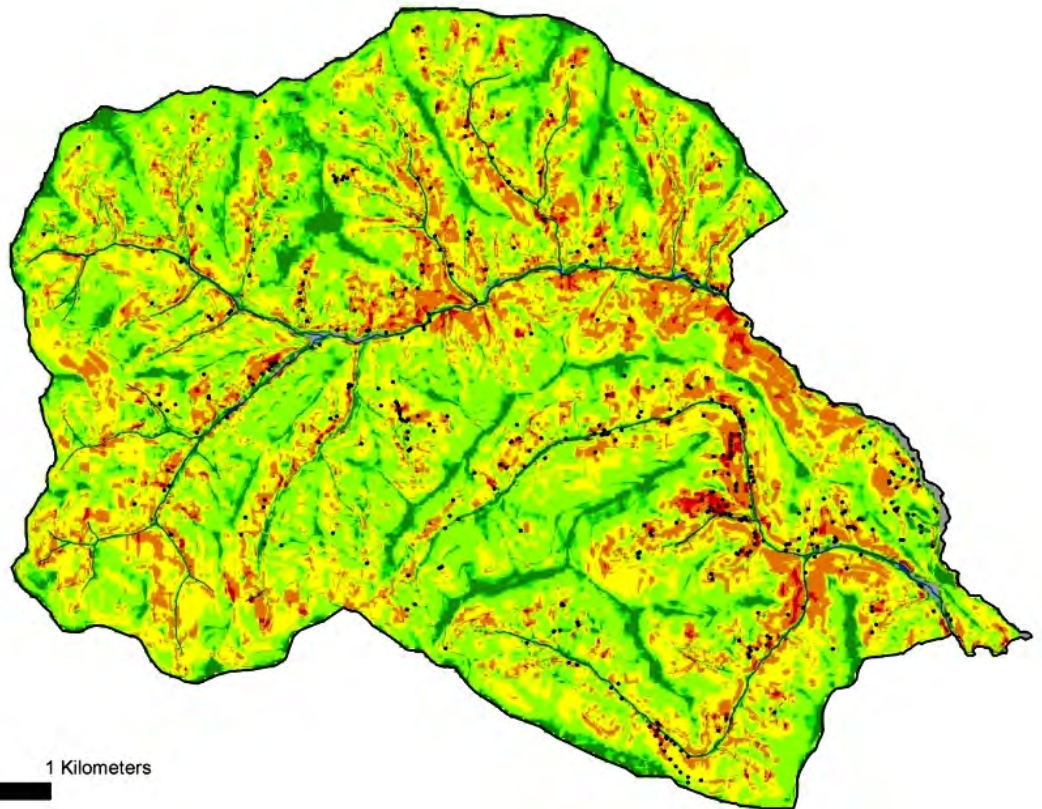
Fig. 7.5.3-7: Result of SINMAP Model run V1 (event August 2005) based on "BK"
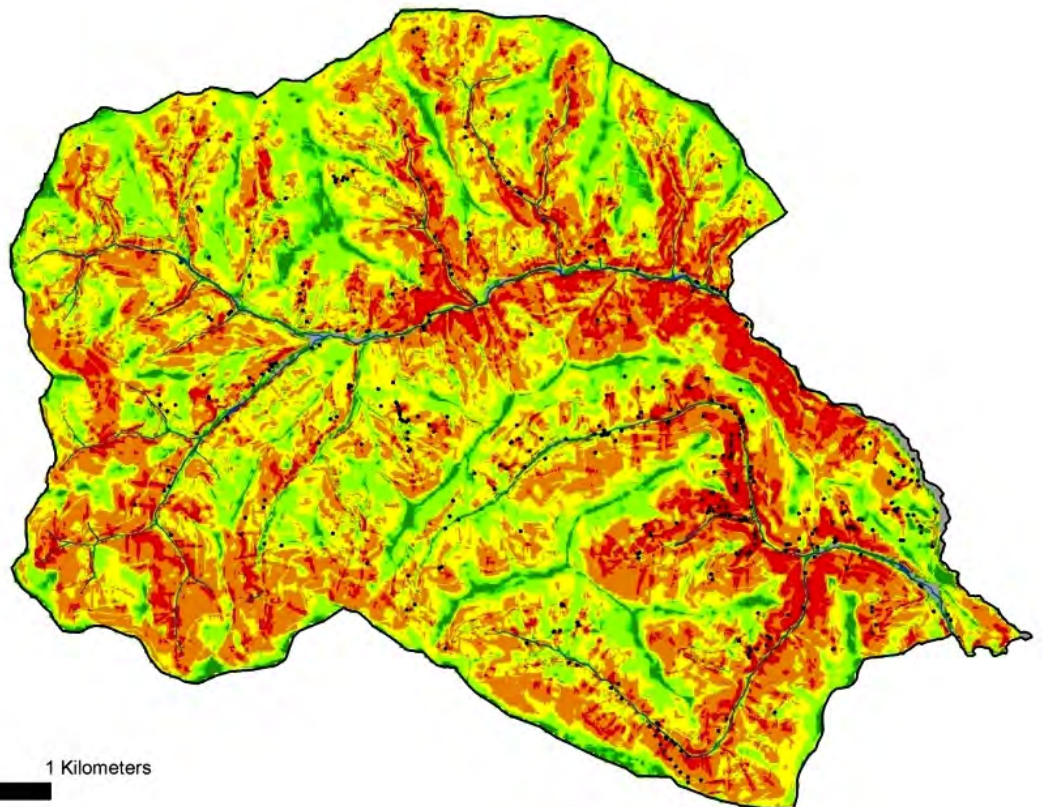
Fig. 7.5.3-8: Result of SINMAP Model run V1 (event August 2005) based on "BK" without forest effect
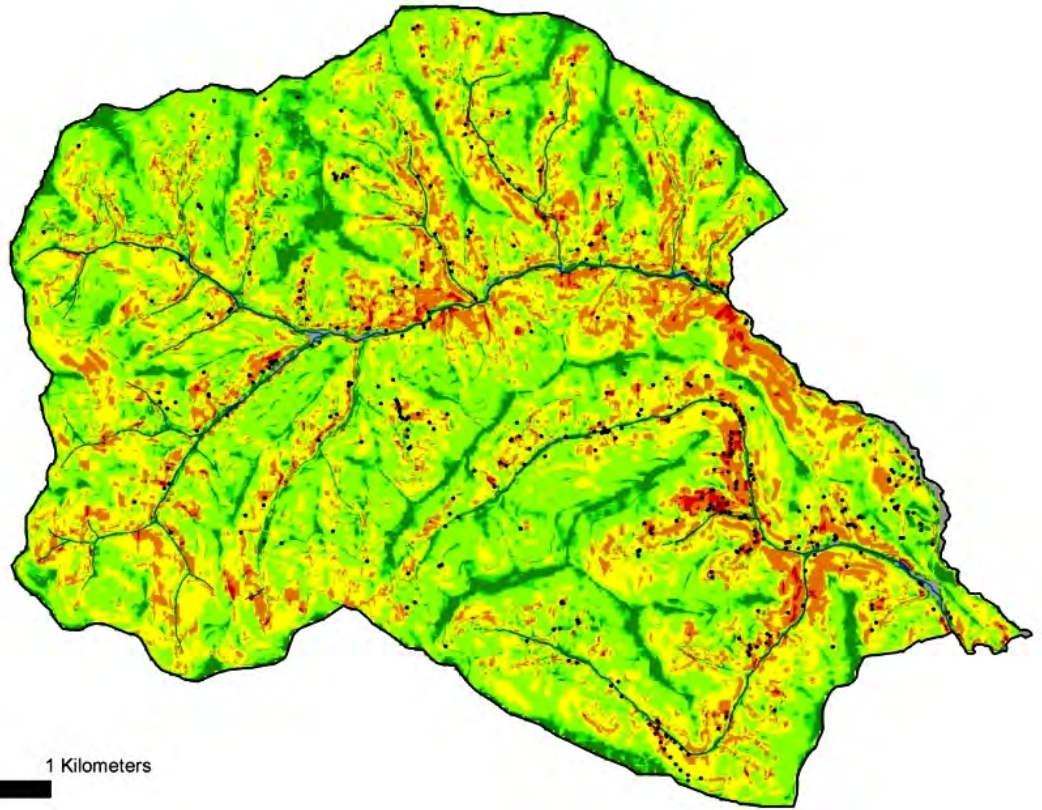
Fig. 7.5.3-9: Result of SINMAP Model run V2 (scenario low) based on "BK"
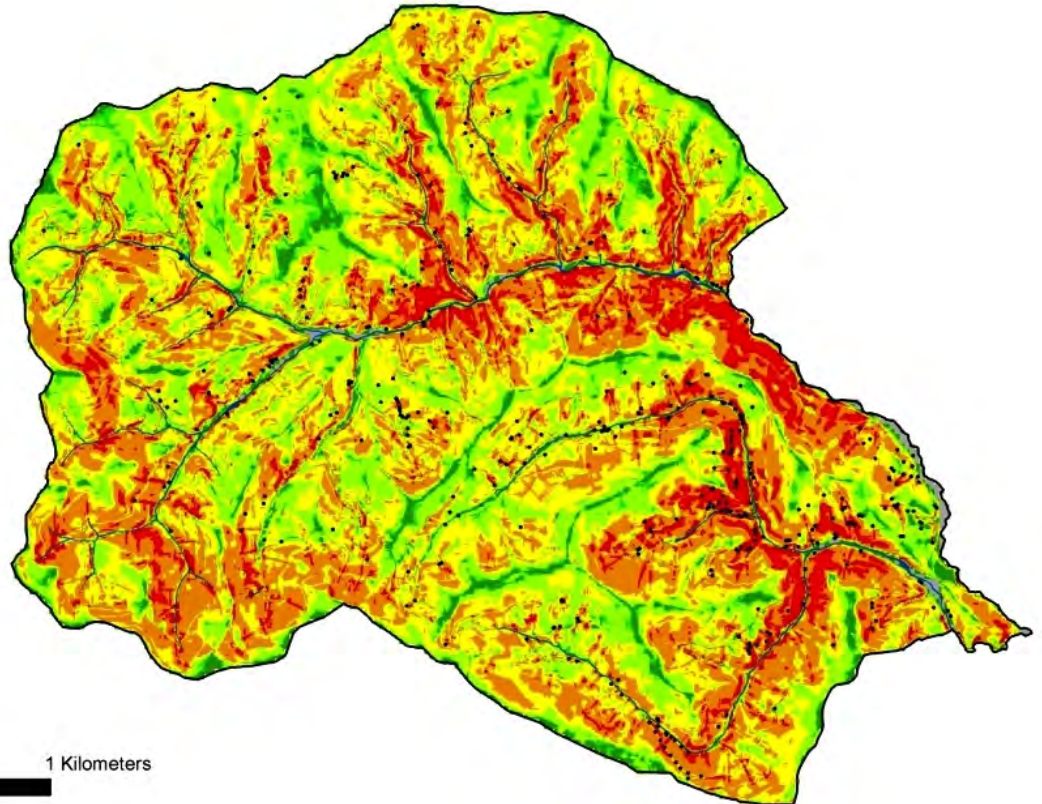
Fig. 7.5.3-10: Result of SINMAP Model run V2 (scenario low) based on "BK" without forest effect
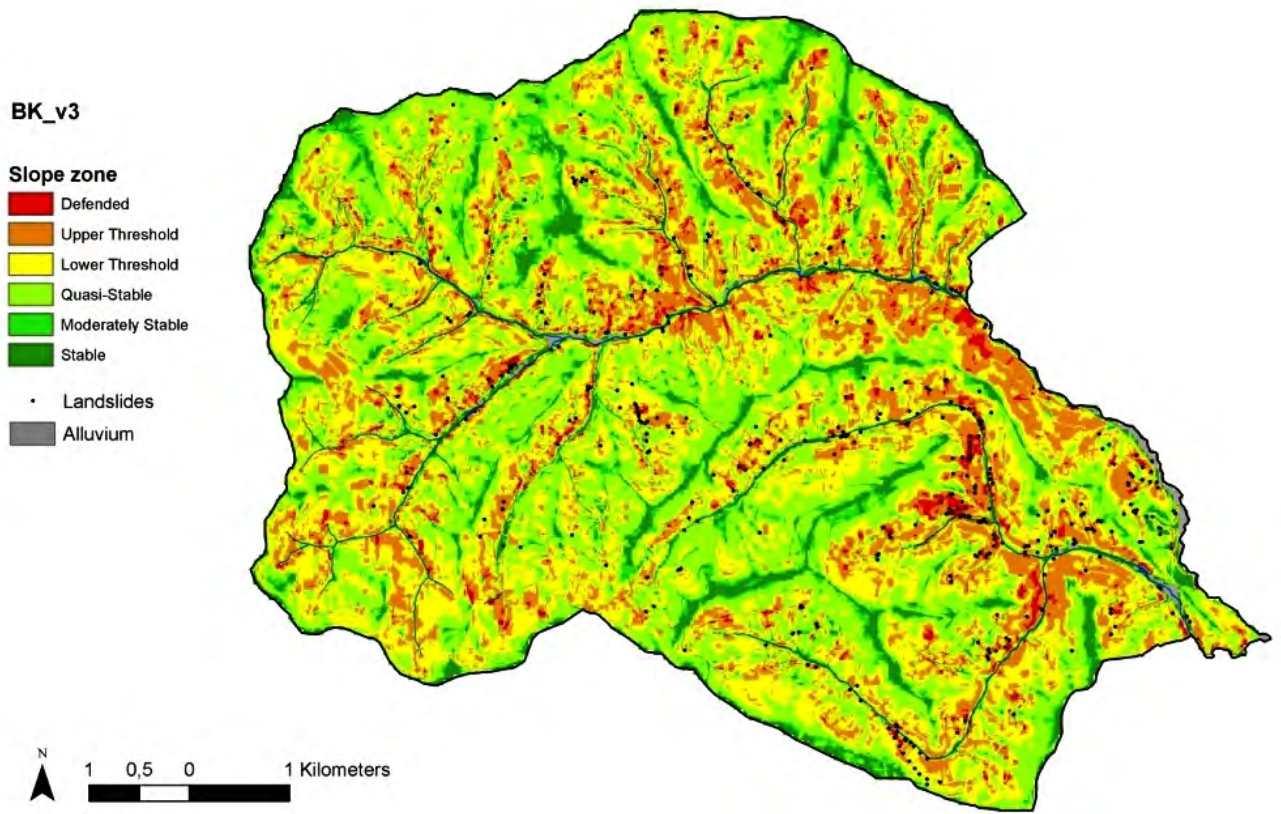
Fig. 7.5.3-11: Result of SINMAP Model run V3 (scenario high) based on "BK"
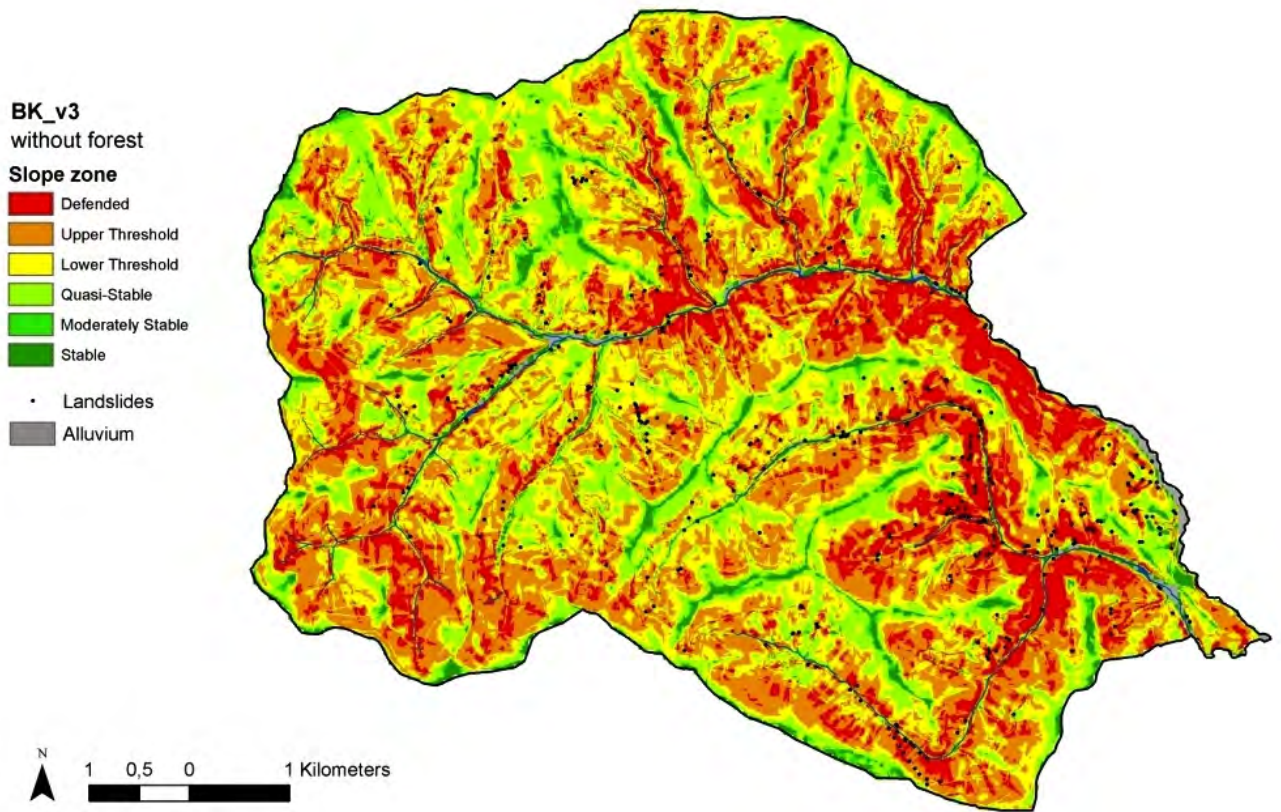
Fig. 7.5.3-12: Result of SINMAP Model run V3 (scenario high) based on "BK" without forest effect

8. Comparisons of Results of Neural Networks and Logistic Regression (GBA, JR)

The following discussion will contrast, and as far as possible compare the modelling results of the methods used in the AdaptSlide project, which were neural networks (Chapter 7.2) and logistic regression (Chapter 7.4). This comparison is made by means of the validation results that were obtained by taking into account the test data. Therefore direct comparison of statistic and deterministic modelling results is not possible as the only reasonable validation method of the SINMAP modelling approach is by calculating the ratio of landslides situated in areas defined by stability indices < 1,0 (Chapter 7.5.3.). This data was used for validation of logistic regression, but it was applied to a limited extent only in the validation of neural networks due to the validation scheme used there (Chapter 7.2). The standard validation methods ROC and validation according to Chung & Fabbri (1999, Chapter 7.1) were applied there. The weight-of-evidence method (Chapter 7.3) was excluded from this process, because direct comparison is impossible due to the different initial database (process data was purely pixel-based, environmental parameters were exclusively categorical).

Because of the strategy used for successive parameter map integration (Chapter 6.2), model runs with the same code numbers in many instances include different parameter combinations for the two methods used. For that reason, there was only comparison, on the one hand, of runs with the same parameter combinations, and on the other hand of the respective "best 5" results (Chapter 7.2. & 7.4) for "level low" and "level high" and the "best of all" results for the two methods. Hence, the latter are usually not based on results with the same parameter combinations. This fact, along with the observation stated several times before in this report that the summarized area-wide validation methods have their limitations, demonstrate the rather limited significance of the validation comparisons of the two modelling methods that will now be presented.

Lastly, those final-result maps that were produced on the basis of an independent parameter map 'precipitation' (for example run 23), were additionally evened out with mean precipitation for the entire study area in order to obtain generally valid susceptibility maps that are independent of events.

8.1. Modelling Results using the "Level Low" Parameter Maps

Comparison of the "level low" results

Neural networks and logistic regression generally produce quite similar susceptibility maps in the "level low" runs, although logistic regression differentiates somewhat more strongly between high and low susceptibilities. The validation comparisons showed that the results of logical regression and neural networks, based on the validation methods used, could be considered "equally good" to "slightly better in the case of neural networks." However, due to the limited significance of the comparisons (for example summarized area-wide validation), neither of the two models can be definitely favoured. The uncertainties in the final results obtained from the five best susceptibility maps are generally very minor for both models, and when compared, more or less equally minor.

The comparisons of the results obtained with neural networks and logistic regression using the same parameter combinations show that the susceptibility maps generated exhibit quite similar susceptibility distributions. As an example of the "level low" results, the susceptibility map for run 10, which was calculated using neural networks (Fig. 7.2.2.1-8), is now compared to the susceptibility map calculated from run 14a (Fig. 8.1-1) by means of logistical regression. Both runs were calculated with the same parameter combination. The similarity of the two maps with respect to the distribution of susceptibility classes is readily visible, and it can also be seen that logistic regression differentiates rather more strongly between high and low susceptibilities.

This is particularly obvious in Fig. 8.1-2, which shows the difference map for the two susceptibility maps. This map exhibits quite small differences in many areas, most values lying between -0.02 and +0.1. Negative differences (red), which show higher values for logistical regression, most often appear in areas of higher susceptibility (valley areas and lower slope areas), whereas positive differences (blue), i.e. higher values for neural networks, occur predominantly in areas of lower susceptibility. This in turn verifies the stronger differentiation by logistical regression. These statements apply to most comparisons of results obtained using the two methods within "level low" results.

Run 14

Susceptibility
- < 0,1
- 0,1 - 0,2
- 0,2 - 0,3
- 0,3 - 0,4
- 0,4 - 0,5
- 0,5 - 0,6
- 0,6 - 0,7
- 0,7 - 0,8
- 0,8 - 0,9
- > 0,9
- Landslides
- Alluvium
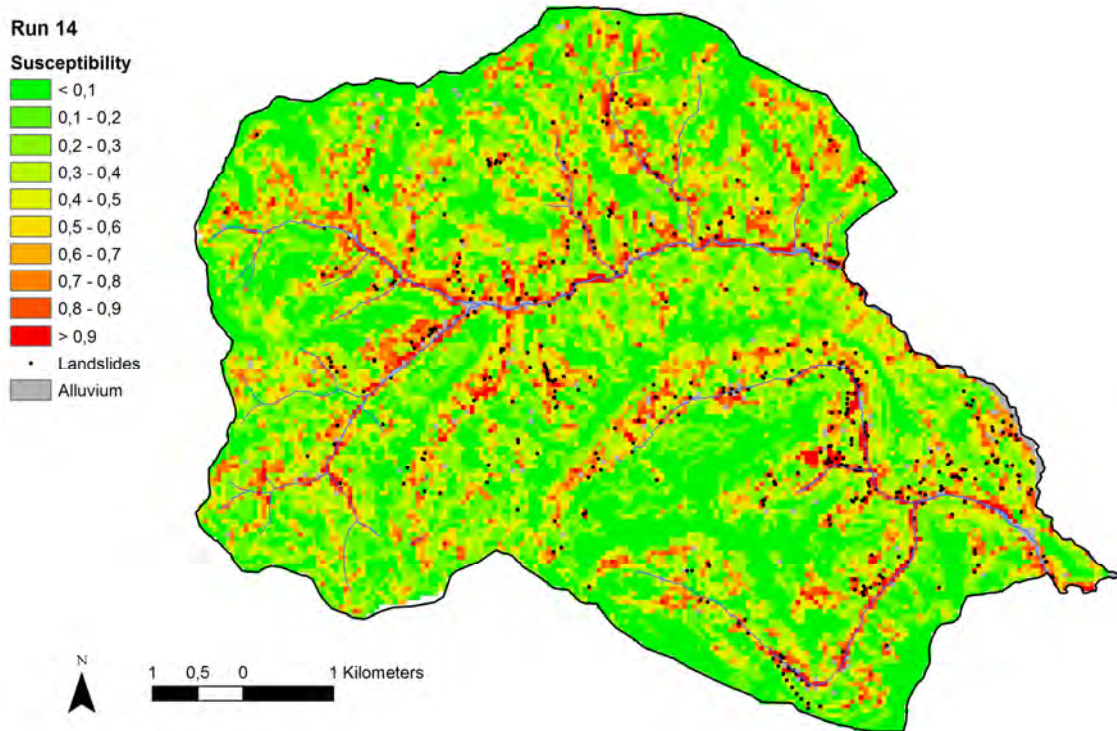
Fig. 8.1-1: Susceptibility map of run 14a (logistic regression)

Difference between run 10 (neural network) and run 14 (logistic regression)

Susceptibility
- < -0,2
- -0,2 - -0,1
- -0,1 - -0,05
- -0,05 - -0,01
- -0,01 - 0,01
- 0,01 - 0,05
- 0,05 - 0,1
- 0,1 - 0,2
- > 0,2
- Alluvium
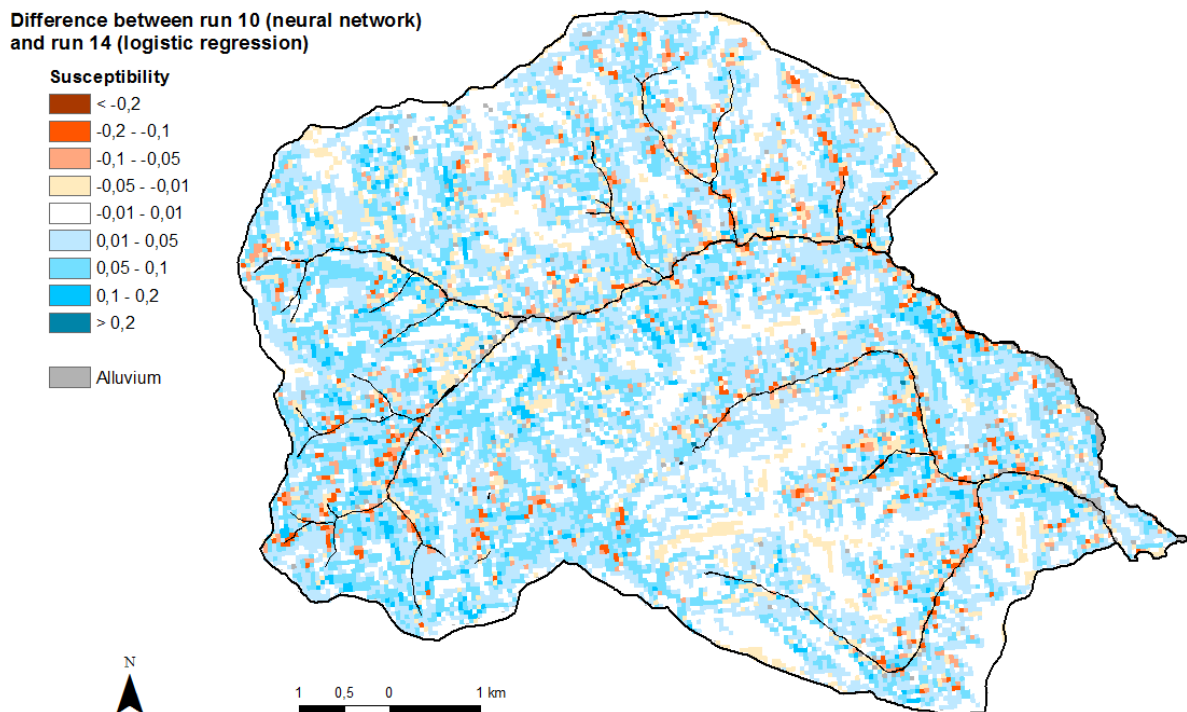
Fig. 8.1-2: Difference between map of neural network (run 10) – map of logistic regression (run 14a)

Tab. 8.1-1 shows the comparison of the validation measured values (AUC of ROC and Chung & Fabbri 1999) of the "level low" runs for both modelling methods, as well

as their differences. Therefore the results of all runs that had the same parameter combinations for both methods were used. The differences in the runs corresponding to the validation measured values are positive (black) when there is better model performance with neural networks, and negative (green) when there is better model performance with logistic regression.

Viewing these differences it is evident that they are usually positive, however quite small, so that model performance with logistic regression and neural networks can generally be described as good. In the interest of a better overview, the differences that exceed the threshold value for equally good model performance (Chapter 7.2.1) are printed in bold. When using the method-specific threshold values for the Chung & Fabbri method (1999), the results for both models can be described overall as "equally good," whereas when using the ROC method, the neural network results tend to be slightly better. That picture is also seen when considering the mean differences for all of these results (Tab. 8.3-1): at +0.65% with the ROC method, it is in the region of the threshold value, which indicates slightly better model performance with neural networks, whereas at +0.44% with the method according to Chung & Fabbri (1999), it is below the threshold value, which indicates equally good model performance for both methods.

Tab. 8.1-1: Validation measured values (AUC) of the test data for "level low" runs with the same parameter combination of logistical regression and neural networks, as well as their differences

Run	Logistic Regression		Neural Network		Difference NN-Log Reg	
	ROC	Chung & Fabbri	ROC	Chung & Fabbri	ROC	Chung & Fabbri
1	88.60%	88.63%	89.03%	88.70%	0.43%	0.08%
2	88.70%	88.75%	89.11%	89.05%	0.41%	0.30%
3	91.40%	91.25%	91.77%	91.59%	0.37%	0.34%
4	91.10%	90.84%	91.65%	91.23%	0.55%	0.39%
5	90.80%	90.61%	91.64%	91.26%	**0.84%**	0.65%
6	90.70%	90.55%	91.52%	91.17%	**0.82%**	0.62%
10 LR, 14a NN	90.70%	90.57%	91.67%	91.36%	**0.97%**	0.79%
11	88.80%	88.83%	89.49%	89.04%	**0.69%**	0.21%
14a LR, 10 NN	90.80%	90.62%	91.68%	91.34%	**0.88%**	0.72%
15	91.50%	91.31%	92.13%	91.77%	0.63%	0.46%
21	90.80%	90.61%	91.62%	91.24%	**0.82%**	0.63%
22	90.70%	90.56%	91.75%	91.42%	**1.05%**	**0.86%**
23	90.70%	90.49%	91.25%	90.87%	0.55%	0.38%
24	91.00%	90.78%	91.89%	91.53%	**0.89%**	0.75%
25	91.00%	90.77%	91.86%	91.52%	**0.86%**	0.75%
26	90.80%	90.65%	90.63%	90.30%	-0.17%	-0.35%
27	90.90%	90.69%	90.10%	89.85%	**-0.80%**	**-0.84%**
31	80.10%	80.34%	82.02%	81.52%	**1.92%**	**1.18%**

A similar situation is seen when considering the best 5 "level low" results (which for logistical regression and neural networks are comprised of runs with the same parameter combinations in both cases, Tab. 8.1-2). Here too there are very slight positive differences, the threshold value for the method according to Chung & Fabbri (1999) never being exceeded, which indicates equally good results. On the other hand, the threshold value of the ROC method is exceeded almost everywhere. The same applies to the average differences with +0.80% for the ROC method and +0.62% for validation according to Chung & Fabbri (1999, Tab. 8.3-1). This validation comparison therefore demonstrates that neural networks show somewhat better model performance.

Tab. 8.1-2: Measured validation values (AUC) for the test data of the "best 5"–"level low" runs with logistic regression and neural networks, as well as their differences

Run	Logistic Regression		Neural Network		Difference NN-Log Reg	
	ROC	Chung & Fabbri	ROC	Chung & Fabbri	ROC	Chung & Fabbri
5	90.80%	90.61%	91.64%	91.26%	**0.84%**	0.65%
6	90.70%	90.55%	91.52%	91.17%	**0.82%**	0.62%
14a LR, 10 NN	90.80%	90.62%	91.68%	91.34%	**0.88%**	0.72%
23	90.70%	90.49%	91.25%	90.87%	0.55%	0.38%
24	91.00%	90.78%	91.89%	91.53%	**0.89%**	0.75%

Even though there are only very minor differences in validations of results within individual modelling methods, and therefore no unequivocally best result could be cited, *one* result, the best validation value from the test data in purely mathematical

terms, was nevertheless selected for each method, and these two results were then compared. For both methods, this was the result of run 24. The result for neural networks was also somewhat better in this validation comparison for a single result (Tab. 8.1.-1 and 8.3-1).

Generally, therefore, the validation comparisons of "level low" results can be considered "equally good" to "slightly better with neural networks." However, as explained above, due to limited significance of these results, neither of the two models can be clearly favoured.

As seen in both this chapter and in the analyses of results of neural networks and logistic regression (Chapter 7.2 & 7.4), the validation results of many runs were very similar, and thus no *single* and clearly best "level low" result could be chosen. The "best 5"–"level low" results were therefore combined into a common final result for the "level low" runs. This was done for the results of both neural networks and logistic regression by means of cell-specific calculation of mean susceptibility based on the respective maximum and minimum (= mid-range). Because the uncertainty that arises from the range of these "best 5"–"level low" results must also be taken into account, this uncertainty was also cell-specifically stated (for detailed discussion, see Chapter 8.4).

This common final result for the "best 5"–"level low" runs is now shown for neural networks in the form of the mid-range and the range in Fig. 8.1.-3 and 8.1-4 respectively. Presented in contrast to that is the final result of the "best 5"–"level low" runs for logistic regression, with the corresponding maps in Fig. 8.1-5 and 8.1-6. Because the maps of the two modelling methods were produced using the same parameter combinations, the maps for neural networks and logistic regression are also directly comparable. A comparison of the two maps of the mid-range again shows that the susceptibility maps for both methods exhibit quite similar susceptibility distributions, the map for logistic regression once again showing somewhat stronger differentiation between the higher and lower susceptibilities.

The modelling uncertainty is quite similar for both models, as can be seen from the range-maps. A major share of the cells in both maps therefore display ranges in the region of <0.1, which is very small. A comparison of the two maps shows that the ranges of logistic regression, at an average of 0.026, are smaller than those of neural networks at 0.040, however the maximum range of 0.55 with logistic regression is obviously higher than that of neural networks at 0.30. The two modelling methods are thus probably comparable with regard to the uncertainty of the „level low" final result.
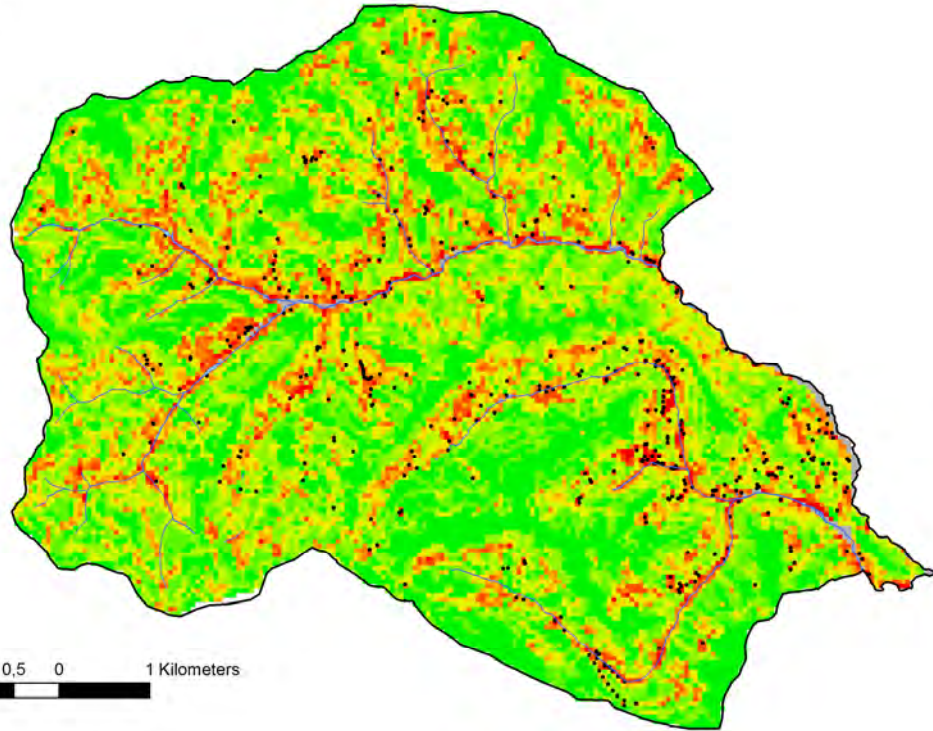
Fig. 8.1-3: "Best 5"–"level low" map (mid-range) generated by neural networks
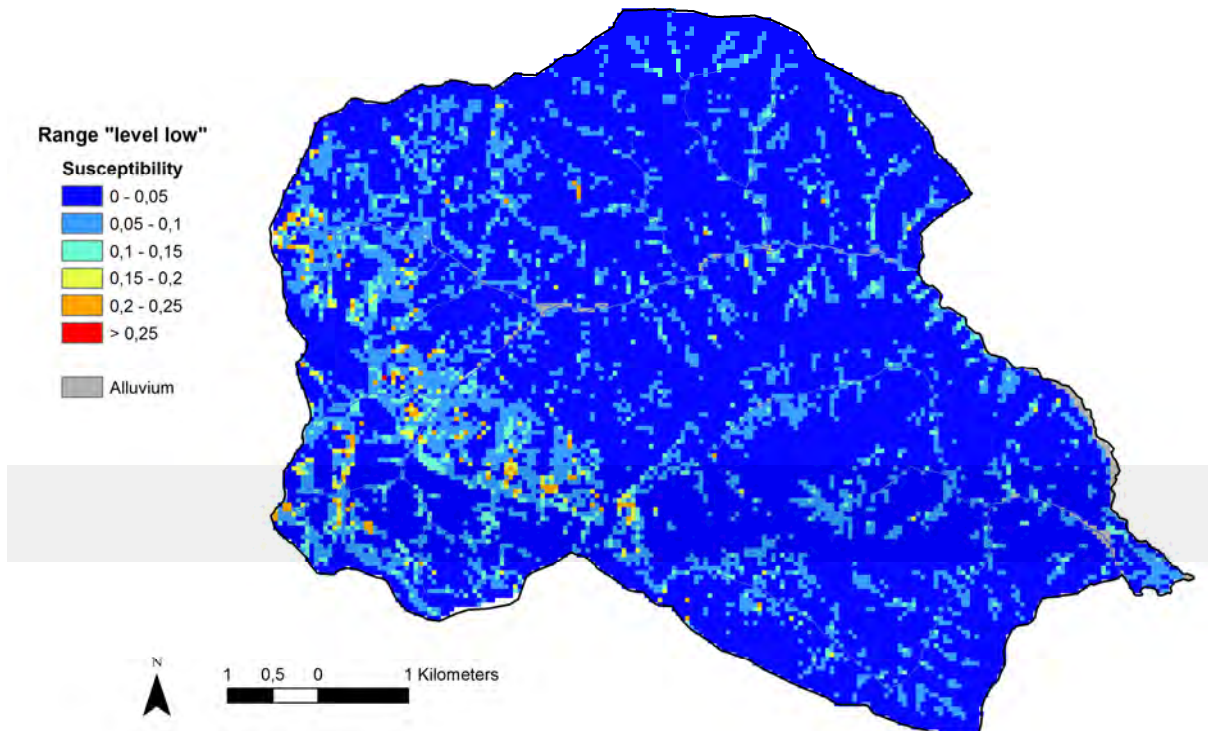
Fig. 8.1-4: Uncertainty – "level low" map (range) generated by neural networks

Fig 8.1-5: "Best 5"–"level low" map (mid-range) generated by logistic regression

Fig 8.1-6: Uncertainty – "level low" map (range) generated by logistic regression

8.2.   Modelling Results using the "Level High" Parameter Maps

<div style="border:1px solid black">

Comparison of "level" results

In the "level high" runs, neural networks and logistic regression generally produce quite similar susceptibility maps, with logistic regression differentiating somewhat more strongly between high and low susceptibilities. The validation comparisons showed that the results of logistic regression and neural networks could be assessed as "equally good" based on the validation methods used. The uncertainties in the final results seen in the 5 best susceptibility maps produced using both models cannot be compared here due to the different parameter maps employed.

</div>

The comparison of the "level high" runs also showed (analogously to the "level low" runs) that the susceptibility maps for neural networks and logistic regression exhibited quite similar susceptibility distributions with the same parameter combinations. Here again, with the use of logistic regression, there was a somewhat stronger differentiation between high and low susceptibilities. This is also seen from the difference map for the runs 58 (neural networks) and 67 (logistic regression), which were calculated using the same parameters (Fig. 8.2-1). Here too, the differences were quite small, the predominant percentage lying between –0.1 and +0.1.
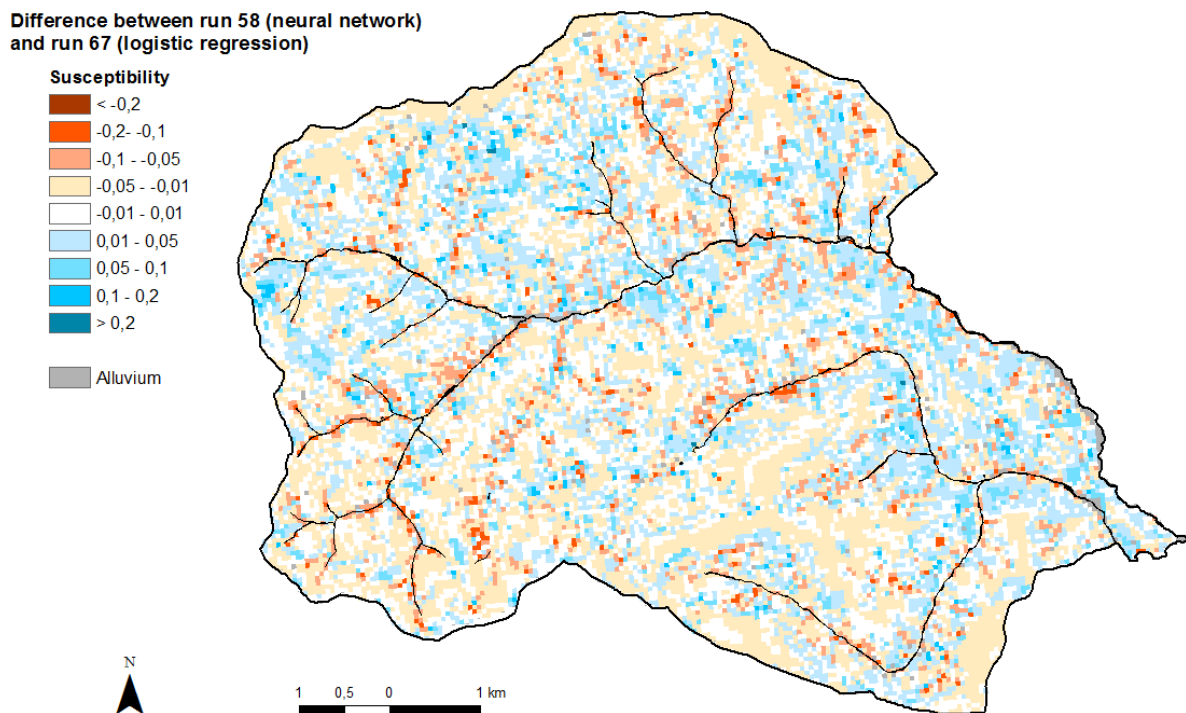
Fig. 8.2-1: Difference between map of neural network (run 58) – map of logistic regression (run 67)

There were obviously fewer results available now for the validation comparison of the "level high" results that had the same parameter combinations (Tab. 8.2-1) than there had been for the "level low" runs. Here too, it was seen that the results of logistic regression and neural networks, due to the minor differences – despite a majority of positive values -- could be termed "similarly good." That statement was

not altered (in contrast to the "level low" results) by the introduction of the threshold value for parity (the values in bold in Tab. 8.2-1 exceed these values). This was also confirmed by the mean differences [+0.06% with ROC, -0.18% with validation according to Chung & Fabbri (1999)] (Tab. 8.3-1).

Tab. 8.2-1: Validation measured values (AUC) of the test data for "level high" runs with the same parameter combination for logistic regression and neural networks, as well as their differences

Run	Logistic Regression		Neural Network		Difference NN-Log Reg	
	ROC	Chung & Fabbri	ROC	Chung & Fabbri	ROC	Chung & Fabbri
33	91.30%	91.03%	92.22%	91.83%	**0.92%**	**0.81%**
35	80.90%	81.14%	81.74%	81.21%	**0.84%**	0.07%
37	90.60%	90.49%	90.71%	90.28%	0.11%	-0.21%
40	91.40%	91.16%	91.55%	91.15%	0.15%	-0.01%
46	91.70%	91.41%	92.07%	91.77%	0.37%	0.36%
67 LR, 58 NN	92.80%	92.40%	92.82%	92.45%	0.02%	0.05%
69	90.40%	90.29%	88.91%	88.48%	**-1.49%**	**-1.81%**
70	90.30%	90.16%	89.88%	89.47%	-0.42%	-0.69%

Because the "best 5"–"level high" results for logistic regression and neural networks are now obviously different with respect to the parameter combinations used, they can no longer be directly compared. They must be indirectly compared via the mean value of the respective validation value. The validation values for logistic regression are entered in Tab. 8.2-2, and those for neural networks in Tab. 8.2-3. The validation values of the other method and its differences could only be entered in the respective table when there were comparable results.

Tab. 8.2-2: Validation measured values (AUC) of test data for the "best 5"–"level high" runs for logistic regression, as well as their differences

Run	Logistic Regression		Neural Network		Difference NN-Log Reg	
	ROC	Chung & Fabbri	ROC	Chung & Fabbri	ROC	Chung & Fabbri
43a LR	91.50%	91.29%				
67 LR, 58 NN	92.80%	92.40%	92.82%	92.45%	0.02%	0.05%
58 LR	93.00%	92.66%				
63 LR	91.40%	91.20%				
66 LR	93.10%	92.74%				

Tab. 8.2-3: Validation measured values (AUC) of test data for the "best 5"–"level high" runs for neural networks, as well as their differences

Run	Logistic Regression		Neural Network		Difference NN-Log Reg	
	ROC	Chung & Fabbri	ROC	Chung & Fabbri	ROC	Chung & Fabbri
33	91.30%	91.03%	92.22%	91.83%		
67 JR, 58 NN	92.80%	92.40%	92.82%	92.45%	0.02%	0.05%
59 NN			91.89%	92.22%		
61 NN			91.41%	91.74%		
P2a NN			92.28%	92.68%		

The mean differences of the "best 5"–"level high" results, at -0.08% for ROC and +0.62% for validation according to Chung & Fabbri (1999), are also quite low and within the threshold values for parity (Tab. 8.3-1). The "best 5"–"level high" results for logistic regression and neural networks can therefore, for the most part, be considered equally good.

For the "level high" runs as well, despite the substantial uniformity of the results for each method, *one* result per method was selected that exhibited the best validation result for the test data in purely mathematical terms. For logistic regression, this was run 66, and for neural networks run 58. When comparing these two single results, it was once again seen that the differences in validation values, at - 0.28% for ROC and - 0.29% for validation according to Chung & Fabbri (1999), were clearly within the threshold values (Tab. 8.3-1), so that these results could also be seen as equally good.

It was therefore seen from the validation comparisons of the "level high" results, that the results of logistic regression and neural networks could be considered "equally good" based on the validation methods used.

For neural networks, the common final result for the "best 5"–"level high" runs is presented in the form of the mid-range and range in Fig. 8.2-2 and 8.2-3. This is compared to the final result for the "best 5"–"level high" runs using logistic regression with the corresponding maps in Fig. 8.2-4 and 8.2-5. Here too, it was seen that the susceptibility maps for both methods showed quite similar pixel distributions, although the distribution for logistic regression did differentiate somewhat more strongly between high and low susceptibilities.

Major differences were however seen in the range-maps: whereas the range-map of logistic regression, with an average of 0.028 and a maximum of 0.31 achieved similarly high values to those of "level low" (Chapter 8.1), the range-map for neural networks, with an average of 0.09 and a maximum of 0.48, exhibited much higher values than either "level low" or logical regression at "level high." These major differences were also very obvious when comparing the map images.

However, it should be stated here that the "level high"-range map for neural networks is not comparable to either the "level low" map for this method or the "level high" map for logistic regression. This is the case because the "level high" map for neural networks was produced from 5 runs with all 3 substrate parameter maps *(Sub_GK_lg, Sub_GK_lh and BK)*, whereas the "level high" map for logical regression was produced from 4 runs with the same substrate map (*Sub_GK_lh*) and only one run with a different substrate map (*BK*). The "level low" map for neural networks was produced with only one substrate map (*Sub_GK_lg*) for all 5 runs. That was the case, because it had been noted that the large-area differentiating substrate maps also caused quite different large-area modifications in the susceptibility maps. While all of the other input parameters for the respective runs were the same, except for the subsurface flow dispositions, which were always similar, and the evened precipitation. The high values of the "level high"-range map of the neural networks is therefore not a result of the methodology of neural networks, but rather the use of several different parameter maps.
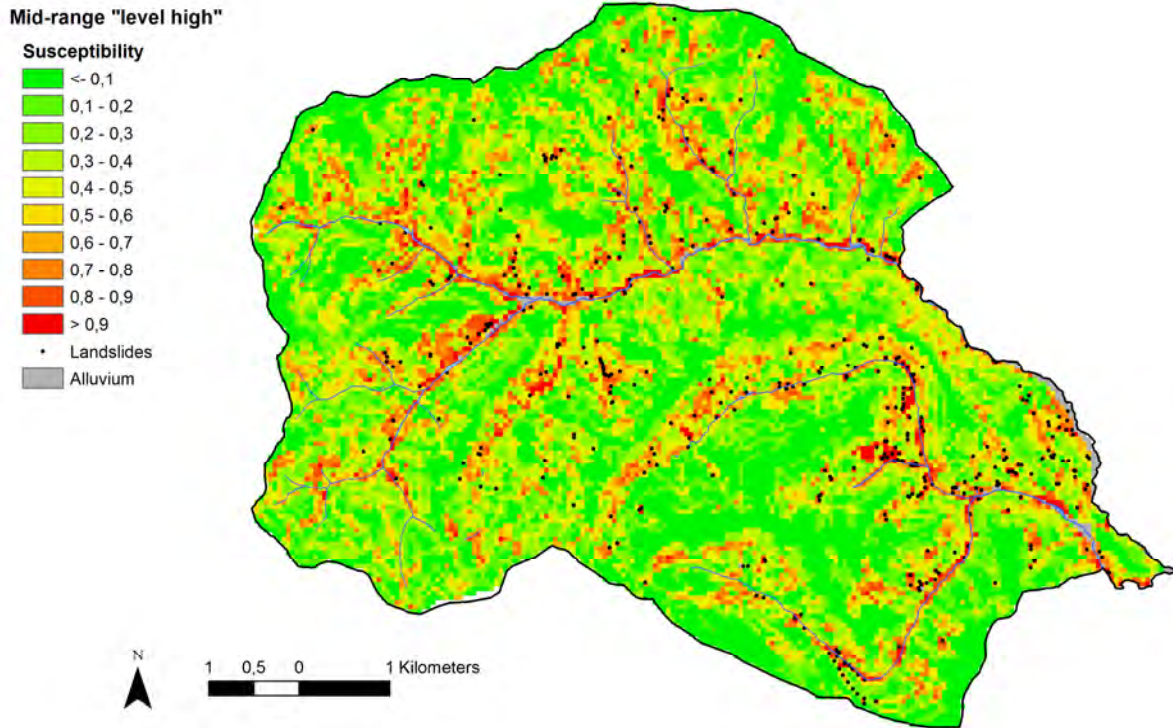
Fig. 8.2-2: "Best 5"–"level high" map (mid-range) generated by neural networks
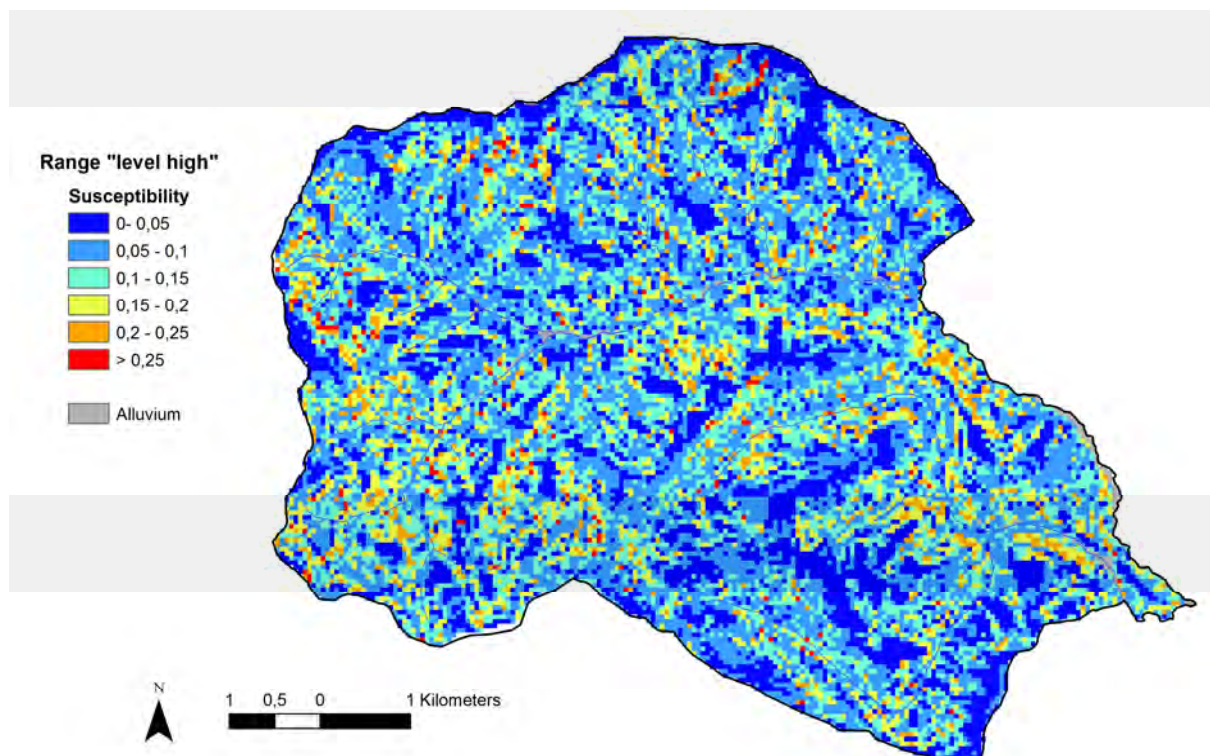
Fig. 8.2-3: Uncertainty – "level high" map (range) generated by neural networks
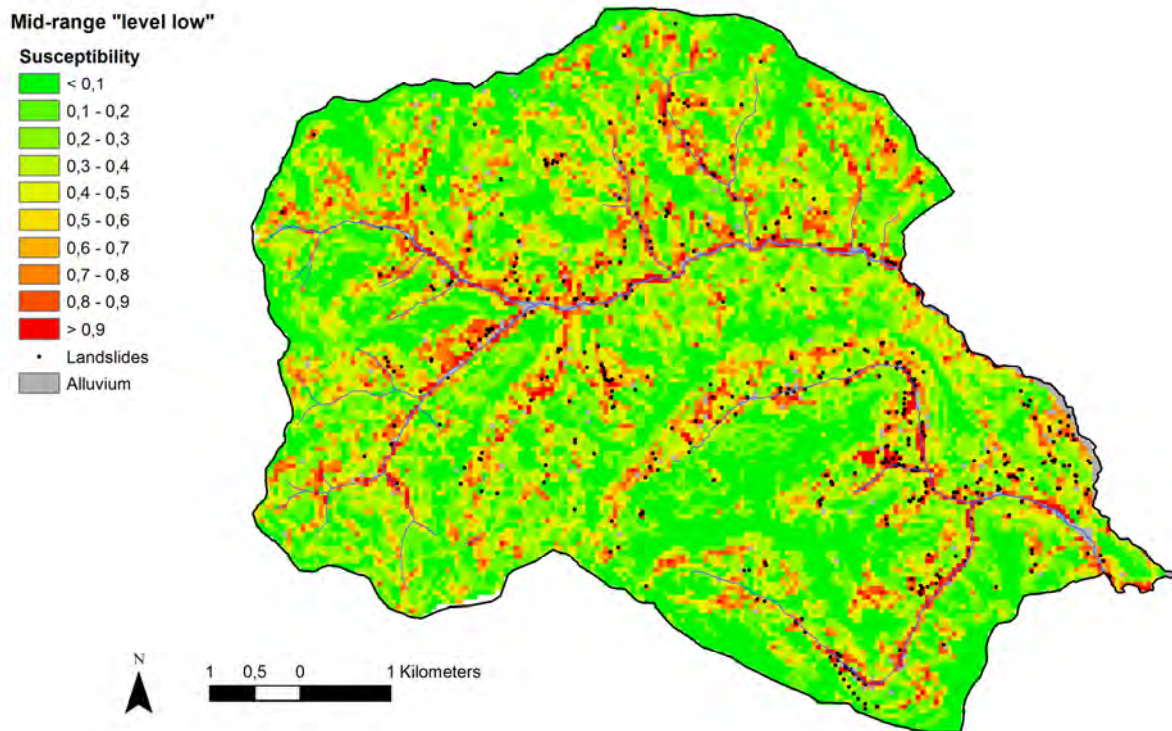
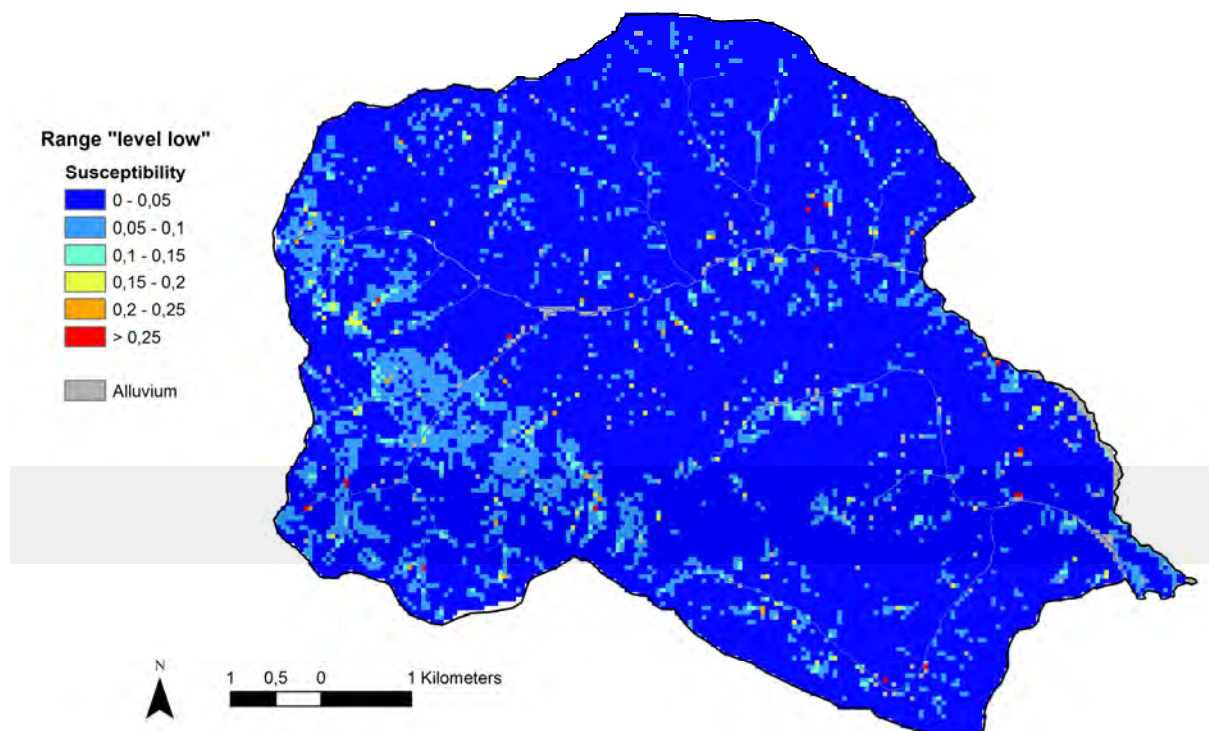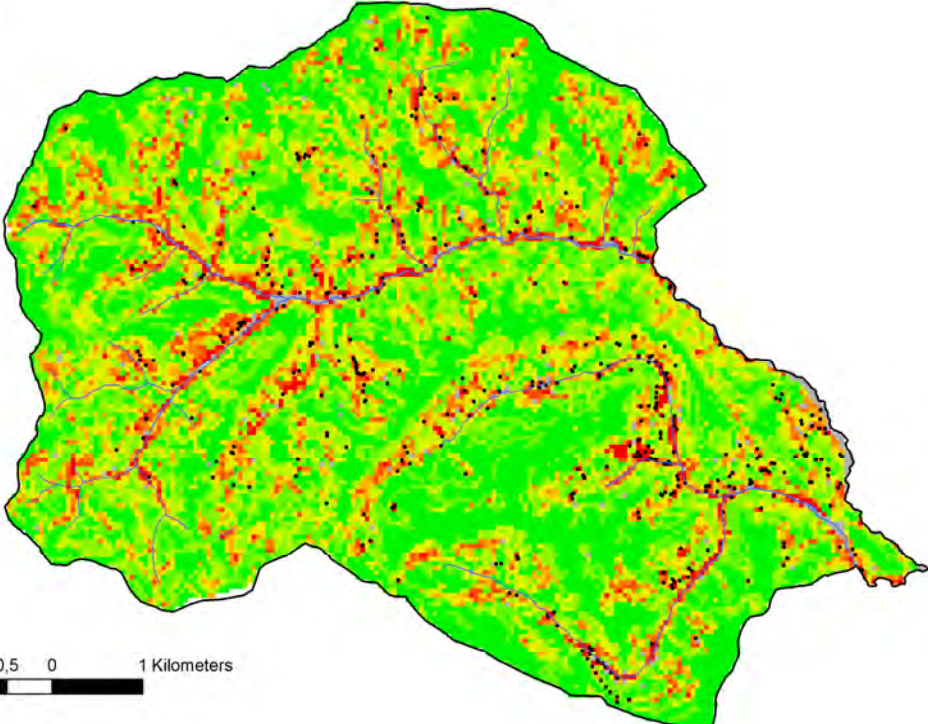*Fig. 8.2-4: "Best 5"–"level high" map (mid-range) generated by logistic regression*
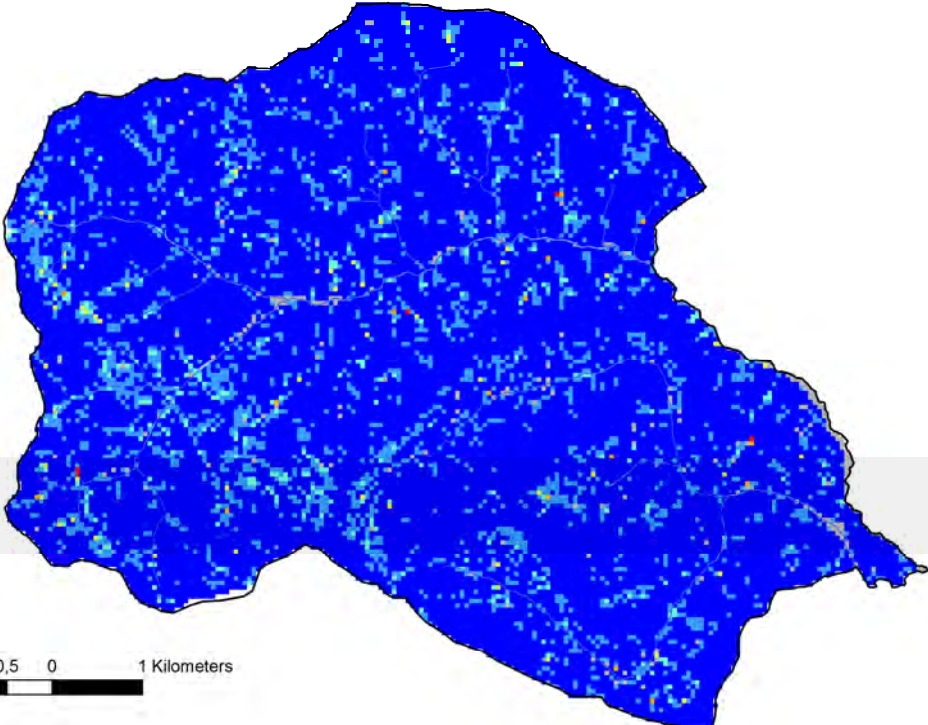
Fig. 8.2-5: Uncertainty – "level high" map (range) generated by logistic regression

8.3.   Comparison of "Level Low" and "Level High" Results

Comparison of "level low" and "level high" results
In these runs, neural networks and logistic regression generally produce quite similar susceptibility maps, although logistic regression differentiates somewhat more strongly between high and low susceptibilities. It was seen in the validation comparison, that the results of logistic regression and neural networks, based on the validation methods used, could be termed "equally good" to "slightly better in the case of neural networks." However, due to the limited significance of these comparisons (for example summarized area-wide validation), neither of the two models can be clearly favoured.

On the whole, the susceptibility maps for neural networks and logistic regression exhibit quite similar pixel distribution with the same parameter combinations. With the use of logistic regression, there was somewhat stronger differentiation between high and low susceptibilities.

The validation comparison in Tab. 8.1-1 and 8.2-1 of all "level low" and "level high" results from runs with the same parameter combinations demonstrates that the values from neural networks and logistic regression are similarly high. However, on closer examination, it is seen that the positive differences predominate, both in general and when the threshold value criterion for parity is used. However, the latter applies only to ROC, whereas here, the values for validation according to Chung & Fabbri (1999) are approximately equally high. Because positive differences indicate higher validation values for neural networks, it can be assumed on the basis of this validation comparison, that the model performance of results with neural networks is "equally good" to "slightly better" compared to that of the results with logistic regression. When the mean differences (Tab. 8.3-1) are compared, two positive values: +0.47% for ROC and +0.25% for validation according to Chung and Fabbri (1999) also occur, however they do not exceed the threshold criterion for parity.

When the validation comparisons for the "best 5"-"level low" and -"level high" results are summarized (Chapter 8.1 and 8.2 and Tab. 8.3-1), it is also seen that the model performance of the results with neural networks is "equally good" to "slightly better" than the model performance of the results with logistic regression. This also applies to comparisons of the "best" single results (Tab. 8.3-1), for which, despite the high degree of similarity of the best results of one modelling method, *one* result per level was selected by means of the best purely mathematical test data validation.

Finally, for both modelling methods, **one** "overall" (best of all) result was selected on the basis of the respective validation strategy used. Here too, the best results lay so close together that the selection is somewhat arbitrary. For both neural networks and logistic regression, this was the result of the respective run 58. However the two results, due to the different successive parameter integration in the two kinds of modelling, also had different parameter combinations. Here run 58 for logistic regression had an AUC for the test data of 93.00% with ROC and 92.66% with Chung and Fabbri (1999). For the neural-networks run 58, these values were 92.82% and 92.45% respectively.

The resulting differences (Tab. 8.3-1) were also small and still lay within the threshold-value range for parity, so the two results should also be assessed as equally good.

Tab. 8.3-1: Summary of the differences between the validation measures values (AUC) of the test data for neural networks and logistic regression

	Difference NN-Log Reg	
Multiple runs	**ROC (Mean)**	**Chung & Fabbri (Mean)**
Runs with same parameter maps "level low"	**0.65%**	0.44%
Runs with same parameter maps "level high"	0.06%	-0.18%
Runs with same parameter maps "all"	0.47%	0.25%
Best 5 runs "level low"	**0.80%**	0.62%
Best 5 runs "level high"	-0.08%	0.62%
Single runs	**ROC**	**Chung & Fabbri**
Run with highest test date value „level low"	**0.89%**	0.75%
Runs with highest test date value „level high"	-0.28%	-0.29%
Best run of all	-0.18%	-0.21%

In general, therefore, in the validation comparisons between the two methods, the results for logistic regression and neural networks can be termed "equally good" to "slightly better for neural networks" based on the validation methods used. As mentioned above, due to the limited significance of these comparisons, neither of the two models can be definitely favoured.

8.4.   Discussion and Conclusions

As shown above, both intermethodological validation results and those from method-specific runs are quite similar, although the results for neural networks are in part somewhat better. From the authors' point of view, the summarized area-wide validation methods (Chapter 7.2) used here (and also internationally) are not adequate to provide unequivocal, reliable statements on model performance, particularly when there are results of similar quality. For that reason, the authors have refrained from stating that one modelling method, or a single modelling result, is clearly superior to others. The inadequacy of the validation methods was seen, for example, from the fact that the susceptibility map for one result was completely changed by the integration of precipitation, and probably also improved due to the definite influence of this parameter, however the validation result was still virtually unchanged (Chapter 7.2.2.2).

As neither of the methods and no result can be singled out as the best, all of the results of both modelling methods and several results for each level, were used to produce a common final result. That also made it possible to depict the spatial variability and the uncertainty of susceptibility. This was done by selecting the 5 best runs for each level of each method and then combining them to make a common map. These "best 5"–"level low" and "level high" maps for the two modelling methods were then combined into a common, intermethodological, "level low" or "level high" map, in which there was, in each case, cell-specific calculation of the mean susceptibility from all maximum and minimum values (= mid-range) and the fluctuation range (= half range).

This mid-range, which, due to the small number of outliers, comes very close to the arithmetic mean, was selected, because with this value, a good combined presentation with the fluctuation range as a measure of uncertainty can be guaranteed. The final-result map is thus a "mid-range +/- half range." This form of presentation therefore covers the entire potential range of values in **one** combined map, and it is very clear and easy to understand. It was used for the final-result map for "level low" (Fig. 8.4-1), and for "level high" (Fig. 8.4-2), which are also shown in a larger scale and with a legend in the Annex (Fig. A1 and A2). Here, the susceptibilities of the mid-range were shown in the usual colours (high values in red, low values in green), the half range (fluctuation range = uncertainty), on the other hand, is shown by means of superimposed black circles/dots (not visible in the case of very low values).
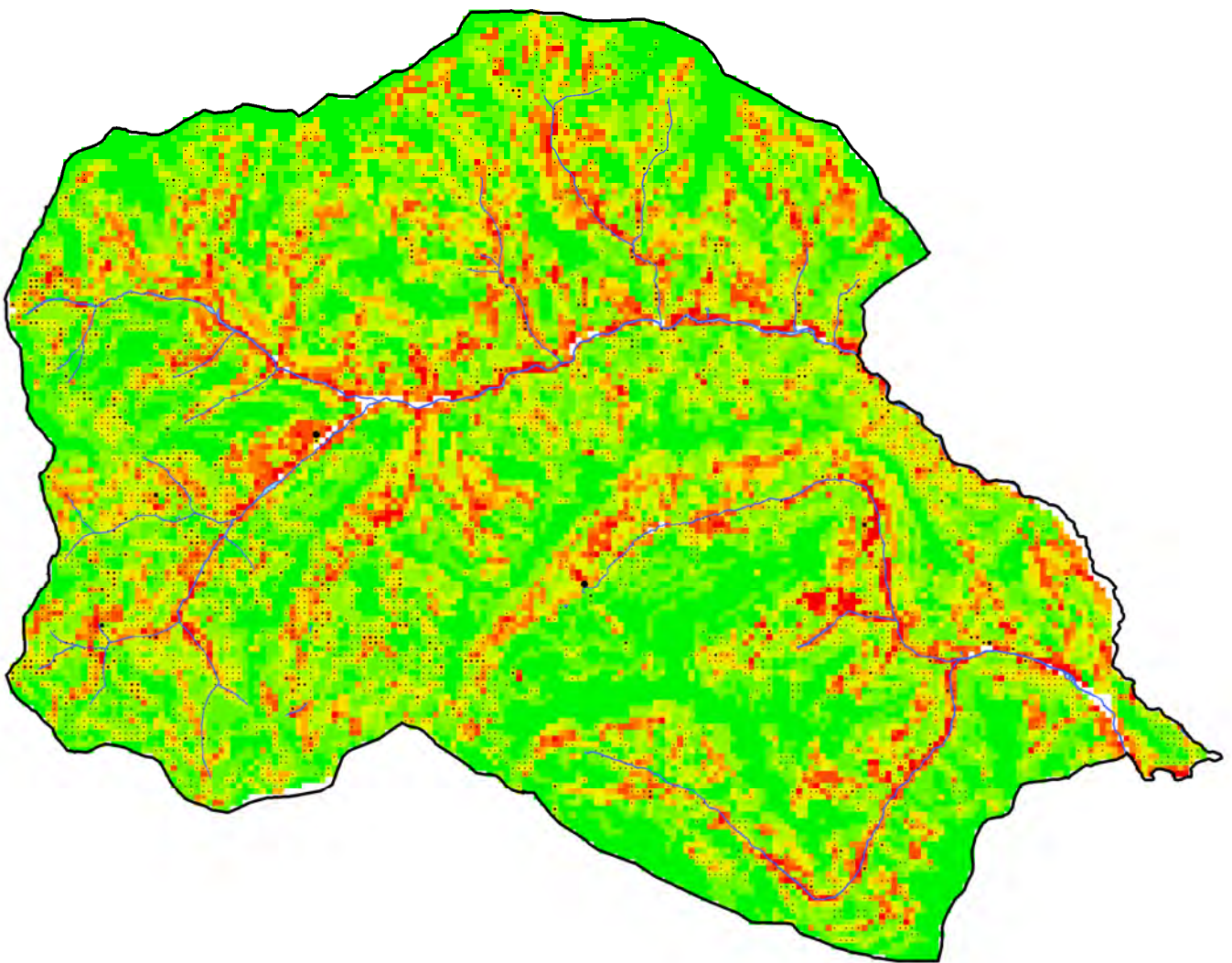
Fig. 8.4-1: Combined final-result map "level low" of susceptibility and uncertainty for both methods (for legend see map in Annex A1)

As in the case of Fig. 8.2-5, it can be seen from Fig. 8.4-1 that the uncertainties in the "level low" final-result map are very small, whereas somewhat greater

uncertainties extend mainly along the black/green schists (in the west). There are only a few, isolated areas of major uncertainty.

The "level high" final-result map is quite similar to the susceptibility distribution of the "level low" map, however greater uncertainties are clearly recognizable, which derive from the "best 5" map of neural networks (explanation in Chapter 8.2). It is clearly seen that little uncertainty/few fluctuations appear primarily in areas that were always shown as very stable (many forest areas) or as very instable (many lower slope areas).
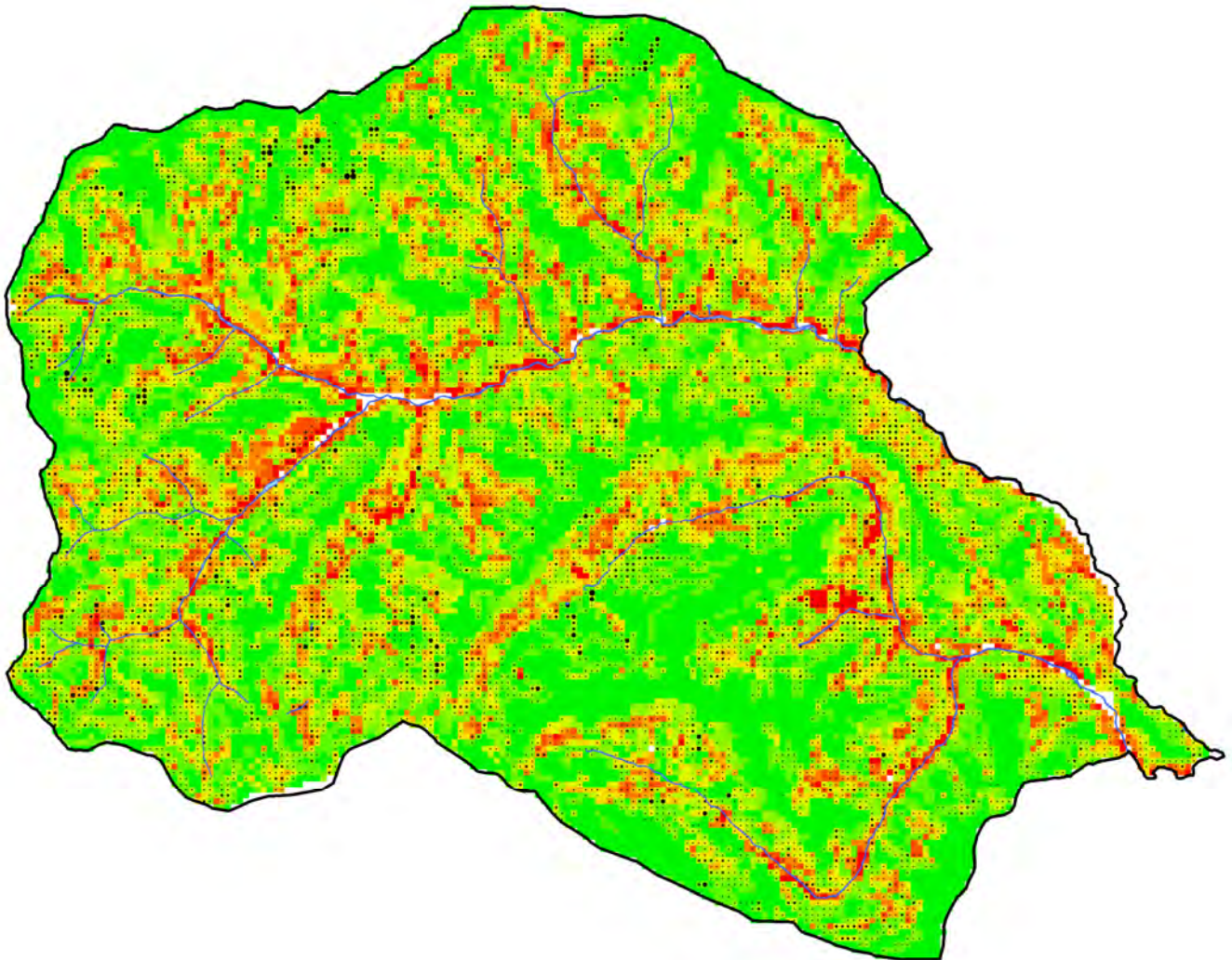
Fig. 8.4-2: Combined final-result map "level high" of susceptibility and uncertainty for both methods (for legend see map in Annex A1)

Mean susceptibility (= mid-range) in combination with fluctuation range (= half range) are causing several possible disposition classes in many cells, which are illustrated in the final-result map for "level high" in Fig. A3 in the Annex.

As a rule, it can also be said that because of the similarity of the validation results and the inadequacy of the summarized area-wide validation methods, a combination of several results from both modelling methods should always be used in the

Adaptslide project and subsequent projects. With the currently available validation methods, only obviously better results can be recognized as such, whereas with moderate to minor differences in the validation results – and these made up the major portion of results obtained during the Adaptslide project – the issue of the better result inevitably remains unclear. Singling out one best result or one best method would therefore be a randomly decision and could not be justified. Thus, in order to make reliable statements concerning both model performance and the possibilities of improving final results, as well as the capacities of individual modelling methods, it will be urgently necessary to develop new validation methods in the future.

9. Modelling the Process Areas under Consideration of the Spatial Variation of the Landslide Disposition (BFW)

On the basis of a comprehensive documentation of numerous landslides in the communities of Gasen and Haslau (South East Austria, Province of Styria) in 2005, a method was developed to estimate the runout length of shallow landslides and the resulting debris flow events. The aim was to complete the landslide disposition maps by estimating not only the starting zones of the landslide, but the whole area affected by the process. A modified empirical approach, based on several avalanche applications, was developed in order to allow regional applications with usually limited data availability. Starting from documented events or susceptibility maps (raster information), the flow path was calculated by a multiple flow approach. In addition, parameters to consider the effects of concave or convex terrain on the lateral spread and the runout length were developed.

9.1 Basics and Aims

As shown in Chapter 7 there are several methods to estimate the landslide disposition of spontaneous landslides in loose material.

However, these maps do not allow conclusions on the affected areas. When spontaneous landslides in loose material result in debris flow, they affect an area which is far larger than the starting (sliding) area. Hence, for compiling maps showing endangered areas in detailed scales, it is necessary to determine the flow paths and the spread of the moving masses, too. Due to the high possible transport velocities, the forces are high compared to the transported masses. The occurrence of the process is abrupt and often surprising. These reasons cause high risks of casualties and the loss of property.

There are hardly any available methods and models, which can meet the demands specified as following:

> ➢ The runout length and, if possible, the affected area of landslide-triggered transport processes should be calculated.
> ➢ The method should be applicable on an area-wide basis.
> ➢ The method should have moderate model input requirements.
> ➢ The method should complete the contents of the landslide-disposition maps generated in the test area (scale,…)
> ➢ The method should be able to deal with varying types of starting point information.

The comprehensive documentation of numerous landslide events in the communities of Gasen and Haslau (Chapter 4) offered the possibility to develop a simple method to estimate the runout length of spontaneous landslides and landslide-caused transport processes like debris flow on slopes on an area-wide basis, using just a few key parameters.

The developed method should complete the raster-based slope susceptibility maps and result in "advanced" hazard index maps. It is mentioned that the displayed process areas cannot fulfill the requirements of hazard maps due to the unknown frequency and magnitude of the events. The approach aims at simulating small and medium-sized spontaneous landslides in loose material.

The model input requirements are defined as follows:

➢ DEM10 (Digital Elevation Model, 10 * 10 m) or higher resolution for morphologic information.

➢ Documented events (triggering, transport and deposition zones) to support the determination of the model input parameters and to calibrate the model.

9.2 State of the Art

The implementation of most of the available models requests a sound knowledge of basic data, such as detailed morphological information (e.g. DEM with high resolution and additional information about constructions, data on physical parameters (e.g. inner and external friction coefficients, masses) or the type of transport process, which are usually not available or ascertainable in sufficient quality. These approaches are therefore suited for selective assessments. Some more or less established models and approaches, which are designed to determine the flow path and runout distances and partially additional information on the flow velocity and deposition issues are e.g.:

➢ FLO2D: This commercial model needs comprehensive information on the volume, hydrographs (which do not exist in the usual manner in the case of debris flow caused by spontaneous landslides on slopes) and rheologic conditions (FLO-2D User's Manual 2004, Garcia et al. 2004, Jäger & Moser 2008)

➢ RAMMS: The Rapid Mass Movements Software package has also been available for debris flow for some time. High requirements of the models input data and the limitation to single debris flow assessment are anticipated (Stähli & Bartelt 2007, RAMMS 2010).

Several approaches are available to estimate the area potentially affected by landslide runout masses:

A promising approach of area wide estimation of debris flow range and flow paths was realized in the SIVAProtect –CH project. The main objective was to quantify the vulnerability of settlements and infrastructure and to identify protection forests throughout Switzerland in case of rockfall, avalanches, landslides and debris flow (BAFU 2008). For determining the triggering areas of landslides, the model SLIDISP (Liener & Kienholz 2000, Liener et al. 2008) was implemented. This approach calculates the slope stability by infinite slope analyses for each single raster cell. Starting from these raster cells, transit and depositions area from slope debris flow (triggered by spontaneous, shallow landslides) where calculated with the model SlideSim (geo7, 2010). It requires user defined external and internal friction

coefficients. These data have to be identified in a deterministic way e.g. by calibrating the model in well documented test areas. Unfortunately, SlideSlim is not available – simulations have to be charged by GEO7.

Similar approaches are currently tried out in tests in smaller regions in some European countries; e.g. Dahl et al. (2010) presented a simple approach for mapping regional landslide susceptibility and runout on the Faroe Islands.

Generally, for predicting landslide runout, two types of models are used: Statistically based models and physically based models. Good overviews are presented in Rickenmann (2005), Hürlimann et al. (2008) and McKinnon (2010). Statistical models correlate physical properties of the landslide, landslide prone slope and/or geomorphologic characteristics of the flow path with the extent of the runout zone. Best practice dictates that statistical models should only be applied in conditions similar to the events used in the statistical analysis (Rickenmann, 2005 cf. McKinnon, 2010). This especially holds true for issues of the initial volume, the detachment position of the unstable mass and the conditions of the transport and deposition zones (McKinnon, 2010).

Statistical approaches for runout calculation of mass movements originate from the concept of Heim (1932). Heim (1932) deviated the first linear regression to use the volume of rock avalanche hazards for predicting the ratio H/Lh between the vertical fall height (H) and the length of the horizontal projection of the track, called travel distance (Lh) from the starting to the end point of the mass movement. He denominated H/Lh the 'travel angel' (also called angle of reach, AOR). H/Lh corresponds to the angle of the line between the start and the end point of the mass movement and the horizon level. It is possible to determine the travel distance of mass movements by the intersection of this line with the terrain profile along the movement path. During practical implementation the minimum or medium observed H/Lh ratio is often used for the runout calculation, because it is difficult to estimate the factors, which determine the H/Lh ratio locally, e.g. the potential volume (V) or area (A) of the failure. This is called the general gradient concept. The problem is that the H/Lh ratio of observed mass movements varies widely and the variations cannot be explained only by the variance of slide volume and area. Therefore, Corominas (1996) performed H/Lh – volume regressions for subsets of landslides, categorized by movement and path morphology adapted to different scopes. According to our field observations, the travel distance especially of smaller spontaneous landslides in loose material, correspond more to the water saturation of the debris, the grain size and the morphology of the path (curvature, roughness) than to the initial or deposition volume. This is also confirmed by the observations and analyses of other authors, e.g. Corominas (1996), Iverson (1997), Rickli and Bucher (2003), Okura et al. (2003) and Dahl et al. 2010. Data of landslides tabled by Iverson (1997) and Legros (2002) suggest a significant decrease of the H/Lh ratio with increasing flow volume.

Other empirical runout calculation approaches are based on mass reduction factors and the concept of volume balance along the flow path (Hungr et al., 1987; Cannon, 1993). They require detailed and precise data on the flow path and the initial volume. The lateral spreading of debris can be considered with multiple flow direction algorithms, Monte Carlo and random walk approaches.

Dynamic runout models are based on physical relationships to establish runout characteristics, such as applying the lays of the conservation of momentum to the kinematics of a failing mass. Dynamic models account for the progression of time and for terrain anomalies, and thus may be used to predict a complete description of landslide motion (McKinnon, 2010). In principle, there are two kinds of dynamic models: point mass models and continuum models.

Point mass models (mainly 1D analytical models), presume the failure volume to be a single mass without interaction between the moving debris parts. They reduce the landslide mass to a single point and calculate its dynamics along a previously selected flow path. The implied physical model of mass movement is Coulombs law of friction (frictional rheology) or the frictional-turbulent Voellmy fluid flow rheology. The Voellmy model (Voellmy 1955) has been successfully applied to both point mass and continuum models (Hürlimann et al., 2008).

Continuum models (1D, 2D and 3D numerical models) treat the flow volume as mixture of elements that interact with each other. This allows for modelling the source mass deforming throughout the runout, incorporating both solid (dislocation along a failure surface) and fluid (continuous flow) deformation, which are characteristic of landslides (Hungr, 1995 cf. McKinnon, 2010).

The downsides of physical-based models and especially continuum models are the computational intensity and the demanding rheological parameterization.

9.3 Method

Due to the difficulties of the practical implementation of dynamic models and limited model and data availability, focus has been layed on empirical approaches of runout calculation. Empirical approaches have already been implemented successfully for snow avalanches. Körner (1980) adopted the concept of Heim (1932) for snow avalanches and compared it with the Voellmy model (Voellmy 1955). Lied and Bakkehoi (1980) extended the approach and introduced the α/β -model. The model was applied to numerous snow avalanches in Iceland (Jóhannesson, 1998), Spain (Furdada and Vilaplana, 1998), Austria (Lied et al., 1995), Canada (McClung et al., 1989; Delparte et al., 2008), Japan (Fujisawa et al., 1993) and Norway (e.g. Mears, 1989). Latest investigations concerning this statistical approach were carried out by Gauer et al. (2010). They used avalanche data from numerous countries and applied different snow avalanche models in order to make statistical conclusions. Klebinder et al. (2009) applied a simple travel angle model to detect the danger for forests from small snow avalanches in the eastern Alps.

Basis for the model are susceptibility maps, which may be generated in different ways. There are various methods to combine, adjust and improve the basic approaches of landslide susceptibility (probability) assessment. Modelling of the process area depends on the quality of this data base; therefore its development is emphased. Starting points are raster cells with a certain degree of landslide disposition. Experts and authorities are challenged to identify this value dependent on the specific needs of security and interests of area use.

Within the present study (AdaptSlide) different approaches (weight of evidence, logistic regression, neural network, SINMAP) and various parameter combinations were generated. The release areas are defined using the base of this raster

information. From each cell within the release areas, tracks were determined. Starting from such a cell, the tracks were calculated, by determining the path to all of the eight neighbouring cells which had lower elevations (multiple flow approach). A cell was part of the track, if the slide passed over the cell. Two criteria stopped a track:

(1) Either no neighboring cell with a lower altitude (addition of a selectable tolerance possible) exists, or

(2) the critical angle decreases to $\alpha_N < \alpha_{crit}$.

Fig. 3 shows the vertical profile of a path (continuous line). The point (x_0, z_0) is the centre of a cell in the release area. The distance to the next cell centre Δx is either the cell size Δc in north-south/east-west direction or $\sqrt{2}\ \Delta c$ along the diagonals. The downward slope angle α_N for the cell N is defined by eq. (1).

$$\alpha_N = \operatorname{atan}\ \frac{z_0 - z_N}{\sum_{i=0}^{N}\Delta d_i} \qquad (1)$$

z_0 is the altitude of the cell in the release area and z_N the altitude in the cell of interest. The denominator is equivalent to the horizontal distance from the cell i = 0 to the cell i = N along the track.

If $\alpha_N < \alpha_a$ (thin line) the maximum travel length is reached at x_a caused by criteria (ii). In the example shown in Fig. 3 the lower critical angle α_b (dotted line) for the travel length is marginally longer; the higher elevations trigger the criteria (i).
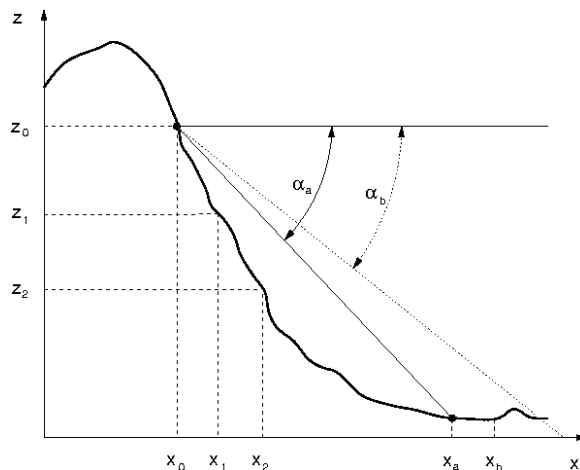
Fig. 9.3-1: The main principle of the exit conditions based on the vertical profile (details see text)

In order to avoid abrupt stopping caused by criteria (i) depressions of the DEM were filled by standard hydrological grid functions in a GIS (Tarboton et al., 1991).

The critical angle α_N is defined by eq. (2).

$$\alpha_N = \alpha_0 + k_1 c_N + k_2 s_N \qquad (2)$$

α_0 represents the basic user-defined angle, c_N is the curvature at the cell N (eq. 3) and s_N the standard deviation of the elevations along the track from the cell in the release area to the actual cell I = N (eq. 4). Curvature and standard deviation of elevations are used as indicators of flow path confinement and roughness and are calculated by the model. k_1 and k_2 are weighting coefficients which have to be defined by the user.

$$c_N = \frac{\frac{z_n - z_N}{\Delta c} - \frac{z_N - z_s}{\Delta c}}{\Delta c} + \frac{\frac{z_e - z_N}{\Delta c} - \frac{z_N - z_w}{\Delta c}}{\Delta c} \tag{3}$$

The indices n, s, e, w represent the surrounding cells of cell N in the main directions to north, south, east and west.

$$s_N = \sqrt{\frac{1}{N-1} \sum_{i=0}^{N} (z_i - \bar{z})^2} \tag{4}$$

$\bar{z}$ is the arithmetic mean of the elevations along the track from cell $i = 0$ to $i = N$.

If the exit criteria were not satisfied at a cell, the same procedure (Fig. 1) is applied to all neighbouring cells with lower elevations.

The factor f_{spread} is defined as the percentage of cells which is used for the further calculation. It was found that $f_{spread} = 0.3$ is a good choice. This means that only the 2 cells with the lowest altitude may be used in the next calculation step. The above procedure was implemented in a recursive manner. The results are paths of slides.

The model can be parameterized with three coefficients:

1. Alpha angle (α_0)
2. Weighting of curvature (k_1)
3. Weighting of standard deviation (k_2)

Further basic model settings are to specify:

➢ Method of distance determination (geometric, travel)
➢ Spread factor (typically 0.3)
➢ Threshold for release (value of disposition, e.g. 0.5)
➢ Upslope threshold (tolerance for abort criterion (1))

9.4 Model Calibration

Basis of the model calibration are digital information on the starting – transport and deposition zones with accurate position information (Fig. 9.4-1). The best data can be gained from aerial photographs, which are recorded close to the event. Due to the uncertainness of aerial photograph interpretation (Fig. 9.4-1, e.g. B), caused by clearings in settlements and near roads (unclear transport and deposition zones) and limited quality of interpretation in case of forest cover (Fig. 9.4-1, e.g. A), only data checked by in-situ and/or by photo documentation should be used. It has to be considered, that confined debris flow (e.g. because of deposition in tributaries Fig. 4 C) may lead to overestimations of the alpha angle and result in underestimations of the travel length. First results show that the aerial photo polygons (Fig. 9.4-1, brown) cannot be intersected with the DEM to determine the alpha angles "automatically". Hence, for well documented landslides/debris flows trajectories (yellow lines) have been inserted manually to describe the flow path and the range of the debris flow.
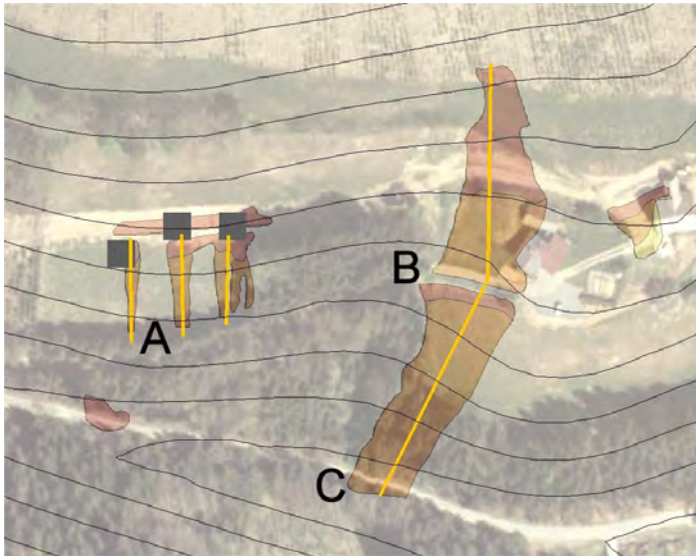
Fig. 9.4-1: Aerial photo information (brown polygons) and manually inserted trajectories. A: Uncertainties of the range due to forest cover; B: Misinterpretation due to an already cleared road; C: confined runoff area due to debris flow discharge in a tributary

When calibrating the model, it is proposed to start with the alpha angle. The alpha angle is defined as the quotient of $\Delta H/\Delta L$ of the trajectories. Statistical analyses of all (112 landslides) reconstructable travel paths of landslides result in a whole area with a mean alpha angle of about 26° (arithmetic average). The alpha angles of landsides with very short sliding distances showed sometimes unrealistic values and a spread above average. Simultaneous calculations in the section, where also a DEM1 (Digital Elevation Model 1*1 m) was available, produced a mean alpha angle of 29°. Thereby, variances of the alpha angles calculated with DEM 1 and DEM 10 where recognized up to 10° especially (of course) in the case of small ΔL. Due to these reasons, only landsides >20 m where elected for further analyses. The mean alpha angle based on this dataset (95 landslides) is 27.6 °. Fig. 9.4-2 shows the distribution of the landslide – length and alpha angels of the data set.

Fig. 9.4-2: Distribution of landslide - length and alpha angles of the selected dataset

The calculated regression between the horizontal landslide length (ΔL) and difference in altitude (ΔH) shows a slight increase of the alpha angle with increasing length, which is interpreted as being stochastic within the quality of the data and the correlation respectively (Fig. 9.4-3).
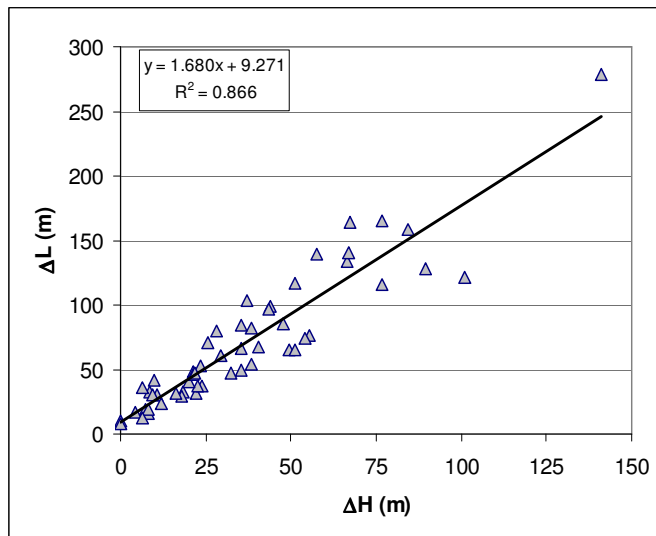
Fig 9.4-3: Correlation between ΔH and ΔL of the runoff paths of selected landslides

For determining the alpha angle, well documented, unconfined landslides and debris flow and a DEM with an adequate resolution are preferable. Included landslides with confined runoff caused an overestimation of the alpha angle and therefore short travel length.

The calibration of the weighting for curvature has to be determined in an iterative way by interpreting the effects of changed weights of curvature to spread and travel distance for the model runs. Higher weighting of curvature produce longer travel distances in concave surface structures caused by material-concentration and reduced surface-friction.

The standard deviation of the elevations along the track that influence the alpha angle, have to be determined in the same way.

9.5 Modelling Based on Single Point Starting Zones

The model (ASlide 1.0) is developed to handle with different kinds of raster based starting information, as single point (Pixel) information or susceptibility maps are.

Single point starting zones will be applied by known starting points e.g. on the basis of well-documented past landslides/debris flow and/or possibly compared to other models. Furthermore, it is the adequate way to calibrate the model and check the results for plausibility. Therefore, insights from model application are discussed first on this basis, while being aware that the validation of model results on single slide events involves scale factor problems – the model is not developed to produce results for travel length and spreading in detailed planning scales.

The mean value of the model is certainly the alpha angle. Identification should be done for unconvinced, well documented landslides and debris flow and a DEM with an adequate resolution. The area-wide availability of the DEM with 10*10 m resolution in the test area facilitates the rejection of landslides with a length of less than 20 m. Furthermore, implausible runaway values have to be removed from the database. These steps reduced the difference of the mean alpha angle determined by DEM10 and DEM1 to 0,47° in the test area.

As model calibration showed, the average alpha values can be seen as the upper limit. Applications showed that for the whole test area, alpha angles around 22° (75 % of the documented trajectories are steeper) showed the best results. The lower limit for the alpha angle in the test area is 17 – 18 ° (90 % of the documented trajectories are steeper). With this alpha angle and the further model parameterization shown below, most of the documented process areas were marked by the model with coevally overestimation of the affected areas in several sub-regions. In particular cases, the DEM could not reproduce the surface correctly. In these cases the model results differ from the documented process areas and can not be improved by varying the model parameters (e.g. with reduced lower alpha angles, Fig. 9.5-1). Using the average alpha angle of the test area (26 °) tends to underestimate the process area in many cases.
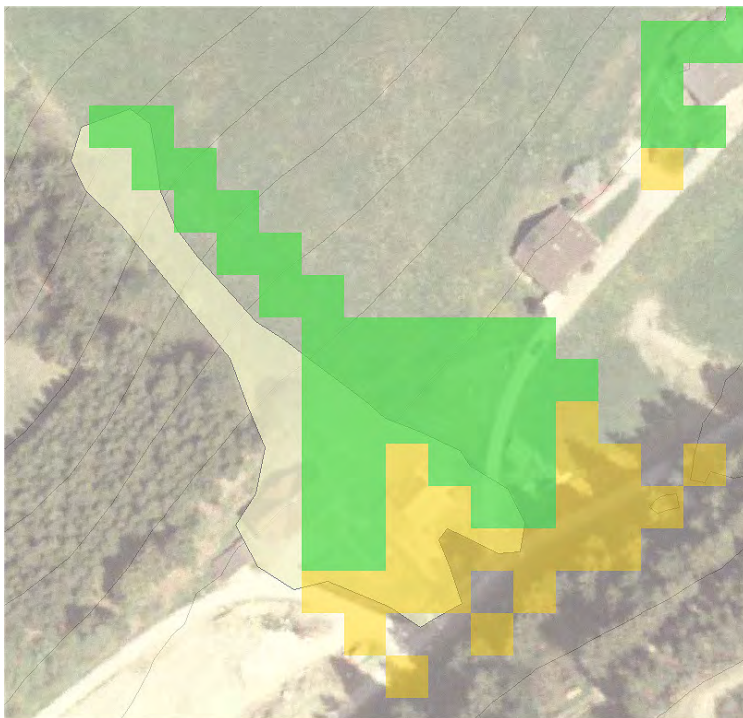
Fig 9.5-1: ASlide 1.0 – Single point starting zone, landslide and ongoing debris flow in Gasen (one example of about 50 assessed process areas). White: Documented (reconstructed) process area. An alpha angle of 17 ° (yellow) overestimates the process area in this case. The alpha angle of 22 ° leads to a slight underestimation of the process area. However, an essential part of the deviation (model results - documented process area) is caused by the impreciseness of the DEM

Based on practical experience and application of other models, it is known that concave surface structures increase the range of debris flow by concentrating the mass and reducing friction forces. In the model, these structures are calculated for each cell from the DEM to consider these effects by changing the alpha angle. Applications based on the DEM10 showed that information on small structures had been inadequate. But as small debris flow volumes mostly occurred in the test area, this information is crucial. Generally, effects of increasing weighting of curvature in the model include the concentration of the flow to concave structures and the increase of runout length. The spread is increased by convex structures and the runout length decreased. Although the model is designed to simulate landslides and debris flow on planar slopes and not for channels, model results considering the curvature show enhanced and generally plausible results.

Model approaches with higher resolutions certainly showed better adjustment to surface structures, especially channels. However, with increasing resolutions, new challenges arise. Small structures which are not displayed in a DEM 10 but displayed e.g. in a DEM1 (e.g. forest roads) lead to a changed flow path. These effects may lead to an increase and/or misinterpretation of affected areas because, in reality, debris flows often cross such structures without relevant changes of the flow direction. Therefore, higher resolutions do not necessarily lead to better results. Considering the aim of the assessment at a regional scale and the usual resolution of the base indicating the starting points of the model runs (susceptibility map 50 * 50 m), a DEM10 or DEM5 calculated on the base of a DEM1 might be most suited for this area. However, further verifications in this issue were not possible because a an area-wide DEM1 was not available.

9.6 Modelling Based on Susceptibility Maps

The real aim for developing this model was to complete the information of landslide susceptibility maps. Therefore, the ASlide model is designed to calculate area-wide information of starting information in raster (pixel) form. For the model runs and to show the results, the starting information of the "best of five" landslide disposition map, level low (compare Chapter 8) are the basis. The Annex comprises the corresponding model results for the starting information of the landslide-disposition map level high.

The first issue running the model on this starting information concerns the starting criterion. The model allows to define a threshold regarding the landslide disposition. When the pixel information exceeds this threshold, the model identifies the pixel as triggering point and starts to calculate the runout length.

The determination of this threshold affects the calculated process area considerably. Though there are functional aspects determining this threshold, it is finally also a political decision which "residual hazard" will be acceptable. For the test area, a threshold of 0.5 is supposed, which is on the one hand the medium disposition value (0 – 1). On the other hand, this disposition level seems to be a suitable compromise between the recognition rate of the mapped landslide starting zones (nearly 80%) and the percentage of the indicated area in relation to the whole test area (about 25 %). It is also the breakpoint in the relation between recognition rate and indicated area, where the "area consumption" passes the recognition rate (angle of the function > 45 ° Fig. 9.6-1; compare also Chapter 8). However, this value displays the

relative disposition of landslide probability on the base of the mapped events and cannot be transformed to absolute, comparable values of probability (Chapter 7).
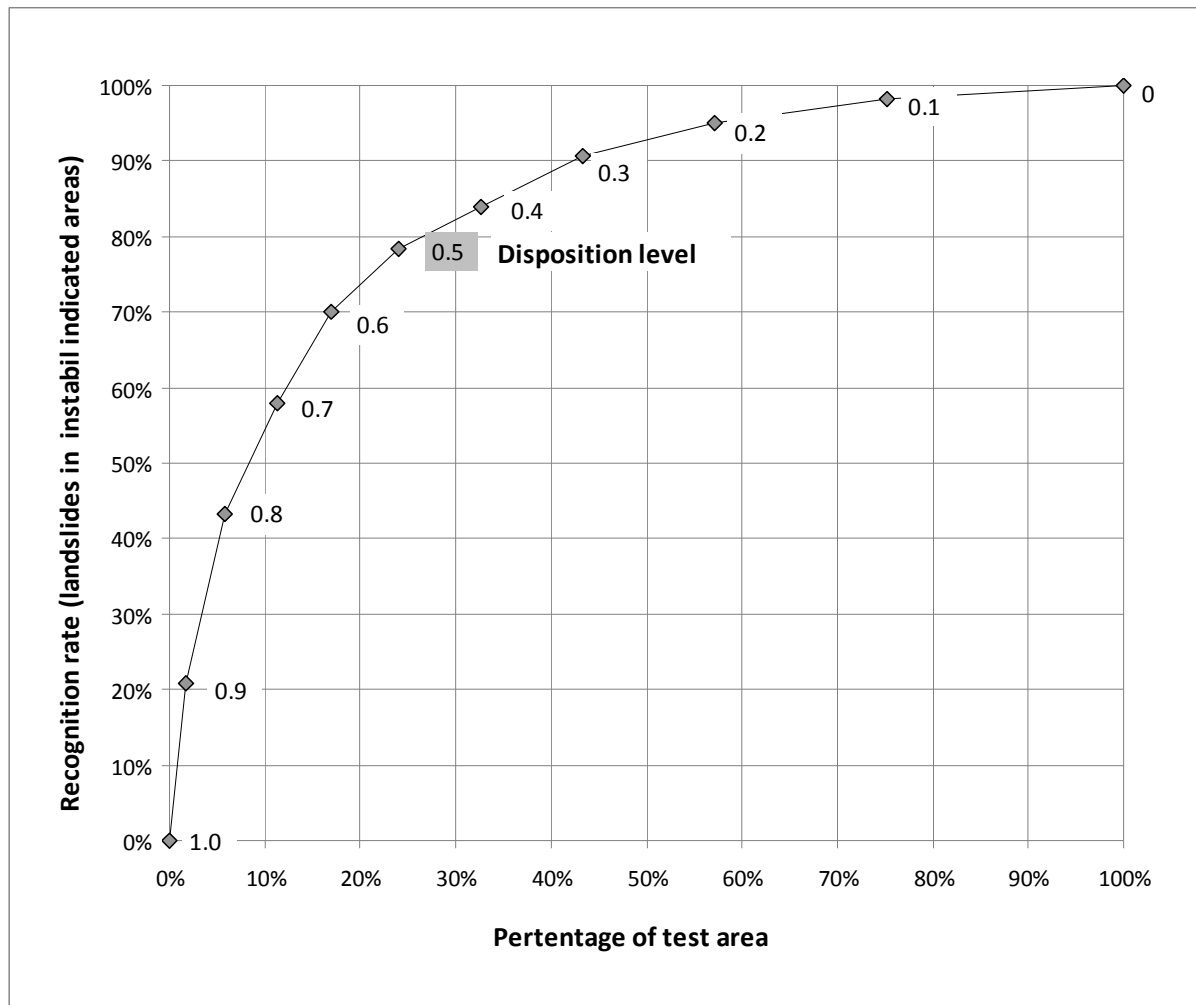
Fig. 9.6-1: Relation between disposition level, recognition rate (of the susceptibility map, complete dataset best result, level low) and percentage of the test area

Running the model the user has to decide between two opportunities of results. Either all effected areas can be marked by

1. an unique value or
2. the disposition value can be overtaken

Add. 1:

Fig. 9.6-2 shows the simplest kind of results which can be achieved with the model, compared with the massmovement – hazard map and mapped areas affected in the 2005 event. Each pixel which is affected by landslides will be marked with 1. This kind of result allows only the interpretation "affected of landslides or not" – it is not evident if this classification results from the disposition map or from the ASI-model.
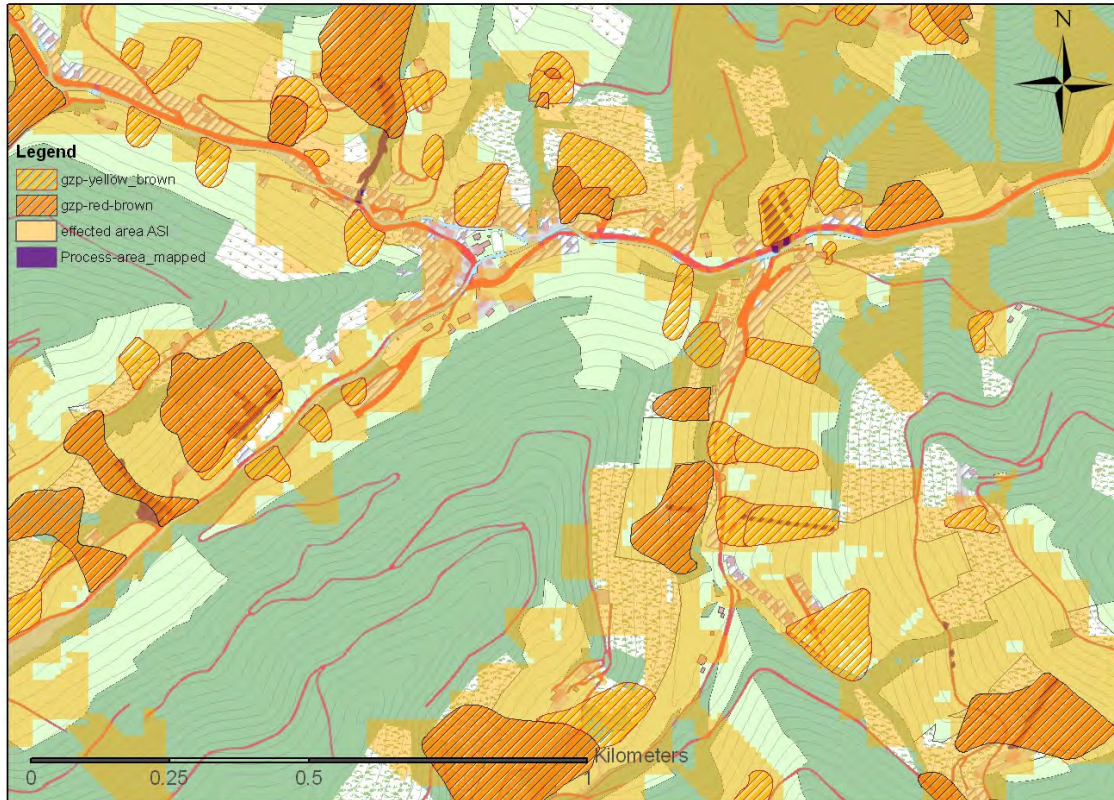
Fig. 9.6-2: ASI model run for the centre of Gasen (with alpha = 17 ° - lower limit/ maximum extent and other adjusted model-parameters, marked yellow). The process area of all selected and mapped landslides (violet) is indicated as process area as well as most of the area indicated as endangered by the hazard map. Considerable parts of the area are indicated as process-area only by the model results

Transferring the model results into a GIS allows to merge them with the disposition map and to receive therefore the additional information, if the indication results from the disposition map or from the runout-length model (Fig. 9.6-3). The relation of the area indicated by the disposition model and additional areas indicated by the runout-length model can be displayed as well as parts of the process areas which are only affected by the transport processes. As shown in Fig. 9.6-3, most of the affected areas as determined by the "runout length-model" have already been identified as areas of high landslide disposition by the hazard index map. This is reasonable because of the importance of the slope angle in both models. Furthermore, the test area has small surface structures and a predominant landslide disposition on lower slopes causes a short transport length. Combined with the 50 * 50 m resolution of the disposition model, which also covers flat areas, the extent of additional areas displayed as endangered areas because of transport processes may be assessed as being relatively low in this area. This underlines the high relevance of the quality of starting information as appointed by the quality of the disposition map and the starting criteria (threshold) – agreements.

Merging model runs with different parameterization allow estimating areas with higher and lower probability of landslide transport processes (Fig. 9.6-4). It is noted

that this information contains only the probability of the transport process (if the landslide is already triggered) but not the probability of landslide triggering.
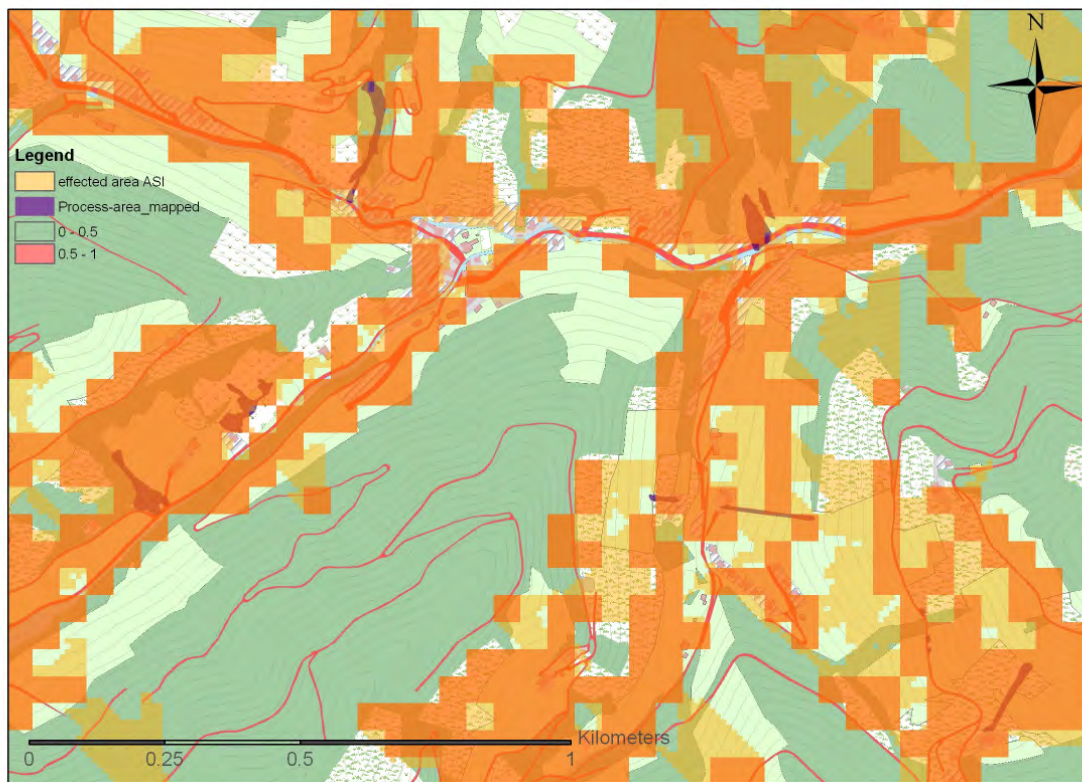
*Fig. 9.6-3: Comparison of endangered areas based on a susceptibility map (50*50 m Susceptibility >0.5 orange and modelling results (basis 10 * 10 m DEM with the runout-length model (yellow), same features as in Fig. 9.6-2. The yellow areas have to be additionally considered as affected by mass-transport processes*
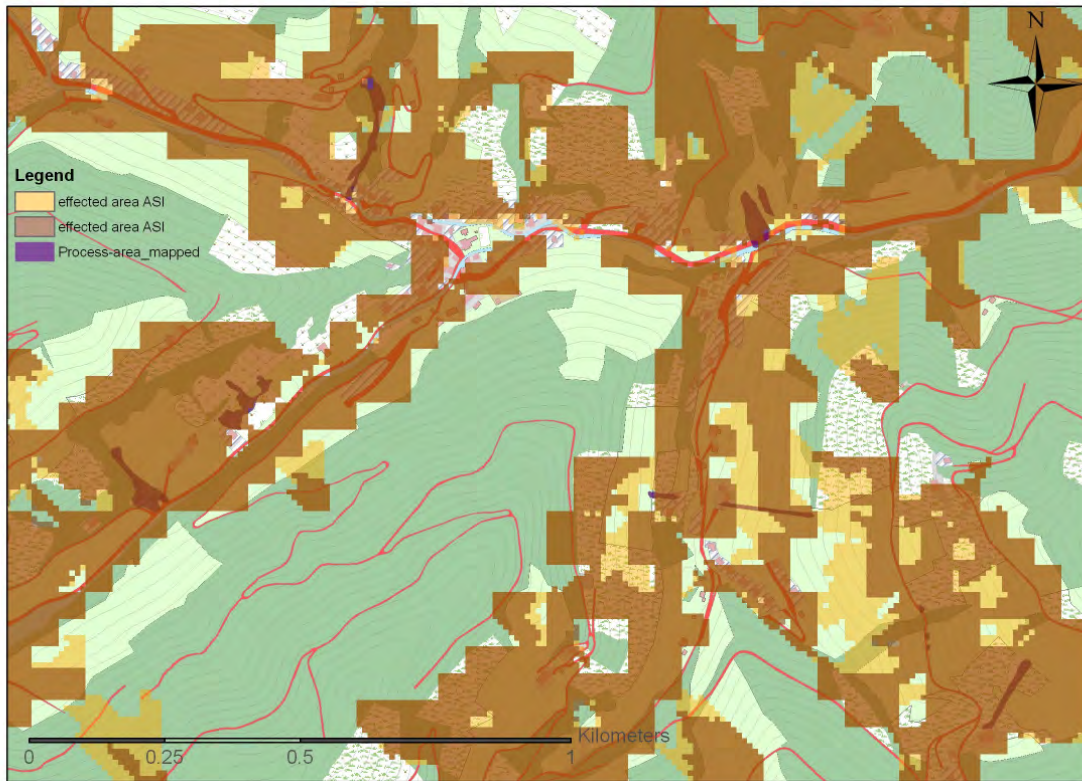
Fig. 9.6-4: Comparison of (by the ASI model) indicated areas with alpha best results (22 °, brown) and alpha lower limit (17 °, yellow). For the area of the existing buildings in Gasen the modification of the alpha angle has a low impact, only in the SE of the shown section the sensitivity is higher, other features are the same as in Fig. 9.6-2

Add. 2:

Fig. 9.6-5 (Fig A4 in the Annex for the whole test-area) shows the model results overtaking the disposition level from the disposition map. The affected areas are not marked with a static value as in 1 but with the level of disposition of the starting zone. In case of competing values, the highest disposition value will be stored (in each pixel). The added value of this approach is that the (relative) endangerment for each cell in combination with the disposition map and the runout-length model is shown. So, areas with a moderate landslide disposition may have to be reclassified being highly endangered because of mass transport processes from higher endangered areas above (e.g. example in Fig. 9.6-5 - circle). The results offer the best possible model information, thus the interpretation of such maps is more ambitious.
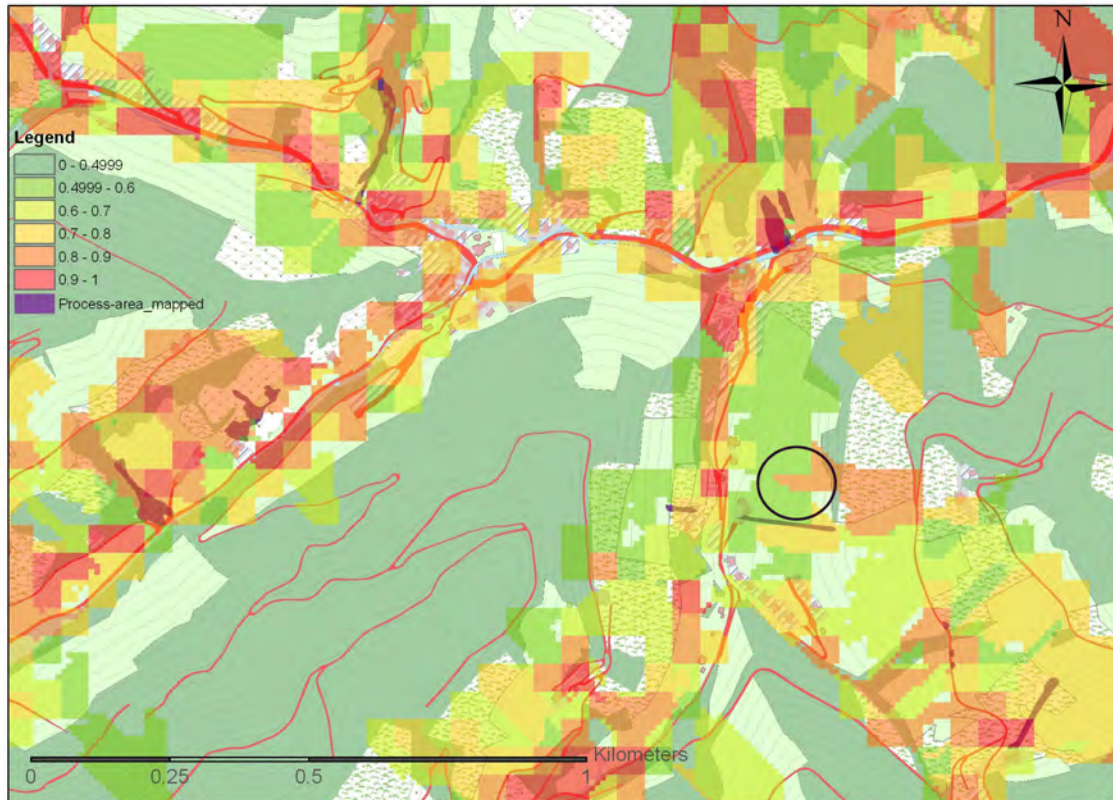
Fig. 9.6-5: Model-run with disposition values overtaken from the susceptibility map. In several areas, the endangerment is higher than indicated by the disposition map because of mass transport processes above (example see circle: The disposition value of 0.5 - 0.6 have to be raised up to 0.8 - 0.9). Other features are the same as in Fig. 9.6-2, ASl modelling with "best alpha" (22 °)

9.7 Discussion

The introduced model is designed for a local to regional determination of area-wide runout length of landslides in case of limited data availability. Hence, for detailed local-scale use, results have to be verified by additional studies. The approach estimates areas affected by mass transport processes triggered off by spontaneous, more or less shallow landslides in loose material. Thus "hot spots" should be identified.

The application of this empirical approach requires an adequate date base of documented landslides and/or slope debris flow. Since landslides and especially the runout length of landslides are not reliably recorded in detail, the application of the approach is limited.

Furthermore, the resolution of the DEM needs to display the transport-relevant surface structures. There is no generally admitted agreement concerning the scale of the DEM. It varies with different landscapes and different landslide characteristics (volume etc.) and should be revised by single point modelling. In the test area, the available DEM 10 met this requirement not always in a satisfying manner, because of the small spatial surface structures and the accuracy of the DEM which appeared to be less than 10 m.

Finally, the quality of the landslide starting information (e.g. susceptibility maps) must be as good as possible, because of its significant impact to the model results. For the determination of the starting criterion (threshold), the scientific considerations indicate a threshold of 0.5. However, this decision depends also on substantial socio-economic and administrative reasons. Further applications and the feedback of practitioners should give insights into how to deal with this issue.

The implementation of a multiple flow approach in the flow path resulted in a more realistic determination of affected areas, especially in case of convex structures such as alluvial fans. The concomitant implementation of a parameter considering the surface curvature produces more plausible model results, although the effect of this parameter is limited by the rough model resolution in relation to the small surface structures and the small debris flow volumes in the test area.

At this stage of model development, the parameterization of the model is static, which means that it is not modified by area information. For this reason, the model quality depends on the homogeneity of the modeled area. For the test region, this pre-condition was not met perfectly. An area within the community of Haslau (Amasseggerbach) showed differing landslide transport conditions. Unfortunately, there was no significant correlation found between the (assumed) area and given parameter information of the area.

Since the ASI model was designed as a simple, empiric approach, the result can only display the area affected by landslide processes, whereat the displayed results on pixel basis have to be interpreted as an assumption with limited demands of accuracy, which do not keep up with the highly displayed resolutions. Of course, the results do not allow any quantification of transport volumes, velocity and resulting forces. They have to be assessed in crucial areas with enhanced models or by expert knowledge in the field to define obligations restrictions or protection measures. The optionally displayable probability is overtaken from the disposition map and are therefore (in this project) of an area-specific, relative value.

When assessing the model results, it turned out that we do not have adequate methods to evaluate regional model results in an objective and transparent way. Assessment of model results on the basis of documented single events amended by expert knowledge and other model approaches may be sufficient for model calibration, but it is not an adequate tool to evaluate the model results in a comparable way.

10. Potential of Methods regarding Susceptibities Under Changed Frameconditions (Climate Change, Land-Use Change)

10.1 Basics (Climate Change, Land Use)

While the complex systems of landslide processes depend on several parameters, climatic and especially precipitation conditions are the major direct triggering factor. Different kinds of land use may considerably influence the pre-triggering conditions on the one hand and on the other hand, they are relevant for the possible damages eventually caused by a landslide-event. Due to that fact, changes of these factors are relevant for the landslide process itself, and for the magnitude of property loss (Fig. 10.1-1, Hagen & Andrecs 2011). Climate Change became a quiet popular theme within the last years, land use changes have been associated with socioeconomic development since a long time.
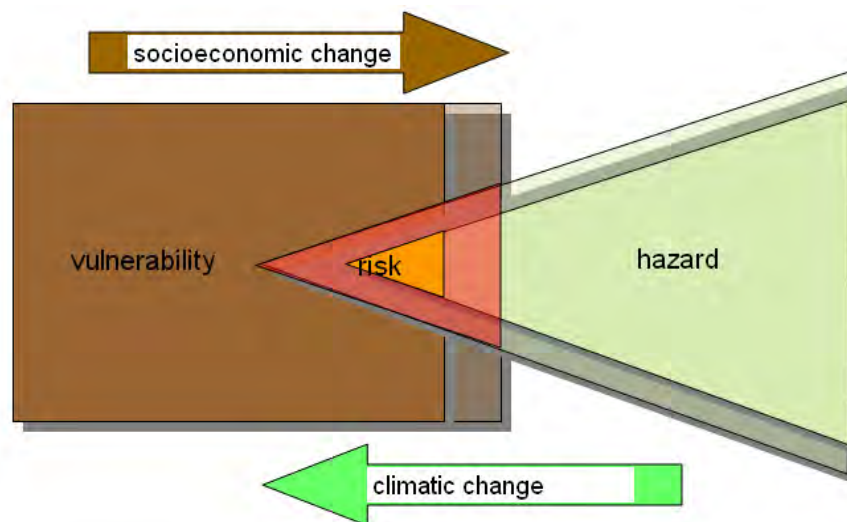
Fig. 10.1-1: Schematic relation between risk, hazard and vulnerability. Changes of hazard as well as vulnerability (caused by socioeconomic development) may abate or boost the risk

10.1.1 Climate Change – Facts and Assumptions

Earth history tells us that there have always been temperature changes driven by various reasons. However, according to the Fourth Assessment Report of IPCC (2007), global warming is already a fact (amount to about + 1,5 °C in the Alps, including regional variations (e.g. Reinhard Böhm, 2009). It will continue (which is virtually certain) in the 21st century, depending on the development of greenhouse gas emissions (Fig. 10.1.1-1).
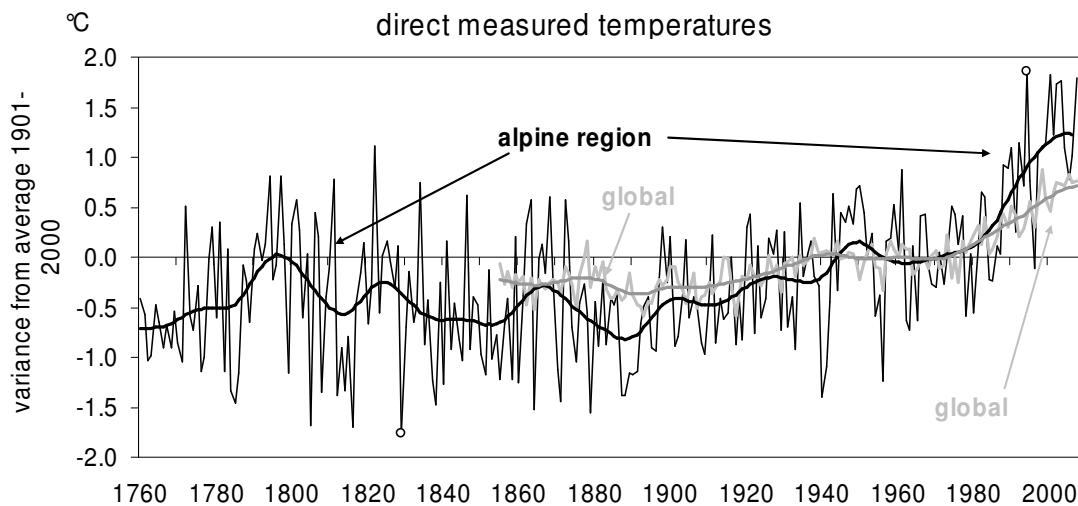
Fig. 10.1.1-1: The region of the Alps seems to be particularly susceptible to climatic impacts; the variance of temperature is more visible in this region than in the global trend. HISTALP (Auer at al. 2007 and Böhm et al. 2009)

Since the parameter temperature is not relevant to landslide processes, its rise will not affect landslide processes and dispositions directly. A fortiori, the assumed accompanying effects, namely the impact of precipitation behavior have to be considered. Changes of land cover due to climatic change (changed forest species, increasing number of forest fires and wind blows etc.) may also influence the dispositions of slopes for landslides, but this thematic field is far too complex to deal with in this project.

According to the IPCC report, it is very likely that heavy precipitation events have already increased in most areas, and this trend is likely to continue. For Central Europe (Christensen et al 2007, Andrecs et al. 2010) summer precipitation will decrease with drought but extreme precipitation events are likely to increase (prediction highly model-dependent). Winter precipitation will increase as well as extreme precipitation events (in magnitude and frequency) while snow cover will decrease.

Presumably, in Austria, precipitations during the summer months are likely to decrease while winter precipitation will increase. However, conclusions on heavy rainfall events can only be drawn to a limited extent.

For the test bed (communities of Gasen and Haslau) the precipitation event (including the high preprecipitation amount) must be considered as not having been measured before, which means a period of about 120 years (Tab. 10.1.1-1, Andrecs et al 2007). Although this was an extreme event, it is not serious to draw conclusions from this single event to an ongoing climate change. Linked with other extreme events it might be a small part of the "Global Puzzle".

Tab. 10.1.1-1: Precipitation sums of the gauging stations of the Hydrographische Landesdienst Steiermark in the region of Gasen and Haslau, (2005). It shows up a significant spatial variation which can not be explained by topographical issues – compare Chapter 5.5)

Station	Lage Gebiet	Stationsdaten		Ereignis	
		SH (m)	N seit	$N_{Tag/Max}$ (mm)	N_{2T} (mm)
Birkfeld	O	680	neu/ 1893	64	124
Breitenau/Mixnitz	W	560	1921	60	118
Fladnitzberg	SW	1070	1988	100	169
Hohenau a.d.Raab	S	702	1981	**135**	**191**
Schanz	N	1230	neu	85	107
Stanz	NW	648	1936	67	128
Teichalm	W	1175	neu/ 1897	(58)	(92)

10.1.2 Land Use Change

The history of settlement and socioeconomic development is (not only in the Alpine space) also the history of land use and its changes. Land use is a relevant factor within landslide triggering conditions.

Generally, forest cover is assumed to decrease the landslide disposition because of the mechanical stabilisation of the soil by the roots and an increased Evapotranspiration potential. However, also the additional weight of forest stands might be relevant.

In Austria, the forest cover is continuously increasing (Fig. 10.1.2-1), mainly because of the artificial or natural reforestation of former agricultural used areas (meadows, mountain pastures).
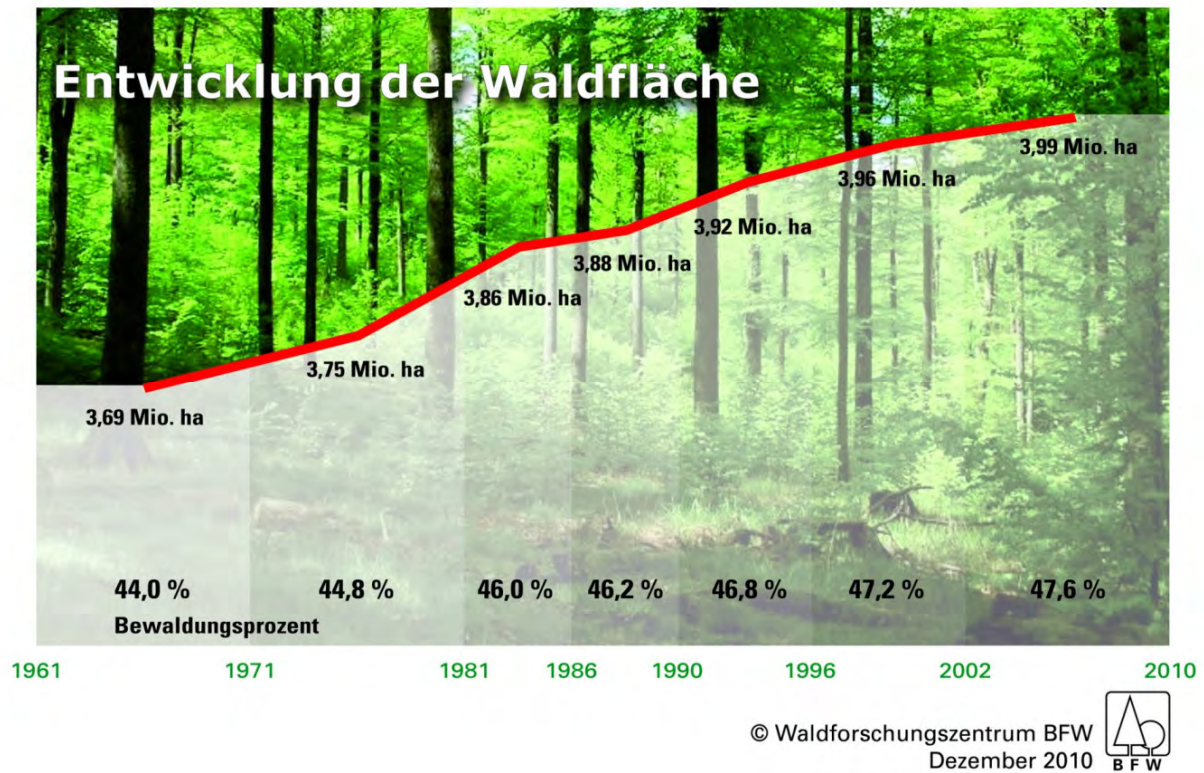
Fig. 10.1.2-1: Development of forest cover in Austria (Russ 2011)

Constructions can influence the landslide disposition in both directions. Slope draining, retaining walls, geotextiles etc. should reduce it, constructions with steep slopes, raised and inadequately stabilized material may increase the landslide disposition considerable as it was observed in the test bed in 2005.

Our awareness of natural disasters such as landslides is primarily associated with the extent of losses, respectively with the risk of losses. The term risk is defined as the product of hazard and vulnerability. Calculating vulnerability means to determine the number of affected objects and their resistance against the potential damage. Fig. 10.1.2-2 shows the increase of buildings in Austria, from 1951 to 2001 (from 916.448 to 2.047.712 buildings). It indicates that, in Austria, the socioeconomic development is probably more responsible for increasing losses than effects of climate change. Furthermore, it is necessary to consider not only the absolute monetary losses, but also the consequences of these losses for the communities.
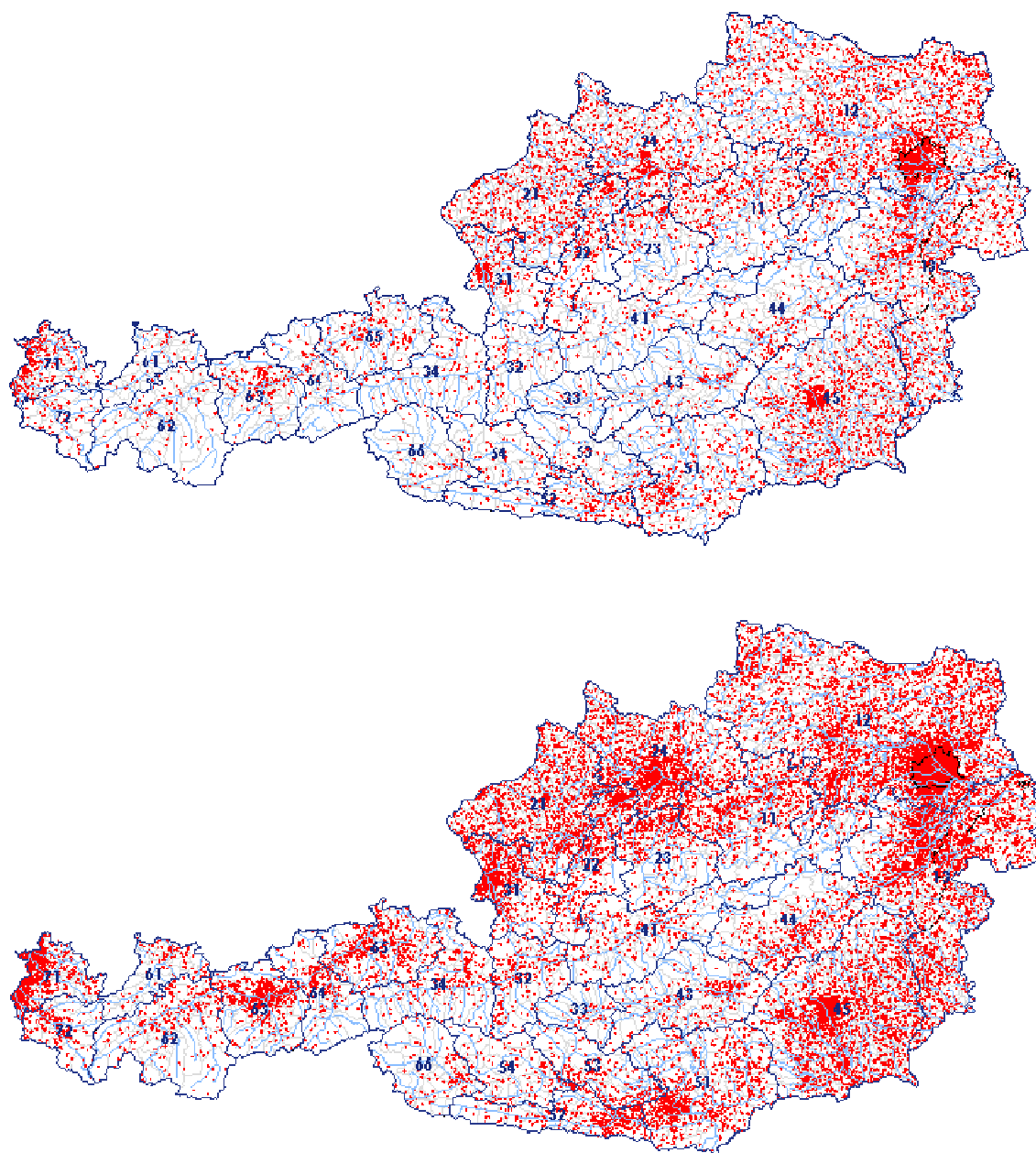
Fig. 10.1.2-2: Building census, Austria 1951 – 2001, every red point is representing 100 buildings. (WIFO, 2008 based on Statistics Austria)

10.2 Producing Susceptibility Maps based on Neural Networks that take into Account Variable Precipitation Sums and/or Changes in Land-use

Summary of scenario calculations

Plausible scenarios for changed land-use and variable precipitation can be calculated using neural networks. Concrete information for spatial planning can be derived on the basis of these scenarios, and the methodology used also makes it technically possible to incorporate climate-change precipitation scenarios into landslide-disposition modelling.

With the **land-use scenarios** "complete deforestation" and "complete reforestation," there was a strong increase in process-oriented susceptibility in large areas of deforested land and a strong reduction in process-oriented susceptibility in reforested areas respectively. This underlines the strong influence of the parameter map "forest" on modelling and thus on susceptibility.

In the case of the **scenarios "area-wide maximum event-precipitation**," the results calculated with the parameter map *precipitation "level low"* showed only a moderate rise in susceptibility in areas that originally had low precipitation, although some false or implausible values did occur. On the other hand, the results calculated for these areas on the basis of the parameter map *precipitation "level high"* displayed a strong increase in susceptibility, which almost equalled the magnitude of the increase with land-use scenarios. No more false values occurred here. This can be attributed to the parameter map *precipitation "level low"* having only a weak and unclear influence on modelling, whereas the parameter map *precipitation "level high"* has a strong and clear impact.

For the model results obtained using "level low" and "level high" parameter maps, only one "worst case" (complete deforestation) land-use scenario was calculated in each case, and one "best case" (complete reforestation). In addition, "worst case" (maximum) and "best case" (minimum) precipitation scenarios were calculated, assuming an area-wide equal precipitation based on the parameter maps "level low" and "level high." The values for minimum and maximum precipitation sums are based on the event-precipitation in the area studied during the period 21-23 August 2005. The land-use scenarios were calculated using runs without the parameter *event precipitation*, in which by using the runs 10 and 33, one of the best "level low" and "level high" runs respectively were chosen. For the precipitation-scenarios, it was necessary to select runs that contained the parameter *event-precipitation*. Here, with run 23 for "level low and run 58 for "level high" respectively, one of the best results was selected in each case.

10.2.1 Changed land-use scenarios

Fig. 10.2.1-1 now shows the "worst case" land-use scenario (complete deforestation) for the "level low" run 10. The large areas of greater susceptibility are clearly visible here, which can be attributed to a strong increase in susceptibility in the formerly forested areas of the result for run 10 (Fig. 7.2.2.1-8). This in turn underlines the strong influence of forest on modelling, and thus on process susceptibility.
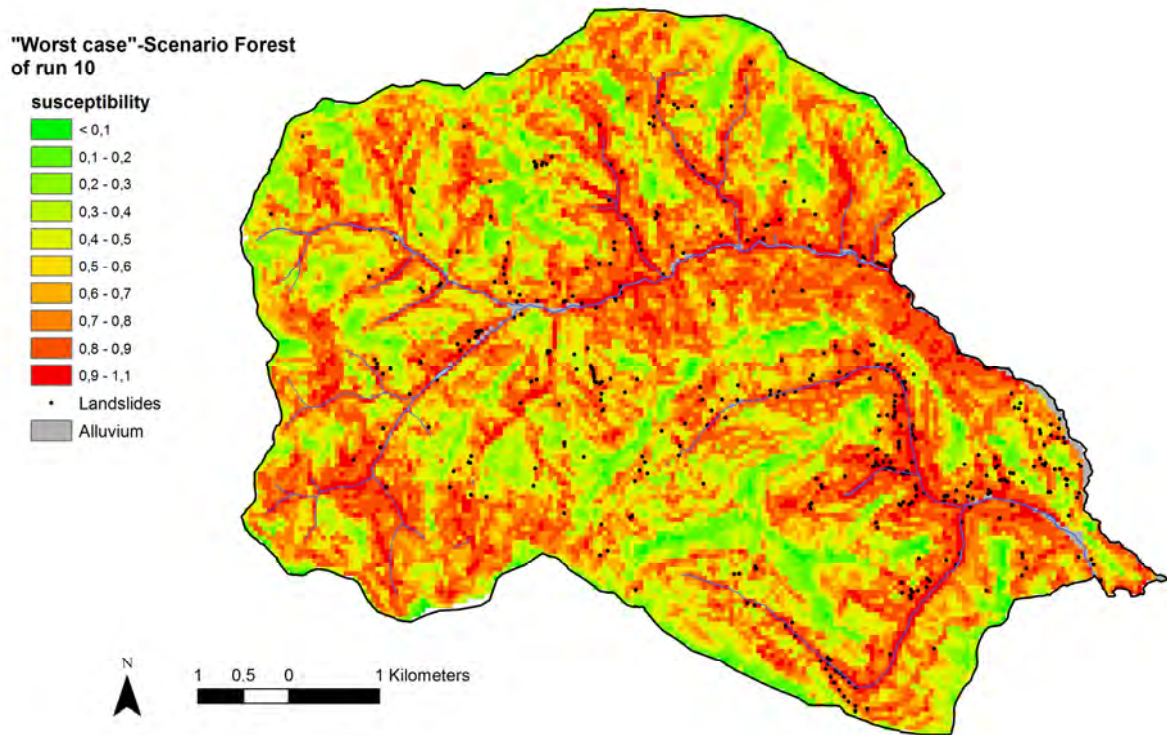
Fig. 10.2.1-1: "Worst case" scenario, forest (complete deforestation) of run 10

Fig. 10.2.1-2 presents the difference map of the result of run 10 and the "worst case" land-use scenario of run 10. The map clearly shows very negative differences. This would mean that deforestation had now resulted, without exception, in an increase in susceptibility (blue) in formerly forested areas, and had resulted in no change in susceptibility (white) in the areas without forest. The differences are obviously greater than those seen with the precipitation scenario "level low" (Chapter 10.2.2), and nowhere is there a decrease in susceptibility (red), as is the case with the precipitation scenario "level low." This illustrates, on the one hand, that the neural networks react in the desired and expected way to changes in land-use. On the other hand, it also demonstrates the obviously stronger and more unequivocal influence of forest compared to precipitation "level low."

Difference of run 10 and "worst case"-scenario forest of run 10

susceptibility

- < -0,5
- -0,5 - -0,4
- -0,4 - -0,3
- -0,3 - -0,2
- -0,2 - -0,1
- -0,1 - -0,01
- -0,01 - 0

Alluvium

N

1   0.5   0   1 km
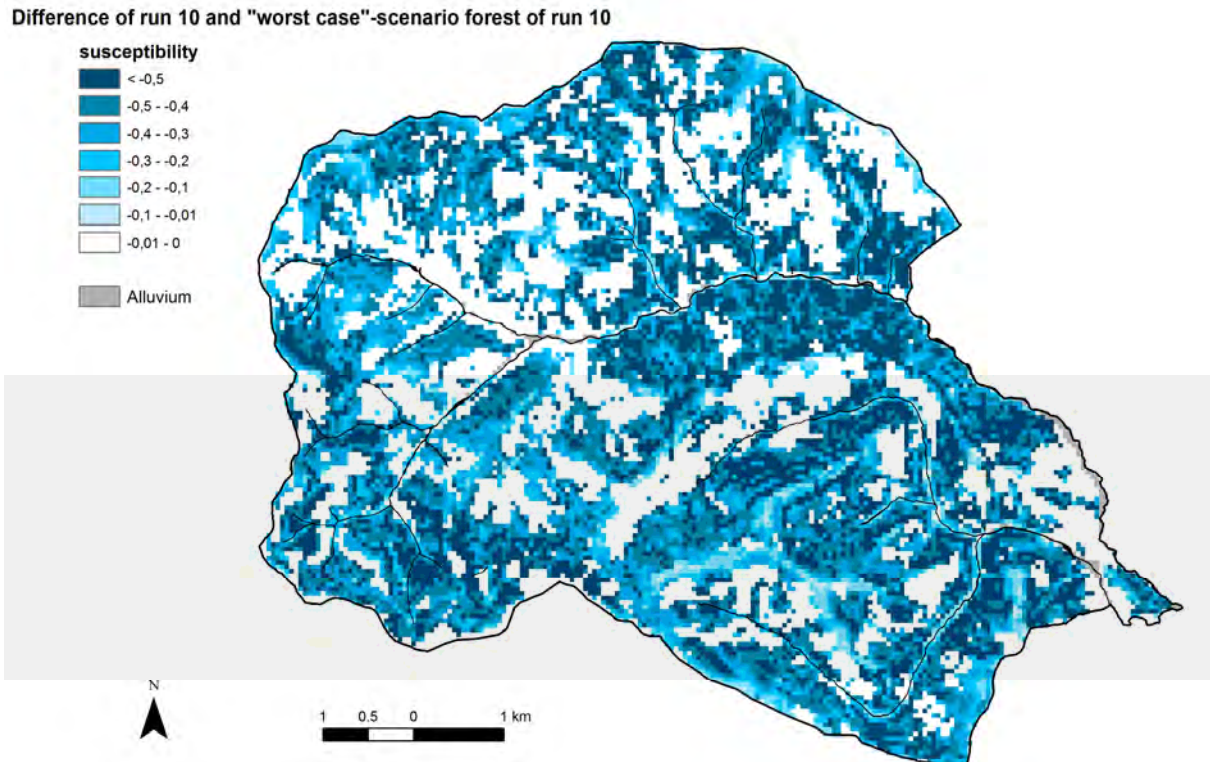
Fig. 10.2.1-2: Difference between run 10 and "worst case" scenario forest of run 10

Fig. 10.2.1-3 shows, by comparison, the "best case" land-use scenario (complete reforestation) for the "level low" run 10. It shows very large areas of low susceptibility and also major changes compared to the result of run 10 (Fig. 7.2.2.1-8). Due to reforestation, there is now usually a clear decrease in susceptibility in formerly unwooded areas compared to the result of run 10, while susceptibility remains equally high in forested areas. Here too, the decrease in susceptibility is stronger than that seen with precipitation "level low," and nowhere is there an increase in susceptibility, which again points to the obvious and unequivocal influence of forest on modelling.

"Best case"-Scenario Forest
of run 10

susceptibility

- < 0,1
- 0,1 - 0,2
- 0,2 - 0,3
- 0,3 - 0,4
- 0,4 - 0,5
- 0,5 - 0,6
- 0,6 - 0,7
- 0,7 - 0,8
- 0,8 - 0,9
- 0,9 - 1,1
- Landslides
- Alluvium
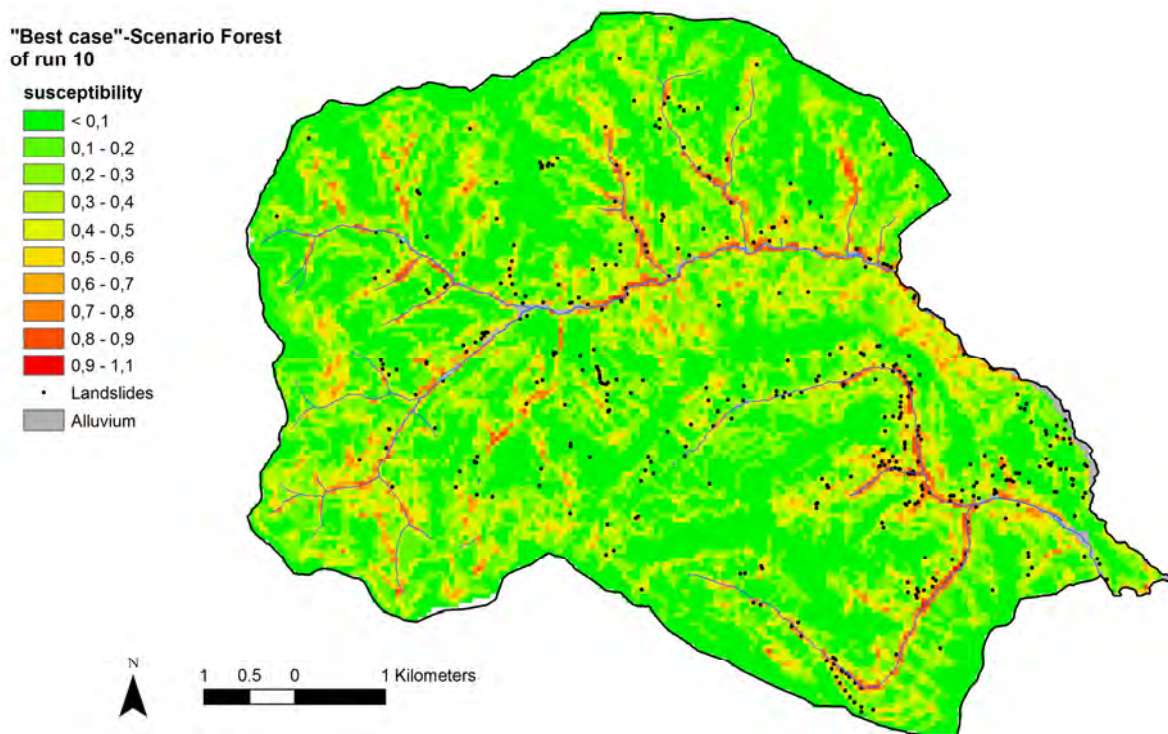
Fig. 10.2.1-3: "Best case" scenario forest (complete reforestation) of run 10

The land-use scenarios of the "level high" run 33 show largely the same picture as the "level low" results of run 10. The changes in susceptibility here occur in approximately the same dimension as in run 10, however they are slightly higher than those of the precipitation scenario "level high." This is due to precipitation "level high" having an obviously stronger influence on the result than "level low" precipitation (Chapter 7.2.2.2).

The possible negative and positive consequences of deforestation and reforestation respectively are impressively reflected by these scenarios. These kinds of land-use scenarios could be a valuable tool for spatial planning, because concrete statements can be made about the way area-specific deforestation or reforestation will affect process susceptibility (Where should forest by no means be cleared, and where would clearing have no impact?). Where could reforestation have a positive effect on process susceptibility, and where would it not?

10.2.2 Variable precipitation scenarios

Fig. 10.2.2-1 now shows the "worst case" precipitation scenario for the "level low" result 23. Compared to the result of run 23 (Fig. 7.2.2.1-11), it generally shows an in increase in susceptibility in areas with originally lower precipitation in the east and west, and approximately constant susceptibility levels in areas of originally very high precipitation in the north and south of the study area. However, the changes compared to run 23 are moderate and thus obviously smaller than the changes in the

land-use scenarios (Chapter 10.2.1). This is due to the rather weaker influence that precipitation "level low" has on the modelling result (Chapter 7.2.2.1).
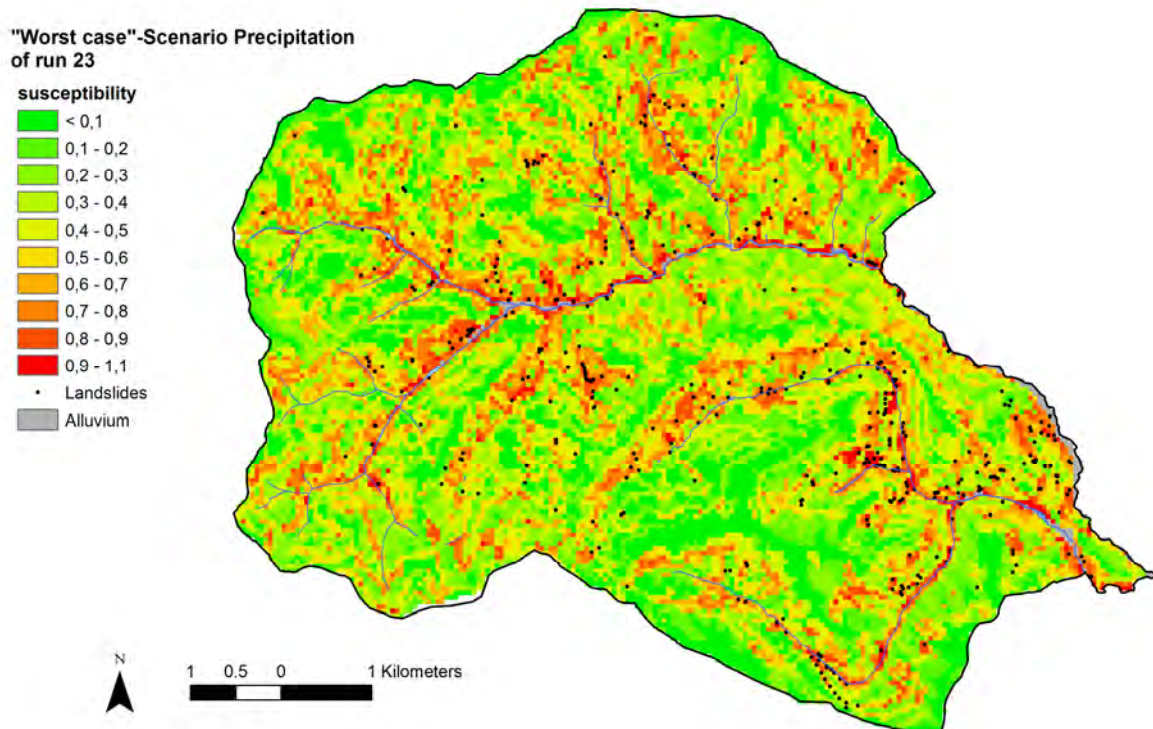
Fig. 10.2.2-1: "Worst case" scenario, precipitation of run 23

These facts can be seen even more clearly in Fig. 10.2.2-2, which shows the difference map of the "worst case" precipitation scenario of run 23 and run 23. Here, the increases in susceptibility with this scenario, compared to run 23, are shown in red, constant susceptibilities are shown in white, and decreases in susceptibility in blue. It is shown that with this scenario, despite the increase in precipitation, there are isolated examples of a decrease in susceptibility, which does not correspond to reality from a process-oriented point of view. The reason for this is that the connection between mass-movement distribution and the parameter precipitation "level low" is not that clear to the neural network, which is why this parameter plays only a rather weak role in the modelling, which in turn does not produce unequivocal results.

Difference of run 23 and "worst case"-scenario precipitationof run 23

susceptibility

- < -0,2
- -0,2 - -0,1
- -0,1 - -0,05
- -0,05 - -0,01
- -0,01 - 0,01
- 0,01 - 0,05
- 0,05 - 0,1
- 0,1 - 0,2
- > 0,2

Alluvium
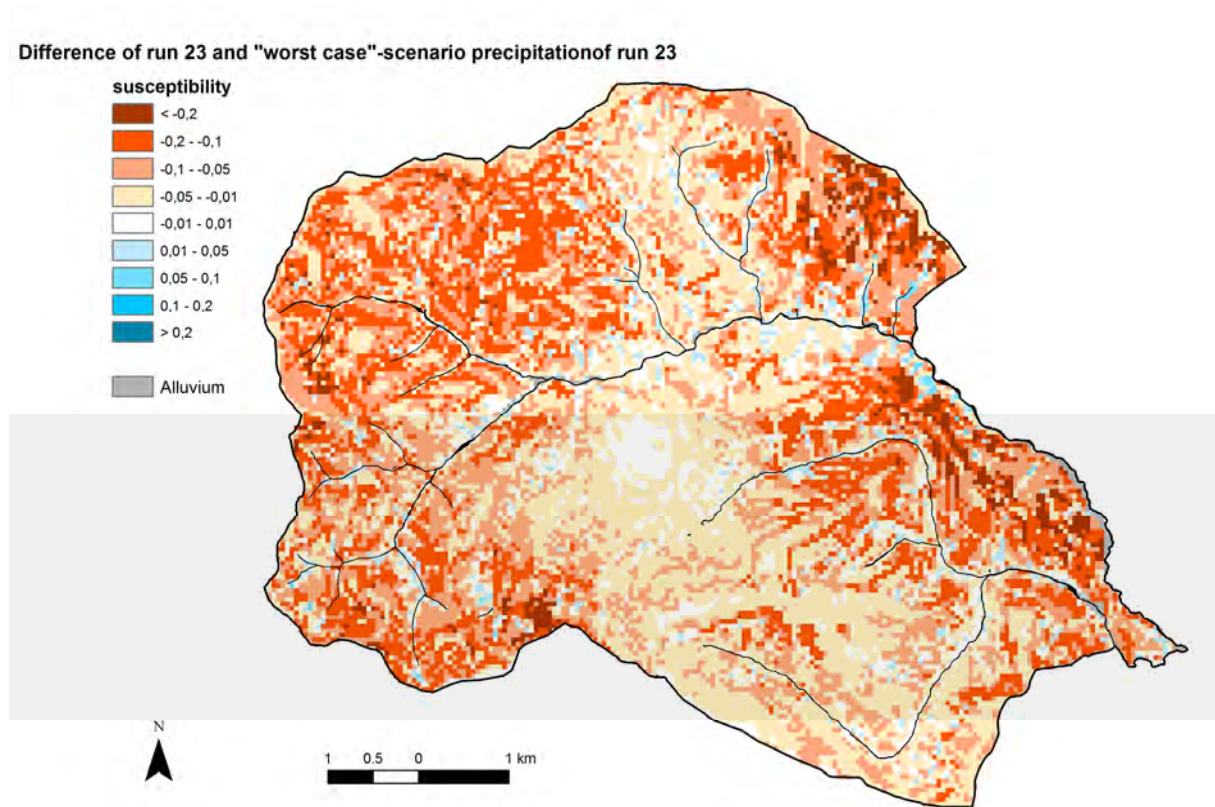
Fig. 10.2.2-2: Difference between run 23 and "worst case" scenario precipitation of run 23

However, the situation is presented differently in the "worst case" precipitation scenario of "level high" run 58 (Fig. 10.2.2-3 and 10.2.2-4). Here there is an obvious increase in susceptibility compared to run 58 in the areas that originally had low precipitation in the northeast and west. These increases are much more pronounced here than they are in the "worst case" scenario of run 23 (Fig. 10.2.2-2). Furthermore, these increases display almost the same magnitude as the changes caused by the land-use scenarios (Chapter 10.2.1). Also, in contrast to the "level low" precipitation scenario, no decreases in susceptibility (blue) can be seen with higher precipitation. All of this can be attributed to the obvious influence of "level high" precipitation on modelling, this influence being much greater than that of "level low" precipitation (Chapter 7.2.2.2). Generally speaking, this strong increase in susceptibility strikingly demonstrates that in case of precipitation reaching the maximum level of the event in August 2005, large areas that had remained stable due to the distribution of precipitation during the 2005 event might still become unstable.

"Worst case"-Scenario Precipitation
of run 58

susceptibility

- < 0,1
- 0,1 - 0,2
- 0,2 - 0,3
- 0,3 - 0,4
- 0,4 - 0,5
- 0,5 - 0,6
- 0,6 - 0,7
- 0,7 - 0,8
- 0,8 - 0,9
- 0,9 - 1,1
- · Landslides
- Alluvium

Fig. 10.2.2-3: "Worst case" scenario precipitation of run 58

Difference of "worst case"-scenario precipitation of run 58 and run 58

susceptibility

- < -0,2
- -0,2 - -0,1
- -0,1 - -0,05
- -0,01 - -0,05
- 0,01 - -0,01
- 0,01 - 0,05
- 0,05 - 0,1
- 0,1 - 0,2
- > 0,2

- Alluvium

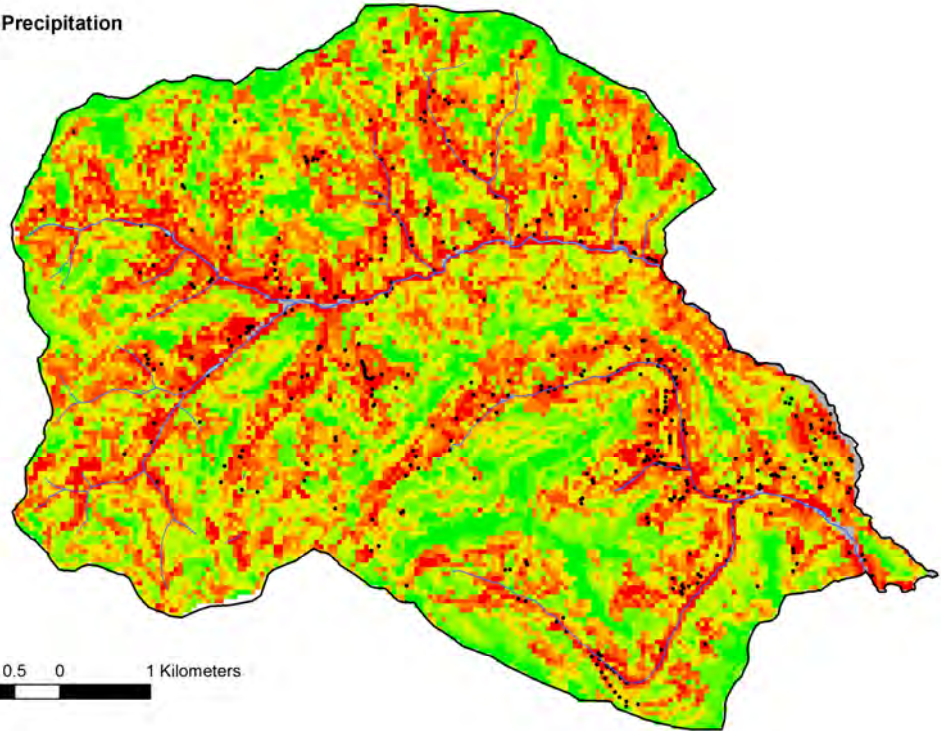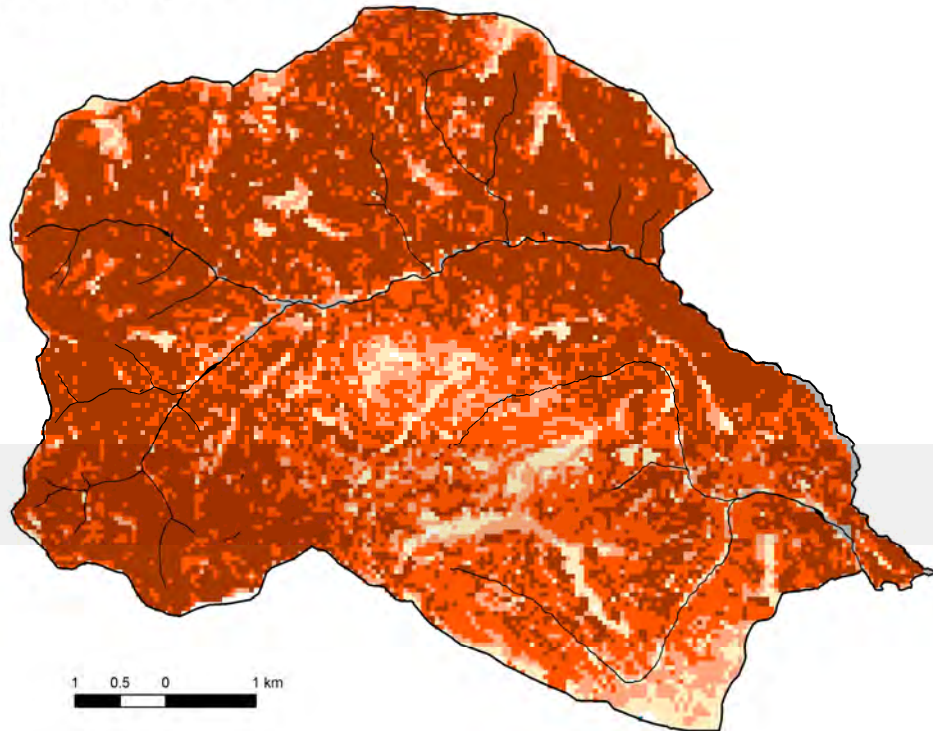*Fig. 10.2.2-4: Difference between "worst case" scenario precipitation of run 58 and run 58*

It was therefore demonstrated that using neural networks, it is basically possible to calculate plausible scenarios based on an assumption of changed precipitation conditions, because the parameter *precipitation* had the expected and correct influence on the results. Therefore, in the future, scenarios relating to changed precipitation conditions due to climate change can be calculated in a similar way, provided reliable data on these conditions is available. However, it should be kept in mind that such scenarios, like the scenarios calculated here, do not take into account the important variables of antecedent soil moisture, precipitation intensity, and precipitation duration. Furthermore, it is unclear at what threshold values the correlations between precipitation-sum and existing/previous gravitational mass movements that have been incorporated into the model will still be valid (exceedance of soil infiltration capacity, for example).

Based on the model calculations carried out, it can be said that the parameter precipitation "level high" is better suited for modelling than the "level low" variant, because it plays a stronger role in modelling, and no unrealistic differences in process susceptibility were calculated.

10.3 Susceptibility Maps Based on Logistic Regression with Consideration of Variable Precipitation Sums and/or Changes in Land-use

The development of the statistical models was based on the landslide inventory of the August 2005 event exclusively (Chapter 6.1). Furthermore when involving precipitation related parameter maps in specific modelling runs also the data of this event were used (*NS_lg* and *NS_lh*, cf. Chapter 5.5). Therefore strictly speaking these modelling results are valid only for the specific scenario of the August 2005 event.

In order to overcome these limitations and to exclude influences caused by the specific precipitation pattern of the August 2005 event some runs showing the best validation indices and involving *NS_lg* (run23) or *NS_lh* (run 58, 66 and 67) were recalculated with the scenario of uniform precipitation (arithmetic mean of the realistic precipitation as presented in *NS_lg* and *NS_lh*). These runs were named 23mc, 58mc, 66mc and 67mc, the "mc" standing for "mean case".

Aiming at hypothesising a different precipitation event run 58 was recalculated as well with highest intensities uniformely covering the whole test area (runs 58c, 58d - worst case, cf. Chapter 10.3.2).

Furthermore a different scenario with respect to landcover (worst case: complete deforestation) was recalculated in order to identify those areas with high sensitivities to landuse modifications.

Altogether an additional 8 modelling runs were calculated aiming at modelling different scenarios with regard to precipitation and forest cover. These additional modelling runs are listed in Tab. 10.3-1.

Tab. 10.3-1: List of scenario model runs calculated with Logistic Regression

Run	Parameter Maps (abbreviations cf. Tab. 6.2.2)
23mc	Wald_Sat_lg_mb + HN-DHM10 + VW-DHM10 + Wegenetz_lg_mb + Sub_GK_lg + QDisp_lg_GK_lh_fa + NS_lg(mc)
58mc	Wald_Sat_lg_mb + HN-DHM10 + VW-DHM10 + Wegenetz_lg_mb + QDisp_lh_fa + Sub_GK_lh + NS_lh(mc)
58b	HN-DHM10 + VW-DHM10 + Wegenetz_lg_mb + QDisp_lh_fa + Sub_GK_lh + NS_lh
58c	HN-DHM10 + VW-DHM10 + Wegenetz_lg_mb + QDisp_lh_fa + Sub_GK_lh + NS_lh(max)
58d	Wald_Sat_lg_mb + HN-DHM10 + VW-DHM10 + Wegenetz_lg_mb + QDisp_lh_fa + Sub_GK_lh + NS_lh(max)
58e	Wald_DKM_lg_80 + HN-DHM10 + VW-DHM10 + Wegenetz_lg_mb + QDisp_lh_fa + Sub_GK_lh + NS_lh
66mc	Wald_Sat_lg_mb + HN-DHM10 + VW-DHM10 + Wegenetz_lg_mb + QDisp_lh_fa + Sub_GK_lh + NS_lh(mc) + BK
67mc	Wald_Sat_lg_mb + HN-DHM10 + VW-DHM10 + Wegenetz_lg_mb + BK + QDisp_lg_BK_fa + NS_lh(mc)

explanations of run numbers:

58mc = run 58 hypothesising mean case with regard to precipitation amount of August 2005 event

58b = run 58 hypothesising no forest cover

58c = run 58 hypothesising no forest cover and maximum precipitation considering August 2005 event

58d = hypothesising maximum precipitation considering August 2005 event

58e = run 58 considering Wald_DKM_lg_80 instead of Wald_Sat_lg_mb (abbreviations cf. Tab. 6.2.2)

66mc = run 66 hypothesising mean case with regard to precipitation amount of August 2005 event

67mc = run 67 hypothesising mean case with regard to precipitation amount of August 2005 event

Summarizing the results of the scenario calculations which are presented in detail in the following sections, the same conclusions can be drawn as for neural networks (Chapter 10.2): plausible scenarios for modified land-use and variable precipitation can be calculated using the logistic regression approach. Practical information for spatial planning purposes can be derived on the basis of these scenarios, and the methodology used also makes it technically possible to incorporate climate-change precipitation scenarios into landslide-disposition modelling.

10.3.1 Changed land-use scenarios

Past events (without strong winds) have indicated a significant correlation between the susceptibility of shallow landslides in loose material and the forest cover. By hypothesising a "worst case" land-use scenario (complete deforestation) and visualizing the differences in difference maps areas with particular sensitivity towards deforestation can be identified.
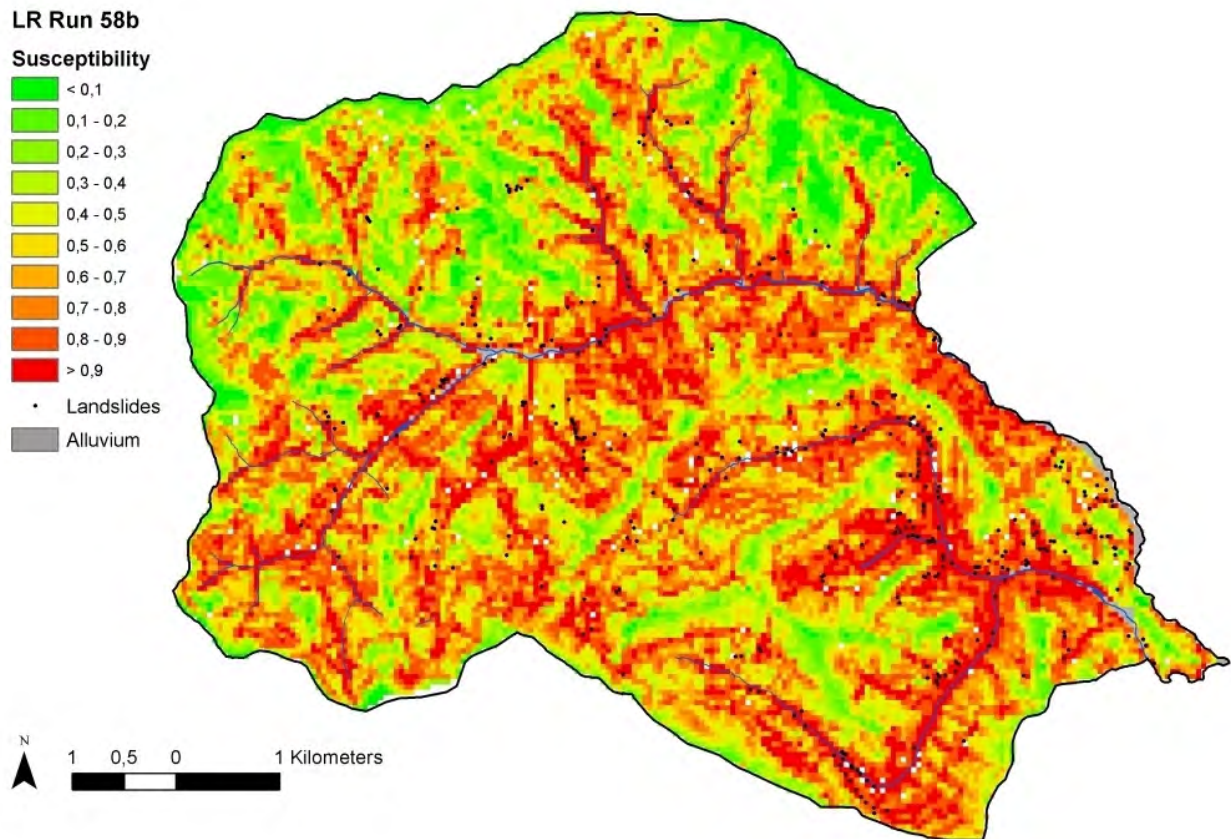
Fig. 10.3.1-1: "Worst case" scenario, forest (complete deforestation) of run 58

Fig. 10.3.1-1 shows the "worst case" land-use scenario (complete deforestation) for the "level high" run 58. Very similar to the results obtained by neural networks (cf. chapter 10.2) the large areas of higher susceptibility are clearly visible, which can be attributed to a strong increase in susceptibility in the formerly forested areas of the result of run 58 (Fig. 7.4.2.2-2). This in turn underlines the strong influence of forest on modelling, and thus on process susceptibility.

Fig. 10.3.1-2 presents the difference map of the result of run 58 and the "worst case" land-use scenario 58b for forested areas (currently open areas are shown in white), highlighting small (yellow) and large differences (red). The map clearly shows high negative differences indicating that deforestation results, without any exception, in an increase of susceptibility in formerly forested areas. However the scale of differences is quite heterogeneous. High dfferences (> 0,5, red) can be observed mostly in very steep areas whereas small differences (< 0,1, yellow) are restricted to forested areas on gentle slopes. This illustrates that - like the calculation based on neural networks - the calculation based on logistic regression reacts in the desired and expected way to changes in land-use.
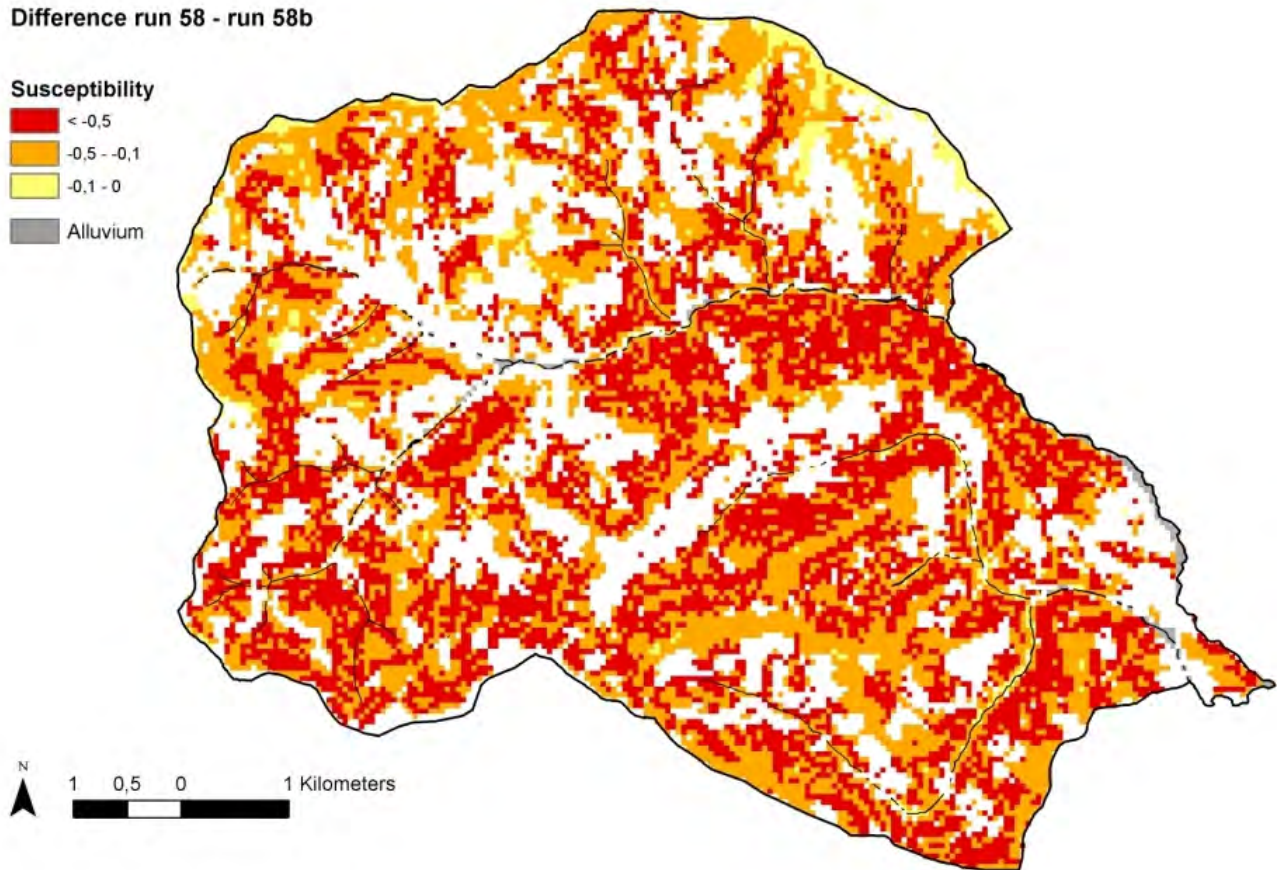
Fig. 10.3.1-2: Differences between run 58 and "worst case" scenario forest of run 58b

10.3.2 Variable precipitation scenarios

Regarding precipitation scenarios models were developed with the real precipitation distribution as presented by the respective August 2005 event analyses and regionalised afterwards with highest (worst case) intensities.

The following simulation refers to run 58 representing the best result of the "level high" modelling stage which was trained and validated with the NS_lh parameter map (cf. Chapter 5.5).

Fig. 10.3.2-1 shows the "worst case" precipitation scenario for the result 58 (58d, see Tab. 10.3-1). Fig. 10.3.2-2 presents the difference map of the result of run 58 and the "worst case" precipitation scenario 58d. A significant increase in susceptibility compared to run 58 in the areas that originally had relatively low precipitation in the northeast and west can be observed. These increases display almost the same magnitude as the changes caused by the "worst case" land-use scenario (complete deforestation, cf. Chapter 10.3.1). No reductions of susceptibility (blue) can be observed with higher precipitation. These results can be attributed to the obvious influence of NS_lh on modelling. The calculation based on logistic regression reacts in the desired and expected way to changes in precipitation.
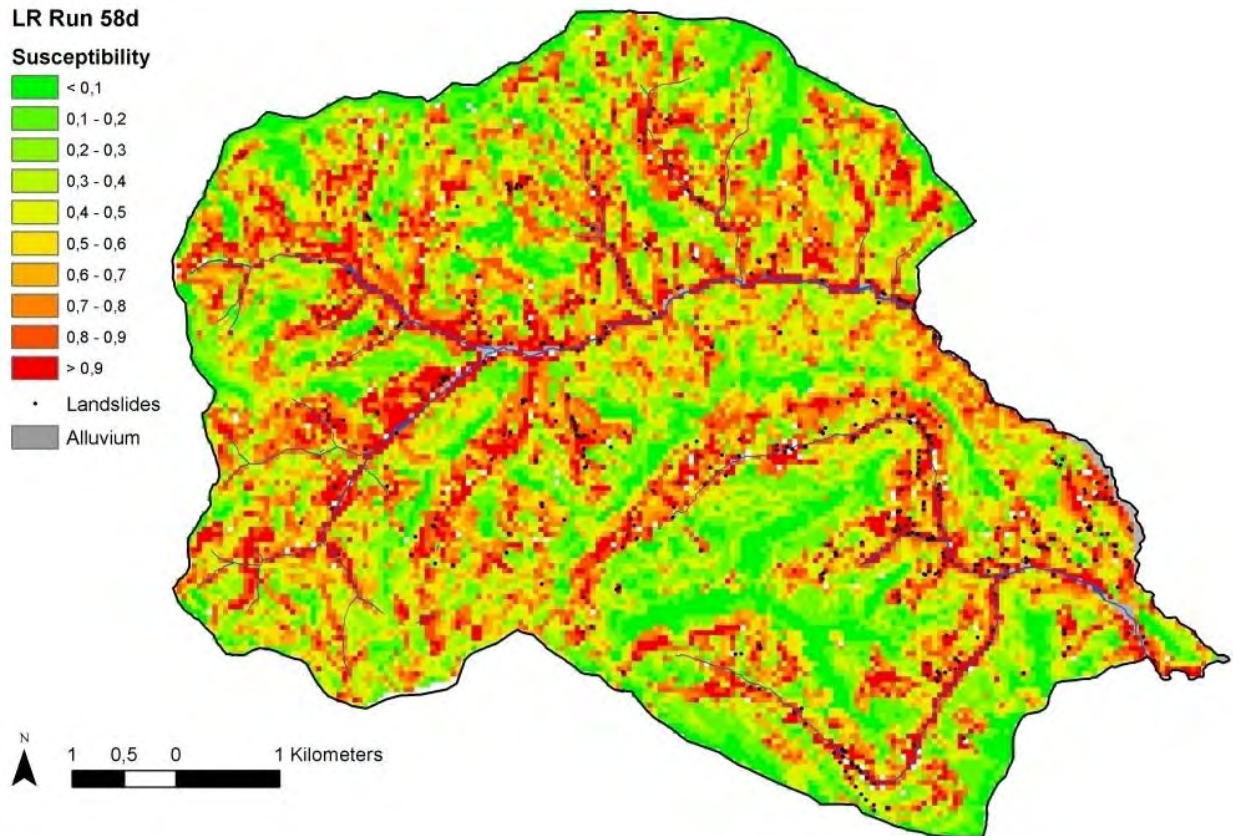
Fig. 10.3.2-1: "Worst case" scenario 58b, precipitation of run 58

For visualisation purposes the high negative differences as displayed in Fig. 10.3.2-2 covering large areas in the northern and western part of the study area have been split up and are presented in Fig. 10.3.2-3.

The results of logistic regression based scenarios with respect to precipitation give approximately equivalent results as the neural network based calculations: the strong increase of susceptibilities indicates that in case of precipitation reaching the maximum level of the event in August 2005, large areas that were not affected by landslides due to the distribution of precipitation during the 2005 event might still become unstable.
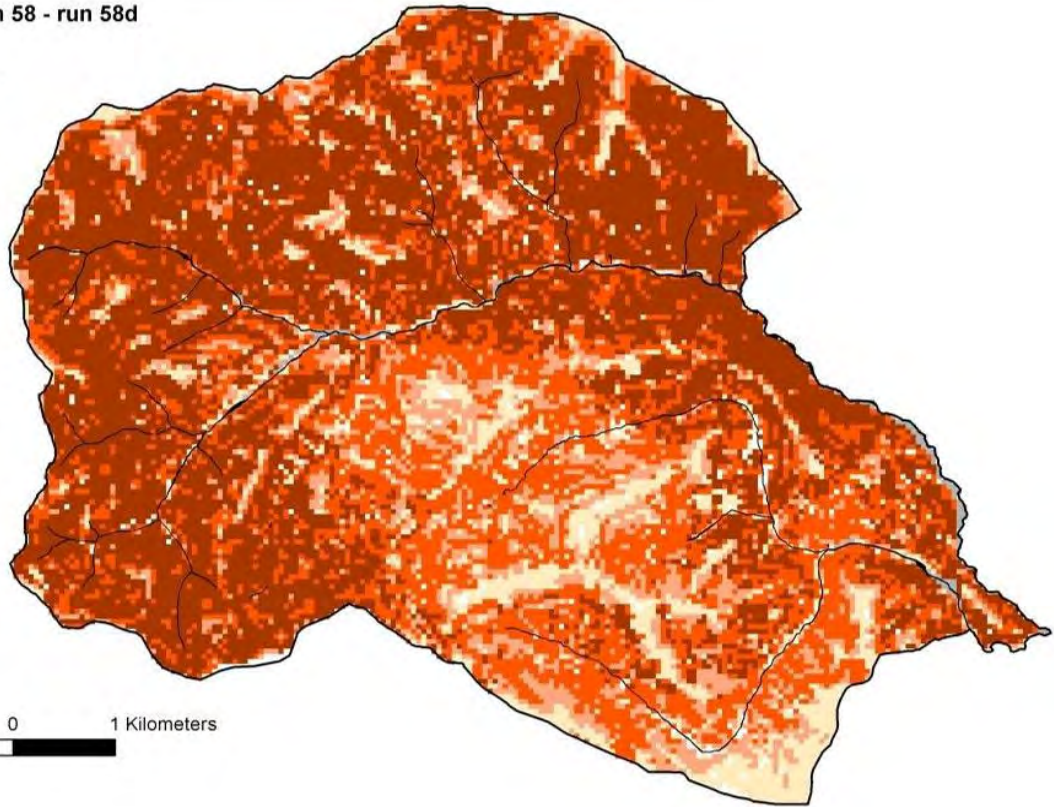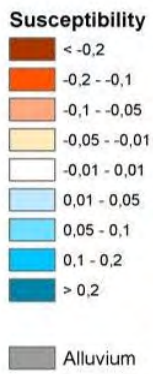
Fig. 10.3.2-2: Differences between run 58 and "worst case" scenario precipitation
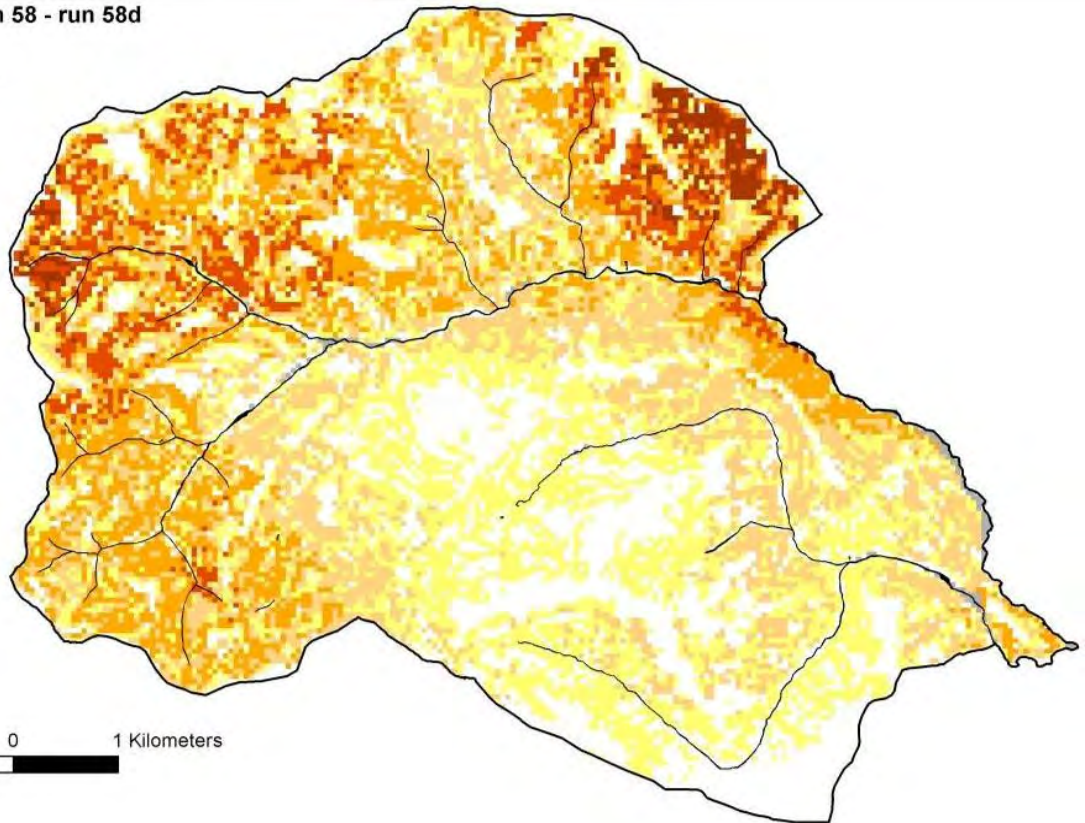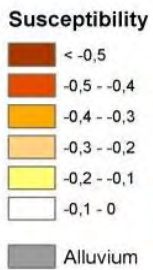
Fig. 10.3.2-3: Differences between run 58 and "worst case" scenario precipitation (split version)

11. Summary and conclusions

The AdaptSlide project was implemented to analyse, compare and improve different modelling techniques for creating susceptibility maps regarding spontaneous landslides in loose material in the region of Gasen-Haslau (about 50 km^2), especially by studying the improvement possibilities of the input data quality.

It was carried out within the framework of the AdaptAlp project and co-financed by the Federal Ministry of Agriculture, Forestry, Environment and Water Management (BMLFUW). Project partners were the Geological Survey of Austria (GBA), the Federal Research and Training Centre for Forests, Natural Hazards and Landscape (BfW), the Joanneum Research (JR), and the Central Institute for Meteorology and Geodynamics (ZAMG).

It was investigated in which way different parameter maps which describe the temporal and spatial variable site conditions, influence susceptibility maps for soil slips and earth flows. On the one hand, we analysed which improvements could be achieved by integrating a parameter map into the modelling process compared to the parameter map in question not being used. On the other hand, we studied the improvement potential resulting from the use of parameter maps that had been improved by applying expert knowledge, additional calculations, and field mapping (="high level" parameter maps). They where compared to parameter maps produced in the standard manner, using generally available data (="level low" parameter maps). In addition, we performed a number of model runs with exclusively process-oriented combinations of parameter maps selected on the basis of the authors' expert knowledge.

All parameter maps for this project were generated and analysed by the project partners. In some cases, methods developed by the partners were used to generate the maps. The expenditure required to produce the parameter maps was recorded in order to determine the cost-benefit ratio of the parameter maps generated in this way.

The empirical approach to estimate the runout length of landslides area-wide was attuned to the formats and information of the compiled landslide maps and commonly available data.

11.1. Modelling of Susceptibility Maps

The methods used for modelling susceptibility maps were: neural networks, logistic regression, weight of evidence and the deterministic approach SINMAP. The results of neural networks and logistic regression were subjected to more precise validation and comparative analysis. Because the authors consider conventional validation methods as inadequate, a combination of several validation methods was used and an advanced validation strategy developed.

Several examples of best results were ultimately selected from the modelling, employing neural networks and logistic regression and combined to produce two final-result maps. These maps served as a basis for process area modelling. Neural networks and logistic regression were also tested for their suitability to establish scenarios for changed land-use and variable precipitation sums.

In the case of both modelling methods studied in detail (neural networks and logistic regression), major improvements in model performance (= improvements in the validation of results) were observed only with the **integration of the following parameters:** *forest, road network, profile curvature,* (and definitely *slope* as well, even though this was not studied) and to a limited extent with the integration of different *subsurface flow dispositions* (for the most part in the case of neural networks, but not with logistic regression) and *precipitation* (for logistic regression, but not for neural networks). The biggest differences in validation, and thus the greatest improvements in model performance, were achieved by the integration of the parameter *forest*. However, the integration of the parameters *Flowaccumulation, geological basic disposition*, *basic disposition based on soil map, curvature classification* and to a limited extent *subsurface flow disposition* and *precipitation* did generally not result in any improvement of the results of either modelling method.

All these observations can be found for the different modelling methods in Tab. A4 to A6 in the Annex (see column "Improvements in the quality of the susceptibility map"), which list all the parameter maps studied and their improvement potential, i.e. the influence on the validation result (+/- "no influence to slightly positive influence" to +++ "very high positive influence"). The assessments of the improvements made in these tables and in the chapter described herein differ sometimes slightly from those in the individual chapters of the modelling (Chapter 7). This is the case, because in the authors opinion conventional international validation methods (Chapter 7.1) used in the project AdaptSlide are inadequate to provide exact and reliable assessments of the quality of results and should be considered only as rough assessment methods (see below). For that reason, comparisons of results that are described as "slightly better/worse" in the modelling chapter are assessed here as more or less "equally good" (+/- "no influence to slight influence").

The results for **improvement potential of the improved parameter maps** can also be seen in Tab. A4 to A6 in the Annex. The column "Improvement caused by compared parameter map" shows the improvement that was possible to achieve by means of the improved parameter map (= "level high") compared to the original parameter map (= "level low"). The improved parameter map as well as the different parameter map versions with which it is compared, are listed in the column "Compared parameter map".

It was shown that in most cases the improved parameter maps did not improve the model performance. In almost all modelling runs using "level high" parameter maps there was no improvement in model performance ("+/-" in the table) compared to the modelling runs with corresponding "level low" parameter map. Improvements compared to the "level low" ("+" in table) were to some extent possible for *"level high" precipitation as an independent parameter* (mainly for logistic regression, however not for neural networks). *"Level high precipitation"* is therefore the only "level high" parameter map that produced any kind of improvement. The lack of improvement with "level high" parameter maps is remarkable and might possibly be explained by inadequate validation methods.

In the case of the parameters *forest* and *subsurface flow disposition*, it was possible to generate several parameter-map versions, where each version was derived in a different way. It was shown that none of these versions could be preferred, because they all produced similarly good validation results (see "+/-" in Tab. A4 to A6 in the Annex). Furthermore, all runs with exclusively process-oriented parameter combinations resulted in a deterioration of the model performance.

Very large differences in validation, and thus the greatest improvements in model performance, could however always be achieved in the case of **parameters with fieldwork based land-use information on forest and road network** compared to these parameters without field data (Tab. A4 to A6 in the Annex). The improvement when comparing the parameter forest with/without field data was always assessed as "++" in the tables.

This improvement potential of the improved parameter maps was subsequently examined in terms of a **cost-benefit analysis** with regard to the expenditure required to produce the maps. Fig. 11.1-1 shows the assessment scheme for this cost-benefit analysis: The relative expenditure of time (expenditure of time as the proportion of the expenditure of time to produce the parameter map with maximum expenditure) to produce a parameter map (x-axis) was compared to the improvement in the quality of results that was achieved by using this parameter map (y-axis). The y-axis corresponds to the validation in the column "improvements in the quality of the susceptibility map" in Tab. A4 to A6 in the Annex, which specifies the improvement of the model performance (=improvement in the validation of the result) caused by the integration of the particular parameter map in comparison to not using this parameter map. For example, the basic map 2 in Fig 11.1-1 was produced with very low expenditure (5%), but has improved the result by raising its quality over two levels.

In the case of a combined parameter map, the total expenditure of time is given, i.e. the expenditure of time needed to generate the basic parameter maps used for producing the combined parameter map is included as well (for example the combined parameter map based on *geological map „level low"* and *flow accumulation*). In this way, the time expenditure for the combined parameter map might turn out to increase considerably (total expenditure for basic maps 1 & 2), while the improvement remains at the same level as for the basic map 2 (Fig. 11.1-1). This is because the quality of the result is mainly evoked by one parameter map (basic map 2). In this case basic map 1 as well as its combination with basic map 2 did not result in an improvement of the quality of the output. So the use of basic map 1 has to be questioned.
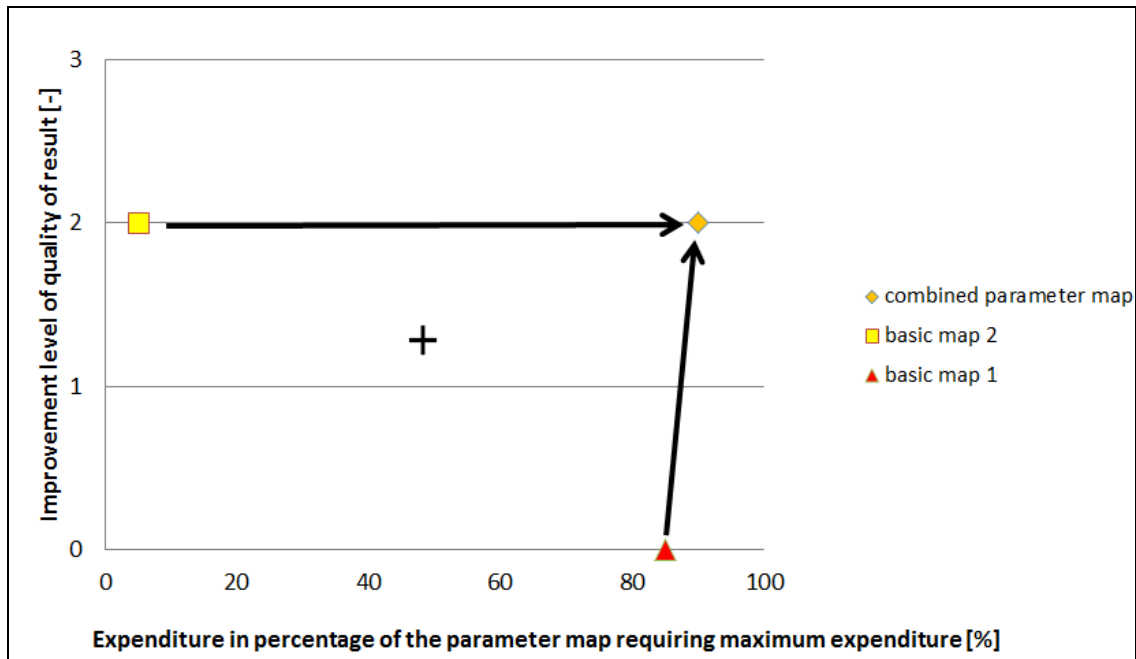
Fig. 11.1-1: Expenditure calculation of combined parameter map. In the example, the combination of map 2 and map 1 did not improve the output-quality

Fig. 11.1-2 and 11.1-3 show these cost-benefit analyses for all of the parameter maps studied for the modelling methods of neural networks and logistic regression. Orange dots represent "level high" parameter maps, whereas "level low" parameter maps are represented by the other colours. Green dots show the versions of the "level low" parameter *forest*, light-blue dots the versions of the "level low" parameter *subsurface flow disposition,* while all other "low level" parameters appear as dark-blue dots. The arrows (having a different meaning here than in Fig. 11.1-1) in each case connect a "level low" parameter map with a corresponding "level high" parameter map, or in the case of the forest map with and without field data of land use.

The graphics provide further clarification of the statements made above: Almost all "level high" parameter maps did not produce any improvement in the quality of the result compared to the corresponding "level low" parameter maps (indicated by horizontal arrows). So the additional expenditure spent for the production of the "level high" maps was in vain in most cases. Only in the case of the *precipitation map* when using logistic regression it was possible to get an improvement (ascending arrow) in the "level high" map, with relatively high expenditure. On the other hand, in the case of the parameter *road network* when using neural networks, there was even a deterioration of the result to be observed (descending arrow).

Another ascending arrow shows Fig. 11.1-2, which marks the improvement evoked by using the parameter map *forest including field mapped land use information* in comparison to *forest without field mapped land use information* when using neural networks. Furthermore the production of this map involved relatively low expenditure (field data must already be available, however). By comparing the versions of one parameter it was observed in the case of both forest (green dots) and subsurface flow disposition (light-blue dots) that the quality level of the results did not differ (all points remain at same improvement level) regardless of the invested expenditure.

Here, however, we refer once again to the limitations of the validation methods that also formed the basis for these analyses.
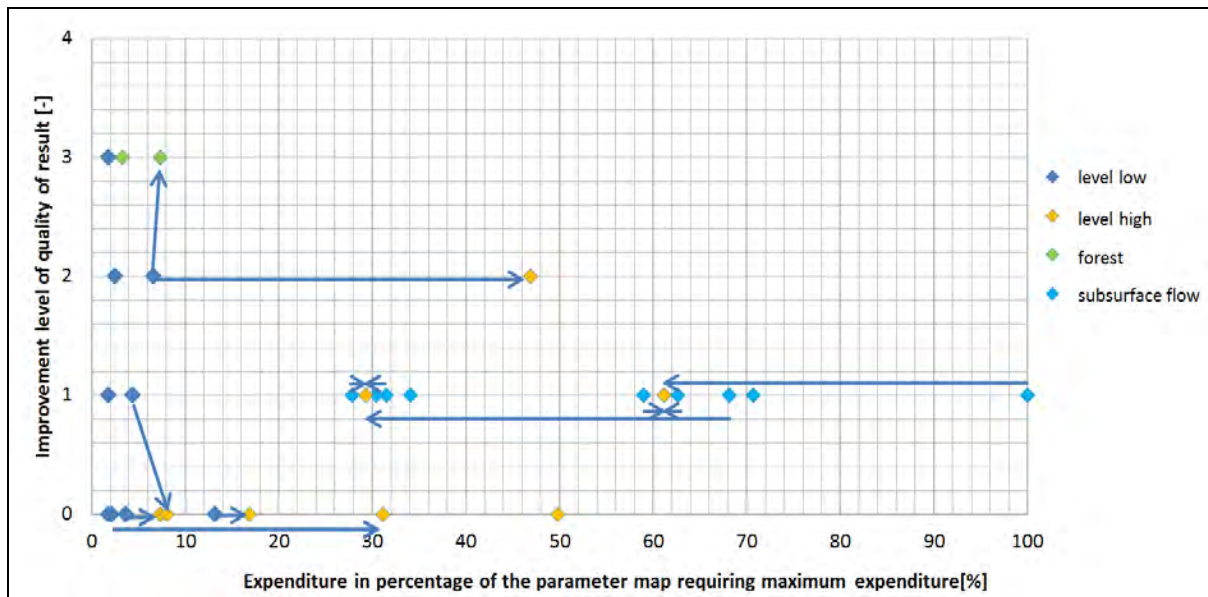
Fig. 11.1-.2: Costs and benefits of applied parameter maps using neural networks
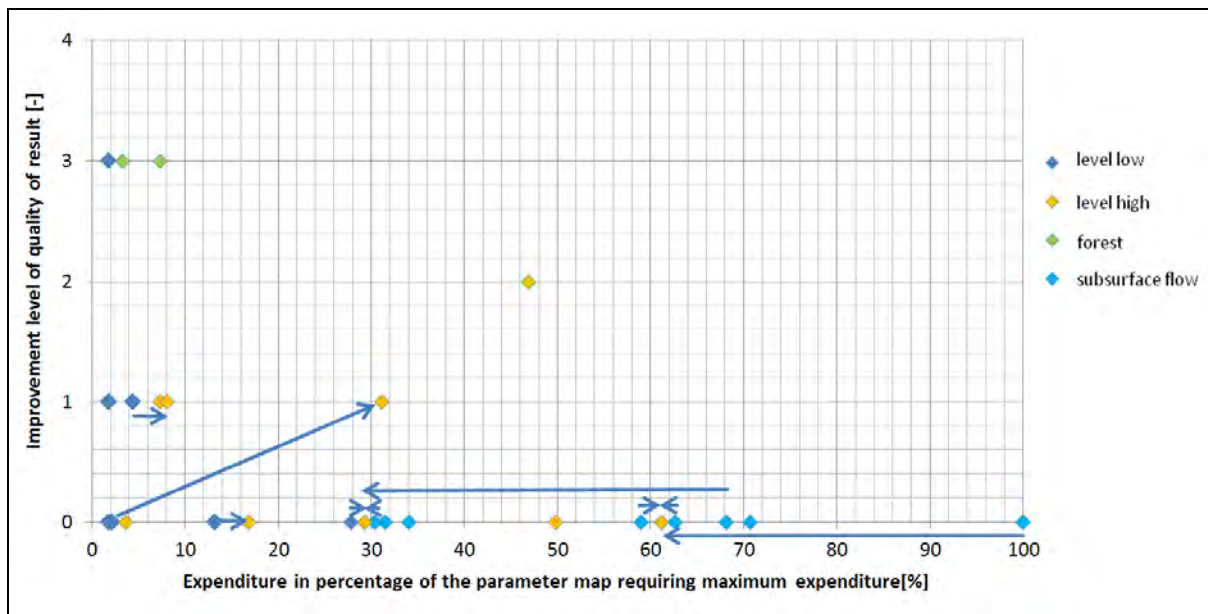
Fig. 11.1-3: Costs and benefits of applied parameter maps using logistic regression

When **comparing the two modelling methods neural networks and logistic regression**, it was seen that both methods generally produced quite similar susceptibility maps, although logistic regression differentiated somewhat more strongly between high and low susceptibilities. The validation comparison based on the applied validation methods indicated that the results from logistic regression and neural networks can be termed "equally good" to "slightly better" using neural networks. However, due to the limited validity of these comparisons (for example,

summarized area-wide validation, see below), neither of the two modelling methods could be definitely preferred.

Also, as no definite "best result" could be selected due to similarly good validations of the results and inadequate validation methods, the best 5 results for each level of the two modelling methods were combined in order to produce a common, final-result map that involved both methods. These two final-result maps were calculated cell-specifically as a combination of mean susceptibility from the respective maximum and minimum (= mid-range) on the one hand, and the fluctuation range (= half-range) on the other. Thus, the combined final-result maps presented susceptibility and its spatial variability and uncertainty caused by the different modelling methods and the incomplete (or simplified) status of the data. This causes several possible susceptibility classes in many cells, which are illustrated in the final-result map for "level high" in Fig. A2 in the Annex.

Using neural networks and logistic regresssion, it was possible to calculate plausible **scenarios for changed land-use and variable precipitation**. Based on these scenarios, it is possible in principle to make concrete statements for spatial planning and forestry concerning favourable areas for reforestation and areas that are at risk due to deforestation. With the methodology used, it would also be possible, in a general sense, to integrate climate-change precipiation scenarios into landslide-susceptibility modelling.

The lack of improvement with nearly all "level high" parameter maps is remarkable, and there might be several reasons for this, as there might also be for the similarly well validated parameter-map versions and best results, and for the deterioration in model performance with process-oriented parameter combinations. Actually, it might be that the "level high" parameter map used in each case does not depict the respective situation in a more realistic and process-oriented manner than the "level low" map, so that the expenditure of producing the "level high" parameter map for modelling can be questioned. Furthermore, it is also possible that the improvements in the parameter map cannot be captured by the model, because the data is insufficient, given the complexity of the material.

However, it is also likely that some "level high" parameter maps are indeed more realistic and process-oriented than the corresponding "level low" map, but that the validation method is not able to recognize the improvements in the susceptibility map. This might be the case because, in the authors' opinion, the validation methods used, are too simplified offering only summarized area-wide validation (Chapter 7.1). These validation methods can therefore not detect partial differences in map quality, so that small, well-modelled partial areas with many mass movements strongly affect the validation result for an entire area. This inadequacy of the validation methods was also shown, for example, by the way in which the integration of precipitation completely modified the appearance of the map and probably also improved the map due to the obvious importance of this parameter. Nevertheless, the validation result remained virtually unchanged.

This deficit underlines the necessity of developing **new, partial validation methods**, so that in future, reliable statements can be made on both, model performance and the possibility of improvement in final results, as well as the capabilities of individual modelling methods.

Based on the inadequacy of the validation methods, it can also be concluded, as demonstrated by the AdaptSlide project that in subsequent projects several validation methods should be used in combination, as long as no single reliable

validation method has been developed. Likewise, no *single* result of a *single* modelling method should be selected as the best final result, but rather **combinations of several results** from both modelling methods should be provided as final results, in order to illustrate the **uncertainty** of the modelling results.

The obvious improvement of the results using field data for forest and road network clearly shows the enormous importance of **mapping this land-use information** in the framework of an event documentation of gravitational mass movements in the field. In future projects, particular attention should be paid to collect as much high-quality and comprehensive data as possible.

11.2. Modelling the Process Area

For any kind of spatial planning considering landslides, it is not only necessary to consider the starting zone but to look at the whole area affected by this process. Thus, in the AdaptSlide project a model was developed to estimate the **process-area of spontaneous (shallow) landslides on an area wide** basis (for the test area). It is based on a simple travel angle model for small snow avalanches.

To run the model, an adequate data base of documented landslides and/or slope debris flow to determine the α-angle to calibrate the model and to evaluate the results is required. Further, the DEM have to adequately display the transport-relevant surface structures. The DEM 10, which was available for the test area has not always fulfilled these requirements in a satisfying manner.

Most important for estimating the process area is the starting information (e.g. susceptibility maps) and the definition of the threshold for the starting criterion (disposition). Scientifically a threshold of 0.5 is justified, but this decision depends also on substantial socio-economic and administrative reasons.

The model displays the area affected by landslide processes area wide on pixel basis to identify "hot spots". Optionally, the probability of the landslide disposition map can be overtaken from the disposition map. The results have to be interpreted as estimation with limited demands of accuracy, considering the empirical, area-wide model approach.

When assessing the model results, it turned out that there are no adequate methods to evaluate the area-wide model results. The assessment on the basis of documented single events amended by documentations, expert knowledge and other model approaches may be sufficient for model calibration, but it is inappropriate to evaluate the model results in a comparable way. Thus, a coherent evaluation of the approach could not be accomplished.

12. References

Abraham, J. & Adolt, R. (2006): Stand height estimation using aerial images and laser datasets. EARSeL - Proceedings of the Workshop on 3D Remote Sensing in Forestry, Austria.

Alemayehu, L. (2007): Landslide Susceptibility Modeling Using Logistic Regression and Artificial Neural Networks in GIS: a Case Study in Northern Showa Area, Ethiopia. Unpubl. Thesis, Addis Ababa University, http://shawndra.pbworks.com/f/Landslide+Susceptibility+Modeling+Using+Logistic+Regression.pdf.

Andrecs P., Hagen K., Fromm R., Gauer P., Höller P., Klebinder K., Kohl B., Lang E., Markart G., Perzl F., Stary U., Zeidler A 2010: AdaptEvent. Analyse der Sicherheit und Genauigkeit von Bemessungswerten bei gravitativen alpinen Naturgefahren und Ableitung von Anpassungsstrategien an den Klimawandel. Endbericht des BFW im Auftrag des BMLFUW im Rahmen des EU Projekts AdaptAlp ("Adaptation to Climate Change in the Alpine Space"), Wien: 321 S

Andrecs P., Hagen K., Lang E., Stary U.,Gartner K., Herzberger E., Riedel F., Haiden T. (2007): Documentation and Analyses of Disasters 2005 in the Communities of Gasen and Haslau (Styria), BFW-Domumentation 6, 75 p.

Andrecs, P., Hagen, K., Lang, E., Stary, U., Gartner, K., Herzberger, E., Riedel, F. & Haiden, T. (2007): Dokumentation und Analyse der Schadensereignisse 2005 in den Gemeinden Gasen und Haslau (Steiermark). BFW-Dokumentation; Schriftenreihe des Bundesforschungs- und Ausbildungszentrums für Wald, Naturgefahren und Landschaft,Wien, Nr. 6, 75 p.

Arpa Piemonte (ed.) (2005): CatchRisk – Mitigation of Hydro-Geological Risk in Alpine Catchments. Final report, 189 p., Milano.

Auer I, Böhm R, Jurkovic A, Lipa W, Orlik A, Potzmann R, Schöner W, Ungersböck M, Matulla C, Briffa K, Jones PD, Efthymiadis D, Brunetti M, Nanni T, Maugeri M, Mercalli L, Mestre O, Moisselin J-M, Begert M, Müller-Westermeier G, Kveton V, Bochnicek O, Stastny P, Lapin M, Szalai S, Szentimrey T, Cegnar T, Dolinar M, Gajic-Capka M, Zaninovic K, Majstorovic Z, Nieplova E, (2007). HISTALP – Historical instrumental climatological surface time series of the greater Alpine region 1760-2003. International Journal of Climatology 27: 17-46

Ayalew, L. & Yamagishi, H. (2005): The Application of GIS-based Logistic Regression for Landslide Susceptibility Mapping in the Kakuda-Yahiko Mountains, Central Japan. Geomorphology, 65, pp. 15-31.

Backhaus, K., Erichson, B., Plinke, W. & Weiber, R. (2000): Multivariate Analysemethoden. Springer, Berlin.

BAFU (Bundesamt für Umwelt CH) 2008: Sivaprotect-CH, Eidgenössisches Departement für Umwelt, Verkehr, Energie und Kommunikation, Bern

Barbieri, G. & Cambuli, P. (2009): The Weight of Evidence statistical Method in Landslide Susceptibility Mapping of the Rio Pardu Valley (Sardinia, Italy). 18th World IMACS / MODSIM Congress, Cairns, Australia 13-17 July 2009, http://mssanz.org.au/modsim09.

Beguería S. (2006). Validation and evaluation of predictive models in hazard assessment and risk management. In: Natural Hazards 37(3), pp. 315—329.

Bell, R. (2007): Lokale und regionale Gefahren- und Risikoanalyse gravitativer Massenbewegungen an der Schwäbischen Alb. Diss. Rheinische Friedrich-Wilhelms-Universität Bonn., http://hss.ulb.uni-bonn.de/diss_online.

Beven, K.J. & Kirkby, M.J. (1979): A Physically Based Variable Contributing Area Model of Basin Hydrology. Hydrological Sciences Bulletin, 24(1), pp. 43-69.

Bishop, M. C. (1995): Neural Networks for Pattern Recognition. Oxford University Press. New York. pp. 482.

BMLFUW (2006): Hochwasser 2005 –Ereignisdokumentation, Teilbericht der Wildbach- und Lawinenverbauung

Böhm R., Jones P.D., Hiebl J., Frank D., Brunetti M., Maugeri M., (2009): The early Instrumental warm bias. A solution for long central European temperature Series 1760-2007

Bonham-Carter, G.F. (1994): Geographic Information Systems for Geoscientists. Modelling with GIS. Pergamon Press, Oxford and Elsevier Science Inc, New York, 398 p.

Bonham-Carter, G.F., Agterberg, F.P. & Wright, D.F. (1989): Weight of Evidence Modelling: A New Approch to Mapping Mineral Potential. In: Statistical Applications in Earth Sciences, Nr. 89-9, pp. 171-183, Geological Survey of Canada.

Bundesamt für Bodenkartierung und Bodenwirtschaft (1967): Die österreichische Bodenkarte 1:10.000, Anweisung zur Durchführung der Kartierung, Wien

Bunza, G. and T. Schauer (1989): Der Einfluss von Vegetation, Geologie und Nutzung auf den Oberflächenabfluss bei künstlichen Starkregen in Wildbachgebieten der Bayerischen Alpen. Informationsber. 2/89 d. Bayer. Landesamtes f. Wasserwirtschaft, München

Burch, G.J., Moore, I.D. and J. Burns (1989): Soil hydrophobic effects on infiltration and catchment runoff. Hydrol. Processes, 3: 211-222

Cannon, S. H. (1993): An empirical model for the volume-change behavior of debris flows. In: Shen, H. W., Su, S. T. and F. Wen (eds.), Hydraulic Engineering 1993, Vol. 2, pp. 1768-1773.

Carrara, A., Guzzetti, F., Cardinali, M. & Reichenbach, P. (1999): Use of GIS Technology in the Prediction and Monitoring of Landslide Hazard. Natural Hazards, 20, pp. 117-135.

Chen, Z. & Wang, J. (2007): Landslide Hazard Mapping using Logistic Regression Model in Mackenzie Valley, Canada. Natural Hazards, 42, pp. 75–89.

Chifflard, P. & Tilch, N. (2010): Learning from Nature – Mapping of Complex Hydrological and Geomorphological Process Systems for More Realistic Modelling of hazard-related maps.-Poster und abstract, EGU 2010, Wien (http://www.geologie.ac.at/pdf/Poster/poster_2010_chifflard_tilch.pdf)

Chigira, M., Duan, F., Yagi, H. & Furuya, T. (2004): Using airborne laser scanner for the identification of shallow landslides and susceptibility assessment in an area of ignimbrite overlain by permeable pyroclastics. Landslides 1, pp. 203-209.

Christensen, J.H., B. Hewitson, A. Busuioc, A. Chen, X Gao, I. Held, R. Jones, R. K. Kolli, W.T. Kwon, R. Laprise, V. Magana Rueda, L. Mearns, C.G. Menendez, J. Räisänen, A. Rinke, A. Sarr and P. Whetton 2007: Regional Climate Projections. In: Climate Change 2007: The Physical Science Basis. Contribution of Working Group I to the Fourth Assessment Report of the Intergovernmental Panel on climate Change [Solomon, S., D. Qin, M. Manning, Z. Chen, M. Marquis, K. B. Averyt, M. Tignor and H.L. Miller (eds)]. Cambridge University Press, Cambridge, UK and New York USA

Chung, C.F., Fabbri, A.G. (1999): Probabilistic Prediction Models for Landslide Hazard Mapping. Photogrammetric Engineering & Remote Sensing 65 (12), pp. 1389-1399

Chung, C.J. & Fabbri, A.G. (2003): Validation of spatial prediction models for landslide hazard mapping. Natural Hazards, 30, pp. 451-472.

Corominas, J. (1996). The angle of reach as a mobility index for small and large landslides. Canadian Geotechnical Journal, 33(2), pp. 260–271.

Costa-Cabral, M. and S.J. Burges (1994): Digital Elevation Model Networks (DEMON): a model of flow over hillslopes for computation of contributing and dispersal areas, Water Resources Research, 30:1681-1692

Czell, A. (1972): Wasserhaushaltsmessungen in subalpinen Böden. Mitt. Forstl. Bundesversuchsanstalt, Bd. 98

Dahl, M.-P. J., Mortensen, L. E., Veihe, A. and N. H. Jensen (2010): A simple qualitative approach for mapping regional landslide susceptibility in the Faroe Islands. Nat. Hazards Earth Syst. Sci., 10, pp. 159-170.

Dai, F.C. & Lee, C.F. (2002): Landslide characteristics and slope instability modeling using GIS, Lantau Island, Hong Kong. Geomorphology, vol 42, pp. 213–228.

Dai, F.C. & Lee, C.F. (2002): Landslides on Natural Terrain. Physical Characteristics and Susceptibility Mapping in Hong Kong. Mountain Research and Development, vol. 22, No. 1, pp. 40-47.

Dai, F.C., Lee, C.F., Tham, L.G., Ng, K.C. & Shum, W.L. (2004):Logistic Regression Modelling of storm-induced shallow Landsliding in Time and Space on natural Terrain of Lantau Island, Hong Kong. Bull. of Eng.-Geol. and the Environment, Vol 63, No. 4, pp. 315–327.

Delparte, D., Jamieson, B. and N. Waters (2008): Statistical runout modeling of snow avalanches using GIS in Glacier National Park, Canada. Cold Regions Science and Technologies, 54, pp. 183-192.

Dixon, M.D. (2003): Landslide Computer Modeling Potential. Engineering Field Notes, Vol. 35/1, Washington DC, U.S. Department of Agriculture, Forest Service, Engineering. 8 p.

eBod (2010): www.bodenkarte.at

Fell, R., Corominas, J., Bonnard, C., Cascini, L., Leroi, E. & Savage, W.Z. on behalf of the JTC-1 Joint Technical Committee on Landslides and Engineered Slopes (2008): Guidelines for Landslide Susceptibility, Hazard and Risk Zoning for Land Use Planning. Engineering Geology 102, pp. 85–111.

FLO-2D User Manual Version 2004.10, Nutrioso, USA

Flügel, H.W., Hötzl, H. & Neubauer, F. (1990): Geologische Karte der Republik Österreich 1:50.000, Blatt 135 Passail; Geologische Bundesanstalt, Wien.

Fowze, J.S.M., Buena, D., Daag, A.S., Hazarika, M.K. & Samarkoon, L. (2007): Spatial Modeling of Rain-triggered Landslides. A case study in Southern Leyte Province, Philippines. Proc. 28th Asian Conference on Remote Sensing 2007, Kuala Lumpur, Malaysia (www.a-a-r-s.org/acrs/proceeding/ ACRS2007/Papers/TS2.4.pdf).

Fujisawa, K., Tsunaki, R. and I. Kamiishi (1993): Estimating snow avalanche runout distances from topographic data. Annals of Glaciology, 18, pp. 239-244.

Furdada, G. and J.M. Vilaplana (1998): Statistical prediction of maximum avalanche run-out distances from topographic data in the western Catalan Pyrenees (northeast Spain). Annals of Glaciology, 26: 285-288.

García R., Rodríguez J., O'Brien J., 2004: Hazard Zone Delineation for Urbanized Alluvial Fans, American Society of Civil Engineers

Gauer, P., Kronholm, K., Lied, K., Kristensen, K. and S. Bakkehøi (2010): Can we learn more from the data underlying the statistical α-β model with respect to the dynamical behavior of avalanches? Cold Regions Science and Technology, 62, pp. 42-54.

Geo7 2010: Modellierung von Hangmuren und spontanen flachgründigen Rutschungen, http://www.geo7.ch/uploads/media/Hangmurenmodellierung.pdf (7.10.2010)

Geofast (2005): Provisorische Geologische Karte der Republik Österreich 1:50. 000 - 135 Birkfeld / Stand 1999, Ausgabe 2005 / Kompilation: Joanneum Research, GIS-STMK / erstellt im Rahmen des GBA-Projektes Geofast; Geologische Bundesanstalt, Wien.

Granica, K., Schardt, M. & Gallaun, H. (2000): Monitoring of Protection Forests by Means of SPOT4 Satellite Data. Proc. 20th EARSEL-Symposium 'A decade of Transeuropean Remote Sensing Cooperation', Dresden, Germany.

Granica, K., Schardt, M., Hirschmugl, M. & Gallaun, H. (2004): The Observation of Protection Forests in Critical Zones using New Satellite Technology. Proc. INTERPRAEVANT 2004, vol. 5, pp. 37-48.

Greco, R., Sorriso-Valvo, M., & Catalano, E. (2007): Logistic Regression Analysis in the Evaluation of Mass Movements Susceptibility: the Aspromonte Case Study, Calabria, Italy. Engineering Geology, 89, pp. 47-66.

Guzzetti, F., Carrara, A., Cardinali, M. & Reichenbach, P. (1999): Slide Hazard Evaluation: A Review of current Techniques and their Application in a multi-scale Study, Central Italy. Geomorphology, 31, pp. 181–216.

Haberler, A., Schwarz, L., Lotter, M. & Kociu, A. (2009): Rutschungen in der Katastrophenregion Feldbach (Steiermark) im Sommer 2009 - eine vorläufige Bestandsaufnahme.- Geoforum Umhausen, Niederthai, 15./16.10.2009. (http://www.geoforum-umhausen.at/aktuelles2009/Tagungsband_2009.pdf)

Haiden, T., A. Kann, G. Pistotnik, K. Stadlbacher, and C. Wittmann, 2009: Integrated Nowcasting through Comprehensive Analysis (INCA) – System description. ZAMG documentation, 60p. http://www.zamg.ac.at/fix/INCA_system.pdf

Haiden, T., 2008: INCA re-analysis of a heavy precipitation event 2005 in Styria. Interne Dokumentation, 10p.

Haiden, T., A. Kann, G. Pistotnik, K. Stadlbacher, and C. Wittmann, 2009: Integrated Nowcasting through Comprehensive Analysis (INCA) – System description. ZAMG documentation, 60p. http://www.zamg.ac.at/fix/INCA_system.pdf

Haiden, T., G. Pistotnik, 2009: Intensity-dependent parameterization of elevation effects in precipitation analysis. Adv. Geosci., 20, 33-38.

Hair, J.F., Anderson, R.E., Tatham, R.L. & Black, W.C. (1998): Multivariate data analysis. 5ed., Prentice-Hall, London.

Hamby, D.M. (1994): A Review of Techniques for Parameter Sensitivity Analysis of environmental Models. Environmental Monitoring and Assessment, 32, pp. 135-154.

Hammond, C., Hall, D., Miller, S. & Swetik, P. (1992): Level I Stability Analysis (LISA) Documentation for Version 2.0.- General Technical Report INT-285, USDA Forest Service Intermountain Research Station, 190 p.

Haneberg, W.C., Creighton, A.L., Medley, E.W. & Jonas, D.A. (2005): Use of LiDAR to assess slope hazards at the Lihir gold mine, Papua New Guinea. In: Hungr, O., Fell, R., Couture, R. & Eberhardt, E. (eds.): Landslide Risk Management. Proceedings of International Conference on Landslide Risk Management, Vancouver, Canada.

Heim, A. (1932). Bergsturz und Menschenleben. Fretz & Wasmuth Zürich.

Hosmer, D.W. & Lemeshow, S. (1989): Applied Logistic Regression. Wiley, New York, 1989.

Hungr, O., Morgan, G. C., VanDine, D. F. and D. R. Lister (1987): Debris flow defences in British Columbia. In: Costa, J.E. and Wieczorek, G.F. (eds.), Debris Flow: Process, Description and Mitigation. Geological Society of America, Reviews in Engineering Geology 7, pp. 201-222.

Hungr 0. (1995): A model for the runout analysis of rapid flow slides, debris flow and avalanches. Canadian Geotechn. Joournal V. 32, p 610-623

Hürlimann, M., Rickenmann, D., Medina, V. and A. Batemann (2008): Evaluation of approaches to calculate debris-flow parameters for hazard assessement. Engineering Geology 102, pp. 152-163.

IPCC (2007): Fourth Assessment Report: Climate Change 2007 (AR4)

Iverson, R. M. (1997): The physics of debris flow. Reviews of Geophysics, 35, 3 / 1997, pp. 245-296.

Jäger G., Moser M. 2008: Numerische hydrologische und hydraulische Simulation der Auswirkungen einer möglichen Flutwelle im Rahmen einer Risikoanalyse und Risikomanagements am Suggadinbach, Interpraevent 2008 – Conference Proceedings, Vol 1, S 355-365, Dornbirn

Jayathissa, H. (2010): Combined statistical and dynamic Modelling for real time Forecasting of Rain induced Landslides in Matara District, Sri Lanka - a Case Study. Dissertation Mathematisch-Naturwissenschaftliche Fakultät, Eberhard Karls Universität Tübingen.

Jelem, H., Anninger, P., Helm, G: Standortserkundung im Umstellungsgebiet Gasen-Heilbrunn oststeirisches Bergland; Schriftenreihe des Institutes für Standort.- Wien : Forstliche Bundesversuchsanstalt ; 5

Jóhannesson, T. (1998): Icelandic avalanche runout models compared with topographical models used in other countries. Norwegian Geotechnical Institute, Publ. Nr. 203, pp. 43-52.

Klebinder K., R. Fromm, F. Perzl (2009): Ausweisung von Lawinenschutzwald mittels GIS und einfachen Modellrechnungen. In: Strobl, Blaschke, Griesebner (Hrsg.): Angewandte Geoinformatik 2009. Beiträge zum 21. AGIT- Symposium, Salzburg.

Klebinder K., Kohl B., Markart G. und B. Sotier (2008): Regionalisierung der Oberflächenabflussdisposition, Oberflächenrauigkeit und der hydrologischen Vegetationseinheiten. Unveröffentlichter Projektbericht des BFW im Auftrag des FTD f. WLV, GBL Südliches Niederösterreich und Burgenland.

Kleinbaum, D.G., Kupper, L.L., Muller, K.E. & Nizam, A. (1998): Applied Regression Analysis and Other Multivariable Methods. Duxbury Press, 1998.

Klingseisen, B. & Leopold, Ph. (2006): Early Landslide Prediction in non-alpine Areas. Proc. of the 26th International ESRI User Conference, San Diego, USA, http://proceedings.esri.com/library/ userconf/proc06/papers/papers/pap_1173.pdf.

Klingseisen, B. & Leopold, Ph. (2006): Landslide Hazard Mapping in Austria.- GIM International 20 (12): pp. 41–43.

Körner, H.J. (1980): The energy-line method in the mechanics of avalanches. Journal of Glaciology, Vol. 26, No. 94, pp. 501-505.

Kuthari, S. (2007): Establishing Precipitation Thresholds for Landslide Initiation along with Slope Characterisation using GIS-based Modelling. Unpubl. Thesis, 82 p., ITC, Enschede.

Lan, H., Wu, F., Zhou, C. & Wang, L. (2003): Spatial Hazard Analysis and Prediction on Rainfall-induced Landslide using GIS. Chinese Science Bulletin, Vol. 48, No. 7, pp. 703-708.

Lee, S., Choi, J. & Min, K.D. (2002): Landslide Susceptibility Analysis and Verification using the Bayesian Probability Model. Environmental Geology, 43, pp. 120-131.

Legros, F. (2002): The mobility of long-runout landslides. Engineering Geology 63 (2002), pp. 301-331.

Lied, K. and S. Bakkehøi (1980): Empirical calculations of snow-avalanche run-out distance based on topographic parameters. Journal of Glaciology, Vol. 26, No. 94, pp. 165-177.

Lied, K., Weiler, C., Bakkehøi, S., and Hopf, J. (1995): Calculation methods for avalanche runout distance in the Austrian Alps. ANENA, Chamonix 1995.

Liener S. Kienholz H. 2000: Modellierung von Flachgründigen Rutschungen mit dem Modell SLIDISP, Interpraevent 2000, Villach

Liener, S., Pfeifer, R. and M. Giamboni (2008): Simulation von Gefahrenhinweisflächen als Grundlage zur Schutzwaldausscheidung in der Schweiz. In: Proceedings of Interpraevent 2008, Vol. 2, pp. 529-538.

Löhmannsröben, R., Altfeld O., Bunza G., Eidt M., Fischer A., Jürging P., Schauer T. and R. Ziegler (2000): Geländeanleitung zur Abschätzung des Abfluss- und Abtragsgeschehens in Wildbacheinzugsgebieten, in Bayerisches Landesamt für Wasserwirtschaft, Materialien Nr. 87

Long, N.T. (2008): Landslide Susceptibility Mapping of the mountainous Area in A Luoi District, Thua Thien Hue Province, Vietnam. Thesis Vrije Universiteit Brussel, Faculty of Engineering, Department of Hydrology and Hydraulic Engineering, http://twws6.vub.ac.be/hydr/download/nguyenthanhlong.pdf.

Markart G., Kohl B., Sotier B., Schauer T., Bunza G. and R. Stern (2004): Provisorische Geländeanleitung zur Abschätzung des Oberflächenabflussbeiwertes auf alpinen Boden-/Vegetationseinheiten bei konvektiven Starkregen (Version 1.0). BFW-Dokumentation, Nr.3

Markart, G., Kohl B., Kirnbauer R., Pirkl H., Bertle H., Stern R., Reiterer A. and P. Zanetti (2006): Surface runoff in a torrent catchment in Middle Europe and its prevention. Geological and Geotechnical Engineering, 24, 1403-1424

Markart, G., Perzl, F., Kohl, B., Luzian, R., Kleemayr, K., Ess, B., Mayerl, J. (2007): 22. und 23. August 2005 - Analyse von Hochwasser- und Rutschungsereignissen in ausgewählten Gemeinden Vorarlbergs. 22nd and 23rd August 2005 - Analysis of flooding events and mass movements in selected communities of Vorarlberg. BFW-Dokumentation, Wien, (5).

Mathew, J., Jha, V.K. & Rawat, G.S. (2007): Weights of Evidence Modelling for Landslide Hazard Zonation Mapping in Part of Bhagirathi Valley, Uttarakhand. Current Science, Vol. 92, No. 5, pp. 628–638, Bangalore.

May, R.J., Maier, H.R. & Dandy, G.C. (2010): Data splitting for artificial neural networks using SOM-based stratified sampling. Neural Networks, 23 (2), pp. 283-294.

McClung, D.M., Mears, A.I. and P. Schaerer (1989): Extreme avalanche run-out: data from four mountain ranges. Annals of Glaciology, 13, pp. 180-184.

McKean, J. & Roering, J. (2003): Objective landslide detection and surface morphology mapping using high resolution airborne laser altimeter. Geomorphology 57, pp. 331-351.

McKinnon, M. (2010): Landslide runout. Statistical Analysis of Physical Characteristics and Model Parameters. Master Thesis. University Of British Columbia, Vancouver.

Mears, A.I. (1989): Regional comparisons of avalanche-profile and runout data. Arctic and Alpine Research, Vol. 21, No. 3, pp. 283-287.

Montgomery, D.R. & Dietrich, W.E. (1994): A physically based Model for the topographic Control on shallow Landsliding. Water Resour. Res. 30, pp. 1153–1171.

Naef, F., Margreth M., Schmocker-Fackel P. and S. Scherrer (2007): Automatisch hergeleitete Abflussprozesskarten – ein Werkzeug zur Abschätzung von Hochwasserabflüssen. Wasser Energie Luft, 99. Jg., Heft 3, 267-262

Neuhäuser, B. & Terhorst, B. (2007): Landslide Susceptibility Assessment using "Weights-of-Evidence" applied to a Study Area at the Jurassic Escarpment (SW-Germany). Geomorphology, 86, pp. 12-24.

Okura, Y., Kitahara, H., Kawanami, A. and U. Kurokawa (2003): Topography and volume effects on travel distance of surface failure, Eng. Geol., 67, pp. 243-254.

Pack, R.T., Tarboton, D.G. & Goodwin, C.N (1998): The SINMAP Approach to Terrain Stability Mapping. Proc. Int. Congress of the International Association of Engineering Geology and the Environment 8, Vol 2, A A Balkema, Rotterdam, pp. 1157–1165.

Pack, R.T., Tarboton, D.G., Goodwin, C.N. & Prasad, A. (2005): SINMAP User's Manual. A Stability Index Approach to Terrain Stability Hazard Mapping. www.engineering.usu.edu/dtarb/sinmap.html.

Picard, R.P. & Berk, K.N. (1990): Data Splitting. The American Statistician, Vol. 44, No. 2, pp. 140-147.

Porwal, A.K., Carranza, E.J.M. & Hale, M. (2003): Knowledge - driven and Data - driven Fuzzy Models for predictive Mineral Potential Mapping. Natural Resources Research, 12(1), pp. 1-25.

Pradhan, B., Ab Talib, J. & Saro Lee, S. (2006): Application of Remote Sensing Data in determining regional Landslide Hazard Analysis by using Logistic Regression Model and GIS. Proc. 27th Asian Conference on Remote Sensing, Asian Association on Remote Sensing (AARS).

Proske, H., Granica, K., Hirschmugl, M. & Wurm, M. (2008): Landslide Detection and Susceptibility Mappping using innovative Remote Sensing Data Sources. Proc. Internationales Symposion INTERPRAEVANT 2008, Vol. 2, pp. 219 – 230, Feldkirch 2008.

RAMMS (2010) http://ramms.slf.ch/ramms/ 7.10.2010

Regmi, N.R., Giardino, J.R. & Vitek, J.D. (2010): Modelling Landslides Using the Weight of Evidence Approach: Western Colorado, USA. Geomorphology 115, pp. 172-187.

Rezaei Moghaddam, M.H., Khayyam, M., Ahmadi, M. & Farajzadeh, M. (2007): Mapping Susceptibility Landslide by Using the Weight-of-evidence Model: A Case Study in Merek Valley, Iran. Journal of Applied Sciences 7(22), pp. 3342–3355.

Rickenmann, D. (2005): Runout prediction models. In: Jakob, M., Hungr, O. (editors), Debris-flow Hazards and Related Phenomena. Springer, Berlin, pp. 305–324.

Rickli, C. and F. Forster (1997): Einfluss verschiedener Standortseigenschaften auf die Schätzung von Hochwasserabflüssen in kleinen Einzugsgebieten. Schweiz. Zeitschr. f. Forstwesen. Vol. 148, Heft 5, 367-385.

Rickli, C. and H. Bucher (2003): Oberflächennahe Rutschungen, ausgelöst durch die Unwetter vom 15.-16.7.2002 im Napfgebiet und vom 31.8.-1.9.2002 im Gebiet Appenzell. Projektbericht zuhanden des Bundesamtes für Wasser und Geologie BWG. Bundesamt für Wasser und Geologie BWG, Eidgenössische Forschungsanstalt WSL.

Russ W. 2011: Mehr Wald in Österreich, in: BFW Praxis Information Nr. 24-2011 S3-9, BFW-Wien

Sabto, M. (1991): Probabilistic modelling applied to landslides in central Colombia using GIS procedures. Unpubl. Msc Thesis, ITC, Enschede, 26 p.

Schardt, M. & Schmitt, U. (1996): Klassifikation des Waldzustandes für das Bundesland Kärnten mittels Satellitendaten. Österr. Zeitschrift für Vermessung und Geoinformation, Heft 1/96, 84. Jahrgang.

Schauer, T. (1992): Der Beitrag der Vegetationskartierung für die Abschätzung und Prognose des Abflusses, des Abtrags und der Belastung bei spezifischen Nutzungen in alpinen Wildbacheinzugsgebieten. Internationales Symposium INTERPRAEVENT, Bern

Scherrer, S. and F. Naef (2003): A decision scheme to indicate dominant hydrological flow processes on temperate grassland. Hydrological Processes, 17, 391-401

Schwarz S., Englisch M., Aichberger K., Baumgarten A., Blum W. Danneberg O., Glatzel G., Huber S., Kilian W., Klaghofer E., Nestroy O., Pehamberger A., Wagner J., Gerzabek M. (2001): Bodeninformation in Österreich, aktueller Stand und Ausblick. Mitt. d. Österr. Bodenkundl. Ges., H. 62.

Schwarz, L., Haberler, A., Tilch, N., Lotter, M., Koçiu, A. (2009): Massenbewegungen in der Katastrophenregion Bezirk Feldbach im Juni 2009, Zwischenbericht. Interner Bericht für Land Steiermark, 19 S., 6 Abb., Geol.B.-A. (Wien).

Schwarz, L., Tilch, N. & Kociu, A. (2009): Landslide susceptibility mapping by means of artificial neural networks performed for the region Gasen-Haslau (eastern Styria, Austria). 6th EUREGEO - European Congress on Regional Geoscientific Cartography and Information Systems, München, 9.-12. Juni, 2009; [http://www.geologie.ac.at/pdf/Poster/poster_2009_euregio.pdf]

Sekiguchi, T. & Sato, H.P. (2004): Mapping of micro topography using airborne laser scanning. Landslides 1, pp. 203-209.

Smith, M. (1993): Neural Networks for Statistical Modeling, Van Nostrand Reinhold, New York.

Spiegelhater, D. & Kill-Jones, R.P. (1984): Statistical and knowledge approaches to clinical decision-support systems, with an application in gastroenterology. Journal of the Royal Statistical Society, 147, pp. 35-77.

Spiegelhater, D. J. (1986): A statistical View of Uncertainty in Expert Systems. In: Gale, W. (Ed.): Artificial Intelligence and Statistics. Addison-Wesley, Reading, MA, pp. 17–55.

Stähli, M., Bartelt, P., 2007: Von der Auslösung zur Massenbewegung, in Forum für Wissen, WSL – Birmensdorf.

Sulaiman, W.N.A. & Rosli, M.H. (2010): Susceptibility of Shallow Landslides in Fraser Hill Catchment, Pahang Malaysia. EnvironmentAsia 3 (special issue), pp. 66-72, Chantaburi, Thailand.

Tarboton, D.G., Bras, R.L. and I. Rodriguez–Iturbe. 1991. On the Extraction of Channel Networks from Digital Elevation Data. Hydrological Processes. 5: 81-100.

Thiebes, B., Bell, R. & Glade, T. (2007): Determinitische Analyse flachgründiger Hangrutschungen mit SINMAP - Fallstudie an der Schwäbischen Alb / Deterministic landslide susceptibility analysis using SINMAP - case study in the Swabian Alb, Deutschland. In: Proc. of the Conference 'Geomorphology for the Future', Obergurgl, Österreich, pp. 177–184.

Thiery, Y., Malet, J.-P., Sterlacchini, S., Puissant, A. & Maquaire, O. (2007): Landslide Susceptibility Assessment by bivariate Methods at large Scales: Application to a complex mountainous Environment.- Geomorphology, 92, 1-2 (2007) pp. 38–59, DOI : 10.1016/j.geomorph.2007.02.020.

Tilch N, Kociu A. 2007: Bericht zum Projekt: Abschätzung der Risikodisposition für Rutschungen und Hangbewegungen am Beispiel Gasen/Haslau (Stmk), GBA Wien

Tilch, N. & Koçiu, A. (2006): Massenbewegungen in der Katastrophenregion Gasen-Haslau (Oststeiermark) im August 2005.- Tagung Pangeo06, 17. – 20. 09.2006 in Innsbruck, Posterpräsentation S3 Alpine Naturgefahren – Massenbewegungen. (http://www.geologie.ac.at/pdf/Poster/poster_2006_pangeo06_tilch.pdf)

Tilch, N. (2007): Abschätzung der Risikodisposition für Rutschungen und Hangbewegungen am Beispiel Gasen/Haslau (Stmk) – „state of the art" der Datenkompilation .- Vortrag im Rahmen eines Projekttreffens am 12.10.2007; Gasen (Steiermark).

Tilch, N. (2009): Gravitative Massenbewegungen in der Katastrophenregion Klingfurth (Walpersbach, Südliches Niederösterreich) im Juni 2009 – Erkundungsergebnisse und eine erste Abschätzung des rutschungsinduzierten Gefahrenpotentials .- 11. Geoforum Umhausen 15.-16.10.09, Niederthai. (http://www.geologie.ac.at/pdf/Poster/poster_2009_geoforum_tilch.pdf)

Tilch, N., Kociu, A., Ribitsch, R., Schmid, F., Proske, H., Andrecs, P., Hagen, K., Lang, E., Hermann, S. & Loizenbauer, J. (2009): Abschätzung der Risikodisposition für Rutschungen und Hangbewegungen am Beispiel Gasen/Haslau (Stmk).- FloodRisk II - Vertiefung und Vernetzung zukunftsweisender Umsetzungsstrategien zum integrierten Hochwassermanagement. Ergebnispräsentationsveranstaltung 29./30.06.2009, Wien; Poster. (http://www.geologie.ac.at/pdf/Poster/poster_2009_floodrisk_II.pdf)

Van Westen, C.J. (1993): Training package for geographic information systems in slope instability zonation. Vol. 1: Theory: Application of geographic information systems to landslide hazard zonation. ITC Publication No. 15, International Institute for Aerospace Survey and Earth Sciences, Enschede.

Voellmy, A. (1955): Über die Zerstörungskraft von Lawinen. Schweizerische Bauzeitung, 73.

Wack, R. & Wimmer A. (2002): Digital Terrain Models From Airborne Laser Scanner Data – A Grid Based Approach. IAPRS, Vol XXXIV, Part 3B, ISPRS Commission III Symposium, Graz, Austria, pp. 293□296.

Wack, R., Schmidt, M., Kubista, E., Schönhuber, M., Richter, M., Koudelka, O. & Raggam, H. (2006): Fluggestützte Plattform für Katastropheneinsätze – Basisstudie. Unpubl. Report b.o. of Styrian Government/Dep. for Science and Research, Graz.

Wagner, W., Ullrich, A. & Briese, C. (2003): Der Laserstrahl und seine Interaktion mit der Erdoberfläche. Österreichische Zeitschrift für Vermessung & Geoinformation 4, pp. 223-235.

Wehr, A. & Lohr, U. (1999): Airborne laser scanning – an introduction and overview. ISPRS Journal of Photogrammetry & Remote Sensing, 54 (2-3), pp. 68-82.

WIFO - Austrian Institute of Economic Research (2008): Eine volkswirtschaftliche Analyse der Wildbach- und Lawinenverbauung.

Zhu, L. & Huang, J. (2006): GIS-based Logistic Regression Method for Landslide Susceptibility Mapping in regional Scale. Journal of Zhejiang University Science A

13. Annex

See: ASlide_Endreport_Annex_201107

Content

Tab. A1: Validation of runs of neural networks according to validation strategy Chapter 7.2.1

Tab. A2: Comparison of the validation of runs of neural networks according to validation strategy Chapter 7.2.1 (bold: run showing better validation measured value)

Fig. A1: Combined map of final result „level low" of susceptibility (mid-range) and its uncertainty (half range of) for both methods

Fig. A2: Combined map of final result „level high" of susceptibility (mid range) and its uncertainty (half range) for both methods

Fig A3: Combined map of final result „level high" of susceptibility range (version for practical application, attached as A= plot)

Fig A4: Process areas with calculated with the ASlide model based on starting information landsilde disposition, level high (best fit), starting criterion 0.5 and alpha = 22 (best fit), shp files in dig. version attached

Tab. A3 part 2: Parameter maps and their expenditure of time

Tab. A4 part 1: Improvements in the quality of the susceptibility maps by adding parameter maps and comparisons of the improvements caused by different parameter maps – susceptibility maps modelled by neural networks (for exact definition of parameter map: cf. Tab A3)

Tab. A4 part 2: Improvements in the quality of the susceptibility maps by adding parameter maps and comparisons of the improvements caused by different parameter maps – susceptibility maps modelled by neural networks (for exact definition of parameter map: cf. Tab A3)

Tab. A5 part 1: Improvements in the quality of the susceptibility maps by adding parameter maps and comparisons of the improvements caused by different parameter maps – susceptibility maps modelled by logistic regression (for exact definition of parameter map: cf. Tab A3)

Tab. A5 part 2: Improvements in the quality of the susceptibility maps by adding parameter maps and comparisons of the improvements caused by different parameter maps – susceptibility maps modelled by logistic regression (for exact definition of parameter map: cf. Tab A3)

Tab. A6 part 1: Improvements in the quality of the susceptibility maps by adding parameter maps and comparisons of the improvements caused by different parameter maps – susceptibility maps modelled by weight of evidence (for exact definition of parameter map: cf. Tab A3)

Tab. A6 part 2: Improvements in the quality of the susceptibility maps by adding parameter maps and comparisons of the improvements caused by different parameter maps – susceptibility maps modelled by weight of evidence (for exact definition of parameter map: cf. Tab A3)